Controls on seasonal elemental variation in tropical rivers in Goa, India

Controls on seasonal elemental variation in tropical rivers in Goa, India

Chris Hibbert

Birkbeck, University of London

PhD Thesis

31st July 2017

Declaration

This thesis is a presentation of my original research work. Wherever contributions of others are involved, every effort is made to indicate this clearly, with due reference to the literature, and acknowledgement of collaborative research and discussions.

The work was done under the guidance of Professor Karen Hudson-Edwards, Birkbeck, University of London and Dr Mike Widdowson, University of Hull.

Name: Chris Hibbert

Signed:

Acknowledgements

Firstly, I would like to express my sincere gratitude to my supervisors; Prof. Karen Hudson-Edwards and Dr Mike Widdowson for their continuous support throughout my PhD study, and for their patience, motivation, and continuous advice. Their guidance helped me throughout all aspect including, research, analysis, interpretation and writing of this thesis. I could not have imagined having better supervisors and mentors for my PhD study.

Besides my advisor, I would like to thank Professor Andy Carter, Dr Philip Pogge von Strandmann and Dr Philip Hopley for their constructive comments during my transfer viva which led to a greater understanding of my field of study. Likewise I would like to thank my examiners, Professor Balz Kamber and Dr Kate Heppell for their thorough evaluation of my thesis which has substantially improved the documentation of the study.

However, my greatest gratitude must go to my wife for supporting me throughout this incredible journey and for not letting me give up in those numerous difficult times.

Abstract

This study focuses upon chemical variation in fluvial discharge over a 15 month period (May 2007 – July 2008) in a sub-tropical, monsoonal climatic regime in western India. Here, highly seasonal rivers rising at the Western Ghats escarpment discharge into the Arabian Sea. The Ghats present a topographical barrier to the SW monsoon, and thus generate one of the world's highest orographic gradients.

Two river basins were selected for this study, the Zuari and the Chapora, both characterised by high seasonal precipitation and run-off, with c. 85% occurring during the monsoon months (June – September). The rivers flow steeply down the Ghats then across the low-lying Konkan - Kanara coastal plateaux much of which is heavily weathered and covered by laterite. The water samples (n = 13 per month) were collected from seven sites along the Zuari River and six sites along the Chapora River. The samples were analysed using ICP-MS for cations and ion chromatography for anions.

Major and trace element concentrations were found to be very low throughout both basins, although a marked increase was observed for various elements (e.g., Ca, K, Mg, Na, Rb, Sr, V, Cr, Mn, Fe, Co, HCO_3^-) shortly after the onset of the monsoon. We interpret this as a 'rinse-out effect'. Despite absolute concentrations decreasing with increasing river run-off, total element fluxes increase during the monsoon. Additionally, due to the low elevation of the coastal plain, tidal effects are observed c. 40 km inland becoming forced seaward during the monsoon by high river flows.

Silicate weathering is of primary importance in the long term global climate due to associated CO_2 sequestration, and continental weathering is controlled by numerous factors, including lithology, climate, vegetation and anthropogenic effects; it is highest in the humid tropics due to high temperatures and precipitation. However, this study also identifies additional controls, these being the degree of weathering and the extent of weathering residuum, which are major limiting factors for elemental fluxes in tropical catchments.

Table of Contents

Table of Figures

List of Tables

Thesis Title: Controls on seasonal elemental variation in tropical rivers in Goa, India

Acknowledgements: Dr Karen Hudson-Edwards, Dr Mike Widdowson and Mr Orlando Fernandez.

PART I: BACKGROUND

Chapter 1. Introduction

Continental weathering and erosion exerts a fundamental control on the delivery of particulate and dissolved products from the continents to the oceans, and is therefore a major factor in the global cycling of many chemical elements, including carbon (Berner et al., 1983, Dessert et al., 2001). For the purposes of understanding this cycling, the continents may be considered as comprising a range of lithologies, which can be broadly sub-divided into carbonates, evaporites and silicates. It is the weathering of silicates that affects the carbon cycle (Dessert et al., 2003), and in particular the weathering of Ca and Mg silicates which leads to the permanent (million year timescale) removal of CO_2 (Berner et al., 2003). This process converts atmospheric CO_2 into bicarbonate which is transported in rivers and streams to the oceans where it is precipitated as Ca and Mg carbonates (Dessert et al., 2003). The second major control on atmospheric CO_2 is the weathering and subsequent burial of organic carbon during sediment deposition (Dessert et al., 2001). During the Phanerozoic, approximately 80% of the carbon removed from the ocean-atmosphere system was due to carbonate deposition, with the remaining 20% being due to organic carbon burial (Raymo and Ruddiman, 1992). Therefore, weathering and erosion can affect the long-term ocean-atmosphere budget of CO_2 through the consumption of carbonic acid during silicate weathering, and through changes in the weathering and burial rates of organic carbon (France-Lanord and Derry, 1997) The majority of organic carbon burial takes place in shallow marine environments such as estuaries, continental shelves and deltas (Raymo and Ruddiman, 1992). Changes in the weathering and burial rates of these deposits can provide a negative feedback control on atmospheric CO_2 as they release CO_2 back to the atmosphere during weathering (Raymo and Ruddiman, 1992). Since CO_2 is a greenhouse gas, weathering and erosion play a vital role in regulating the Earth's climate, and over geological timescales (10^6 to 10^9 years) continental silicate weathering is the main sink for carbon (Dupre et al., 2003). For example, the chemical weathering of Ca-silicates (e.g. key rock forming minerals such as plagioclase feldspar, pyroxene etc.) can be generically described as follows (Dupre et al., 2003):

$CaSiO_3 + CO_2 + H_2O \leftrightarrow Ca^{2+} + 2HCO_3^- + SiO_2 + H_2O$ *Equation 1.1*

Calcium silicate + carbon dioxide + water ↔ Calcium ions + bicarbonate ions + silicon dioxide + water

This dissolution reaction releases cations and HCO_3^- into rivers and the oceans, where they are consumed by carbonate precipitation on the seafloor (Dupre et al., 2003).

$Ca^{2+} + 2HCO_3^- \leftrightarrow CaCO_3 + H_2CO_3$ *Equation 1.2*

Calcium ions + bicarbonate ions ↔ calcium carbonate + carbonic acid

The net budget of silicate weathering can be written as follows:

$CaSiO_3 + CO_2 \leftrightarrow CaCO_3 + SiO_2$ *Equation 1.3*

Calcium silicate + Carbon dioxide ↔ Calcium carbonate + Silicon dioxide

CO_2 is also involved in the weathering of carbonate minerals such as calcite and dolomite (Berner et al., 1983). The calcite and dolomite weathering equations are written below:

$CaCO_3 + H_2CO_3 \leftrightarrow Ca^{2+} + 2HCO_3^-$ *Equation 1.4*

Calcite + carbonic acid ↔ calcium ions + bicarbonate ions

$CaMg(CO_3)_2 + 2H_2CO_3 \leftrightarrow Ca^{2+} + Mg^{2+} + 4HCO_3^-$ *Equation 1.5*

Dolomite + carbonic acid ↔ calcium ions + magnesium ions + bicarbonate ions

From the above equations it can be seen that no CO_2 is permanently sequestered and precipitated during carbonate weathering; only Ca, Mg ions and bicarbonate ions are generated. The bicarbonate ions form part of the Dissolved Inorganic Carbon (DIC) cycle.

$CO_2 + H_2O \leftrightarrow H_2CO_3 \leftrightarrow H_2CO_3 + H^+ \leftrightarrow HCO_3^- \leftrightarrow HCO_3^- + H^+ \leftrightarrow CO_3^{2-}$ *Equation 1.6*

Carbon dioxide + water ↔ carbonic acid ↔ Carbonic acid + hydrogen ion ↔ bicarbonate ion ↔ Bicarbonate ion + hydrogen ion ↔ carbonate ion

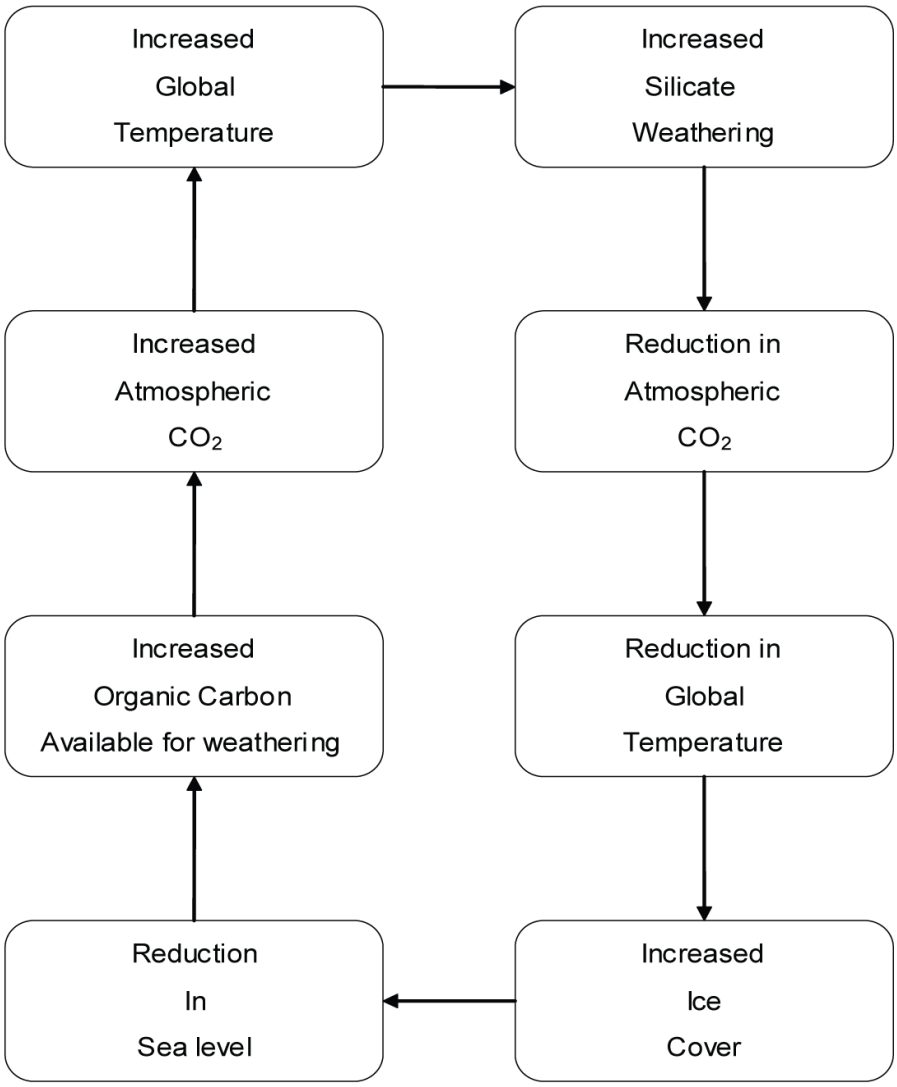

Figure 1.1 Flow diagram depicting the interconnectedness of silicate weathering rate, organic carbon burial and atmospheric CO_2 variation (after Raymo and Ruddiman, 1992).

Chemical weathering rates (CWR) and silicate weathering rates (SWR) are regulated by numerous co-dependent factors, including lithology, temperature, run-off, vegetation and relief. Lithology is a key control, with basalts known to weather more rapidly than other silicates such as granites and gneisses (Meybeck, 1986, Amiotte Suchet and Probst, 1993). This is due to the relative stability of the minerals contained within the various lithologies at the temperatures and pressures found at the Earth's surface. Goldich (1938) demonstrated that there was a consistent variation in the stability of the common rock-forming silicate minerals that occur in a range of igneous and metamorphic rocks. This variation is similar to Bowen's reaction series, which describes the order in which minerals precipitate from a melt.

Weatherability is essentially the opposite of Bowen's reaction series, with the minerals that precipitated at the highest temperatures (least stable) weathering first and the minerals precipitated at the lowest temperatures (most stable) being typically more resistant to weathering (Figure 1.2). Basalts are relatively high temperature (i.e., 1000 – 1175°C) extrusive igneous rocks of mafic composition and are dominated by the relatively unstable mafic minerals like pyroxene, anorthite and olivine. By contrast, granite is an intrusive igneous rock emplaced within the continental crust at much lower temperatures (i.e., 650 - 750°C); it is of felsic composition and is dominated by the more stable minerals quartz, plagioclase feldspar and biotite mica. Additionally, igneous and metamorphic rocks are typically more susceptible to chemical weathering than sedimentary rocks since sedimentary rocks, (excluding examples such as tephra fall), by their very nature, have already undergone at least one stage of weathering, erosion and transport prior to their deposition. Accordingly, through each cycle they retain an increasing proportion of the most stable components.

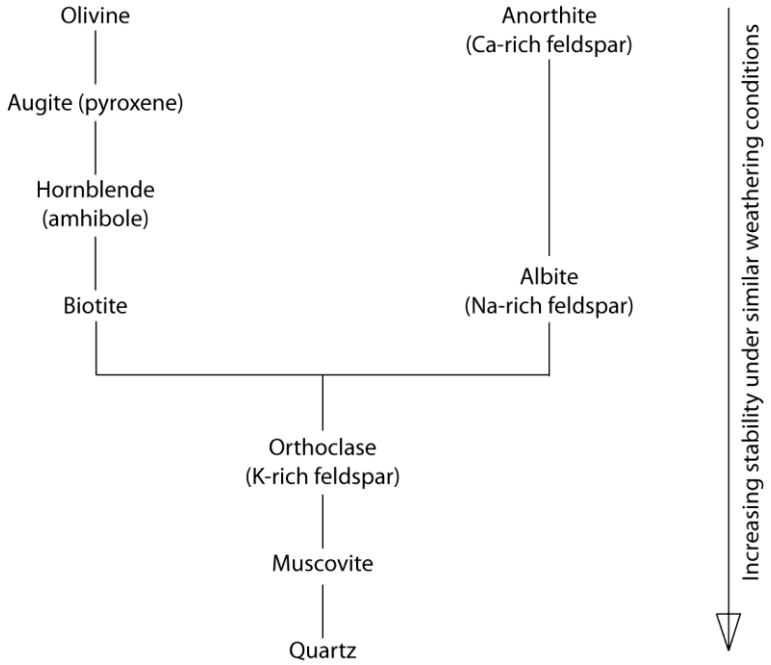

Figure 1.2 Diagram describing the relative stability of various common rock forming minerals under similar weathering conditions (after Goldich, 1938).

Importantly, basalt is one of the most common rocks (c.80%) occurring at the Earth's surface (ocean crust and Large Igneous Provinces), and therefore its weathering and decomposition necessarily must play an important role in the chemical cycling processes described above. Although the ocean floors are composed almost exclusively of basaltic crust, this material is unavailable for the usual weathering processes except where preserved sub-aerially (e.g., in ophiolitic successions).

Most important, however, are basaltic successions emplaced either as volcanic edifices (on land or emerging from the ocean – Hawaii etc.), and the immense remains of continental flood basalt events, examples of which are preserved on every major continental mass. For instance, Louvat et al. (1997) studied weathering on the volcanic islands of Reunion and Sao Miguel (Azores), and concluded that basalt weathering acts as a significant sink for atmospheric CO_2 due to high precipitation (up to 7000 mm yr^{-1} for Reunion and 740 – 2400 mm yr^{-1} for Sao Miguel) and high relief leading to high rates of run-off (Louvat and Allegre, 1997, Louvat and Allegre, 1998, Taylor and Lasaga, 1999). This observation is further supported by studies on the weathering of large igneous provinces such as the Columbia River Basalts (Taylor and Lasaga, 1999) and the Deccan Traps (Dessert et al., 2001). After lithology, degree of run-off and temperature are widely believed to be the dominant controls on chemical weathering (Dessert et al., 2001, Dessert et al., 2003, Dupre et al., 2003, Das et al., 2005b). In locations where extensive weathering has created a thick laterite or soil cover this reacted material then alters the controls by creating a buffer between the unaltered bedrock and the prevailing climate. This becomes especially important where particular climate extremes exist, such as high temperatures and seasonally high precipitation. Accordingly, run-off and temperature are fundamental controls in monsoon affected areas where seasonal fluctuations predominate.

The seasonal variation of the Inter Tropical Convergence Zone (ITCZ) brings a monsoon climate to many low latitude parts of the globe. The large pressure differential between the Indian Ocean high-pressure zone, and the intense low-pressure zone located over Southern Asia, makes the South West Monsoon most dramatic in Southern Asia and the Arabian Sea due to the extreme elevation of the Himalayas. This monsoonal circulatory pattern is not a new phenomenon but is the result of the collision of India and Asia over the past 50 Ma and the subsequent uplift of the Tibetan plateaux c. 15 - 17 Ma (Raymo et al., 1988, DeConto and Pollard, 2003), the elevation of this plateaux has remained relatively constant over the past 15 Ma (Spicer et al., 2003). On a global scale, such plateau uplift may have enhanced silicate rock weathering (Raymo and Ruddiman, 1992) and a drawdown of atmospheric CO_2 that may be linked to cooling across the Oligocene and the onset of glacial conditions. This monsoonal climate results in high temperatures, with the hottest months occurring pre and post monsoon where temperatures reach 30 - 33ºC (Government of India, 2010) and highly seasonal precipitation (e.g. annual precipitation of 1500 – 3500 mm, of which c. 80 – 85% occurs during June - September), and thus potentially provides significantly enhanced chemical weathering rates. As such, monsoon-affected areas

are important to consider when calculating global CO_2 drawdown values (Dessert et al., 2001, Dessert et al., 2003, Dupre et al., 2003, Das et al., 2005). For instance, considerable research has been conducted on the silicate weathering rates of the Deccan Basalts of NW peninsular India (Figure 1.9), which are well-known for their high weathering rates (Dessert et al., 2001, Dessert et al., 2003, Dupre et al., 2003, Das et al., 2005). These support the previous assertion that after lithological control, run-off and temperature are the main parameters controlling CWR and CO_2 consumption during basaltic weathering. Further, the effects of variation in run-off upon CWR are demonstrated by the observation that chemical and silicate weathering rates of the west-flowing rivers along the western coast of India are of the order of four times higher than those draining the peninsula to the east (Das et al., 2005b); this corresponds to the higher rainfall and run-off in the western region of 463 mm yr^{-1} for the easterly flowing rivers and 1690 mm yr^{-1} for the westerly flowing rivers. These co-dependent factors are discussed in more detail in section 2.4.

1.1. Thesis Aims and Objectives

The aim of this PhD research is to determine the characteristics, controls, and effects on atmospheric CO_2 drawdown of chemical weathering in a sub-tropical, monsoonal climatic regime in high CWR westerly-draining river basins of western peninsular India. In order to achieve this, two river basins were chosen in Goa state which drain from the scarp slope of the Western Ghats, and across the low-lying Konkan plain; the more southerly basin, the Zuari is adjacent to extensive areas of iron ore (banded iron formation; BIF) mining and is used as a route way for bulk ore carrying barges; the more northerly Chapora basin is unaffected by mining activities. Through studying these two basins, the following specific objectives are identified:

1) determine the variation in chemical composition of fluvial discharge into the Eastern Arabian Sea over a 15 month period from June 2007 to July 2008;
2) determine the extent of tidal influence on river chemistry, spatially, throughout the drainage basins and temporally, throughout the sampling period in order to ensure that only riverine samples unaffected by estuarine influence are used in subsequent discussions;
3) determine the role of lithology on the elemental concentrations within the chosen fluvial systems;
4) determine the effect of the laterite cover on the elemental concentrations within the chosen fluvial systems;
5) determine the effect of Fe-Mn mining on dissolved riverine fluxes.

6) calculate the CO_2 drawdown resulting from the chemical weathering of the underlying lithology of the Chapora and Zuari River basins.

The results of the study will provide information to allow the evaluation of the following broader themes:

i) Continental weathering and erosion and their effects on atmospheric CO_2 and global climate. In this context, the current work provides important documentation and data supplementing the growing global body of research detailing river catchments and their fluxes. Most crucially this research documents chemical fluxes in a previously uncharacterised setting of high rainfall, a high orographic gradient and a mature weathering (lateritised) hinterland.

ii) This mature weathered (lateritised) hinterland can act to protect the underlying unaltered protolith, therefore the variation in elemental reactivity with increasing depth has been evaluated by means of a column experiment. In which the material used in each column is derived from a different zone within a weathering profile (Merces Quarry). This research clearly demonstrates that the majority of chemical weathering occurs at depth at the weathering front with diminishing contributions moving upwards towards the surface;

iii) A comparison of river chemistry between adjacent basins affected and unaffected by BIF mining activities, i.e., (Zuari and Chapora drainage basins, respectively). In this context, the current work provides important documentation and data regarding the magnitude and effect of Fe-Mn mining affecting the nature of the dissolved riverine fluxes.

Chapter 2. Literature review

The main focus of the current research is to investigate weathering and element mobility resulting from the alteration of the lithologies that form the solid geology exposed across Goa State. This is achieved by detailed chemical investigation of river waters within key drainage systems of the Chapora and Zuari rivers. To provide context, a brief summary of the key aspects of weathering and erosion is presented Figure 2.1. This diagram provides a framework for the ensuing discussion since each heading is considered in turn. Beginning with the high energy environments where physical weathering dominates, before moving onto the low energy environments where chemical weathering dominates. Each section considers the main mechanisms and factors controlling their respective rates. The section then discusses existing published weathering studies, beginning with more global examples before focusing in on India and then Goa.

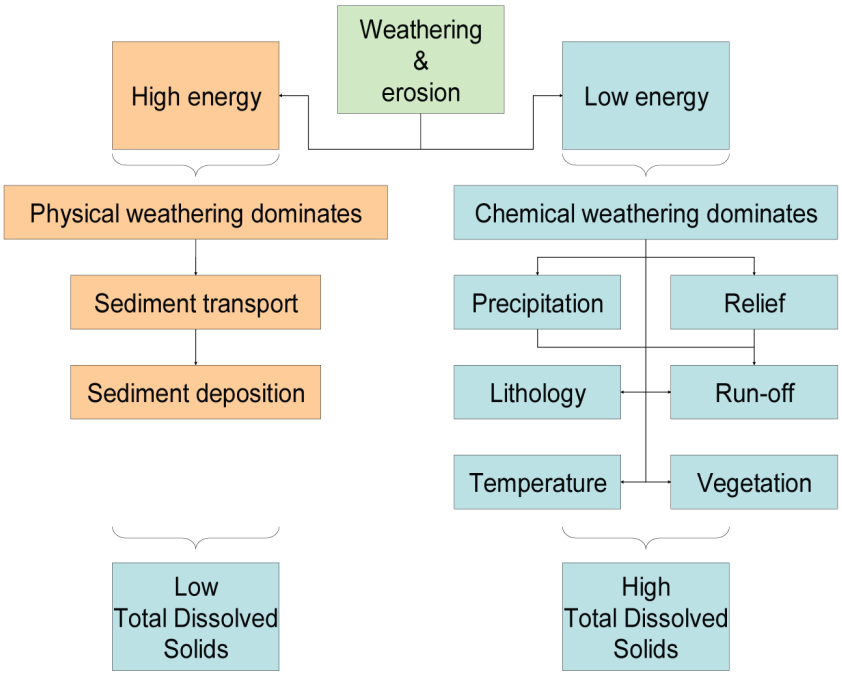

Figure 2.1 Diagram highlighting how high and low energy environments favour either physical or chemical weathering resulting in low or high Total Dissolved Solids (TDS), respectively, compiled from previous author's summaries.

Weathering can be divided into those processes that involve chemical reactions and the formation of new minerals (chemical weathering) and those that involve physical changes (physical weathering or breakdown) However, in practice these two processes rarely work independently of each other. For example, a rock shattered by physical weathering will provide greater surface area for chemical weathering; conversely,

chemical weathering along a joint or fissure will weaken it and make it more susceptible to physical weathering (Summerfield, 1991). Additionally, biological weathering can accelerate both chemical and physical weathering; this is discussed in more detail in section 2.5. Also, depositional environments themselves can provide additional opportunity for chemical weathering to take place; this may be of particular importance for highly seasonal environments where a protracted dry (low energy) season exists between successive Monsoonal (high energy) periods which may favour more physical weathering.

2.1. Physical weathering

The physical breakdown of a rock is always manifested with some form of volumetric change and / or change in the exposed surface area. This may involve an overall volumetric change in the rock, or be related to changes in the volume of material introduced into voids or fissures within the rock (Summerfield, 1991, Thomas, 1994). Rocks formed at depth can undergo volumetric changes caused by their expansion or dilation as they become uplifted to the surface as the overlying strata is removed by erosion; this is known as pressure release, and in turn this promotes the formation of joints. These joints, along with other naturally occurring features such as foliations and micro-fissures associated with the original pattern of mineral crystallisation, can provide lines of weakness where exfoliation (i.e., spalling off of thin sheets of rock) or granular disintegration (disintegration of individual crystals or grains) can occur. Thermal expansion is another way that stresses can be created within the rock. This can be purely as a result of large fluctuations between day time and night time temperatures, by lightning strike, or by the occurrence of vegetation fires. The effect of these processes may be more effective when differential thermal expansion in individual minerals occurs (Summerfield, 1991, Thomas, 1994).

Volume changes due to material introduced into voids or fissures can be considered in two processes; 1) stresses caused by crystal growth and expansion of primarily salt and ice and 2) stresses caused by biological activity including both flora and fauna. Frost weathering involves the breakdown or rocks by stresses induced by the freezing of water. This is thought to be due to the 10% volume expansion during the phase change from water to ice (Holden, 2005). Under ideal conditions this can lead to pressures of around 200 MPa. However, since the tensile strength of most rocks is c. 25 MPa for this to occur it is necessary to have a closed system so that water cannot just be expelled into voids elsewhere in the system.

Salt weathering involves the precipitation of salts in voids and the expansion of salt crystals through either hydration or heating. Salt weathering is most active in arid environments where evaporation rates are high relative to precipitation and therefore surface and soil waters can become saturated in certain salts. Also the high salinity of seawater makes it likely that salt is an active weathering agent in coastal areas. When saline solutions in the pore spaces of rocks become saturated as a result of temperature change or evaporation, salt crystals begin to form which can generate considerable pressures (Nash and McLaren, 2011). In this study area the dominant processes are floods and landslides.

2.2. Sediment transport and deposition

The majority of rivers do not cut directly into bedrock but rather flow in alluvial channels formed of unconsolidated sediments of various sizes, ranging from clay-sized particles to boulders depending on the flow regime of the river at any given time (Summerfield, 1991). The initial setting in motion of a solid particle is called entrainment and this occurs when the forces acting on a particle are greater than the resistive forces, the ratio of these forces is known as the safety factor (SF), if SF is greater than one then movement will begin (Holden, 2005). The resistive forces are the immersed weight of the particle resulting from its size and density and the constraining effects of its neighbouring grains. Particles can also be subjected to a lifting force; this can arise from the acceleration of water over projecting grains. This increase in velocity over the grain leads to a reduction in pressure, if this lift force is sufficient to overcome the resistive force the grain will rise from the channel bed, this is called the Bernoulli effect (Summerfield, 1991). It is unlikely that the river flow force will be sufficient to retain these larger particles in the flow and they will slowly fall back towards the channel bed at a low angle, this type of flow is called saltation. Other forms of transport include suspension, rolling and sliding. River load can be split into dissolved or solute load which is derived from chemical weathering and is dispersed throughout the flow. Solid load can be sub-divided into bed load which includes all rolling, sliding or saltating loads and suspended load. Suspended load can also be further sub divided to include wash load which comprises very small particles that can remain in suspension provided there is some flow maintained. The suspended load, also known as suspended particulate matter (SPM) varies in proportion to energy and is therefore linked to rainfall and hence river run-off (Purnachandra Rao et al., 2011). For example, Figure 2 in their paper shows clear correlation between rainfall peaks and SPM peaks for both the Zuari and Mandovi rivers.

Where rivers do cut through bedrock channels they can erode the channels through abrasion, cavitation and corrosion (Summerfield, 1991). Abrasion is the wearing away or detachment of bedrock by particles moved by the water flow, these particles can be any size depending on the prevailing flow velocity. The effectiveness of abrasion depends on concentration, hardness and kinetic energy of the impacting bodies. Since kinetic energy is proportional to the square of the velocity, rates of abrasion increase rapidly with increasing velocity (Summerfield, 1991). Cavitation is essentially when an acceleration of flow in a fluid causes a pressure drop, which if sufficiently large can cause air bubbles to form. Cavitation occurs when these air bubbles implode and emit tiny jets of water at very high velocity as high at 130 ms^{-1}. Such velocities can generate sufficient stresses to fracture solid rock. Although this process is likely to occur in stream flows above 10 ms^{-1} its effects are usually obscured by the effects of abrasion. Finally, corrosion is the chemical weathering of minerals in contact with stream water.

2.3. Chemical weathering

Chemical weathering is concerned with the dissolution of pre-existing minerals, and formation of new minerals (often termed 'secondary minerals') that are stable at conditions prevailing at the Earth's surface. The rates at which these new minerals are formed are often difficult to model through analogue experimentation. Therefore it is necessary to consider two complementary approaches when studying chemical weathering (Summerfield, 1991). Thermodynamics considers the energy changes occurring during the chemical reactions, whilst kinetics is concerned with the rates and mechanisms of change. When chemical reactions occur energy is usually liberated in the form of heat (although, in certain reactions heat is absorbed). This liberation of heat represents a net release of free energy (ΔG) that is known as Gibbs Free Energy. The net free energy is calculated by subtracting the sum of all the free energies of the reacting substances from the sum of the free energies of the reaction products. If the calculated free energy change is negative the reaction will occur spontaneously, the larger the negative value the more readily the reaction will occur and the more stable the products will be compared to the original reactants. However, many mineral forms occur at the Earth's surface even though thermodynamic considerations tell us that they are unstable. Therefore it is necessary to consider the kinetics of weathering processes and hence the factors that affect the rate of change. These include the instability of the reacting system, the concentration of the reactants, temperature, catalysts and the intensity of leaching. For example, weathering by ground water will react differently dependent of the rock being weathered, i.e., a fine grained permeable

rock will weather faster than an impermeable well cemented or crystalline rock due to the difference in surface area available as reaction surfaces. Temperature is another crucially important factor which is expressed by the Arrhenius Equation which indicates that reaction rates approximately double for every 10ºC rise in temperature (Summerfield, 1991).

2.4. Climate controls

Temperature

Chemical weathering, like all chemical reactions, operates more quickly at higher temperatures. The most standard mathematical expression for the consumption flux of CO_2 by the weathering of a given exposed surface of silicate rocks F_{sil} might be written as follows (Dupre et al., 2003):

$$F_{sil} = k_{sil} R_f \cdot exp\left(\frac{Ea}{R}\left(\frac{1}{T} - \frac{1}{T_0}\right)\right)$$

Where R_f & T are the run-off across and temperature of the considered surface, k_{sil} is the kinetic rate constant for silicate weathering (Hilley and Porder, 2008), R is the gas constant and E_a is the activation energy, which, for basalt and granite are reported as 42,300 J mol^{-1} (Dessert et al., 2001) and 48,700 J mol^{-1} (Dupre et al., 2003), respectively and T_0 is the absolute temperature (298ºK). In practice this results in a doubling of reaction rate for every 10ºC rise in temperature (Goudie and Viles, 2012). The continental surface where this law can be applied is at best the size of small catchments (10^6 m^2). This kind of law is not appropriate for smaller spatial scales such as the microscopic scale (Dupre et al., 2003).

Since CO_2 is a greenhouse gas, a rise in atmospheric CO_2 causes a concomitant rise in Global Mean Surface Temperature (GMST). Moreover, because the weathering rate is temperature sensitive, a rise in temperature should be offset by a rise in weathering rate and CO_2 drawdown, thereby providing a strong negative feedback for variations in atmospheric CO_2 (Ruddiman, 1997). When one considers the mass of carbon stored in the atmosphere (0.06 x 10^{18} mol) compared with the estimated out-gassing flux (8 x 10^{18} mol Ma^{-1}) it is clearly important that the sources and sinks be closely balanced in order to maintain the atmospheric CO_2 concentration at a reasonable level (Berner et al., 1983, Ruddiman, 1997).

Precipitation and Run-off

Run-off is also a major controlling factor in weathering rate (Dessert et al., 2003). In a hydrologically closed watershed run-off (R) and precipitation (P) are related by the expression:

$R = P - ET$

Where R is run-off, P is precipitation and ET is the evapotranspiration all expressed as mm yr^{-1}. White and Blum (1995) provide average ET for alpine/temperate and tropical climates as 500 mm yr^{-1} and 1400 mm yr^{-1}, respectively, but also point out that tropical climates with very high precipitation can also have low ET possibly due to higher humidity. For example, one tropical location included in their study, Rio Icados in Puerto Rico was recorded as having a mean annual temperature of 22ºC, precipitation of 4300 mm yr^{-1} and a run-off of 3680 mm yr^{-1}, which equates to 620 mm yr^{-1} (14%) evapotranspiration.

High run-off rates often result in high weathering rates. In studies on coastal rivers c.100 km north of Goa in Maharashtra State, weathering rates of the westerly flowing rivers (Vashishthi, Shashtri, Kajli, Arjuna, Sukh and Gad) of c. 54 t km^{-2} y^{-1} were shown to be approximately four times higher than those flowing to the east (Krishna and its tributaries; Bhima, Koyna, Varna, Panchganga, Dudhganga and Ghataprabha as well as tributaries of the Bhima river; the Ghod, Mutha and Nira) with values of c. 14 t km^{-2} y^{-1} (Das et al., 2005) (Figure 2.2).

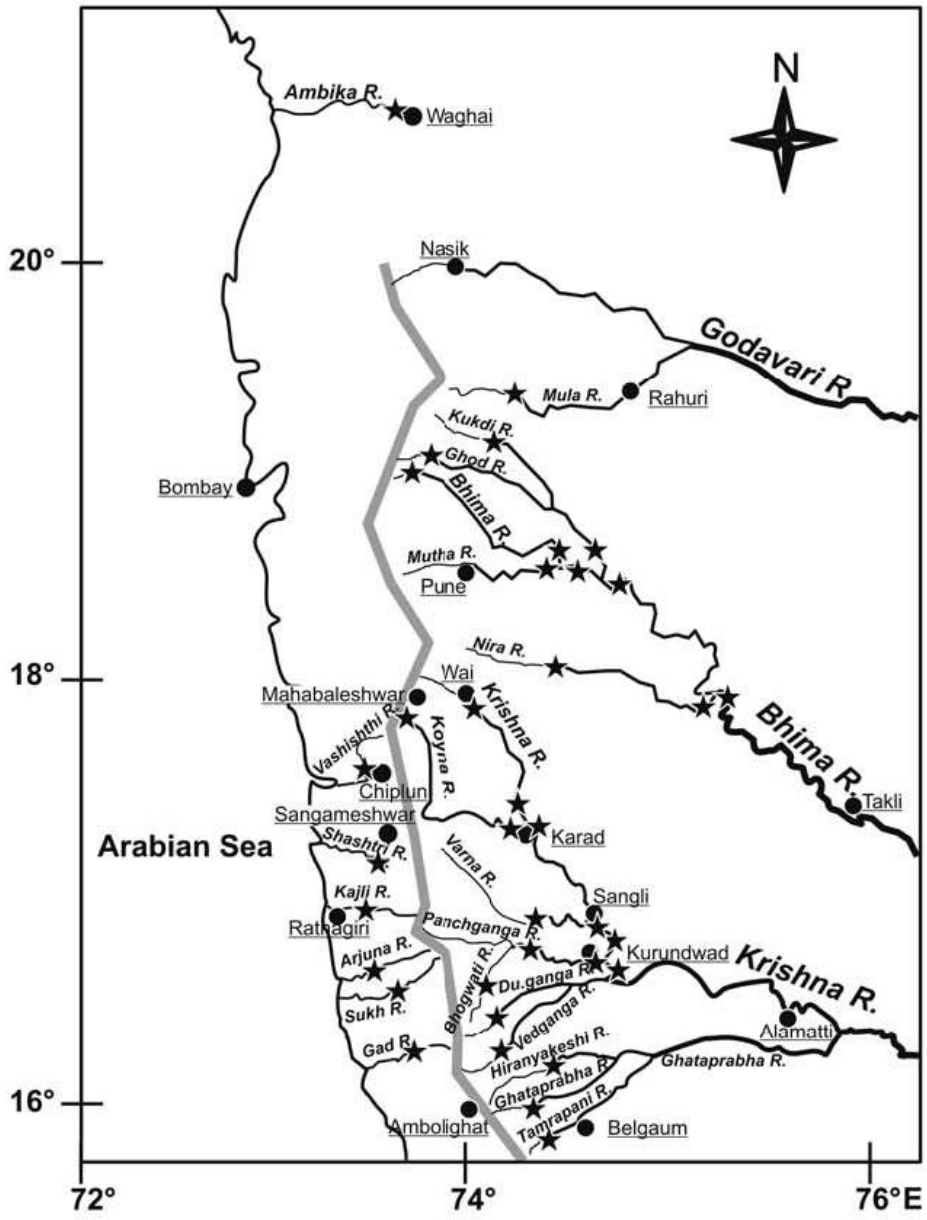

Figure 2.2 Location map showing the rivers sampled by Das et al. (2005); the sample localities are depicted by filled stars and major cities are depicted by filled circles (after Das et al, 2005).

This was attributed to the higher precipitation and subsequent run-off in the western region of 1690 mm y^{-1} compared to 463 mm y^{-1} for the east flowing rivers the headwaters of which lie in the 'rain shadow' of the Ghats escarpment (Das et al., 2005). Data available for the Zuari River record a run-off value of 2000 mm y^{-1} (Subramanian, 2000), similar in magnitude to that of the westerly flowing rivers observed by Das et al. (2005). Element flux tends to vary in response to increased river discharge with fluxes increasing as discharge increases, however, element concentrations do not appear to increase in the same way. Instead the opposite is often evident with element concentrations reaching their highest values during dry

periods and their lowest values during periods of high discharge. This is particularly evident for rivers draining seasonally dry lands. For instance, the Pilcomayo River in Bolivia shows a gradual decline in river discharge during the dry winter season (May until October) while concentrations of major anions and cations increase concomitantly (Smolders et al., 2004). Their 1998 – 99 study revealed that when water discharge was lowest (2 m^3 s^{-1}) during October, Na and Cl concentrations reached levels as high as 11,200 and 9600 µmol L^{-1}, respectively. Conversely, when discharge was highest (January 1999, peak discharges >1000 m^3 s^{-1}), Na and Cl concentrations became as low as 680 and 370 µmol L^{-1}, respectively (Smolders et al., 2004). Sulphate, magnesium and calcium concentrations were also lowest in January 1999 and highest in the first week of October, although the differences between the concentrations at high river discharge and low river discharge were significantly less (Smolders et al., 2004). At the beginning of the rainy season major ion concentrations initially decreased with increasing river discharge due to dilution of solutes in the base flow as a result of surface run-off derived from rainfall. As discharge continued to rise over subsequent weeks major ion concentrations showed a sudden sharp increase, which was explained by dissolution of precipitated salts formed during the dry season and the flushing of highly concentrated waters accumulating in the soil pores during the dry season (Smolders et al., 2004). This phenomenon has been termed 'the rinse out effect' (House and Warwick, 1998, Smolders et al., 2004), and is an important concept revisited later in this thesis.

The effects of run-off as a function of relief are most evident in areas affected by orogenesis. Tectonically uplifted areas such as the Himalayas, the Andes and the Tibetan Plateaux are key study areas especially as the uplift of the Himalayas coincides with the global cooling around the Cenozoic (Raymo and Ruddiman, 1992). However, it is not merely the weathering of silicates that increases, but there is also a concomitant increase in the burial of organic carbon. For example, Neogene sediments from the Bengal Fan have been used to estimate the CO_2 flux as a result of organic carbon burial and silicate weathering following the Himalayan uplift (France-Lanord and Derry, 1997). The estimated CO_2 consumption resulting from organic carbon burial and silicate weathering was calculated for two types of sediments; the first was dominated by illite and chlorite (the IC assemblage), this represents sedimentation before 7 Myr and after 1 Myr, the second was dominated by smectite and kaolinite (the SK assemblage) which represents sedimentation between 7 yr and 1 Myr when weathering was more intensive (France-Lanord and Derry, 1997). The CO_2 consumption resulting from silicate weathering was calculated as 0.17 mol kg^{-1} for the IC assemblage and 0.23 mol kg^{-1} for the SK assemblage, whilst the CO_2 consumption

due to organic carbon burial was calculated as 0.27 mol kg^{-1} for the IC assemblage and 1.1 mol kg^{-1} for the SK assemblage, between 1.7 and 4.7 times that of their silicate weathering sinks (France-Lanord and Derry, 1997). The extreme relief of the Himalaya and the monsoon climate lead to very rapid physical denudation and fast transport of sediment to the ocean. This results in a weathering limited system in which the kinetics of chemical weathering are slow relative to the transport time of erosion products, their storage in flood plains and eventual delivery to the ocean (France-Lanord and Derry, 1997, Pogge von Strandmann and Henderson, 2015).

Increased rates of uplift following orogenesis results in enhanced physical erosion providing a congruent increase in the surface area of fresh minerals available for chemical attack (Sarin, 2001). For instance, around the Palaeocene-Eocene boundary (c. 55 Ma) India's northward movement slowed as it began its collision with Asia and the Himalayas began to form. Evidence from mammalian distribution and pollen assemblages suggest that the Himalayas have risen c. 2.5km since the Late Miocene / Early Pliocene (c. 5 Ma) (Raymo et al., 1988). Likewise, in the Eastern Cordillera and Altiplano of the Bolivian Andes evidence from dated pairs of apatite and zircon shows that uplift here has approximately doubled over the past 5 Ma (Benjamin et al., 1987). These increased rates of tectonic uplift could have a significant effect on the chemical weathering rate and organic carbon burial, in turn leading to decreasing global climate by lowering atmospheric CO_2 (Raymo et al., 1988, Spicer et al., 2003). The Yangtze, Amazon and Ganges-Brahmaputra Rivers draining the Tibetan Plateaux are, today, the World's three largest fluvial supplies of dissolved material into the oceans, In fact, the Andes and Himalayas respectively account for c. 20% of the total dissolved and suspended solids and water discharge to the oceans (Raymo et al., 1988). Chemical weathering determines the flux of dissolved materials whereas physical erosion determines the flux of particulates in the riverine environment. Data from eight of the largest rivers draining the Himalayan-Tibetan region (Ganga, Brahmaputra (India), Irrawady (Burma), Chang Jiang, Xijiang, Indus, Mekong and Huanghe (China)) show that almost 25% of the Global dissolved load that is transported to the oceans comes from only c. 5% of the total land area (Sarin, 2001).

2.5. Vegetation controls

Rooted vascular plants accelerate the rate of mineral weathering in a number of ways. These can be grouped into chemical and physical processes (Berner et al., 2003). Vegetation not only accelerates the weathering process but also cycles elements, such as, Ca, Mg, K, Na, Si and Fe as nutrients, although >90% of these nutrients are

returned as forest litter where they can be reused. The remainder is stored in the woody parts of the plants or removed to secondary minerals in the soil, however there is an annual loss of nutrients in the form of run-off to rivers and streams, particularly Ca, Mg, K, Na and Si. These nutrients need to be replaced via rock weathering (Berner et al., 2003).

Atmospheric CO_2 is taken up during photosynthesis and is released into the soil via the roots during respiration, forming carbonic acid by its combination with water, thereby removing the CO_2 from the atmosphere (Velbel, 1993). This carbonic acid acts as a weathering agent for minerals. The roots also affect mineral weathering due to ion exchange and the secretion of organic acids (Berner et al., 2003). For example, the secretion of organic acids by lower plants such as lichens has been found to be highly efficient at accelerating chemical weathering (Brady et al., 1999). The same is true for higher plants, where experimental studies on the basalt weathering activity of plant roots found weathering rates one to five times that of abiotic experiments (Hinsinger et al., 2001). The exchange of H^+ ions for cationic nutrients such as Mg^{2+}, Ca^{2+}, NH_4^+ and K^+ in order to retain an ion charge balance occurs around fine roots, in an area called the rhizosphere (Lucas, 2001), thereby reducing the pH in the vicinity of the roots. Dissolution rates for silicates are generally independent of pH at neutral pH, but increase with increasing acidity below pH 4-5 and above pH 8 with increasing alkalinity (Berner et al., 2003). The root-induced acidity caused by the ion exchange has been shown to have significant effects on the dissolution of Ca carbonates, phosphates and phyllosilicates (Hinsinger et al., 2001). Rhizospheric microorganisms secrete organic acids such as oxalic, citric and tartaric acid amongst others, which attack primary minerals, which also increase the availability of cationic nutrients. For example, oxalic acid increases the availability of PO_4^{3-} (Berner et al., 2003). Oxalic acid also forms soluble complexes through enhanced dissolution of normally insoluble Fe and Al from their host minerals (Hinsinger et al., 2001).

Plants play a crucial role in the water cycle, via transpiration or release of water from the leaves stomata and via evaporation of water from the ground. Together these two processes are termed evapotranspiration. By increasing evapotranspiration, more water vapour is available to form rain, in fact it is estimated that up to 50% of the Amazonian rainfall is due to evapotranspiration (Viers et al., 2007). This evapotranspiration also causes water to be extracted from the rocks by fine roots before the water can become saturated with dissolved products, which would otherwise inhibit further chemical dissolution. This water can then be replaced by unsaturated downward percolating rainwater (Lucas, 2001). Plant roots also affect weathering rates by retaining water, which allows chemical weathering to continue during dry spells

(Drever, 1994). Increased rainfall means that saturated soils are replaced with fresh water, again increasing the weathering rate (Berner et al., 2003). From a more physical point of view, plant roots anchor the soil thereby slowing down physical erosion; this is especially true for steep topography (Drever, 1994). This has the effect of prolonging the water contact time with primary minerals undergoing dissolution again increasing weathering potential (Berner et al., 2003).

2.6. Lithological controls

Different lithologies weather at different rates under the same climatic conditions. Accordingly, the degree of weathering will be fundamentally dependent on the relative abundance of specific minerals in specific lithologies, and their individual sensitivity to weathering. Expressed as a weathering scale from most resistant to least resistant are: quartz, K-feldspars, micas, Na-feldspars, Ca-feldspars, amphiboles, pyroxenes, dolomite, calcite, pyrite, gypsum, anhydrite and halite (Stallard and Edmond, 1983) (Figure 1.2). In general, mafic volcanic rocks such as basalt weather about eight times faster than intrusive rocks such as granite (Dupre et al., 2003), and as a result, the weathering of basaltic surfaces consumes between five and ten times more atmospheric CO_2 than equivalent areas of granitic surfaces under the same conditions. These basaltic lithologies account for approximately 30-35% of the total consumption of atmospheric CO_2 due to the weathering of continental silicate rocks (Dupre et al., 2003), which can be compared to the percentage of continental basalts relative to the global silicate area of 8.4% (Dessert et al., 2003). Consequently, it appears that the products of mafic volcanic activity not only act as a major source of supply to atmospheric CO_2, but also creates a significant sink through subsequent alteration of these products.

Berner created a theoretical model called GEOCARB to consider factors affecting the carbon cycle and atmospheric CO_2 on a multi-million year timescale (Berner, 2006a). This is based on Ca and Mg silicate weathering reactions as shown below:

$$CO_2 + CaSiO_3 \rightarrow CaSiO_3 + SiO_2$$

$$CO_2 + MgSiO_3 \rightarrow MgSiO_3 + SiO_2$$

The model also considers the diagenetic, metamorphic and volcanic degassing of CO_2 and the weathering and burial of sedimentary organic matter. In addition the model also takes into account the various factors affecting the rate of weathering. These include

the uplift of mountains as they affect the rate of erosion and the exposure and availability of fresh Ca and Mg silicate rocks, the evolution of land plants, continental drift since it affects the temperature and hydrology of the continents, the constant increase in solar radiation and the feedback effects of increased CO_2 on global temperature and enhanced hydrological cycle and plant growth and hence plant-assisted weathering (Berner et al., 2003). This model was later modified to consider the combined long term cycles of carbon and sulphur and as such was renamed GEOCARBSULF (Berner, 2006a). Here as in the earlier GEOCARB model calculations are done by means of a succession of steady states for exchanges of total carbon and total sulphur between the rocks and the surficial system (ocean, atmosphere, life and soils) calculated for each one million year time step (Berner, 2006a). The most dominant factor affecting CO_2 and O_2 over the past 550 Ma was the rise of vascular plants (Berner, 2006a). They brought about large increases in the rates of chemical weathering of silicates and rates of burial of organic matter resulting in a dramatic rise in O_2 and a drop in CO_2 during the mid to late Palaeozoic, although this came to an abrupt end at the Permian-Triassic boundary as a result of the massive biological extinction at that time (Berner, 2006a).

Within the updated GEOCARBSULF model, Berner also made the distinction between the weathering of silicates into volcanic and non-volcanic rocks. The reason for this separation is essentially twofold: 1) the chemical weathering of Ca and Mg silicate minerals that are abundant in volcanic rocks dominates the uptake of atmospheric CO_2 during weathering and 2) volcanic rocks weather faster than non-volcanic rocks (Berner, 2006b). Volcanic rocks weather approximately twice as fast as non-volcanic rocks under the same environmental conditions (Taylor and Lasaga, 1999).

The most extensive sub-aerial examples of basaltic volcanism are the large igneous provinces (LIP). These eruptions produced huge quantities of basalt in a relatively short time. The Deccan Traps, covering much of north western peninsular India, is one of largest igneous provinces, covering an area of c. 500,000 km^2, (Mahoney, 1988, Bondre et al., 2006). Total eruptive volumes in the entire Deccan LIP are usually estimated to have been between 1×10^6 km^3 (Widdowson, 1997) and 2×10^6 km^3 (Pascoe, 1964, Vandamme et al., 1991) but more recent work has calculated the total eruptive volume to be 1.3×10^6 km^3 (Jay and Widdowson, 2008). $^{40}Ar/^{39}Ar$ dating and paleomagnetic dating indicate that Deccan volcanism (c. 64 – 67 Ma) spanned the Cretaceous-Tertiary (K-T) boundary (Chenet et al., 2007, Richards et al., 2015) and as such has attracted significant interest regarding its effects on Cretaceous-Tertiary boundary biota (Jay and Widdowson, 2008).

Based on a number of studies of basaltic rivers by Dessert et al. (2003), it appears that knowledge of temperature and run-off are sufficient enough to characterise chemical weathering and associated CO_2 consumption rates. Figure 5 of Dessert et al (2003), recreated here as Figure 2.3, shows a clearly improved correlation between calculated and measured CO_2 consumption rates based on both run-off and temperature (black symbols) compared to those based solely on run-off (open symbols).

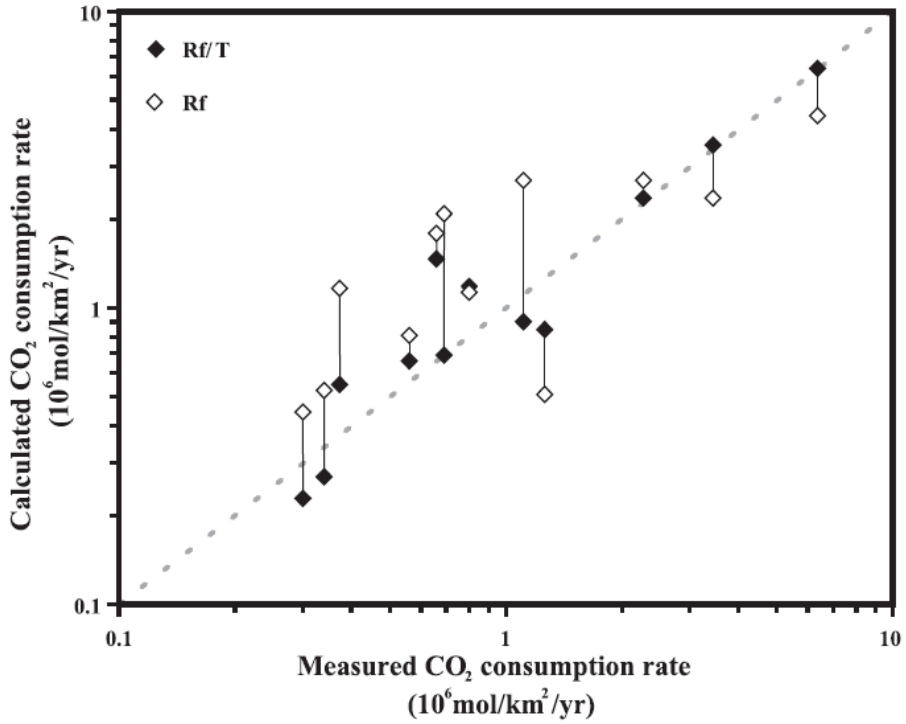

Figure 2.3 Calculated CO_2 consumption rates versus measured CO_2 consumption rates. The rates determined by Dessert et al (2003) as a function of both run-off and temperature are represented by black symbols, whilst those calculated as a function of run-off are represented by white symbols. Measured rates are represented by the dotted diagonal line (after Dessert et al., 2003, Figure 5).

Moreover, Dessert et al (2003) provides CO_2 consumption rates for each of the world's major basaltic LIP provinces. These rates are determined using digitised maps of the LIP areas, lithological maps, global run-off data and global temperature data, and are summarised in Table 2.1.

Table 2. 1 Area, annual run-off, annual temperature and annual CO_2 consumption data for a selection of basaltic provinces (Dessert et al., 2003).

Name	Area (10^6 km^2)	Run-off (mm y^{-1})	Annual temp (ºC)	CO_2 consumption flux (10^{12} mol y^{-1})
Ethiopia	0.807	129	21.3	0.121
Siberia	0.796	402	-10	0.053
Parana	0.568	498	19.8	0.318
SE Asia & Indonesia	0.538	1372	25	1.033
Deccan	0.532	424	26.9	0.392
Japan & East Russia	0.373	731	3	0.151
Australia & Tasmania	0.327	176	20.4	0.047
Central America	0.309	763	22.8	0.356
Arabic Peninsular	0.219	4	23.3	0.001
South Africa	0.216	102	19.3	0.024
Patagonia	0.209	151	9.3	0.018
Kamchatka	0.173	750	-3.5	0.031
Columbia River	0.154	371	9.5	0.034
Iceland	0.105	1889	2	0.070
Greenland	0.099	364	-11	0.004
Cascade & Snake river	0.081	404	7.2	0.017
East Canada	0.038	441	1.4	0.006
Other (Antarctica not included)	1.305	420	18.6	0.433
Total	6.849			3.109

Table 2.1 shows CO_2 consumption is not merely a function of area. For example, South East Asia and Indonesia have an area of 0.538 x 10^6 km^2, which is similar to the Deccan area of 0.532 x 10^6 km^2. However, the CO_2 consumption for South East Asia and Indonesia (1.033 x 10^{12} mol y^{-1}) is approximately three times higher than that of the current Deccan CO_2 consumption (0.392 x 10^{12} mol y^{-1}). This is seen more clearly if these values are expressed as CO_2 flux relative to area.

South East Asia and Indonesia:

1.033 x 10^{12} mol y^{-1} / 0.538 x 10^6 km^2 = 1.92 x 10^6 mol y^{-1} km^{-2}

Deccan:

0.392 x 10^{12} mol y^{-1} / 0.532 x 10^6 km^2 = 0.74 x 10^6 mol y^{-1} km^{-2}

These data can be best explained by considering the climatic regimes of the two locations. South East Asia and Indonesia has a slightly lower annual temperature of 25ºC compared to 26.9ºC for the Deccan. However, the real difference comes from the run-off, with South East Asia and Indonesia having over 3 times more runoff than the Deccan, 1372 mm y^{-1} compared to just 424 mm y^{-1}. Similarly, Iceland has a higher run-off than South East Asia and Indonesia; but due to its low annual temperature of just 2ºC it has a low CO_2 flux of 0.070×10^{12} mol y^{-1}. As a function of its area this equals 0.67×10^{6} mol y^{-1} km^{-2}.

Figure 2.4 plots CO_2 consumption rate as a function of area, rather than just as consumption rate as presented by Dessert et al (2003). This clearly shows how both temperature and run-off play key roles in the amount of CO_2 consumption as a consequence of basalt weathering. It also shows that the Deccan has the third highest CO_2 drawdown after South East Asia and Indonesia and Central America.

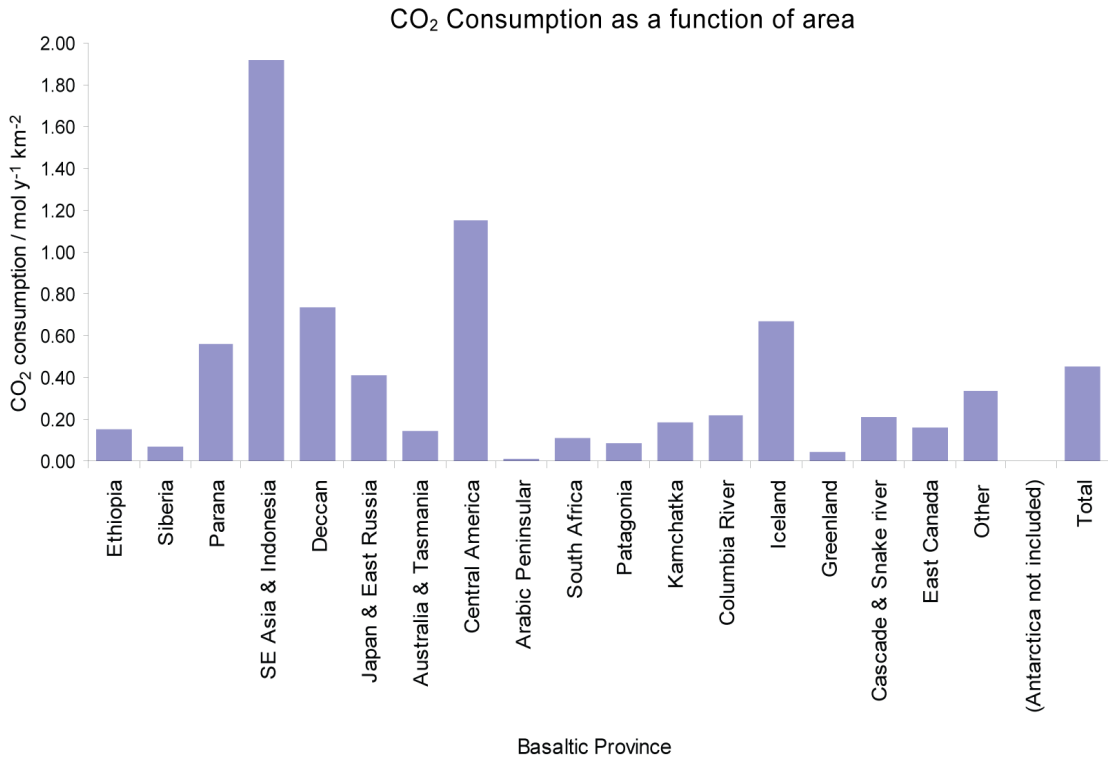

Figure 2.4 CO_2 consumption rate plotted as a function of area for a selection of Basaltic Provinces (After Dessert et al., 2003).

2.7. Weathering profiles

Laterite

Laterite comprises an important subset of the wider range of ferruginous and aluminous weathering and alteration products which also include ferricretes and bauxites (Widdowson, 2008). Strictly speaking, laterites are residual materials formed directly by in-situ rock breakdown, and should not contain any significant allocthonous (introduced or externally derived) component (Widdowson, 2009). Their compositional characteristics are the result of relative enrichment of immobile elements such as Fe and Al and other less mobile residual elements as a result of low temperature alteration and associated mineralogical breakdown leading to the release of mobile elements into groundwater and fluvial systems. The degree of weathering usually diminishes with depth producing a weathering profile, that if retained in its entirety, should range from unaltered protolith at the base, through increasingly altered parent rock (saprolite), iron enriched zones (mottled zone) culminating at the top as an iron rich duricrust. Laterites form as a result of intense tropical or sub-tropical weathering on a variety of lithologies (McFarlane, 1976, Summerfield, 1991), although protoliths that have inherently higher Fe contents are most suited to lateritization (e.g., mafic igneous rocks and immature sedimentary rocks such as greywackes). The conditions under which laterites form include (Widdowson, 2009):

1. favourable geomorphological environment, characterised by limited run-off and lack of aggressive erosion where the ingress of rainfall and the establishment of a water table can promote the flushing, leaching and chelation of the more mobile elements;
2. favourable climatic conditions, such as seasonal, high annual rainfall (a monsoon type climate). High humidity and high annual temperatures to produce high weathering rates;
3. relative tectonic stability characterised by minimal or slow uplift, crustal deformation and/or erosion.

The Bidar weathering profile

The Bidar weathering profile, located North West of Hyderabad (17º54'42"N, 77º32'48"E) developed on a basaltic lithology and was formed during the early Palaeocene (c. 64 – 60 Ma; Schmidt & Prasad, 1983) after the eruption of the Deccan Traps flood basalt (c, 64 – 67 Ma) has ceased (Widdowson and Cox, 1996). The Bidar profile is c. 50 m deep and is an excellent example of an autochthonous laterite weathering profile, preserving a complete profile from unaltered basalt protolith at its base to an indurated laterite cap at its upper surface (Figure 2.5), BB1 to BB9 represent the locations from which samples were collected and analysed, not discussed further here (Widdowson, 2009).

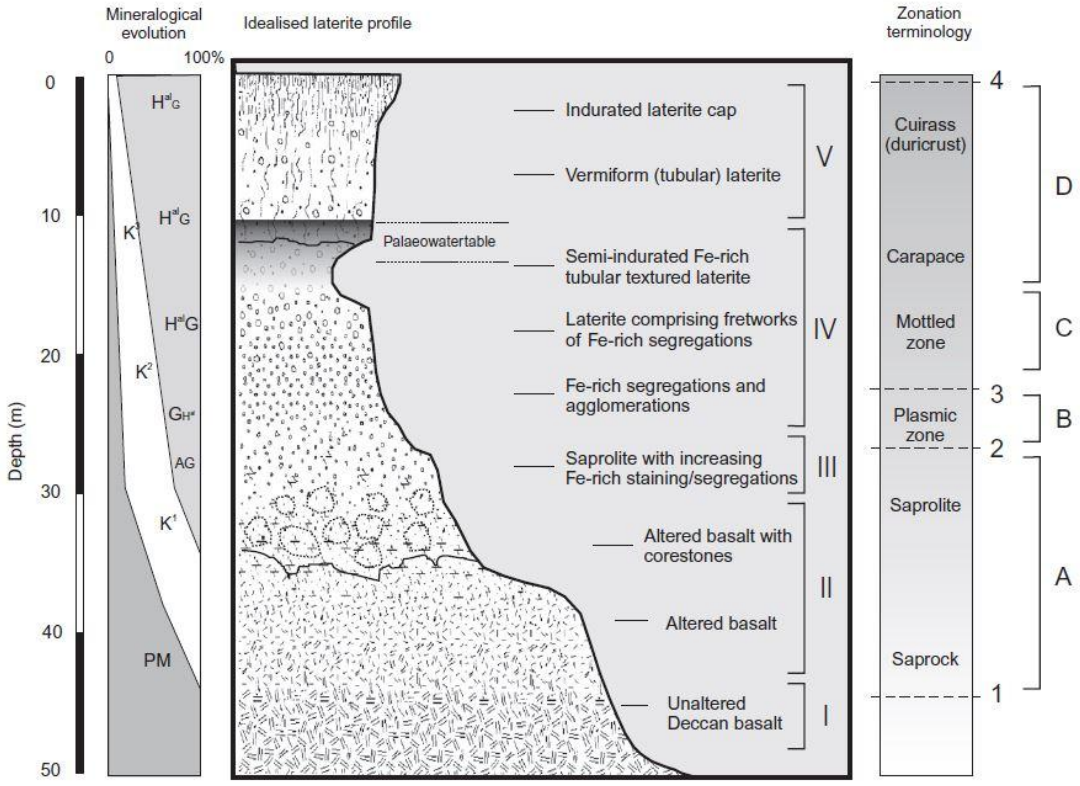

Figure 2. 5 Generalised vertical section through the Bidar weathering profile, showing the compositional and textural progression from unaltered protolith at the base to indurated laterite cap at the surface. The left hand column indicates the idealised vertical distribution of minerals through the profile, PM, parent minerals; K^1 to K^3, well-crystallised to poorly-crystallised kaolinite; AG, amorphous goethite; G, goethite; $H^{al}G$, aluminous haematite and goethite. The right hand column shows the terminology of the various zones and alteration fronts within a typical laterite weathering profile (after Widdowson, 2009). For more detail see Widdowson (2009).

Soil cover.

In low relief areas where low physical erosion rates are prevalent, thick clay-like soil (often termed saprolite) is often formed as a result of chemical weathering. This thick layer then acts to protect the primary minerals in the buried bedrock from further chemical weathering because the bedrock becomes isolated from precipitation (Berner et al., 2003).

2.8. Weathering Indices

As discussed in the previous sections, chemical weathering is controlled by numerous factors including lithology, climate, vegetation and human activities. However, the mechanisms at various spatial and temporal levels are often poorly understood and difficult to quantify. Therefore, over the years various geochemical proxies have been proposed to quantify the intensity of continental weathering. Conventionally these weathering indices fall into two categories based upon their underlying approach, in that they quantify the degree of weathering by either monitoring the decomposition of an unstable mineral or tracing the mass transfer of a labile element (Ohta and Arai, 2007). The most commonly used weathering indices monitoring the decomposition of an unstable mineral, or mineral combinations are the Chemical Index of Alteration (CIA) (Nesbitt and Young, 1982), the Chemical Index of Weathering (CIW) (Harnois, 1988) and the Plagioclase Index of Alteration (PIA) (Fedo et al., 1995). Since the CIA index is concerned with the conversion of feldspar minerals which are the most abundant rock-forming minerals occurring at the Earth's crust, this index has been most widely used. Of the second category based on tracing the mass transfer of labile elements the most widely used is the Weathering Index of Parker (WIP) first proposed by Parker (1970) and later developed by Hamdan and Burnham 1996. The CIA and WIP are defined as follows:

$$CIA = Al_2O_3 / (Al_2O_3+CaO^*+Na_2O+K_2O) \times 100, \text{ (Nesbitt and Young, 1982)}$$

$$WIP = (2\ Na_2O/0.35+MgO/0.9+2K_2O/0.25+CaO^*/0.7) \times 100 \text{ (Parker, 1970)}$$

Where CaO* represents the CaO content in the silicate fraction of the sample. Stronger chemical weathering is indicated by the smaller WIP values, whereas for the CIA index it is indicated by larger values.

Despite their merits and subsequent wide use over the years, the above geochemical indices are founded on assumptions that can pose significant problems in practical use (Ohta and Arai, 2007). The principle assumption associated with chemical indices monitoring the decomposition of an unstable mineral is that the geochemistry of the un-weathered protolith is invariant in terms of mineral composition, and that certain elements reside in specific minerals. For example the CIA index assumes that all the Al_2O_3, Na_2O, CaO and K_2O is only present in feldspars, therefore if significant amounts of other minerals, such as amphiboles, contain these elements then variation in the calculated CIA values may actually reflect variation in protolith chemistry rather than the desired variation of degree of weathering (Price and Velbel, 2003). Indices tracing the mass transfer of labile elements rely on the behaviour of the specific element used in the ratio rather than considering the effects of multiple elements. During the weathering process elements can behave in an inconsistent manner depending on the prevailing physico-chemical conditions (Nesbitt and Young, 1984, Hamdan and Burnham, 1996, Price and Velbel, 2003). For example, Fe is often leached in the early stages of weathering, and then accumulates in the later stages (Hamdan and Burnham, 1996). Since both types of weathering indices appear to have potential for producing biased results an alternative index is proposed by (Ohta and Arai, 2007). Ohta and Arai, (2007) suggest that a weathering index should take account of the behaviour of multiple elements and should be independent of geochemical variability of the un-weathered protolith in order to reduce the likelihood of obtaining biased results. This they propose can be achieved using a principle component analysis (PCA), this is a statistical technique designed to extract orthogonal (independent) latent components expressed as a linear combination of multiple elements. The authors also propose a ternary diagram based on the orthogonal coordinates of the principle component analysis, which depicts the weathering profiles of felsic to mafic igneous rocks.

More recently the mafic index of alteration (MIA) has been developed which extends the chemical index of alteration to include the mafic elements Fe and Mg and is therefore most suitable for, but not restricted to studying mafic rock weathering and more accurately records the differences in alteration of these related lithologies (Babechuk et al., 2014). Many mafic minerals such as pyroxene and olivine are susceptible to chemical weathering, leading to the loss of Mg from the remaining weathering profile. This loss of Mg can be evaluated using the Mg index, however, by contrast the fate of Fe is dependent on whether the environment is oxidising or reducing. In oxidising environments Fe is retained by the formation of highly insoluble ferric iron (Fe^{3+}) oxides or hydroxides, therefore the total Fe ($Fe_2O_{3(T)}$) is regarded as

an immobile element along with Al (Al_2O_3) as shown below as $MIO_{(O)}$. However, in reducing environments where ferrous iron (Fe^{2+}) can be mobile and can be leached along with Mg, the total Fe is regarded as mobile along with Mg, Ca, Na and K as shown below as $MIA_{(R)}$.

$$MIA_{(O)} = (Al_2O_3+Fe_2O_{3(T)}) / (Al_2O_3+Fe_2O_{3(T)}+MgO+CaO^*+Na_2O+K_2O) \times 100$$

$$MIA_{(R)} = Al_2O_3 / (Al_2O_3+Fe_2O_{3(T)}+MgO+CaO^*+Na_2O+K_2O) \times 100$$

As is the case for CIA, the MIA uses molar ratios of the major element oxides by converting the wt% into moles and the CaO is corrected for the presence of carbonate to consider only the silicate derived Ca (CaO*). Again, in line with CIA values, the higher the value the more altered the rock, with a value of 100 representing complete removal of all mobile elements, including those which may have been subsequently incorporated into secondary minerals and clays (Babechuk et al., 2014).

2.9. Atmospheric CO_2

As mentioned earlier, the Earth's climate has remained stable within limits tolerable for life over millions of years. This is believed to be largely dependent on the rate of CO_2 released via volcanic degassing being balanced by the rate of CO_2 consumption through silicate weathering (Walker et al., 1981), as well as complex biological feedbacks (Lovelock and Margulis, 1996). Throughout the Cenozoic era, spanning the last 66 Ma, the marine isotopic ratios of strontium, osmium and lithium (McArthur et al., 2001, Klemm et al., 2005, Misra and Froelich, 2012) suggest that extensive uplift of mountain ranges may have enhanced CO_2 consumption by silicate weathering (Raymo et al., 1988). However, reconstructions of sea floor spreading (Muller et al., 2008) do not indicate a corresponding increase in CO_2 release through volcanic degassing; this imbalance would have depleted the atmosphere of all CO_2 within a few million years (Berner and Caldeira, 1997). A number of hypotheses have been proposed; for example, that excess CO_2 consumption by silicate weathering over the Cenozoic could have been balanced by a net decrease in the size of the organic C reservoir (Raymo and Ruddiman, 1992). However, recent work has shown that orogenic activity increases organic C burial and stabilises petrogenic C, through graphitization (Galy et al., 2008). Model results also suggest that changes in organic C burial during this time were insufficient to balance CO_2 consumption (Katz et al., 2005, Li and Elderfield, 2013). The release of CO_2 during thermal decomposition of carbonate minerals during metamorphism has also been suggested as a contributor towards the missing CO_2

required to balance the Cenozoic C cycle (Bickle, 1996). However, petrologic and geochronologic data on the timing and potential magnitude of the fluxes bring this hypothesis into question, additionally, since any CO_2 released during metamorphism is subject to high levels of uncertainty regarding the fraction of CO_2 that makes it through kilometres of rock of variable permeability and reactivity to reach the surface and enter the atmosphere (Kerrick and Caldeira, 1998). Another recent suggestion was that the acceleration of continental weathering was balanced by a decrease of weathering of oceanic islands basalts by a factor of 2 (Li and Elderfield, 2013), whilst this is reasonable there is currently no direct evidence to test this prediction (Torres et al., 2014). Torres et al provide another alternative hypothesis regarding the oxidation of sulphide coupled with carbonate dissolution, which like silicate weathering would also be enhanced by Cenozoic uplift. The oxidation of sulphides produces sulphuric acid as follows:

$$4FeS_2 + 15O_2 + 14H_2O \rightarrow 4Fe(OH)_3 + 8H_2SO_4$$

The dissolution of carbonate minerals in the presence of this sulphuric acid results in the transfer of sedimentary C into the ocean-atmosphere system as CO_2 as follows:

$$CaCO_2 + H_2SO_4 \rightarrow CO_{2(g)} + H_2O + Ca^{2+} + SO_4^{2-}$$

And

$$2CaCO_2 + H_2SO_4 \rightarrow 2Ca^{2+} + SO_4^{2-} + 2HCO_3^-$$

For the second equation CO_2 is released immediately whereas for the third equation CO_2 is still released but on a timescale of carbonate precipitation in the ocean (10^6 Ma) as follows:

$$Ca^{2+} + 2HCO_3^- \rightarrow CaCO_3 + CO_{2(g)} + H_2O$$

2.10. Calculating CO_2 consumption rate (CCR)

The sources of major ions to rivers are broadly classified into three groups; (i) rain / precipitation, (ii) chemical weathering and (iii) anthropogenic inputs and seawater, which is an important source of ions in localities subjected to tidal influences. Rainwater composition forms the baseline for the evolution of river water composition and is location dependent; being dominated by sea salt (Na and Cl) near the coast changing to Ca, HCO_3 and SO_4 dominated further inland. Krishnaswami and Singh (2005) provide data on the rainwater composition for a range of coastal and inland locations across India, including Goa; these data are recreated in Table 2.2.

Table 2. 2 Chemical composition of rainwater over India, all values are in μEq l^{-1} (Krishnaswami and Singh, 2005).

Location	*Na*	*K*	*Mg*	*Ca*	*Cl*	*NO_3*	*SO_4*	*F*	*HCO_3*	*NH_4*
Coastal										
Goa	*115*	*3*	*30*	*46*	*135*	*6*	*32*	*-*	*-*	*7*
Chembur	*96*	*28*	*57*	*175*	*141*	*-*	*421*	*5*	*-*	*117*
Kalyan	*103*	*26*	*39*	*93*	*112*	*31*	*108*	*6*	*-*	*21*
Kalyan	*147*	*6*	*48*	*130*	*134*	*66*	*110*	*-*	*-*	*14*
Colaba	*179*	*6*	*59*	*155*	*171*	*34*	*52*	*-*	*-*	*12*
Alibag	*220*	*5*	*64*	*133*	*236*	*9*	*36*	*-*	*-*	*8*
Thumba	*207*	*5.6*	*38*	*46*	*228*	*-*	*14*	*-*	*-*	*-*
Bombay	*115*	*3.6*	*24*	*36*	*138*	*-*	*10*	*-*	*-*	*-*
Inland										
Pune	*39*	*3*	*17*	*68*	*44*	*18*	*23*	*-*	*-*	*26*
Silent Valley	*46*	*4*	*14*	*43*	*43*	*21*	*20*	*-*	*-*	*3*
Hyderabad	*40*	*36*	*20*	*119*	*47*	*10*	*32*	*-*	*22*	*13*
Korba	*21*	*4*	*43*	*183*	*32*	*25*	*213*	*5*	*-*	*15*
Gopalpura	*21*	*4*	*94*	*153*	*38*	*43*	*19*	*29*	*44*	*48*
Dayalbagh	*18.4*	*7.6*	*45.6*	*56.1*	*32*	*23*	*36*	*18*	*-*	*40*
Delhi	*82*	*44*	*70*	*134*	*140*	*67*	*90*	*-*	*-*	*26*
Himalaya										
Nepal	*10*	*2*	*12*	*44*	*7*	*4*	*10*	*-*	*68*	*-*

Chemical weathering in drainage basins occur primarily in two forms, the first of which are dissolution reactions (e.g., NaCl forming Na^+ and Cl^- ions; these are congruent reactions and are important in terrains draining evaporites and saline / alkaline soils). The second form is reactions requiring protons, the common source of which is carbonic acid. Other acids, such as sulphuric acid from the oxidation of pyrites and organic acids (humic, fulvic, oxalic), can also be important. Weathering mediated by acids can be either congruent or incongruent, with many silicate weathering reactions falling into the latter category which results in the formation of secondary minerals such as clays and Fe and Al oxides.

Anthropogenic inputs are the third source of major ions to rivers, and can be from the discharge of sewage, industrial and mining effluents and fertilizers. It is estimated that c. 30% of Na, Cl, SO_4 and nutrients can be of anthropogenic origin (Berner and Berner, 2012) however, the contribution from this source can be very different from the mean. Additionally, two other potential sources of major elements to rivers exist; organic matter, which during its growth incorporates nutrients (N, P and K) but during its decay releases them back to the rivers, nitrogen and phosphorus are generally recycled but potassium is derived from silicate weathering. The other source is springs and groundwater, which occurs due to the chemical weathering of aquifer rocks, although this is hard to quantify.

Silicate weathering rate per unit area is the riverine flux of dissolved major cations and silica derived from silicates within the basin and can be described as follows (Krishnaswami and Singh, 2005):

$$SWR = Q\sum(Na + K + Mg + Ca)_{sil} + SiO_2 = Q\{TDS(s)\}$$

Where $(X)_{sil}$ is the dissolved riverine concentration of cations derived from silicate weathering and Q is the water discharge per unit area. The difficulty here is to extract the silicate contributions from the various cations from the measured major ion composition of the water. This relies on a suitable proxy; a common choice is Na_{sil} which is calculated as follows:

$$Na_{sil} = Na_r - (Na_{rain} + Na_s)$$

Where the subscripts sil, r, rain and s refer to silicate, river, rainwater and halite/saline/alkaline soils and or anthropogenic inputs and Na_{rain} is appropriately corrected for evapotranspiration. For K the dominant source is silicate weathering with only minor concentrations in rainwater as can be seen in Table 1.3. Therefore K_{sil} can be calculated by subtracting the rainwater contribution from the measured riverine value. The silicate contributions for Ca and Mg are more difficult to quantify since they have multiple sources, therefore these are calculated assuming that they are released to rivers in proportion to their abundance in the basin rocks relative to Na. This can lead to quite a wide range of ratios depending on the rocks present within the basin.

2.11. Weathering reactions

Table 2.3 lists common silicate minerals, complete with their respective generic chemical formulae, their rock type and their main weathering reaction type.

Table 2. 3 After Berner and Berner (2012, Table 4.3).

Mineral	Generic chemical formula	Rock type	Main weathering reaction
Quartz	SiO_2	Igneous Sedimentary Metamorphic	Generally resistant to dissolution, but small amounts break down to form silicic acid (H_4SiO_4)
Biotite	$K(Mg, Fe)_3(AlSi_3O_{10})(OH,F)_2$	Igneous Metamorphic	Incongruent dissolution by acids. Oxidation of Fe.
Muscovite	$K\ Al_2\ (AlSi_3O_{10})(OH,F)_2$	Metamorphic	Incongruent dissolution by acids.
Clinopyroxene	$Ca\ (Mg, Fe)\ Si_2O_6$	Igneous	Oxidation of Fe. Congruent dissolution by acids.
Orthopyroxene	$(Mg, Fe)\ SiO_3$	Igneous	Oxidation of Fe. Congruent dissolution by acids.
Garnet	$(Mg, Fe, Mn, Ca)_3\ (Al, Fe, Cr)_2Si_3O_{12}$	Metamorphic	Oxidation of Fe. Congruent dissolution by acids.
Plagioclase	$NaAlSi_3O_8 – CaAlSi_2O_8$ Albite - Anorthite	Igneous Metamorphic	Incongruent dissolution by acids.
Orthoclase K-feldspar	$K\ AlSi_3O_8$	Igneous Sedimentary Metamorphic	Incongruent dissolution by acids.
Microcline K-feldspar	$K\ AlSi_3O_8$	Igneous Sedimentary Metamorphic	Incongruent dissolution by acids.
Amphibole	$NaCa_2(Mg, Fe)_4\ Al_3Si_6O_{22}(OH,F)_2$	Igneous Metamorphic	Oxidation of Fe.

Weathering reactions are classified in the table above according to the nature of the attacking substance and whether the primary mineral completely dissolves or whether it partially dissolves with a proportion of it being reprecipitated as a secondary mineral or minerals (Berner and Berner, 2012). Attacking substances are categorised into soil acids, dissolved oxygen or water. Dissolved oxygen only attacks minerals that contain reduced forms of elements such as Fe and S. Most minerals are attacked by soil acids with very few dissolved in the presence of water alone (Berner and Berner, 2012). Minerals that completely dissolve undergo what is termed congruent dissolution whereas minerals that partially dissolve with reprecipitation of a proportion of its components undergo what is termed incongruent dissolution (Berner and Berner, 2012).

Congruent dissolution:

Congruent dissolution of silicate minerals is rare and is limited to olivine, pyroxene and amphibole that are relatively free of Fe.

Pyroxenes:

Pyroxenes are a large group and can be split into clinopyroxenes (monoclinic) and orthopyroxenes (orthorhombic). The most widespread clinopyroxenes include aegirine, augite and diopside whilst the most common form of orthopyroxenes is enstatite. The weathering equation below is for clinopyroxene without Fe (Berner and Berner, 2012).

$CaMgSi_2O_{6\,(s)} + 4CO_{2\,(g)} + 6H_2O_{\,(l)} \rightarrow Ca^{2+}_{(aq)} + Mg^{2+}_{(aq)} + 4HCO_3^-{}_{(aq)} + 2H_4SiO_{4\,(l)}$

Pyroxene + carbon dioxide + water → Ca ions + Mg ions + Bicarbonate ions + Silicic acid

If Fe is present in pyroxene then this will weather by oxidation of Fe (Berner and Berner, 2012).

Amphiboles:

Like pyroxenes, the amphibole group comprises a large number of different solid solutions; however, they all have similar crystal structures despite the variety of possible chemical substitutions possible. The most common amphibole in igneous rocks is hornblende and the chemical formula given is representative of this mineral. Congruent weathering of hornblende is shown below but with F removed for simplicity:

$2NaCa_2(Mg,Fe)_4\,Al_3Si_6O_{22}(OH)_{2\,(s)} + 26CO_{2\,(g)} + 29H_2O_{\,(l)} \rightarrow 2Na^+_{(aq)} + 4Ca^{2+}_{(aq)} + 8(Mg,Fe)^{2+}_{(aq)} + 26HCO_3^-{}_{(aq)} + 3Al_2Si_2O_5(OH)_{4\,(s)} + 6H_4SiO_{4\,(l)}$

Hornblende + carbon dioxide + water → Na, Ca, Mg and Fe ions + bicarbonate + kaolinite + silicic acid

Incongruent Dissolution:

The majority of other silicate minerals especially those containing Al dissolve incongruently with the consequent formation of Fe oxides or clay minerals (fine grained aluminosilicates such as kaolinite, smectite and vermiculite). The most abundant crustal silicate mineral which is readily weathered is plagioclase feldspar (Berner and Berner, 2012).

Plagioclase feldspar:

Incongruent weathering of Na-plagioclase feldspar (albite) can be weathered by hydrolysis, by organic acid such as oxalic acid, strong acid such as sulphuric acid or in the presence of a carbonic acid, which is considered below (Berner and Berner, 2012).

$2NaAlSi_3O_{8\,(s)} + 2CO_{2\,(g)} + 11H_2O_{\,(l)} \rightarrow 2Na^+_{(aq)} + 2HCO_3^-{}_{(aq)} + 4H_4SiO_{4\,(l)} + Al_2Si_2O_5(OH)_{4\,(s)}$

Albite + carbon dioxide + water → Na ions + bicarbonate ions + silicic aid + kaolinite

Plagioclase feldspar can range in composition between two end members, Na-rich albite and Ca-rich anorthite. In addition alkali feldspar can also range between two end members, from Na rich albite to K rich orthoclase feldspar and microcline. The reaction shown above would occur for all the other forms of feldspar, but would yield varying proportions of Na, Ca or K ions according to their original composition.

Micas (Biotite and Muscovite):

Two varieties of mica are common in rocks, the colourless muscovite mica and the brown biotite mica. The main difference between muscovite and biotite is that muscovite does not contain any Fe or Mg, which leads to its colourless appearance. The incongruent weathering reactions for muscovite (Smolders et al., 2004) and biotite are shown below:

$2KAl_3Si_3O_{10}\,(OH)_{2\,(s)} + 2CO_{2\,(g)} + 5H_2O_{\,(l)} \rightarrow 2K^+_{(aq)} + 2HCO_3^-{}_{(aq)} + 3Al_2Si_2O_5(OH)_{4\,(s)}$

Muscovite + carbon dioxide + water → K ions + bicarbonate + kaolinite

$2KMg_3AlSi_3O_{10})(OH)_{2\,(s)} + 14CO_{2\,(g)} + 15H_2O_{\,(l)} \rightarrow 2K^+_{(aq)} + 6Mg^{2+}_{(aq)} + 14HCO_3^{1}{}_{(aq)} + Al_2Si_2O_5(OH)_{4\,(s)} + 4H_4SiO_{4\,(l)}$

Biotite + carbon dioxide + water → K and Mg ions + bicarbonate ions + kaolinite + silicic acid

Chlorite

Chlorites are a group of phyllosilicates minerals and can be described by the following four ends members; clinochlore $(Mg_5Al)(AlSi_3)O_{10}(OH)_8$, chamosite $(Fe_5Al)(AlSi_3)O_{10}(OH)_8$, nimite $(Ni_5Al)(AlSi_3)O_{10}(OH)_8$, and pennanite $(Mn_5Al)_6(AlSi_3)O_{10}(OH)_8$. Also Zn, Ca and Li species are known. This wide range of compositions allows chlorite minerals to occur throughout a broad range of pressure and temperature conditions, they are therefore ubiquitous in low to medium temperature metamorphic rocks.

$(Mg,Fe)_5Al_2Si_3O_{10}(OH)_{8\,(s)} + 10\ CO_{2\,(g)} + 5\ H_2O_{\,(l)} \rightarrow 5\ (Mg,Fe)^{2+}{}_{(aq)} + 10\ HCO_3^-{}_{(aq)} + Al_2Si_2O_5(OH)_{4\,(s)} + H_4SiO_{4\,(l)}$

Chlorite (Clinochlore) + carbon dioxide + water → Mg and Fe ions + bicarbonate ions + kaolinite + silicic acid

Garnet

Garnets are a group of silicate minerals with a general formula $X_2Y_2Si_3O_{12}$. The main types are pyrope, almandine, spessartine, andradite, grossular and uvarorite, although there are numerous less common species. For the purposes of this section grossular garnet has been used.

$Ca_3Al_2Si_3O_{12\,(s)} + 6\ CO_{2\,(g)} + 7\ H_2O_{\,(l)} \rightarrow 3\ Ca^{2+}{}_{(aq)} + 6\ HCO_3^-{}_{(aq)} + Al_2Si_2O_5(OH)_{4\,(s)} + H_4SiO_{4\,(l)}$

Grossular garnet + carbon dioxide + water → Ca ions + bicarbonate + kaolinite + silicic acid

Quartz

Quartz is very resistant to weathering and is therefore extremely slow to breakdown, also it does not involve the drawdown of atmospheric CO_2, therefore it is insignificant in the study of weathering reactions and the global CO_2 cycle, however it is included here purely for completion of the weathering reactions tabulated in Table 2.3.

$SiO_{2\ (s)} + 2\ H_2O_{\ (l)} \rightarrow H_4SiO_{4\ (l)}$

Quartz + water → Silicic acid

The following table lists the various minerals discussed above along with their respective ratios of moles of mineral weathered versus moles of CO_2 sequestered. It can be seen that the amount of CO_2 sequestered per mole of mineral weathered varies markedly from zero for quartz, 1 for feldspars up to 13 for hornblende.

.

Table 2. 4 Moles of CO_2 sequestered for each mole of mineral weathered

Mineral	*Moles of mineral*	*Moles of CO_2 sequestered*
Olivine	*1*	*4*
Hornblende	*2*	*26*
Pyroxene	*1*	*4*
K-Feldspar	*2*	*2*
Albite	*2*	*2*
Anorthite	*2*	*2*
Biotite	*2*	*14*
Muscovite	*2*	*2*
Grossular Garnet	*1*	*6*
Albite - Gibbsite	*1*	*1*
Quartz	*1*	*0*
Chlorite (Clinochlore)	*1*	*10*

2.12. Isotopic evidence of silicate weathering

As discussed above, various isotopes are valuable in testing the hypothesis that mountain uplift caused an increase in silicate weathering and led to the cooling trends associated with the Cenozoic era. Initially, marine carbonate strontium isotopic ratio ($^{87}Sr/^{86}Sr$) was used as a weathering flux proxy. The $^{87}Sr/^{86}Sr$ ratio of seawater today is believed to be constant and represents a mixture of essentially two sources: weathered continental lithosphere with a high average value and hydrothermal fluids with a low average value. The combined $^{87}Sr/^{86}Sr$ ratio can be calculated by a simple mass balance equation as shown below:

$$R_{sw} \times (F_1 + F_2) = (F_1 \times R_1) + (F_2 \times R_2)$$

The problem with this calculation is that all continental rocks have different $^{87}Sr/^{86}Sr$ ratios depending on their mineralogy, their age and the relative weatherability of the key components of the parent lithology. Additionally, anomalously radiogenic Himalayan carbonates are shown to dominate the riverine Sr flux in the Bhote Kosi–Sun Kosi river system, central Nepal, a major Himalayan tributary to the Ganges (Oliver et al., 2003). Mass balance analysis of the contributing sources to the dissolved load identifies the weathering of Palaeoproterozoic impure carbonates (comprised largely of dolomite and mica) from the Lesser Himalaya as the most significant lithological control upon elevated $^{87}Sr/^{86}Sr$ ratios (Oliver et al., 2003). Nevertheless, Sr isotopes have proved valuable in identifying key ancient weathering inputs into the ocean system; these are recorded in deep sea sediments comprising pelagic oozes. Of these, that most geographically relevant to the current study is the anomalous juvenile $^{87}Sr/^{86}Sr$ signal that predates the Cretaceous – Palaeogene (K-Pg) boundary and which has been convincingly linked, together with a $^{187}Os/^{188}Os$ spike, to the weathering of the neo-formed lava field of the Deccan (Ravizza and Peucker-Ehrenbrink, 2003).

Li isotopes are a potential alternative, whose behaviour is solely controlled by silicate weathering processes. Further, Li isotopes are not fractionated by biological processes (Lemarchand et al., 2010) and are unaffected by carbonate weathering (Kisakurek et al., 2005, Millot et al., 2010).

Fluvial δ^7Li is effectively independent of primary lithology with the highly variable δ^7Li in rivers being controlled by the extent of uptake of Li into secondary minerals which preferentially removes ^6Li (Pistiner and Henderson, 2003, Wimpenny et al., 2010). Therefore; riverine δ^7Li reflects the ratio of primary rock dissolution (driving rivers to

low, rock-like δ^7Li ratios with high Li) relative to secondary mineral formation (driving rivers to high δ^7Li and low Li (Pogge von Strandmann et al., 2010). This behaviour has also been described as weathering congruency, where if the riverine δ^7Li is low (close to that of the primary rock value) then less Li is being taken into secondary minerals; therefore, weathering is described as congruent, i.e. not forming secondary minerals during the weathering process (Misra and Froelich, 2012, Pogge von Strandmann et al., 2013). The Li isotopic ratio of seawater has been assessed and shows increasing values of δ^7Li from c 40 Ma to the present, which Misra and Froelich (2012) interpret as being the result of Himalayan uplift, increased denudation and increased incongruent weathering in the mountain belt (increased amount of clay formation). However, the problem with this interpretation is that the rivers draining the Himalayas have δ^7Li values lower than the global average (Kisakurek et al., 2005) suggesting that Himalayan weathering is more congruent meaning that increased Himalayan weathering should have driven seawater δ^7Li to lower values instead of higher values (Pogge von Strandmann and Henderson, 2015).

In their paper Pogge von Strandmann and Henderson identify a negative correlation between δ^7Li and uplift for a selection of catchments from South Island, New Zealand (their figure 1b). This observation suggests that higher uplift rates continually supplying fresh primary material, combined with high run-off rates lead to higher rates of dissolution of primary material compared with the formation of secondary minerals (congruent weathering). This is in contrast with the eastern side of South Island, where uplift and run-off are significantly lower and waters become more super-saturated and more secondary minerals are precipitated (incongruent weathering) leading to higher δ^7Li ratios. Since for a given denudation rate congruent weathering provides more cations to the ocean than incongruent weathering, where a proportion of the cations released are retained in clay minerals. Cenozoic uplift provided a continuous supply of fresh material for weathering and thus CO_2 drawdown, however, it is likely that a significant amount of weathering occurred in the surrounding flood plains and as such a significant proportion of the cations would have been retained in secondary minerals thus limiting the effectiveness of uplift in driving CO_2 removal (Pogge von Strandmann and Henderson, 2015). Therefore Li isotopes can provide a record of the efficiency of continental weathering in driving CO_2 removal (Pogge von Strandmann and Henderson, 2015).

2.13. Transport and kinetic limited weathering

As observed in the previous section, mountain uplift has provided an increased supply of fresh material to be chemically weathered, leading to enhance CO_2 drawdown; however, it is unlikely that this chemical weathering actually took place in the high mountain environments. More probably the majority of chemical weathering takes place in the surrounding low elevations and flood plains. This can be explained by considering the time it takes for minerals to be chemically weathered compared with their residence time in a particular environment, and can be described as a) transport limited or b) kinetic limited weathering.

2.13.1. Transport limited weathering

In catchments where the supply of water and acids relative to the supply of silicate minerals is large and where the residence time in the weathering environment compared to the reaction time is long, minerals are almost completely altered before they are removed from the environment (West et al., 2005). In circumstances such as these, silicate weathering rates (ω) – variables and units are directly related to erosion rates by the following relationship:

$$\omega = A \times \varepsilon$$

Where the constant A, is the weight fraction of soluble cations in the silicate rock and ε is the erosion rate (West et al., 2005). When removal processes are slow relative to chemical weathering rates, chemical weathering rates become 'transport limited' as determined by the rate supply of fresh material by erosion.

2.13.2. Kinetic limited weathering

In those cases where the erosion rate is high relative to the reaction time the situation arises where chemical weathering is incomplete, and is therefore dependent on the kinetics of the reactions regulated by temperature, run-off and vegetation (kinetic limited or weathering limited). In such cases the silicate weathering rate (ω) depends instead on the kinetic rate of mineral dissolution *(W),* the supply of material by erosion *(ε)* and the time available for the reaction *(τ):*

$\omega = W \times \varepsilon \times \tau$

Where W depends on the environmental conditions such as temperature and run-off (West et al., 2005). In the theoretically limiting case of the highest erosion rates, silicate minerals will pass through the weathering environment rapidly and will undergo infinitely limited dissolution. Most importantly, in the natural world, variability of run-off and temperature means that the transition from kinetic limitation to transport limitation is also variable.

2.14. Summary

The key observations following the literature review are as follows:

- Run-off is a dominant control on chemical weathering in river systems;
- Before using any fluvial data it is necessary to account for other input sources, such as atmospheric, anthropogenic, carbonate and evaporite weathering;
- Atmospheric inputs can be corrected using Cl as a proxy;
- With coastal rivers it is necessary to identify any sample localities that may be subject to a tidal influence prior to using the data for calculating silicate weathering rates and CO_2 consumption;
- When collecting samples, the date of sampling is important, due to variations in temperature, precipitation and run-off, dry season versus wet season and its effects on calculated silicate weathering rate and CO_2 consumption
- Carbonate weathering can be corrected for by studying the molar ratios of Ca and Mg relative to Na in the river water samples and comparing these ratios with those of the lithologies within the drainage basin;
- CO_2 sequestered per mole of mineral weathered varies markedly from zero for quartz, 1 for feldspars up to 13 for hornblende.

Chapter 3. Area of Study

The rivers studied in this project are the Chapora and Zuari Rivers which both lie within the state of Goa. This chapter provides background into the location, tectonic history, geology, geomorphology, drainage systems and climate of Goa, with more detailed information on the Chapora and Zuari Rivers to follow in chapter 4.

3.1. History and Location

Goa is located on the western coast of Peninsular India between the latitudes 14°53'54" N and 15°40'00" N and longitudes 73°40'33" E and 74°20'13" E (Figure 1.4). Its total land area is c. 3700 km^2, of which 1736 km^2 is in North Goa and 1966 km^2 is in South Goa. It is bounded by the state of Maharashtra to the north and by Karnataka to the east and south, while the Arabian Sea forms its western coast. Within North Goa 20% is forested and 48% is used for agriculture, whilst within South Goa 46% is forested and 27% is used for agriculture. The population of North Goa as per the latest 2011 Census is 818,008 giving a population density of 471 people per square kilometre compared with 640,537 giving a population density of 326 people per square kilometre for South Goa (www.census2011.co.in). Goa is India's richest state with a GDP per capita two and a half times that of the country as a whole.

Goa was a Portuguese colony until annexation and incorporation into the post-colonial Indian Republic on December 19th 1961. Goa was then accorded the status of Union Territory until on May 30th 1987 when it became India's 25th state, with Panjim (now renamed Panaji) as its capital. Goa is the smallest state in India, and can be found on the western coast. Administratively the state is separated into North Goa and South Goa, which are further sub-divided into 11 Talukas (administrative districts). North Goa comprises seven Talukas (Mormugao, Pernem, Bardez, Bicholim, Satari, Tiswadi and Ponda), whilst South Goa comprises four Talukas (Sanguem, Salcete, Quepem and Canacona; Figure 3.1) Its main industries are tourism based around stretches of its sandy coastline, and iron ore mining of its inland occurrences of Banded Iron Formation (BIF) lithologies.

Figure 3.1 The Talukas (administrative districts) of Goa, western India (Fernandes, 2009).

3.2. Tectonic History and Geology of Peninsular India

Peninsular India represents a fragment of the Gondwanan supercontinent which began rifting c. 180 Ma ago. The fragment which now forms peninsular India, together with Madagascar, separated from east Africa at c. 140 Ma, whilst still in the southern hemisphere. Madagascar separated at c. 88 Ma, then Seychelles at c. 65 Ma (Storey et al., 1995, Collier et al., 2008), both events being associated with the eruption of huge volumes of basaltic magma (Volcan de l'Androy and Deccan Traps, respectively). Peninsular India continued its northward movement gradually closing the Tethys Ocean and eventually colliding with Eurasia c. 55-50 Ma. This northward movement continued and caused the formation of the Himalayas and the uplift of the Tibetan Plateau around 17 Ma (Storey et al., 1995).

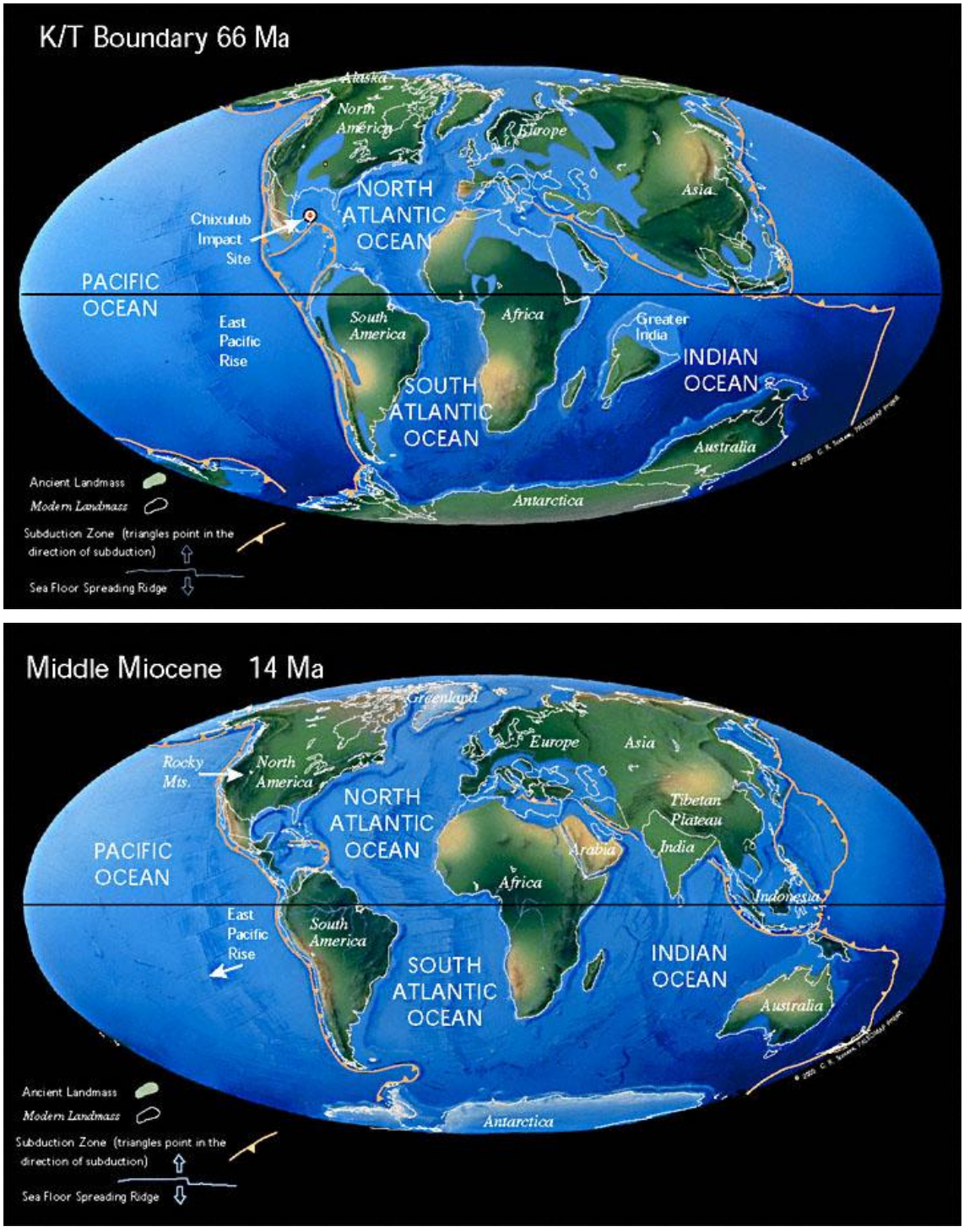

Figure 3. 2 Palaeolatitudinal reconstruction maps showing the location of the continents at 66 Ma (K/T Boundary and 14 Ma (Middle Miocene) (Scotese, 2001) (www.scotese.com, date accessed 22/11/2012).

The structural configuration of the western margin of India is the result of two major rifting episodes during the Mesozoic, these being the separation of Madagascar at c. 88 Ma and then the separation of the Seychelles c. 65 Ma (Storey et al., 1995, Collier et al., 2008). Both of these rifting episodes are linked to mantle plumes or hot spots. The first episode is linked with the Marion (Prince Edward) hotspot now situated beneath Marion and Prince Edward Islands. This hot spot caused the eruption of the Madagascar continental flood basalt province (CFBP) (Storey et al., 1995). The second and more recent episode is linked to the Reunion hotspot currently located beneath Reunion Island, which led to the emplacement of the Deccan continental flood basalt province (CFBP) or Deccan Traps (Mahoney, 1988, Courtillot and Renne, 2003).

Peninisular India can be divided into five discrete crustal areas on the basis of geology and bounding faults and/or lineaments which may represent cratonic units that were assembled during the Archaean and Proterozoic (Rogers, 1986, Naqvi and Rogers, 1987). These units include the Bhandara, Singhbhum and Aravalli Cratons, the Eastern Ghats, and a block in southern India consisting of the Dharwar Craton and adjoining Southern Granulites (Rogers, 1986). The combined units of this southern crustal block is often termed the Dravidian Shield (Rogers, 1986) or the South Indian Shield (Narain and Subrahmanyam, 1986). These five crustal blocks are separated by four major features: the Eastern Ghats Front, Godavari Rift, the Mahanadi Rift / Sukinda Thrust and the Namarda-Son Lineament (Figure 3.3) (Rogers, 1986).

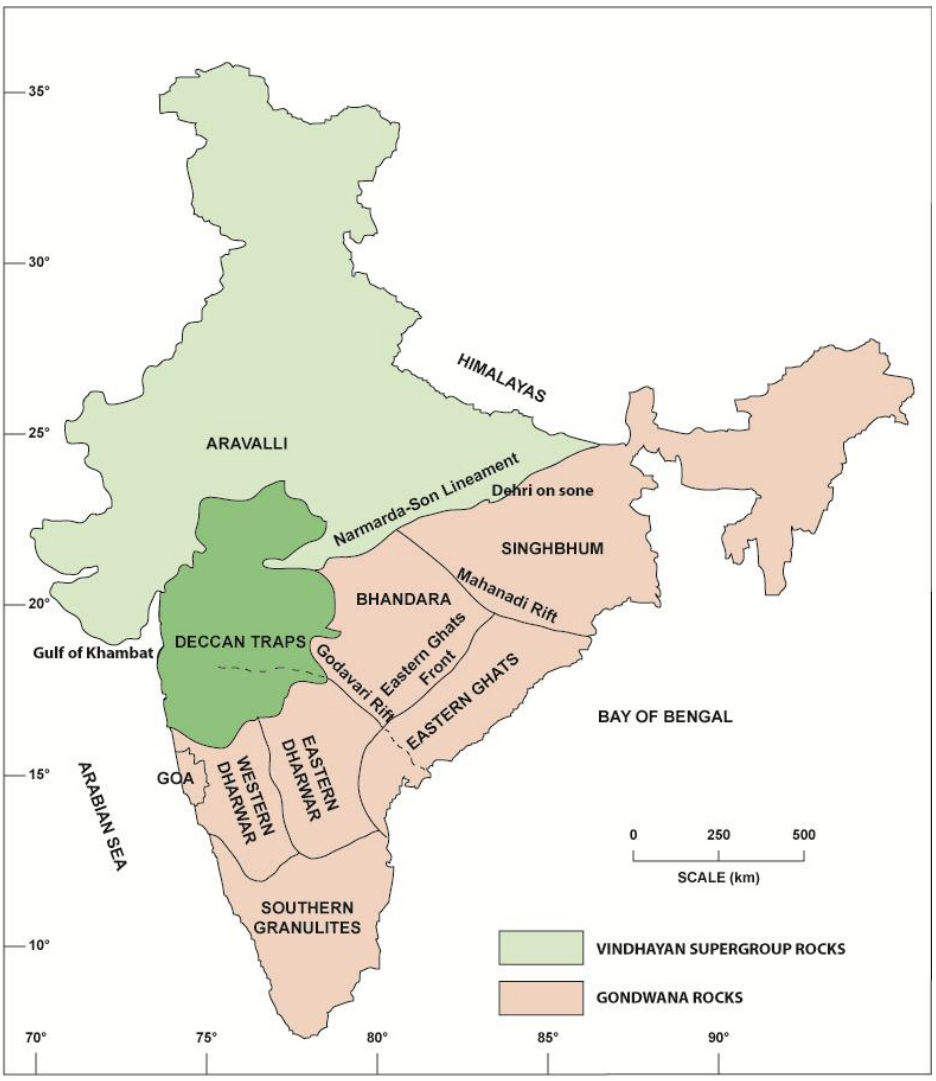

Figure 3.3 Map of India, detailing the five main tectonic components and their respective separation features (after Naqvi and Rogers, 1985).

The Narmarda-Son Lineament, a broad zone comprising fracturing and faulting, is a complex structural feature in northern India and of significant importance regarding the structural evolution of the sub-continent separating cratonic cores (Patro et al., 2005). It has a total length of 1200 km and trends in an ENE-WSW direction from the Gulf of Khambat (72.5ºE, 21ºN) to Dehri on Sone (82.5ºE, 24ºN) where it drains into the Ganges (Anand and Rajaram, 2004). During the Mesozoic its western reaches were a major depocentre resulting from north-south crustal extension prior to the India – Asia collision. It separates the Vindhyan Supergroup rocks in the north from the Gondwana rocks of the South Indian Shield (Narain and Subrahmanyam, 1986) (Figure 3.3).

The South Indian Shield (SIS) comprises the Dharwar Craton (DC) and the southern granulite terrain. The Dhawar Craton is further subdivided into the Western Dharwar Craton (WDC) and the Eastern Dharwar Craton (EDC) separated by the Closepet Granite (Swami Nath and Ramakrishnan, 1976). However, an alternative boundary has been identified along the eastern boundary of the Chitradurga Belt (Drury, 1984). More recently these tectonic boundaries have been defined as TB1 and TB2 which now subdivide the Dharwar Craton into three parts, the Western Dharwar Craton (WDC), Eastern Dharwar Craton -1 (EDC-1) and the Eastern Dharwar Craton-2 (EDC-2) (Raval and Veeraswamy, 2011). It is the western region of the Western Dharwar Craton, and more specifically that part of it occurring in the state of Goa, that is the subject of this thesis.

3.3. The Geology of Goa

Figure 3.4 shows a simplified geological map of Goa. The state of Goa represents the north-west extension of the South Indian Precambrian shield region (Dhoundial et al., 1987). The oldest of these basement rocks consist of trondhjemitic (Peninsular or Basement) gneiss of Middle to Late Archaean age (c. 3.2 to < 2.5 Ga) (Gokul, 1985). These basement rocks, known hereafter as the Peninsular Gneissic Complex (PGC), are overlain by the Goa group of rocks that form part of the Dharwar super-group (Dhoundial et al., 1987). The Goa Group consists of low grade (greenschist facies) metamorphic rocks and is divided from oldest to youngest into Barcem, Sandvordem, Bicholim-Rivona and Vageri Formations (Gokul, 1985) (Table 3.1.) More recent work has identified two unconformities and now proposes the renaming of the Goa Group into the Barcem Group consisting of just the Barcem Formation, and the Ponda Group comprising the Sandvordem, Bicholim-Rivona and Vageri Formations (Dessai, 2011). However, for the purposes of this thesis the term Goa Group will be used generically to identify all the supracrustal formations in Goa. In Goa state the Goa Group are intruded by mafic and ultra-mafic complexes of lower Proterozoic age. In places the PGC, the Goa Group and the mafic-ultramafic complexes are all intruded by K-rich granites such as the Chandranath Granite (2650 ± 100 Ma), the Dudhsagar granite (2565 ± 95 Ma) and the Canacona granite (2395 ± 390 Ma), which occur as plutons and plugs (Dhoundial et al., 1987). In the north-east the Late Cretaceous - early Palaeocene Deccan Traps are found. Finally, as a result of intense tropical weathering, a considerable amount of the area is covered by laterite, which is thought to be of late Cenozoic age.

Table 3.1: Stratigraphic sequence of rock formations in Goa (Fernandes, 2009)

<table>
<tr><td colspan="2">Late Cenozoic to Recent</td><td>Sand, alluvium, lateritic soil and laterite</td></tr>
<tr><td colspan="2">Upper Cretaceous to Lower Eocene</td><td>Deccan Trap volcanics and dolerite dykes</td></tr>
<tr><td colspan="2">Paleoproterozoic (<2500 Ma)</td><td>Acidic and basic intrusives including granites, gabbros, dolerite dykes and ultramafics</td></tr>
<tr><td rowspan="5">ARCHEAN</td><td rowspan="4">(DHARWAR SUPERGROUP)
GOA GROUP
(3000 – 2500 Ma)</td><td>Vageri Fm: detrital metasediments (quartzite, metagreywacke and argillite) with some metavolcanics</td></tr>
<tr><td>Bicholim - Rivona Fm: mainly chemogenic sediments (phyllites with banded-hematite-quartzite and limestone)</td></tr>
<tr><td>Sandvordem Fm: detrital metasediments including meta-conglomerates, quartzites, metagreywackes and argillites</td></tr>
<tr><td>Barcem Fm: mainly metavolcanics and metabasites with few metasediments</td></tr>
<tr><td>(>3000 Ma)</td><td>Basement trondhjemite gneiss (Peninsular Gneissic Complex)</td></tr>
</table>

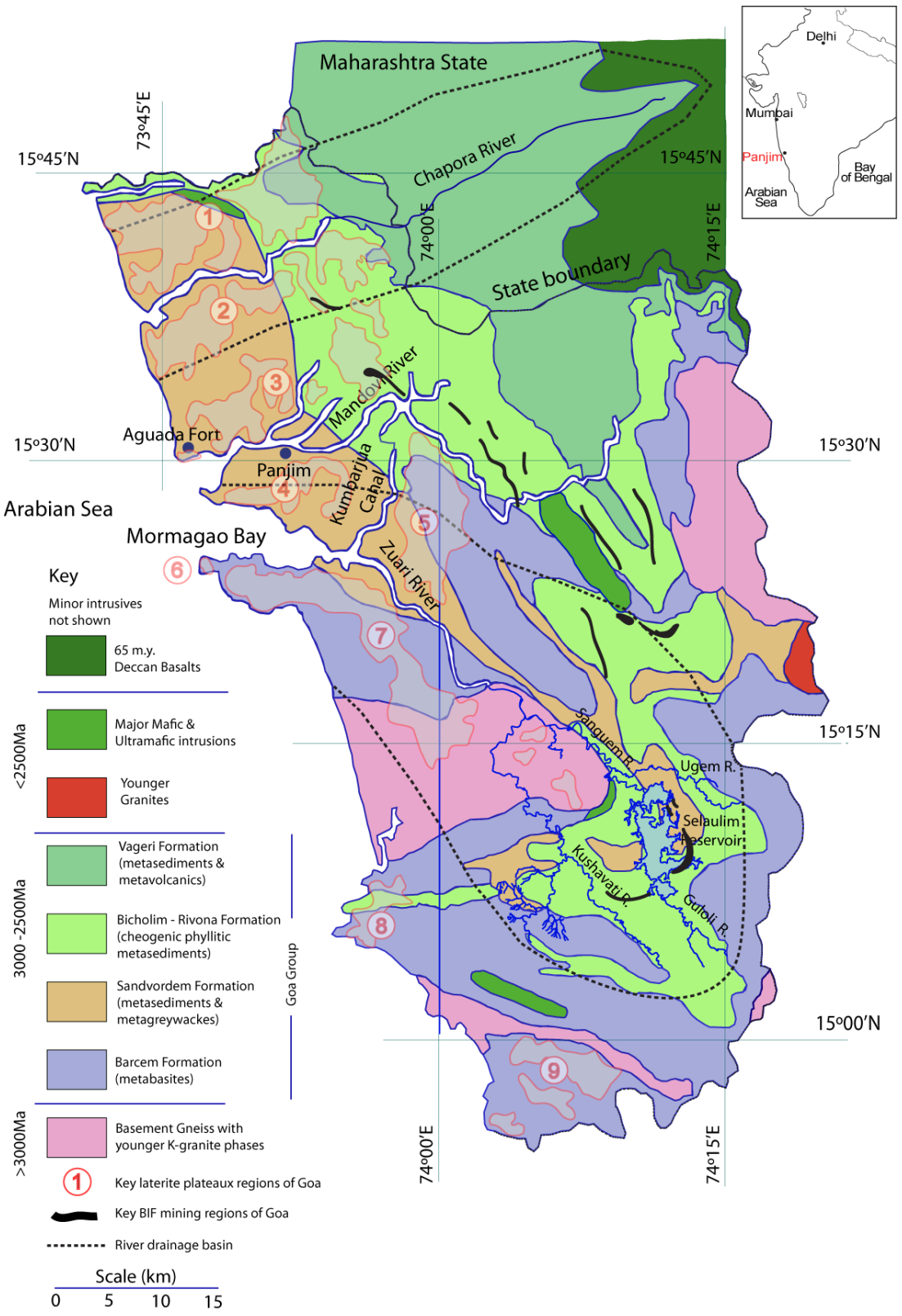

Figure 3. 4 Solid geological Map of Goa (adapted from GSI, 1996 maps) showing the Chapora and Zuari River systems along with their respective drainage basins. Also shown is the geology of Maharashtra pertinent to the Chapora River. Note that many areas of the outer Konkan are currently covered with significant thicknesses of laterite. For details of laterite distributions see Section 3.3.4 and Figure 3.5). Also shown are the main BIF mining areas, which predominantly occur in the Bicholim Fm.

3.3.1. The Dharwar Super-Group and the Goa Group.

The Dharwar Super-Group is made up of greenschist supracrustal rocks that occur as NNW-SSE trending linear schistose belts that have been folded in within the Peninsular Gneiss of the Indian Shield. These rocks have been metamorphosed, folded and faulted in several episodes, and have also been intruded numerous times by various volumes of igneous melts ranging in composition from felsic to mafic to ultramafic. All these folding and intrusive events appear to have taken place during the Archaean and early Proterozoic, after which no major orogenic activity has affected the rocks. The Goa Group is defined as the north western extension of the Dharwar Super-Group (Gokul, 1985) and their lithology may be summarised from oldest to youngest as follows:

The Barcem Formation

The Barcem Formation is the oldest of the four Goa Group formations and it dominates the south of Goa. It comprises ortho-quartzite, meta-basalt, meta-gabbro, meta-acid volcanics (quartz-porphyry meta-rhyodacite and tuffs) and quartz-amphibole schist with bands of agglomerate (GSI, 1996).

The Sandvordem Formation

The Sandvordem Formation is the second oldest of the Goa Group and consists of polymictic meta-conglomerate/breccia, overlain by thick succession of mainly turbiditic deposits now forming meta-greywacke, quartz-chlorite schist and lenses of quartzite. The formation varies in thickness, reportedly up to 400 m. The meta-conglomerate/breccia contains rounded to angular, pebble to boulder size clasts of quartzite, gneissic granite, granodiorite and mica schist. The conglomerate is widely but irregularly distributed at various stratigraphic levels and is also reported to show transitional contact with the overlying quartz-chlorite-biotite schist of the Bicholim-Rivona Formation (GSI, 1996).

The Bicholim-Rivona Formation

The Bicholim-Rivona Formation is dominated by quartz-chlorite-bioitite-amphibole schist with thin lenses of meta-basalt, meta-gabbro, carbonaceous and manganiferous chert, quartzite, banded iron formation (BIF), quartz sericite schist and magnesian Mn-rich limestone (GSI, 1996). This formation occupies a considerable part of Goa, running almost the full length along the centre of the state, and occurs at thicknesses

up to 250 m to 500 m. In the south of Goa the formation is manganiferous. The BIF occur in a belt 95 km long by 1-14 km wide, and is intercalated with quartz-chlorite-biotite-amphibole schist, chert, quartzite, limestone and meta-volcanics. Two types of oxide facies are identifiable; the lower one is reported as haematitic, a banded haematite quartz (BHQ) and upper one magnetite banded magnetic quartz (BMQ) (GSI, 1996).

The Vageri Formation

The Vageri Formation consists of carbonate-quartz schist and meta-greywacke with thin lenses of meta-basalt and quartzite. Some of the meta-greywackes found to the north are known to be garnet-bearing (GSI, 1996).

3.3.2. Intrusions

The Goa Group as a whole is intruded by mafic and ultramafic complexes of lower Proterozic age. In the Bondla-Durgini (Figure 1.12) hills the complex is layered, and comprises dunite, serpentinite, peridotite, pyroxenite and gabbro with chromite lenses. In the Pernem taluka, near the town of Ibrampur, is an occurrence of an undifferentiated peridotite – gabbro – norite complex with radial dykes of pyrozenite – gabbro. The parentage of these complexes is believed to be komatitic, tholeiitic or calkalkaline lavas, that were emplaced late in the Dharwarian tectonic regime (GSI, 1996), and altered to their present state by later tectonic events.

3.3.3. Granite intrusions

The Goa Group and the mafic – ultramafic intrusions are in places intruded by K-rich granites, which occur as plutons and plugs. Very often they occur within the banded and migmatitic gneisses of the PGC, into which they grade imperceptibly. These K-rich granitoids formed as younger phases of melts, are often correlated with Dharwarian tectonic activity, and are termed syntectonic or post-tectonic. For example, the Chandranath Granite is believed to be syntectonic with the first phase of folding and has been dated at 2650 ± 100 Ma (Dhoundial et al., 1987), whereas the Canacona porphyritic granite, exposed in the far south of Goa, is post-tectonic and has been dated at 2395 ± 390 Ma (Dhoundial et al., 1987, Fernandes, 2009).

3.3.4. Laterite

Laterite is common along the length of the Konkan coastal lowland of Goa. This coastal plain evolved during Cenozoic times and is bounded to the east by the Western Ghats escarpment. The coastal plain comprises a gently dipping discontinuous ramp of dissected laterite-capped mesas or tablelands, which slope gently from maximum elevations of 150-200 m in the east to less than 50-100 m at the coast (Widdowson, 2009). These represent the remnants of a once extensive, semi-continuous laterite belt that extended along the length of peninsular India, along the Konkan – Kanara coastal plain (Widdowson and Gunnel, 1999).

Conditions suitable for laterite formation have prevailed in western peninsular India since the Late Miocene and as such laterite is common and it was an example from Malabar (i.e. modern-day Kerala State) that the first scientific description was given for 'laterite' (Buchanan, 1807). However, the definition and classification of laterite remains a polemic issue, as can be seen in several studies (Bourman and Ollier, 2002, Bourman and Ollier, 2003, Schellmann, 2003, Summerfield, 1991).

Within western India laterites may be recognized in two distinct geomorphological zones: 1) capping the elevated basalt mesas of the Western Ghats, running from Pune to Belgaum and often termed 'high-level laterites' (Sahasrabudhe and Deshmukh, 1981, Widdowson and Cox, 1996, Widdowson, 1997) and 2) an extensive, semi-continuous belt lying to the west of the main Western Ghats escarpment between Mumbai and Trivandrum capping the coastal plateaux of the outer Konkan and Kanara coastal plain. These are often termed 'low-level', or 'coastal belt' laterites (Figure 3.5). It is important to note however, that since Goa is almost completely devoid of Deccan basalt terrain; there are no high level laterites present in the study area.

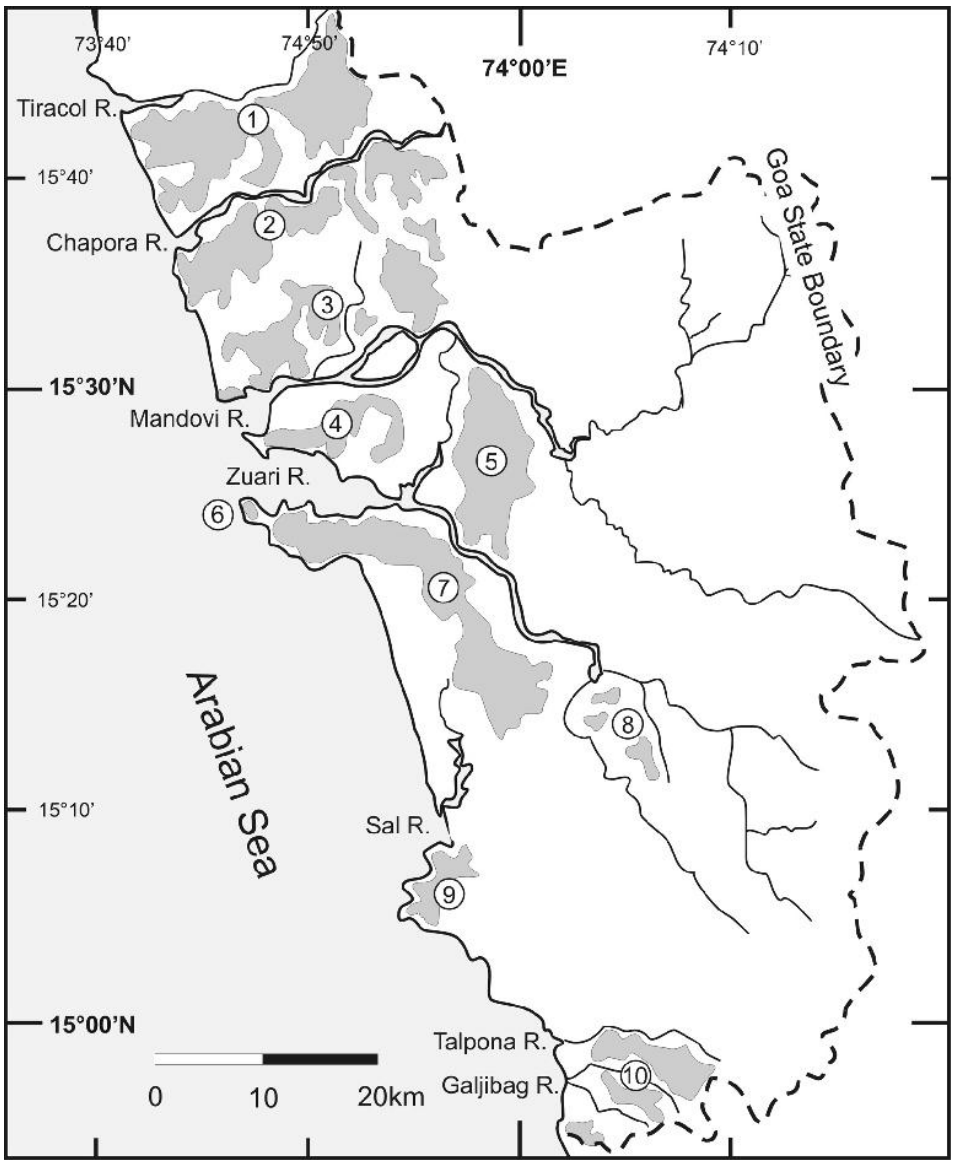

Figure 3. 5 Distribution of key laterite-capped table-land (plateaux) regions of Goa. 1, Pernem Plateaux; 2, Mapusa Plateaux; 3, Porvorim Plateaux; 4, Panjim Plateaux; 5, Ponda Plateaux; 6, Vasco de Gama Plateau; 7, Dabolim – Madgaon Plateaux; 8, Quepem Plateaux; 9, Cabo de Rama Plateaux; 10, Canacona Plateaux (after Widdowson, 2009).

3.4. Geomorphology

Immediately north of Goa, in Maharashtra State, the geology is dominated by Deccan Basalt (c. 64 - 67 Ma) (Widdowson and Cox, 1996, Widdowson et al., 2000) which overlies, to the south, a complex Precambrian basement lithology (Dhoundial et al., 1987). Outcrops of the southernmost Deccan basalt exposures occur around the NE periphery of Goa. Denudation has affected both these lavas and the pre Deccan basement in a similar way, creating a commonality of broad geomorphological divisions across the various lithologies (Widdowson and Gunnel, 1999). Accordingly, the continental margin region may be delineated into four distinct geomorphological zones which, from the coast inland, are as follows (Widdowson, 2009) (Figure 3.6):

i) A low lying, 50 – 200 m high coastal plain, 5-70 km wide, called the Konkan - Kanara lowlands which includes the Midland Hilly region, characterised by short westerly flowing rivers;
ii) A continental scale, 600 – 1000 m high escarpment called the Western Ghats that runs broadly parallel with the coast;
iii) The Western Ghats summit zone. This is a narrow zone of discrete, elevated mesas in the basaltic zone or ridges and domes in the cratonic zone;
iv) The inland Karnataka and Maharashtra plateaux, an area of elevated land c. 600 – 800 m elevation characterised by slow easterly flowing rivers.

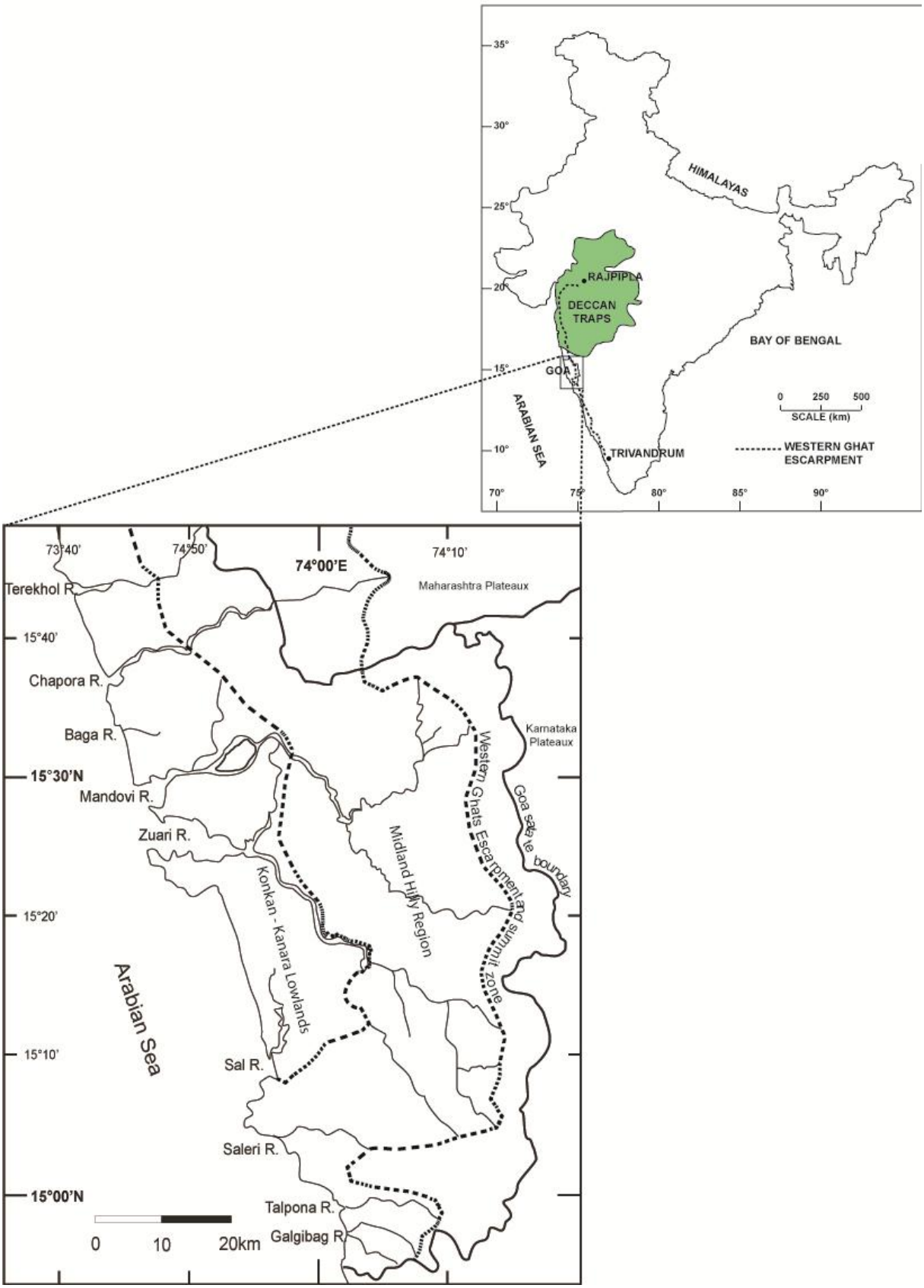

Figure 3.6: Map of the Indian sub-continent showing the location of Goa and the extent of the Western Ghats Escarpment, with an enlarged map of Goa depicting the various geomorphological zones including Western Ghats Escarpment (after Widdowson, 2009) and the Midland Hilly Region (after Fernandes 2009).

3.5. Drainage systems

3.5.1. Evolution of the Western Ghats escarpment

The c. 1600 km Western Ghats escarpment is a continuous large-scale geomorphological feature, running from the state of Gujurat in the North (c. 20ºN), the escarpment beginning near the village of Rajpipla (21.78ºN, 73.57ºE), to the city of Trivandrum (8.44ºN, 76.92ºE) in the south (Gunnell and Fleitout, 1998, Widdowson, 2009). It is of fundamental geographical importance since it demarcates the drainage divide for all of peninsular India (Watts and Cox, 1989), and separates the coastal plains from the elevated interior (Figure 3.6). Most rivers in peninsular India rise at this escarpment and drain to the east into the Bay of Bengal, although north of the Narmada river drainage is to the north-east into the Ganga valley. Also in the north there are occasional examples of westerly drainage into the Arabian Sea (Cox and Summerfield, 1989). Cox and Summerfield (1989) interpret the whole of peninsular India as the flank of the remaining eastern half of the original plume related dome created during the separation of India and the Seychelles micro-continent c. 65 Ma. Therefore the rivers draining to the east are generally slower flowing compared to the highly erosive upper courses of the rivers draining to the west down the escarpment and across the Konkan coastal plain into the Arabian Sea. For example, the Godavari and Krishna River systems flow from the high Western Ghats escarpment all the way to the Bay of Bengal, whereas the Narmada River, which, in terms of discharge and drainage basin size, is the fourth largest river in India after the Brahmaputra, Ganges (Bhandari et al., 2005) and Tapti Rivers, flows via fault controlled valleys from the Deccan Plateau to the Gulf of Cambay (Cox and Summerfield, 1989).

The Western Ghats escarpment is believed to have its origins following the plume-related surface uplift that occurred as India moved northwards over the Reunion Hotspot (Collier et al., 2008). Immediately following the eruption of the Deccan Traps Continental Flood Basalt Province, c. 65 Ma ago (Watts and Cox, 1989), India and the Seychelles micro-continent became detached (Widdowson and Cox, 1996, Campanile et al., 2008, Ganerod et al., 2011), thus leaving a seaward facing fault escarpment complex at the rift locus on the western coast of peninsular India; it is this structural feature that is thought to have formed the proto-escarpment which later evolved during the Cenozoic into the eastwardly-retreating Western Ghats escarpment (Widdowson and Cox, 1996).

Following separation of the Seychelles micro-continent c. 65 Ma ago this escarpment has retreated inland as a result of weathering and erosion (Widdowson and Cox, 1996, Campanile et al., 2008). The recession of the escarpment and subsequent weathering and erosion in the latter Cenozoic has left behind a low-lying coastal plain capped by a shallowly-dipping discontinuous ramp of dissected laterite-capped mesas or 'tablelands', which slope from maximum altitudes of 150-200 m in the east to less than 50-100 m at the coast (Widdowson, 2009). Since the initial formation of the escarpment, its elevation and the 'pinned drainage' patterns have essentially been maintained by denudationally driven isostatic uplift of the lithosphere in response to the erosion (Widdowson, 1997; Figure 3.7). Rejuvenation and uplift across the coastal plain has since led to the formation of steeply incised meandering rivers cutting through the uplifted lateritised pediment resulting in coastal sea cliffs and extensive tracts of laterite preserved on the uplifted resistant laterite duricrust.

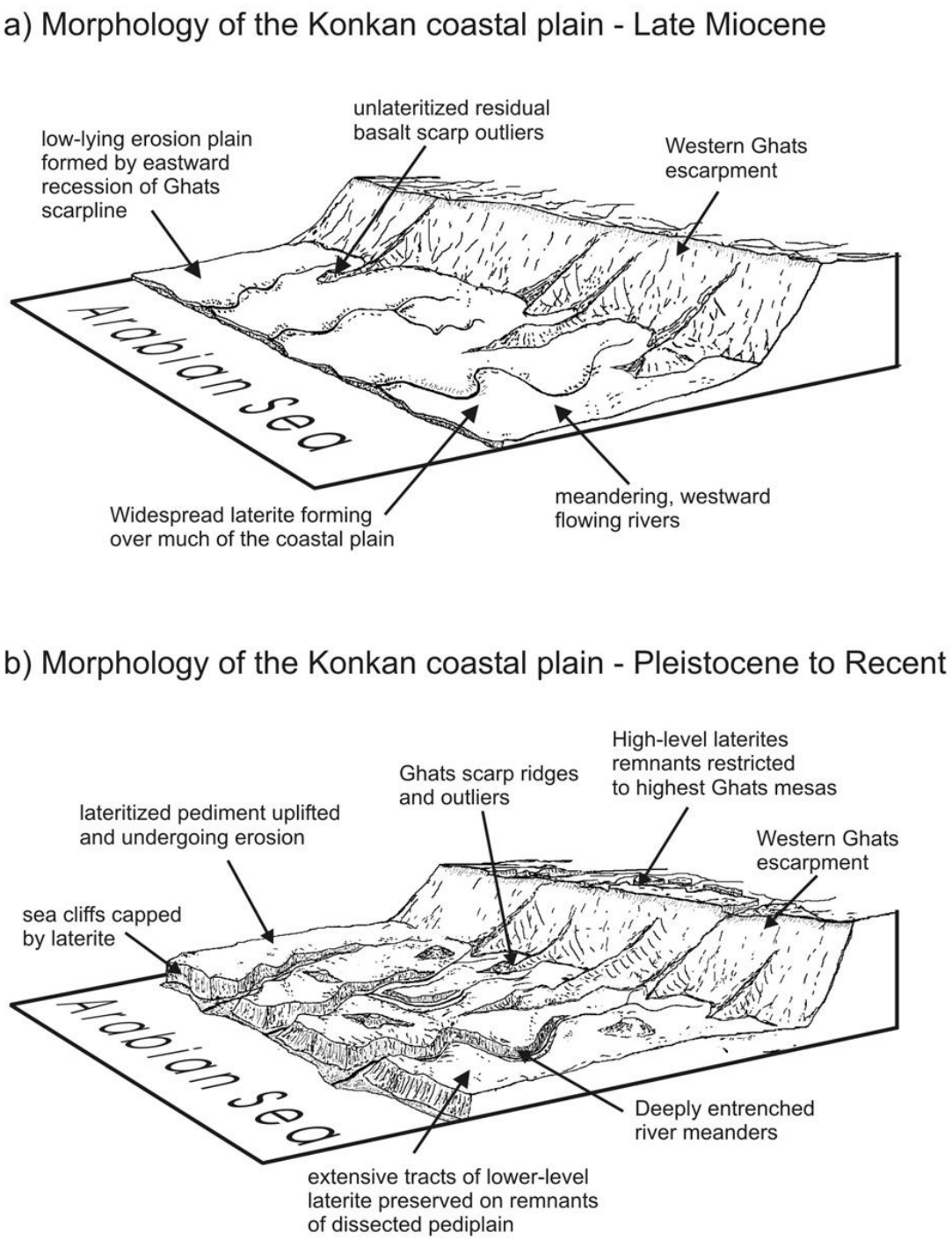

Figure 3. 7 Schematic block diagrams showing the main geomorphological features during the evolution of the coastal (Konkan) laterite belt, Goa, India and its subsequent dissection by the eastward-flowing drainage (after Widdowson, 2009).

Since Goa is completely contained between the Western Ghats escarpment and the coast, it is dominated by high energy, westerly flowing rivers. There are nine major rivers in the state of Goa flowing from east (Western Ghats) to west (Arabian Sea) (ENVIS, 2012). From north to south these are the Terekol, Chapora, Baga, Mandovi, Zuari, Sal, Saleri, Talpona and Galgibag (ENVIS, 2012) (Figure 1.8). The Mandovi and

Zuari River systems are the two major westerly flowing river systems. They are connected by the Kumbarjua Canal, which was constructed to provide a transport link between the Mandovi and Zuari Rivers to facilitate the transport of iron and manganese ore to Mormugao Port (Mesquita and Kaisary, 2007) (Figure 3.1). These two rivers drain over 2500 km^2 (68%) of the total land area of Goa (Nair, 2003). The Mandovi has an annual run-off of c. 16 km^3, of which only 0.06 km^3 occurs as dry season run-off. The Zuari has an annual run-off of c. 9 km^3, of which only 0.03 km^3 occurs as dry season run-off (Nair, 2003). The rivers are typically c. 5 m deep at the estuary, reducing to c. 2 m deep 50 km upstream and their cross sectional area decreases hugely from mouth to head (Unnikrishnan et al., 1997).

All the rivers are tidal, and tidal effects are observed up to c. 40 km upstream due to the low gradients of the rivers dissecting the Konkan coastal plain. They display uniform diurnal and semi-diurnal amplitudes up to the point at which fresh water influx can arrest tidal influx, after which the amplitude rapidly diminishes (Unnikrishnan et al., 1997). This tidal range varies throughout the year in response to fresh water influx as a result of the monsoon climate. Unnikrishnan et al. (1997) observed the water levels within the Mandovi and Zuari river system over a 72 hour period at 15 locations using tide poles during two separate periods: 7-9th April 1993 and 19-21st August 1993. During the period 19-21st August 1993, when the fresh water influx was close to maximum (monsoon season), the tides were forced further downstream (c. 30 km from the coast) by the large influx of fresh water. By contrast, during the period 7-9th April 1993 (dry season) the tides reached further inland (c. 40 km from the coast) where the river cross sectional area is lower and a lower fresh water influx is sufficient to arrest the upstream flow of the tide. This observation is also supported by Shetye et al. (1995), who observed that even during the driest quarter (March-May 1993), there was still sufficient fresh water to keep the salinity of the river water close to zero upstream of 40 km from the mouth of the rivers. This is attributed mainly to the fact that the cross sectional area of the rivers diminishes rapidly upstream, with the Zuari decreasing from c. 35,000 m^2 at the mouth to c. 20 m^2 at the head (Unnikrishnan et al., 1997).

3.5.2. Fe and Mn mining

Important iron ore deposits in Goa are located in Bicholim, Sanguem, and Sattari talukas (Figure 3.8). Approximately 18,000 ha of land are currently under mining operations in Goa (IBM, 2002). The present mining rate of 16–21 million tonnes of ore and the high ore:over burden ratio of around 1:3, means that there is a need for

removal and disposal of 40–50 million m^3 of waste per year (Yellishetty et al., 2008). Both the Mandovi and Zuari Rivers flow through Fe and Mn mining areas. The Zuari has 10 mines located within its basin, and together they contribute to about two-thirds of the total exploitation of Fe, Mn and ferromanganese ores from Goa. About 90% of all Fe and ferromanganese ores are transported through these estuaries in barges to Mormugao harbour (Nair, 2003). The mines along the Zuari River generate between 1000-4000 tonnes of waste per day per mine, inevitably, some of these waste products finding their way into the rivers (Nair, 2003).

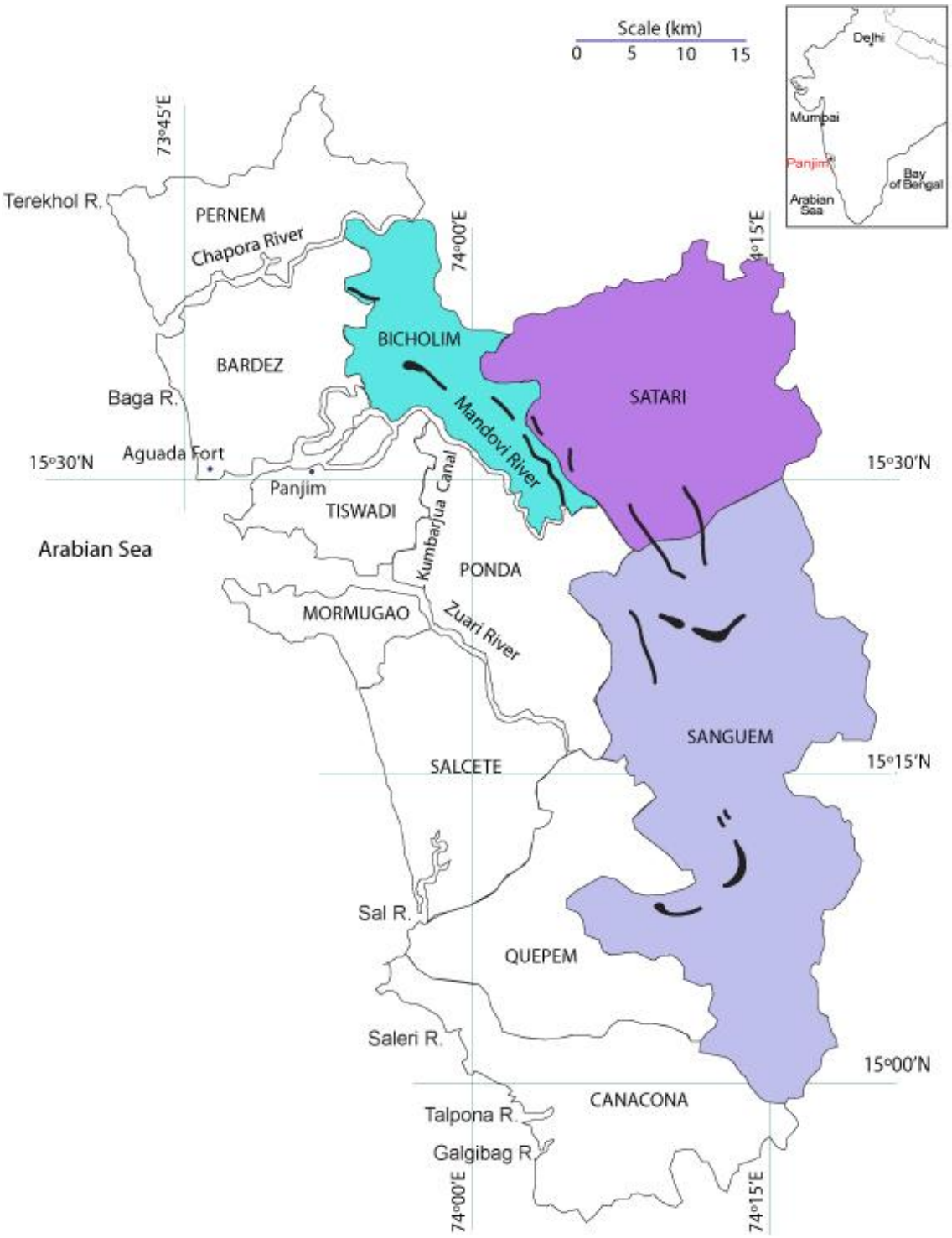

Figure 3. 8 Map of Goa showing the location of the nine major rivers and the location of the iron ore ranges as represented by the black shaded areas as located in the Bicholim, Satari and Sanguem Talukas (after Yellishetty et al., 2008). Colours used to highlight the three Talukas and are not representative of the underlying geology, for this information see Figure 3.4.

3.6. Climate (temperature, humidity, precipitation)

The westernmost region of the Deccan Province on the western coast of India (Gujurat, Maharashtra, and Goa States) is subject to a sub-tropical climate with highly seasonal, monsoonal rainfall. Around 85% of the rainfall occurs during the summer monsoon months of July – October (NOAA, 2012). This pattern is also reflected in the river discharge, with 80% of their flow occurring in this period (UNESCO, 1993).

Accordingly, since Goa lies within this monsoonal belt at near equatorial latitudes, its climate is highly cyclical, with precipitation varying widely between the dry season (October – May) and the wet season (June – September). The National Oceanic and Atmospheric Administration (NOAA) website through its National Climatic Data Centre (NCDC) provides historic daily and monthly precipitation and temperature records via its Global Daily Climatology Network (GDCN) and Global Historical Climatology Network (GHCN) datasets (Watts and Cox, 1989). From these useful data sets, details regarding the rainfall frequency and variability in western India and Goa may be extracted. The monthly Global Historic Climatology Network (GHCN) dataset provides a monthly precipitation record for Panjim. This has been temporally limited to the years 1978 to 2008, and clearly shows the cyclic nature of the monsoonal climate (Figure 3.9). The Global Daily Climatology Network (GDCN) record for Panjim is not available after 1984, but it does demonstrate the highly variable nature of the monsoon rainfall, ranging from 0 to 437 mm, with an average of almost 50 mm during June to September 1984 (Figure 3.10).

In Figure 3.11 the data have been interrogated to create a graph of annual precipitation. Like Figure 3.9 this graph has also been temporally limited to the years 1978 to 2008. The precipitation graphs shown in Figures 3.9, 3.10 and 3.11 highlight the huge variability in rainfall during different monsoon seasons, not only on an annual basis but also on a monthly and even weekly basis. For example, the highest annual rainfall recorded during this period was 3583 mm and 3690 mm which occurred in 1983 and 2007, respectively, whilst the lowest annual rainfall was 1723 mm and 1987 mm, occurring in 1986 and 1996, respectively, whilst the annual precipitation for 2008 was 2803 mm (close to the calculated average of 2800 mm).

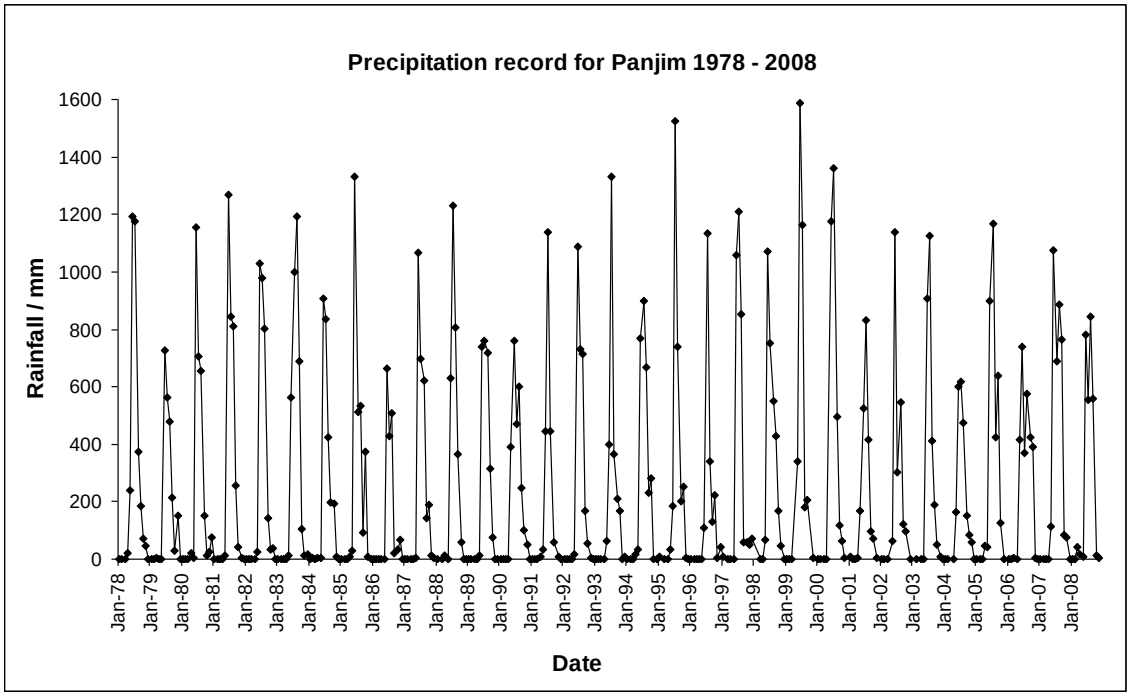

Figure 3.9 Monthly precipitation records for Panjim, India (1978 - 2008) (data from NOAA, 2012).

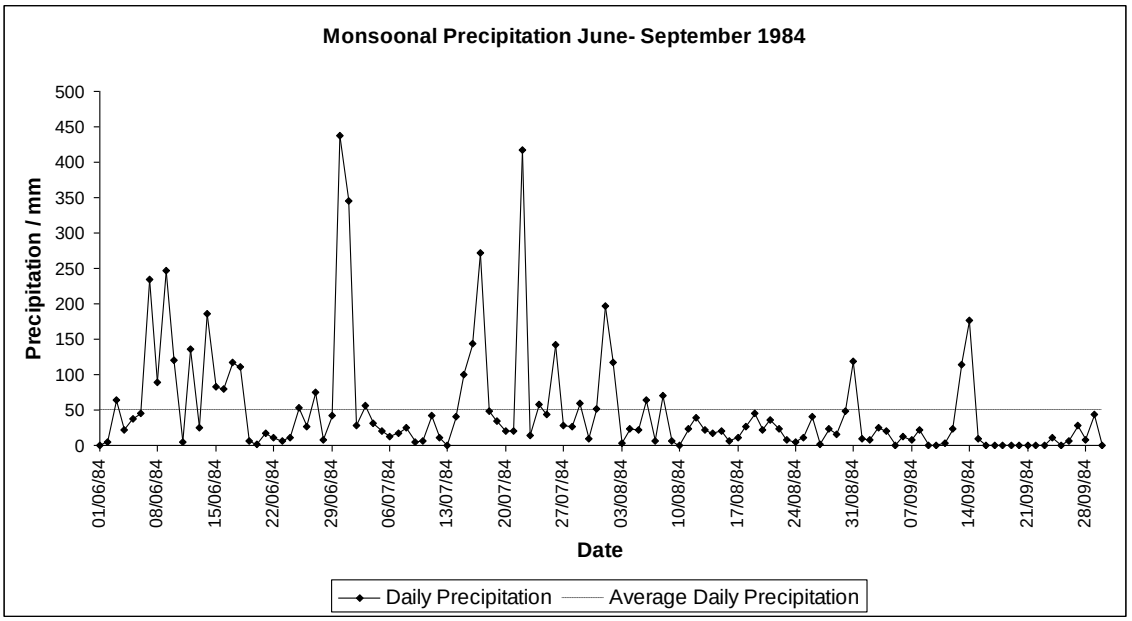

Figure 3.10 Precipitation records for Panjim, India (June - September 1984) including a calculated average daily precipitation (data from NOAA, 2012).

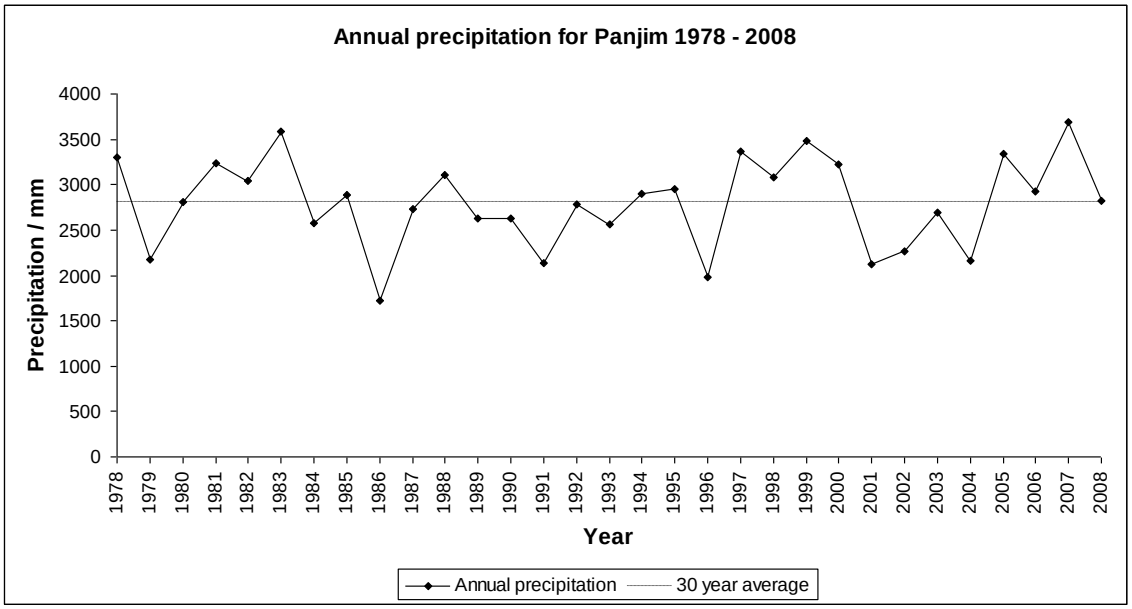

Figure 3.11 Annual precipitation records for Panjim, India (1978-2008) including a calculated 30 year average of 2800 mm (data from NOAA, 2012).

Summary

- The geology of Goa comprises a complex juxtaposition of Precambrian basement rocks of the Dharwar Craton, which in itself is part of the South Indian Shield (SIS);

- In detail this basement complex consists predominantly of low grade (greenschist facies) metamorphic rocks of the Goa Group, which are sub-divided into the Barcem, Sandvordem, Bicholim-Rivona and Vageri Formations;

- The Goa Group rocks have subsequently been intruded by various mafic and ultramafic complexes, most significantly the Chandranath (2650 ± 100 Ma), Dudhsager (2565 ± 95 Ma) and Canacona (2395 ± 390 Ma) granites, as well as a series of mafic intrusive bodies and associated dykes;

- A major unconformity exists between this basement complex and the overlying Deccan Basalt succession,; this latter was erupted onto the eroded surfaces of the Dharwar Craton. A small area of these Deccan Basalts occur in the Northeast corner of Goa, and cap the uppermost few hundred metres of the Ghats escarpment;

- The broad geomorphology of Goa comprises a low lying, 50 – 200 m high coastal plain, 5 – 70 km wide, called the Konkan-Kanara lowlands and which includes a

Midland Hilly Region forming the foothills to the Ghats escarpment. The lowlands are characterised by short westerly flowing rivers draining into the Arabian Sea. Inland of these geomorphological regions there is a continental scale, 600 – 1000 m high escarpment called the Western Ghats which runs broadly parallel with the coast; to the east this becomes the Western Ghats summit zone and then the extensive Karnataka and Maharashtra plateaux, an elevated area c. 600 – 800 m high characterised by slow easterly flowing rivers;

- The Ghats summit zone provides the main drainage divide for Peninsular India;

- Goa is subjected to a monsoonal climate with high temperatures throughout the year; almost all rainfall occurs during the monsoon months of June, July, August and September;

- Fluvial systems respond to this monsoonal climate through vastly changing annual riverine fluxes/discharge.

PART II: FIELD-BASED RESEARCH

Chapter 4. Selection of fluvial systems, river water and rock sampling rationale

This chapter contains three sections; the first providing a rationale for how the rivers and the sample localities were selected along with descriptions of the rivers, water sample collection and in situ analysis methods. The second section provides a rationale for river bed rock sample collection, including a description of the analysis techniques employed. The third and final section provides a rationale for the study of a weathering profile based on a metagreywacke protolith accessible in the Merces Quarry.

4.1. Rationale for river selection

As discussed in part I, numerous studies have already been completed on rivers draining the Deccan Traps (Dessert et al., 2001, Das et al., 2005). By contrast, this study will focus on the heterogeneous lithology of Goa, which can be broadly described as Proterozoic basement gneiss overlain by a variety of metamorphosed lithologies that comprise the Goa Group, much of which is capped by laterite. Laterite forms preferentially on lithologies that have inherently higher Fe and or Al contents, for example, mafic igneous rocks such as the Deccan basalt and immature sedimentary rocks such as greywackes. Initial desk studies showed that to the very north of Goa around the Chapora River the geology is dominated by the Goa Group and here the laterite covers the majority of the Chapora River drainage basin. This is also true for the remainder of Goa, with the exception of the Chandranath Granite Basement Gneiss and the Canacona Granite to the south and the Anmod Ghat Granite Gneiss to the east, none of which are susceptible to lateritisation. It was decided that a compare and contrast study would be undertaken to study the difference in elemental concentrations in the Chapora River draining predominantly Goa Group geology and the more southerly Zuari River draining a mixture of Goa Group and Basement Gneiss geology.

It was also noted that large areas of Goa are subject to open cast Fe and Mn mining operations. These are located towards the east of Goa running roughly north – south below the Western Ghats Escarpment in the Bicholim, Sanguem, and Sattari Talukas (Figure 3.1). The Mandovi and Zuari Rivers flow through these areas and are both widely used for transportation of ore. Therefore potential contamination arises from mine waste, transportation of the mined material by road to reprocessing plants, and

then by river barges out to sea (Figure 4.1). This provided an additional opportunity to compare and contrast the effects of mining and natural weathering effects on the rivers draining these areas. The Zuari River was used to monitor elemental concentrations draining the areas affected by mining. The more northerly Chapora River was used to monitor elemental concentrations draining an area largely unaffected by mining.

(a)

(b)

Figure 4. 1 Photographs showing the transportation of mining products (a) by road to the processing plant and (b) by river to the loading barges in the Arabian Sea.

However, neither river is completely unaffected by anthropogenic activity because large dams have been constructed upstream to create the Salaulim Reservoir on the Zuari River and the Tilari Reservoir on the Chapora River. The water in both rivers is also widely used for agricultural irrigation via irrigation channels and for domestic activities (e.g. washing of clothes, motorbikes and even trucks (Figure 4.2).

(a)

(b)

(c)

Figure 4. 2 Photographs showing (a) and (b) mining ore lorries being washed in the river and (c) manual sediment dredging of the river bed.

4.1.1. Description of Rivers.

Zuari River description

The Zuari River is the second largest river in Goa, after the Mandovi. It drains an area of c. 1059 km^2 and is formed by three main tributaries. From north to south these are the Ugem River, the Guloli River and the Kushavati River. The main channel formed by the Ugem River begins c. 70 km inland at the Western Ghats escarpment at an elevation of c. 550 m. From here a series of ephemeral minor streams and rivulets cascade down the hillsides and gather into feeder streams with more persistent flow, and thence into the river channel proper. The river elevation drops rapidly at first, losing around 500 m in the first 5 km (Figure 4.3), after which the gradient declines to just a few m per km as the river meanders in a north westerly direction, passing the first two sampling sites (Zua 01 and Zua 02) before encountering the first tributary. It is here the Guloli River delivers its flow from the huge Selaulim Reservoir where, just 1 km upstream, the third sampling locality (Zua 03) can be found. The river continues in a north westerly direction for a further 12 km passing the fourth sampling locality (Zua 04) before converging with the Kushavati River. The fifth and sixth sampling localities (Zua 05 and Zua 05opt) are to be found 3.7 km and 12.4 km upstream, respectively, along the Kushavati River. From here all three flows converge to travel the final 40 km past the seventh and final locality (Zua 06) eventually entering the Arabian Sea at Mormagao Bay.

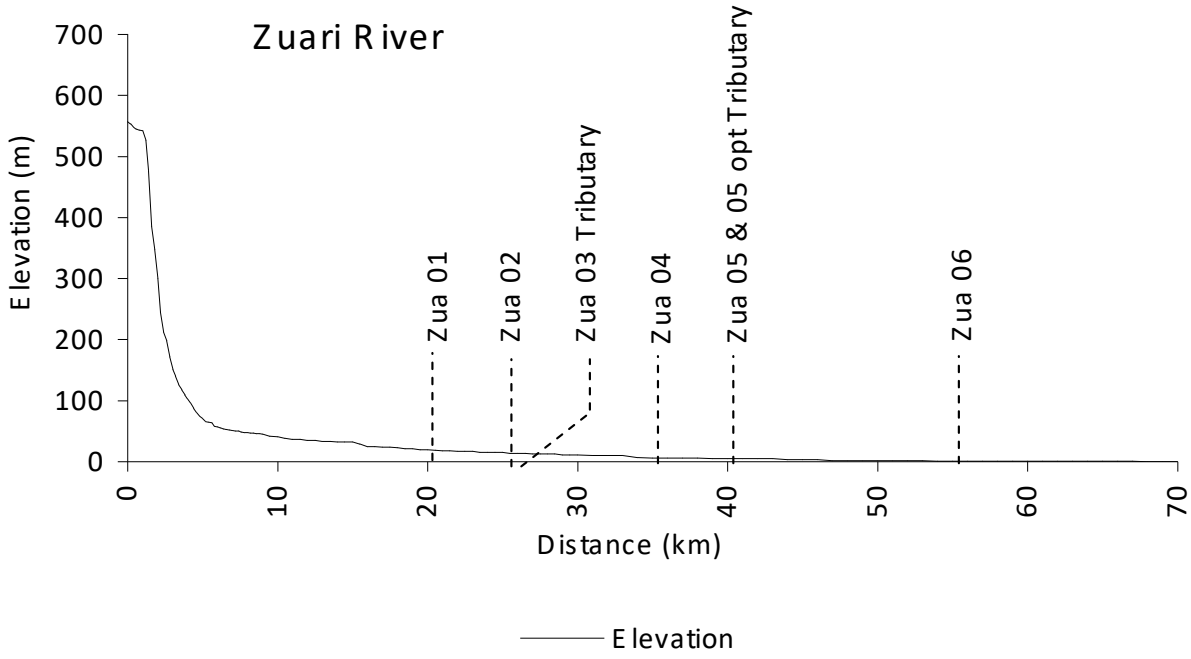

Figure 4. 3 Elevation profile for the Zuari River, showing the location of the sampling sites. The profile was created using Google Earth 6.2 to establish the elevation above sea level along the river. Elevations were taken every 200 m for the first 10 km of the river course, increasing to 500 m for the next 20 km and 1000 m for the lower course where it crosses the coastal plain and becomes tidally influenced.

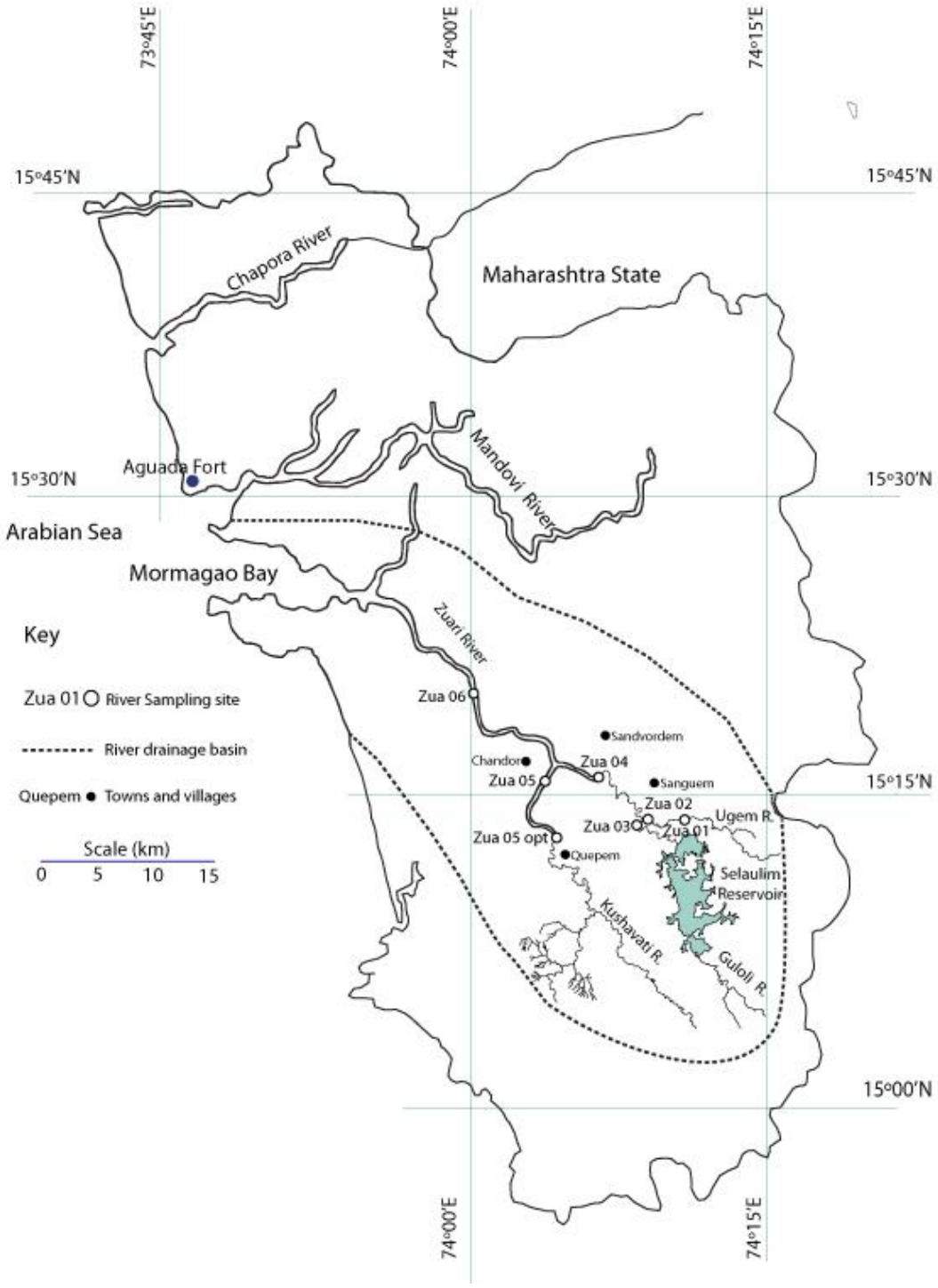

Figure 4. 4 Sampling localities in the Zuari River drainage basin

The Zuari River

Zua 01

Zua 02 and 03

Zua 04

Zua 05

Zua 05 opt

Zua 06

Figure 4. 5 Satellite photos of the Zuari River sampling localities (from Google Earth).

Figure 4. 6 Photographs of the Zuari sampling localities during June 2007. All photographs are viewed downstream.

Zua 01

The river at this locality is at an elevation of 20 m and flows through a shallow densely vegetated valley in a NNW direction (345º). The river is approximately 35 m wide from bank to bank. The river width varies seasonally to as little as 5 m in the dry season, during which small pebble bars can be seen as well as some in-situ exposures of soft weathered meta-sediments (fine sandstone). Boulders of laterite and phyllite c. 30-40 cm across (occasional larger c. 1 m) occur in the river channel. The banks of the river are overgrown with a mix of dense jungle and coconut plantation.

Zua 02

This locality, near Sanguem, is c. 200 m east of a main tributary convergence. The river here is approximately 40 m wide from bank to bank, although the river width varies seasonally. The river flows in a westerly direction (270º) through a densely vegetated valley (c. 25 m deep). The vegetation is a mixture of dense jungle and coconut plantation and the river banks are so overgrown that it was not possible to gain access to the river to collect samples. Outcrops of ferricrete can be seen on the downstream section of the riverbank. On closer inspection the ferricrete is made up of cobbles of banded haematite quartz (BHQ) which have been re-cemented together, although the upper surfaces do take the form of a duricrust.

Zua 03

This locality also near Sanguem is c. 900 m south west of a main tributary convergence. The river is approximately 40 m wide from bank to bank although the river width varies seasonally. The river flows in a northerly direction (360º). Scattered boulders of ferricrete occur upstream of the sampling site. Alluvium is red coloured sandy silt. The banks of the river are dominantly vegetated by coconut plantation mixed with areas of jungle.

Zua 04

At this locality near Sandvordem, the river is c. 100 m wide from bank to bank and flows in a westerly direction (300º). There are no visible outcrops or river bed sediments. The banks of the river are moderately vegetated with a mix of coconut plantation and jungle. A mine reprocessing plant occurs downstream of the sampling

site, where mining products are transferred from trucks to barges. Conurbations can be seen on either side of the river at this locality.

Zua 05

Locality Zua 05, near Chandor, is located on a tributary feeding into the main channel from the south. This tributary drains the Chandranath Granite Terrain and was chosen to determine if there are any discernible differences between its aqueous chemistry and that of the main channel. The river here is c. 40 m wide from bank to bank, although the river width varies seasonally. The river flows in a northerly direction (360º). There are no river deposits or outcrops visible. Both river banks are densely vegetated primarily with coconut plantation interspersed with jungle.

Zua 05 opt

Locality Zua 05 (opt) near Quepem is also located on the same feeder channel as locality Zua 05, although this locality is 5 km further south east. Here the river flows in a north westerly direction (294º). The river channel is c. 40 m wide from bank to bank, although the river width varies seasonally to as little as 10 m. The valley floor exposes rock outcrops and substantial pebble / gravel bars; these are heavily vegetated, suggesting that the valley is not often flooded to its maximum width. The rock outcrops are fine-grained, Fe-Mg mineral-poor microgranite, which are foliated and fractured and generally weathered. The pebble - gravel bars comprise coarse sand with 1 -15 cm diameter sub-rounded to angular pebbles of vein quartz, quartz with biotite mica, banded ferricrete, haematite, goethite, micaceous metamorphic (mafic), meta-sandstone and sandstone.

Zua 06

The river here flows in a westerly direction (294º). The main channel is c. 165 m wide with an additional 500 m wide flood plain (rice paddies) either side. These are flanked by low hills with dissected laterite mesas that are formed on meta-greywacke. The banks are moderately vegetated with a mixture of coconut plantation, rice paddies and jungle.

Chapora River description

The Chapora River rises in the state of Maharashtra just north of the small village of Tilari Nagar at 15º49'42.56"N, 74º11'35.75"E at an elevation of c. 700 m on the summit of the Western Ghats escarpment. From here it descends through a steep sided, densely vegetated valley, losing over 500 m in less than 4 km (Figure 4.7). The river then flows across the low coastal Konkan / Kanara plateau in a south westerly direction, meandering past numerous low vegetated hills on its way into Goa state and on towards the Arabian Sea.

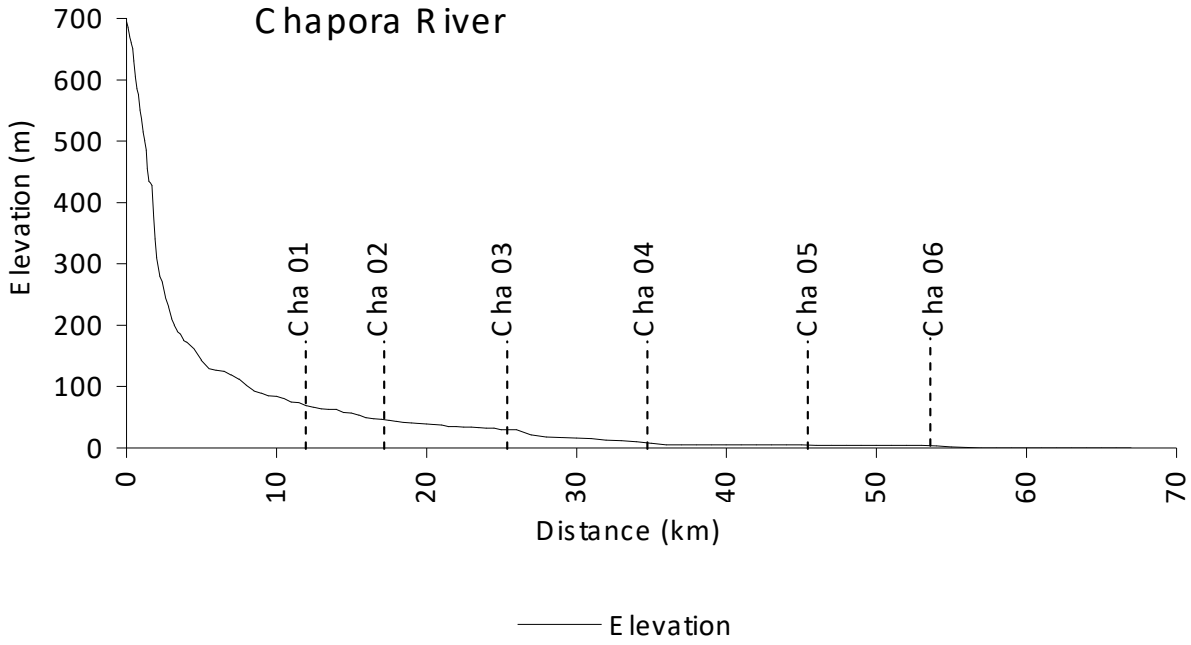

Figure 4. 7 Elevation profile of the Chapora River, showing the location of the sampling sites. The profile was created using Google Earth 6.2 to establish the elevation above sea level along the river. Elevations were taken every 200 m for the first 5 km of the river course, increasing to 500 m for the next 20 km and 1000 m for the lower course where it crosses the coastal plain and becomes tidally influenced.

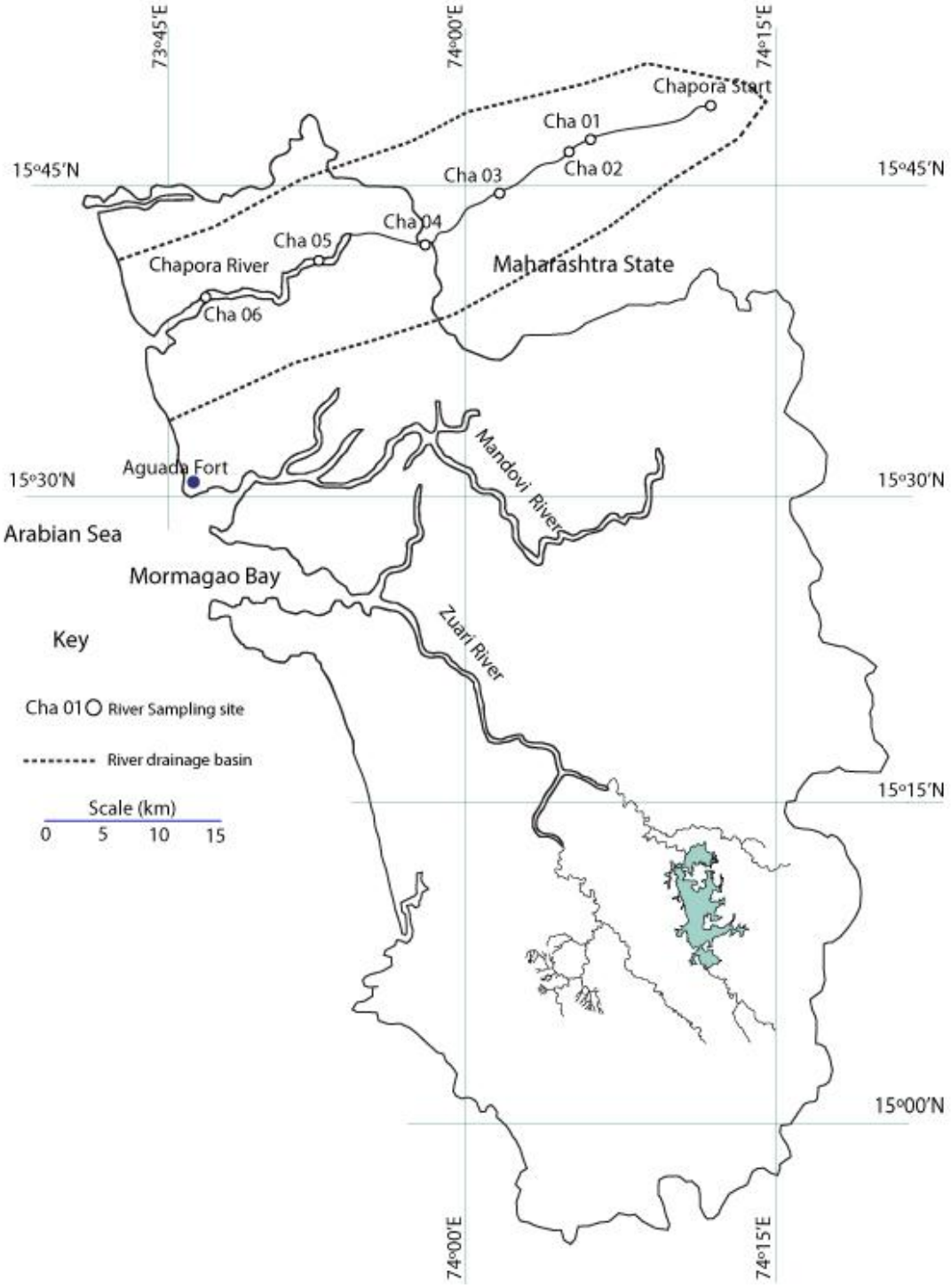

Figure 4. 8 Sampling localities in the Chapora River drainage basin.

The Chapora River

Cha 01

Cha 02

Cha 03

Cha 04

Cha 05

Cha 06

Figure 4. 9 Satellite photos of the Chapora sampling localities (from Google Earth).

Figure 4. 10 Photographs of the Chapora sampling localities during June 2007. All photographs are viewed downstream.

Cha 01

The river at this locality is at c. 75 m elevation and flows in a south westerly direction (230º). The width of the river is approximately 70 m from bank to bank, although this is seasonally variable. The June photographs (Figure 4.10) which were taken during the monsoon show the river in spate with the bridge flooded and almost impassable. However, in March 2007 the river was very different, showing large vegetated pebble bars in both the upstream and downstream sections. The pebble bars on the downstream section split the river into two separate flows (Figure 4.9). These pebble bars are made up of a range of lithologies including meta-greywacke, garnet mica schist, quartz and occasional Deccan basalt of varying sizes with the boulders commonly occurring up to 30-40 cm in size. The pebbles are rounded to sub-rounded and the boulders are angular to sub angular. The vegetation on each side of the river is mainly jungle with occasional banana, mango, palm, bamboo and acacia. The edge of the Western Ghats can be seen some 5 – 10 km to the east.

Cha 02

The river at this locality is at approximately 50 m elevation and flows in a westerly direction (264º). Looking upstream the river splits in two with the main channel flowing to the north and the other channel flowing to the south east, where the river has recently been dammed to form a reservoir. The river width is c. 85 m wide from bank to bank although the river width varies seasonally. Looking upstream there is a large central pebble bar which is vegetated around its river facing edge. The pebble bar was not accessible but appears to comprise mainly cobbles and pebbles with fewer boulders than the previous locality, Cha 01. The cobbles and pebbles appear to be made up of c. 40% basalt, which are identifiable by their often vesicular nature and the presence of large feldspar crystals. These are probably derived from the now dammed river to the south east where the Ghats escarpment can be seen with large basalt flows clearly visible in the topmost 100 m. The remainder of the cobbles and pebbles comprise meta-banded gneisses, fine grained phyllite schist, occasional quartz and occasional granite. The vegetation at this locality is dominated by jungle with occasional mango and palm plantation becoming more prevalent downstream.

Cha 03

At this locality the river is at approximately 33 m elevation and flows in a south westerly direction (235º) through a c. 500 m wide valley bounded by low forested hills to the north and south. The river banks are vegetated with coconut, banana and jungle with numerous fields occurring to the east of the river where the valley opens up into a wide plateau. The river is c. 95 m wide from bank to bank although the actual river width varies seasonally. This can be observed in the photographs (Figure 4.10) and compared with the Google Earth screenshot (Figure 4.9) which was taken during the dry season. Looking upstream no deposited sediments were observed except at the bridge. Looking downstream there are two large vegetated pebble bars in the centre of the channel, which during the dry season split the flow into two smaller channels. It is clear that the channel is much wider during the monsoon period, as can be observed by the vegetated gravel terrace on the northerly edge of the river (Figure 4.9).

Cha 04

Locality Cha 04 is located on the coastal plain, where the river and the surrounding land is at an approximate elevation of 8 m. The river flows in a south westerly direction (242º). As with previous localities the Google Earth screenshot (Figure 6.7) is representative of the dry season whilst the photographs (Figure 4.10) are representative of the monsoon season. Figure 6.7 clearly shows large areas of lightly vegetated gravel terrains or flood plains both on the upstream and downstream stretches. These flood plains are demarcated by the tree line that comprises coconut, mango and banana plantation and jungle. The river at this locality is c. 85 m from bank to bank at the bridge, widening to nearly 150 m c. 200 m downstream, although the river width varies seasonally and during the dry season can be as little as 10 m wide. No rock outcrops were visible at this locality.

Cha 05

The river at this locality is at an elevation of approximately 12 m and flows from the north, bending downstream almost 90º to flow in a south westerly direction (238º). The width of the river from bank to bank is c. 100 m and is bounded by low lying fields to the north and low (c. 25 – 30 m) vegetated hills to the south and east. This locality is a depositional regime of the river course as demonstrated by the numerous small

wooden dredging boats which dredge the river bed to collect sediment which is used as building sand (Figure 4.10).

Cha 06

Locality Cha 06 occurs just to the north of Bardez. The river here is at an elevation of approximately 2 m and flows in a north westerly direction (290º). The river is c. 165 m wide from bank to bank at the bridge; however, within c.1 km downstream the river increases in width to over 600 m. Four hundred metres upstream the river bends sharply towards the north. Vegetation at this location is comprised of coconut and mango plantation near the shore of the river but this gives way to fields after no more than 100 m. As at Cha 05, dredging boats are present.

4.1.2. Water sampling

The number and location of the sampling localities was predominantly based upon spacing along the river system, location of tributaries and lithological changes. However, practical constraints, such as access to the river, also had to be considered. Logistics were a fundamental control on the location and number of sample sites chosen on each river course. Sample sites were chosen close to where tributaries entered the main channel, bearing in mind that these locations also needed to be safe to access during the entire 12 month monsoonal cycle, especially at the height of the monsoon. Therefore, road bridges, from which the water samples could be collected by lowering a bucket into the river flow, were chosen. The initial localities were chosen after a desk study combining local maps and Google Earth 4; final site selection was achieved with the assistance of Mr Orlando Fernandes of Dhempe College using a combination of his detailed local knowledge and reconnaissance fieldwork. Six sites were chosen and visited along the Chapora River and seven sites were chosen and visited along the Zuari River (Figure 4.11, Table 4.1, and Table 4.2).

Table 4. 1 Zuari River sampling sites.

Sample locality	GPS Position	
Zua 01	15º 14.079'N	74º 11.066'E
Zua 02	15º 13.972'N	74º 09.077'E
Zua 03	15º 13.612'N	74º 08.728'E
Zua 04	15º 16.014'N	74º 06.678'E
Zua 05	15º 15.460'N	74º 03.457'E
Zua 05 opt	15º 12.935'N	74º 04.348'E
Zua 06	15º 20.993'N	74º 00.179'E

Table 4. 2 Chapora River sampling sites.

Sample locality	GPS Position	
Cha 01	15º 47.795'N	74º 06.072'E
Cha 02	15º 45.999'N	74º 04.746'E
Cha 03	15º 44.097'N	74º 01.169'E
Cha 04	15º 42.761'N	73º 57.411'E
Cha 05	15º 40.973'N	73º 53.001'E
Cha 06	15º 38.932'N	73º 50.174'E

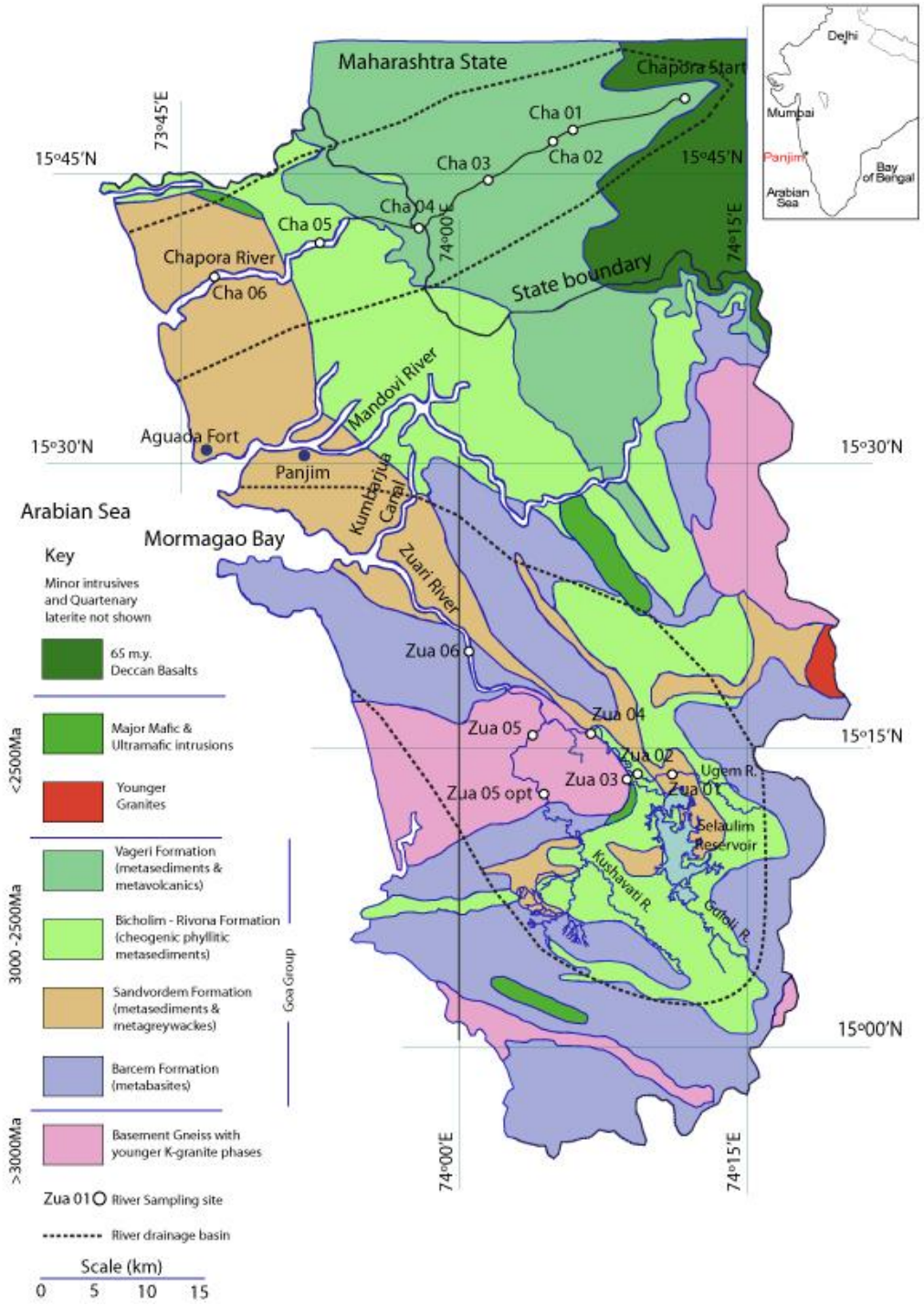

Figure 4. 11 Geological map of Goa showing the location of the Zuari and Chapora drainage basins and sampling localities. The geology of Maharashtra State pertinent to the Chapora River basin is also shown.

4.1.3. Labelling and systematics

In order to study the temporal and spatial variation in elemental concentration of the Zuari and Chapora river water it was necessary to collect river water samples monthly at all thirteen sites throughout an entire year encompassing a full monsoon cycle. A total of 35 samples (including blanks and duplicates) were taken every month resulting in large suite of samples (c. 430) over a twelve month period. Accordingly, it was necessary to put in place a simple labelling strategy which could be easily and reliably deployed in the field. Therefore, to minimise collection errors when taking samples in the field a standard nomenclature was derived and printed on adhesive labels which could be stuck on the bottles on site. These were also taped over using clear tape to prevent damage during storage and transportation. The nomenclature is shown in Table 4.3.

Table 4. 3 Sample label nomenclature.

Label	Detailed interpretation
Apr 08 / Cha / 2C	Cation sample collected from locality 2 of the Chapora River in April 2008
Apr 08 / Cha / 2A	Anion sample collected from locality 2 of the Chapora River in April 2008
Apr 08 / Cha / 2 / FB	Field blank sample collected from locality 2 of the Chapora River in April 2008

Cation labels were printed using blue ink and suffixed with the letter C whilst anion labels were printed using red ink and suffixed with the letter A. Field blanks were printed using black ink and suffixed with the letters FB. Each label also indicates the month and year of collection, the river; Cha for the Chapora or Zua for the Zuari and sample site.

The six localities on the Chapora River provided six cation and six anion samples, two duplicate cation, two duplicate anion samples and one field blank, resulting in 17 samples each month. The Zuari River provided seven cation and seven anion samples, two duplicate cation, two duplicate anion samples and one field blank, resulting in 19 samples each month, and together making 35 samples per month.

In order to collect the full suite of samples a team of eight undergraduate students from Dhempe College were trained by myself and placed under the supervision of Mr Orlando Fernandes (Senior Lecturer in Geology at Dhempe College, Panjim) to conduct the regular monthly sampling of the two rivers throughout the 15 month sampling period. The samples were stored in a freezer and then dispatched to the UK for analysis. This provided an opportunity to provide training and some real field experience to the students. Additionally, a set of instructions were provided, to be used as a reminder for each month of sample collection (Appendix B) as well as pre printed data sheets for water sample collection and geomorphological surveys. These are described below.

Water sampling data sheets were designed by myself as a method of prompting the user (students) to collect the same set of information at each location and to provide a documentary record of the data in a repeatable and reliable format. The data sheets provide data entry points for sample site, date and time, comments, pH, water temperature, air temperature, dissolved oxygen, conductivity and three sections for titrations to determine bicarbonate concentrations. An example of this data sheet can be seen in Appendix A.

Geomorphological survey sheets were designed to prompt the user to collect a consistent set of data at each location and to provide a documentary record of the data in a repeatable and reliable format. The data sheets provide data entry points for sample site, date and time, GPS location, comments, elevation, river morphology, river bed sediment, samples retrieved, vegetation type and description and local geomorphological setting. An example of this data sheet can be seen in Appendix C.

4.1.4. River water sampling methods

At each location a small bucket was lowered on a rope from a road bridge into the centre of the river, retrieved and rinsed out three times prior to acquiring the sample, taking care not to catch the rope on the bridge so as to minimise dirt falling into the rising bucket. Every effort was made to select sites with good access; but some of the selected sites had no bridge access. Where this was the case the bucket was submerged in a free flowing section of the river close to the bank, again the bucket was rinsed three times prior to acquiring the sample. As soon as the bucket was recovered it was covered to minimise ingress of dust from passing traffic and immediately returned to the vehicle. Once the sample was back at the vehicle the pH, conductivity,

water temperature, air temperature and dissolved oxygen readings were taken and recorded on the standard data sheet.

From the water collected in the bucket two 30 ml water samples were taken and filtered sequentially through 5.0 µm and 0.2 µm Nucleopore filter papers. One sample was acidified with high purity HNO_3 to pH~2 for analysis of cations, while the other sample remained unacidified for analysis of anions. One set of field blanks and two sets of duplicates were taken for each river. Finally, three titrations were performed using 1.6 N acid using a Hach digital titrator to determine bicarbonate concentrations.

4.2. Rationale for rock and sediment collection

Where possible bedrock substrate and riverine sediment samples were collected from in situ outcrops at the water sampling sites in an attempt to establish provenance between the underlying lithology and the river chemistry. At localities where no in situ outcrops were accessible, river bed deposits or dredged sediment samples were collected. It is acknowledged that any river bed samples are not necessarily representative of the rocks at that particular locality but are derived from upstream locations. Nevertheless, these provide the only realistic method of gauging variation in substrate composition. These rock and sediment samples were analysed using X-Ray Fluorescence (XRF).

4.3. Rationale for studying a weathering profile

As mentioned previously, laterite has developed over large areas of Goa; this is particularly true for Northern Goa. Accordingly, it would be insufficient to consider only the underlying unaltered geology since, in many instances, the water/rock interaction is within these highly altered lithologies, and the ‘original’ protolith thus ‘protected’ and buffered from further alteration by tens of metres of overlying weathered material. This weathered material differs significantly from the protolith in that it is depleted of mobile elements and enriched in immobile elements. To better understand the relationship between the thick, lateritised weathering mantle and the underlying unaltered substrate, the Merces Quarry weathering profile, which has developed on a metagreywacke protolith, was studied. This profile had been previously studied in detail (Widdowson, 2009), and is particularly valuable in that displays an uninterrupted series of zones typical of laterite profiles from unaltered protolith at the base through saprolite (altered greywacke), semi-indurated Fe-rich tubular textured laterite to indurated

laterite cap or duricrust at the surface. Further, the chemical and mineralogical variation is well understood, and broadly representative of the lateritic weathering profiles in the western Goa coastal region.

Seventeen individual/discrete samples (MQ1 – MQ17), and seven bulk samples representing (MQBK1 – MQBK7) were collected from various horizons where observable changes occurred. In order to consider how water chemistry may vary with depth and degree of alteration, a column experiment was designed and constructed using the bulk samples from five discrete horizons as detailed in section 4.4.

4.4. Column experiment

The column experiment (reaction columns) was designed to simulate monsoonal rainfall onto a selection of columns composed of material from five different zones from an Indian laterite (weathering) profile. The zones were selected as representing areas of significant and obvious change in colour and/or texture and are detailed below:

Zone 1 - Original protolith
Zone 2 – Saprolite
Zone 3 – Saprolite
Zone 4 – Palaeowater table
Zone 5 – Duricrust.

The samples were collected from the Merces quarry which is used for the quarrying of road aggregate with the laterite being removed as overburden. The quarry faces are accessed via a selection of cut benches. Figure 4.12 shows the locations from which these samples were collected and the diagram is intended to show their locations relative to the cut benches. Also included in Figure 4.12 is a depth table listing the depth below ground level for each sample and a colour bar to represent the approximate change in colour of the rock up through the zonal sequence.

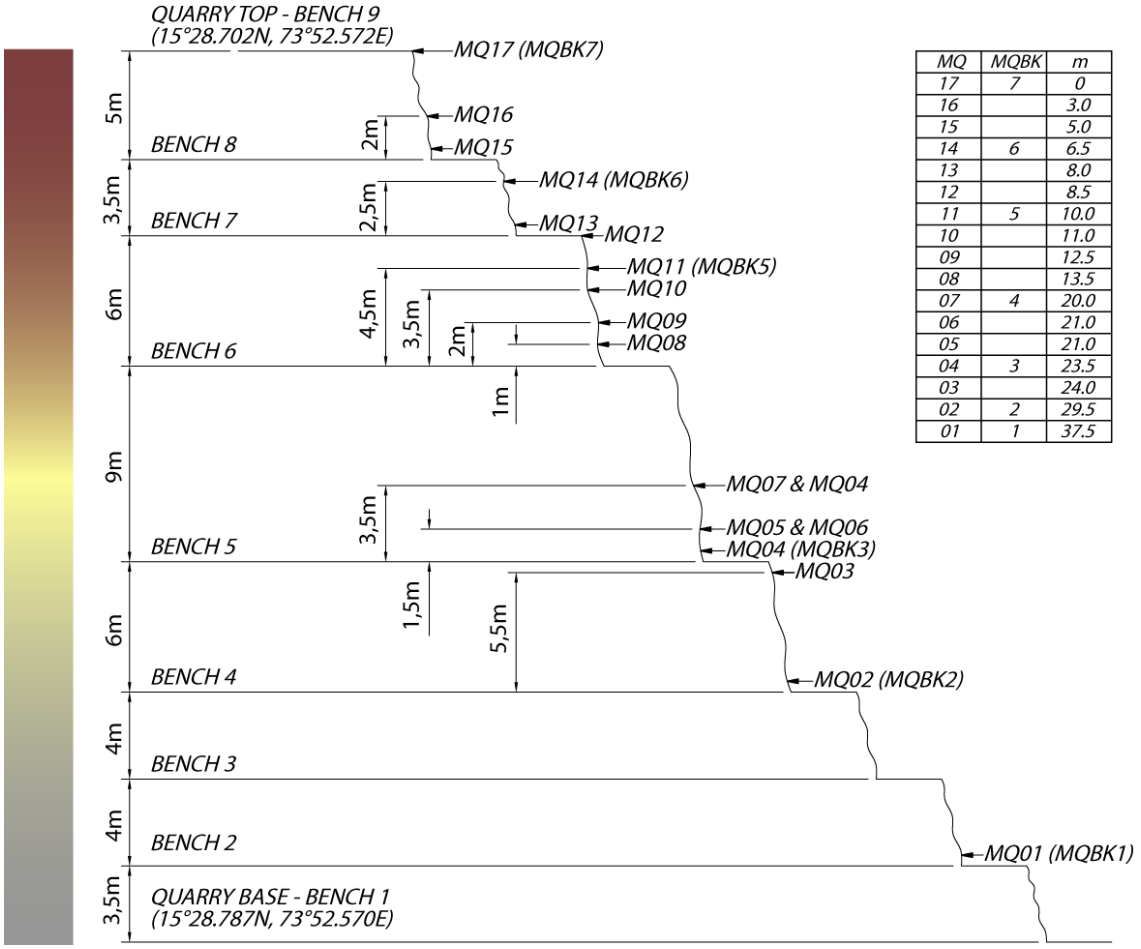

MQ	MQBK	m
17	7	0
16		3.0
15		5.0
14	6	6.5
13		8.0
12		8.5
11	5	10.0
10		11.0
09		12.5
08		13.5
07	4	20.0
06		21.0
05		21.0
04	3	23.5
03		24.0
02	2	29.5
01	1	37.5

Figure 4. 12 Diagram of the Merces Quarry, showing the various cut benches and the locations from which the samples were collected. Also provided is a colour column showing the variation in colour throughout the profile and a depth table showing the depth below the surface for each sample.

4.4.1. Relative reactivity

Ideally undisturbed ‘cored’ samples would be collected at each horizon thus retaining their individual characteristics such as permeability, unfortunately this could not achieved, and therefore it was decided to compare the relative reactivity of the zones. Anstead, c. 5 kg samples were collected thus offering a bulk representative of that particular horizon. Each sample was then crushed and sieved to a chosen grain size of between 1-2 mm – this to offer consistent available surface area for each sample when loaded into the reaction columns. Each column was filled with 250 mm of sample. The use of equal quantities of equal sized grains further intended to provide equal permeability and thus water contact time to react with equivalent surface areas. The columns were also designed to allow for enhanced and consistent contact time by holding the water in the columns for a set amount of time; the time chosen was 10

minutes; this latter chosen for practicalities of allowing time for rock-water interaction, and collection purposes.

4.4.2. Column design

My column design used extruded clear acrylic tube which has an outside diameter of 50 mm and an inside diameter of 44 mm, providing an internal area of 0.00152 m^2. This was chosen to allow visual inspection of progress of the water through the column. The column is sealed at each end using uPVC waste pipe adaptors; these have screw caps to allow water to be added to the top of the column and a ball valve has been mounted to the lower cap to allow water to be held within the columns, then drained, collected and sampled after the allotted time. Additionally, to stop the sample material from blocking and potentially exiting via the discharge tap a 200 µm gauze was installed within the lower cap.

4.4.3. Rainwater addition

The amount of water to be added to the columns is intended to be representative of actual rainfall in the region. Therefore, the average rainfall value of 2800 mm has been used from the annual precipitation records for Panjim calculated from 1978 – 2008 (Figure 3.6). It was then necessary to consider the number of rainwater additions to optimise the number of samples collected and the height of the columns based on the volume of water to be added each time. It was decided to add 270 ml of water every week for 16 consecutive weeks. This equated to an in-tube water height of 175 mm per addition, and would yield 96 water collections from which to collect samples for analysis of anions, cations and duplicates. Blanks were also collected each week. During each weekly water addition the quantity of water added was measured using a weigh scale base on the specific gravity of water meaning that 1 ml or water weighs one mg and the amount of water added and recovered was measured using the weigh scale and recorded.

The rainwater composition was also considered with early thoughts of trying to engineer a water sample based on a collected rainwater sample from the study area, however, the decision was made to use deionised water instead as this could be more easily obtained and be of a more constant chemical composition for the volumes required.

4.4.4. Experiment temperature

The experiment was to be conducted from early September to the end of December 2009 and was located in a room which was subjected to varying daily temperatures due to external temperatures and the effects of the central heating. It was decided that the experiment needed to be controlled at a constant fixed temperature. This was achieved by designing the experiment to be fully enclosed and to incorporate a thermostatically controlled, 60 cm x 30 cm heat mat. A separate temperature data logger was located inside the box and set to record the internal temperature every 30 minutes for the entire duration of the experiment (Figure 4.13).

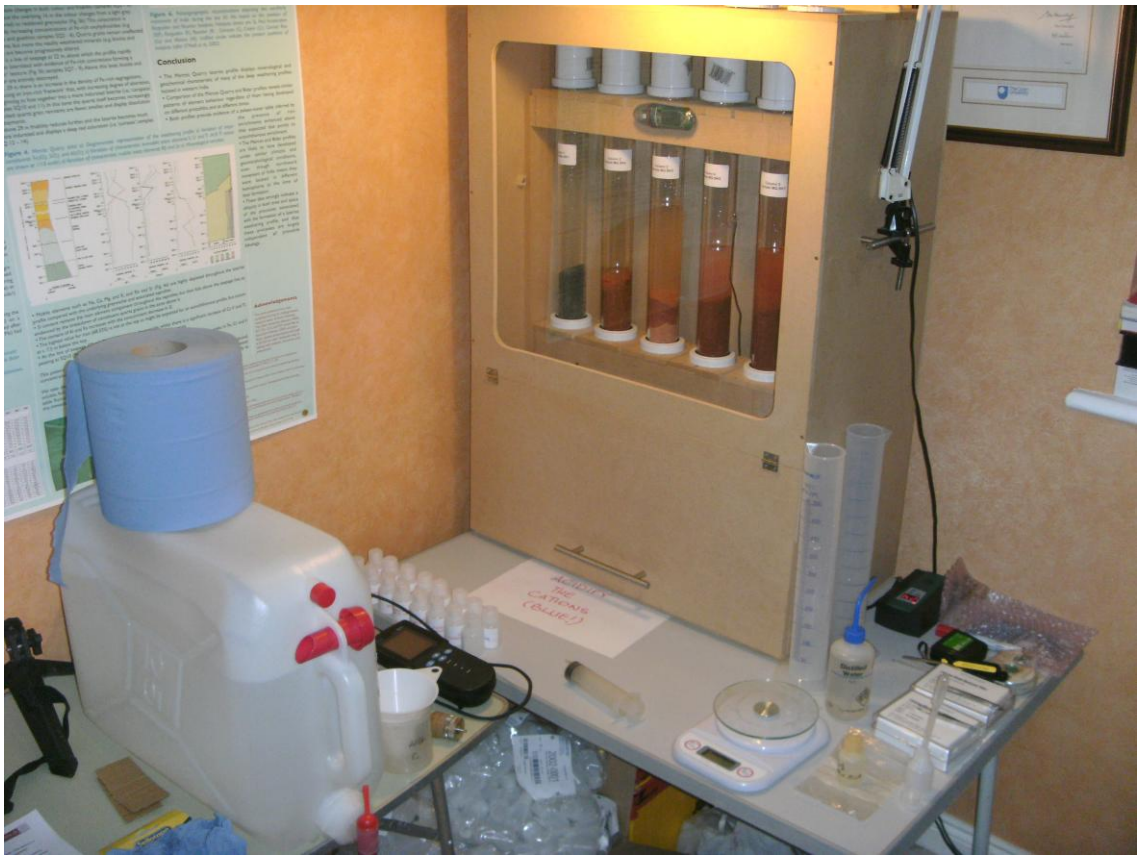

Figure 4. 13 Photograph of the column experiment showing the enclosed experiment box, which is fitted with a thermostatically controlled heat mat in its base. Visible through the Perspex window are the sample filled columns complete with water addition and the temperature data logger (experiment designed and constructed by C.Hibbert).

4.5. Analytical techniques

4.5.1. X-Ray Fluorescence (XRF)

Rock samples were cleaned of any weathering crusts, and then dried in an oven at 100ºC for 24 hours. The samples were then homogenised by crushing in a steel jaw crusher and milled to a fine powder in an agate Tema mill. The powder was then used to create fused glass discs for major element analysis and powder pellets for trace element analysis. Fused glass discs were manufactured using 1 part rock powder (dried at 110ºC) and 5 parts dried lithium metaborate / tetraborate flux (Johnson Matthey Spectroflux 100B) in Pt-5% Au crucibles at 1100ºC. Percentage loss on ignition (LOI) of volatile elements such as H_2O, CO_2 etc was determined separately by calculating the weight loss after ignition at 1000 ºC for 1 hour. The powder pellets were created by mixing 9-10 g of rock powder with 0.1 ml per gram of binder. The mixture was then placed in a stainless steel press which was loaded to c. 5 t for 30 seconds. The pellets were then left to dry before analysis.

Analyses were performed using an ARL 8420+ dual goniometer wavelength dispersive X-ray Fluorescence (XRF) spectrometer employing routine procedures and analytical packages. Elemental intensities are corrected for background and known peak overlap interferences. Medium term instrumental intensity drift was taken into account using a drift normalisation monitor. Accuracy was determined by calibrating the machine against reference materials that included USGS basalt standards AGV-1, BCR-1 and BHVO-1 and the laterite standards VL-1 and VL-2 (Labrecque and Schorin, 1987). After calibration the standards were run as unknowns, producing values typically within <0.5% of the recommended values.

4.5.2. Inductively Coupled Plasma – Optical Emission Spectroscopy (ICP-OES) and Mass Spectroscopy (ICP-MS)

Analysis of the major cations calcium (Ca), sodium (Na), potassium (K), magnesium (Mg), aluminium (Al) and silicon (Si), trace elements rubidium (Rb), strontium (Sr), vanadium (V), chromium (Cr), manganese (Mn), iron (Fe), cobalt (Co), nickel (Ni), copper (Cu), zinc (Zn), lead (Pb) and barium (Ba) and rare earth elements (REE) in the river water samples and field blanks was determined using an Agilent 7500 ICP-MS at The Open University. Approximately 1000 µl of each sample was decanted into 1500 µl vials and loaded into a sample rack. Analyses were standardised against a suite of synthetic reference materials, measured at the beginning and end of each analytical

run. These synthetic standards were made up from single element plasma grade solutions (Alfar Aesar), the concentrations of which were to replicate those found in the unknowns. In addition, the Certified Reference Material (CRM) National Institute of Standards and Technology (NIST) 1640 standard and SLRS 4 (NRC-CNRC, National Research Council Canada) were also analysed as unknowns every 7 to 10 samples in order to monitor instrumental drift and to assess the external reproducibility of the data. The samples were analysed, undiluted in batches of c. 30. Every standard and sample was internally mixed with a known volume of tellurium as the internal standard. The average major and trace element cation values obtained for the NIST 1640 samples are documented in Tables 4.7 and 4.8.

Estuarine samples that were too highly concentrated to be analysed using ICP-MS were analysed using ICP-OES. Analysis of cations calcium (Ca), sodium (Na), potassium (K), iron (Fe), manganese (Mn), magnesium (Mg), phosphorous (P) and silicon (Si) in the river water samples and field blanks was performed using ICP-OES (JY Ultima 2). Initially all samples were diluted by adding 0.1 ml of sample to 0.9 ml of deionised water into a vial. Then all non monsoon samples (January 2008 to May 2008) were diluted to 25 parts deionised water to 1 part sample by adding 0.04 ml of sample to 0.96 ml of deionised water into a vial. At the beginning of each batch a set of standards (S1, S2, S3 and S4) were used to calibrate the instrument. These are documented in Table 4.4. The sample positions along with the locations of any CRMs and standards were documented using an ICP-MS tray template (Appendix E).

Table 4. 4 Element concentrations for standards used for ICP-OES, note Si was calibrated separately.

Cation	Standard			
	S1	S2	S3	S4
Al	0	0.5	2	5
B	0	1	5	10
Ba	0	0.5	1	2
Ca	0	10	50	100
Fe	0	1	5	10
K	0	1	5	10
Mg	0	10	20	30
Mn	0	1	2	5
Na	0	10	20	40
P	0	1	5	10
Sr	0	0.5	1	2
Si*	0	5	10	20

The top standard for the major cations (S4) and the top standard for Si (S4i) were analysed at the beginning of a batch and then again after every ten analyses. In addition to these standards a certified reference material (CRM) and a lab blank (deionised water) was analysed at regular intervals throughout the batch. The CRM used was Ion 96.3. During the analysis the results were observed and any samples that were out of detection range were noted for further dilution and reanalysis.

4.5.3. Ion Chromatography (IC)

Ion chromatography using a Dionex ICS-2500 instrument was used to analyse the anions, chloride (Cl^-), nitrate (NO_3^-), sulphate (SO_4^{2-}) and fluoride (F^-). Initially all samples were run undiluted. One thousand µl of each sample was decanted into its own 1500 µl vial. These were placed in the sampling tray and their position recorded. For each batch of analyses a set of standards were analysed, along with a set of lab blanks and a certified reference material (CRM). The CRM used was Ion 96.3, which was diluted one part CRM to four parts deionised water. The standards were as follows; Cl - 5, 15 and 25 mg l, NO_3 - 5, 10 and 15 mg l, SO_4 - 5, 15 and 25 mg l and F - 1, 3 and 5 mg l. Any samples that were deemed to be out of the detection range were diluted to appropriate ratios and reanalysed. The sample positions along with the locations of any CRMs and standards were documented using an Ion Chromatography tray template (Appendix D).

4.6. Limits of detection

Limits of detection can be calculated in a variety of ways; however, where a blank is analysed the following method can be used. A blank is defined as a sample which has undergone all the processes applied to the sample itself without the introduction of the sample. This method is therefore readily applied to ICP-OES, ICP-MS and IC analysis.

$$LOD = \frac{Concentration\ of\ lowest\ standard - Concentration\ of\ blank}{Intensity\ signal\ of\ lowest\ standard - Intensity\ signal\ of\ blank}\ x\ 3\sigma\ on\ blank$$

Since the concentration of the blank is normally taken as zero because deionised water is used for its preparation the equation can be simplified to:

$$LOD = \frac{Concentration\ of\ lowest\ standard}{Intensity\ signal\ of\ lowest\ standard - Intensity\ signal\ of\ blank}\ x\ 3\sigma\ on\ blank$$

Unfortunately no intensity data were available for the ICP-MS analyses or for the IC analyses. The only intensity data available for the ICP-OES analyses are for the top standard. Therefore, manufacturers' reported detection limits have been used where appropriate. These are documented in Table 5.6.

4.7. Statistical analysis

Statistical analysis was used to verify whether the methods were sufficiently rigorous to produce reliable and repeatable results. For this study this was considered in two separate parts, firstly, water sample collection and secondly water sample analysis. The sample collection methods were evaluated by comparing element concentrations of duplicate samples. For example, duplicate samples were collected every month at sample localities Cha 02, Cha 03, Zua 02 and Zua 03. The sample analysis methods were evaluated by comparing the element concentrations of a known certified reference material (CRM), for example Ion 96.3 (ICP-OES and Ion Chromatography) or NIST 1640 (ICP-MS), against analysed values.

4.7.1. Water sample collection

The percentage difference and standard deviation have been calculated and compared .The percentage difference and standard deviation values differ widely for different elements and for different months depending on the particular element concentration prevailing at the time (Table Appendix F1 – F4). Figures 4.14, 4.15, 4.16 and 4.17 present cross plots for the comparison of duplicates for cations and anions for the months of April, May, June and July, respectively.

Tables Appendix F1 – F4 shows that the range of percentage difference and standard deviation between the samples and their respective duplicates are very good for the majority of the major cations analysed. Only Al displays a particularly large range of values which is due to the low values recorded. The same is also true for the anions with all except F having reasonably low ranges of percentage difference and standard deviation.

Tables Appendix F5 – F12 present precision of duplicate data for the trace elements analysed (Tables Appendix F5, F6, F7 and F8) for April, May, June and July respectively and the REE analysed (Tables Appendix F9, F10, F11 and F12) again for April, May, June and July, respectively.

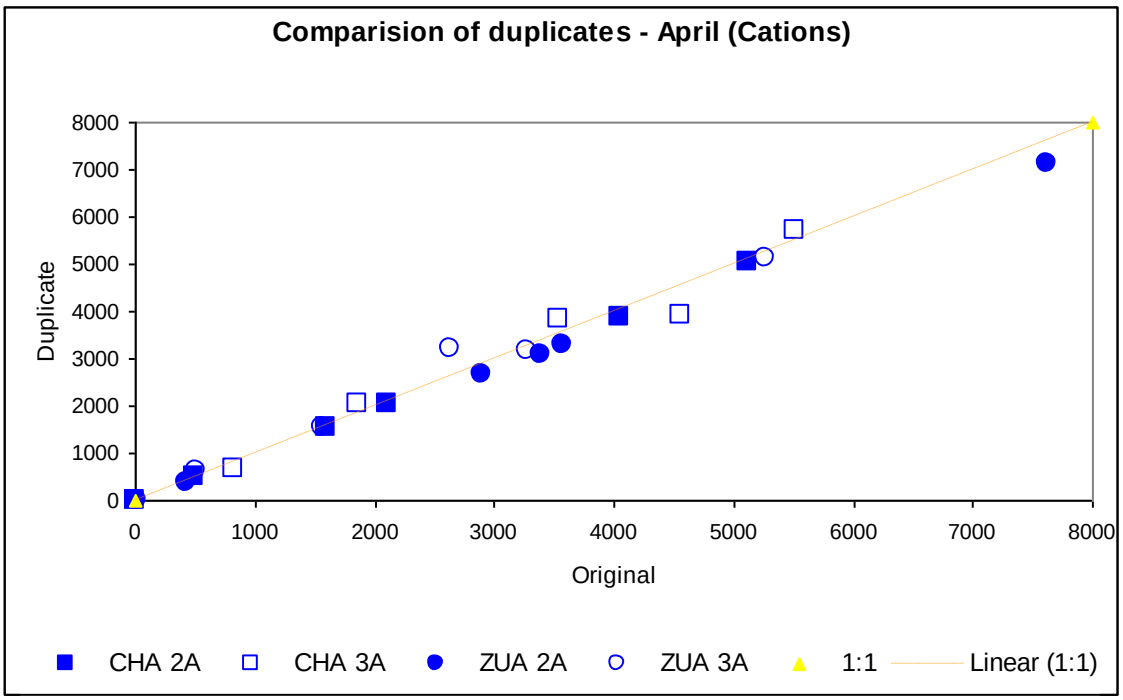

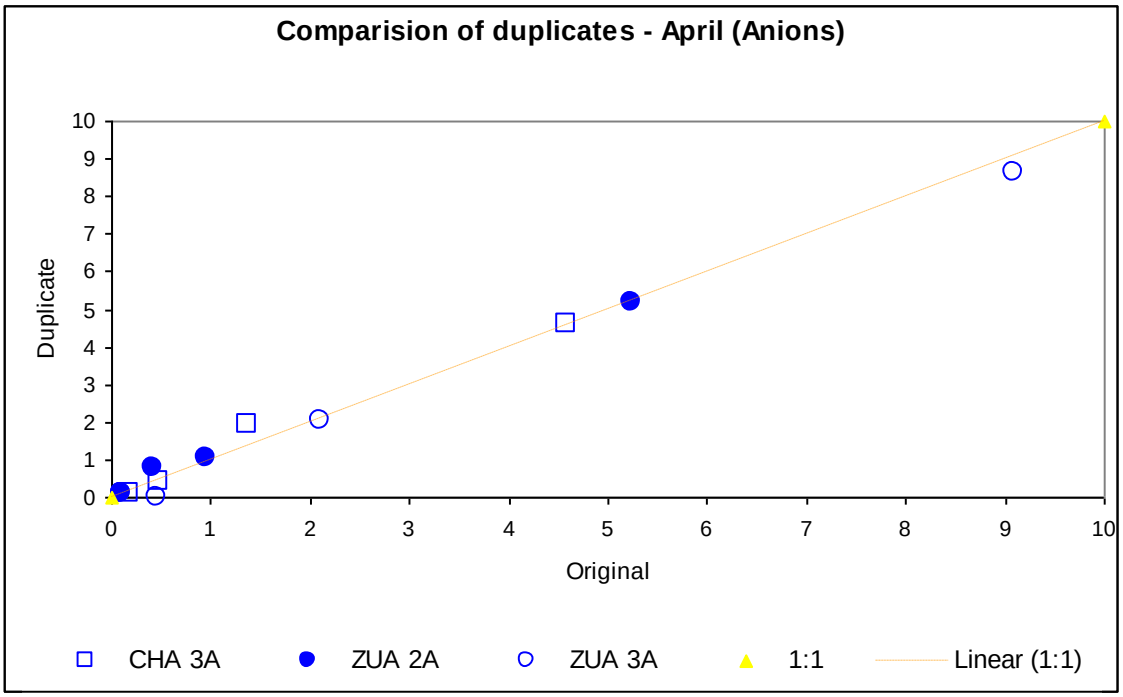

Figure 4.14 Cross plots of Chapora and Zuari samples (x-axis) and duplicates (y-axis) for cations and anions for the moth of April 2008.

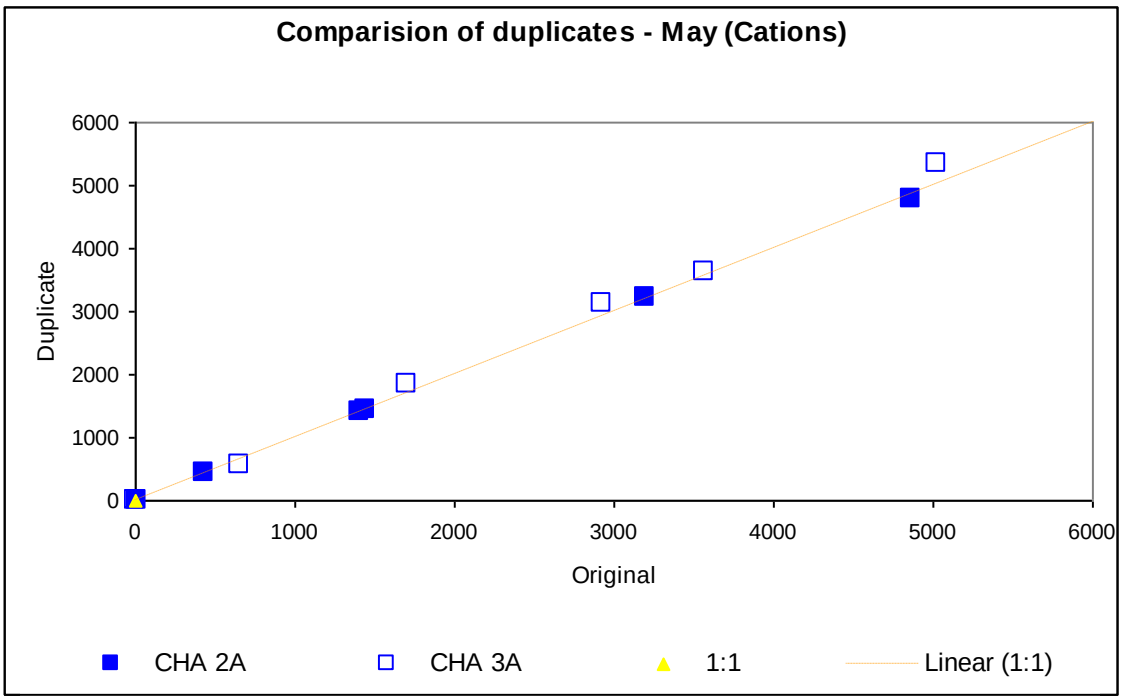

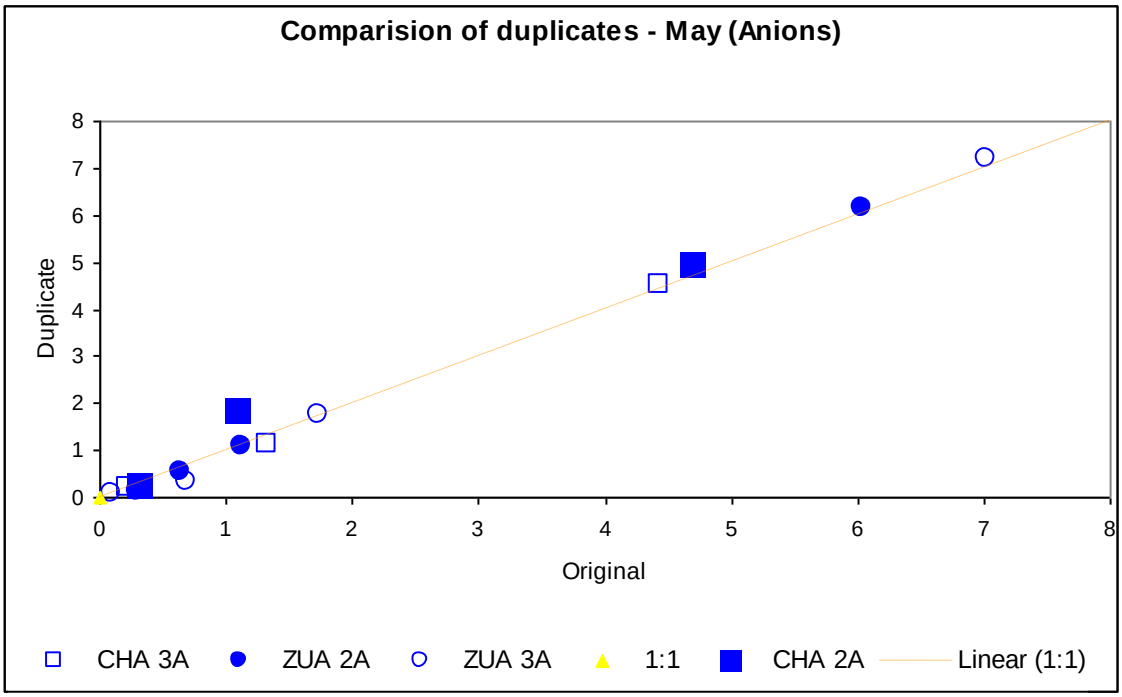

Figure 4.15 Cross plots of Chapora and Zuari samples (x-axis) and duplicates (y-axis) for cations and anions for the moth of May 2008.

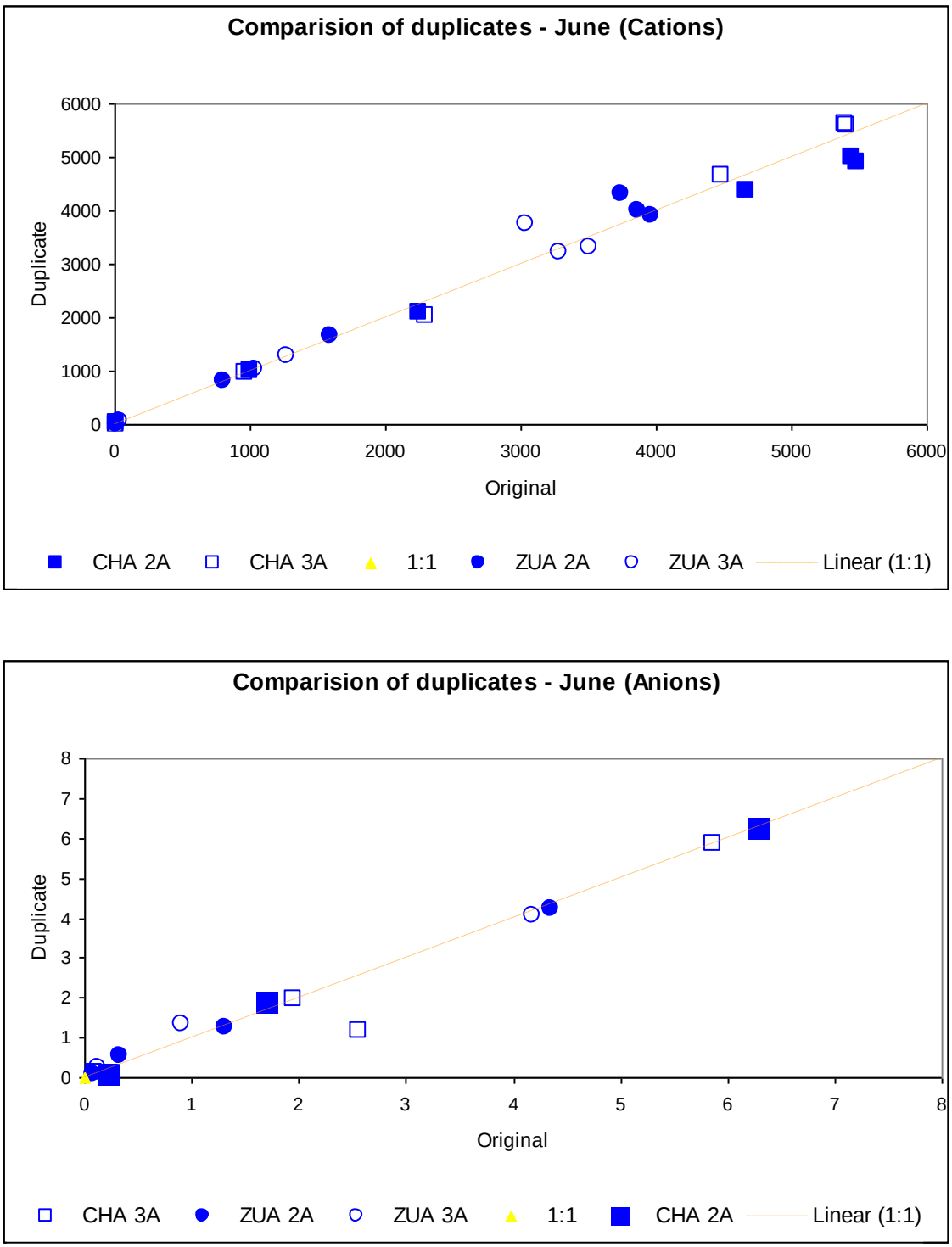

Figure 4.16 Cross plots of Chapora and Zuari samples (x-axis) and duplicates (y-axis) for cations and anions for the moth of June 2008.

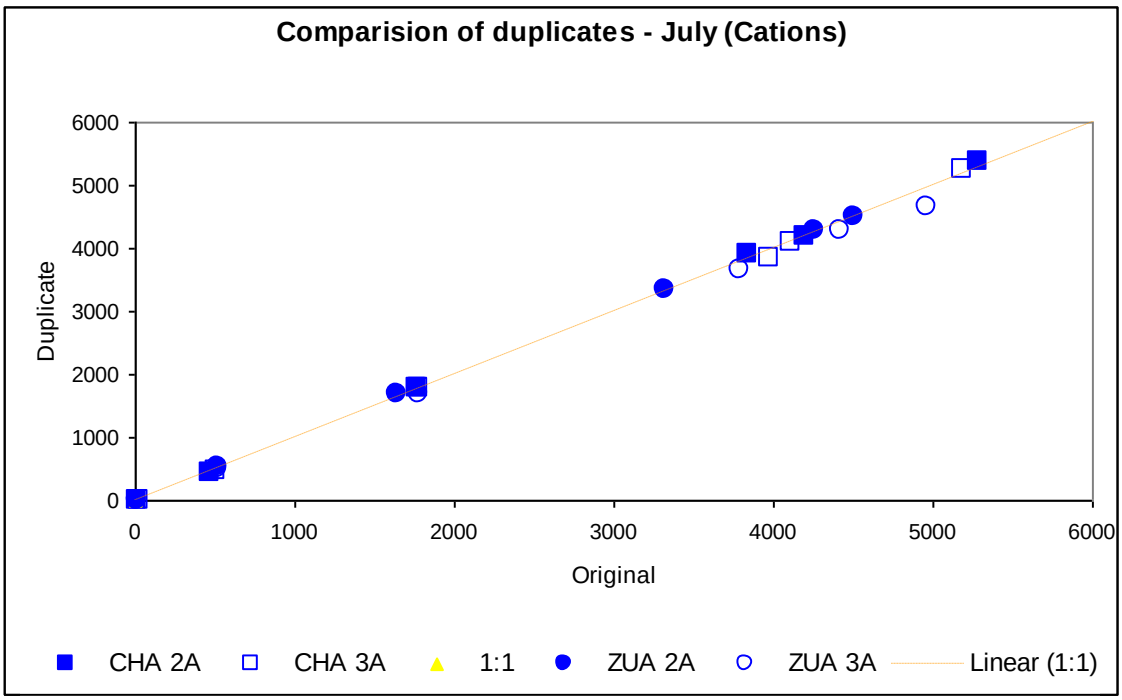

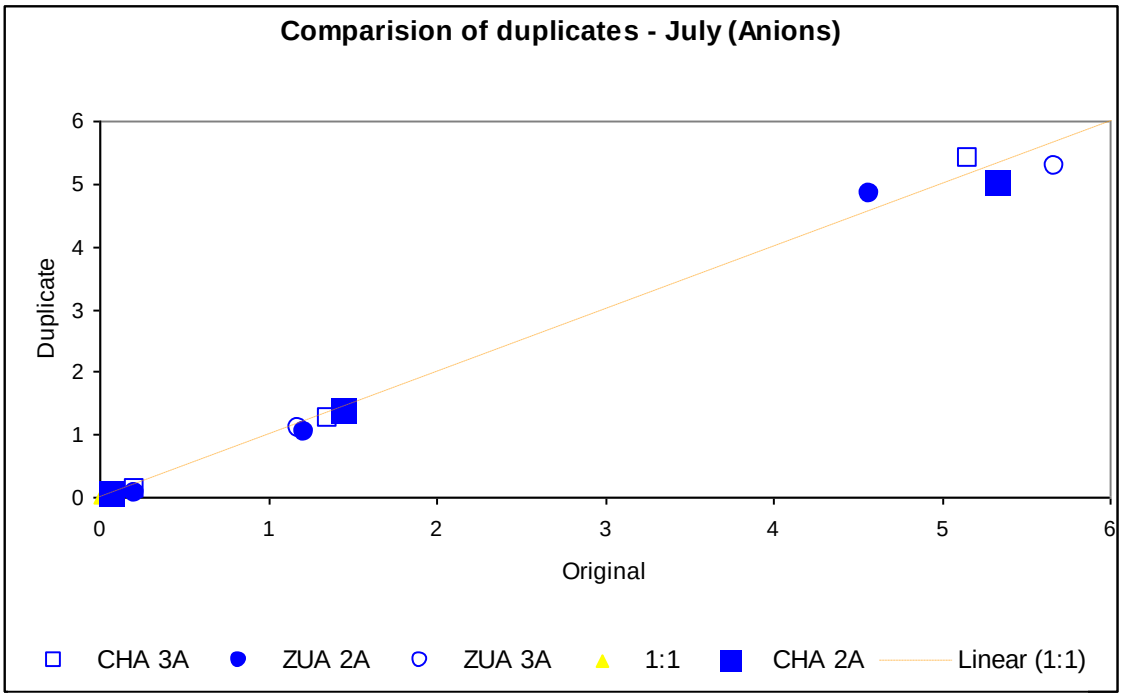

Figure 4.17 Cross plots of Chapora and Zuari samples (x-axis) and duplicates (y-axis) for cations and anions for the moth of July 2008.

4.7.2. Water sample analysis

In order to ensure that the analytic equipment being used is performing correctly it is necessary to include Certified Research Materials (CRMs) within the suite of samples. These CRMs have closely defined elemental concentrations and are used to check the accuracy of the equipment and are included throughout the sample suite at regular intervals. The CRMs used include Ion 96.3, NIST 1640 and SLRS4.

Ion 96.3

This CRM provided by the Canada Centre for Inland Waters was used in the analysis of anions using Ion Chromatography (IC) and in the analysis of estuarine influenced cations using Inductively Coupled Plasma - Optical Emission Spectroscopy (ICP-OES).

Table 4. 5 Percentage difference between the Certified Research Material (CRM), Ion 96.3 and the average measured values, reported with their Relative Standard Deviation (RSD) for the major anions analysed using IC.

Element	*SO_4^{2-}*	*Cl*	*F*	*NO_3*
	Certified values reported as ±2σ.			
Analysis 1 (17th February 2010)				
Ion 96.3: Average measured value	*147.6±5.7*	*118.5±7.3*	*0.23±11.8*	*6.6±2.5*
Ion 96.3: Certified value	*110±8.5*	*93.0±5.9*	*0.16±0.06*	*4.3±0.35*
% difference from our values	***34.2***	***27.4***	***44.1***	***55.0***
Analysis 1 (18th February 2010)				
Ion 96.3: Average measured value	*141.9±3.4*	*117.3±2.65*	*0.2±8.05*	*6.1±6.65*
Ion 96.3: Certified value	*110±8.5*	*93.0±5.9*	*0.16±0.06*	*4.3±0.35*
% difference from our values	***29.0***	***26.1***	***29.4***	***42.7***
Analysis 1 (19th February 2010)				
Ion 96.3: Average measured value	*150.7±5.4*	*123±3.0*	*0.3±4.2*	*7.8±0.2*
Ion 96.3: Certified value	*110±8.5*	*93.0±5.9*	*0.16±0.06*	*4.3±0.35*
% difference	***37.0***	***33.6***	***93.9***	***80.0***

Table 4. 6 Percentage difference between the Certified Research Material (CRM), Ion 96.3 and average measured values, reported with their Relative Standard Deviation (RSD) for the major cations analysed using ICP-OES.

Element	*Na*	*K*	*Mg*	*Ca*	*Si*
Ion 96.3-1	*52.0*	*4.0*	*26.6*	*92.0*	*1.1*
Ion 96.3-2	*51.5*	*3.9*	*26.8*	*89.9*	*1.2*
Ion 96.3-3	*51.0*	*3.7*	*26.6*	*90.6*	*1.1*
Ion 96.3: Average measured value ± RSD	*51.5±1.03*	*3.9±4.32*	*26.7±0.48*	*90.8±1.19*	*1.1±1.96*
Ion 96.3: Certified value	*48.6±5*	*4.0±0.45*	*25.7±1.8*	*90.6±8.5*	*1.16±0.17*
% difference	***0.25***	***3.6***	***3.7***	***6.0***	***1.8***

NIST 1640

This CRM provided by the National Institute of Standards and Technology was used in the analysis of cations using Inductively Coupled Plasma - Mass Spectroscopy (ICP-MS). Table 4.7 and Table 4.8 show the percentage difference between the average measured NIST 1640 values for each analysis (c. 5 per analysis) and the CRM values for major cations and trace elements, respectively. Each average NIST 1640 measured value is quoted with its calculated Relative Standard Deviation (RSD). The percentage difference is calculated only for the average value and not for the error range. Since REE are not included in NIST 1640 no table is provided for these elements. In general the percentage difference is lower for the major cations compared to the trace elements, which, is as expected due to the higher concentrations for the major cations compared to those of the trace elements.

Table 4. 7 Percentage difference between the Certified Research Material (CRM), NIST 1640 and average measured values reported with their Relative Standard Deviation (RSD) for the major cations analysed using ICP-MS.

Element	*Na*	*K*	*Mg^{24}*	*Ca^{43}*	*Al*	*Si*
Analysis 1 (14th & 15th January 2014)						
NIST 1640: Average measured value	*30108±4.3*	*999±7.5*	*5774±4.3*	*7857±4.1*	*59.8±4.0*	*5042±4.3*
NIST 1640: Certified value	*29350±310*	*994±27*	*5819±56*	*7045±89*	*52±1.5*	*4730±120*
% difference from our values	***2.6***	***0.6***	***0.8***	***11.5***	***15.1***	***6.6***
Analysis 2 (17th January 2014)						
NIST 1640: Average measured value	*26890±7.1*	*884±7.5*	*5090±7.0*	*6941±6.4*	*48.4±5.9*	*4565±6.9*
NIST 1640: Certified value	*29350±310*	*994±27*	*5819±56*	*7045±89*	*52±1.5*	*4730±120*
% difference from our values	***8.4***	***11.1***	***12.5***	***1.5***	***6.9***	***3.5***
Analysis 3 (29th January 2014)						
NIST 1640: Average measured value	*29557±3.2*	*925±3.2*	*5707±3.4*	*7345±3.5*	*50.6±3.2*	*4766±3.7*
NIST 1640: Certified value	*29350±310*	*994±27*	*5819±56*	*7045±89*	*52±1.5*	*4730±120*
% difference from our values	***0.7***	***7.0***	***1.9***	***4.3***	***2.8***	***0.8***
Analysis 4 (13th February 2014)						
NIST 1640: Average measured value	*34545±3.2*	*1056±3.9*	*6690±2.8*	*8572±3.8*	*60.2±7.3*	*5654±3.6*
NIST 1640: Certified value	*29350±310*	*994±27*	*5819±56*	*7045±89*	*52±1.5*	*4730±120*
% difference from our values	***17.7***	***6.2***	***15.0***	***21.7***	***15.7***	***19.5***
Analysis 5 (17th February 2014)						
NIST 1640: Average measured value	*33629±8.9*	*1049±9.3*	*6508±9.1*	*8304±8.6*	*69.0±9.4*	*5668±9.1*
NIST 1640: Certified value	*29350±310*	*994±27*	*5819±56*	*7045±89*	*52±1.5*	*4730±120*
% difference from our values	***14.6***	***5.6***	***11.8***	***17.9***	***32.8***	***19.8***
Analysis 6 (19th March 2014)						
NIST 1640: Average measured value	*33315±1.1*	*1059±1.2*	*6474±0.9*	*8070±1.1*	*62.4±1.2*	*5539±0.6*
NIST 1640: Certified value	*29350±310*	*994±27*	*5819±56*	*7045±89*	*52±1.5*	*4730±120*
% difference from our values	***13.5***	***6.5***	***11.3***	***14.5***	***20.0***	***17.1***
Analysis 7 (20th March 2014)						
NIST 1640: Average measured value	*31986.0±3.5*	*996.9±3.6*	*6176.4±3.7*	*7820.4±3.5*	*61.3±3.6*	*5267.2±3.2*
NIST 1640: Certified value	*29350±310*	*994±27*	*5819±56*	*7045±89*	*52±1.5*	*4730±120*
% difference from our values	***9.0***	***0.3***	***6.1***	***11.0***	***17.8***	***11.4***

Note: Attempts to reanalyse samples that were outside acceptable limits were not successful.

Table 4. 8 Percentage difference between the Certified Research Material (CRM), NIST 1640 and average measured values reported with their Relative Standard Deviation (RSD) for the trace elements analysed using ICP-MS.

Element	*Rb*	*Sr*	*V*	*Cr*	*Mn*	*^{56}Fe*	*Co*	*Ni*	*Cu*	*Zn*	*^{206}Pb*	*Ba*
Analysis 1 (14th & 15th January 2014)												
NIST 1640: Average measured value	*2.23±2.3*	*136.4±2.5*	*16.0±3.7*	*42.1±3.6*	*136.2±3.2*	*40.0±17.2*	*24.5±3.2*	*29.6±2.5*	*95.2±2.6*	*61.2±2.8*	*26.8±2.6*	*158.9±2.0*
NIST 1640: Certified value	*2±0.02*	*124.2±0.7*	*12.99±0.37*	*38.6±1.6*	*121.5±1.1*	*34.3±1.6*	*20.3±0.31*	*27.4±0.8*	*85.2±1.2*	*53.2±1.1*	*27.9±0.14*	*148±2.2*
% difference (not including error)	***11.4***	***9.9***	***23.0***	***9.1***	***12.1***	***16.5***	***20.1***	***7.9***	***11.7***	***15.1***	***3.9***	***7.4***
Analysis 2 (17th January 2014)												
NIST 1640: Average measured value	*1.9±6.8*	*114.6±6.1*	*13.5±7.1*	*35.7±6.3*	*116.6±6.7*	*15.1±37.1*	*20.8±6.2*	*27.3±7.1*	*79.9±6.6*	*52.2±6.4*	*25.1±4.3*	*137.9±5.7*
NIST 1640: Certified value	*2±0.02*	*124.2±0.7*	*12.99±0.37*	*38.6±1.6*	*121.5±1.1*	*34.3±1.6*	*20.3±0.31*	*27.4±0.8*	*85.2±1.2*	*53.2±1.1*	*27.9±0.14*	*148±2.2*
% difference (not including error)	***7.6***	***7.7***	***3.8***	***7.4***	***4.0***	***56.1***	***2.4***	***0.5***	***6.2***	***1.9***	***10.2***	***6.9***
Analysis 3 (29th January 2014)												
NIST 1640: Average measured value	*2.2±3.2*	*134.9±2.8*	*15.3±2.8*	*40.3±3.5*	*132.5±3.1*	*9.7±32.4*	*23.9±3.2*	*30.9±3.4*	*93.6±3.5*	*60.2±3.4*	*28.0±2.5*	*163.9±2.6*
NIST 1640: Certified value	*2±0.02*	*124.2±0.7*	*12.99±0.37*	*38.6±1.6*	*121.5±1.1*	*34.3±1.6*	*20.3±0.31*	*27.4±0.8*	*85.2±1.2*	*53.2±1.1*	*27.9±0.14*	*148±2.2*
% difference (not including error)	***8.7***	***8.6***	***17.8***	***4.5***	***9.0***	***71.7***	***17.7***	***12.8***	***9.8***	***13.1***	***0.3***	***10.7***
Analysis 4 (13th February 2014)												
NIST 1640: Average measured value	*2.5±4.9*	*154.7±3.6*	*17.2±3.3*	*46.0±3.0*	*151.8±3.2*	*<dl*	*26.8±3.8*	*33.1±4.1*	*114.3±3.7*	*69.5±3.3*	*35.4±1.8*	*189.3±3.0*
NIST 1640: Certified value	*2±0.02*	*124.2±0.7*	*12.99±0.37*	*38.6±1.6*	*121.5±1.1*	*34.3±1.6*	*20.3±0.31*	*27.4±0.8*	*85.2±1.2*	*53.2±1.1*	*27.9±0.14*	*148±2.2*
% difference (not including error)	***23.2***	***24.5***	***32.2***	***19.1***	***24.9***	*-*	***32.1***	***20.8***	***34.1***	***30.7***	***26.7***	***27.9***
Analysis 5 (17th February 2014)												
NIST 1640: Average measured value	*2.6±9.7*	*160.7±8.7*	*17.8±8.9*	*48.8±9.0*	*154.6±8.4*	*39.3±27.9*	*27.5±9.1*	*34.3±8.6*	*111.3±9.0*	*72.3±8.6*	*36.4±8.2*	*193.8±8.5*
NIST 1640: Certified value	*2±0.02*	*124.2±0.7*	*12.99±0.37*	*38.6±1.6*	*121.5±1.1*	*34.3±1.6*	*20.3±0.31*	*27.4±0.8*	*85.2±1.2*	*53.2±1.1*	*27.9±0.14*	*148±2.2*
% difference (not including error)	***31.7***	***29.4***	***36.8***	***26.5***	***27.3***	***14.6***	***35.6***	***25.3***	***30.7***	***35.9***	***30.5***	***31.0***
Analysis 6 (19th March 2014)												
NIST 1640: Average measured value	*2.3±0.4*	*141.3±1.1*	*15.4±1.2*	*41.7±1.2*	*136.2±0.6*	*49.5±14.2*	*24.4±1.1*	*30.2±1.3*	*105.9±1.2*	*62.5±1.3*	*28.5±0.5*	*165.0±0.9*
NIST 1640: Certified value	*2±0.02*	*124.2±0.7*	*12.99±0.37*	*38.6±1.6*	*121.5±1.1*	*34.3±1.6*	*20.3±0.31*	*27.4±0.8*	*85.2±1.2*	*53.2±1.1*	*27.9±0.14*	*148±2.2*
% difference (not including error)	***13.6***	***13.7***	***18.5***	***8.1***	***12.1***	***44.2***	***20.5***	***10.0***	***24.3***	***17.5***	***2.0***	***11.5***
Analysis 7 (20th March 2014)												
NIST 1640: Average measured value	*2.2±3.7*	*135.2±3.4*	*14.8±3.6*	*39.4±3.7*	*128.5±4.2*	*17.0±16.9*	*23.1±3.6*	*28.5±3.8*	*98.8±3.8*	*59.9±3.6*	*26.8±3.0*	*157.3±2.8*
NIST 1640: Certified value	*2±0.02*	*124.2±0.7*	*12.99±0.37*	*38.6±1.6*	*121.5±1.1*	*34.3±1.6*	*20.3±0.31*	*27.4±0.8*	*85.2±1.2*	*53.2±1.1*	*27.9±0.14*	*148±2.2*
% difference (not including error)	***7.9***	***8.9***	***13.9***	***2.2***	***5.8***	***50.5***	***13.8***	***3.9***	***16.0***	***12.6***	***3.9***	***6.3***

Note: Attempts to reanalyse samples that were outside acceptable limit were not successful.

SLRS4

This CRM provided by the National Research Council Canada was also used in the analysis of cations using Inductively Coupled Plasma - Mass Spectroscopy (ICP-MS). Table 4.9 and Table 4.10 show the percentage difference between the average measured SLRS4 values for the complete analysis (c. 2 per analysis) and the CRM values for major cations and trace elements, respectively. Each average SLRS4 measured value is quoted with its calculated Relative Standard Deviation (RSD). The percentage difference is calculated only for the average value and not for the error range. Since REE are not included in SLRS4 no table is provided for these elements. In general the percentage difference is lower for the major cations compared to the trace elements, which, is as expected due to the higher concentrations for the major cations compared to those of the trace elements.

Table 4. 9 Percentage difference between the Certified Research Material (CRM), SLRS4 and average measured values reported with their Relative Standard Deviation (RSD) for the major cations analysed using ICP-MS. Units quoted are µg l^{-1}.

Element	*Na*	*K*	*Mg^{24}*	*Ca^{43}*	*Al*
Analysis 1 (14th & 15th January 2014)					
SLRS4: measured value sample 16	*2159*	*649*	*1470*	*6095*	*61*
SLRS4: measured value sample 65	*2389*	*751*	*1646*	*6816*	*68*
Analysis 2 (17th January 2014)					
SLRS4: measured value sample 16	*1996*	*581*	*1338*	*5364*	*50*
Analysis 3 (29th January 2014)					
SLRS4: measured value sample 16	*2309*	*641*	*1580*	*5991*	*56*
SLRS4: measured value sample 49	*2223*	*624*	*1522*	*5900*	*54*
Analysis 4 (13th February 2014)					
SLRS4: measured value sample 16	*2928*	*805*	*2033*	*7804*	*78*
SLRS4: measured value sample 51	*2770*	*749*	*1911*	*7270*	*68*
Analysis 5 (17th February 2014)					
SLRS4: measured value sample 17	*2726*	*763*	*1894*	*7088*	*80*
SLRS4: measured value sample 58	*2705*	*768*	*1871*	*7145*	*80*
Analysis 6 (19th March 2014)					
SLRS4: measured value sample 16	*2683*	*779*	*1896*	*6897*	*73*
SLRS4: measured value sample 38	*2644*	*750*	*1853*	*6684*	*70*
Analysis 7 (20th March 2014)					
SLRS4: measured value sample 16	*2680*	*746*	*1849*	*6921*	*73*
SLRS4: measured value sample 47	*2513*	*701*	*1736*	*6459*	*68*
Average value ± RSD	*2517±11.0*	*716±9.7*	*1738±12.0*	*6649±10.0*	*68±14.7*
SLRS4: Certified value ± abs error	*2400±200*	*680±20*	*1600±100*	*6200±200*	*54±4*
% difference (not including error)	*4.9*	*8.6*	*5.3*	*7.2*	*25.1*

Note: Attempts to reanalyse samples that were outside acceptable limits were not successful.

Table 4. 10 Percentage difference between the Certified Research Material (CRM), SLRS4 and average measured values reported with their Relative Standard Deviation (RSD) for the trace elements analysed using ICP-MS.

Element	*Sr*	*V*	*Cr*	*Mn*	*^{56}Fe*	*Co*	*Ni*	*Cu*	*Zn*	*^{206}Pb*	*Ba*
Analysis 1 (14th & 15th January 2014)											
SLRS4: measured value sample 16	*30.8*	*0.40*	*0.37*	*3.87*	*101.0*	*0.03*	*0.75*	*2.11*	*1.15*	*0.09*	*14.1*
SLRS4: measured value sample 65	*32.3*	*0.43*	*0.39*	*4.19*	*127.8*	*0.04*	*0.79*	*2.22*	*1.17*	*0.08*	*13.8*
Analysis 2 (17th January 2014)											
SLRS4: measured value sample 16	*25.2*	*0.33*	*0.30*	*3.19*	*73.3*	*0.03*	*0.70*	*1.74*	*0.91*	*0.08*	*11.7*
Analysis 3 (29th January 2014)											
SLRS4: measured value sample 16	*32.4*	*0.40*	*0.34*	*3.97*	*92.7*	*0.03*	*0.82*	*2.11*	*1.11*	*0.09*	*14.4*
SLRS4: measured value sample 49	*31.2*	*0.39*	*0.33*	*3.87*	*92.4*	*0.03*	*0.81*	*2.08*	*1.06*	*0.08*	*13.9*
Analysis 4 (13th February 2014)											
SLRS4: measured value sample 16	*39.6*	*0.47*	*0.35*	*4.06*	*<dl*	*0.01*	*0.89*	*2.61*	*1.51*	*0.13*	*18.2*
SLRS4: measured value sample 51	*36.2*	*0.45*	*0.24*	*3.51*	*<dl*	*<dl*	*0.64*	*2.40*	*1.41*	*0.13*	*17.2*
Analysis 5 (17th February 2014)											
SLRS4: measured value sample 17	*39.2*	*0.49*	*0.52*	*4.40*	*136.9*	*<dl*	*0.94*	*2.46*	*1/47*	*0.13*	*17.9*
SLRS4: measured value sample 57	*39.8*	*0.51*	*0.52*	*4.67*	*104.3*	*<dl*	*0.90*	*2.47*	*1.50*	*0.12*	*18.0*
Analysis 6 (19th March 2014)											
SLRS4: measured value sample 16	*34.2*	*0.42*	*0.37*	*4.15*	*141.4*	*0.03*	*0.86*	*2.39*	*1.22*	*0.10*	*15.1*
SLRS4: measured value sample 38	*33.4*	*0.41*	*0.37*	*4.04*	*123.1*	*0.04*	*0.79*	*2.32*	*1.15*	*0.10*	*14.7*
Analysis 7 (20th March 2014)											
SLRS4: measured value sample 16	*33.9*	*0.43*	*0.34*	*4.07*	*102.2*	*0.04*	*0.82*	*2.25*	*1.21*	*0.08*	*14.9*
SLRS4: measured value sample 47	*31.5*	*0.41*	*0.31*	*3.78*	*91.8*	*0.03*	*0.74*	*2.11*	*1.14*	*0.08*	*13.9*
Average value ± RSD	*33.8±12.2*	*0.43±11.0*	*0.36±21.5*	*3.98±9.3*	*107.9±19.9*	*0.03±27.1*	*0.80±10.4*	*2.25±10.1*	*1.23±15.0*	*0.10±19.3*	*15.2±13.2*
SLRS4: Certified value ± abs error	*26.3±3.2*	*0.32±0.03*	*0.33±0.02*	*3.37±0.18*	*103±5*	*0.033±0.006*	*0.67±0.08*	*1.81±0.08*	*0.93±0.1*	*0.086±0.007*	*12.2±0.6*
% difference (not including error)	*28.6*	*32.9*	*10.5*	*18.1*	*4.8*	*4.0*	*20.1*	*22.4*	*32.3*	*15.4*	*24.7*

Note: Attempts to reanalyse samples that were outside acceptable limit were not successful.

Chapter 5. Results – Geological observations

This chapter comprises three main sections and are presented here to address objectives 3 and 4. Section 5.1 describes the geological observations beginning with a description of the Zuari and Chapora drainage basins, including descriptions of any rock and sediment samples collected. Section 5.2 documents the XRF data for the rock and sediment samples collected from the river beds and section 5.3 describes preliminary results of the column experiment (Section 4.4).

5.1. Attributes of the Chapora and Zuari rock and sediment samples

This section evaluates the rock and sediment samples collected from the sampling localities, first in hand specimen and thin section and later as analysed using XRF beginning with those collected from the Zuari River basin and then those collected from the Chapora River basin.

5.1.1. Lithology of the Zuari drainage basin

The Zuari drainage basin covers an area of c. 1059 km^2 and is underlain by rocks of the Goa Group, including meta-basites of the Barcem Formation, meta-sediments and meta-greywackes of the Sandvordem Formation, and cheogenic phyllitic meta-sediments of the Bicholim – Rivona Formation. In addition to these metamorphosed sediments the Zuari River also flows through a significant section of basement gneiss (Chandranath Granite). Samples were collected from localities Zua 01, Zua 03 and Zua 05 opt (Figure 5.1).

Zua 01 is located on the Ugem River at GPS – 15º14.051' 74º11.049' where the underlying geology is the Sandvordem Formation comprising metasediments and metagreywacke. Three samples were collected from the river bed of this site; these were Zua 01 S1 – laterite, Zua 01 S2 – phyllite and Zua 01 S3 – river bed sand.

Zua 03 is located on the Guloli River at GPS – 15º13.612' 74º08.730' where the underlying geology is at a boundary between the Bicholim – Rivona Formation comprising cheogenic phyllitic meta-sediments and the Basement Gneiss of the Chandranath Granite. One sample was collected from this locality: Zua 03 S1 – red silt.

Zua 05 opt is located on the Kushavati River at GPS – 15º12.935' 74º04.348' where the underlying geology is Basement Gneiss of the Chandranath Granite. Two samples

were collected from this locality: Zua 05 opt S1 – amphibolite and Zua 05 opt S2 – gravel and pebbles.

Sample Zua 05 opt S1 is a meta-pelite, which outcrops upstream of the sampling locality which itself is located within the Chandranath granite. It is a light grey, fine grained (<1 mm) friable rock with a very fine foliation. The sample comprises c. 40% quartz and 40% FeMg minerals, with the remainder of the groundmass made up of opaques.

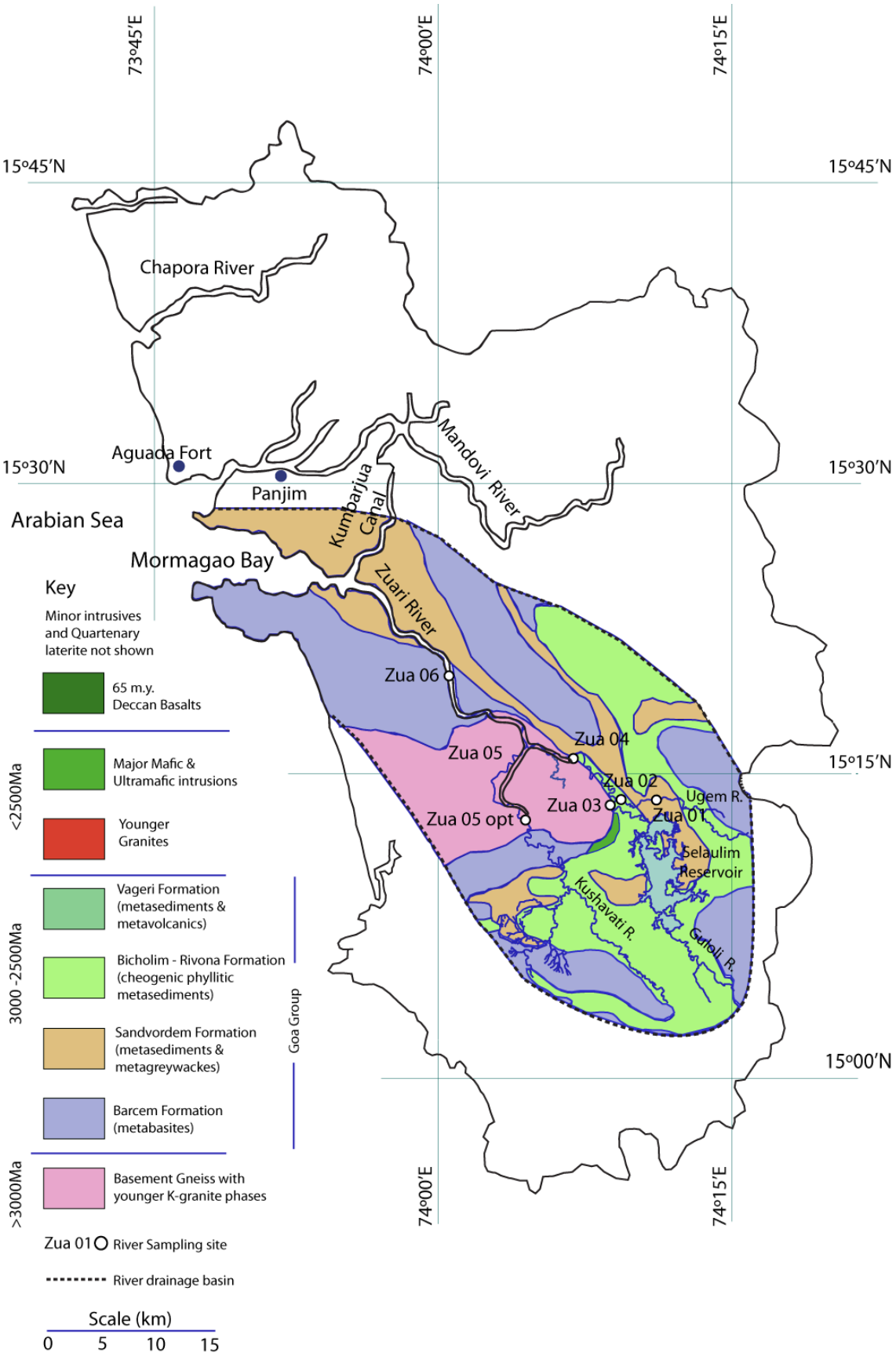

Figure 5. 1 Map of the Zuari River drainage basin, showing underlying geology and sampling sites.

5.1.2. Lithology of the Chapora drainage basin

The Chapora drainage basin covers an area of c. 588 km^2 and is underlain by rocks of the Goa Group, including, meta-sediments and meta-greywackes of the Sandvordem Formation, and cheogenic phyllitic meta-sediments of the Bicholim – Rivona Formation and meta-sediments and meta-volcanics of the Vageri Formation. In addition to these metamorphosed sediments the Chapora River rises in the state of Maharashtra at the Western Ghats escarpment where it drains Deccan Basalt. Samples were collected from localities Cha 01, Cha 02, Cha 03, Cha 05 and Cha 06 (Figure 5.2).

Cha 01 is located at GPS – 15º47.795' 74º06.072' where the underlying geology is the Vageri Formation; four samples were collected from this locality.

Sample S1 is a meta-greywacke. This is a grey, fine grained rock showing distinct light and dark foliations. Viewed as a thin section it is well foliated with bands of 1 mm quartz (55%-60%) and 5 mm x 1 mm biotite (40%), with small amounts of sieve textured high relief 5 mm pyroxene altering to muscovite.

Sample S2 is a garnet mica schist. It is a light grey, fine grained , weakly foliated rock comprising c. 65% 1-3 mm quartz grains and 20-25% 3-5 mm x 1 mm biotite grains with c. 3-5% 1-2 mm garnets. Viewed as a thin section biotite defines the foliation; this is at an angle to the garnet inclusions indicating at least two stages of deformation.

Sample S3 is a light coloured, very fine grained rock (<1 mm) showing extremely distinct dark, cream and green foliations. Viewed as a thin section there is clear foliation comprising distinct bands of light and dark green minerals separated by areas dominated by quartz (75%) and smaller amounts of plagioclase feldspar (15%) showing typical lamellar twinning. The green minerals are pleochroic, suggesting they are an amphibole possibly hornblende.

Sample S4 is an amphibolite. It is a dark green, very fine grained rock displaying very fine foliations. Viewed as a thin section the sample is dominated by a green mineral (90%) that is pleochroic from dark green to light green and is probably an amphibole possibly hornblende. The remainder of the ground mass is made up of quartz (5%) and plagioclase (5%).

Cha 02 is located at GPS – 15º47.795' 74º06.072' where the underlying geology is the Vageri Formation; one sample, Cha 02 S1 – granitic rock was collected from this

locality. Also observed was considerable proportion of Deccan basalt cobbles and pebbles. The composition of these was most likely of from the Ambenali group (Mitchell and Widdowson, 1991, Jay et al., 2009).

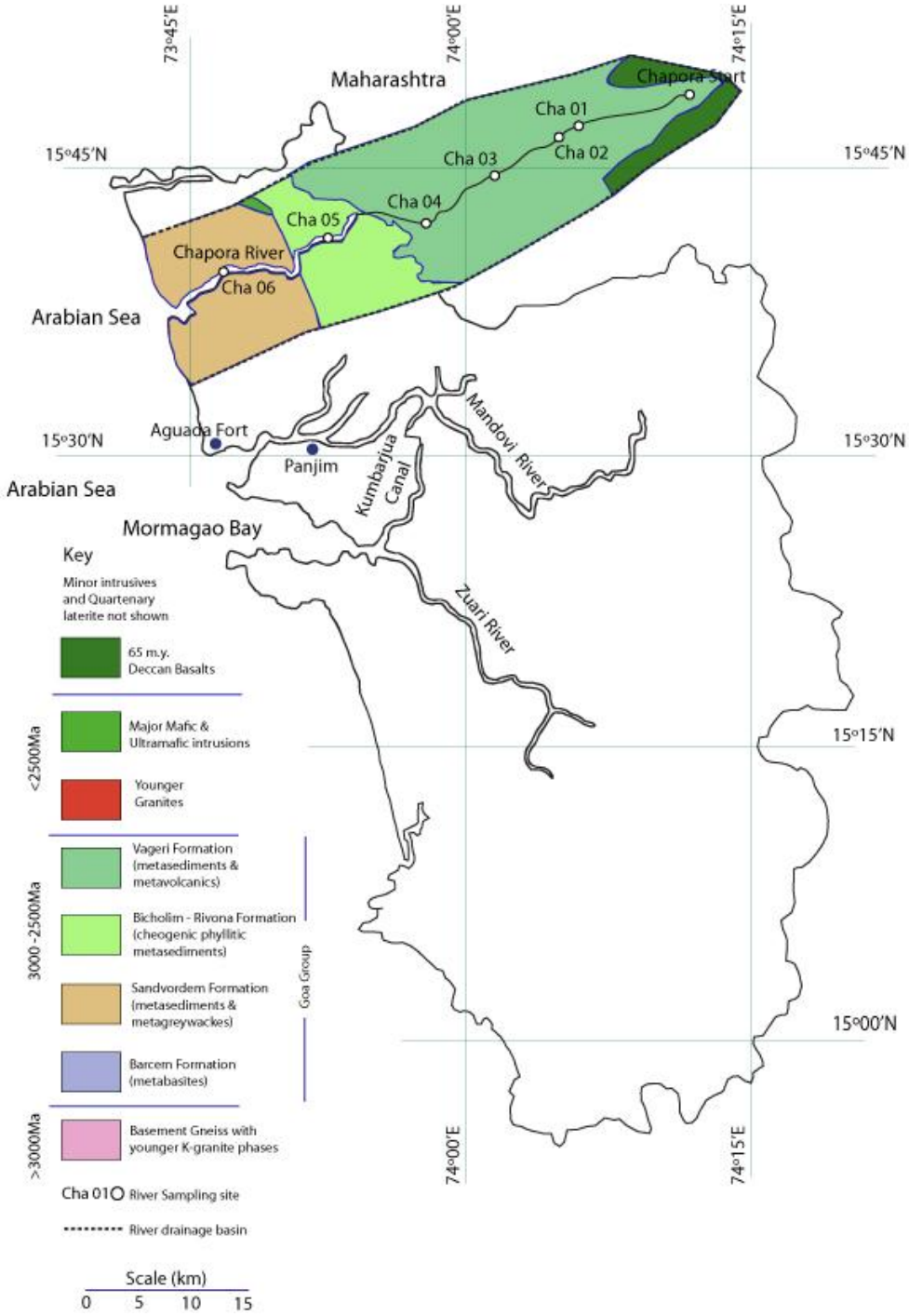

Figure 5. 2 Map of the Chapora River drainage basin, showing underlying geology and sampling sites.

Cha 03 is located at GPS – 44.215' – 74º.00.487' where again the underlying geology is the Vageri Formation; four samples were collected from this locality.

Sample S1 is a meta-greywacke. It is a grey, fine grained rock dominated by equal amounts of quartz and amphibole (c. 45% each) with the remainder comprised of 2% muscovite, 2% plagioclase and 5% opaques. The sample has no sign of foliation. Viewed as a thin section there are green high relief, slightly pleochroic minerals, probably amphibole and quartz.

Sample S2 is a meta-basite. This is a dark grey-green, coarse grained rock with crystalline texture and no foliation. It comprises mostly (c. 80%) FeMg minerals, including highly reacted pyroxenes; feldspar makes up the majority of the remaining groundmass (c. 15-18%) along with c. 2% muscovite and c. 2% opaques.

Sample S3 is a quartzite. It is coarse grained (6-10 mm diameter grains) rock comprised of c. 100% quartz with inclusions of biotite (<1%). The quartz comprises inter-grown crystals with no cementation, which is also indicated by undulose extinction.

Sample S4 is quartz chlorite schist, which under thin section appears to be dominated by chlorite (50%) which shows clear pleochroism varying from light green to light straw colour. Under crossed polars the chlorite crystals show strong birefringence colours from green to blue. In addition to the chlorite there are quartz (35%) and biotite (15%) crystals present.

Cha 05 is located at GPS – 15º40.973' 73º53.001' where the underlying geology is still the Bicholim – Rivona Formation; one sample Cha 05 S1 was collected from this locality. This was a river sediment sample which had been dredged from the river bed and was being stored in large heaps awaiting transport and subsequent use as a building sand.

Cha 06 is located at GPS – 15º38.932' 73º50.175' where the underlying geology is the Sandvordem Formation; one sample Cha 06 S1 was collected from this locality. This was also a river sediment sample which had been dredged from the river bed.

Table 5. 1 Lithology and mineralogy of Chapora and Zuari River rock and sediment samples – determined by petrographic analysis.

Sample locality	Sample	Rock Type	Formation	Quartz (%)	Biotite (%)	Muscovite (%)	Chlorite (%)	Pyroxene (%)	Garnet (%)	Plagioclase (%)	Orthoclase (%)	Microcline (%)	Amphibole (%)	FeMg minerals (%)	Opaques (%)	Lithic fragments (%)	Basalt fragments (%)	Laterite fragments (%)
Chapora River Samples																		
Cha 01	S1	Meta-greywacke	Vageri	50-55	40	2		2										
Cha 01	S2	Garnet Mica schist	Vageri	65	20-25				3-5						<1			
Cha 01	S3	Meta-greywacke	Vageri	75						15				5	5			
Cha 01	S4	Amphibolite	Vageri	5						5				90				
Cha 02	S1	Gneissic granite	Vageri	70-75		5				15			5					
Cha 03	S1	Meta-greywacke	Vageri	45		2				1-2			45		5			
Cha 03	S2	Meta-basite	Vageri			2				15-20				80	2			
Cha 03	S3	Quartzite	Vageri	100	<1													
Cha 03	S4	Quartz chlorite schist	Vageri	35		15	50											
Cha 05	S1	Channel Sediment	Bicholim	70-80	2	1				<1		1					5	5
Cha 06	S1	Channel Sediment	Sandvordem	80-90	1	1						<1					2	5
Zuari River Samples																		
Zua 01	S1	Laterite	Sandvordem								No thin section							
Zua 01	S2	Phyllite	Sandvordem	40										40	3-5			
Zua 01	S3	River bed sand	Sandvordem	10											50-60			
Zua 03	S1	Red silt	Bicholim															
Zua 05 opt	S1	Meta-pelite	Sandvordem	50	5										50-60			
Zua 05 opt	S2	Selection of pebbles	Barcem	10-20												20		60-70

5.2. XRF Data

Tables 5.2 and 5.3 provide major and trace element data for the rock and sediment samples collected from the various sampling localities along the Chapora and Zuari Rivers.

Table 5. 2 Major element compositions (wt%)of Chapora and Zuari rock and sediment samples, all values quoted are as wt%. CIA and MIA values and Ca/Na and Mg/Na ratio values all use the molar ratios of the major oxides by converting the wt% concentrations into moles (Babechuk et al., 2014).

Location	Cha 01				Cha 02	Cha 03				Cha 05	Cha 06	Zua 01			Zua 03	Zua 05 opt	
Sample	S1	S2	S3	S4	S1	S1	S2	S3	S4	S1	S1	S1	S2	S3	S1	S1	S2
Rock type	Meta-greywacke	Garnet mica schist	Meta-greywacke	Amphibolite	Gneissic granite	Meta-greywacke	Meta-basite	Quartzite	Quartz chlorite schist	River bed sediment	River bed sediment	Laterite	Phyllite	River bed sand	Red silt	Meta-pellite	Selection of pebbles
SiO_2	59.90	62.79	62.17	49.56	66.12	60.49	48.68	97.22	50.49	76.14	75.52	14.27	64.00	67.28	64.52	74.76	50.62
TiO_2	0.69	0.66	0.29	0.58	0.45	2.00	0.69	0.03	0.79	0.67	1.34	0.98	0.63	1.95	1.42	0.19	0.79
Al_2O_3	15.48	15.57	16.47	14.65	15.47	11.63	16.91	0.26	13.69	9.01	8.78	22.13	15.94	11.41	9.94	13.94	13.19
Fe_2O_3	9.06	7.96	5.04	12.67	3.66	12.29	11.35	0.07	12.17	10.22	8.92	60.93	10.29	13.06	15.07	2.07	32.28
MnO	0.15	0.10	0.10	0.24	0.11	0.17	0.17	0.00	0.21	0.07	0.16	0.34	0.25	0.20	1.95	0.29	0.85
MgO	4.47	3.21	1.56	7.53	1.32	3.45	7.93	0.04	7.21	0.95	2.01	0.13	2.66	2.34	0.64	0.46	0.43
CaO	2.70	3.07	7.23	11.04	9.01	6.41	10.52	0.02	10.91	1.18	2.28	0.03	0.17	2.31	0.22	0.53	0.24
Na_2O	3.78	3.40	4.37	2.29	1.26	2.57	2.55	0.00	2.53	0.68	1.07	0.03	2.90	1.21	0.17	4.54	0.14
K_2O	2.72	2.55	0.25	0.27	0.18	0.14	0.49	0.06	0.16	0.76	0.81	0.41	2.87	0.75	0.77	3.07	0.56
P_2O_5	0.15	0.16	0.07	0.10	0.11	0.26	0.06	0.01	0.07	0.11	0.10	0.51	0.14	0.10	0.08	0.04	0.13
LOI	0.59	0.67	0.46	0.87	0.63	0.41	1.35	0.06	0.80	3.72	5.24	14.51	3.96	4.20	6.23	0.93	7.45
Total	99.10	99.46	97.53	98.91	97.69	99.42	99.35	97.70	98.23	99.79	100.99	99.76	99.85	100.61	94.78	99.89	99.24
CIA	52.4	52.8	44.4	37.8	45.3	42.0	41.5	72.0	36.2	68.8	56.4	97.6	66.1	62.0	86.8	54.3	91.2
MIA(o)	52.8	54.9	49.0	43.0	48.4	54.0	42.9	64.0	42.2	78.4	64.4	99.6	67.2	69.9	90.9	56.6	96.2
MIA(r)	28.8	31.8	34.2	19.3	36.3	21.6	22.0	46.3	18.7	30.0	26.4	20.2	35.1	26.6	28.8	46.8	21.5
Ca/Na	0.39	0.50	0.91	2.66	3.95	1.38	2.28	0.55	2.38	0.96	1.18	0.55	0.03	1.06	0.72	0.06	0.95
Mg/Na	0.91	0.73	0.27	2.53	0.81	1.03	2.39	1.54	2.19	1.07	1.44	3.33	0.71	1.49	2.89	0.08	2.36

Table 5. 3 Trace element compositions (ppm) for the Chapora and Zuari rock and sediment samples, all values quoted are in ppm.

Location	Cha 01				Cha 02	Cha 03				Cha 05	Cha 06	Zua 01			Zua 03	Zua 05 opt	
Sample	S1	S2	S3	S4	S1	S1	S2	S3	S4	S1	S1	S1	S2	S3	S1	S1	S2
Rock type	Meta-greywacke	Garnet mica schist	Meta-greywacke	Amphibolite	Gneissic granite	Meta-greywacke	Meta-basite	Quartzite	Quartz chlorite schist	River bed sediment	River bed sediment	Laterite	Phyllite	River bed sand	Red silt	Meta-pellite	Selection of pebbles
Rb	85	88	4	3	4	4	31	2	8	18	22	15	132	13	33	75	19
Sr	315	245	568	99	486	105	183	1	139	65	94	15	53	27	21	158	16
Y	18.7	17.1	13.0	26.4	27.1	62.7	16.0	2.1	18.9	10.6	18.0	12.6	47.2	17.6	20.8	6.7	12.1
Zr	125	127	104	65	93	196	41	37	47	85	90	153	178	93	193	110	94
Nb	7.9	7.3	2.8	4.1	6.4	8.6	2.6	1.2	2.9	5.2	6.6	15.2	12.8	8.4	10.9	6.3	6.7
Ba	779	651	90	80	99	34	55	3	26	126	138	96	820	177	289	604	134
Pb	14	15	11	0	13	3	5	5	4	9	4	26	8	26	19	7	29
Th	10	8	0	2	9	1	1	0	1	4	3	15	11	5	5	11	6
U	2	2	0	0	0	2	0	0	0	2	2	7	4	0	1	2	0
Sc	19	18	11	42	8	37	31	1	43	19	16	32	15	13	25	1	24
V	150	166	166	233	64	327	209	5	262	218	206	290	126	102	214	8	136
Cr	174	137	39	86	59	19	182	7	74	672	510	206	139	145	329	8	435
Co	19	17	5	35	8	22	43	0	39	8	11	8	39	1	8	3	14
Ni	72	51	24	57	27	22	204	3	78	59	63	45	59	32	99	6	89
Cu	9	38	4	72	20	17	128	3	95	37	35	63	116	59	58	4	98
Zn	87	79	36	97	34	66	73	4	85	39	50	35	163	64	84	19	79
Ga	21	18	25	13	18	17	15	1	16	11	12	23	20	11	14	17	18
Mo	0	2	0	0	1	0	0	0	0	1	0	5	2	0	0	1	2
As	0	2	0	0	3	0	0	0	1	6	4	79	10	22	11	2	31
S	8	420	3	0	107	82	138	0	457	420	761	515	20	108	385	1	395

5.3. Column experiment – Preliminary results

This section details the preliminary results of the column experiment. These include those measurements that were recorded during the experiment, such as pH, HCO_3^-, and conductivity. Water samples were collected for cation and anion analysis but due to time constraints these were not analysed. Additionally, XRF data are presented for all of the collected samples MQ1 – MQ17.

5.3.1. pH

Figure 5.3 shows that the pH of both the water input and of the collected water samples varied by column and over time. The sharp decrease in pH for the water input coinciding with week 2 was peculiar and it was noticed that the sides of the water supply container had begun to be sucked inwards as water was repeatedly removed. This was overcome by providing an air entry point above the water level allowing air to be sucked in as the water was removed. Subsequently, the pH of the water supply input gradually recovered and if we ignore the week 2 value the pH varied from pH 5.66 in week 3 to pH 6.57 in week 13. The cause for this observed change in water pH remains unknown.

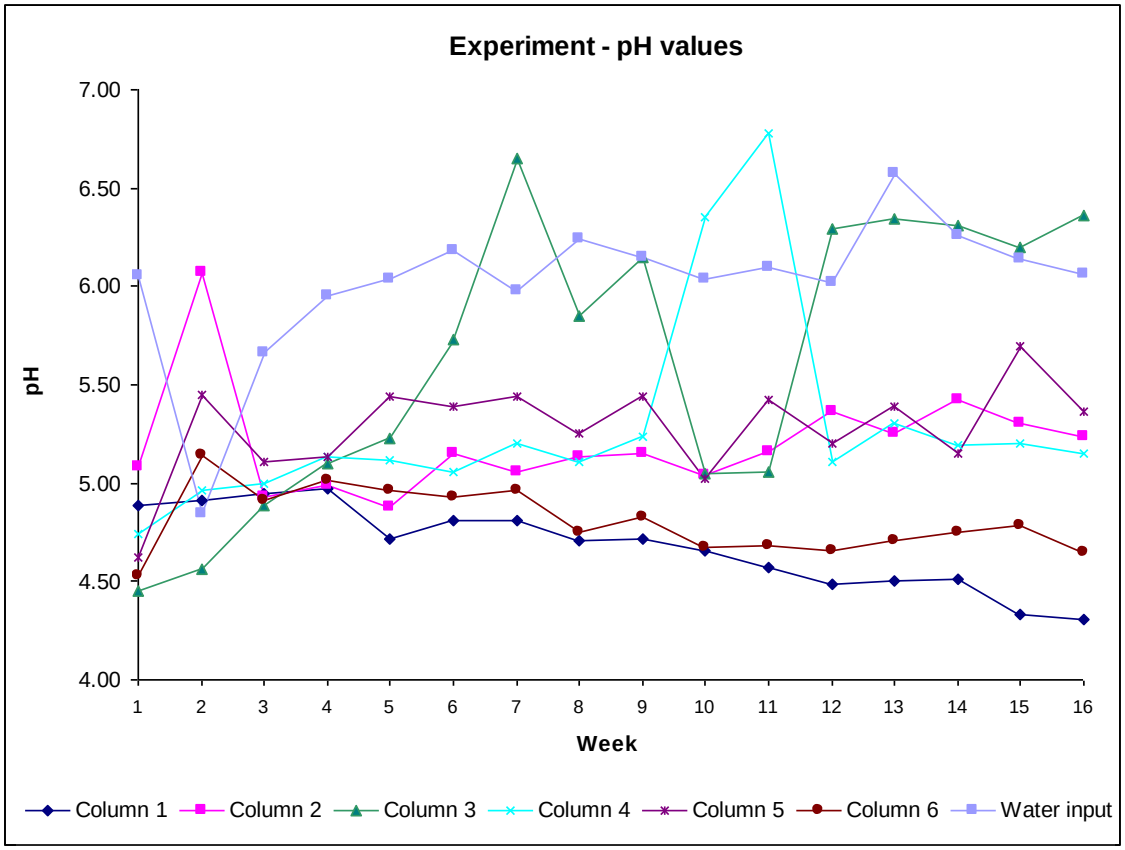

Figure 5.3 pH values for the water samples collected from the column experiment over a 16 week period.

Column 1, unaltered protolith; the data show that the pH remained fairly consistent around pH 5.0 up to week 4 before gradually declining over the subsequent weeks to pH 4.31 at week 16.

Column 2, saprolite; the data show that pH remains fairly consistent ranging between pH 4.85 during week 5 and pH 5.42 during week 14. However, there is a prominent positive excursion up to pH 6.07; this coincides with the low pH data recorded for the anomalous water supply input occurring during week 2.

Column 3, saprolite; pH values for this column are very different to those described previously. Here the data show pH starting off quite low at pH 4.45 for week and rising continuously up to a high of pH 6.65 during week 7. Values then drop sharply in two stages to pH 5.05 and pH 5.06 for weeks 10 and 11, respectively, before rising once more to level off between pH 6.2 and pH 6.36 for weeks 12 to week 16.

Column 4, palaeowater table zone; data for this column show a relatively flat profile with a slight rise in values from week 1 to week 16, however, there are two clear positive excursions to pH 6.35 and pH 6.78 during weeks 10 and 11, respectively.

Column 5, duricrust; data for this column show values ranging between pH 4.62 during week 1 to a high of pH 5.70 during week 15, other than the relative high value of pH 5.45 coinciding with week 2 there is no clear discernible pattern with an almost saw-toothed profile being recorded.

Column 6, combination column; data show that the values begin low at pH 4.53 and like columns 2 and 5 records an obvious positive excursion at week 2 to pH 5.14 coinciding with the low pH value of the water input. After which values decline gradually to a low of pH 4.65 during week 16.

5.3.2. Bicarbonate

Figure 5.4 presents the HCO_3^- concentrations for the column experiment. The general pattern shows slightly elevated values at the beginning of the experiment gradually diminishing over time, with the exception of the peaks associated with weeks 9, 10 and 11. The following paragraphs describe each column in turn.

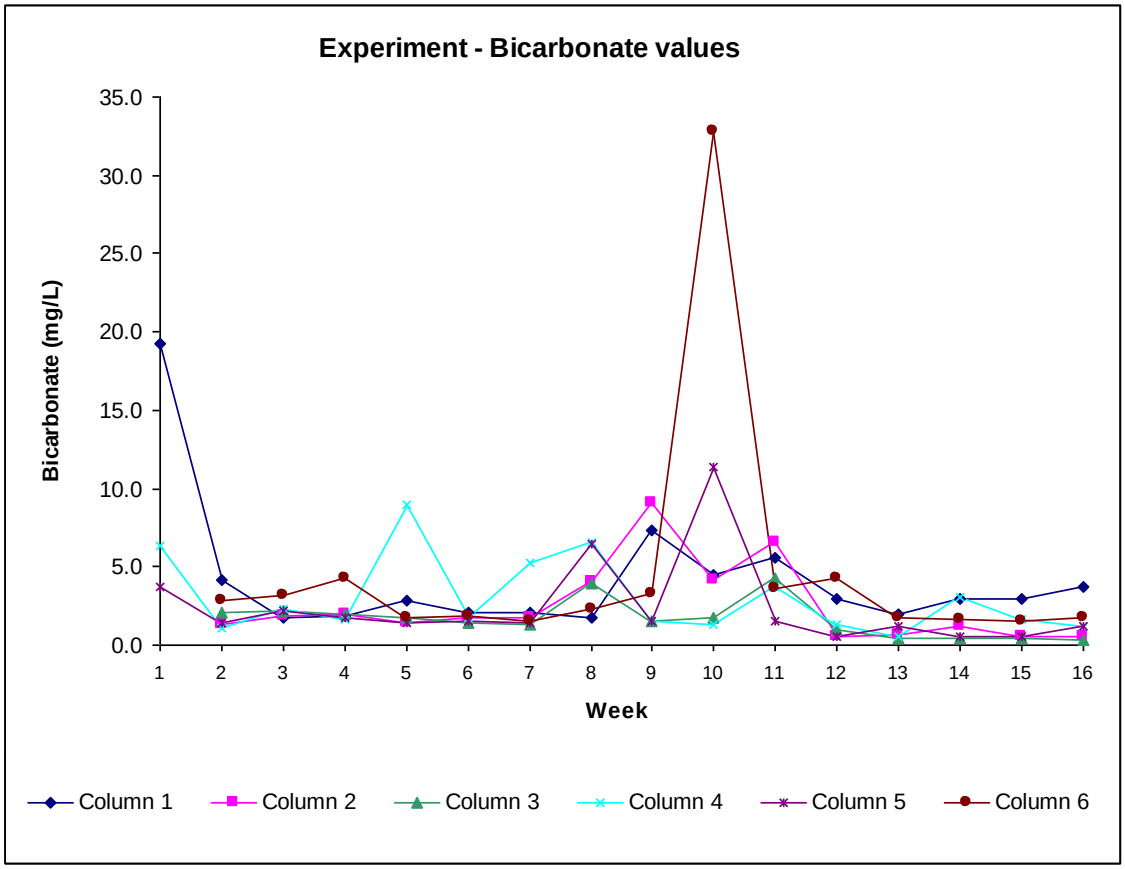

Figure 5.4 HCO_3^- values for the water samples collected from the column experiment over a 16 week period.

The following summarises the bicarbonate behaviour in the columns over the duration of the experiment. It important to note that for the first week there was an issue with draining columns 3 and 6, on week two all samples except column 3 had drained after 1 hour, this was ultimately overcome by allowing the samples 24 hours to drain before analysing the collected water sample.

Column 1, unaltered protolith; bicarbonate values initiate at relatively high levels of 19.2 mg l^{-1} before falling to an experimental low of 1.7 mg l^{-1}, after which the values generally range between this low value and 3.0 mg l^{-1}. However, there are three positive excursions to 7.3 mg l^{-1}, 4.5 mg l^{-1} and 5.6 mg l^{-1} for weeks 9, 10 and 11, respectively.

Column 2, saprolite; no titration was completed for week 1 for this column due to the very slow nature of the water seeping through the column. The remaining values recorded are between 0.7 mg l^{-1} and 2.0 mg l^{-1} with the obvious exceptions of four positive excursions of 4.1 mg l^{-1}, 9.1 mg l^{-1}, 4.2 mg l^{-1} and 6.6 mg l^{-1} for weeks 8, 9, 10 and 11, respectively.

Column 3, saprolite; again data for week 1 is missing (due to column drainage problems). The general trend is one of a gradual reduction in values from 2.1 mg l^{-1} and 2.2 mg l^{-1} for weeks 2 and 3, respectively down to 0.4 mg l^{-1} and 0.3 mg l^{-1} for weeks 15 and 16, respectively. However, as with column 2 there are positive excursions for weeks 8, 9, 10 and 11 with values of 3.9 mg l^{-1}, 1.5 mg l^{-1}, 1.8 mg l^{-1} and 4.3 mg l^{-1}, respectively.

Column 4, Palaeowater table zone; the data for this column do not appear to show any discernible trends, and in fact they show a saw tooth pattern with alternating highs and lows and as such is difficult to interpret, other than there does appear to be a general reduction in values from week 1 to week 16, this can be seen more clearly if a logarithmic trend line is used.

Column 5, duricrust; the initial HCO_3^{-1} concentrations for this column are recorded as 3.7 mg l^{-1}, from this point they show a general gradual decline down to values of 0.5 mg l^{-1} for week 15 and 1.2 mg l^{-1} for week 16. Once again, there are positive excursions at week 8 and week 10 with values of 6.5 mg l^{-1} and 11.4 mg l^{-1}, recorded respectively.

Column 6, combination column; again the data for week 1 is missing. The most striking observation for this column is the large positive excursion to 32.8 mg l^{-1} during week 10. Other than this values range between 1.5 mg l^{-1} during week 7 and 4.3 mg l^{-1} during week 4 and week 12.

5.3.3. Conductivity

The conductivity of the water was measured as soon as the water samples were collected from the columns. Since conductivity is the measure of the waters ability to pass an electrical current it is directly related to element concentration, with high conductivity coinciding with higher element concentrations, Figure 5.5 presents the conductivity values for the column experiment.

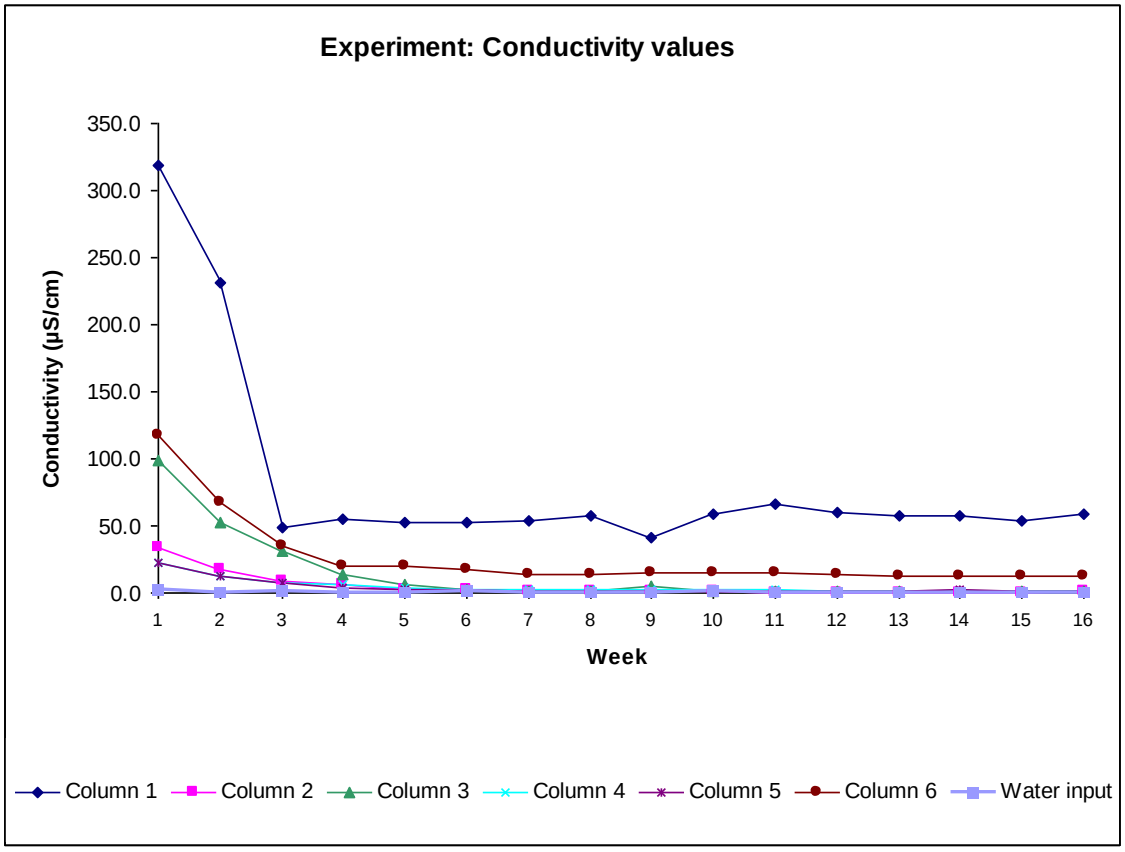

Figure 5.5 Conductivity values for the water samples collected from the column experiment over a 16 week period.

All columns showed similar trends with conductivity starting off high and then gradually falling over the subsequent 4 to 5 weeks before levelling off at fairly consistent values. Column 1, unaltered protolith recorded by far the highest conductivity values, beginning at 319 µS cm^{-1} before dropping sharply over the next two weeks to 49 µS cm^{-1} after

which values level off. All the other columns display gently diminishing conductivity values, with the next highest values occurring for column 6 which is a combination of the previous five columns and its higher value could be due to the presence of unaltered material from column 1. Column 3 records the third highest values, starting at 117 µS cm^{-1}, which are almost three times lower than those for column 1. The higher conductivity of this column relative to that of column 2 which should be more reactive may be due to the higher contact time between the water and the column material due to poorer permeability, which is also linked to smaller average grain sizes which would provide a greater surface area with which to react. This is followed by column 2 with an initial value of 34 µS cm^{-1} and finally by columns 4 and 5 with initial values of 23 µS cm^{-1} and 22 µS cm^{-1}, respectively.

5.3.4. XRF data for Merces Quarry samples

XRF data for the Merces Quarry samples MQ1 – MQ17 are tabulated in Table 5.5 for major elements and Table 5.6 for trace elements; selected data are then plotted against profile depth in Figures 5.6 and 5.7 and described in the following pages.

Table 5. 4 Location, elevation and descriptions of the zones from which the various discrete (MQ) and bulk (MQBK) samples were collected along with observations documented during field sampling. The terminology of the zones and descriptions is from Widdowson, 2009. See Figure 3.4 for detail.

Zone	Observation	Elevation above quarry base (m)	Bench	Sample	Bulk Sample
Laterite cuirasse	Highly indurated vermiform laterite	37.5	TOP (9)	MQ17	MQBK7
Laterite cuirasse	Base of vermiform laterite	34.5	8	MQ16	
Laterite carapace	Fe nodules / stringer zone	32.5	8	MQ15	
Laterite carapace	Fe nodules / stringer zone	31	7	MQ14	MQBK6
Laterite carapace	Fe nodules / stringer zone	29.5	7	MQ13	
Fe mottled	Fe stringer zone	29	7	MQ12	
Fe mottled	Fe stringer zone	27.5	6	MQ11	MQBK5
Fe mottled / Plasmic	Base of Fe stringer zone	26.5	6	MQ10	
Plasmic	Fe segregations (spots small diffuse nodules)	25	6	MQ9	
Plasmic	Fe segregations (spots small diffuse nodules)	24	6	MQ8	
Saprock / Plasmic	Fe segregations (spots small diffuse nodules)	17.5	5	MQ7	MQBK4
Saprock	Fe segregations start / remnants of bedding	16.5	5	MQ6	
Saprock	Red saprock / visible seedy bedding	16.5	5	MQ5	
Saprock	Grey saprock (with some leisegang structures)	14	5	MQ4	MQBK3
Saprock	Spheroidal weathering of protolith	13.5	4	MQ3	
Saprock	Altered protolith / weathering front	8	4	MQ2	MQBK2
Protolith	Unaltered greywacke	0	2	MQ1	MQBK1

Table 5. 5 Major element compositions of Merces Quarry weathering profile samples, all values quoted are as wt% and depth is in metres above quarry base CIA and MIA valus and Ca/Na and Mg/Na ratio values all use the molar ratios of the major oxides by converting the wt% concentrations into moles (Babechuk et al., 2014).

Sample	MQ01	MQ02	MQ03	MQ04	MQ05	MQ06	MQ07	MQ08	MQ09	MQ10	MQ11	MQ12	MQ13	MQ14	MQ15	MQ16	MQ17
Element / Depth (m)	0	8	13.5	14	16.5	16.5	17.5	24	25	26.5	27.5	29	29.5	31	32.5	34.5	37.5
SiO_2	67.06	68.89	68.09	69.83	61.21	31.92	45.21	61.40	49.52	68.23	67.57	69.08	18.99	16.45	15.34	14.73	10.66
TiO_2	0.55	0.51	0.68	0.49	0.69	1.06	0.75	0.80	0.86	0.46	0.67	0.64	1.14	1.50	2.10	2.29	1.42
Al_2O_3	14.36	13.87	12.13	14.99	18.40	23.35	16.02	19.84	20.42	15.27	17.97	18.10	23.20	25.42	32.77	26.71	25.01
Fe_2O_3	5.90	5.21	6.52	4.51	6.94	31.70	28.95	8.61	18.58	8.33	5.59	4.66	43.05	42.54	31.67	40.79	47.61
MnO	0.13	0.12	0.12	0.09	0.12	0.03	0.02	0.02	0.02	0.01	0.02	0.01	0.03	0.03	0.02	0.04	0.12
MgO	2.98	2.78	3.94	2.19	2.76	0.15	0.16	0.33	0.35	0.28	0.31	0.32	0.09	0.08	0.12	0.12	0.08
CaO	0.73	0.78	0.66	0.18	0.06	0.01	0.01	0.02	0.03	0.01	0.01	0.01	0.02	0.02	0.02	0.02	0.02
Na_2O	2.96	2.97	0.92	2.52	0.73	0.05	0.05	0.06	0.06	0.05	0.05	0.06	0.05	0.05	0.08	0.10	0.06
K_2O	3.78	3.11	2.26	2.86	3.09	0.70	0.70	1.59	1.44	1.44	1.72	1.66	0.38	0.43	0.60	0.75	0.30
P_2O_5	0.12	0.10	0.11	0.01	0.02	0.16	0.21	0.04	0.09	0.05	0.02	0.02	0.27	0.24	0.19	0.28	0.30
LOI	1.15	1.53	4.06	2.48	5.98	11.57	8.67	7.37	8.66	5.82	6.00	6.06	12.90	13.52	16.85	14.42	14.34
Total	99.74	99.87	99.50	100.15	99.99	100.70	100.76	100.08	100.03	99.95	99.93	100.61	100.14	100.27	99.76	100.25	99.92
TiO_2 x 100	55.40	51.25	68.12	48.51	69.18	105.89	74.58	79.90	86.06	45.58	66.66	63.90	114.35	149.93	209.66	229.42	141.80
MnO x 100	12.61	11.63	11.69	8.60	11.51	3.17	1.83	1.79	2.31	0.86	1.85	1.23	3.23	2.53	2.10	4.29	11.72
Summed Alkalis	10.46	9.64	7.79	7.75	6.64	0.91	0.93	2.01	1.87	1.78	2.09	2.05	0.55	0.58	0.82	0.99	0.46
CIA	65.8	66.9	75.9	73.0	82.6	96.9	95.4	92.2	93.1	91.1	91.0	91.3	98.1	98.1	97.9	96.9	98.5
MIA (o)	66.0	66.4	70.5	71.6	79.2	98.4	98.0	93.4	95.4	93.0	91.9	91.8	99.2	99.2	98.7	98.6	99.4
MIA (r)	46.7	48.3	45.9	55.0	57.5	41.7	34.9	65.1	50.0	60.2	70.1	73.0	34.7	37.1	50.2	39.0	34.2
Ca/Na	0.14	0.14	0.40	0.04	0.04	0.11	0.15	0.20	0.25	0.06	0.06	0.06	0.26	0.18	0.16	0.14	0.18
Mg/Na	0.77	0.72	3.28	0.67	2.92	2.16	2.35	4.29	4.64	4.15	4.34	4.36	1.32	1.15	1.12	0.94	0.98

Table 5. 6 Trace element compositions for the Merces Quarry weathering profile, all values quoted are in ppm and depth is in metres above quarry base.

Sample	MQ01	MQ02	MQ03	MQ04	MQ05	MQ06	MQ07	MQ08	MQ09	MQ10	MQ11	MQ12	MQ13	MQ14	MQ15	MQ16	MQ17
Element / Depth (m)	0	8	13.5	14	16.5	16.5	17.5	24	25	26.5	27.5	29	29.5	31	32.5	34.5	37.5
Rb	123	100	90	93	148	27	30	39	36	30	31	33	18	17	25	35	16
Sr	105	103	49	47	13	25	17	13	15	7	8	7	25	29	47	54	26
Y	18.5	12.8	22.0	15.4	34.9	16.0	19.2	12.1	14.8	9.2	7.4	6.2	13.5	16.8	26.7	31.3	17.0
Zr	187	165	180	141	220	222	205	234	234	133	200	177	214	248	380	453	265
Nb	13.3	12.6	17.9	11.7	15.4	18.5	15.3	16.4	16.9	10.1	14.2	13.4	17.7	21.0	32.9	38.0	21.1
Ba	741	614	437	760	756	262	267	741	612	722	746	809	60	61	155	138	33
Pb	11	14	13	10	18	39	29	9	15	9	5	5	55	55	48	56	50
Th	17	18	31	12	20	22	27	21	26	11	19	16	22	24	28	26	17
U	6	5	3	3	7	3	7	4	5	4	2	3	7	6	5	7	8
Sc	12	11	15	11	15	28	28	21	28	16	11	11	<dl	<dl	20	13	<dl
V	95	93	128	98	155	192	165	164	175	121	107	106	<dl	<dl	232	<dl	<dl
Cr	121	128	298	692	167	380	231	129	220	134	114	87	<dl	<dl	485	50	<dl
Co	11	10	12	4	12	<dl	<dl	<dl	<dl	<dl	<dl	<dl	<dl	<dl	<dl	0	0
Ni	36	29	46	29	49	60	74	48	61	22	33	26	75	56	54	66	54
Cu	31	35	44	16	113	57	67	25	28	20	18	11	66	55	42	62	56
Zn	89	76	86	67	128	35	80	25	28	19	24	14	32	29	23	34	28
Ga	17	16	16	17	21	35	28	26	28	18	18	19	41	48	60	61	43
Mo	1	2	1	2	3	9	5	2	2	1	2	1	19	22	14	15	20
As	5	6	4	5	5	59	28	14	13	13	4	6	142	139	72	96	167
S	477	322	62	60	46	875	820	241	543	272	142	88	1154	1298	646	1017	1536

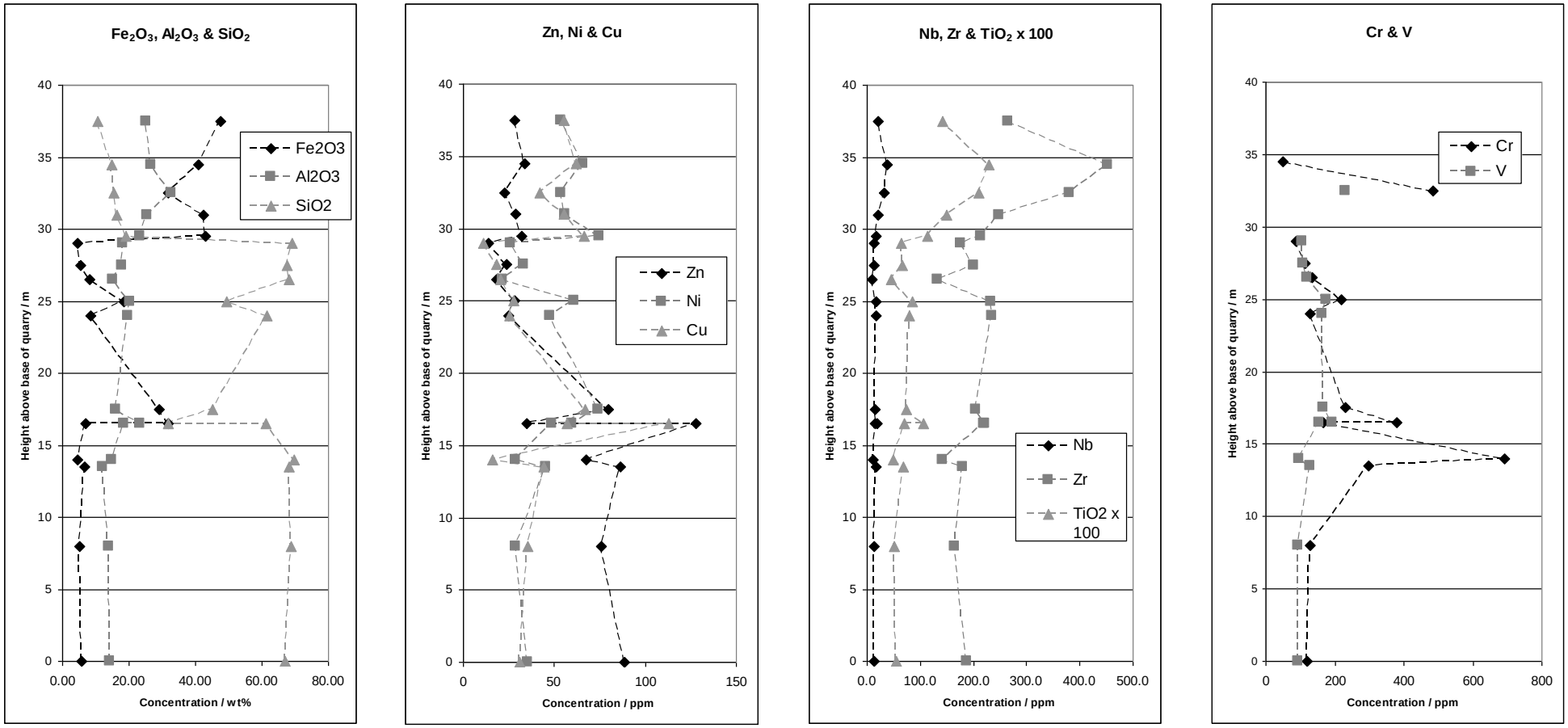

Figure 5. 6 Element concentration plots showing concentration versus profile depth for (a) Fe_2O_3, Al_2O_3 & SiO_2 (b) Zn, Ni & Cu (c) Nb, Zr & TiO_2 x100 and (d) Cr & V.

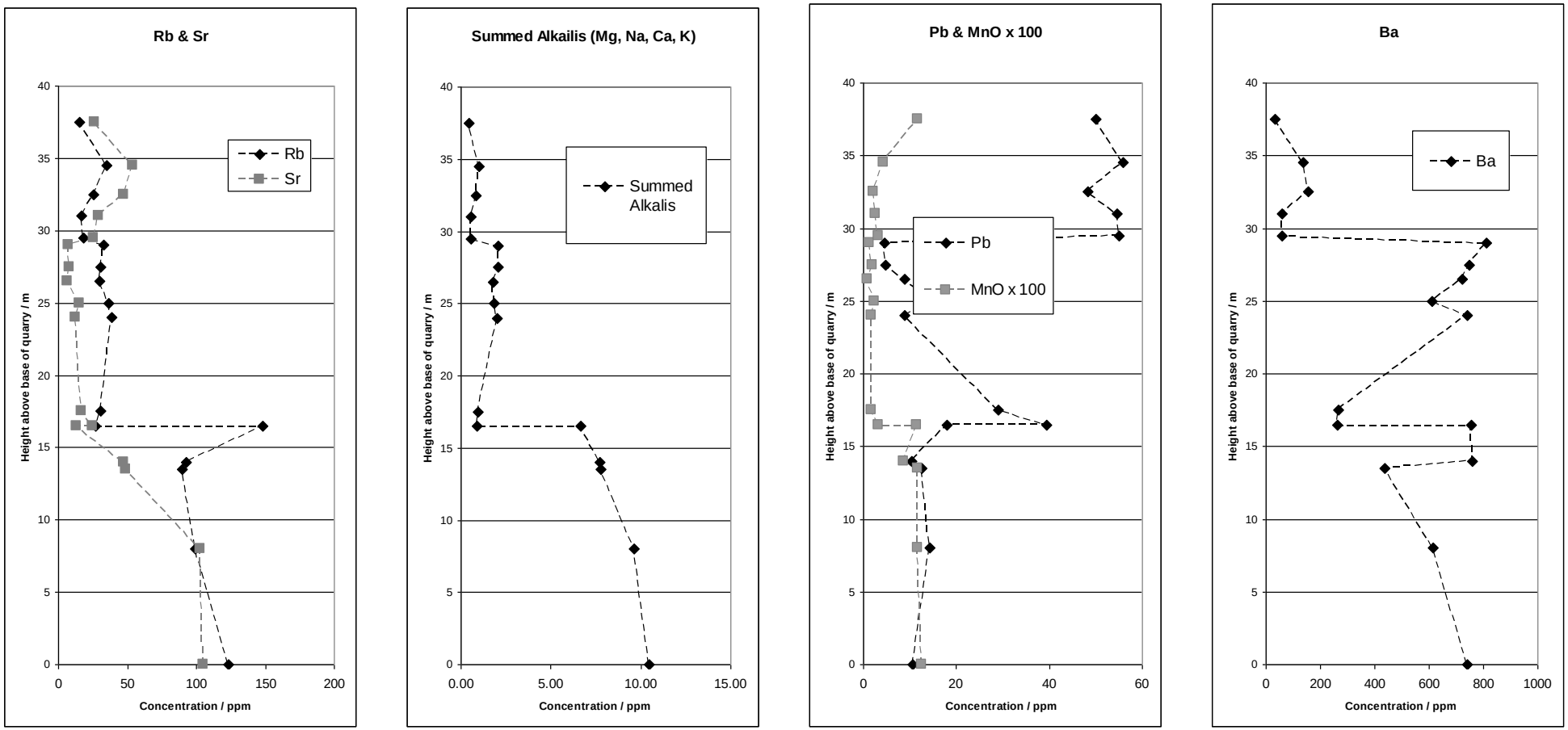

Figure 5. 7 Element concentration plots showing concentration versus profile depth for (a) Rb & Sr (b) Summed Alkalis (c) Pb, Zr & MnO x100 and (d) Ba.

The following paragraphs describe the elements as displayed in Figures 5.6 & 5.7.

Fe_2O_3, Al_2O_3 and SiO_2 (Figure 5.6a).

Staring at the base of the quarry the composition of all three oxides remains fairly consistent for the first 6 m or so with Fe_2O_3 ranging between 4.51 wt% and 6.52 wt%, Al_2O_3 ranging from 12.13 wt% and 14.99 wt% and SiO_2 ranging between 67.06 wt% and 69.83 wt%. From this point SiO_2 values reduce significantly to 31.92 wt% over a very short depth of just 2.5 m with the majority of the change occurring from 8 m to 8.5 m. Over the same depth there is a rise in Fe_2O_3 and Al_2O_3 values reaching 31.7 wt% and 23.5 wt%, respectively for sample MQ6. Above 8.5 m, SiO_2 rises gradually towards original values of between 68.23 wt% and 69.08 wt% for samples MQ10 at 13.5 m and MQ12 at 21 m, respectively, whilst Fe_2O_3 reduces to 8.33 wt% for MQ10 and 5.59 wt% for MQ12 and Al_2O_3 reduces to 15.27 wt% for MQ10 and 18.1 wt% for MQ12. Due to an obvious physical change at the depth of 21 m two samples were collected at the same level, albeit a few cm apart and MQ13 records very different values with Fe_2O_3 rising to 43.05 wt%, Al_2O_3 rising to 23.2 wt% and SiO_2 falling to 18.99 wt%. Above this level SiO_2 fell gradually to 10.66 wt% for MQ17, Fe_2O_3 remained fairly consistent; albeit with a slight reduction to 31.67 wt% for MQ15 at 24 m, whilst Al_2O_3 rose steadily to a peak of 32.77 wt% for MQ15 and then fell again towards MQ17 with a valie of 25.01 wt%.

Zn, Ni and Cu (Figure 5.6b).

Again the concentrations are reasonably consistent with Zn ranging between 67 ppm and 89 ppm, Cu ranging from 16 ppm to 44 ppm and Ni ranging between 29 ppm and 46 ppm. Above this point a major increase occurs for Zn and Cu with values reaching 128 ppm and 113 ppm, respectively for MQ5 at 8 m above the quarry base. A smaller increase to 49 ppm is also present for Ni. From here values for Ni continue to increase to 60 ppm and 74 ppm for MQ6 and MQ7 at 8.5 m and 10 m, respectively, however, for Zn and Cu there are sharp falls in values to 35 ppm and 57 ppm, respectively. This is followed by another smaller rise for Zn and Cu to values of 80 ppm and 67 ppm with Ni also showing a small rise to 74 ppm. For the next 11 m all three elements show a steady reduction reaching some of their lowest values of 14 ppm, 11 ppm and 26 ppm for Zn, Cu and Ni, respectively. Immediately above this zone values rise markedly to 32 ppm, 66 ppm and 75 ppm for Zn, Cu and Ni, respectively and then remain fairly consistent towards the surface

Nb, Zr and TiO_2 (x100) (Figure 5.6c)

Considering Nb and Zr first, again concentrations are fairly consistent over the first 6 m with values ranging between 165 ppm and 187 ppm for Zr and 12.6 ppm and 17.9 ppm for Nb, although, there is a slight change from 5 m to 6.5 m with values falling to 141 ppm for Zr and 11.7 ppm for Nb. Above this level values rise markedly for MQ5 at 8 m above the quarry base with values of 220 ppm for Zr and 15.4 ppm for Nb, these values remain fairly consistent through to MQ9 at 12.5 m, after which values fall again for MQ10 to 133 ppm and 10.1 ppm for Zr and Nb, respectively, before rising again to 200 ppm and 14.2 ppm for MQ11. MQ12 sees another small reduction with values of 177 ppm and 13.4 ppm for Zr and Nb, respectively before another rise for MQ13 to 200 ppm for Zr and 14.2 ppm for Nb from which point values continue to increase up profile peaking at 454 ppm for Zr and 38 ppm for Nb for MQ16 before falling once more to 265 ppm and 21.1 ppm for Zr and Nb, respectively.

TiO_2 follows much the same profile with values ranging from 0.55 wt% to 0.68 wt% over the first 5 m with a small reduction to 0.49 wt% for MQ4 at 6.5 m. Values then rise steadily through MQ5 to a value of 1.06 wt% for MQ6 before falling again to 0.75 wt% for MQ7 at 10 m above the quarry base. Above this level values increase for MQ8 and MQ9 with values of 0.8 wt% and 0,86 wt%, respectively, before falling once more for MQ10 to a value of 0.46 wt%. MQ11 sees another increase, this time to 0.67 wt% and then concentrations continue to rise steadily, peaking at a value of 2.29 wt% for MQ16 at 26.5 m above the quarry base, prior to falling again to 1.42 wt% for MQ17.

Cr and V (Figure 5.6d)

On the whole Cr and V behave similarly, although Cr does show a significant increase in concentration for MQ3 and MQ4 to 298 ppm and 692 ppm, respectively. Whereas, V reports fairly uniform concentrations between 93 ppm and 128 ppm for these samples. Above this level Cr and V values become similar with V values increasing to 155 ppm and Cr values decreasing to 167 ppm for MQ5 at 8.5 m above the quarry base. After which both element concentrations for MQ6 increase to 380 ppm and 192 ppm for Cr and V, respectively, before falling through MQ7 with values of 231 ppm for Cr and 165 ppm for V to MQ8 with values of 129 ppm and 164 ppm for Cr and V, respectively. MQ9 sees another increase in concentrations to 220 ppm for Cr and 175 ppm for V, before falling steadily through MQ10, MQ11 and MQ12 to values of 87 ppm for Cr and 106 ppm for V. MQ13 reports a significant fall in concentrations with values becoming highly negative as is the case for MQ14. At 24 m above the quarry base, MQ15 returns

values to the positive with concentrations of 485 ppm for Cr and 232 ppm for V. Cr remains in the positive with a concentration of 50 ppm for MQ16 before falling again into highly negative values, whilst V falls back to negative values for MQ16 and MQ17.

Rb and Sr (Figure 5.7a)

Rb reports fairly consistent concentrations for the first 6.5 m above the quarry base with values ranging from 93 ppm to 123 ppm, whereas, Sr seems to report two sets of figures one set for MQ1 and MQ2 with values of 105 ppm and 103 ppm, respectively and the other set for MQ3 and MQ4 with figures of 49 ppm and 47 ppm, respectively. Above this level, MQ5 shows an increase for Rb to 148 ppm and a decrease for Sr to 13 ppm. Rb concentrations then fall significantly to 27 ppm whilst Sr concentrations increase slightly to 25 ppm. From here Rb increases slightly up profile to MQ8 at 11 m above the quarry base and remains within a few ppm until MQ12 at 21 m. MQ13 also from the 21 m zone, reports the Rb concentration as decreasing from 33 ppm to 18 ppm. Sr concentrations consistently diminish up profile from 25 ppm at MQ6 to 7 ppm for MQ12 at 21 m above the quarry base, whilst MQ13 concentration increases to 25 ppm. Sr continues to increase up profile to MQ16 with a concentration of 54 ppm before finally decreasing to 26 ppm for MQ17. Rb also continues to increase up profile to MQ16 with a concentration of 35 ppm before falling to 16 ppm for MQ17.

Summed Alkalis (Figure 5.7b)

Concentrations of the summed alkalis starts at 10.46 wt% for MQ1 and gradually decrease up profile to 9.64 wt % for MQ2, 7.79 wt% for MQ3, 7.75 wt% for MQ4 and 6.64 wt% for MQ5 at 8 m above the quarry base. Above this level concentrations fall sharply to 0.91 wt% and 0.93 wt% for MQ6 and MQ7, respectively, before increasing to 2.01 wt% for MQ8. From here concentrations remain fairly consistent, ranging between 1.78 wt% and 2.09 wt%. Again MQ13 reports a discernible change with concentration decreasing to 0.55 wt% and then increasing slightly up profile to 0.99 wt% for MQ16 before finally decreasing again to 0.46 wt% for MQ17.

Pb and MnO (x100) (Figure 5.7c)

Firstly considering Pb, concentrations are fairly consistent throughout the lower 6.5 m of the profile ranging from 10 ppm to 14 ppm, rising to 18 ppm for MQ5 and 39 pm for MQ6 at 8.5 m above the quarry base. Concentrations then fall to 29 ppm for MQ7 and then fall further to 9 ppm for MQ8. From here concentrations fall slightly from 9 ppm to

5 ppm for MQ12 at 21 m above te quarry base. Also at 21 m above the quarry base MQ13 again reports a discernible change with concentration increasing to 55 ppm and remaining within a few ppm throughout the remainder of the profile.

MnO concentrations are consistently low throughout the whole profile ranging from a minimum of 0.01 wt% to a maximum of 0.13 wt%. However, the concentrations do start off at the higher end of the range within the lowest parts of the profile (MQ1 to MQ4), with values ranging from 0.09 wt% to 0.13 wt%. MQ5 demarcates the main change where concentration drops to 0.03 wt% and remains within 0.01 wt% throughout the remainder of the profile with the exception of MQ17 where the concentration of 0.12 wt% returns to a similar value to that of the unaltered protolith.

Ba

Ba concentrations begin at 741 ppm for MQ1 and then fall to 614 ppm for MQ2 and 437 ppm for MQ3 before rising again to 760 ppm and 756 ppm for MQ4 and MQ5, respectively. MQ6 at 8.5 m above the quarry base indicates a significant change with concentration falling to 262 ppm and continuing at this level for MQ7 with a value of 267 ppm. MQ8 reports another obvious change as concentrations increase once more to 741 ppm and then remaining fairly consistent up profile to MQ12 at 21 m above the quarry base. MQ13, also at 21 m above the quarry base shows another very discernible change with the concentration falling dramatically to 60 ppm where it remains for MQ14 before increasing to 155 ppm and 138 ppm for MQ15 and MQ16, respectively and then finally falling to 33 ppm for MQ17.

Chapter 6. Results - Hydrochemical observation for the Chapora and Zuari Rivers systems

The following chapter considers the main area of study: the Chapora and Zuari River systems and is presented here to address objectives 2 and 3. The chapter begins with section 6.1 by documenting the method used to estimate the fluvial flux for the rivers based on precipitation and drainage basin area. Section 6.2 follows by considering the hydrochemical observations documenting temporal variation in river water pH, temperature, electrical conductivity and dissolved oxygen before moving on to document and describe the temporal variation in major and trace element concentrations. Section 6.3 discusses the element ratios of Ba/Sr and Y/Ho, section 6.4 discusses REE concentrations for the river water samples, whilst section 6.5 concludes the chapter by documenting and describing the calculated saturation indices.

6.1. Fluvial flux data Zuari and Chapora

Since no fluvial flux data exist for either of these rivers for the sampling period in question, values were calculated based upon monthly precipitation data for Panjim, India (NOAA, 2012) and the drainage area of each river. The drainage area of the Zuari River is stated as 550 km^2 (Nair, 2003), but, the ENVIS website states that it is 973 km^2 (ENVIS, 2012). The drainage area of the Chapora River is 255 km^2 (ENVIS, 2012). As there was such a significant difference in the two published values for the Zuari drainage basin the drainage basins for both rivers was calculated independently using Google Earth 6.2 and topographic maps. The result obtained for the Zuari River was 1059 km^2, and this was within 10% of that published on the ENVIS website. The result calculated for the Chapora River was 588 km^2, of which 235 km^2 is within Goa state, the remainder being located in Maharashtra: this value was also within 10% of the reported value of 255 km^2 (ENVIS, 2012). The independently determined values were used for all subsequent calculations. It was assumed that the whole drainage basin receives the same quantity of precipitation and that 63% of this precipitation enters the rivers. This is based on the expression:

$$R = P - ET$$

Where, R = run-off, P = precipitation and ET = evapotranspiration. White and Blum (1995) provided ET values for alpine/temperate climates and tropical climates of 500 mm yr^{-1} and 1400 mm yr^{-1}, respectively. If we use this tropical value of 1400 mm yr^{-1}

and calculate this as a percentage of the annual precipitation (3748 mm yr^{-1}) we get c. 37% ET or 63% run-off. For example; the precipitation data for Panjim, India for the month of June 2007 was 1077 mm. To calculate the volume of water, this value (converted to metres) was multiplied by the drainage area in square metres: this value was then multiplied by 63% to determine the flux. The values presented are quoted with a tolerance of plus or minus 10%.

Zuari River water volume for June 2007 = (1.077 m x 1.059 x 10^9 m^2) = 1.14 x 10^9 m^3

To convert this to a flow in m^3 s^{-1} the value was divided by the number of seconds in June. There are 30 days in June and 86,400 seconds per day giving 2.59 x 10^6 s for the month.

Flow = 1.14 x 10^9 m^3 / 2.59 x 10^6 s = 440 m^3 s^{-1} x 0.63 = 277 ± 44 m^3 s^{-1}

This calculated value is considerably higher than the value of 115 - 125 m^3 s^{-1} reported for the Zuari River for August 1993 (Unnikrishnan et al., 1997), although their value is documented as discharge at the upstream end of the channel and is taken to be entirely derived from the fresh water influx. The calculated value is taken over the entire drainage basin area and as such appears to be a reasonable estimate. Therefore Table 6.5 lists the monthly precipitation data (NOAA, 2012) and the calculated monthly river flows for the Zuari and the Chapora Rivers based on the above parameterisation.

Table 6. 1 Monthly precipitation data and calculated river flows for the Zuari and Chapora Rivers. Values are quoted with a tolerance range of ± 10%.

Month	Monthly Precipitation (mm)	Calculated River Flow ($m^3 s^{-1}$)	
		Zuari	Chapora
May 2007	114	29.4±5	16.3±3
June 2007	1077	277±44	154±24
July 2007	689	177.5±27	98.5±15
August 2007	887	228.5±35	126.9±19
September 2007	764	196.8±31	109.3±17
October 2007	82	21.1±3	11.7±2
November 2007	76	19.6±3	10.9±2
December 2007	1	0.3±0.04	0.1±0.02
January 2008	0	0	0
February 2008	0	0	0
March 2008	43	11.1±2	6.2±1
April 2008	15	3.95±0.5	2.1±0.3
May 2008	10	2.6±0.5	1.4±0.2
June 2008	783	201.7±32	112±18
July 2008	553	142.4±22	79.1±12
Annual May 2007-April 2008	3748	965.5±148	536.1±82
Discharge weighted mean	425	137	76

The annual river run-off value for the Zuari River as calculated above as 965.5±148 $m^3 s^{-1}$ can be converted to $km^3 yr^{-1}$ as follows:

(965.5 $m^3 s^{-1}$ x 31536000 s yr^{-1}) / 1 x 10^9 m^3 km^{-3} = 30.4±4.7 $km^3 yr^{-1}$

This annual river flux can now be compared to the average annual run-off of 9 $km^3 yr^{-1}$ as quoted by Nair et al, 2003. The calculated value is clearly considerably higher than that previously quoted. One reason for this disparity is that the calculated values above are based on a measured drainage basin area of 1059 km^2 compared to that of 550 km^2 reported by Nair et al (2003). If we increase the Nair et al. value pro rata by the difference in drainage basin area we get a figure of 17.3 $km^3 yr^{-1}$. This is still 43% lower than the calculated value of 30.4 $km^3 yr^{-1}$, so there is still a major discrepancy.

It could be that the evapotranspiration was even higher than the 1400 mm yr^{-1} value used or that %ET varies seasonally, which is a phenomenon observed by White and Blum (1995) where, %ET is much higher in watersheds with low precipitation compared to watersheds with high precipitation. This is especially true in tropical climates where high temperatures exist throughout the entire year.

Alternatively, another assumption that has been made in the calculations due to the limited availability of rainfall data is that the same amount of rainfall occurs over the entire drainage basins of both rivers. Based on the disparity discussed above this is probably not correct. The rainfall data used is from Panjim which is on the coast close to the Zuari River estuary but a few tens of kilometres south of the Chapora River and many tens of kilometres from the escarpment.

6.2. Hydrochemical observations and results

This section evaluates the river water samples collected over a 15 month period (May 2007 – July 2008) as analysed using ICP-OES (estuarine cations), ion chromatography (all anions), ICP-MS (non estuarine cations). The section starts by tabulating the elements that were analysed along with the technique used and the location at which the analysis was completed Table 6.1. This is followed by a section discussing pH, temperature, conductivity and dissolved oxygen, followed by documentation and discussion of the various major and trace elements analysed. The section then moves to discussing Rare Earth Elements (REEs) before concluding with a discussion on calculated Saturation Indices (SI).

Table 6.2 Elements analysed and techniques used, Ion Chromatography (IC), Inductively Coupled Plasma – Optical Emission Spectroscopy (ICP-OES) and Inductively Coupled Plasma – Mass Spectroscopy (ICP-MS) along with their respective detection limits.

Element	Birkbeck ICP-OES (estuarine cations)	Detection limit (ppm)	Birkbeck IC (anions)	Detection limit (ppm)	Open University ICP-MS (Non estuarine cations)	Detection limit (ppt)
Ca	✓	>1			✓	10-100
Na	✓	>1			✓	10-100
K	✓	>1			✓	10-100
Fe	✓	>1			✓	10-100
Mn	✓	>1			✓	10-100
Mg	✓	>1			✓	10-100
P	✓	>1			✓	10-100
Al					✓	10-100
Si	✓	>1			✓	10-100
Sr	✓	>1			✓	<10
Rb					✓	<10
Cl			✓	>1		
F			✓	>1		
N			✓	>1		
S			✓	>1		
V					✓	10-100
Cr					✓	10-100
Co					✓	10-100
Ni					✓	10-100
Cu					✓	10-100
Zn					✓	10-100
Pb					✓	<10
Ba					✓	<10
REE					✓	<10

pH

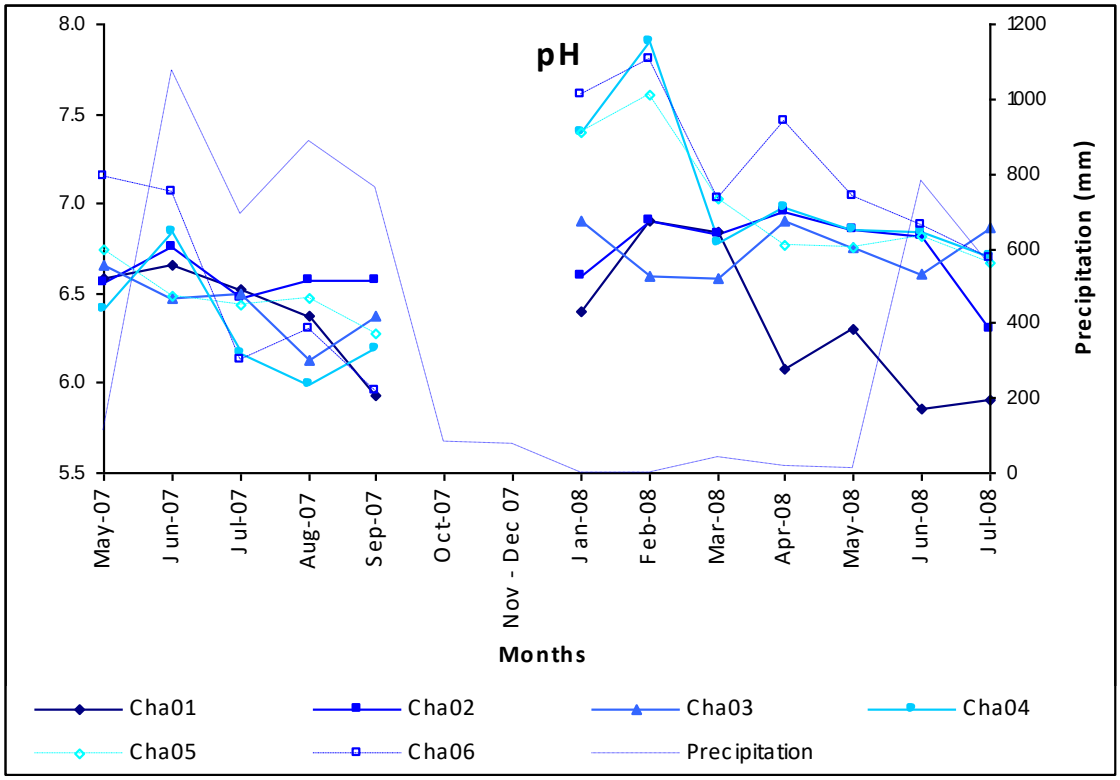

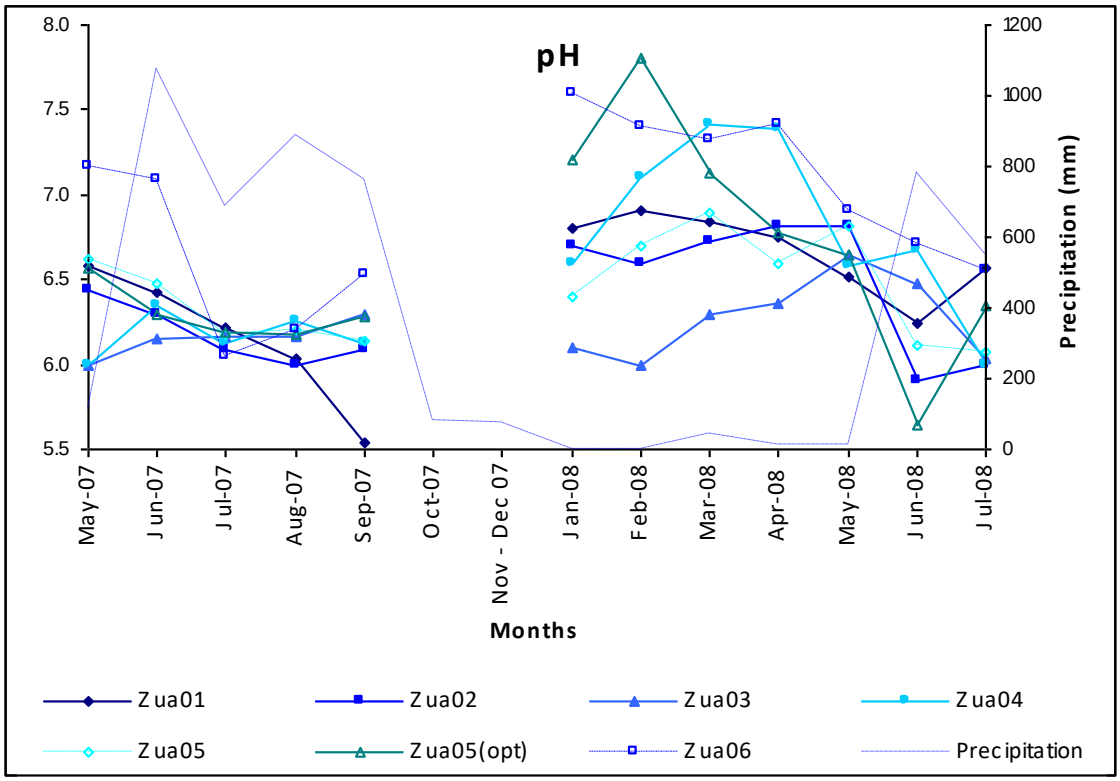

Figure 6. 1 Temporal graphs for pH for the Chapora and Zuari River localities.

It can be clearly seen in Figure 6.1 that pH values vary seasonally, with the highest values occurring during February (dry season) and the lowest values occurring during July and August (monsoon season) for both rivers. Interrogating the actual dataset we can see that the pH varies from 5.86 in June 2008 (monsoon season) to 7.9 in February 2008 (dry season) for the Chapora River and from 5.54 in September 2008 (monsoon season) to 7.8 in February 2008 (dry season) for the Zuari River. In addition, both graphs show a smaller variation during the monsoon periods and a wider variation during the dry season with the largest variation occurring in February for both rivers with values ranging between 6.08 for Cha 03 and 7.9 for Cha 04 for the Chapora River and 6.0 for Zua 03 and 7.8 for Zua 05opt for the Zuari River.

Water temperature

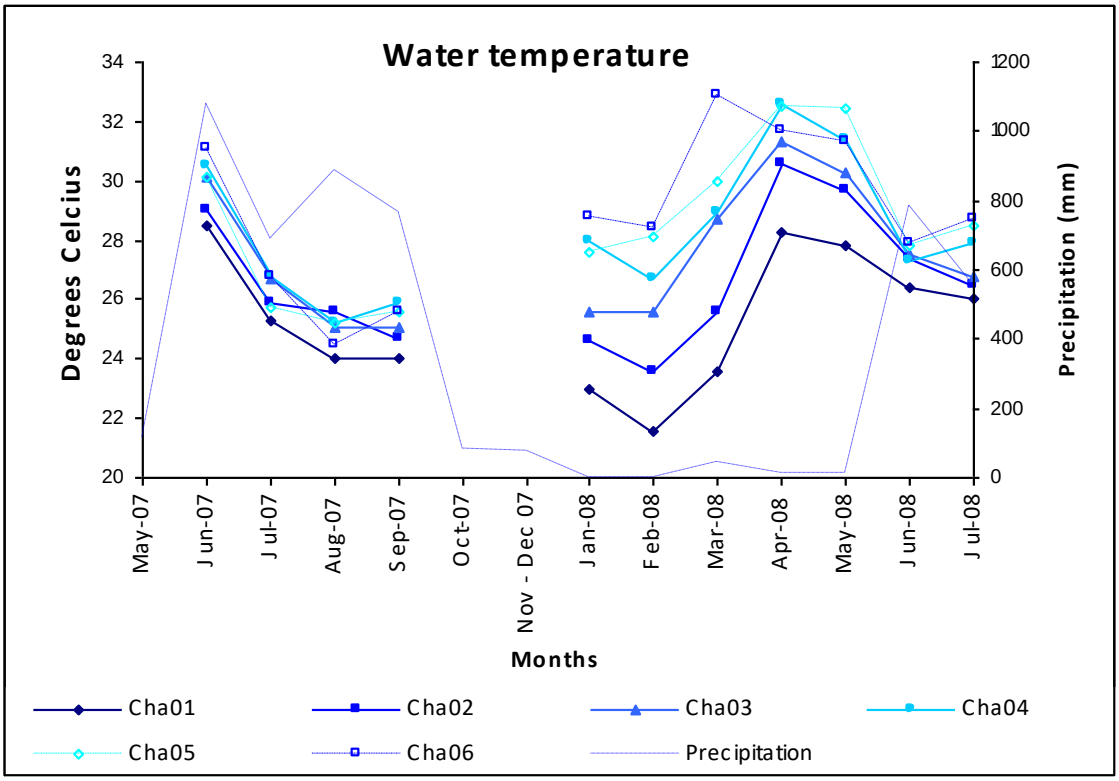

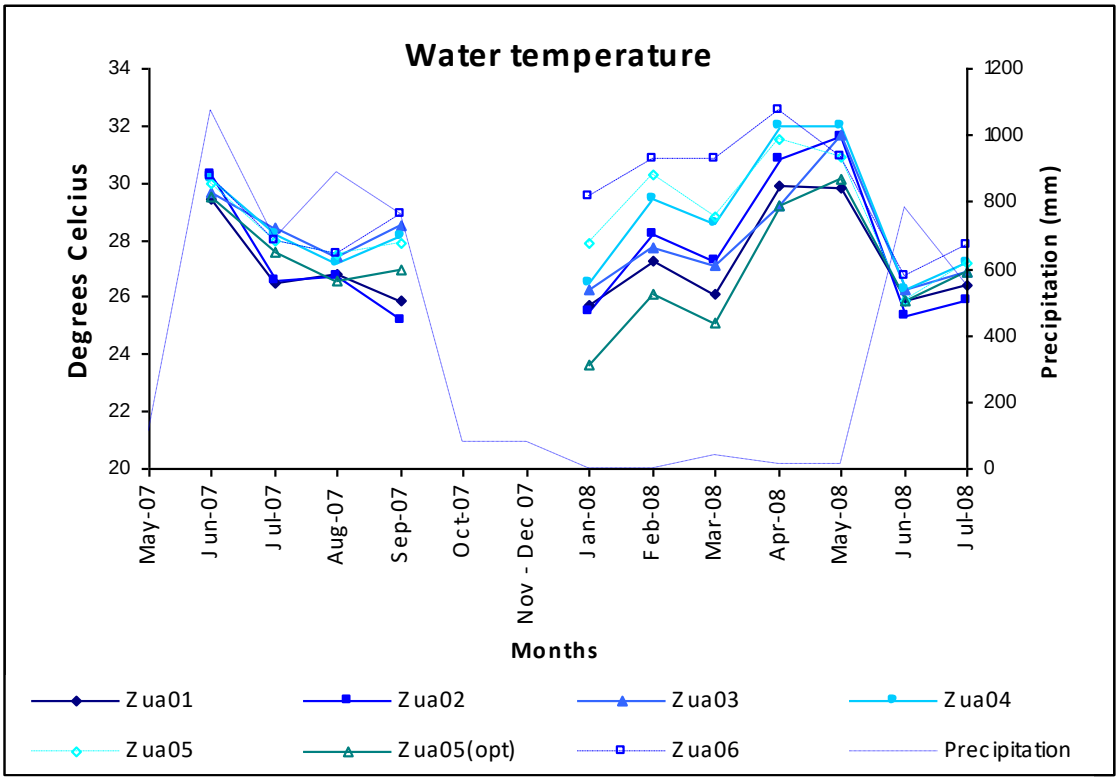

Figure 6.2 Temporal graphs for water temperature for the Chapora and Zuari River localities.

Figure 6.2 shows water temperature for both the Chapora and Zuari Rivers reporting broadly similar trends and values with the higher temperatures occurring towards the end of the dry season and the lowest towards the end of the monsoon period. The Chapora River reports high temperatures of 31.6ºC for Cha 06 in June 2007 and 32.9ºC again for Cha 06 in March 2008, whilst the Zuari River reports high temperatures of 30.3ºC for Zua 02 in June 2007 and 32.5ºC for Zua 06 in April 2008. It is also noticeable that in general water temperature increases travelling downstream, this is particularly evident for the Chapora River, however, a similar trend is apparent for the Zuari River, although, not as consistent, but still with the more estuarine localities reporting the highest temperatures.

Electrical conductivity

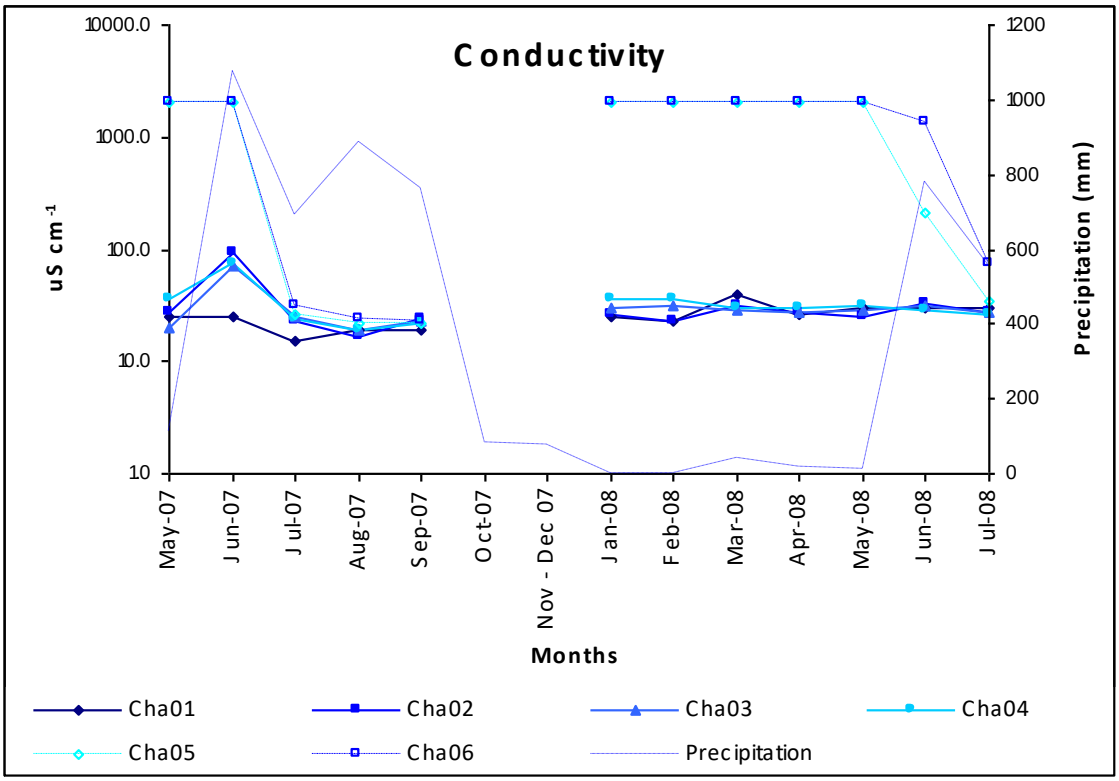

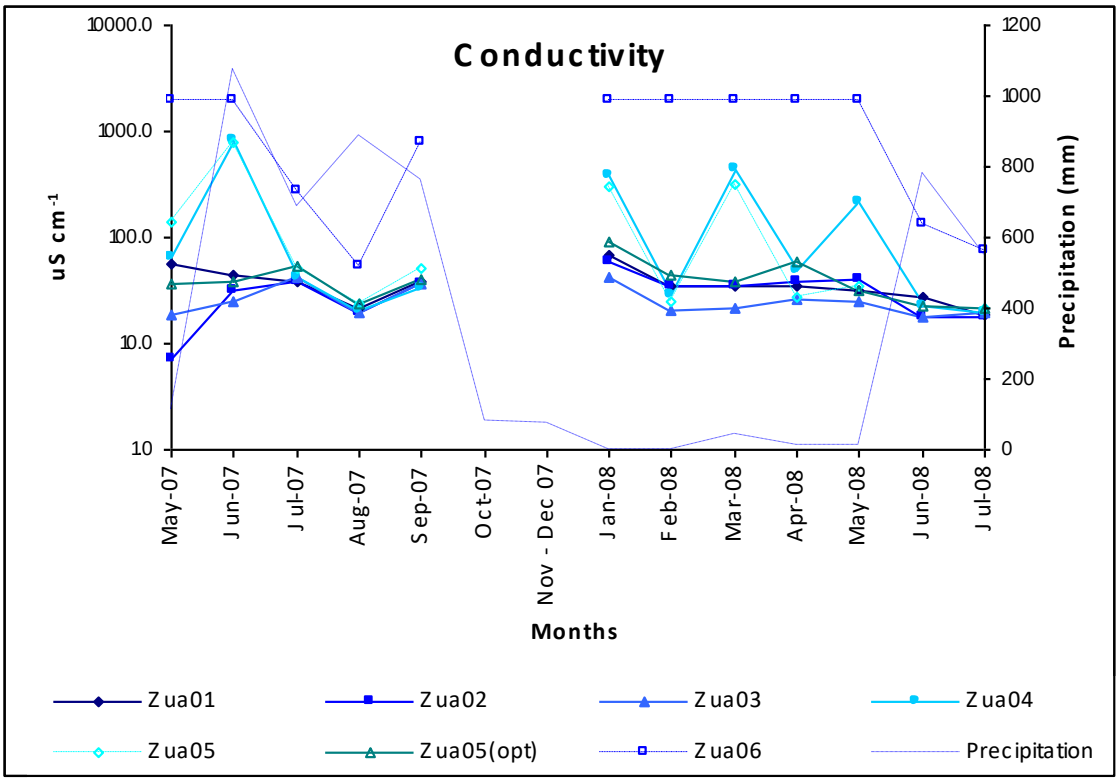

Figure 6.3 Temporal graphs for electrical conductivity for the Chapora and Zuari River localities.

The conductivity data for the upper localities of the Chapora River, Cha 01 – Cha 04 report fairly consistent values ranging between 15 µS cm^{-1} for Cha 01 in July 2007 and 40 µS cm^{-1} for Cha 01 in March 2008. However, there is a distinct rise in values to c.90 µS cm^{-1} for Cha 02, Cha 03 and Cha 04 in June 2007 coinciding with the onset of the monsoon rains. The data for the more estuarine localities, Cha 05 and Cha 06 are very different for the dry season months with all values being significantly higher and most reporting values of 2000 µS cm^{-1}, which is the maximum limit of the conductivity meter.

The data for the Zuari River is slightly more complicated and can best be described in three parts. The first describing the upper localities, Zua 01, 02, 03 and 05opt where the values plot between 7 µS cm^{-1} for Zua 02 in May 2007 and 91 µS cm^{-1} for Zua 05opt in January 2008. The second trend describing the more estuarine localities is similar to that of the Chapora River with the majority of the dry season months reporting values of 2000 µS cm^{-1} again limited by the conductivity meter. The main difference between the Chapora and Zuari graphs is the saw tooth profile for Zua 04 and Zua 05, which show consistent peaks in June 2007, January 2008, March 2008 and May 2008, these are likely representative of estuarine influence.

Dissolved Oxygen

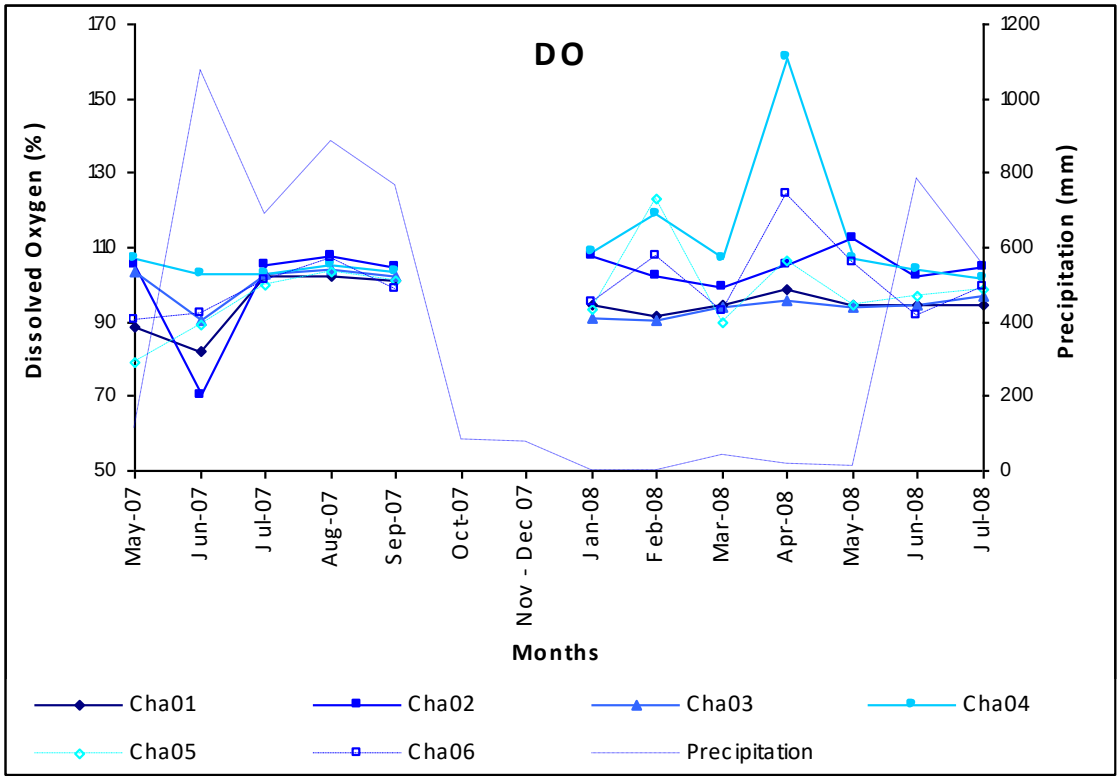

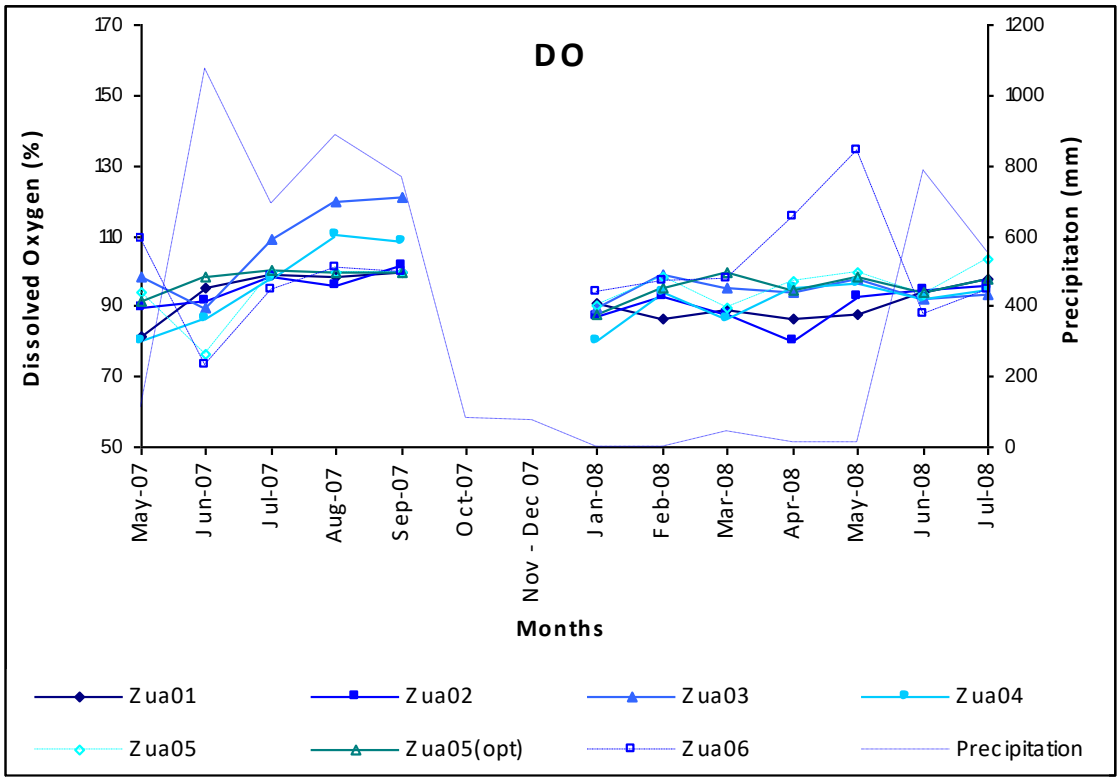

Figure 6.4 Temporal graphs for dissolved oxygen for the Chapora and Zuari River localities.

The dissolved oxygen data for the Chapora River ranges from a low of 70% for Cha 02 in June 2007 to a high of 161.3% for Cha 04 in April 2008. The localities fall into two broad trends, one comprising the upper localities, Cha 01, 02 and 03 and the other comprising the lower localities, Cha 04, 05 and 06. The first trend describing the upper localities can be described as relatively flat with values ranging between 88.7% for Cha 01 in May 2007 and 112.2% for Cha 02 in April 2008, albeit with a distinct reduction in dissolved oxygen values in June 2007 including the low value of 70% for Cha 02. The second trend describing the localities Cha 04, 05 and 06 report relatively flat profiles for the 2007 months with a slight increase in values for Cha 05 and 06, however, the values for the dry season months show a saw tooth profile with values fluctuating on a monthly basis between lows in January, March and May and highs in February and April 2008.

The dissolved oxygen data for the Zuari River can best be described as displaying three trends. The first comprises the upper most two localities, Zua 01 and Zua 02; these begin at between 81.6% for Zua 01 and 89.7% for Zua 02 in May 2007 and gently increase to 99.4% for Zua 01 and 101.4% for Zua 02 in September 2007. Values then reduce slightly to between 90.8% for Zua 01 and 87.0% for Zua 02 in January 2008 remaining relatively consistent through to May 2008 with values of 87.7% for Zua 01 and 92.9% for Zua 02 before rising slightly through June and into July 2008 with values of 97.7% for Zua 01 and 95.9% for Zua 02. The second trend comprises Zua 03, 04 and 05 opt and can be described as being broadly similar to the first trend albeit with more dramatic increases during the 2007 monsoon months with values rising to 121% for Zua 03 in September 2007. The 2008 data ranges between 80.3% for Zua 04 in January to 99.5% for Zua 05opt in March 2008. The final trend comprising the more estuarine localities of Zua 05 and Zua 06 show similar patterns during the 2007 monsoon months starting with values between 93.7% for Zua 05 and 109.1% for Zua 06 in May 2007 before falling sharply in June to 73.4% and 76.7% for Zua 05 and Zua 06, respectively. Values then increase again to similar values to those recorded for May. The values then remain fairly consistent throughout the sampling duration with the exception of two positive deviations for Zua 06 to 115.1% and 134.1% in April and May, respectively.

6.2.1. General trends

The following section describes briefly each element in turn as plotted in the major and trace element plots in order to assist with the identification of patterns and trends. This is particularly important where occasional exceptionally high or low values are present which have a tendency to obscure other trends. In these cases those exceptional values have been temporarily removed to allow for any underlying trends to be described.

6.2.1.1. Major elements

The major cations and anions recorded in both the Chapora River system and the Zuari River system vary both spatially along each river system as it flows from its upper reaches towards the Arabian Sea, and temporally as the rivers experience the extreme variability of the 2007 monsoon season through the dry season and into the beginnings of the 2008 monsoon season. The following section describes some of the trends observed within the temporal data and should be read in conjunction with Figures 6.5 to 6.27. No samples were collected for either river during November and December 2007 due to a breakdown in logistics. No data are available for May 2007 for either river or for October 2007 for the Zuari River due to loss of samples. Only values that are deemed to be unaffected by estuarine influence are included in the graphs, the method for their inclusion or exclusion will be explained in a subsequent section.

Sodium (Na)

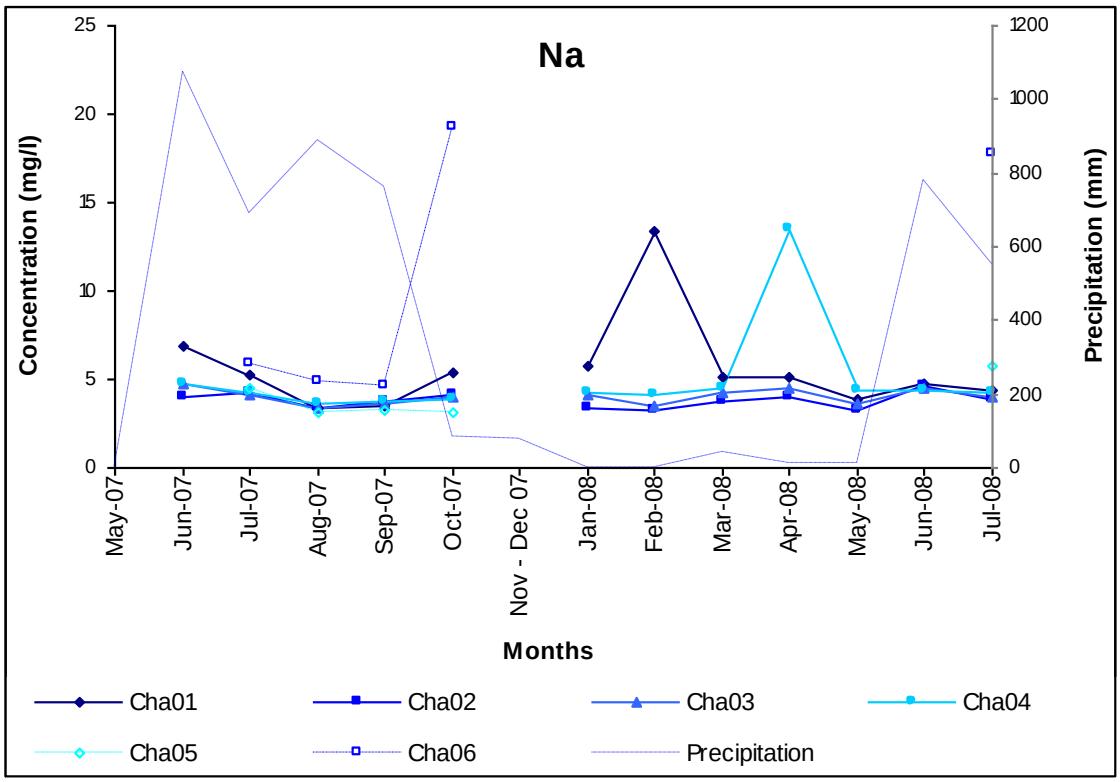

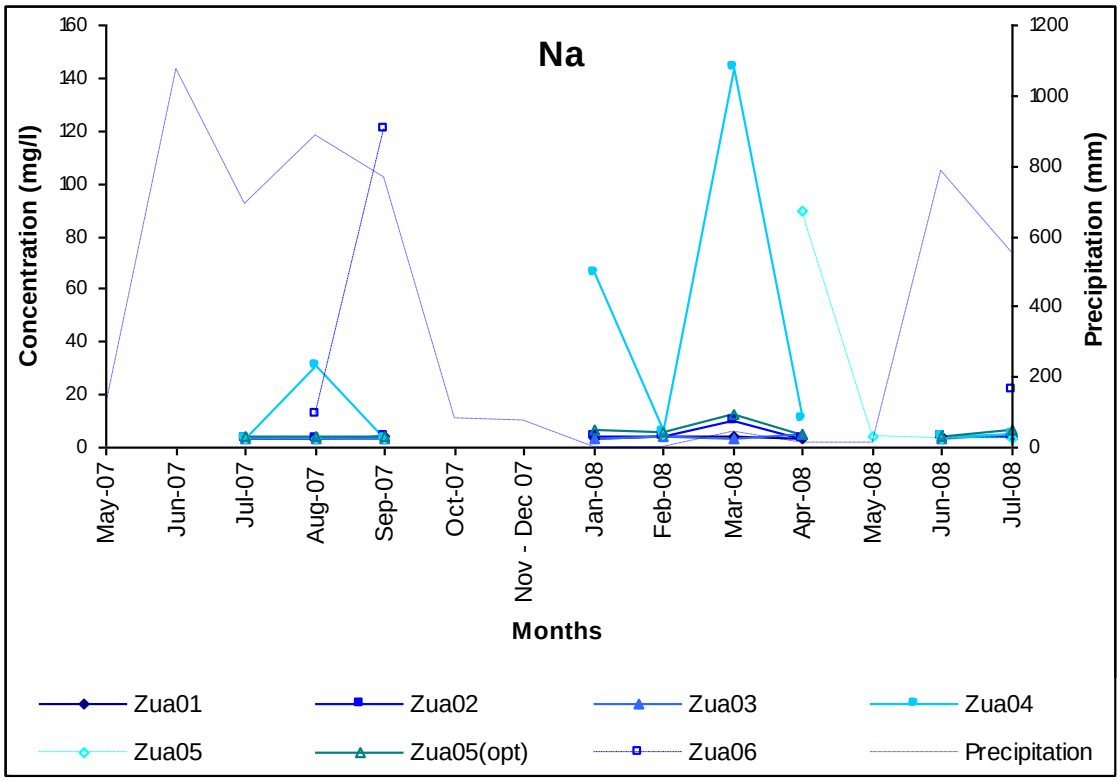

Figure 6.5 Temporal graphs for Na for the Chapora and Zuari River localities.

For the Chapora River the dominant trend for Na is one of fairly low concentrations which remain within a relatively narrow range of values. These values range from a low of 3.17 mg l^{-1} for Cha 05 in August and October 2007 to a high of 6.85 mg l^{-1} for Cha 01 in June 2007. However, there are three pronounced deviations from this general trend, those being, a value of 19.2 mg l^{-1} for Cha 06 in October 2007, a value of 13.4 mg l^{-1} for Cha 01 in February 2008 and a value of 13.5 mg l^{-1} for Cha 04 in April 2008.

For the Zuari River the graph appears a little more complicated but can best be described in three parts; the 2007 monsoon, the 2007 dry season and the 2008 monsoon. During the 2007 monsoon the general trend is similar to that of the Chapora River for the same period, although no data are available for June 2007. The localities Zua 01, Zua 02, Zua 03, Zua 04 and Zua 05opt all displaying fairly low concentrations which remain within a relatively narrow range of values. These values range from a low of 2.99 mg l^{-1} for Zua 03 in August 2007 to a high of 4.42 mg l^{-1} for Zua 05opt in September 2007. However, there is a pronounced deviation from this general trend for Zua 04 in August 2007 with a value of 31.3 mg l^{-1}. During the 2007 dry season again the values are fairly consistent ranging from a low of 3.29 mg l^{-1} for Zua 01 in January 2008 to a high of 12.7 mg l^{-1} for Zua 05opt in March 2008, however, there are 3 significant deviations from this trend with values of 65.9 mg l^{-1} for Zua 04 in January 2008, 145 mg l^{-1} for Zua 04 in March 2008 and 89.7 mg l^{-1} for Zua 05 in April 2008. Finally, the 2008 monsoon season again displays a narrow range of fairly low values ranging from 3.37 mg l^{-1} for Zua 05 in July 2008 to a high of 6.35 mg l^{-1} for Zua 05opt in July 2008. Other than the general trend described above the most significant observation is that no fewer than three localities show a positive deviation in March 2008, which is most likely the result of a slight rinsing out of precipitated minerals (Section 7.1.2) due to the 43 mm of the precipitation occurring in that month.

Potassium (K)

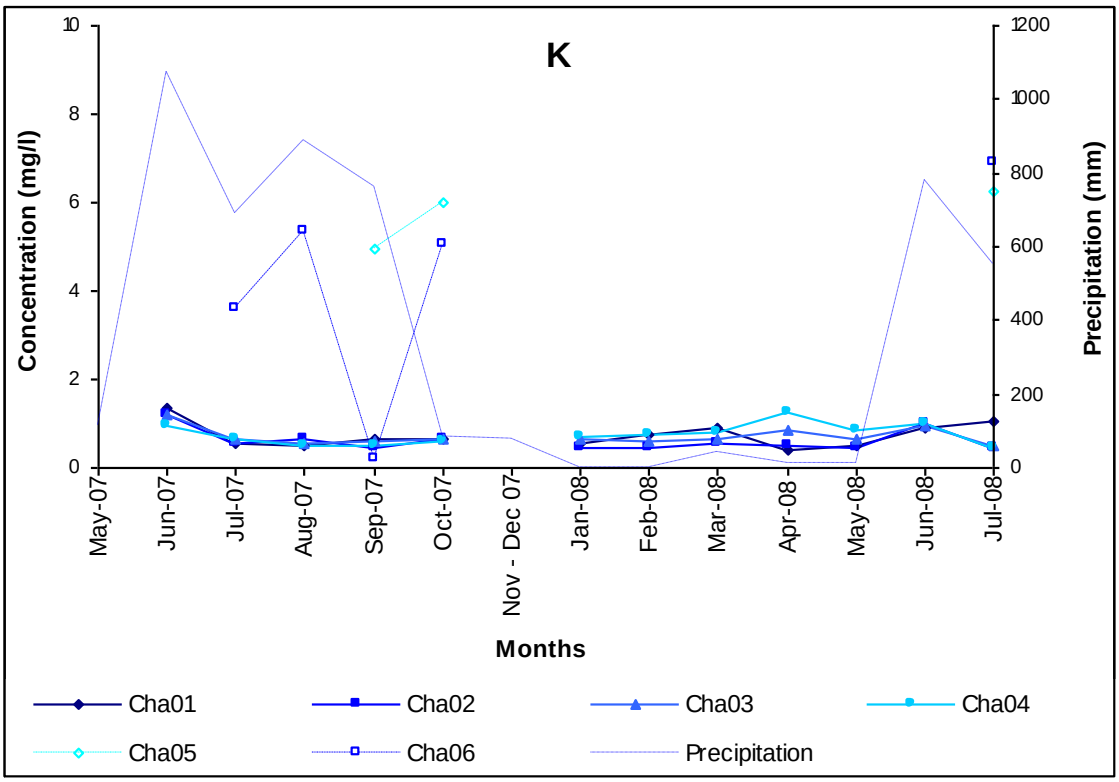

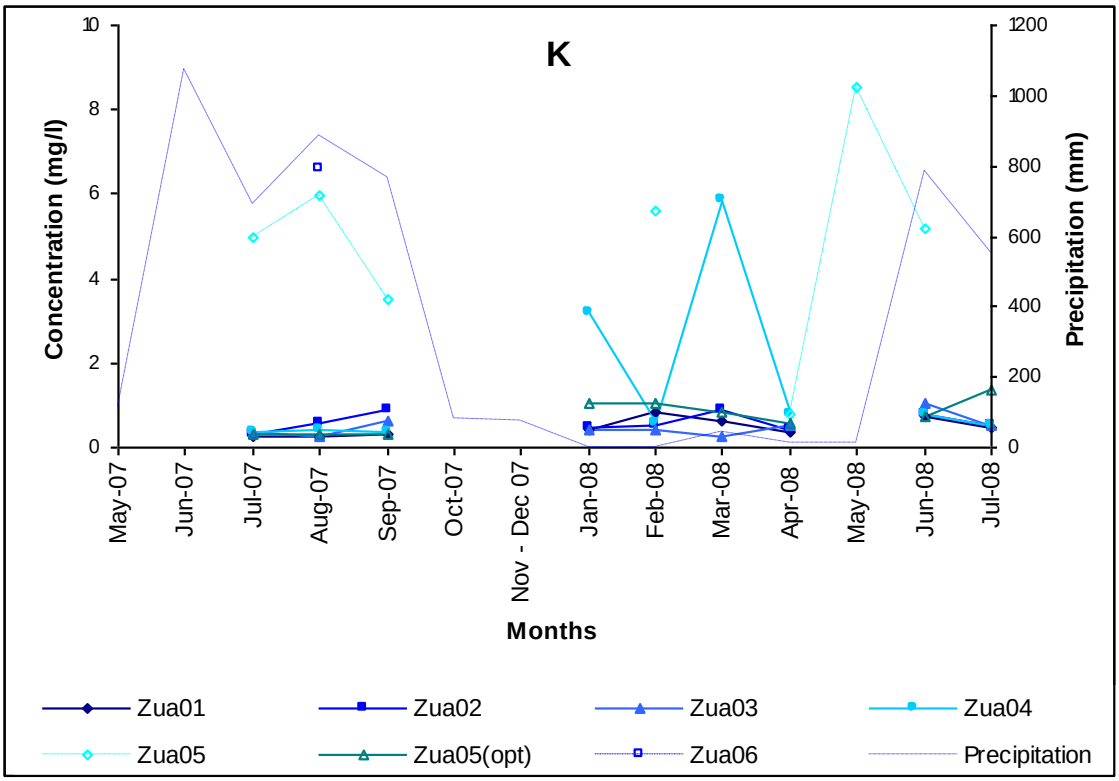

Figure 6.6 Temporal graphs for K for the Chapora and Zuari River localities.

The upper localities of the Chapora, Cha 01, 02, 03 and 04 all have values that are <1.5 mg l^{-1}, although within this there is an observable pattern which starts with relatively high values for all four localities in June 2007, ranging from 1.38 mg l^{-1} for Cha 01 to 0.93 mg l^{-1} for Cha 04. Concentrations then fall sharply to between 0.55 mg l^{-1} for Cha 02 and 0.65 mg l^{-1} for Cha 03 in July 2007. From here the range and size of the values increase towards the next monsoon beginning in June 2008, at which all four localities display a similar peak ranging from 0.89 mg l^{-1} for Cha 01 to 1.0 mg l^{-1} for Cha 04 followed by a subsequent fall in July 2008. However, the values for Cha 05 and Cha 06, whilst still low, vary considerably from the other values. Cha 05 reports peaks of 4.96 mg l^{-1} in September 2007, 5.99 mg l^{-1} in October 2007 and 6.27 mg l^{-1} in July 2008, whilst Cha 06 reports peaks of 3.58 mg l^{-1} in July 2007, 5.34 mg l^{-1} in August 2007, 5.05 mg l^{-1} in October 2007 and 6.92 mg l^{-1} in July 2008.

Like the Na graph for the Zuari River the K graph can best be described in three parts; the 2007 monsoon, the 2007 dry season and the 2008 monsoon. During the 2007 monsoon the general trend is similar to that of the Chapora River for the same period although no data are available for May 2007. Values in July 2007 fall within a small range for Zua 01, 02, 03, 04 and 05opt, ranging from 0.28 mg l^{-1} for Zua 01 to 0.38 mg l^{-1} for Zua 04. These values then rise gradually to between 0.34 mg l^{-1} for Zua 05opt and 0.91 mg l^{-1} for Zua 02 in September 2007. Although there are significant deviations from this trend for Zua 05 and Zua 06, with values of 4.98 mg l^{-1} in July 2007, 5.97 mg l^{-1} in August 2007 and 3.49 mg l^{-1} in September 2007 for Zua 05 and 6.58 mg l^{-1} for Zua 06 in August 2007. Throughout the dry season the values remain fairly consistent between 0.29 mg l^{-1} for Zua 03 in March 2008 and 1.04 mg l^{-1} for Zua 05opt in February 2008, although the values do fall slightly towards April 2008 where the values once again fall within a very small range of 0.38 mg l^{-1} for Zua 01 and 0.55 mg l^{-1} for Zua 05opt. However, Zua 04 also displays two significant deviations from the main trend with values of 3.21 mg l^{-1} in January 2008 and 5.88 mg l^{-1} in March 2008. Throughout the 2008 dry season the values rise slightly to between 0.71 mg l^{-1} for Zua 01 and 1.04 mg l^{-1} for Zua 03 in June 2008 before falling again to between 0.45 mg l^{-1} for Zua 01 and 0.51 mg l^{-1} for Zua 04 in July 2008, with the exception of Zua 05opt which continues to rise to 1.39 mg l^{-1}. Finally, Zua 05 also displays significant deviations throughout both the dry season and subsequent beginnings of the 2008 monsoon with values of 5.59 mg l^{-1} in February 2008, 8.51 mg l^{-1} in March 2008 and 5.19 mg l^{-1} in June 2008.

Magnesium (Mg)

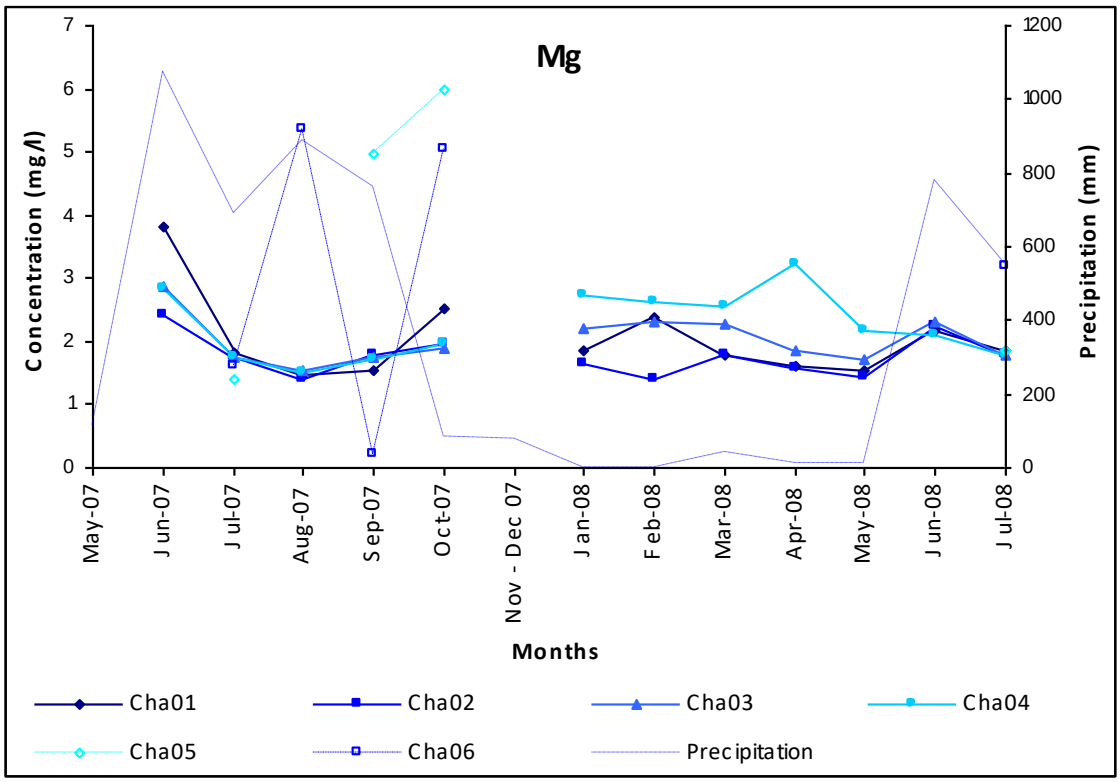

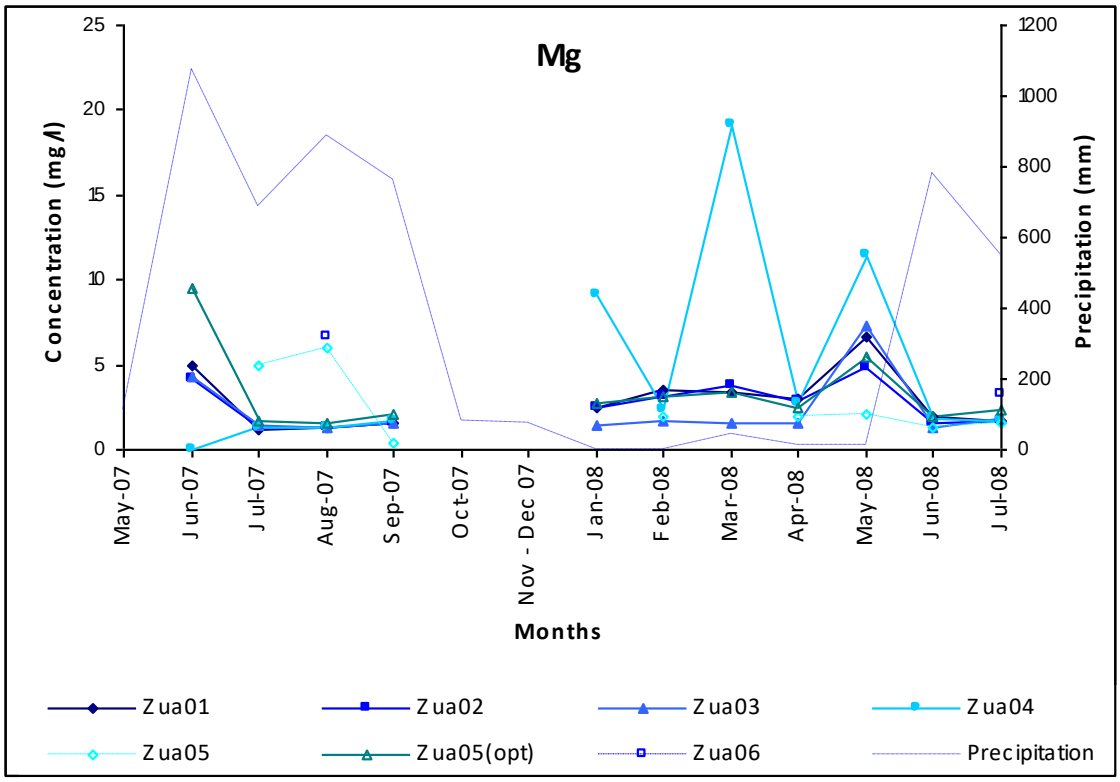

Figure 6.7 Temporal graphs for Mg for the Chapora and Zuari River localities.

Firstly, considering Cha 01, 02, 03 and 04 only, all values fall between 1.39 mg l^{-1} for Cha 02 in February 2008 and 3.8 mg l^{-1} for Cha 01 in June 2007. However, again certain trends can be observed, for example, values start relatively high in June 2007 for all four localities with values ranging from 2.4 mg l^{-1} for Cha 02 and 3.8 mg l^{-1} for Cha 01. Values then fall for these localities for the subsequent two months of July and August to a low of between 1.4 mg l^{-1} for Cha 02 and 1.54 mg l^{-1} for Cha 03, before rising once again through September and October to between 1.91 mg l^{-1} for Cha 03 and 2.53 mg l^{-1} for Cha 01. During the dry season months from January to April 2008 the range of values widen out, showing greater variability between the localities; this is most prominent in April with values ranging from 1.59 mg l^{-1} for Cha 02 to 3.21 mg l^{-1} for Cha 04. However, once moving back towards the monsoon season the range of values tightens once more with all four localities following similar trends, with values falling in May 2008 then rising in June before falling again in July. It appears that the monsoon rainfall is having a significant controlling factor on the river concentrations making values fairly consistent within at least the upper reaches (Cha 01, 02, 03 and 04) of the river, whilst during the dry season other factors appear to be affecting the rivers more locally. However, both Cha 05 and Cha 06 display deviations from the described trend, with values of 4.96 mg l^{-1} in September 2007 and 6.0 mg l^{-1} in October 2007 for Cha 05 and 5.34 mg l^{-1} in August 2007 and 5.05 mg l^{-1} in October 2007 for Cha 06.

Again, initially considering Zua 01, 02, 03 and 05opt only, all values are below 10 mg l^{-1}. Once again, however, there is a clear trend starting with higher values for all these localities in June 2007 ranging between 4.23 mg l^{-1} for Zua 02 to 9.55 mg l^{-1} for Zua 05opt. Values then fall sharply to between 1.2 mg l^{-1} for Zua 02 and 1.67 mg l^{-1} for Zua 05opt before slowly rising again through August and September to between 1.56 mg l^{-1} for Zua 03 and 2.12 mg l^{-1} for Zua 05opt. During the dry season, as with the Chapora River the range of values widen out to once again represent the local controls on river concentration. However, unlike the Chapora River there is a significant positive deviation in May 2008 with values ranging between 4.86 mg l^{-1} for Zua 02 and 7.27 mg l^{-1} for Zua 03 before dropping again in June to between 1.27 mg l^{-1} for Zua 03 and 2.01 mg l^{-1} for Zua 05opt the rising slightly in July 2008. However, Zua 04 also displays a positive deviation in May 2008 with a value of 11.5 mg l^{-1} along with two other positive deviations with values of 9.07 mg l^{-1} in January 2008 and 19.2 mg l^{-1} in March 2008. Other positive deviations also occur for Zua 05 with value of 4.98 mg l^{-1} in July 2007 and 5.97 mg l^{-1} in August 2007 and Zua 06 with a value of 6.58 mg l^{-1} also in August 2007.

Calcium (Ca)

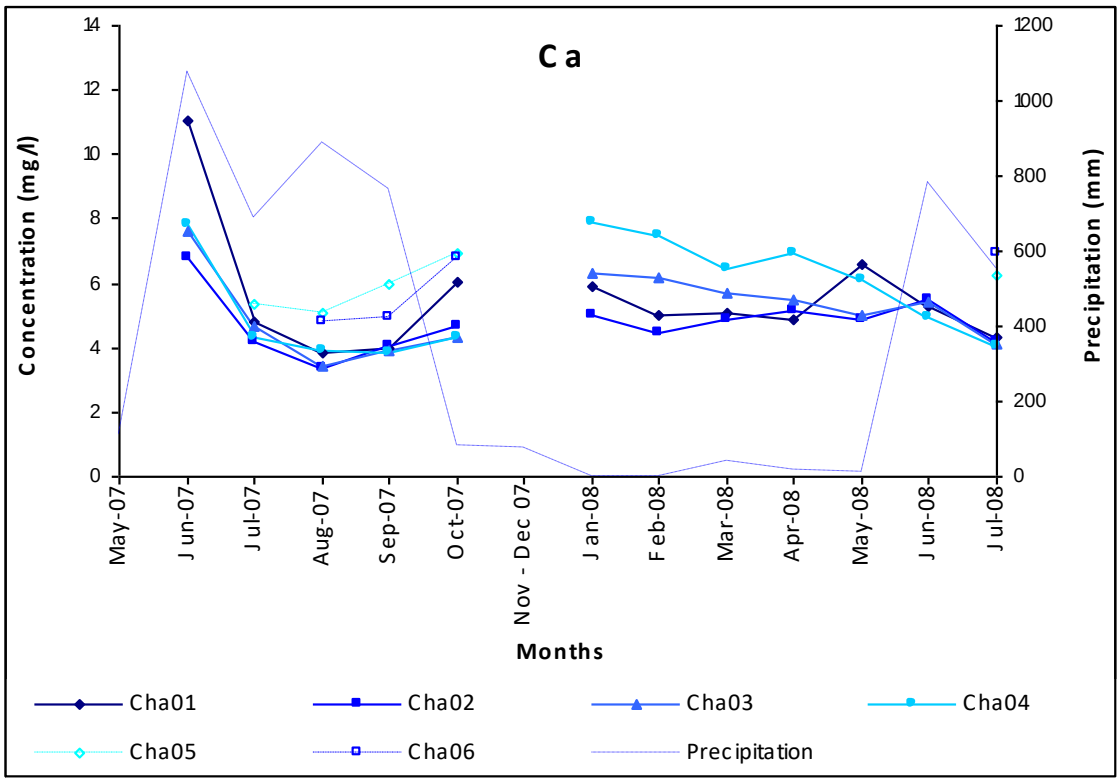

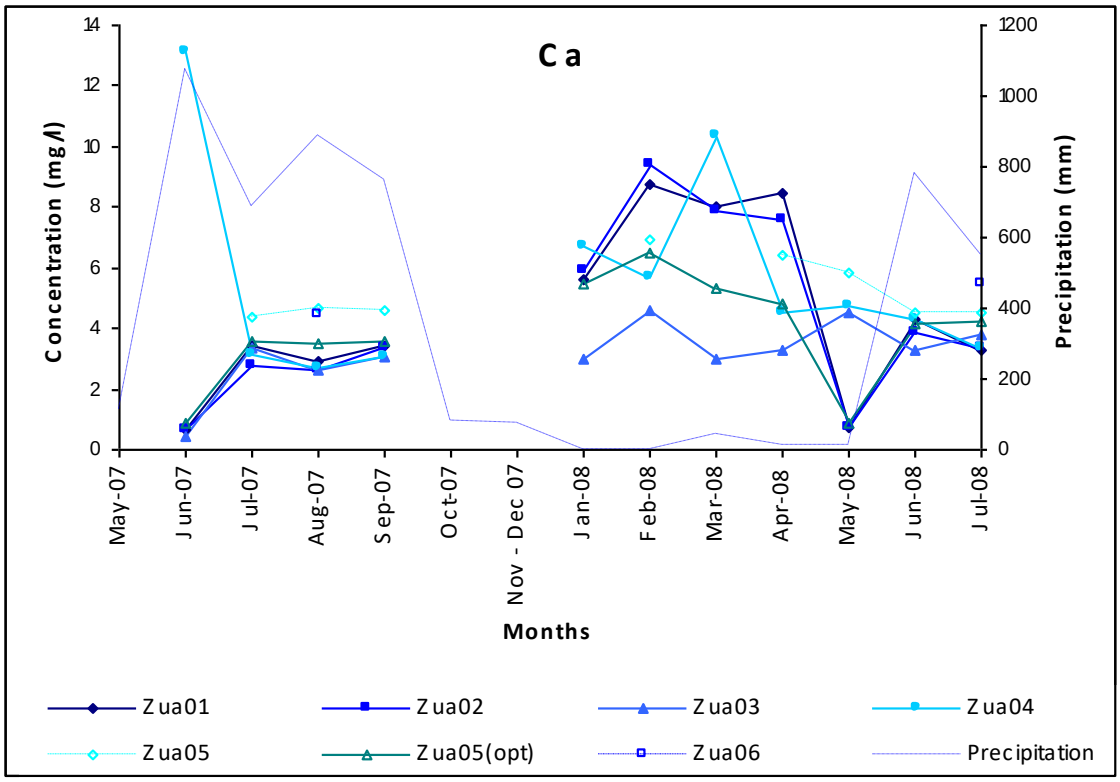

Figure 6.8 Temporal graphs for Ca for the Chapora and Zuari River localities.

As for Mg for the Chapora Rivers very similar trends can be observed for localities Cha 01, 02, 03 and 04, however, in addition, the Ca values for Cha 05 and 06 also follow a similar albeit slightly elevated pattern during the 2007 monsoon period. Other data for these localities are not included due to estuarine influence. The overriding trend is again one of relatively high values in June 2007 ranging between 6.79 mg l^{-1} for Cha 02 and 11.1 mg l^{-1} for Cha 01 before falling sharply to between 4.18 mg l^{-1} for Cha 02 and 4.82 mg l^{-1} for Cha 01 before reaching a low of between 3.45 mg l^{-1} for Cha 03 and 3.93 mg l^{-1} for Cha 04 in August. From here the values begin to rise again through September and October to between 4.30 mg l^{-1} for Cha 03 and 6.04 mg l^{-1} for Cha 04. During the dry season months of January – April 2008 the values increase slightly to between 4.46 mg l^{-1} for Cha 02 and 7.9 mg l^{-1} for Cha 04, but more noticeable is the increased variation of values along the river which is again suggesting more localised controls over the elemental concentrations during the dry season, possible evaporation / crystallisation dominant weathering. The variation in values decreases throughout the dry season, coalescing once again in June 2008 with values between 4.95 mg l^{-1} for Cha 04 and 5.49 mg l^{-1} for Cha 02, and in July 2008 with values between 4.07 mg l^{-1} for Cha 04 and 4.33 mg l^{-1} for Cha 01, suggesting precipitation dominated weathering.

At present the graph for the Zuari River does not show the same dominant trend as is present within all the other graphs, however, this is possibly due to poor data from one of the analyses which contained data for Zuari River for June 2007 and May 2008.

Aluminium (Al)

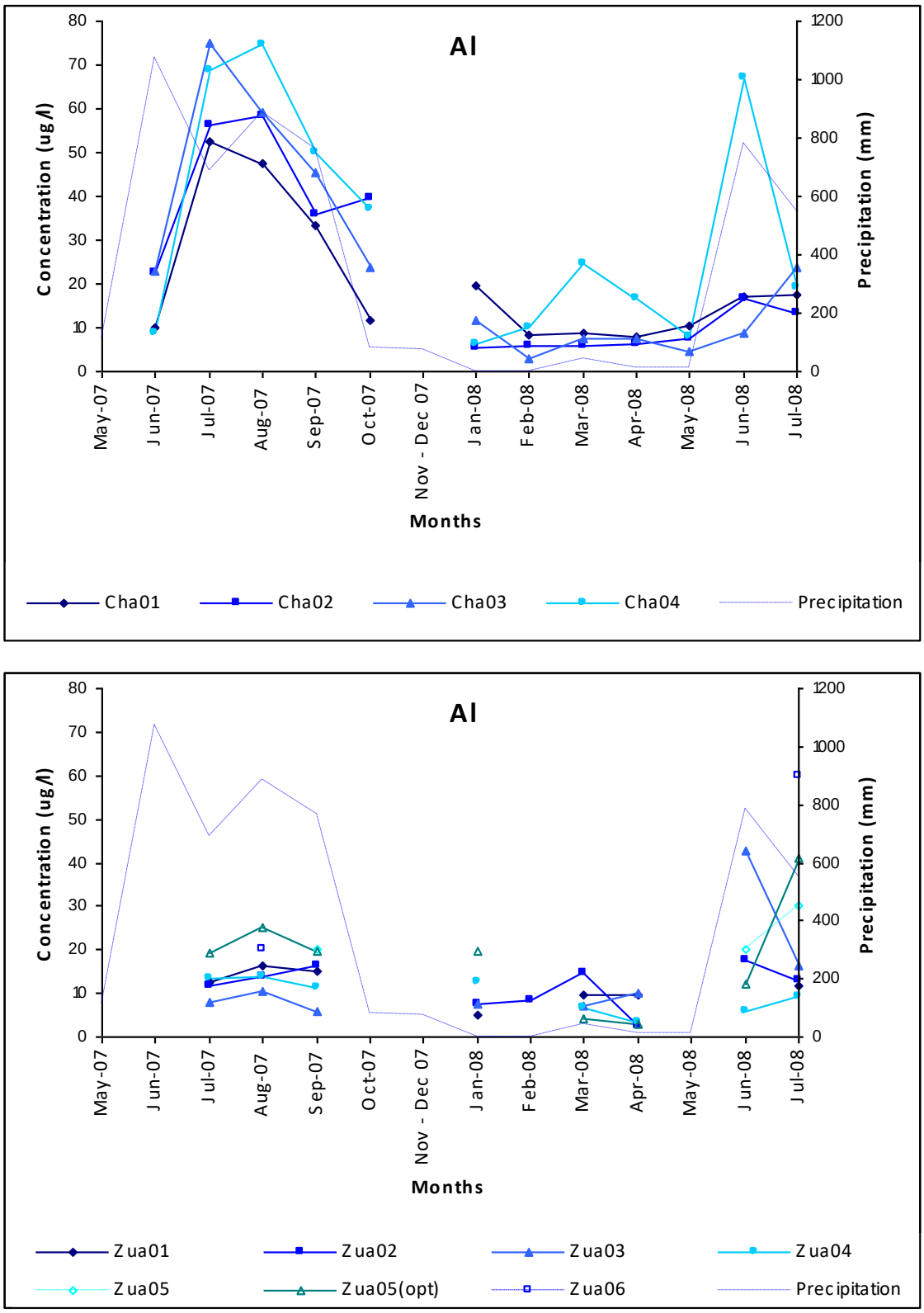

Figure 6. 9 Temporal graphs for Al for the Chapora and Zuari River localities.

Firstly, regarding the Chapora River, the values plotted for Al have units of µg l^{-1} rather than mg l^{-1} suggesting that the Al concentrations are significantly lower than the other major cations, Al could be better classified as a trace element. However, for now it will remain with the major cations. The next observation is that Al does not appear to follow a similar trend to the other major cations having a high peak in June 2007; instead it has relatively low values for June 2007 ranging between 8.65 µg l^{-1} and 22.9 µg l^{-1} before rising to a peak of between 52.4 µg l^{-1} and 74.9 µg l^{-1} In July. The values remain consistently high into August with values ranging between 47.6 µg l^{-1} and 74.6 µg l^{-1} before dropping sharply through September and into October with values between 11.5 µg l^{-1} and 39.5 µg l^{-1}. During the dry season (January to May 2008) the concentrations remain fairly low, but again with a fairly wide variation with values between 2.98 µg l^{-1} and 24.7 µg l^{-1}, before peaking in June 2008 with values between 8.92 µg l^{-1} and 67.0 µg l^{-1}, then falling once more to between 13.5 µg l^{-1} and 23.6 µg l^{-1} in July.

For the Zuari River, the values for Al are also plotted with units of µg l^{-1}. Data are again missing for June 2007 and May 2008. The missing data along with other missing data resulting from lost samples or estuarine influence makes this graph difficult to interpret. With the only clear pattern occurring during the 2007 monsoon, which shows concentrations for Zua 01, 02, 03, 04 and 05opt all following similar trends with values in July 2007 ranging between 8.13 µg l^{-1} for Zua 03 and 19.4 µg l^{-1} for Zua 05opt before rising in August to between 10.4 µg l^{-1} for Zua 03 and 25.1 µg l^{-1} l for Zua 05opt and then falling in September to between 5.88 µg l^{-1} for Zua 03 and 19.6 µg l^{-1} for Zua 05opt.

Silicon (Si)

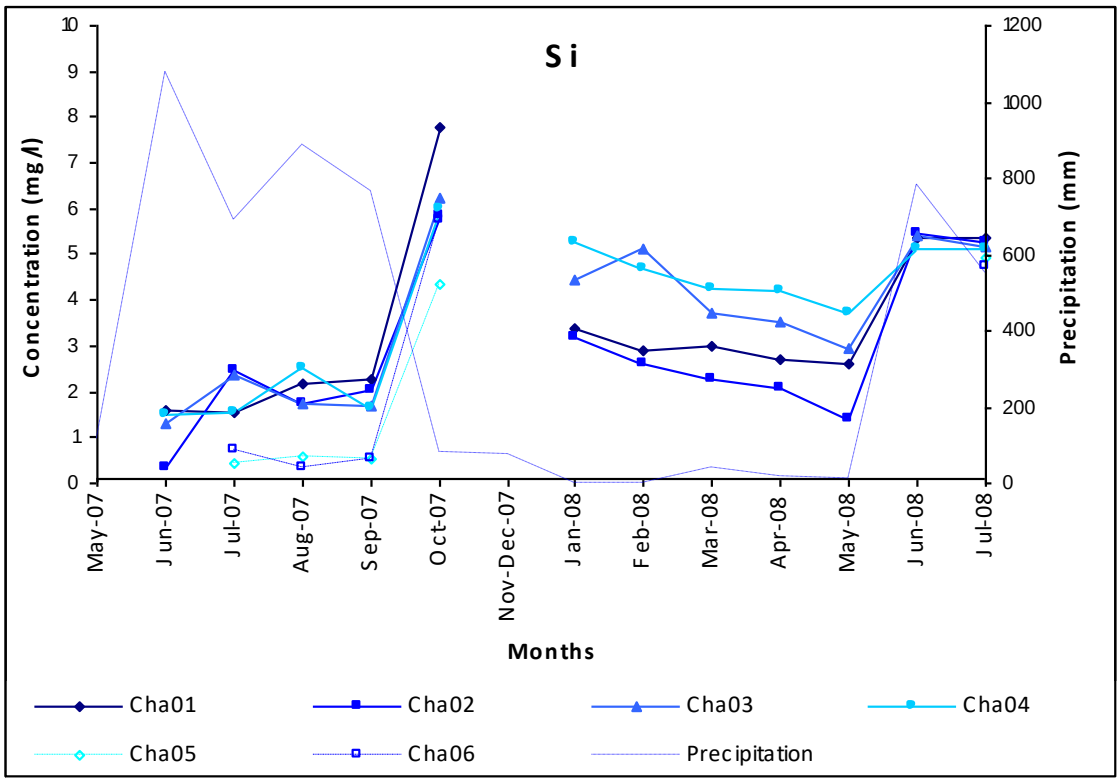

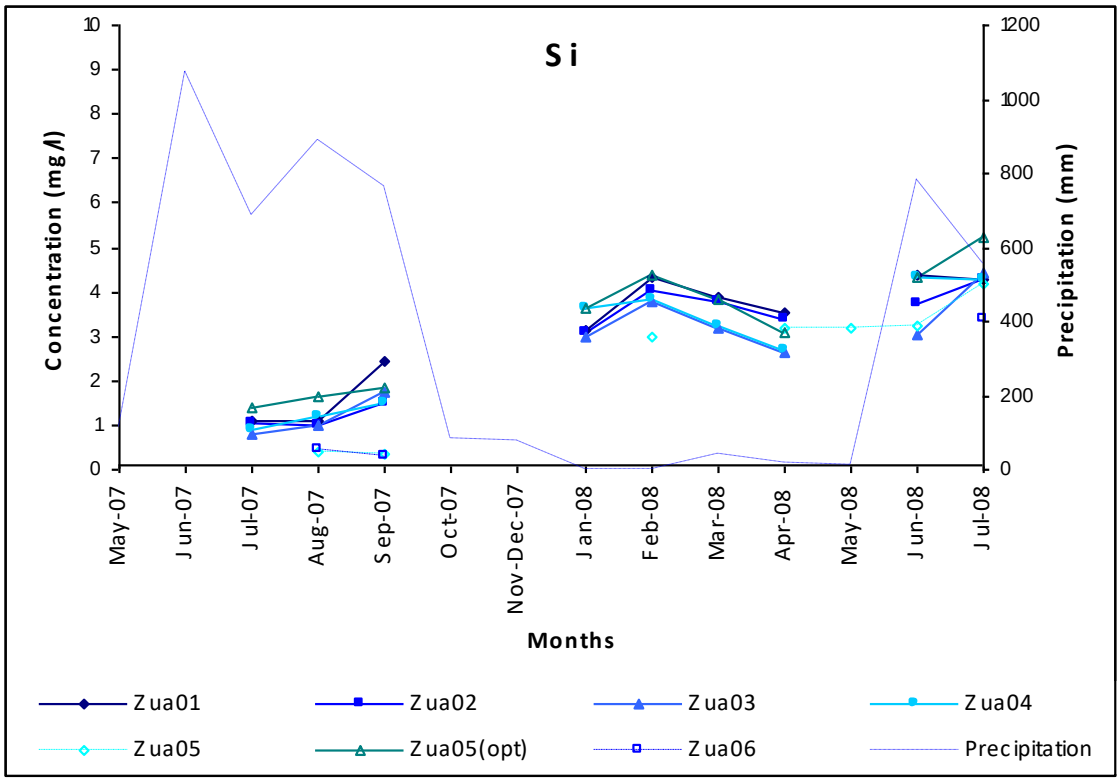

Figure 6.10 Temporal graphs for Si for the Chapora and Zuari River localities.

It is best to consider the more upstream localities in the Chapora River (Cha 01, 02, 03 and 04) separately to the more estuarine localities (Cha 05 and 06) due to significantly higher Si concentrations in the near estuarine localities. Since these have a range of concentrations of between 330 mg l^{-1} and 5750 mg l^{-1} compared to the up stream localities, which all have concentrations <8.0 mg l^{-1}, the upstream concentrations would otherwise be obscured. Considering them separately, patterns can be observed: for example, contrary to all other elements so far studied there is a clear and distinct peak located in October 2007 at the end on the 2007 monsoon period instead of the peak being present at the beginning of the monsoon period in June 2007. In June 2007 the concentration varies between 0.35 mg l^{-1} for Cha 02 and 1.57 mg l^{-1} for Cha 01, increasing gradually through July, August and September where the concentrations vary between 1.65 mg l^{-1} for Cha 04 and 2.28 mg l^{-1} for Cha 01, before rising to between 5.86 mg l^{-1} for Cha 02 and 7.77 mg l^{-1} for Cha 01 in October 2007. During the dry season, concentrations fall initially in January 2008 to 3.21 mg l^{-1} for Cha 02 and 5.27 mg l^{-1} for Cha 04 and continue to fall gradually throughout the dry season months to a low of between 1.40 mg l^{-1} for Cha 02 and 3.73 mg l^{-1} for Cha 02 in May 2008. Concentrations then once again increase in June to between 5.10 mg l^{-1} for Cha 04 and 5.45 mg l^{-1} for Cha 02 and remain fairly consistent into July. The observation of monthly variability decreasing during the wet months and increasing during the dry months is once again apparent. Regarding the more estuarine localities, albeit with significantly greater concentrations, the similar trend of relatively low and consistent concentrations during the early months of the 2007 monsoon followed by a significant peak in October 2007 is still very much apparent.

For the Zuari River, it is unfortunate that in addition to the missing data for October – December 2007 the additional missing data for June 2007 and May 2008 makes it impossible to be certain of similarities between the two rivers; however, from the data available the pattern does look remarkably alike. The pattern appears to once again differ from other major cations previously studied with concentration beginning low during the early 2007 monsoon months followed by a gradual rise in concentration through August and September, one can imagine the values continuing in an upward trend into October as do those from the Chapora River. The dry season values again show slightly elevated concentrations peaking this time in February between 3.79 mg l^{-1} for Zua 03 and 4.39 mg l^{-1} for Zua 05opt rather than January then falling to a low of between 2.64 mg l^{-1} for Zua 03 and 3.54 mg l^{-1} for Zua 01 in April 2008, again it can be imagined that this trend may continue to decrease into May before rising again in June to values of between 3.03 mg l^{-1} for Zua 03 and 4.40 mg l^{-1} for Zua 01 on its way to a peak of between 4.29 mg l^{-1} for Zua 04 and 5.25 mg l^{-1} for Zua 05opt in July.

Bicarbonate (HCO_3^-)

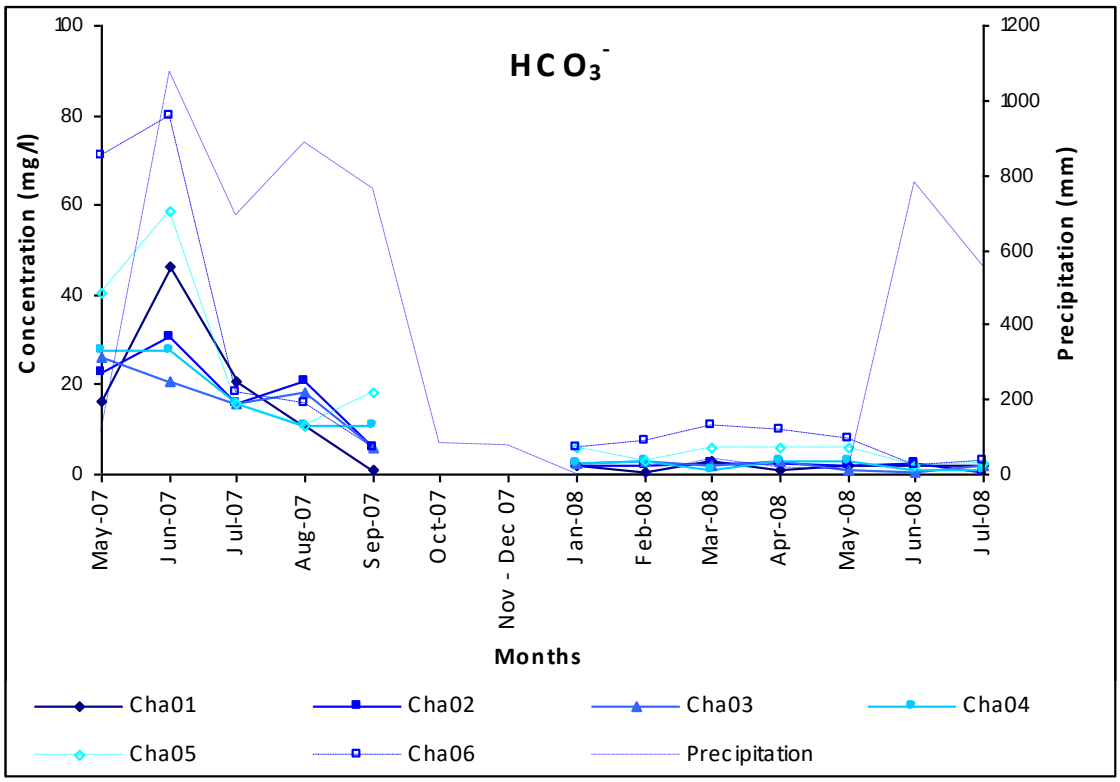

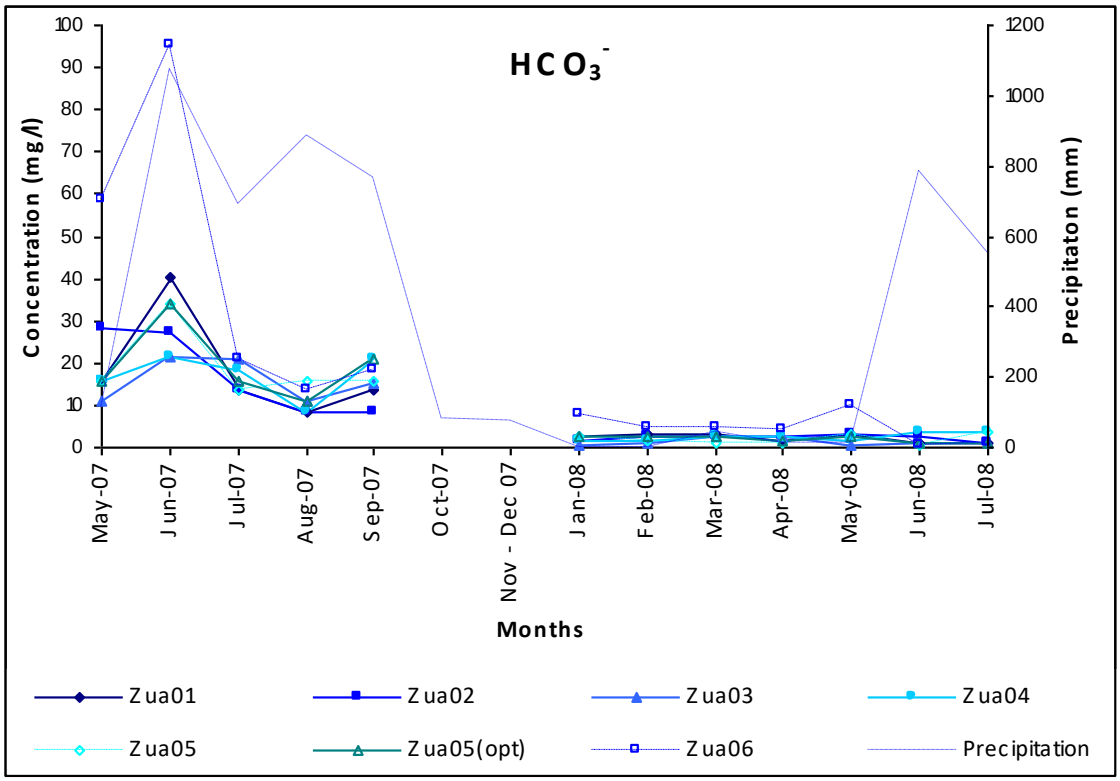

Figure 6.11 Temporal graphs for SO_4^{2-} for the Chapora and Zuari River localities.

It can be seen that both rivers display very similar patterns in which the bicarbonate concentrations are low within both river systems, with the Chapora values peaking at between 20.1 mg l^{-1} for Cha 03 and 79.9 mg l^{-1} for Cha 06 and the Zuari values reaching a high of between 21.4 mg l^{-1} for Zua 04 and 95.2 mg l^{-1} for Zua 06. The peaks for both rivers occurred in June 2007, coinciding with the highest monthly precipitation value of 1077 mm. During the dry season values for both the Chapora River the Zuari River display values of <11 mg l^{-1}, before falling to almost zero in the 2008 monsoon months of June and July.

Sulphate (SO_4^{2-})

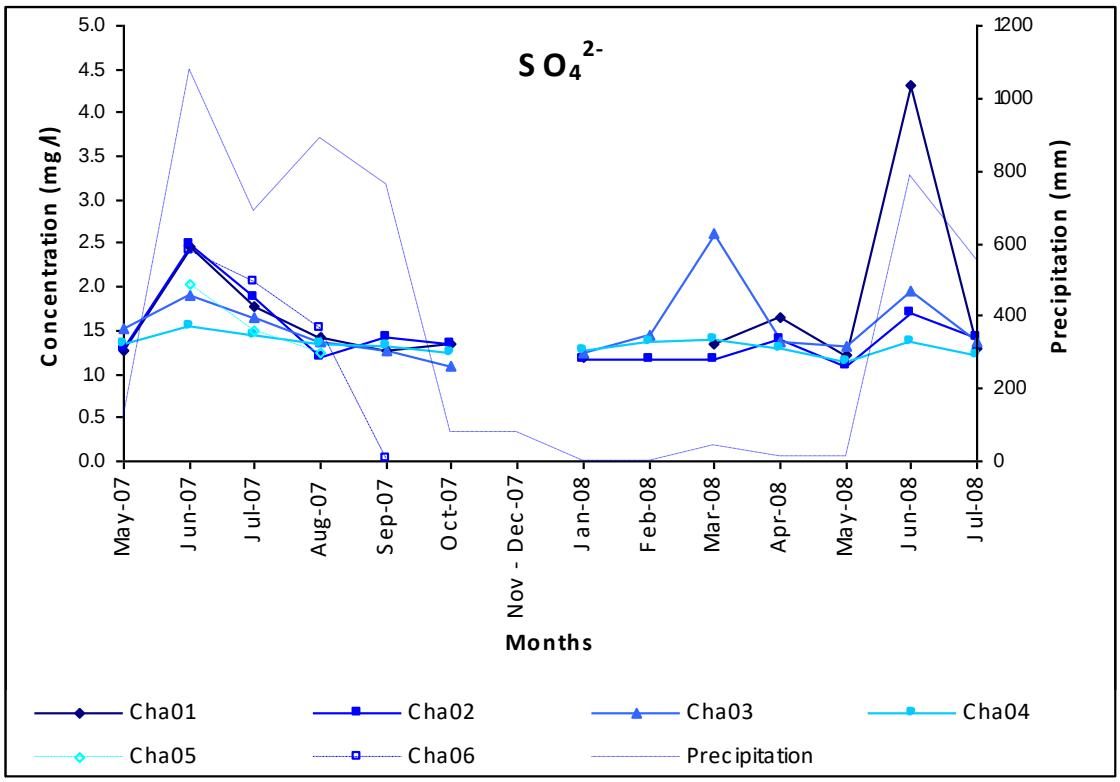

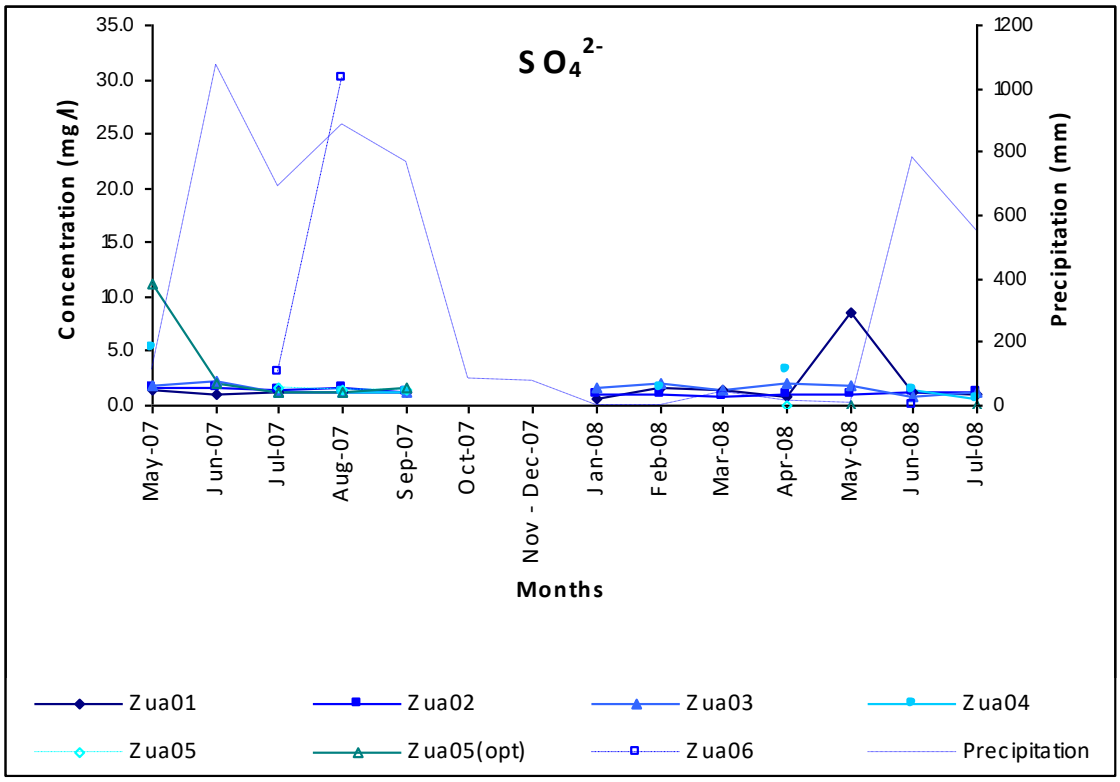

Figure 6.12 Temporal graphs for SO_4^{2-} for the Chapora and Zuari River localities.

For the Chapora River there are two prominent peaks both coinciding with peaks in precipitation occurring in June 2007 with concentrations between 1.54 mg l^{-1} for Cha 04 and 2.5 mg l^{-1} for Cha 02 and in June 2008 with concentration between 1.38 mg l^{-1} for Cha 04 and 4.32 mg l^{-1} for Cha 01, however, another peak is present for Cha 03 in March 2008 with a value of 2.6 mg l^{-1}. Other than these three peaks the concentrations vary little between August 2007 and May 2008 with values ranging between 1.1 mg l^{-1} and 1.6 mg l^{-1}.

Things are not as clear in the Zuari River since there are a number of significantly larger values which obscure the trends. These include a value of 30.1 mg l^{-1} for Zua 06 in August 2007, a value of 11.2 mg l^{-1} for Zua 05opt in May 2007, a value of 8.56 mg l^{-1} for Zua 01 in May 2008 and a value of 5.21 mg l^{-1} for Zua 04 in May 2007. If these values are removed the remaining data can be seen more clearly. Even so, very few patterns can be discerned for the remaining data, with values ranging between 0.61 mg l^{-1} and 3.16 mg l^{-1} and variation in concentration being greatest during the dry season months and smallest during the monsoon months.

Chloride (Cl)

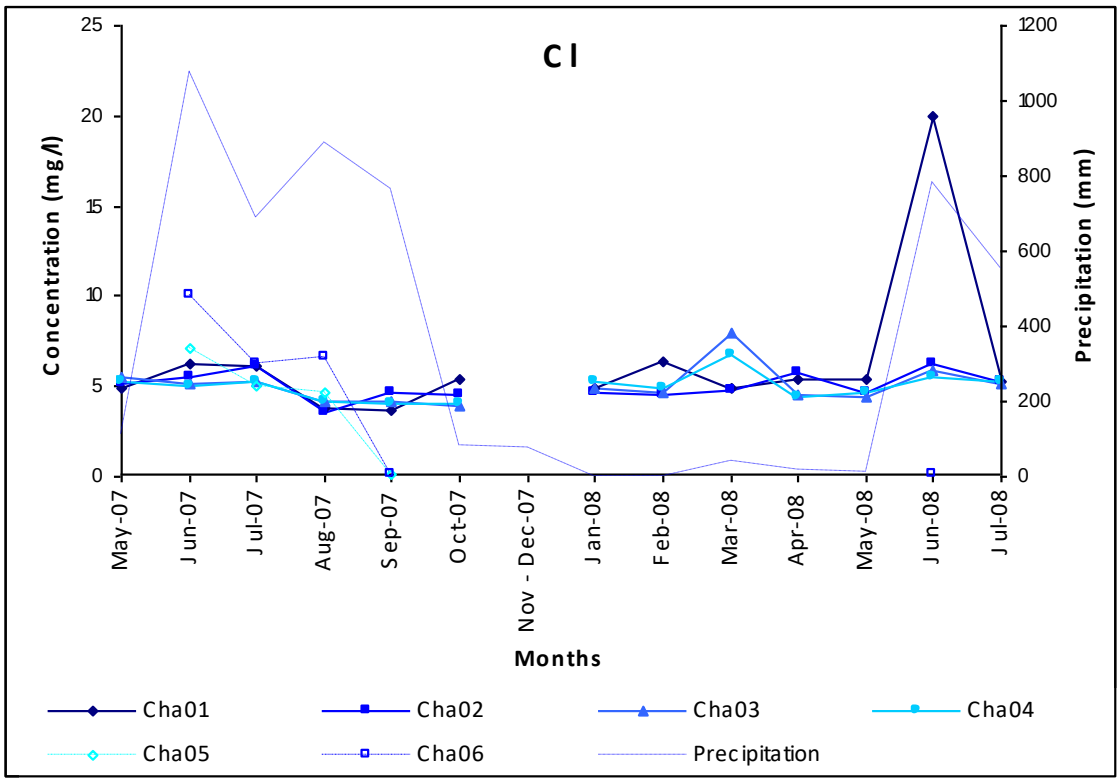

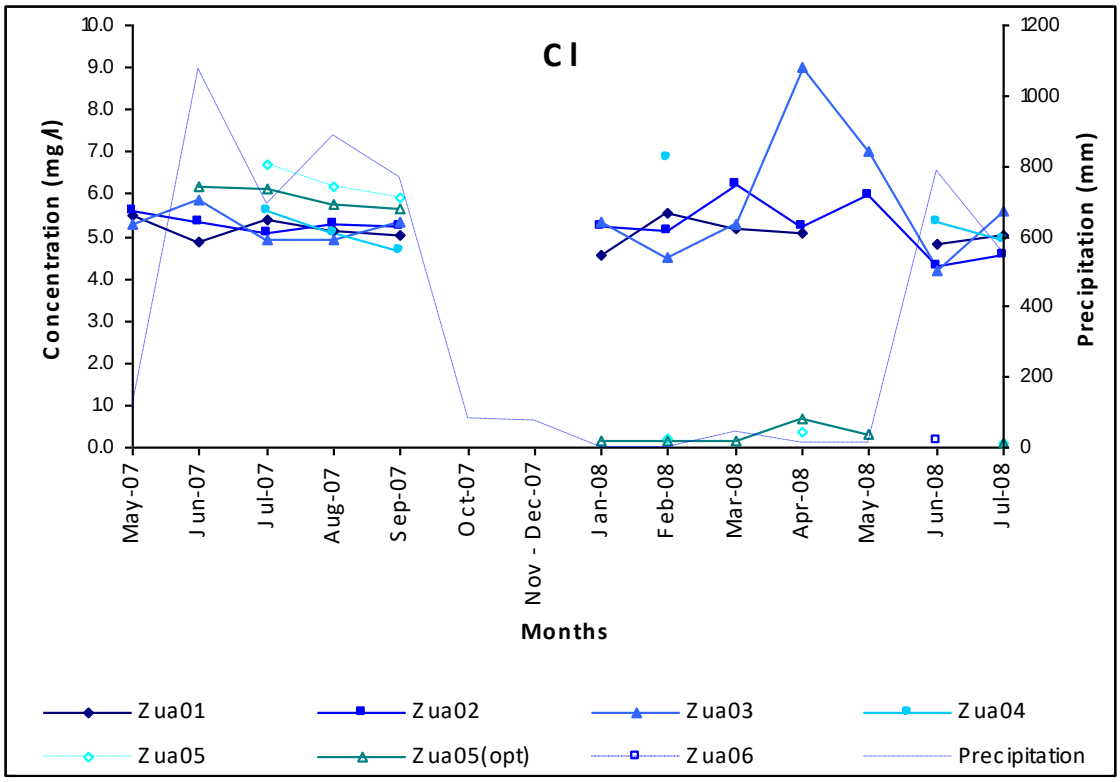

Figure 6.13 Temporal graphs for Cl for the Chapora and Zuari River localities.

The Cl concentrations for the Chapora River remain fairly consistent through the whole sampling period, fluctuating between 3.61 mg l^{-1} and 6.32 mg l^{-1}; however, there are a few notable exceptions. The exceptions have values of 9.99 mg l^{-1} for Cha 06 in June 2007, 6.57 mg l^{-1} for Cha 06 in August 2007, 0.14 mg l^{-1} for Cha 06 in October 2007, 0.13 mg l for Cha 05 in October 2007, 6.72 mg l^{-1} for Cha 04 in March 2008, 7.95 mg l^{-1} for Cha 03 in March 2008 and 20.0 mg l^{-1} for Cha 01 in June 2008. The two highest peaks coincide with the maximum precipitation values at the start of the 2007 and 2008 monsoon periods and the two lowest values coincide with the end of the 2007 monsoon period. These two high values are probably indicating the presence of Cl in the rainfall, with the higher value during these high precipitation events but the remaining data suggest that other than at these times the Cl concentrations are reasonably consistent.

The Zuari River concentrations are again fairly consistent throughout the whole sampling period with concentration varying between 4.19 mg l^{-1} and 6.72 mg l^{-1}; but again with a number of notable exceptions. These exceptions have the following values; 30.8 mg l^{-1} for Zua 04 in May 2007, 32.1 mg l^{-1} for Zua 05opt in May 2007, 21.0 mg l^{-1} for Zua 06 for August 2007, 211 mg l^{-1} for Zua 06 in September 2007, 16.5 mg l^{-1} for Zua 04 in April 2008, 8.99 mg l^{-1} or Zua 03 in April 2008, 7.02 mg l^{-1} for Zua 03 in May 2008 and 57.9 mg l^{-1} or Zua 01 in May 2008. In contrast to the Chapora River none of these exceptions coincide with high precipitation levels.

Fluoride (F)

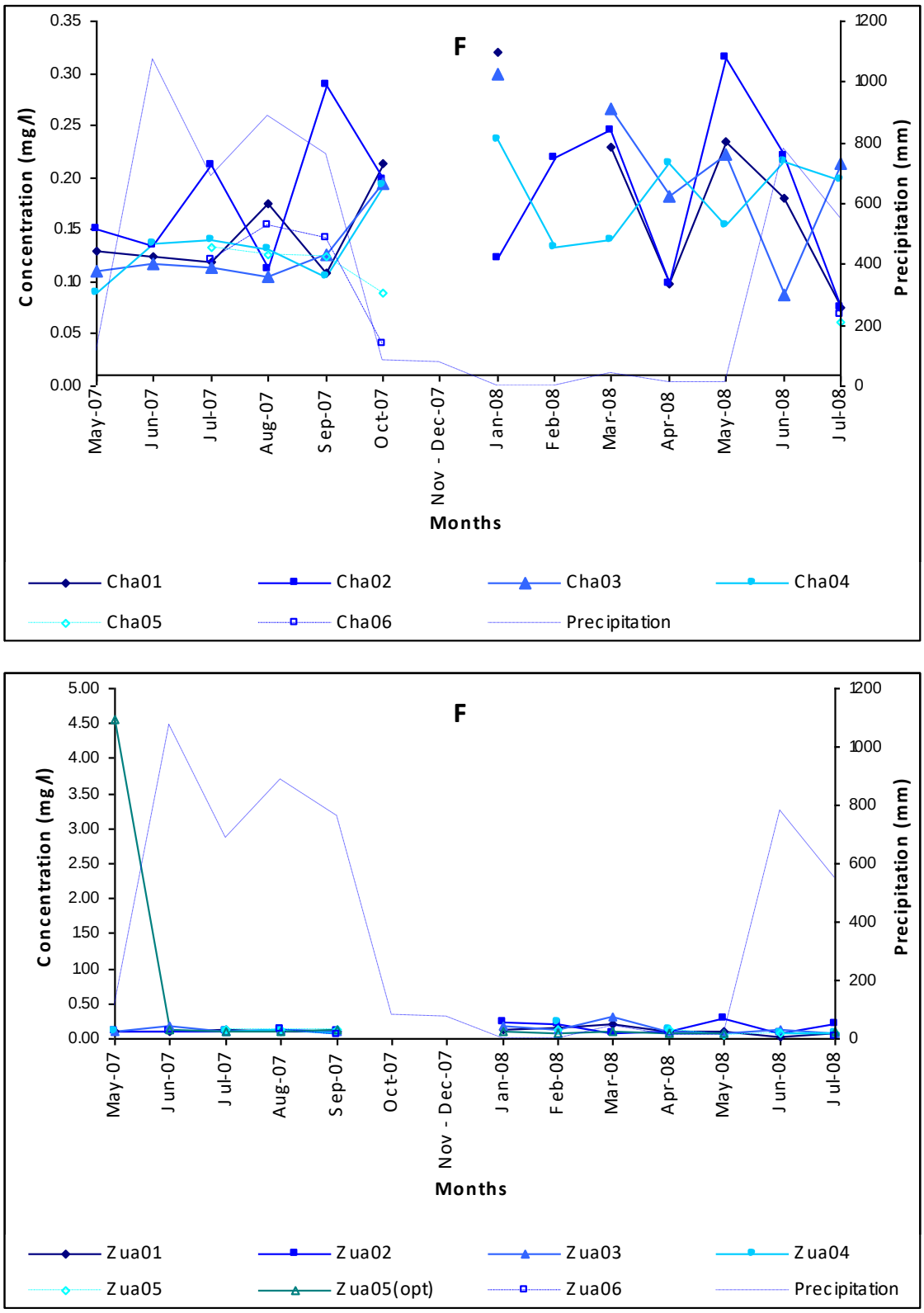

Figure 6.14 Temporal graphs for F for the Chapora and Zuari River localities.

The values for F for both the Chapora River and the Zuari River are very low with values ranging between 0.04 mg l^{-1} and 0.32 mg l^{-1} for the Chapora River and between 0.02 mg l^{-1} and 0.31 mg l^{-1} for the Zuari River, although there is one exception to this for the Zuari River which has a value of 4.57 mg l^{-1} for Zua 05opt in May 2007. The variability in the values and the lack of any significant trends may be due to the low concentrations and their related analytical reliability. The only possible observation that can be made is the difference in concentration variability between the wet and dry months again with reduced variation for the wet months and enhanced variation if the dry months.

Nitrate (NO_3)

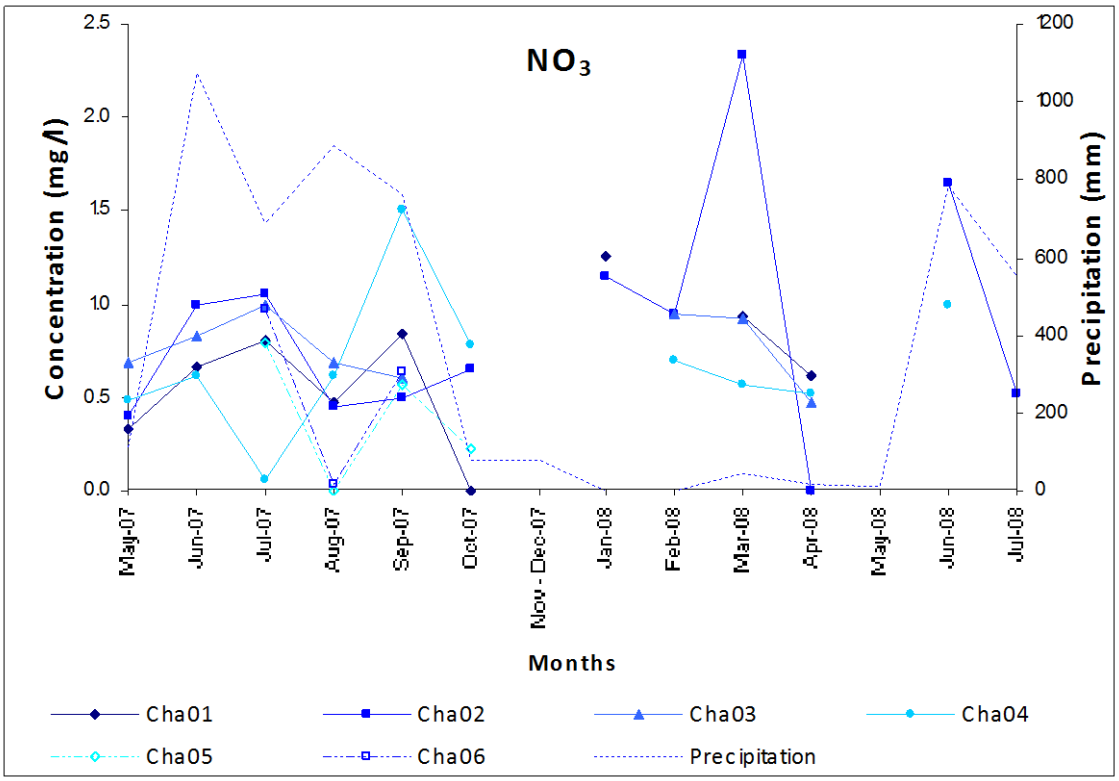

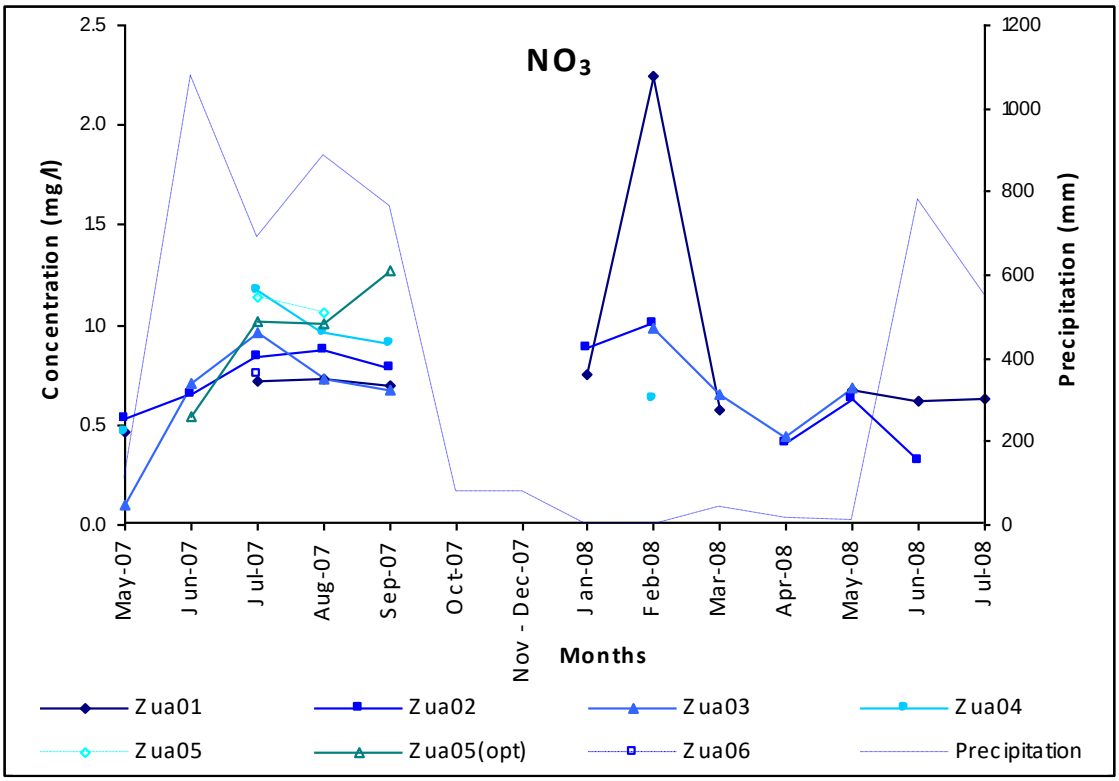

Figure 6.15 Temporal graphs for NO_3 for the Chapora and Zuari River localities.

Values for both rivers are fairly similar with all concentrations ranging between 0 – 2.34 mg l^{-1} for the Chapora River and 0 – 2.25 mg l^{-1} for the Zuari River. Looking first at the Chapora River, throughout the months of May – October 2007 the sample sites Cha 01, 02, 03 and 04 behave similarly with the occasional exception, such as a negative deviation for Cha 04 in July 2007 and a positive deviation for Cha 04 in October 2007. Through this period, values range between 0.33 mg l^{-1} and 0.69 mg l^{-1} in May 2007, rising through June into July with concentrations ranging between 0.79 mg l^{-1} and 1.05 mg l^{-1}. Then concentrations fall in August to between 0 – 0.69 mg l^{-1}, rising again in September to between 0.5 mg l^{-1} and 1.51 mg l^{-1} and falling again in October to between 0 – 0.79 mg l^{-1}. Data are less complete for the dry season months and into the 2008 monsoon season, however, similarities can still be seen for the various localities but again there are a few notable exceptions, such as positive deviations for Cha 02 in March and June 2008 and a negative deviation in April 2008. Concentrations rise again in January to between 1.15 mg l^{-1} and 1.26 mg l^{-1} then gradually fall over the subsequent months to between 0 – 0.62 mg l^{-1} in April 2008, no data are available for May but concentrations then rise once again at the start of the 2008 monsoon with values between 0.99 mg l^{-1} and 1.65 mg l^{-1} before falling with only one value of 0.52 mg l^{-1} in July 2008. The same general observation can be made for the Zuari River with most localities displaying similar trends, with occasional exceptions including a negative deviation to zero for Zua 01 in June 2007 and a positive deviation to 2.25 mg l^{-1} for Zua 01 in February 2008. Concentrations for the Zuari River also begin relatively low in May 2007 with values ranging between 0.1 mg l^{-1} and 0.53 mg l^{-1}, rising through June and in to July with concentration ranging between 0.72 mg l^{-1} and 1.17 mg l^{-1} and concentrations remain fairly consistent through August and into September, when values range between 0.68 mg l^{-1} and 1.27 mg l^{-1}. Like the Chapora, the data become more scarce in the second part of the sampling period, but again the various localities do behave in a similar way, with the odd exception. Concentrations in the dry season start off between 0.76 mg l^{-1} and 0.88 mg l^{-1}, rising slightly in February before falling through March into April with values between 0.41 mg l^{-1} and 0.45 mg l^{-1}. Concentrations then rise once more in May to between 0.64 mg l^{-1} and 0.68 mg l^{-1} and then remain fairly stable with the one slight negative deviation to 0.32 mg l^{-1} for Zua 02 in June 2008.

6.2.2. Trace elements

Rubidium

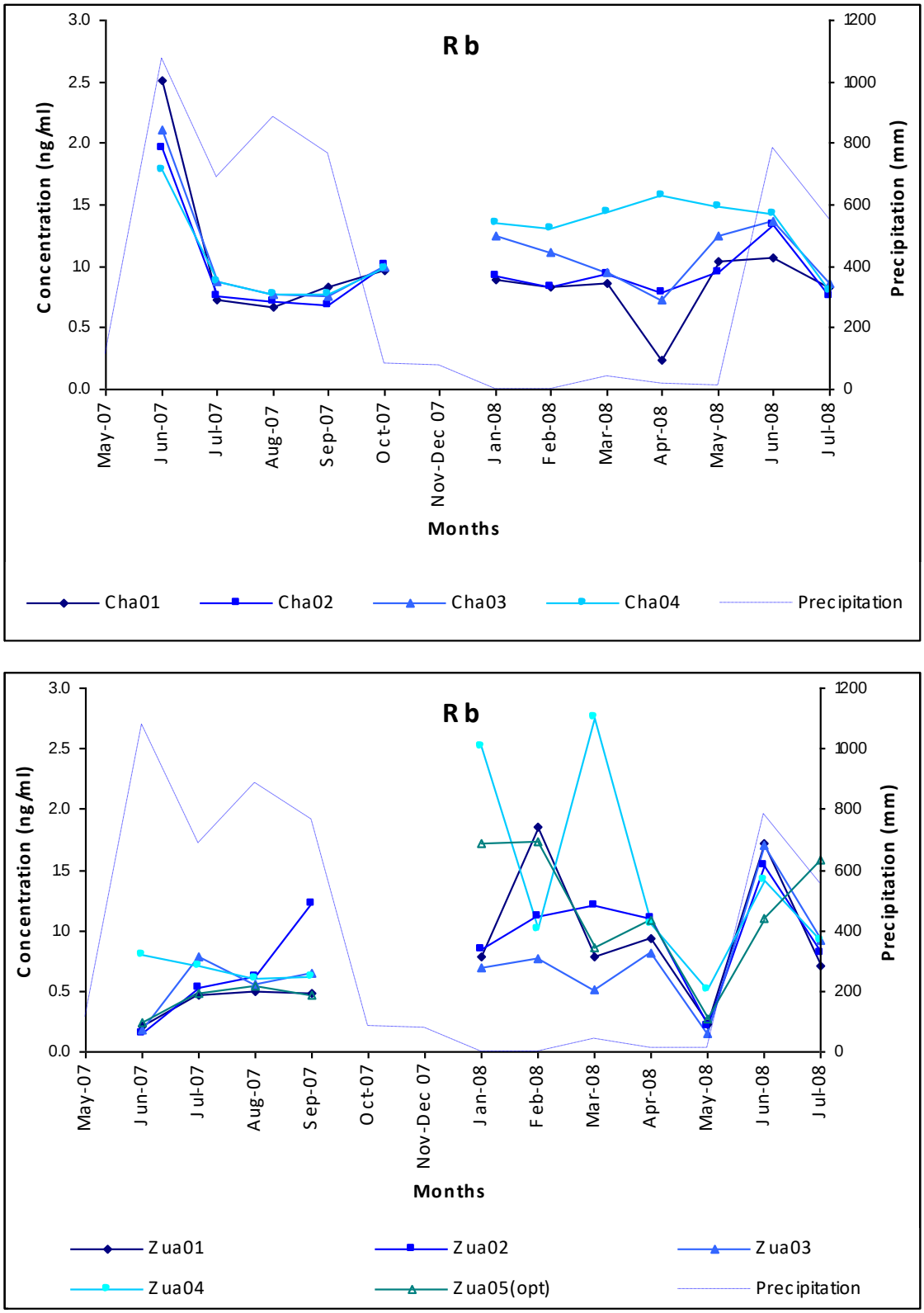

Figure 6.16 Temporal graphs for Rb for the Chapora and Zuari River localities.

For the Chapora River, Rb concentrations for all four localities, Cha 01, 02, 03 and 04 are relatively high in June 2007 with values ranging between 1.78 ng ml^{-1} and 2.5 ng ml^{-1}, coinciding with the onset of the 2007 monsoon period, after which concentrations fall sharply to between 0.73 ng ml^{-1} and 0.88 ng ml^{-1}. They then remain fairly consistent and vary only slightly through August and September, before rising slightly and almost coinciding between 0.97 ng ml^{-1} and 1.02 ng ml^{-1} in October. Moving into January 2008 concentrations continue to rise and variability between the localities increases to between 0.89 ng ml^{-1} and 1.35 ng ml^{-1}, after which trends begin to deviate from each other. Cha 01 and Cha 02 remain very similar to each other through February and March before both recording a significant fall in April followed by a subsequent rise in May and June followed by another fall in July. Cha 03 displays an almost linear reduction in concentration month on month from January into April before rising and falling in broad similarity with Cha 01 and Cha02. Whilst Cha 04, behaves quite differently, instead showing rising concentrations from February to April before falling through May, June and July, where again all four concentration coalesce at between 0.75 ng ml^{-1} and 0.86 ng ml^{-1}.

In regard to the Zuari River, the trends are far from similar to those of the Chapora River. Firstly there are some trends but they are obscured slightly by two positive deviations for Zua 04 with values of 2.51 ng ml^{-1} in January 2008 and 2.76 ng ml^{-1} in March 2008. Describing the graph with Zua 04 removed the trends immediately become clearer. Instead of displaying peak concentrations in June 2007 to coincide with the onset of the monsoon season the values for the Zuari River report some of its lowest concentrations in this month. From this point concentrations show a general increase through July, August and into September to between 0.47 ng ml^{-1} and 1.22 ng ml^{-1}. In 2008 concentrations continue to increase but again the variability of concentration between the various localities increases significantly, with values in February ranging between 0.71 ng ml^{-1} and 1.85 ng ml^{-1}. Moving into March, the concentrations and variability begin to decrease and continue to do so into April where the concentrations almost coalesce between 0.15 ng ml^{-1} and 0.26 ng ml^{-1} before rising sharply to between 1.11 ng ml^{-1} and 1.7 ng ml^{-1} in June to coincide with the onset of the 2008 monsoon before falling again in July.

Strontium

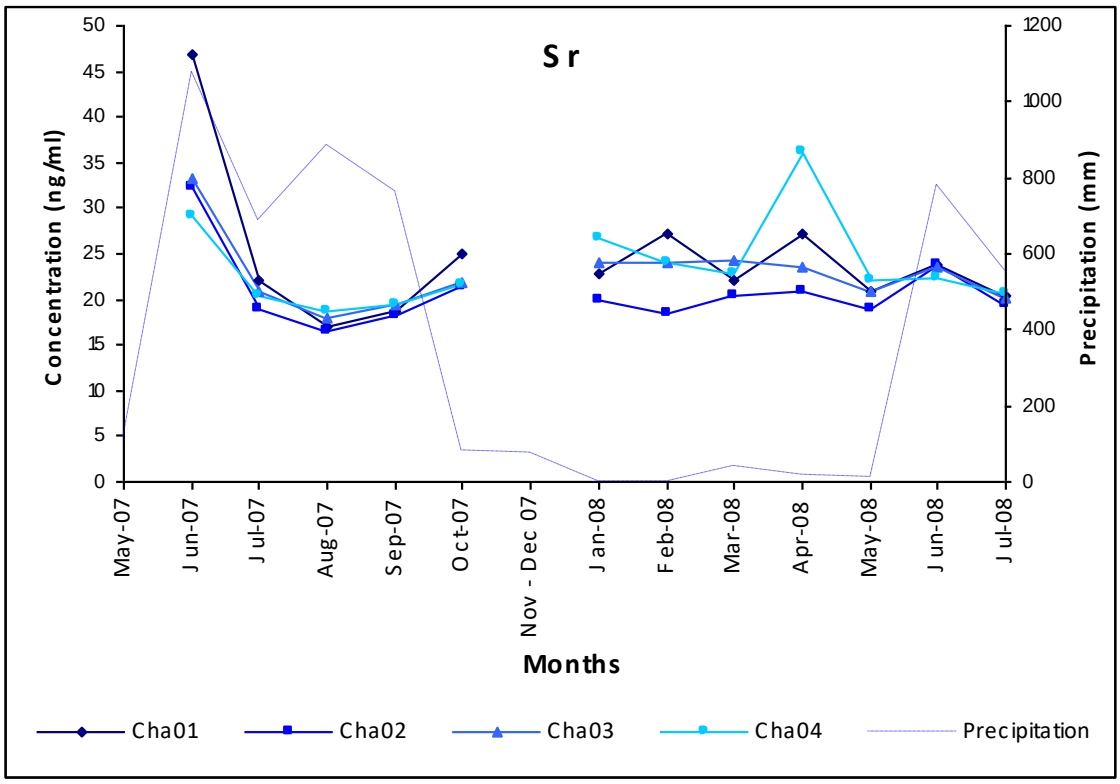

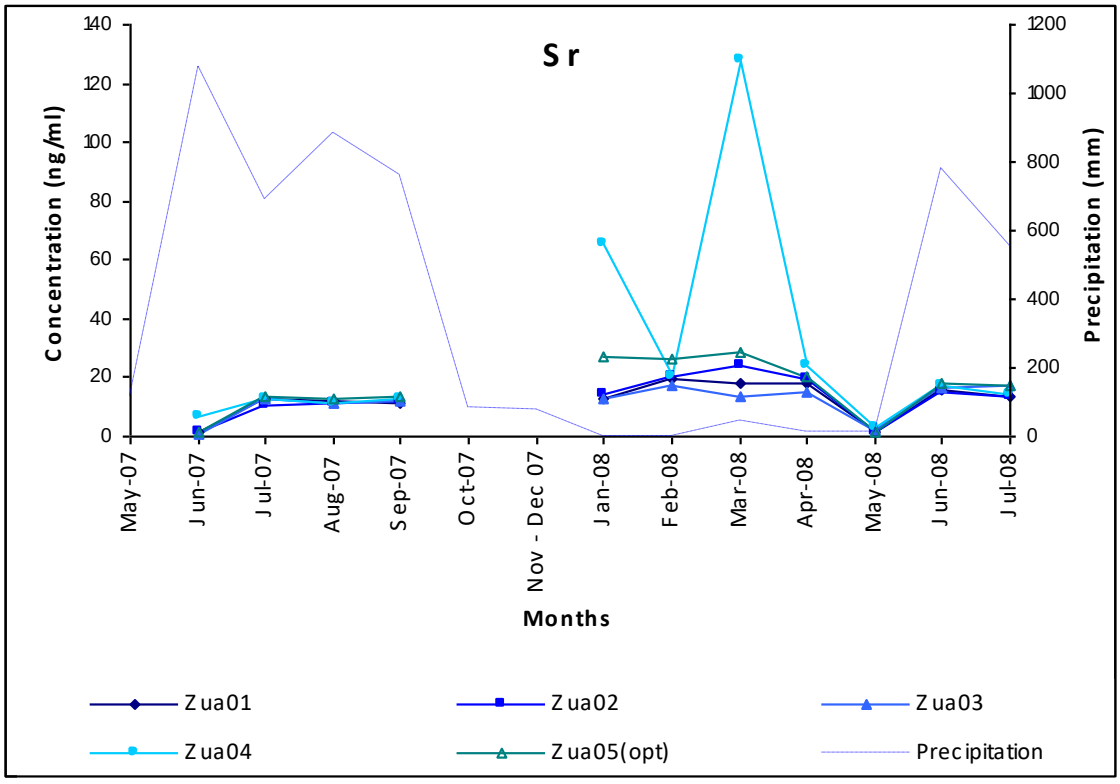

Figure 6.17 Temporal graphs for Sr for the Chapora and Zuari River localities.

Sr concentration trends for the Chapora River localities Cha 01, 02, 03 and 04 are very similar to those for Rb, reporting relatively high concentrations in June 2007 with values ranging between 29.1 ng ml^{-1} and 47.0 ng ml^{-1} coinciding with the onset of the 2007 monsoon period, after which concentrations fall sharply to between 19.0 ng ml^{-1} and 22.1 ng ml^{-1} in July. Concentrations continue to fall further in August to between 16.6 ng ml^{-1} and 18.6 ng ml^{-1} before rising through September and into October where values range between 21.4 ng ml^{-1} and 25.0 ng ml^{-1}. Although the trends are very similar between Rb and Sr the concentration for Sr are at least an order of magnitude higher. Moving into 2008, concentrations remain broadly similar in magnitude, however, the variation between the various localities increases, ranging between 18.6 ng ml^{-1} and 36.1 ng ml^{-1} from January to April. This variation reduces in May 2008 to between 19.0 ng ml^{-1} and 22.0 ng ml^{-1} before rising slightly in June to between 22.5 ng ml^{-1} and 23.8 ng ml^{-1} then falling in July to between 19.4 ng ml^{-1} and 20.7 ng ml^{-1}. As with the majority of elements the key observations are relatively high concentrations coinciding with onset of the 2007 monsoon and increased variability between localities during the dry season months compared to the wet season months where concentrations are fairly uniform throughout the river system.

The trends for the Zuari River, as with those for Rb, are dissimilar to those of the Chapora River. Again the obvious trends are obscured by two positive deviations for Zua 04 with concentrations of 65.3 ng ml^{-1} and 128 ng ml^{-1} in January and March 2008, respectively. Describing the graph with Zua 04 data removed results in the trends immediately becoming clearer. As with Rb concentrations, instead of displaying peak concentrations in June 2007 to coincide with the onset of the monsoon season, the values for the Zuari River report some of its lowest concentrations in this month with values ranging between 1.0 ng ml^{-1} and 1.5 ng ml^{-1}. From this point concentrations increase into July, with values ranging between 10.9 ng ml^{-1} and 13.9 ng ml^{-1} and remain fairly consistent through to September. In 2008 concentrations continue to increase slightly but again the variability of concentration between the various localities increases significantly, with values in January ranging between 12.9 ng ml^{-1} and 26.8 ng ml^{-1}. This variability continues into March before reducing in April to between 15.0 ng ml^{-1} and 20.0 ng ml^{-1} before falling sharply to between 1.7 ng ml^{-1} and 2.5 ng ml^{-1} in May before rising once more to between 14.8 ng ml^{-1} and 17.9 ng ml^{-1} to coincide with the onset of the 2008 monsoon before falling again in July. As with Rb it would appear that, for some reason a ‘rinse-out’ effect is very evident for the Chapora River in 2007 but less so in 2008 whilst it is not present for the Zuari River in 2007 but it is very evident in 2008.

Vanadium (V)

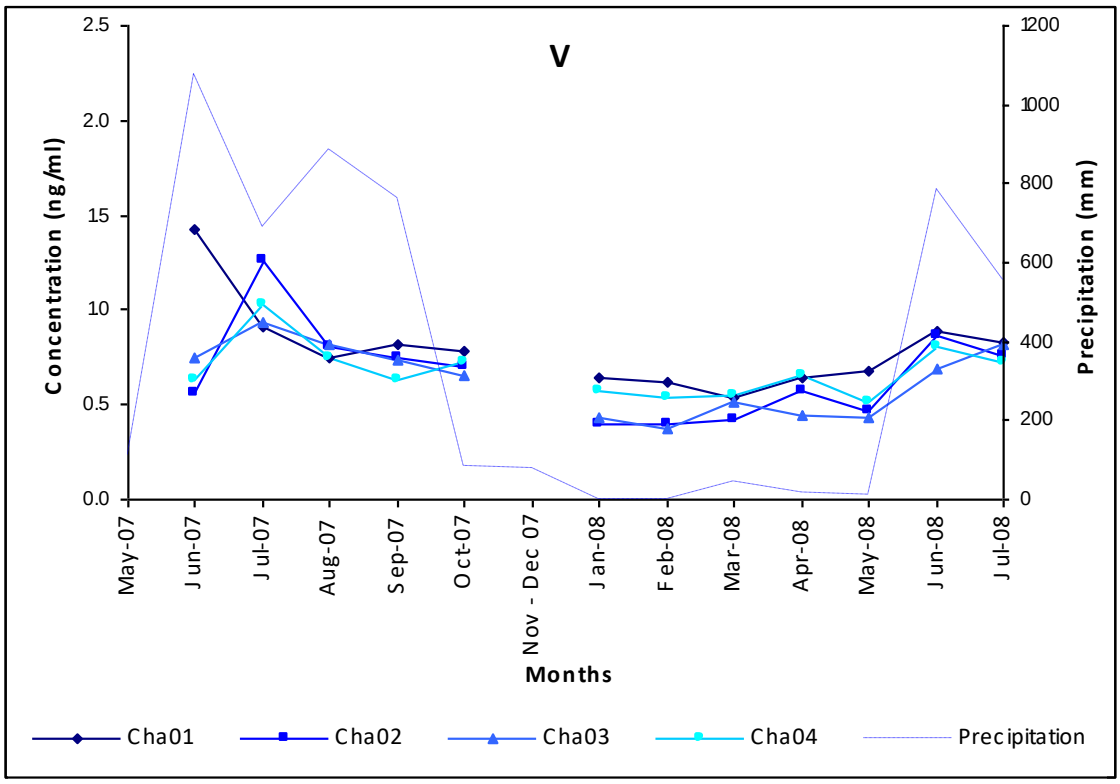

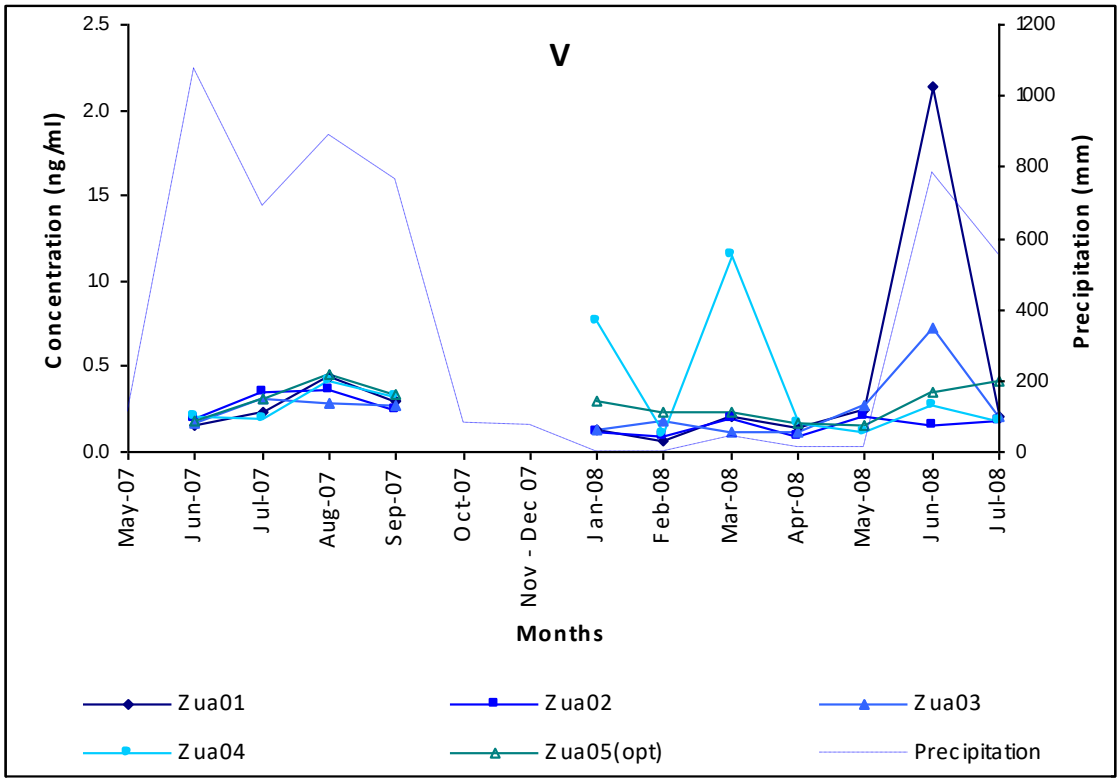

Figure 6.18 Temporal graphs for V for the Chapora and Zuari River localities.

Cha 01 is the only sampling locality to show a relative positive V peak of 1.43 ng ml^{-1} in June 2007 to coincide with the onset of the 2007 monsoon; all the other localities display slight peaks in July ranging between 0.93 ng ml^{-1} and 1.26 ng ml^{-1}. These peaks, whilst not coinciding with the highest precipitation peak of 1077 mm in June, do occur whilst precipitation is still high at 689 mm. After this, concentrations fall to between 0.75 ng ml^{-1} and 0.82 ng ml^{-1} where they remain fairly consistent through to October. In 2008 concentrations are lower still between 0.4 ng ml^{-1} and 0.64 ng ml^{-1} and remain so until they rise slightly in June to coincide with the onset of the 2008 monsoon with values between 0.69 ng ml^{-1} and 0.86 ng ml^{-1}, concentrations then fall very slightly in July.

With regard to the Zuari River, again there are no peaks in concentration coinciding with the onset of the 2007 monsoon; however, on this river the peaks occur in August with values ranging between 0.29 ng ml^{-1} and 0.45 ng ml^{-1}, rising from low values in June ranging between 0.17 ng ml^{-1} and 0.20 ng ml^{-1}. Concentrations then fall in September to between 0.25 ng ml^{-1} and 0.34 ng ml^{-1}. In 2008, concentrations are, as with the Chapora River, slightly lower, where they remain through to May 2008, before they rise quite sharply in June, coinciding again with the onset of the 2008 monsoon, to values between 0.16 ng ml^{-1} and 2.14 ng ml^{-1}, before falling again slightly in July. The presence of a positive peak coinciding with the 2008 monsoon and positive peaks slightly later in the 2007 monsoon season may be due to the amount of precipitation prior to sampling. As with the Chapora River, it may be that each element requires a different amount of precipitation to release it into the river, possibly due to different mineral solubility or sorption efficiencies.

Chromium (Cr)

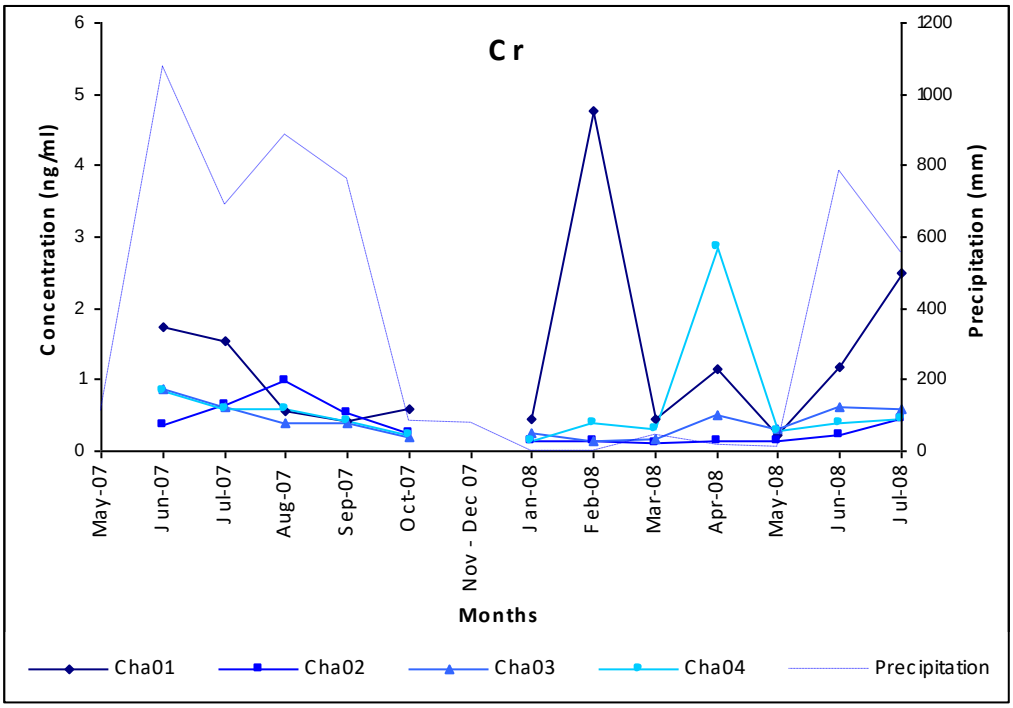

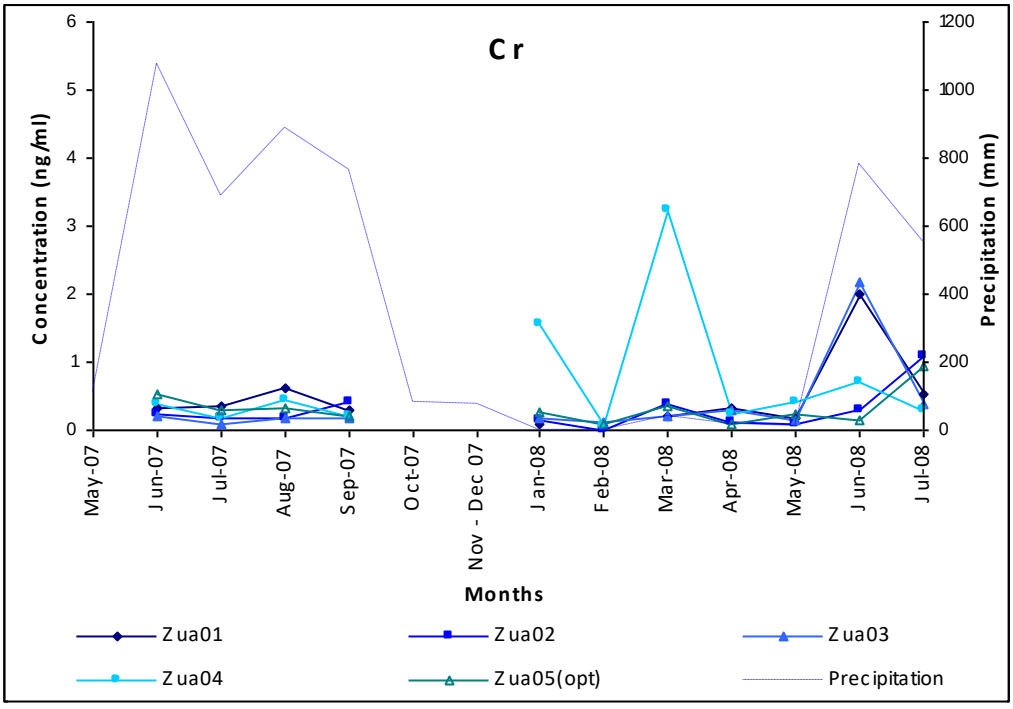

Figure 6.19 Temporal graphs for Cr for the Chapora and Zuari River localities.

In the Chapora River there are three significant positive Cr deviations, two for Cha 01 with values of 4.76 and 2.5 ng ml^{-1} in February and July 2008, respectively, and one for Cha 04 with a value of 2.85 ng ml^{-1} in April 2008. Even if these data points are ignored it is difficult to describe any clear patterns that are similar for the various localities. For example, Cha 02 has a low concentration of 0.36 ng ml^{-1} in June 2007, rising through July to a peak of 0.97 ng ml^{-1} in August before falling sharply through September to concentration of 0.26 ng ml^{-1} in October. Whilst Cha 03 has a relatively high concentration in June 2007 of 0.87 ng ml^{-1} falling constantly through July, August and September to a concentration of 0.21 ng ml^{-1} in October. However, if we consider the trend in more broad terms and try to describe the overall pattern, we could describe the graph as starting with relatively high values in June 2007 which fall gradually through the wet season and remain fairly low through the subsequent dry season before rising again through June and into July 2008, with the occasional deviation in February and April 2008.

The Zuari River graph is possibly a little easier to describe with values fluctuating between 0 and 0.62 ng ml^{-1} throughout much of the sampling period, rising to between 0.92 and 1.08 ng ml^{-1} in July 2008, with the exception of positive deviations of 1.99 and 2.19 ng ml^{-1} for Zua 01 and Zua 03 respectively in June 2008. In addition to this pattern there are two other deviations of 1.56 and 3.23 ng ml^{-1} for Zua 04 in January and March 2008, respectively.

Manganese (Mn)

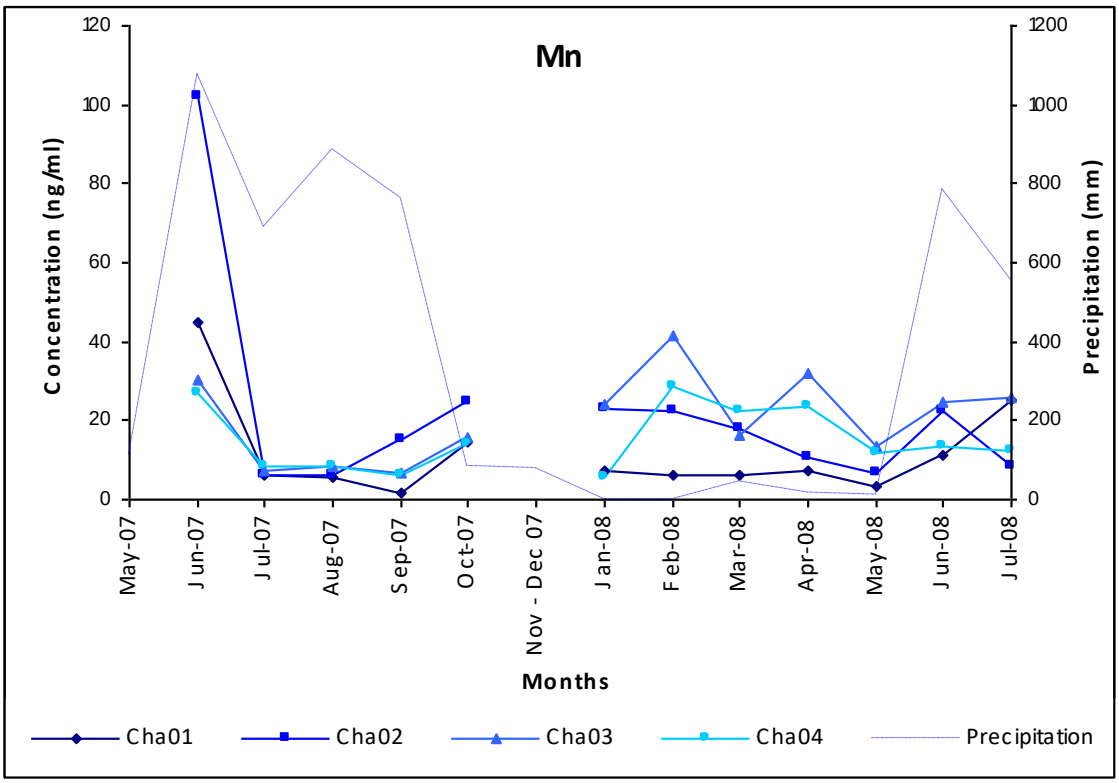

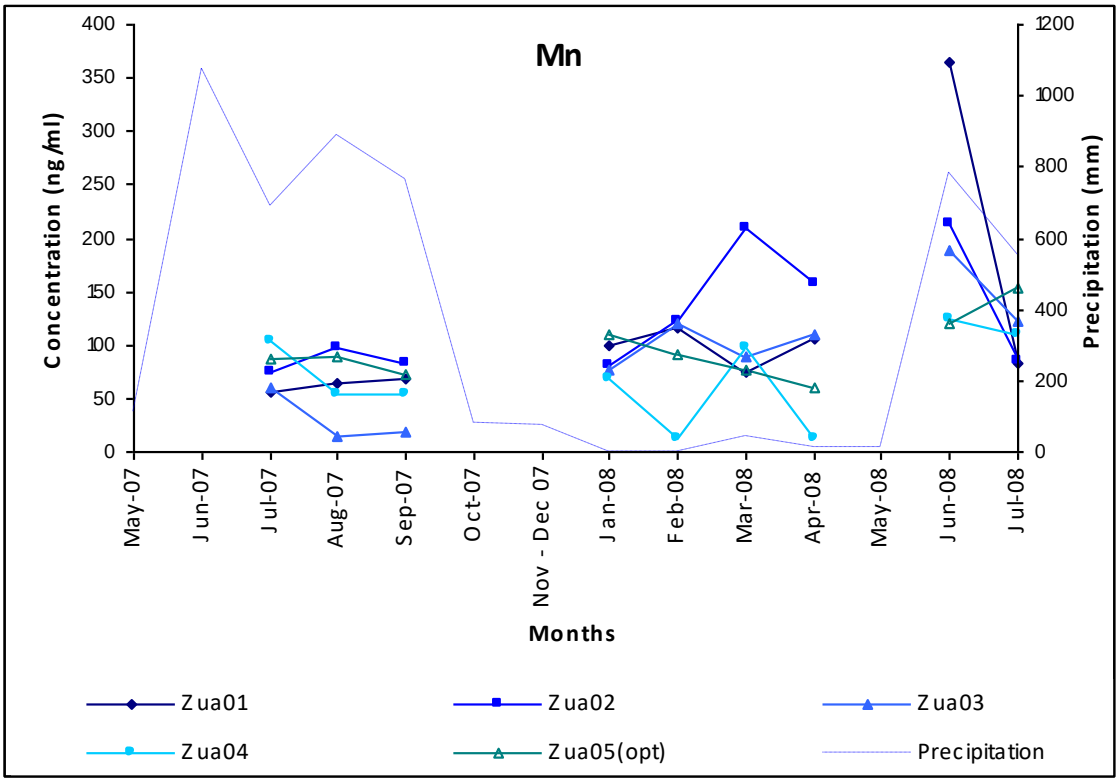

Figure 6.20 Temporal graphs for Mn for the Chapora and Zuari River localities.

For the Chapora River, concentrations in June 2007 are relatively high between 26.9 and 102 ng ml^{-1}, after which they fall sharply to between 6.29 and 8.6 ng ml^{-1} in July and remain fairly constant in August and September, although variability increases in September before concentration rises in October to between 14.0 and 25.0 ng ml^{-1}. In 2008, each locality behaves differently: Cha 01 remains fairly consistent, fluctuating between 3.56 and 7.05 ng ml^{-1} from January to May, before rising to 11.5 ng ml^{-1} and 25.3 ng ml^{-1} in June and July 2008, respectively. One observation is clear, however, and that is again the difference in concentration variability between the various localities for the wet and dry season months, with the wet season months having very little variation and the dry season months having significant variation.

The first point of note for the Zuari is the lack of data for June 2007 and May 2008. So it is impossible to say at present if the Zuari displays a similar 'rinse-out' peak coinciding with June 2007. However, the difference in magnitude of the concentrations between the Chapora and the Zuari Rivers is obvious. For example, the values for the Zuari River for the months of July, August and September are between 53 and 103 ng ml^{-1}, with the exception of two lower values of 15.1 and 18.9 ng ml^{-1} for the Zua 03 locality in August and September, respectively. Comparing these against the concentrations for the same months for the Chapora River, which have values of between 6.29 and 15.1 ng ml^{-1}, again with the exception of one value of 1.75 ng ml^{-1} for Cha 01 in September, it can be seen that the Mn concentrations are between 6.8 and 8.4 times higher for the Zuari compared to the Chapora. Could this be evidence of Mn/Fe mining being far more prevalent along the banks of the Zuari than it is on the Chapora? Without the missing data it is difficult to describe any more trends.

Iron (Fe)

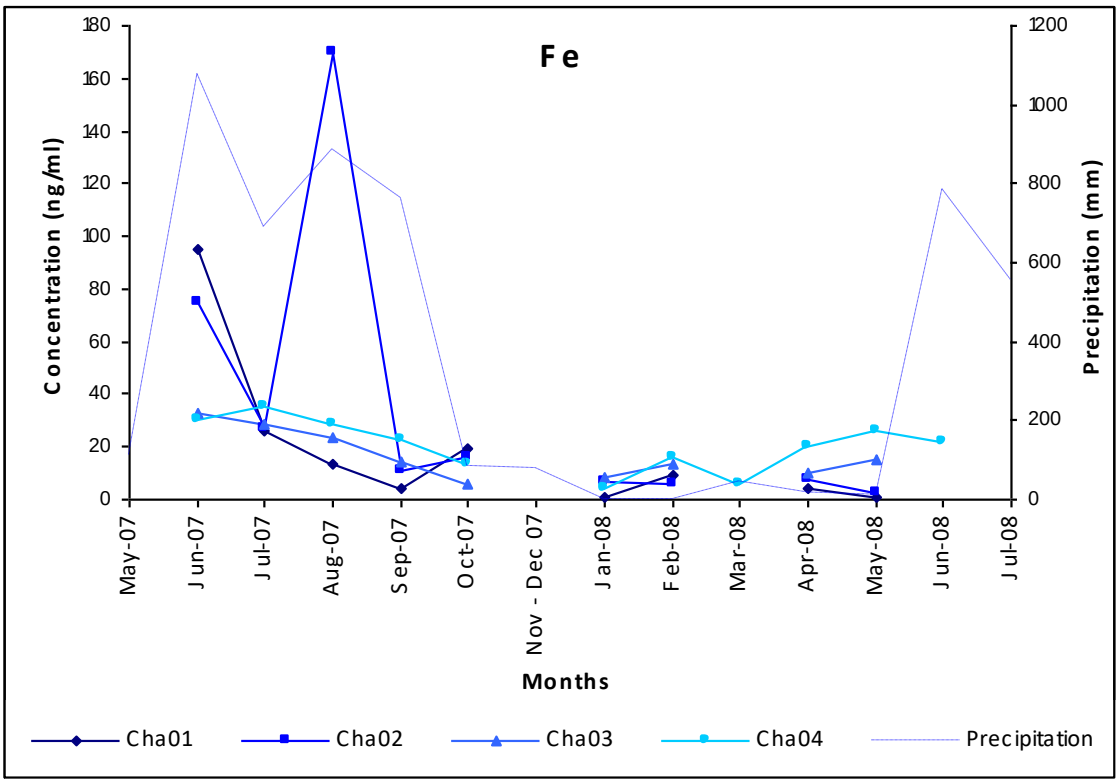

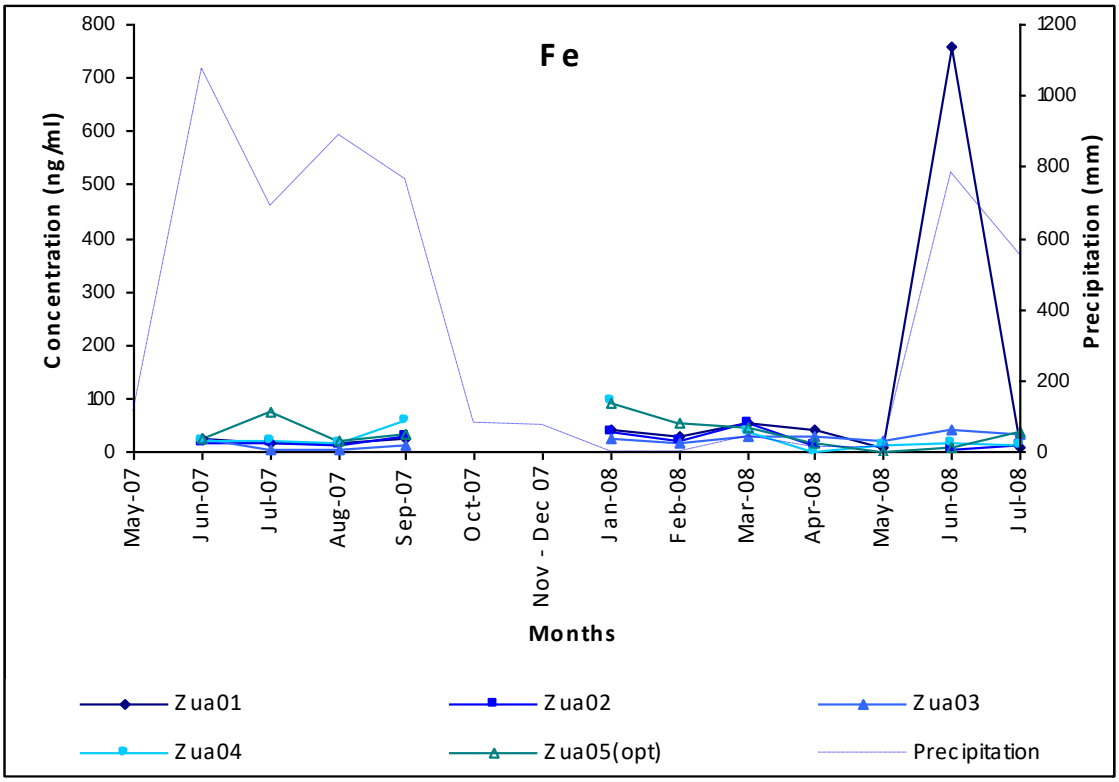

Figure 6.21 Temporal graphs for Fe for the Chapora and Zuari River localities.

The data for Fe are quite poor as a result of two datasets missing some data for the months of June 2007 and May 2008 for the Zuari River. In addition to this, choosing which isotope to plot, ^{56}Fe or ^{57}Fe is also problematic as there are gaps in the data for both isotopes as well as data that yield negative values and as such are deemed below detection limit. Since ^{56}Fe is the main abundant isotope it was preferred to plot this isotope for both rivers, especially since the Chapora River reports an almost complete record of ^{56}Fe concentrations. However, for the Zuari River it is the ^{57}Fe concentrations that are most complete, therefore the Chapora plots ^{56}Fe whilst the Zuari plots ^{57}Fe. An additional difficulty for analysing for Fe is the use of Ar gas in the ICP as the ArO has the same atomic mass as ^{56}Fe.

The Chapora River ^{56}Fe concentrations are interpreted as follows. There are positive peaks in concentration of 95.4 and 74.5 ng ml^{-1} for Cha 01 and Cha 02 in June 2007, respectively, coinciding with the onset of the monsoon period. This is followed by a sharp fall in concentration in July, to values between 26.7 and 35.0 ng ml^{-1} and these for the most part continue to fall gradually through August, September and into October to between 5.58 and 19.7 ng ml^{-1}, with the one exception of Cha 02 in August with a value of 170 ng ml^{-1}. Moving into 2008, the most complete dataset is for Cha 04, which shows concentrations of 3.96 ng ml^{-1} in January, rising to 15.7 ng ml^{-1} in February, before falling to 6.07 ng ml^{-1} in March and then rising gradually through April to a peak of 26.5 ng ml^{-1} in May before falling again in June to 21.9 ng ml^{-1}.
Regarding the Zuari River ^{57}Fe concentrations the first observation is the exceptionally high peak of 757.8 ng ml^{-1} for Zua 01 in June 2008. If we temporarily remove the Zua 01 dataset from the plot the remaining localities can be seen more clearly, although obvious trends are still elusive. However, Zua 02, 03 and 04 do show some similarities during the 2007 monsoon months with values being fairly low and consistent at between 13 – 15 ng ml^{-1} for Zua 02, 5 – 6 ng ml^{-1} for Zua 03 and 18 – 21 ng ml^{-1} for Zua 04 through June, July and August before rising sharply in September 2007 to concentrations of 29.4 ng ml^{-1} for Zua 02, 10.7 ng ml^{-1} for Zua 03 and 56.7 ng ml^{-1} for Zua 04. Looking at the 2008 data, the plots follow a very irregular pattern with concentrations fluctuating widely and for the months of January to April creating an almost saw tooth profile. Whereas during the later months the plots for Zua 03 and Zua 04 do again start to follow a broadly similar trend with values gradually rising through May and June before falling again in July.

Cobalt (Co)

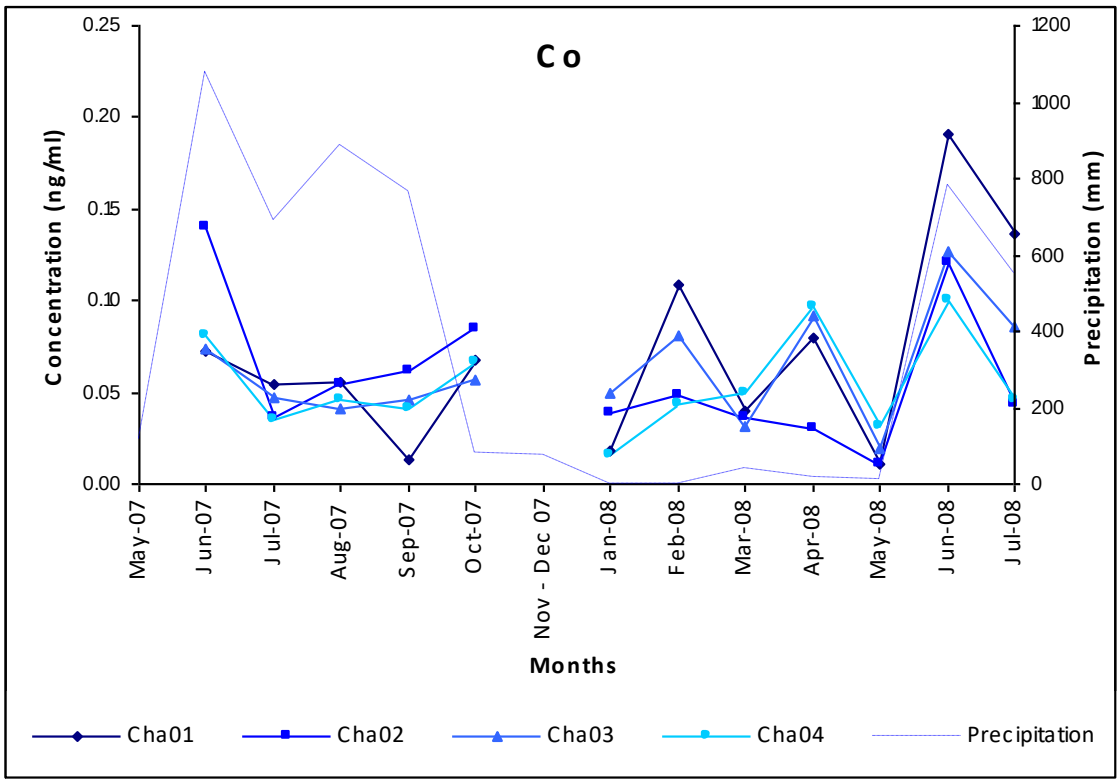

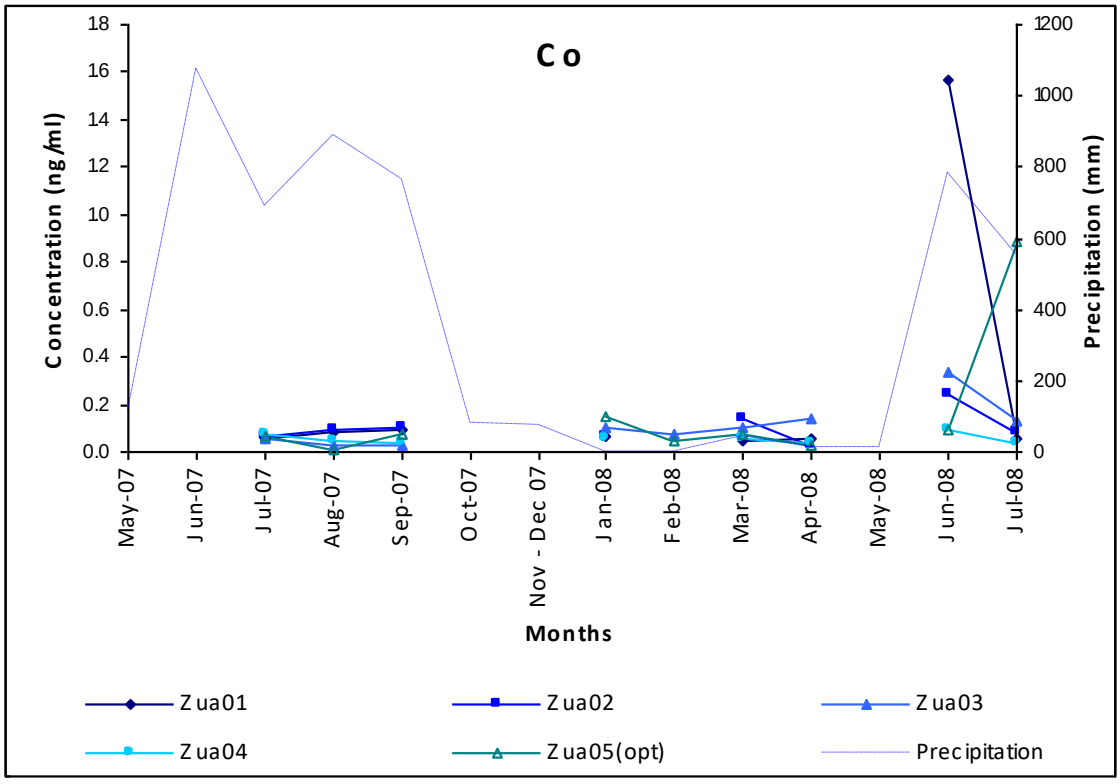

Figure 6.22 Temporal graphs for Co for the Chapora and Zuari River localities.

The concentrations for Co for the Chapora River are all below 0.19 ng ml^{-1}. However, even with these low concentrations there are still obvious peaks in June 2007 and June 2008 for all localities coinciding with the onset of the annual monsoons. In June 2007 concentrations range between 0.07 and 0.14 ng ml^{-1} before falling to 0.04 and 0.05 ng ml^{-1} in July and then rising gradually through August and September to 0.06 and 0.08 ng ml^{-1}in October, with the one exception of Cha 01 in September with a value of 0.01 ng ml^{-1}. Moving on to 2008, values appear to fluctuate in a saw tooth pattern throughout the dry season but all localities display a consistent peak in June 2008 with values ranging between 0.1 and 0.19 ng ml^{-1}.

Once again the Zuari River plot is difficult to describe due to missing data for June 2007 and May 2008, but this is made even more difficult due to data for February 2008 being below detection limits. However, there are a number of consistent peaks in concentration in June 2008 coinciding with the onset of the 2008 monsoon with values ranging between 0.09 and 0.34 ng ml^{-1}, these peaks are significantly higher than the June 2008 peaks for the Chapora River. Other similar higher magnitude concentrations are apparent for the 2007 wet season months with the Zuari values ranging between 0.03 and 0.10 ng ml^{-1} which are also up to twice the magnitude of those for the Chapora River for the same period.

Nickel (Ni)

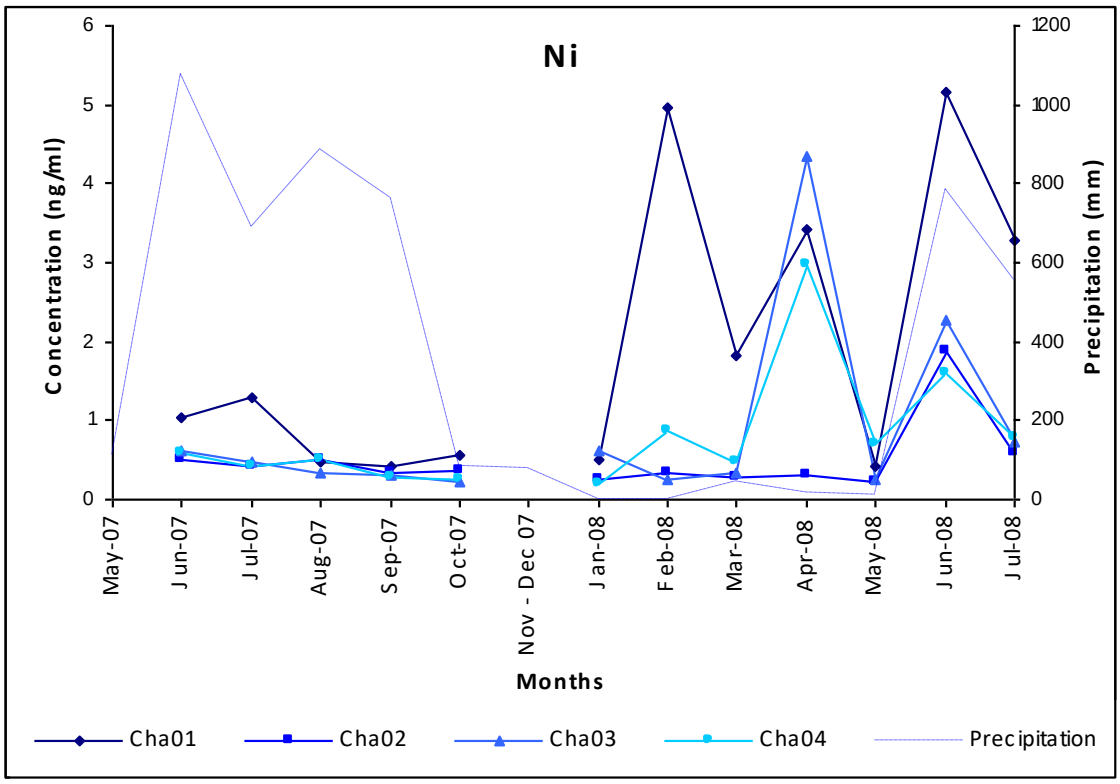

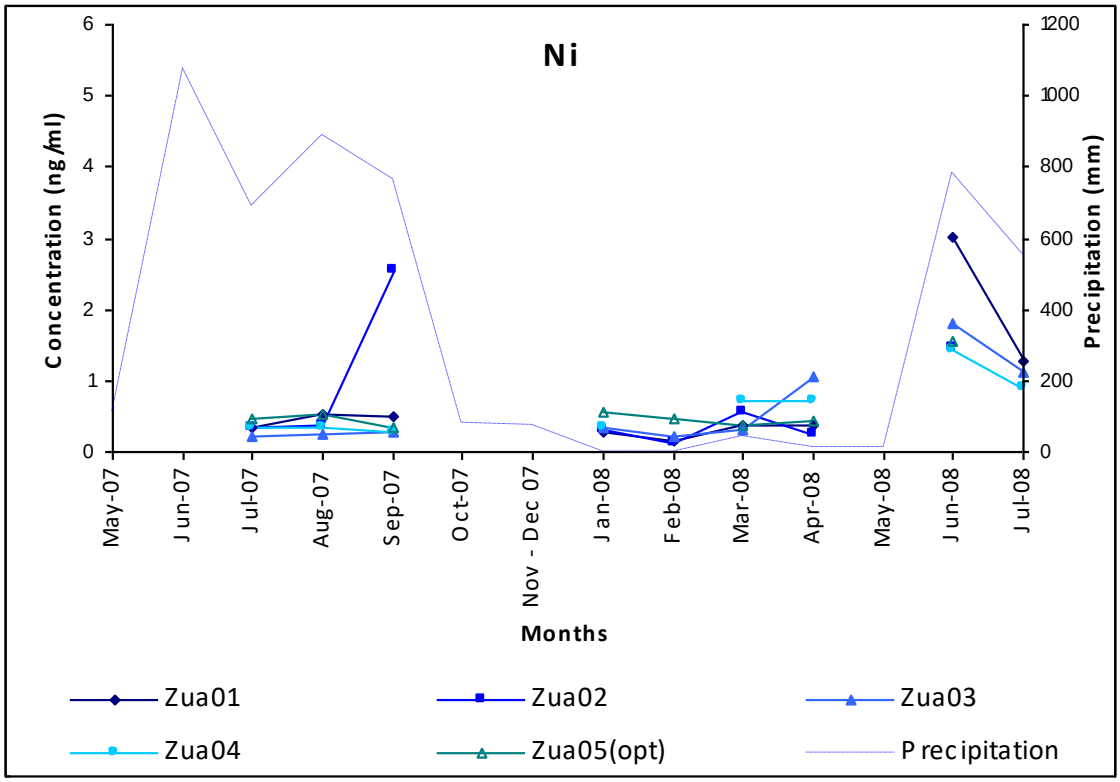

Figure 6.23 Temporal graphs for Ni for the Chapora and Zuari River localities.

For this element the patterns for the four localities are similar to each other during the 2007 monsoon months (June – October) but vary considerably during 2008 dry season before becoming similar again in the 2008 monsoon months of June and July. Therefore, the localities are described in two pairs, Cha 01 and 02 first followed by Cha 03 and 04. Starting with Cha 01 and 02, as previously mentioned they display similar values to each other during the monsoon months with slightly greater variation in concentration in June and July ranging between 0.42 and 1.29 ng ml^{-1} becoming almost identical in August, September and October with concentrations ranging between 0.36 and 0.55 ng ml^{-1}. This similarity in concentration continues in January 2008 but after that the two localities behave very differently with Cha 01 varying markedly between each successive month, e.g., 0.5 ng ml^{-1} in January, 4.96 ng ml^{-1} in February, 1.81 ng ml^{-1} in March, 3.43 ng ml^{-1} in April, 0.43 ng ml^{-1} in May, 5.17 ng ml^{-1} in June and 3.27 ng ml^{-1} in July. By contrast Cha 02 remains very consistent at c. 0.3 ng ml^{-1} until concentrations peak in June to 1.89 ng ml^{-1} before falling to 0.58 ng ml^{-1} in July. Cha 03 and 04, behave in a similar manner during the 2007 monsoon months, displaying consistently low concentrations which reduce slightly through this period, with values starting at c. 0.6 ng ml^{-1} in June reducing to c. 0.25 ng ml^{-1} in October. Moving into 2008, variation increases slightly between the localities ranging between 0.18 and 0.88 ng ml^{-1} for January to March before recording a positive deviation for both localities in April to 4.36 ng ml^{-1} for Cha 03 and 2.98 ng ml^{-1} for Cha 04. The concentrations then fall sharply again in May, before rising and falling in June and July, respectively.

The Ni plot for the Zuari River differs from that for the Chapora River as all of the Zuari localities appear to behave in a similar manner. During the monsoon months concentrations range between 0.23 and 0.53 ng ml^{-1} with one exceptional positive deviation of 2.56 ng ml^{-1} for Zua 02 in September 2007. Moving into 2008, concentrations remain fairly similar through January to March with variation between localities increasing slightly in April to between 0.26 and 1.06 ng ml^{-1}. Unfortunately data are currently missing for May but still a significant positive peak is observable in June with values ranging between 1.42 and 3.03 ng ml^{-1} for all localities before falling in July to between 0.89 and 1.26 ng ml^{-1}.

Copper (Cu)

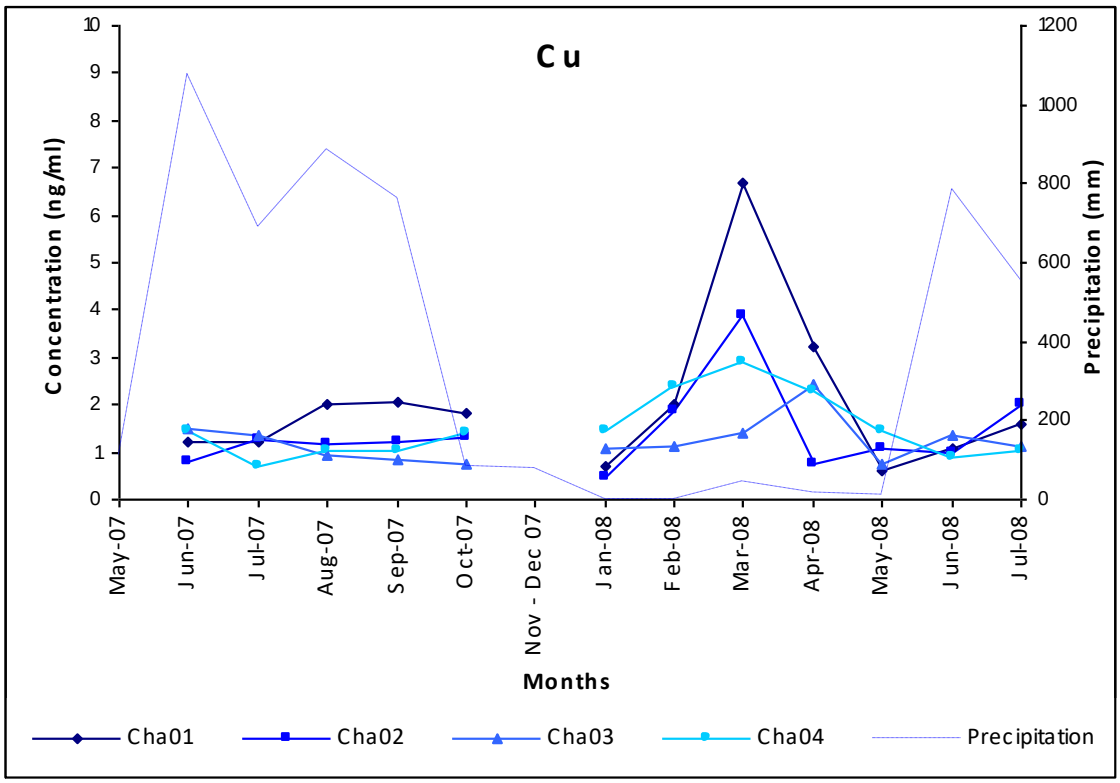

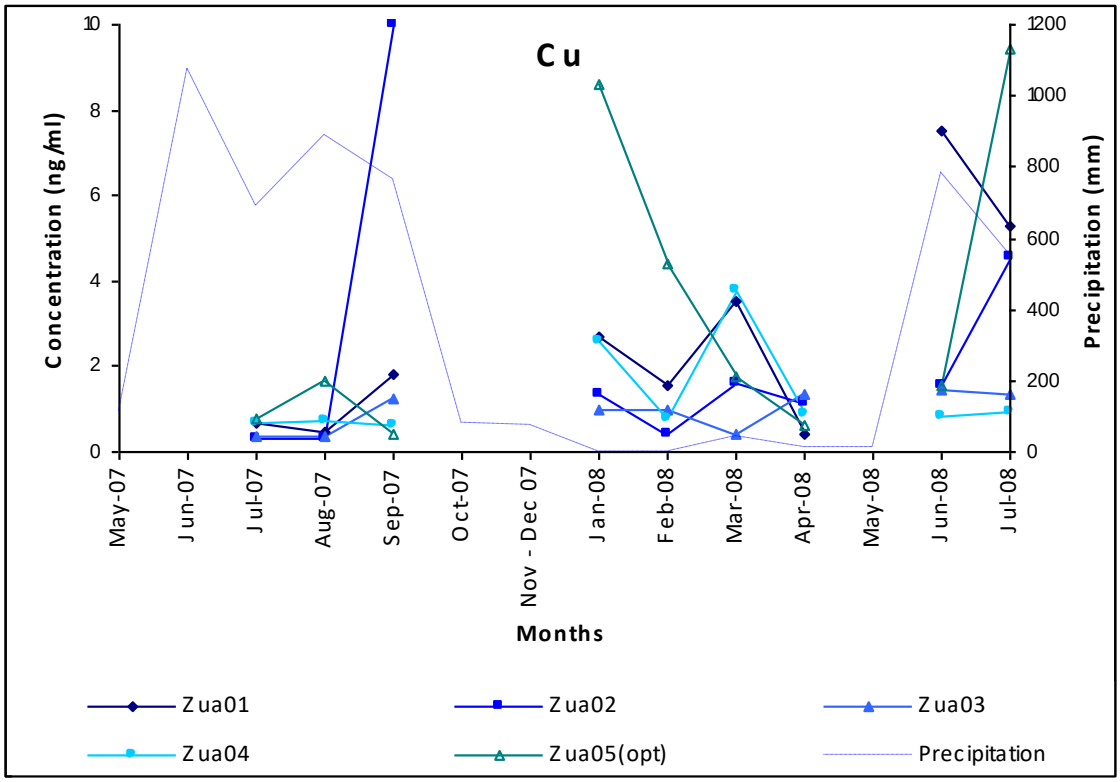

Figure 6.24 Temporal graphs for Cu for the Chapora and Zuari River localities.

Concentrations for all localities are reasonably uniform during the 2007 monsoon months with values ranging between 0.71 and 1.47 ng ml^{-1} for June and July, increasing to between 0.76 and 2.07 ng ml^{-1} in August, September and October, concentrations then fall slightly in January 2008 to between 0.49 and 1.43 ng ml^{-1}. Values for localities Cha 01, 02 and 04 then rise by similar amounts in February before recording their maximum concentrations in March of 6.69 ng ml^{-1}, 3.89 ng ml^{-1} and 2.91 ng ml^{-1}, respectively. However, Cha 03 records its maximum concentration of 2.44 ng ml^{-1} in April. After these peak concentrations all localities show a sharp reduction in to May with concentrations remaining fairly consistent in June and rising slightly in July.

The graph for the Zuari River is much more difficult to describe due to the lack of data for June 2007 and May 2008 and also a number of significant positive deviations that overwhelm other trends, these being; 10.0 ng ml^{-1} for Zua 02 in September 2007, 8.6 ng ml^{-1} for Zua 05opt in January 2008, 4.43 ng ml^{-1} for Zua 05opt in February 2008, 7.53 ng ml^{-1} for Zua 01 in June 2008, 9.43 ng ml^{-1} for Zua 05 opt in July 2008 and 5.3 ng ml^{-1} for Zua 01 in July 2008. If these values are removed the other remaining trends are easier to describe. The concentrations during the 2007 monsoon months of July, August and September begin ranging between 0.35 and 0.7 ng ml^{-1} in July and August with the exception of 1.67 ng ml^{-1} for Zua 05opt in August, rising slightly to between 0.41 and 1.79 ng ml^{-1} in September. Moving into January 2008, the variation in concentration increases to between 0.96 and 2.7 ng ml^{-1} but then the various localities start to behave differently to each other, with Zua 01, 02 and 04 all reporting sharp falls in concentration whilst Zua 03 remains at January levels. Again moving into March the Zua 01, 02 and 04 localities follow similar trends all reporting increases in concentration whilst Zua 03 reports a slight reduction in March. Zua 03 then rises in April, whilst Zua 01, 02, 04 and 05 opt report similar drops in concentration with all values now ranging fairly closely at between 0.44 and 1.37 ng ml^{-1}. The gap in data for May 2008 makes it difficult to be sure but the values for June and July 2008 are reasonably similar to those for April 2008 with the exception of 4.57 ng ml^{-1} for Zua 02 in July.

Zinc (Zn)

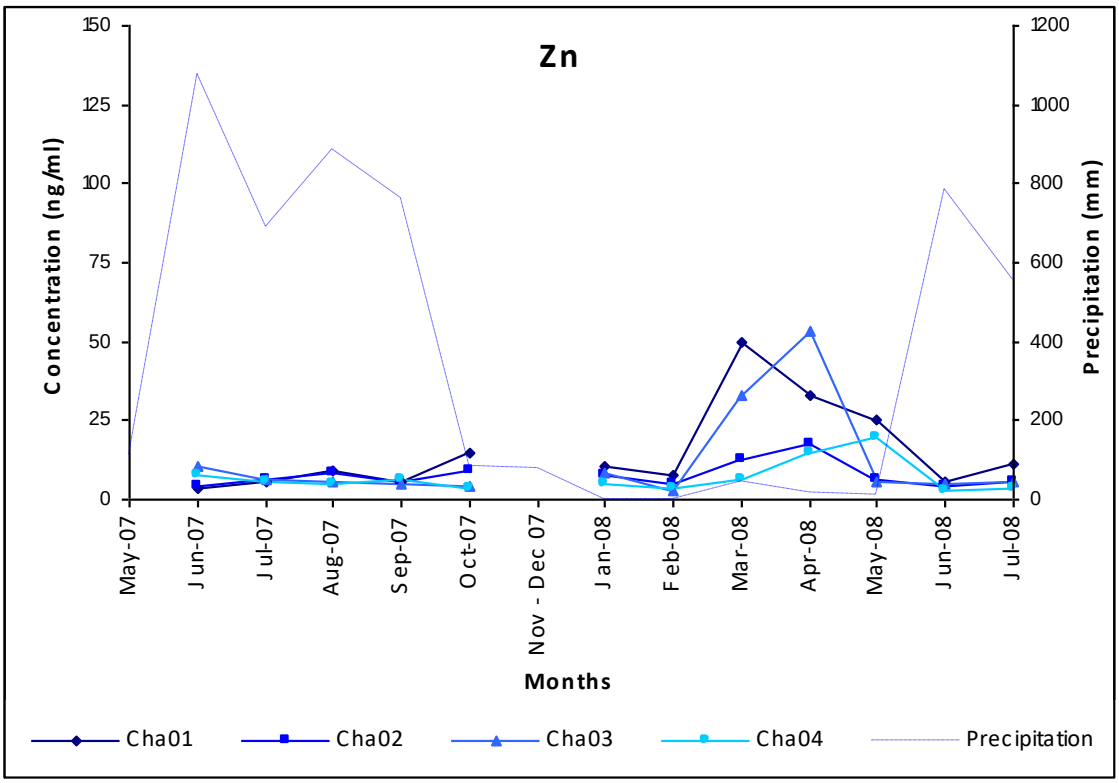

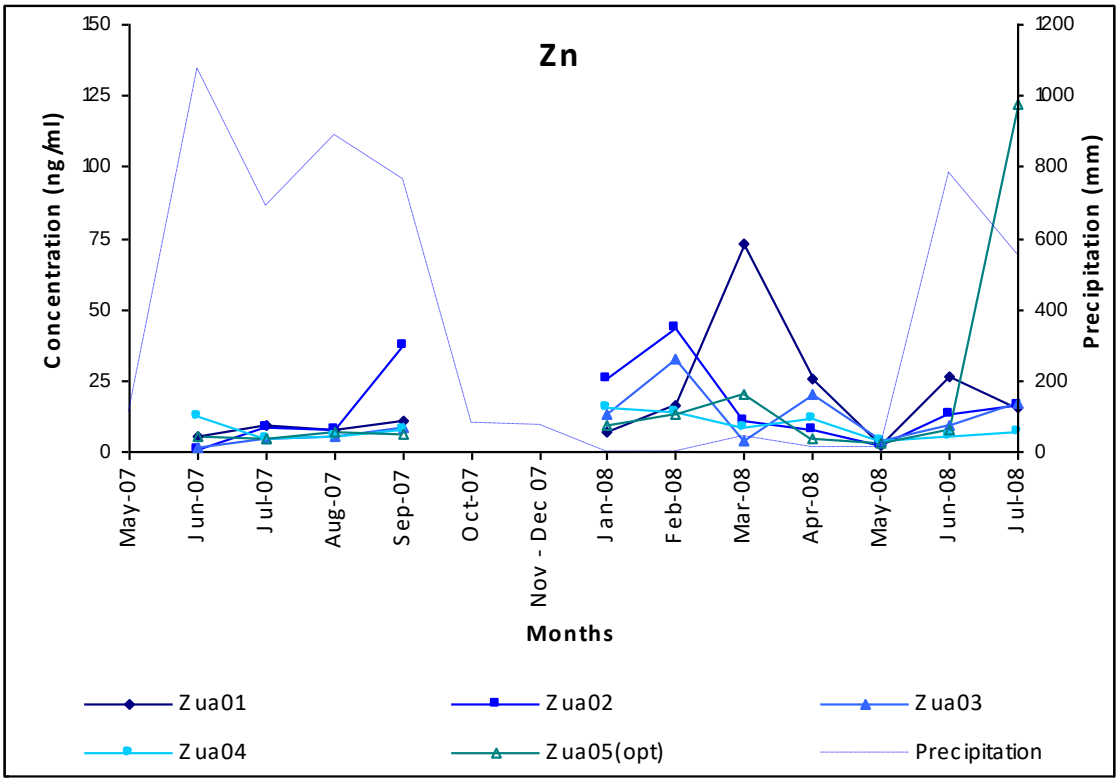

Figure 6.25 Temporal graphs for Zn for the Chapora and Zuari River localities.

During the 2007 monsoon months the concentrations of all four localities vary within a fairly small margin, ranging between 3.20 and 14.5 ng ml^{-1}. However, even within this narrow range there are differences with some localities, Cha 03 and 04 beginning high and reducing through the period whilst others Cha 01 and 02 starting low and fluctuating through the period. However, the greatest variability occurs in the 2008 dry season months. Concentrations continue in similar fashion in January and February before all rising in March with the greatest peaks of 32.9 ng ml^{-1} for Cha 03 and 49.5 ng ml^{-1} for Cha 01 which is its highest concentration. Concentrations remain high in April for all localities; but Cha 01 still represents a fall to 33.3 ng ml^{-1}, whereas Cha 02 and 03 record their highest peaks in April of 17.4 ng ml^{-1} and 53.3 ng ml^{-1} respectively, whilst Cha 04 reaches its peak of 19.3 ng ml^{-1} in May 2008. The concentrations of all four localities come together between 2.5 and 5.0 ng ml^{-1} in June before all rising slightly again in July.

The plot for the Zuari River is similar to that of the Chapora River, in so much as its 2007 monsoon concentrations are similar in magnitude and display similar variations with the slight exception of value of 37.6 ng ml^{-1} for Zua 02 in September 2007. Again it is the dry season where the greatest variation appears, with different localities achieving their peak concentrations at slightly different times. For example, Zua 02 and 03 reach their peak concentrations of 43.7 and 32.1 ng ml^{-1}, respectively, in February 2008, whilst Zua 01 reaches its peak of 73.1 ng ml^{-1} in March, whereas Zua 04 appears to remain at a fairly consistent level throughout the whole sampling period fluctuating between just 3.86 and 15.6 ng ml^{-1}. Concentrations all coincide in May 2008 at between 2.01 and 3.86 ng ml^{-1}.

Lead (Pb)

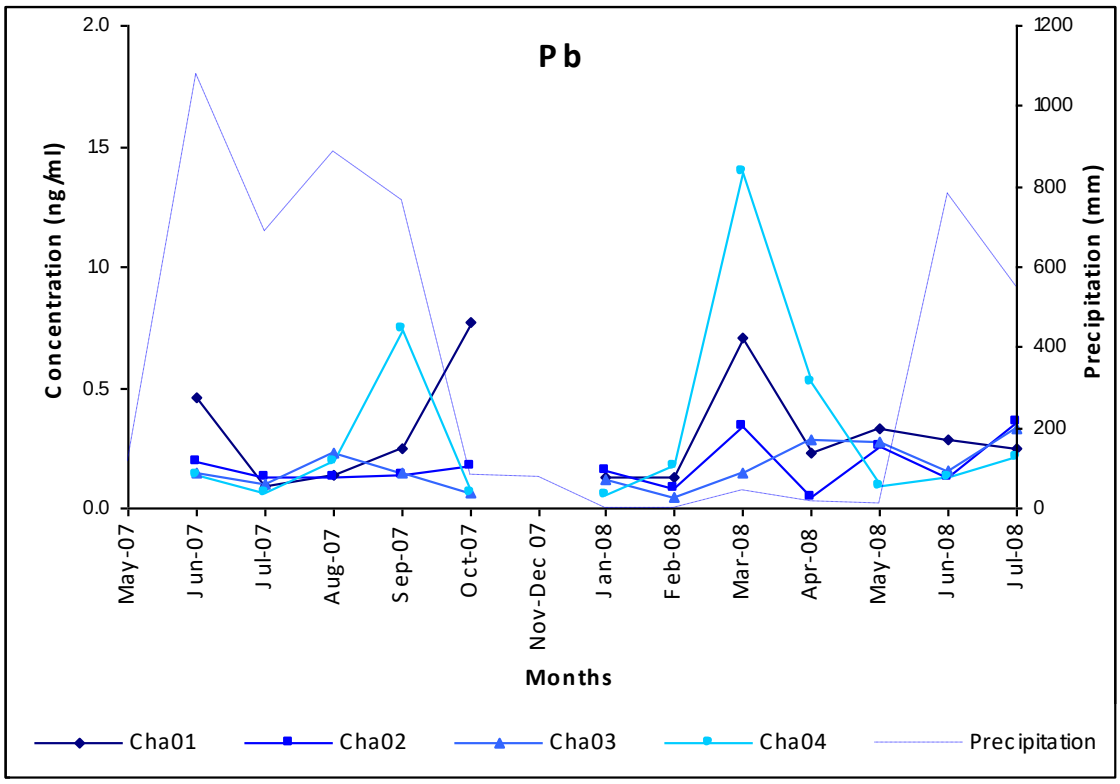

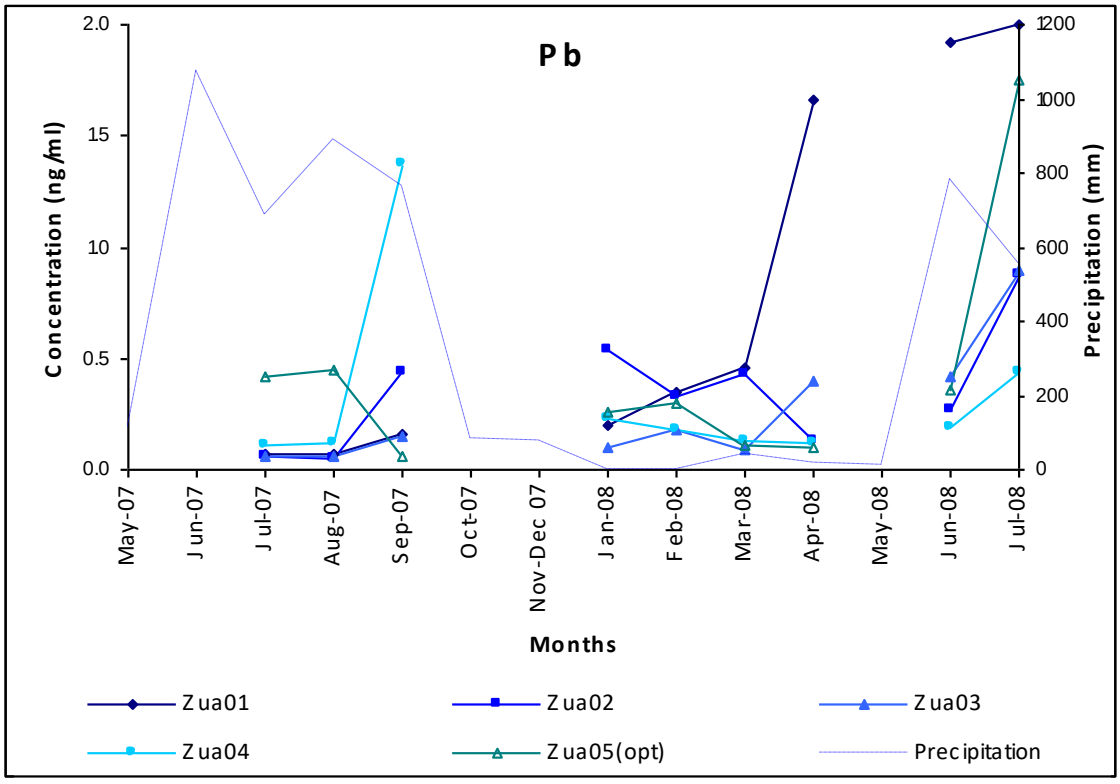

Figure 6.26 Temporal graphs for Pb for the Chapora and Zuari River localities.

In general, the concentrations for Pb during 2007 remain fairly consistent, fluctuating between 0.06 and 0.24 ng ml^{-1}, although there are a few deviations from this, namely, 0.46 ng ml^{-1} for Cha 01 in June, 0.74 ng ml^{-1} for Cha 04 in September and 0.77 ng ml^{-1} for Cha 01 in October 2007. The relatively consistent concentrations continue in to January and February 2008 before reporting significant peaks of 0.34 ng ml^{-1} for Cha 02, 0.71 ng ml^{-1} for Cha 01 and 1.41 ng ml^{-1} for Cha 04 in March 2008. Following these peaks, concentrations fall again through April back to similar levels in May, June and July. It is interesting to note that again the variation in monthly concentration is greater during the dry months than it is during the wet months.

Interpretation of the Zuari graph is more difficult due to lack of data for June 2007, October 2007 and May 2008, but similar peaks to those in the Chapora graph are present in September 2007 with values of 0.43 ng ml^{-1} for Zua 02 and 1.38 ng ml^{-1} for Zua 04. Another difference is that concentrations for Zua 05opt are slightly higher at 0.42 and 0.44 ng ml^{-1} for July and August 2007 respectively, compared to the same months for the Chapora. Looking at 2008, concentrations become more varied ranging between 0.09 and 0.56 for the months of January to June with the exception of 1.66 ng ml^{-1} and 1.92 ng ml^{-1} for Zua 01 in April and June 2008 respectively. Concentrations then rise for all localities reporting values of 2.0 ng ml^{-1} for Zua 01, 0.89 ng ml^{-1} for Zua 02 and 03, 0.43 ng ml^{-1} for Zua 04 and 1.75 ng ml^{-1} for Zua 05opt.

Barium (Ba)

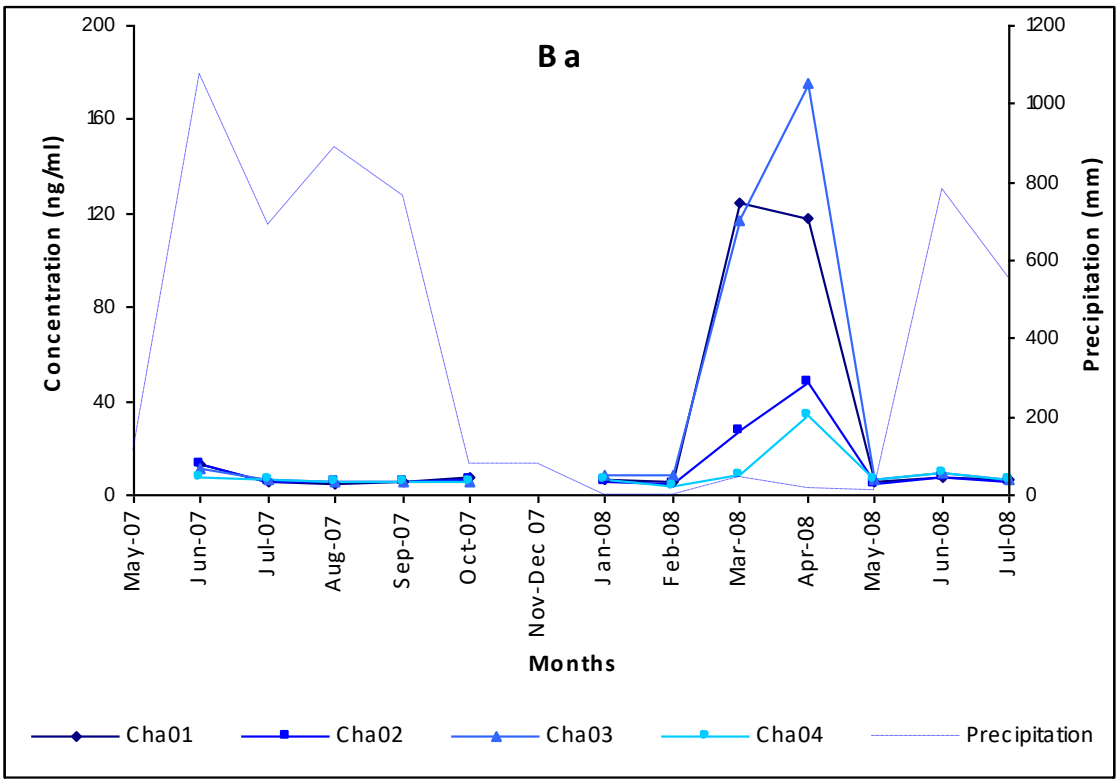

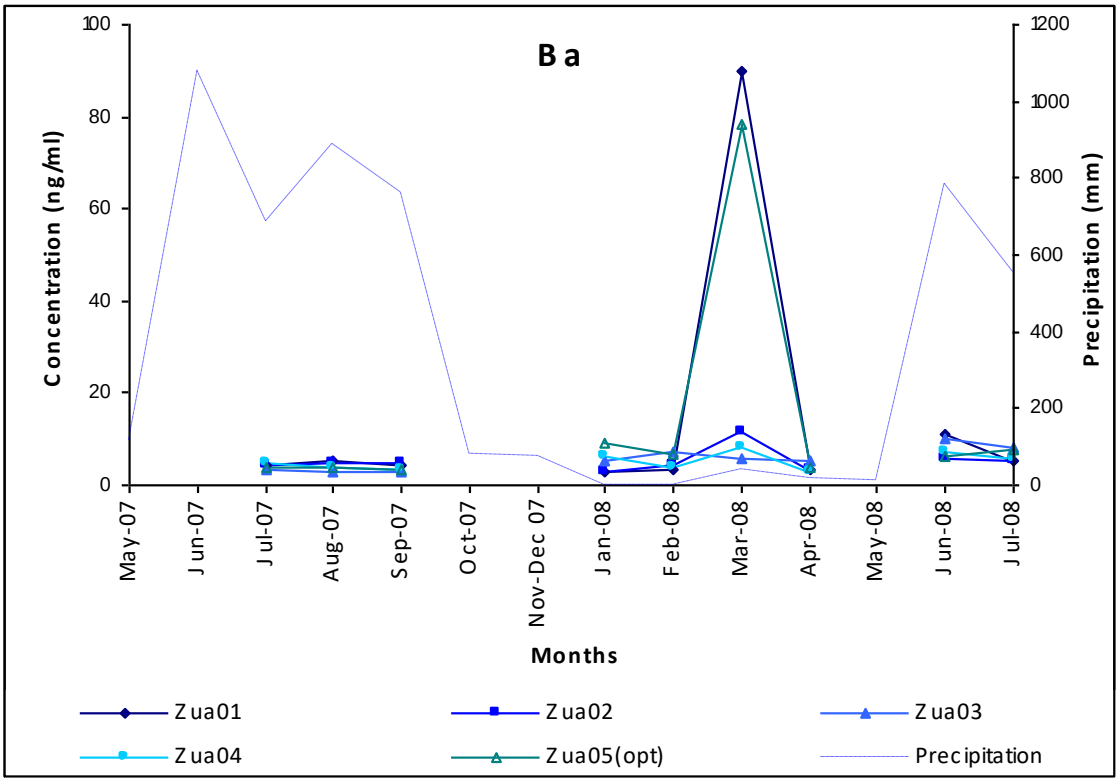

Figure 6.27 Temporal graphs for Ba for the Chapora and Zuari River localities.

The data for Ba for the Chapora River are consistent throughout the whole sampling period, ranging between 4.13 and 9.20 ng ml^{-1}, and the variation between localities for each month is also very small. The only exceptions are for the months of March and April 2008, which report significant increases in concentration with values ranging between 8.83 ng ml^{-1} and 124.4 ng ml^{-1} in March and 33.7 ng ml^{-1} and 175.2 ng ml^{-1} in April.

Very similar patterns exist for the Zuari River, with concentrations ranging between 2.7 and 10.8 ng ml^{-1} for the whole sampling period with the exception of significant peaks in March 2008 with concentrations ranging between 5.58 and 90.1 ng ml^{-1}. Whilst the variation in concentration between localities for each month is still quite small it does increase during the dry months compared with the wet months.

6.3. Element ratios

Ba/Sr versus Y/Ho

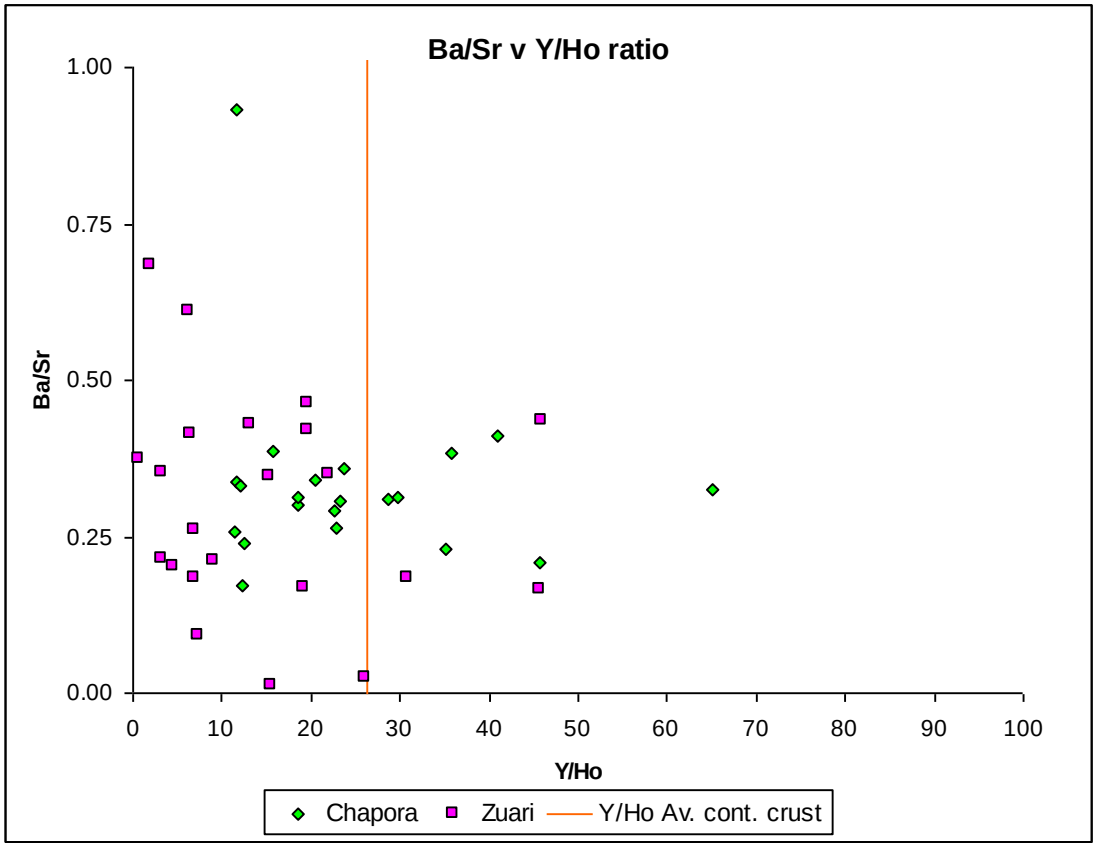

Figure 6. 28 Ba/Sr ratio plotted against the Y/Ho ratio for river water samples from the Chapora and Zuari Rivers. The vertical line represents the average continental crust Y/Ho ratio.

It has only recently been shown that Y loss outweighs that of it geochemical twin Ho during chemical weathering, resulting in measurable Y/Ho fractionation and therefore the Y/Ho ratio can be used as a proxy for silicate weathering (Babechuk et al., 2012). This can be further demonstrated by plotting the Y/Ho ratio versus the Chemical Index of Alteration and/or the Index of Lateritisation in which the Y/Ho ratio is shown to decrease with increasing values of CIA and/or IOL (Babechuk, 2015). Additionally, this element ratio can be used to distinguish riverine waters from marine waters due to the generally higher ratio (40-70) for marine Y/Ho ratios.

Figure 6.28 shows that in general the Y/Ho ratios for both rivers are below 40 and in fact the majority of the values plot below that of the average continental crust at 26.24. There are occasional diversions to higher values which may be due to Y and/or Ho being close to their detection limits or possibly representative of occasional marine signatures.

Sr is significantly more soluble than Ba and therefore a high Ba/Sr ratio is likely to result from enhanced leaching of Sr relative to Ba and is indicative of strong chemical weathering. All the values plotted above are below 1.0 and are therefore suggestive of a weak chemical weathering signature; this is possibly the result of weathering material that is already strongly depleted in mobile elements (laterite).

The Y/Ho versus Ba/Sr plot as a whole is suggestive of weak chemical weathering of material already depleted of mobile elements, which is as expected for the study area where the weathering front is estimated at 25-30m deep.

6.4. Rare Earth Elements (REE)

The Rare Earth Elements (REE) are a group of 17 chemically similar metallic elements including the lanthanide elements plus scandium and yttrium. The lanthanides are elements spanning the atomic numbers 57 (La) to 71 (Lu). The lanthanides all occur in nature; however, promethium (Pm), atomic number 61, is the rarest, occurring only in trace quantities as it has no long lived or stable isotopes (Castor and Hedrick, 2006). Scandium and yttrium are considered REEs as they have similar chemical and physical properties. The lanthanide group of elements possess similar ionic radii, decreasing from 1.016 Å for La to 0.85 Å for Lu (Piper, 2013). The REEs are trivalent (Ln^{3+}) with the exception of Ce^{4+} and Eu^{2+} in certain environments. These similarities mean that

the REEs can substitute for each other in crystal structures and can also impose limitations on their fractionation through weathering, erosion and eventual transport by rivers as suspended or colloidal matter. Therefore they are an ideal group of elements to identify sources of the lithogenous fraction of marine and non marine sedimentary deposits (Piper, 2013). The REE can be separated into three groups; Light REE (La, Ce, Pr, Nd and Pm), Middle REE (Sm, Eu, Gd, Tb, Dy and Ho) and Heavy REE (Er, Tm, Yb and Lu). Yttrium is considered a HREE and scandium is grouped with the LREE due to their chemical similarity.

REE do not occur naturally as metallic elements but occur in a wide variety of mineral types including halides, carbonates, oxides, phosphates and silicates. The REE are generally hosted by rock-forming minerals where they substitute for major ions, Environments in which REE becomes enriched can be divided into two categories; primary deposits associated with igneous and hydrothermal processes and secondary deposits resulting from sedimentary and weathering processes as is the case with this study.

The REE are a prime example of the Oddo-Harkins Rule, whereby, even-numbered elements are more abundant than their odd-numbered neighbours when plotted against atomic number. This is due to the greater nuclear stability gained by the pairing of protons that offsets the spin of the one by the other (Figure 6.29).

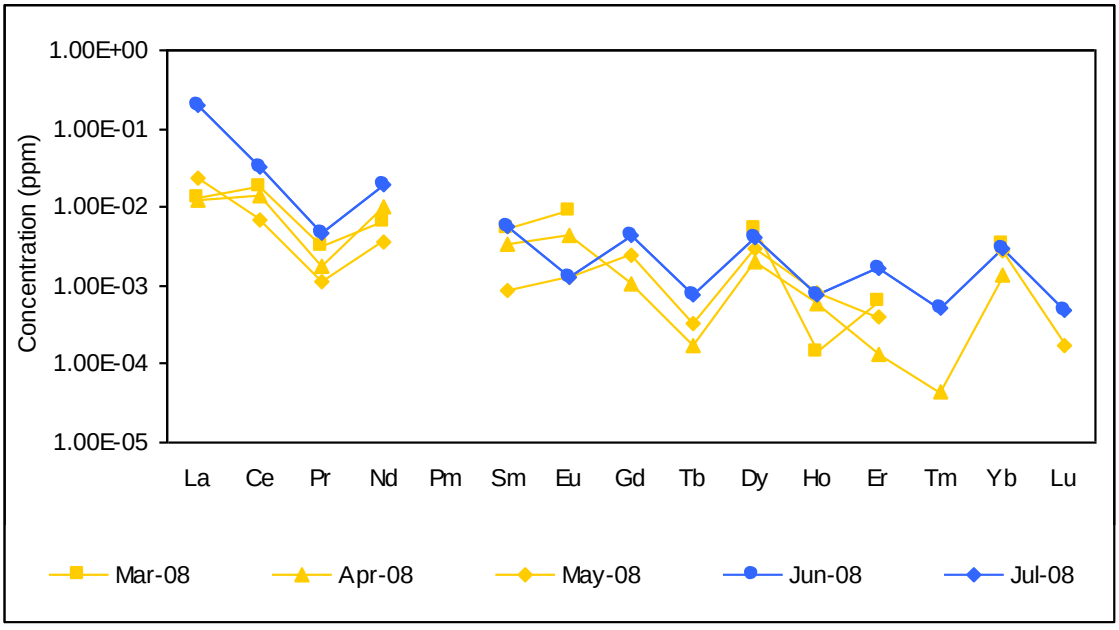

Figure 6.29 Plot of Locality Cha 01 showing the typical herring-bone shaped curves of elemental concentration when plotted against atomic number for the months March 2008 – July 2008.

The herring-bone shaped curve of measured elemental concentration plotted against atomic number can be converted to a more meaningful curve by normalising to a known standard, thus allowing the relative concentrations to be compared visually. A number of standards can be used, including the World Shale Average (WSA), the North American Shale Composite (NASC), the Upper Continental Crust (UCC), the Post Archaean Australian Shale (PAAS) or an average of chondrites (Piper, 2013) (Table 6.3).

Table 6.3 Elemental composition of rock standards – World Shale Average (WSA), the North American Shale Composite (NASC), the Upper Continental Crust (UCC), the Post Archean Australian Shale (PAAS) and average chondrites, all values in μg g^{-1} (Piper, 2013).

Rare Earth Element	*World Shale Average (WSA)*	*North American Shale Composite (NASC)*	*Upper Continental Crust (UCC)*	*Post Archean Australian Shale (PAAS)*	*Average Chondrites*
La	*41.00*	*31.1*	*30*	*38.2*	*0.32*
Ce	*83.00*	*66.7*	*64*	*79.6*	*0.90*
Pr	*10.10*	*7.70*	*7.1*	*8.83*	*0.13*
Nd	*38.00*	*27.4*	*26*	*33.9*	*0.57*
Sm	*7.50*	*5.59*	*4.5*	*5.55*	*0.21*
Eu	*1.61*	*1.18*	*0.88*	*1.08*	*0.074*
Gd	*6.35*	*4.90*	*3.8*	*4.66*	*0.31*
Tb	*1.23*	*0.85*	*0.64*	*0.774*	*0.051*
Dy	*5.50*	*4.17*	*3.5*	*4.68*	*0.30*
Ho	*1.34*	*1.02*	*0.8*	*0.991*	*0.074*
Er	*3.75*	*2.84*	*2.3*	*2.85*	*0.21*
Tm	*0.63*	*0.48*	*0.33*	*0.405*	*0.032*
Yb	*3.53*	*3.06*	*2.2*	*2.82*	*0.18*
Lu	*0.61*	*0.46*	*0.32*	*0.433*	*0.032*

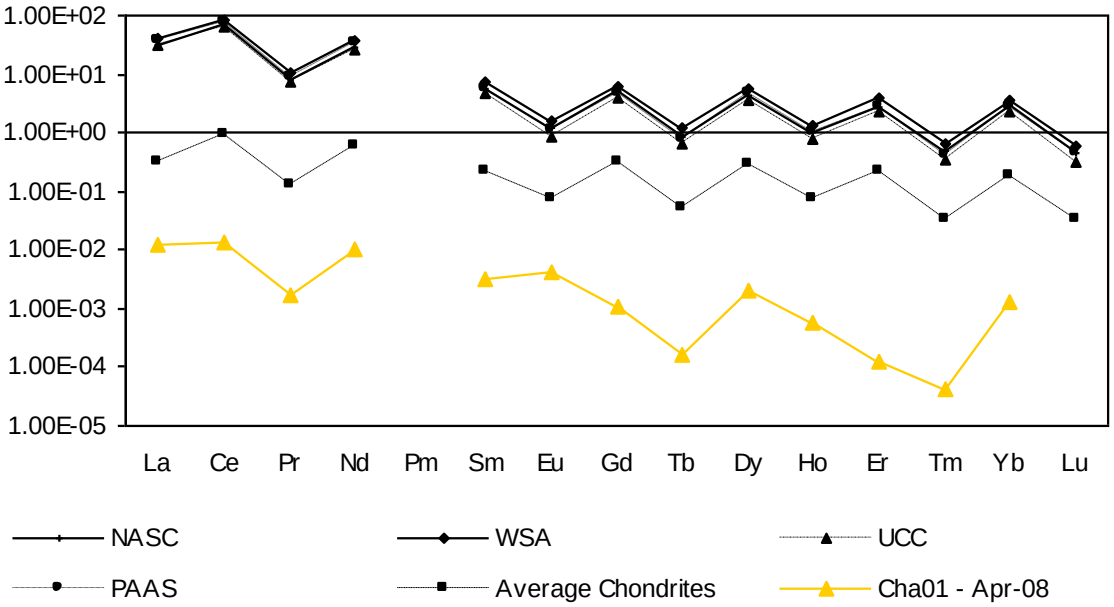

Figure 6.30 The REE curves for all of various standards plotted against the concentrations for locality Cha 01 during April 2008.

Figure 6.30 above clearly shows that the various standards represent two compositional extremes of siliciclastic source rocks: one felsic (NASC, WSA, PAAS and UCC) and the second ultramafic (chondrites). Also plotted on Figure 6.30 are the un-normalised values for locality Cha 01 during April 2008. Since the inter-element concentrations are similar for the sample plotted when compared to any of the above standards, it was decided to use the North American Shale Composite (NASC) standard. Figure 6.30 shows the NASC normalised REE pattern for Cha 01, 02, 03 and 04 and Zua 01, 02, 03 and 04.

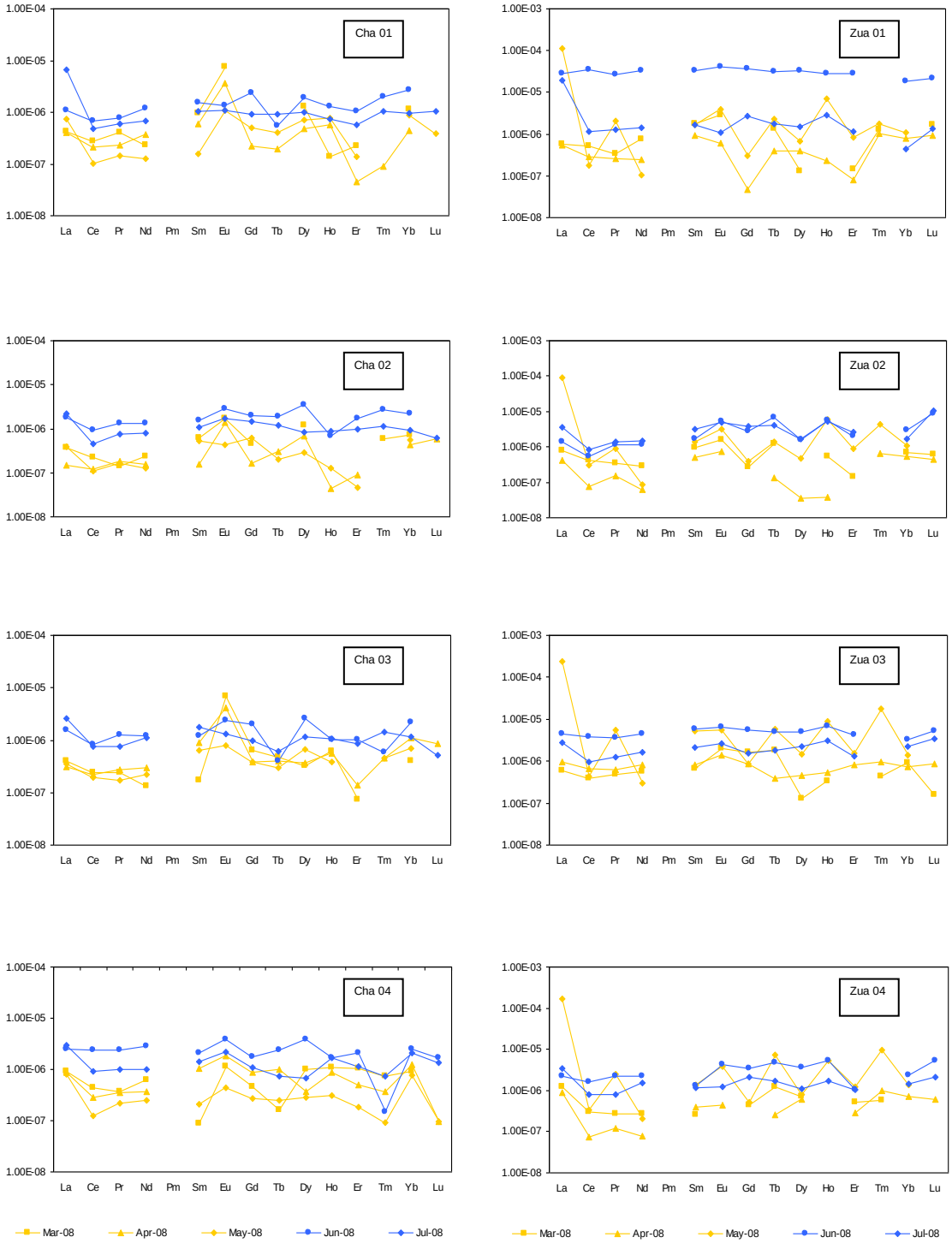

Figure 6.31 NASC normalised Rare Earth Element (REE) plots for Cha 01 – 04 and Zua 01 – 04 for the months March – July 2008.

Figure 6.31 has been plotted for the months of March – July 2008 to provide a compare and contrast between the dry months of March, April and May with the wet months of June and July. There are a number of observations, with the most obvious one being the relatively flat profile of the wet season plots compared to the more fluctuating dry season plots. Particularly clear examples of these flat profiles can be seen on the graphs for Zua 01, 03 and 04 for the month of June 2008; however, the fact that the June 08 data for Zua 01 are c. 1.5 orders of magnitude higher is suspicious and may be due to the possibility that this sample was incorrectly filtered during its collection. Similar flat profiles are also present for the month of July 2008 although most of these also display an elevated La value compared to the other REE for that month. This leads on to the next observation, the elevated La peak, which although present on most of the dry season months for both rivers, is clearly more prominent on the Zuari River for the month of May.

Another observation is that of the positive Eu peak which again is most prominent during the dry season months and can be very clearly seen on the Cha 01 graph for all three dry season months, whereas for the Cha 02, 03 and 04 graphs it is only present for the months of March and April. It seems that the Eu anomaly is predominantly a function of the dry season and appears to be strongest in the dryer months of March and April before weakening in May and becoming imperceptible in June and July. However, this anomaly does not seem to be present for the Zuari River. Since it is only present on the Chapora River it seems most likely that this is due to a difference in lithology (i.e., rocks containing plagioclase) and possibly due to the presence of one or more REE-rich minerals such as monazite or apatite.

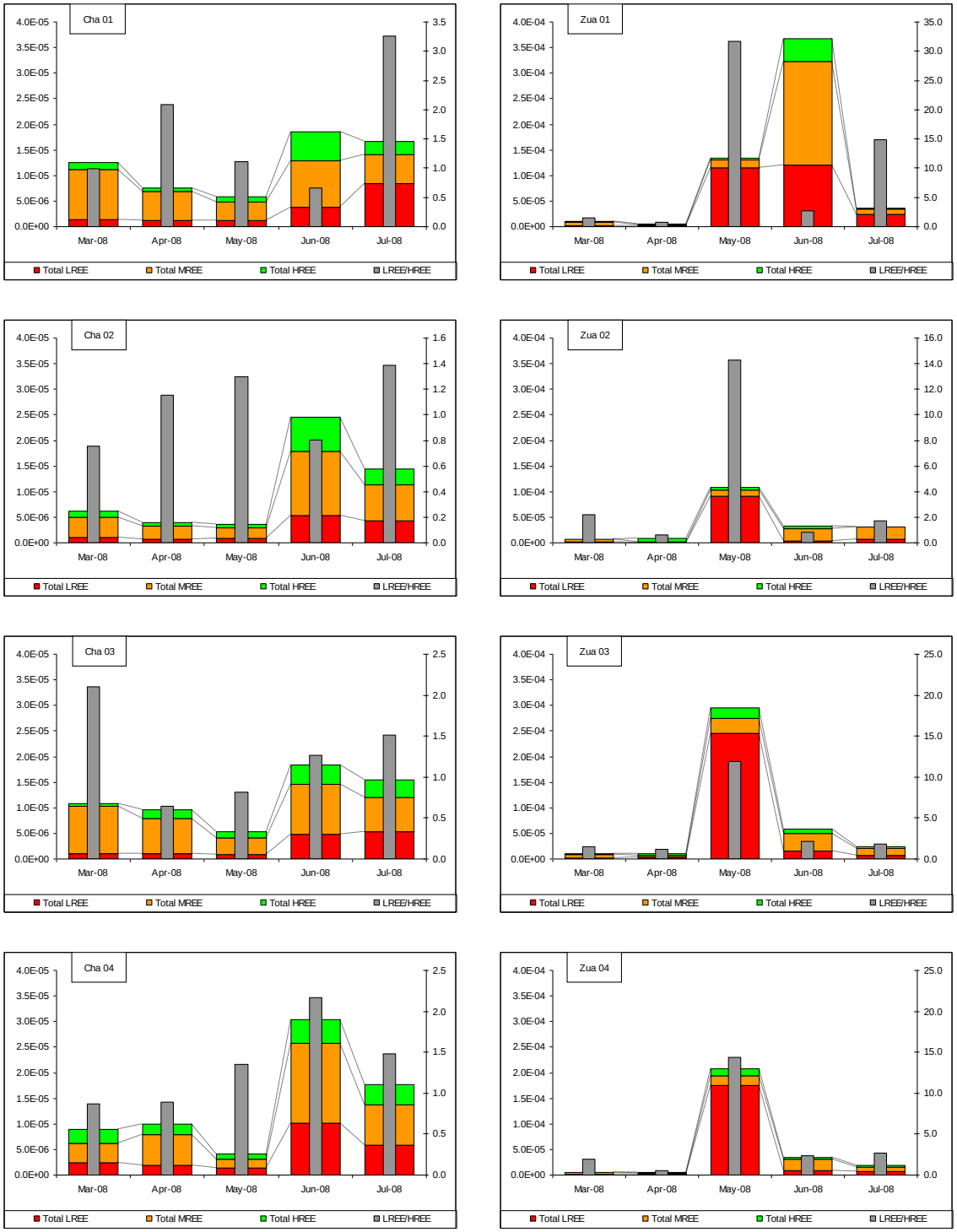

Figure 6.32: REE plots for localities Cha 01 – 04 and Zua 01 – 04 for the months of April – July 2008. The plots show the monthly variation of ∑REE, the proportions of LREE, MREE and HREE and the ratio of LREE/HREE.

Figure 6.32, as the caption describes is a composite plot reporting the monthly variation of ∑REE, the proportions of LREE, MREE and HREE and the ratio of LREE/HREE. The following section will describe each of these components in turn starting with ∑REE.

Total REE

For Cha 01 – 03 the basic trend begins with high values in March 2008 ranging between 1.08 x 10^{-5} for Cha 03 and 8.93 x 10^{-6} for Cha 04, decreasing through April and May to between 3.6 x 10^{-6} for Cha 02 and 6.1 x 10^{-6} for Cha 01, increasing to a peak of between 1.84 x 10^{-5} for Cha 03 and 3.2 x 10^{-5} for Cha 04 in June before decreasing slightly once more in July to between 1.5 x 10^{-5} for Cha 02 and 1.91 x 10^{-5} for Cha 04. Cha 04 is similar with the exception that the March value of 8.93 x 10^{-6} is slightly lower than the April value of 1.01 x 10^{-5}.

Before moving on to describe the Zuari plots in detail it is important to note that the scales for the two Y-axes are one order of magnitude higher than those for the Chapora plots. This is largely the result of the significantly elevated values obtained for May 2008 which are obscuring the other data. As with the data for June 08 this could also be due to lack of correct filtration during sample collection.

For the Zuari localities the pattern is completely different to that of the Chapora samples. Instead values begin very low in March and April with values ranging between 3.77 x 10^{-6} for Zua 02 in April and 1.14 x 10^{-5} for Zua 01 in March. The values then increase markedly in May to between 1.1 x 10^{-4} for Zua 02 and 2.95 x 10^{-4} for Zua 03. After which values decrease significantly to between 2.02 x 10^{-5} for Zua 04 in July and 6.31 x 10^{-5} for Zua 03 in June. However, there is one clear exception, which being the peak value of 3.89 x 10^{-4} for Zua 01 in June.

LREE, MREE and HREE proportions

For the Chapora the months of March, April and May the ∑REE columns are dominated by MREE with relatively similar proportions of LREE and HREE, whilst June and July columns are still dominated by MREE but with varying proportions of LREE and HREE. For example, in June and July for Cha 01 and Cha 02 HREE show a slightly greater proportion than LREE, whereas, for all other plots for June and July throughout the Chapora the opposite is the case with LREE showing a slight dominance over HREE. This dominance of MREE over LREE and HREE could be due to the existence of positive Eu anomalies which have been identified and discussed earlier for the dry season months of March, April and May

For the Zuari localities the most obvious observation is the large dominance of LREE over both MREE and HREE during the May 2008 peaks, interestingly, the higher peak

occurring in June 2008 for the Zua 01 locality doesn't show this feature. If we consider this observation in collaboration with the NASC normalised REE element plots for the Zuari localities we can see that this is in agreement with the positive La anomalies occurring in May for all four localities and it is probably this anomaly that is driving the observed dominance of LREE.

LREE/HREE

As discussed above in the previous section the ratio of LREE compared to HREE varies throughout both river systems. By plotting LREE/HREE we can compare their respective contributions. A value of one would mean an equal amount of each was recorded. A value greater than one informs us that there is a greater proportion of LREE and a value below one informs us that there is a greater proportion of HREE.

For the Chapora River localities the lowest value of 0.66 occurs in June 2008 for the Cha 01 locality, whilst the highest value of 3.26 occurs in July for the same location. For the Zuari graphs the lowest value of 0.58 occurs in April for the Zua 02 & 04 localities, whilst the highest values of between 11.96 and 31.69 are centred on the March samples, with the highest value being recorded for Zua 01 and the lowest for Zua 03. Additionally, there is a fifth high value of 14. 88 reported occurring in July for Zua 01.

Summary

The left hand and right hand Y-axes of Figure 6.32 show the Chapora graphs being an order of magnitude lower than those of the Zuari. This is due to the high ∑REE values and the high LREEs/HREEs ratio present for all of the Zuari River's May data as well as the high ∑REE value for the June data for Zua 01. However, if we compare the individual values of say Cha 01 against Zua 01 etc. for each of the other months (March, April, June and July) we see that the values are of the same order of magnitude, with the exception of Cha 04 versus Zua 04 in April when the Chapora value is 1.01×10^{-5} compared to 5.53×10^{-6} for the Zuari and the Cha 01 versus Zua 01 in June when the Chapora value is 1.85×10^{-5} compared to the Zuari value of 3.89×10^{-4}. This suggests that there is very little difference between the two basins even though they have different lithologies, with the obvious exception of the significantly elevated values occurring in May within the Zuari catchment area.

The Chapora river system displays higher ∑REE values during the wet season months of June and July compared with those of the dry season months of March and April and May, although, the values consistently peak in June before decreasing slightly in July. A similar pattern exists for the Zuari River system, with the exception of the significant May peaks for all localities. These peaks are consistent with the observed 'rinse-out' effect present for many of the major and trace cations and anions.

Spatially there is only one clear trend which displays any consistency, that being for the months of March, April and May for the Chapora River and March and April for the Zuari River. This displays values decreasing from locality 01 to locality 02, increasing from locality 02 to locality 03 and finally decreasing again slightly from locality 03 to locality 04. For the Chapora River the June data show significantly higher values compared to the data for March, April and May but also display an opposite pattern, with values increasing from Cha 01 to Cha 02, then decreasing from Cha 02 to Cha 03 before finally increasing significantly from Cha 03 to Cha 04. The July trend is different again displaying a curving pattern falling gently from Cha 01 to Cha 02 before rising gently through Cha 03 to Cha 04. Considering the Zuari River the data are dominated by the high May values for all localities and the high June value for Zua 01. Although the May values and the Zua 01 June value are significantly higher they do still follow the same broad trend as the March and April values.

The consistently high values occurring in May 2008 for all Zuari River localities cannot be fully trusted as they could be due to a mix up in the field such as accidentally forgetting to filter the sample correctly which was identified for July 2007 and May 2008.

The REE concentrations plotted in Figures 6.31 and 6.32, like all other riverine elemental concentrations, are derived from a variety of sources including atmospheric, lithological and anthropogenic. One of the main lithologies of note within the Zuari River drainage basin is the Banded Iron Formations (BIFs), which are formed by chemical precipitation from seawater and hence are thought to represent the chemical composition of the water body from which they were formed. As such analyses of Banded Iron Formations (BIFs) often deliver negative Ce anomalies, where a strong negative anomaly ($Ce/Ce^* = 0.1 – 0.5$) represents strongly oxygenated conditions similar to modern day seawater (Kato et al., 2006). BIFs also often record positive Eu anomalies ($Eu/Eu^* = 0.8 – 7$) which represent the influence of hydrothermal fluids (Kato et al., 2006). Likewise, one of the key lithologies within the Chapora River basin is Deccan basalt which also often records a strong positive Eu anomaly as discussed

above. Therefore, the REE concentrations of rivers, in both the dissolved and suspended form are strongly controlled by the lithologies of their drainage basins. However, REE concentrations are generally much higher in the suspended fraction compared to the dissolved fraction.

6.5. Saturation Indices (SI)

Saturation Indices have been employed to help predict which minerals are likely to precipitate or dissolve in the presence of the various river water samples. S.I. calculations have been carried out using PHREEQC version 3.17. (Parkhurst, 2013). Positive values predict which minerals may be precipitated from the river waters, whilst negative values predict which minerals may dissolve in the presence of the river waters. Saturation Indices graphs have been created for all none estuarine influenced localities; these include Cha 01, 02, 03 & 04 on the Chapora River and Zua 01, 02, 03 & 04 on the Zuari River (Figures 6.33 and 6.34). Each of these graphs has been populated with data for minerals which report positive values; these include gibbsite, goethite, haematite, Ca-montmorillonite, K-mica, kaolinite and $Fe(OH)_3$, even though Ca-montmorillonite and $Fe(OH)_3$ only record occasional positive values. A number of gaps are present in the data; these are predominantly where no samples were collected, e.g. November and December 2007 for the Chapora River and October, November and December 2007 for the Zuari River. Additionally, a few other gaps are present; these are where there was a lack of reliable data for Fe and / or Al. If no Fe data are recorded there can be no prediction for haematite, goethite, or $Fe(OH)_3$; likewise if no Al data are recorded there can be no prediction for gibbsite, Ca-montmorillonite, K-mica or kaolinite. The following section provides a full set of SI data for Cha 01 (Table 6.4) and Zua 01 (Table 6.5) as well as a graph for each of these localities for phases where positive values are reported, the section then describes the graphs in turn starting with the Chapora localities and then the Zuari localities. Due to similarities in the plots only the Cha 01 and Zua 01 plots are included in the text, however, a full set of graphs is included in Appendix G. The graphs have been separated into Fe-bearing minerals, plotted in black and Al-bearing minerals, plotted in grey. The section concludes with a summary of the key observations.

Table 6.4 Saturation Indices values for Cha 01, phases shown in red bold indicate where positive values are present at some point throughout the sampling period.

Cha 01	Jun-07	Jul-07	Aug-07	Sep-07	Oct-07	Nov- Dec 07	Jan-08	Feb-08	Mar-08	Apr-08	May-08	Jun-08	Jul-08
Phase													
$Al(OH)_3(a)$	-1.47	-1.22	-0.70	-1.21	-2.12		-1.22	-1.72	-1.64	-1.61	-1.50	-1.99	-1.44
Albite	-6.04	-5.12	-5.43	-6.31	-5.43		-5.12	-4.95	-5.31	-6.17	-6.01	-5.92	-5.35
Alunite	-4.67	-4.1	-2.32	-2.49	-5.19		-4.10	-62.55	-6.37	-4.13	-4.63	-3.48	-2.93
Anglesite	-6.32	-6.51	-6.53	-6.17	-5.66		-6.51	-34.35	-5.84	-6.09	-6.09	-5.60	-6.17
Anhydrite	-4.03	-4.55	-4.65	-4.67	-4.49		-4.55	-32.42	-4.57	-4.48	-4.49	-4.05	-4.64
Anorthite	-6.30	-5.9	-5.47	-7.32	-7.90		-5.90	-6.09	-6.03	-7.59	-6.83	-8.18	-7.05
Aragonite	-1.99	-3.9	-3.32	-4.70	-4.50		-3.90	-3.98	-3.30	-4.45	-3.94	-4.47	-4.50
Barite	-1.88	-2.41	-2.47	-2.41	-2.32		-2.41	-30.29	-1.10	-1.02	-2.50	-1.84	-2.39
Ca-Montmorillonite	-1.42	**0.25**	**0.71**	-0.53	-0.66		**0.25**	-0.99	-0.78	-1.13	-0.84	-1.00	**0.29**
Calcite	-1.85	-3.76	-3.18	-4.55	-4.36		-3.76	-3.84	-3.16	-4.31	-3.80	-4.33	-4.36
Celestite	-4.38	-4.94	-4.98	-4.97	-4.85		-4.94	-32.67	-4.90	-4.71	-4.96	-4.38	-4.94
Cerrusite	-3.00	-4.59	-3.93	-4.91	-4.40		-4.59	-4.63	-3.30	-4.79	-4.26	-4.74	-4.76
Chalcedony	-1.07	-0.73	-0.93	-0.90	-0.37		-0.73	-0.80	-0.78	-0.83	-0.85	-0.53	-0.53
Chlorite (14A)	-15.59	-18.11	-18.35	-23.65	-22.85		-18.11	-13.77	-14.79	-22.70	-20.40	-24.15	-22.82
Chrysotile	-12.71	-14.44	-15.25	-17.82	-16.14		-14.44	-11.26	-11.96	-16.76	-15.52	-17.11	-16.97
$CO_2(g)$	-1.88	-3.03	-2.23	-2.73	-2.71		-3.03	-4.05	-3.25	-2.87	-2.92	-2.47	-2.52
Dolomite	-3.77	-7.64	-6.39	-9.14	-8.72		-7.64	-7.63	-6.39	-8.73	-7.84	-8.66	-8.70
$Fe(OH)_3(a)$	**0.22**	-2.4	-1.39	-3.26	-2.56		-2.40	-0.11		-2.76	-3.07		
Fluorite	-3.53	-2.93	-3.68	-4.18	-3.31		-2.93	-58.93	-3.25	-4.02	-3.12	-3.55	-4.34
Gibbsite	**1.20**	**1.44**	**1.96**	**1.45**	**0.55**		**1.44**	**0.95**	**1.02**	**1.05**	**1.17**	**0.67**	**1.22**
Goethite	**6.22**	**3.6**	**4.60**	**2.74**	**3.44**		**3.60**	**5.89**		**3.24**	**2.93**		
Gypsum	-3.76	-4.28	-4.38	-4.40	-4.22		-4.28	-32.15	-4.29	-4.21	-4.22	-3.78	-4.36
$H_2(g)$	-21.38	-20.86	-20.82	-19.92	-19.92		-20.86	-21.86	-21.74	-20.22	-20.66	-19.78	-19.88
$H_2O(g)$	-1.43	-1.43	-1.43	-1.43	-1.43		-1.43	-1.43	-1.43	-1.43	-1.43	-1.43	-1.43
Halite	-8.89	-9.06	-9.40	-9.40	-9.05		-9.06	-8.58	-9.11	-9.06	-9.19	-8.53	-9.15
Hausmannite	-17.61	-21.93	-22.44	-27.49	-24.73		-21.93	-18.08	-18.65	-24.49	-23.62	-25.65	-24.17
Hematite	**14.46**	**9.21**	**11.23**	**7.50**	**8.89**		**9.21**	**13.79**		**8.50**	**7.88**		
Illite	-2.90	-1.76	-1.31	-2.83	-2.99		-1.76	-2.48	-2.31	-3.45	-2.95	-3.29	-1.95
Jarosite-K	-9.07	-17.1	-13.87	-18.11	-16.00		-17.10	-67.21		-17.05	-18.81		
K-felspar	-4.43	-3.83	-3.94	-4.74	-4.04		-3.83	-3.90	-3.76	-4.98	-4.59	-4.34	-3.67
K-mica	**3.58**	**4.67**	**5.61**	**3.79**	**2.68**		**4.67**	**3.62**	**3.90**	**2.76**	**3.37**	**2.62**	**4.39**
Kaolinite	**1.93**	**3.09**	**3.74**	**2.77**	**2.03**		**3.09**	**1.97**	**2.15**	**2.12**	**2.31**	**1.95**	**3.05**
Manganite	-7.56	-9.08	-9.26	-11.09	-10.17		-9.08	-7.63	-7.84	-10.04	-9.68	-10.50	-10.00
Melanterite	-8.44	-10.56	-9.41	-9.97	-9.26		-10.56	-37.57		-9.81	-10.91		
$O_2(g)$	-39.54	-40.58	-40.66	-42.46	-42.46		-40.58	-38.58	-38.82	-41.86	-40.98	-42.74	-42.54
$Pb(OH)_2$	-4.12	-4.56	-4.71	-5.19	-4.70		-4.56	-3.59	-3.06	-4.92	-4.35	-5.28	-5.24
Pyrochroite	-8.08	-9.34	-9.50	-1.09	-9.96		-9.34	-8.39	-8.54	-9.98	-9.84	-10.22	-9.77
Pyrolusite	-12.46	-14.25	-14.45	-16.73	-15.81		-14.25	-12.30	-12.57	-15.53	-14.95	-16.21	-15.65
Quartz	-0.65	-0.31	-0.51	-0.48	0.05		-0.31	-0.38	-0.36	-0.41	-0.43	-0.11	-0.11
Rhodochrosite	-1.76	-4.17	-3.53	-5.40	-4.47		-4.17	-4.24	-3.59	-4.65	-4.56	-4.49	-4.08
Sepiolite	-10.57	-11.17	-12.03	-13.71	-11.70		-11.17	-9.16	-9.60	-12.88	-12.08	-12.61	-12.52
Sepiolite(d)	-13.55	-14.14	-15.01	-16.69	-14.68		-14.14	-12.14	-12.58	-15.86	-15.06	-15.59	-15.50
Siderite	-1.71	-5.22	-3.39	-5.30	-4.59		-5.22	-4.44		-5.09	-5.67		
$SiO_2(a)$	-1.90	-1.56	-1.76	-1.73	-1.20		-1.56	-1.63	-1.61	-1.66	-1.68	-1.36	-1.36
Smithsonite	-4.11	-5.18	-4.50	-6.10	-5.66		-5.18	-5.32	-3.85	-5.16	-4.90	-6.00	-5.62
Strontianite	-3.78	-5.73	-5.09	-6.44	-6.31		-5.73	-5.67	-5.08	-6.13	-5.86	-6.24	-6.25
Sylvite	-9.16	-9.66	-9.79	-9.70	-9.53		-9.66	-9.42	-9.45	-9.75	-9.65	-8.84	-9.35
Talc	-11.10	-12.16	-13.37	-15.89	-13.15		-12.16	-9.12	-9.79	-14.68	-13.47	-14.44	-14.30
Willemite	-7.92	-7.41	-7.87	-10.05	-8.68		-7.41	-5.75	-4.39	-7.81	-7.20	-9.99	-9.13
Witherite	-5.25	-7.17	-6.55	-7.84	-7.75		-7.17	-7.26	-5.24	-6.40	-7.36	-7.66	-7.66
$Zn(OH)_2(e)$	-5.63	-5.54	-5.67	-6.77	-6.35		-5.54	-4.67	-4.00	-5.69	-5.37	-6.93	-6.50

No samples collected

Table 6.5 Saturation Indices values for Zua 01, phases shown in red bold indicate where positive values are present at some point throughout the sampling period.

Zua 01	Jun-07	Jul-07	Aug-07	Sep-07	Oct-07	Nov- Dec 07	Jan-08	Feb-08	Mar-08	Apr-08	May-08	Jun-08	Jul-08
Phase													
$Al(OH)_3(a)$	-	-1.32	-1.35	-2.55			-1.87	-	-1.60	-1.53	-	-	-1.32
Albite	-	-7.11	-7.26	-7.90			-5.72	-	-5.03	-5.22	-	-	-4.85
Alunite	-	-4.13	-3.70	-5.73			-7.87	-	-6.38	-6.68	-	-	-5.07
Anglesite	-	-6.92	-6.83	-6.48			-6.67	-6.11	-6.03	-5.69	-	-5.36	-5.36
Anhydrite	-5.59	-4.79	-4.85	-4.79			-4.83	-4.27	-4.36	-4.62	-4.64	-4.73	-4.83
Anorthite	-	-7.66	-8.13	-10.79			-6.49	-	-5.54	-5.63	-	-	-5.81
Aragonite	-3.50	-3.43	-3.87	-4.11			-3.39	-3.01	-3.11	-3.40	-4.33	-4.42	-4.16
Barite	-	-2.63	-2.51	-2.59			-3.06	-2.62	-1.23	-2.95	-	-2.25	-2.53
Ca-Montmorillonite	-	-1.87	-1.98	-3.67			-1.27	-	-0.25	-0.26	-	-	**0.40**
Calcite	-3.36	-3.29	-3.73	-3.97			-3.24	-2.87	-2.97	-3.26	-4.33	-4.27	-4.02
Celestite	-6.22	-5.2	-5.22	-5.24			-5.44	-4.90	-4.99	-5.27	-5.26	-5.14	-5.19
Cerrusite	-	-4.29	-4.58	-4.52			-3.95	-3.57	-3.50	-3.19	-	-3.77	-3.42
Chalcedony	-29.19	-1.22	-1.21	-0.87			-0.77	-0.63	-0.67	-0.71	-	-0.62	-0.63
Chlorite (14A)	-	-22.5	-24.13	-30.12			-14.86	-	-13.03	-14.17	-	-	-16.48
Chrysotile	-69.92	-17.07	-18.00	-20.09			-11.72	-10.44	-10.93	-11.71	-	-15.16	-13.32
$CO_2(g)$	-1.71	-1.97	-1.99	-1.29			-3.30	-3.30	-3.25	-3.39	-2.92	-3.07	-3.39
Dolomite	-5.44	-6.66	-7.43	-7.89			-6.46	-5.75	-5.93	-6.59	-7.31	-8.50	-7.95
$Fe(OH)_3(a)$	-0.97	-1.8	-2.28	-3.62			**0.29**	**0.38**	**0.48**	**0.15**	-112.0	-0.07	-1.05
Fluorite	-4.82	-4.01	-4.27	-4.20			-3.70	-3.35	-3.11	-3.85	-4.85	-5.48	-4.34
Gibbsite	-	**1.35**	**1.31**	**0.12**			**0.79**	-	**1.06**	**1.13**	-	-	**1.34**
Goethite	**5.02**	**4.19**	**3.71**	**2.38**			**6.28**	**6.37**	**6.48**	**6.14**	**4.88**	**5.93**	**4.95**
Gypsum	-5.31	-4.52	-4.57	-4.52			-4.56	-4.00	-4.09	-4.35	-4.36	-4.46	-4.56
$H_2(g)$	-20.92	-20.5	-21.14	-19.14			-21.66	-21.86	-21.74	-21.56	-21.10	-20.54	-21.20
$H_2O(g)$	-1.43	-1.43	-1.43	-1.43			-1.43	-1.43	-1.43	-1.43	-1.43	-14.30	-1.43
Halite	-38.13	-9.26	-9.25	-9.22			-9.33	-9.14	-9.18	-9.24	-	-9.23	-9.15
Hausmannite	-	-20.68	-21.93	-25.87			-15.29	-14.31	-15.38	-15.62	-	-18.13	-17.35
Hematite	**12.07**	**10.41**	**9.45**	**6.78**			**14.59**	**14.77**	**14.98**	**14.31**	**11.77**	**13.88**	**11.92**
Illite	-	-4.12	-4.35	-6.40			-2.97	-	-1.85	-2.07	-	-	-1.52
Jarosite-K	-40.86	-15.08	-15.98	-18.41			-10.87	-9.85	-9.61	-11.12	-	-9.56	-13.72
K-felspar	-	-5.87	-6.07	-6.67			-4.29	-	-3.55	-3.90	-	-	-3.55
K-mica	-	**2.45**	**2.18**	**-0.81**			**2.92**	-	**4.20**	**3.99**	-	-	**4.75**
Kaolinite	-	**1.92**	**1.88**	**0.16**			**1.72**	-	**2.45**	**2.51**	-	-	**3.09**
Manganite	-	-8.73	-9.21	-10.68			-6.74	-6.38	-6.75	-6.86	-	-7.87	-7.50
Melanterite	-9.27	-9.43	-9.36	-9.20			-9.34	-9.16	-8.94	-9.29	-8.80	-7.77	-9.76
$O_2(g)$	-40.46	-41.3	-42.02	-44.02			-38.98	-38.58	-38.82	-39.18	-40.10	-41.22	-39.90
$Pb(OH)_2$	-	-5.32	-5.60	-6.24			-3.66	-3.27	-3.26	-2.81	-	-3.71	-3.03
Pyrochroite	-	-8.81	-9.11	-10.08			-7.40	-7.14	-7.45	-7.47	-	-7.97	-7.93
Pyrolusite	-	-14.07	-14.73	-16.71			-11.50	-11.04	-11.48	-11.68	-	-13.20	-12.50
Quartz	-28.77	-0.8	-0.79	-0.45			-0.35	-0.21	-0.25	-0.29	-	-0.20	-0.21
Rhodochrosite	-	-2.58	-2.89	-3.17			-2.49	-2.24	-2.50	-2.66	-	-2.84	-3.12
Sepiolite	-95.58	-13.74	-14.34	-15.17			-9.42	-8.32	-8.73	-9.31	-	-11.44	-10.26
Sepiolite(d)	-98.56	-16.72	-17.32	-18.15			-12.40	-11.30	-11.71	-12.29	-	-11.46	-13.23
Siderite	-2.50	-3.39	-3.70	-3.83			-3.20	-3.21	-3.00	-3.38	-3.94	-2.76	-4.39
$SiO_2(a)$	-30.02	-2.05	-2.04	-1.70			-1.60	-1.46	-1.50	-1.54	-	-1.45	-1.46
Smithsonite	-4.15	-4.56	-5.00	-5.15			-4.83	-4.28	-3.70	-4.47	-5.56	-2.17	-5.02
Strontianite	52.82	-5.29	-5.69	-6.00			-5.44	-5.08	-5.18	-5.49	-6.54	-6.27	-5.97
Sylvite	-37.50	-9.9	-9.94	-9.87			-9.78	-9.42	-9.58	-9.80	-	-9.56	-9.72
Talc	-124.5	-15.78	-16.69	-18.10			-9.52	-7.95	-8.54	-9.39	-	-12.66	-10.85
Willemite	-36.47	-8.79	-9.63	-11.00			-6.22	-4.97	-3.96	-5.27	-	-1.20	-6.29
Witherite	-	-6.68	-6.94	-7.32			-7.02	-6.77	-5.39	-7.14		-7.35	-7.27
$Zn(OH)_2(e)$	-5.84	-5.98	-6.41	-7.26			-4.92	-4.37	-3.84	-4.48	-6.04	-2.49	-5.03

Figure 6.32 and Figure 6.33 the show variation in SI data for phases that record more than one positive value for the Chapora River and Zuari River, respectively, these include Ca-montmorillonite, gibbsite, goethite, haematite, kaolinite, K-mica and $Fe(OH)_3$.

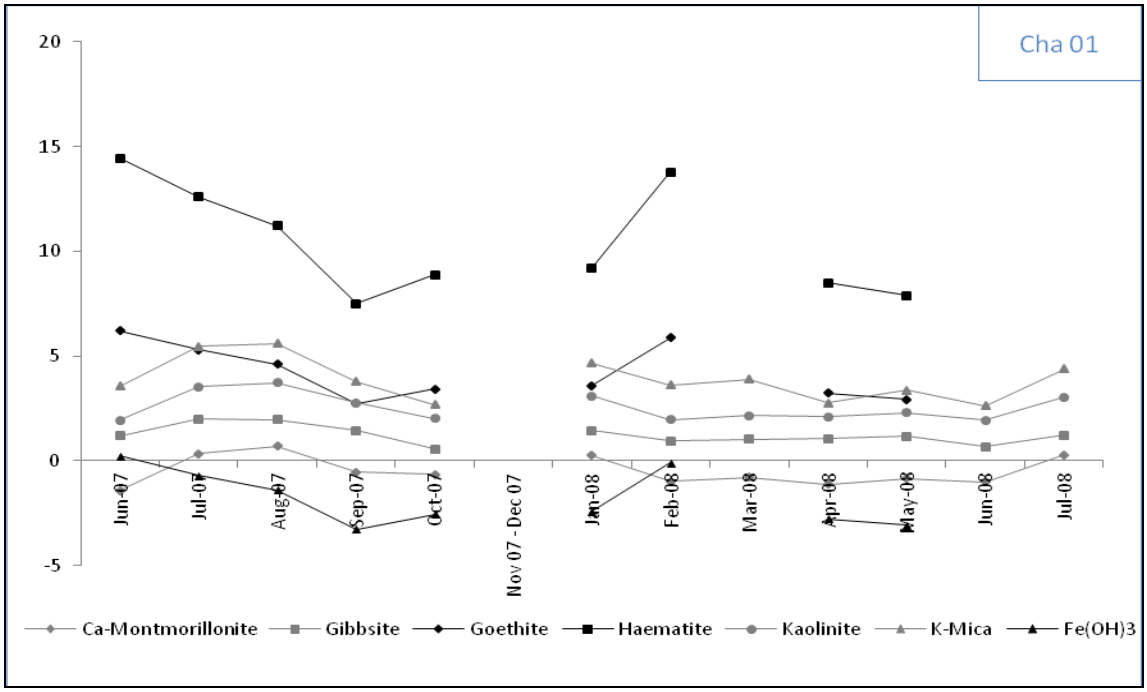

Figure 6.33 Calculated Saturation Indices (SI) values for the Chapora River localities (Cha 01, 02, 03 and 04).

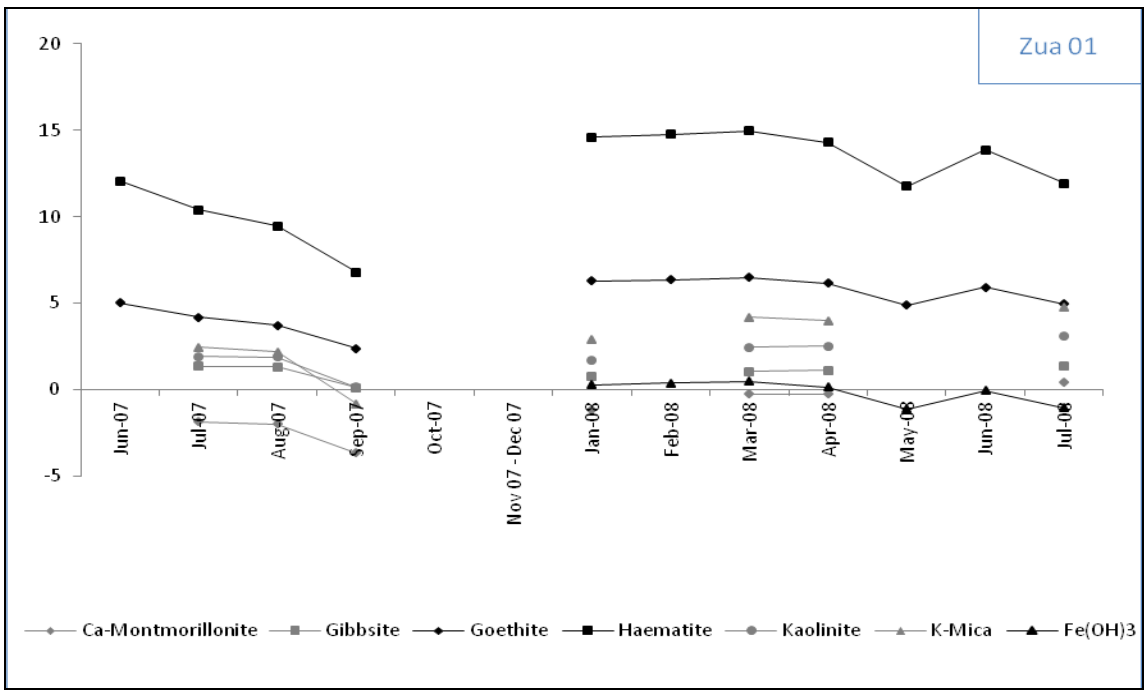

Figure 6.34 Calculated Saturation Indices (SI) values for the Zuari River localities (Zua 01, 02, 03 and 04).

Chapora Localities (Cha 01 – 04)

The most obvious observation for all four localities is that haematite reports by far the highest SI values and as such is the most likely mineral to precipitate throughout the whole sampling regime. This is generally followed by goethite or K-mica SI depending on the season, with K-mica SI being higher in the dry season whilst goethite SI is higher in the wet season. After these, come kaolinite and gibbsite, with Ca-montmorillonite and $Fe(OH)_3$ exchanging position depending on season, with Ca-montmorillonite being higher in the wet season and $Fe(OH)_3$ being higher in the dry season.

Additionally, there are also two broad trends, the first trend shows the Al-bearing minerals, K-mica, kaolinite, gibbsite and Ca-montmorillonite SI values increasing from June 2007 through the wet season months of July and August before decreasing in September and October. Then the SI values of these minerals increase slightly in January 2008 and then retain a fairly flat profile throughout the dry season before increasing once more in July 2008. However, Cha 04 is an exception to this pattern since it reports a slight but significant increase in March 2008 for all four minerals, which coincides with an increase in precipitation of 43 mm compared to the previous two months which are reported as receiving zero precipitation. After which the values decrease once more and follow a similar pattern to the other Chapora River localities.
By contrast the second trend shows the Fe-bearing minerals, haematite, goethite and $Fe(OH)_3$ decreasing from their June 2007 peaks to a low in either September (Cha 01) or October (Cha 02, 03 and 04). In the dry season the SI's of these minerals report an increase in January 2008, which continues to increase in February. Unfortunately no reliable Fe data were available for March, June and July 2008 for Cha 01, Cha 02 and Cha 03 or for July 2008 for Cha 04 and so there are no SI data for these minerals for these months. The more complete dataset for Cha 04, does however, suggest a relatively flat profile with the exception of a slight decrease in SI value in March 2008, again coinciding with the increased precipitation.

Zuari Localities (Zua 01 – 04)

As with all the previous localities of the Chapora River, haematite is again the most likely mineral to precipitate, with SI values consistently approximately twice those of the next most likely mineral to precipitate, goethite. These are followed by K-mica, kaolinite and gibbsite with Ca-montmorillonite and $Fe(OH)_3$ generally reporting similar values and exchanging position depending on the season, with Ca-montmorillonite being higher during the wet season and $Fe(OH)_3$ being higher during the dry season.

Also a clear trend is again present for Fe-rich minerals showing values dropping through the wet season and rising to a relatively uniform level during the dry season. The trend for Al-rich minerals is not so easy to interpret, largely due to missing data. However, looking at the values for July, August and September 2007, it can be seen that values are fairly similar in July and August before dropping in September. This is consistent with the previous trends described and lower values in June would have confirmed this.

Another observation that is present on all Zuari locality plots but not on the Chapora plots is the difference in the range of values for the Al-bearing minerals (in particular K-mica, kaolinite and gibbsite). During the wet season the SI values cluster tightly, whereas during the dry season the range of values increases significantly.

Summary

The saturation Index calculations suggest that haematite is the most likely mineral to precipitate throughout the whole sampling regime; this is consistent for each and every locality. The second most likely mineral to precipitate is generally either goethite or K-mica depending on locality and seasonality.

There appear to be two broad trends; one where the SI values increase slightly in the wet season and reduce to a fairly consistent level during the dry season, and the second being almost the opposite, with values decreasing in the wet season and increasing in the dry season. These trends are notable due to the fact that they are occupied by Al-bearing minerals in the first and Fe-bearing minerals in the second. However, this is not always the case as there are a couple of exceptions to the Al-bearing mineral trends for the Zuari localities Zua 02 and Zua 03. This suggests that Al-

bearing minerals are more likely to be precipitated during the wet season, whilst Fe-bearing minerals are more likely to precipitate during the dry season.

It is interesting to note that for all localities the SI values for $Fe(OH)_3$ are predominantly negative with the occasional positive value, this is in line with the knowledge that $Fe(OH)_3$ is among the first Fe-oxides to form, but later recrystallises to other oxides such as goethite (FeOOH) or haematite (Fe_2O_3).

The range of SI values for the Al-bearing minerals for the Zuari localities consistently shows small variation in values during the wet season and significantly larger variation in values during the dry season. However, this observation does not hold true for the Chapora River localities which show fairly uniform separation. This uniform separation is also the case for the Fe rich minerals which appear to retain an almost parallel separation. This may be due to the environments experiencing different weathering regimes throughout the seasons moving from weathering limited to transport limited.

The slightly elevated SI values reported for the Al-bearing minerals from Zua 04 occurring in March 2008 which coincide with a small but significant amount of precipitation of 43 mm after months of two months of no rainfall suggest a high level of sensitivity.

The only positive SI values being obtained throughout both sampling sites are for Fe-oxides and Al-oxides which is consistent with the formation of secondary minerals as a result of incongruent weathering. There are no positive SI values for sulphates or carbonates which is consistent with the lithology of the basin but also with the fact that the catchment areas are overlain by significant coverings of laterite, which by its very nature has already been depleted of its more mobile elements and enriched by less mobile ones.

6.6. Chapter Summary

- The first observations are the peaks in concentration occurring close to the onset of the monsoon. Although, this is not true for all elements or for both monsoons.

- The second observation in the spatial variation in element concentration. In the monsoon months the concentration at each sampling locality is very similar, whereas, during the dry season months the variability is much greater, suggesting a more localised control on river chemistry during the dry months.

- During the wet season months of June and July the REE profiles appear relatively flat, whilst during the dry season months they are more fluctuating.

- The plots often show elevated La peaks, however, these are present mostly during dry months with the most prominent example occurring on the Zuari River in May 2008.

- The plots also display positive Eu anomalies during the dry season months and are most clearly seen on the Chapora River at locality Cha 01. This anomaly does not manifest on the Zuari River and is therefore most likely due to a difference in lithology.

- The saturation indices suggest that haematite is the most likely mineral to be precipitated for all localities.

- There are two broad trends; one where the SI values increase slightly in the wet season and fall in the dry season and a second trend which displays an opposing pattern.

- The notable observation for these two trends is that the one describes Al-bearing minerals whilst the other is describes Fe-bearing minerals.

- SI values, like major and trace elements concentrations display small spatial variation during the wet season months and large variations during he dry season months.

Chapter 7. Discussion

This chapter discusses the various observations resulting from the previous chapter, beginning with Section 7.1 aqueous geochemistry. This section starts by discussing estuarine influence as this is of significant importance in order to establish which river samples can be regarded as representative of river water and as such be used in the subsequent discussions. The section then discusses aspects such as the rinse-out effect, the column experiment, fluid residence time, spatial downstream variability and seasonal controls on river chemistry. Section 7.2 moves to discuss weathering indices, such as CIA and MIA. Following on from this Section 7.3 provides a comparison of the Chapora and Zuari Rivers in terms of lithological influence and mining influence. The chapter concludes with a discussion on CO_2 drawdown. This is considered using three different approaches; the first method is based on the traditional study of river water chemistry, the second method uses weathering rates of the underlying catchment lithologies whilst the third and final calculation uses an estimate of material loss due to escarpment retreat. These are ultimately compared against each other and against a value for the Nethravati River, which is located a c. 300 miles south of Goa and is subject to a similar climate and tectonic regime. Finally, the river water values are considered in a global context by comparing their values against values calculated by other authors for other river catchments around the world.

7.1. Aqueous geochemistry

The previous sections describing graphical interpretations of cations, anions, trace elements and REE identified a number of clear observations; some of these observations in elemental behaviour were more readily demonstrable. It is important to note that the graphical information only include data deemed to be unaffected by any estuarine influence. This is a highly seasonal observation caused by the large tidal range across the low lying Konkan coastal plain which is offset by the high levels of precipitation occurring during the wet season. This is discussed in more detail in section 7.1.1 – Estuarine influence. Among the most obvious observations derived from the graphs are the relatively high elemental concentrations coinciding with the onset of a monsoon season (June 2007 and June 2008). However, interestingly, not all elements display this trend, and the trend appears to be more widespread, affecting more elements coinciding with the 2007 monsoon than are affected coinciding with the 2008 monsoon. This phenomenon is described here as a ‘rinse-out’ effect, and has been documented elsewhere (Smolders et al., 2004) but does not appear to have been

previously recognised in monsoonal river catchment chemistries. Another very clear and almost ubiquitous observation is the difference in elemental concentration between the dry season and wet season fluvial chemistry. Elemental concentrations remain within a very small range of values for all localities (e.g. Cha 01 – 04) during the wet season months, but display much greater variability during the dry season months. This observation can be best explained using 'Gibbs diagrams' (Gibbs, 1970) to plot total dissolved solids (TDS) against $Cl/(Cl/HCO_3^-)$. These key observations are discussed in detail in the following subsections.

7.1.1. Estuarine influence

The low lying Konkan-Kanara coastal plain of western India is bounded to the west by the Arabian Sea; it varies in width from 5 to 70 km and remains at a consistently low elevation across much of this width until it meets the foothills of the Western Ghats escarpment, where elevation then rises rapidly (Figure 7.1). Accordingly, the tides are thus capable of reaching many kilometres upstream on both the Chapora and Zuari Rivers. Although the study rivers display broadly similar elevation profiles, the Zuari has a more shallow elevation gradient of c. 1 in 600 when compared with the Chapora which has a gradient of c. 1 in 500. This is largely due to the direction of the river relative to the Western Ghats escarpment, with the Chapora running approximately perpendicular to the escarpment, whilst the Zuari runs approximately 15º - 30º parallel to the escarpment. Therefore the tides may be expected to reach slightly further inland on the Zuari system.

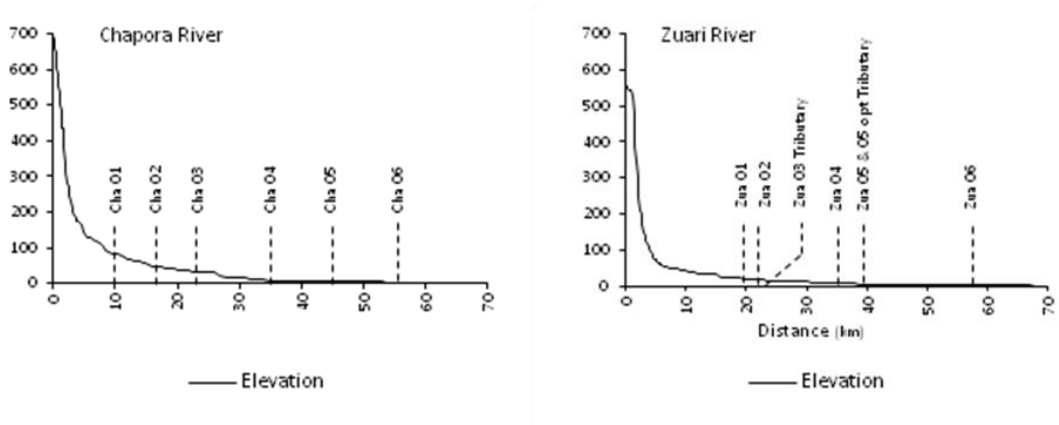

Figure 7.1 Graphical representations of the Chapora and Zuari river profiles showing the sample site locations.

This is not always the case, however, because the extent of tidal influence will also be limited by the amount of fresh water flowing to the Arabian Sea. Therefore, it is expected that the effects of the tides will be detected further upstream during the dry months (October-May) than during the wet months (June-September). This is evident in the Chapora River Cl dataset, which is provided below (Table 7.1 & Figure 7.2) as evidence of estuarine influence.

Table 7. 1 Cl data for the Chapora River (all values are expressed as ng ml^{-1}).

Date	Jun-07	Jul-07	Aug-07	Sep-07	Oct-07	Jan-08	Feb-08	Mar-08	Apr-08	May-08	Jun-08	Jul-08
Cha05	n/a	7.11	5.00	4.60	0.13	14.10	26.30	22.60	9.42	11.40	0.38	n/a
Cha06	n/a	9.99	6.31	6.57	0.14	23.80	32.90	33.80	26.30	28.30	2.44	0.13

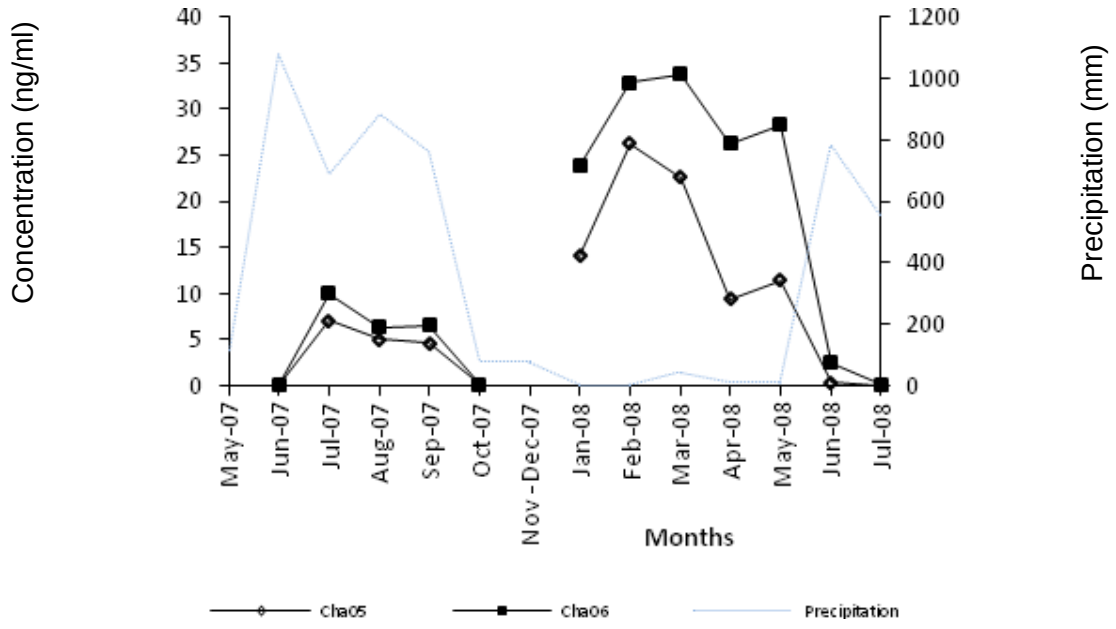

Figure 7.2 Temporal plot showing the Cl data as documented in Table 6.1 for sample localities Cha 05 and Cha 06

Table 7.1 indicates that the highest values of 26.3 ng ml^{-1} for Cha 05 occurs in February 2008, and 33.8 ng ml^{-1} for Cha 06 occurs in March 2008; both of these high values occur during the dry season when the tides are at their most effective, because there is little or no downstream flow counteracting tidal upstream progress. The lowest concentrations occur during the wet season months. For example, during the 2007 monsoon season months (July, August, September and October) values range from 0.13 ng ml^{-1} for Cha 05 and 0.14 ng ml^{-1} for Cha 06 occurring in October 2007 to between 7.11 ng ml^{-1} for Cha 05 and 9.99 ng ml^{-1} for Cha 06 occurring in July 2007.

Values for the 2008 monsoon months of June and July are again relatively low, recorded as 0.38 ng ml^{-1} for Cha 05 and 2.4 ng ml^{-1} for Cha 06 occurring in June and 0.13 ng ml^{-1} for Cha 06 occurring in July. The low Cl concentration reported during the monsoon months suggests that the large influx of fresh fluvial water travelling as surface flow and ground water is effectively pushing the tidal limit towards the coast.

Another indicator to support this observation is conductivity. This is the measure of the ability of water to pass an electric current: it is controlled by the amount of total dissolved solids (TDS) present (µS cm^{-1}). River water has a wide range of conductivities depending on the drainage basin lithology. For example, rivers draining granitic terrains will have lower conductivities than those draining lithologies containing clay minerals (Pritchard, 1989). The spatial (downstream) conductivity variations for the Chapora and Zuari Rivers for the months May 2007 to July 2008 are shown in Figures 7.3 and 7.4, respectively. These graphs clearly show that the conductivity varies significantly for each of the months analysed. The Chapora graphs show that the near-estuarine sample localities (Cha 05 and Cha 06) have values of > 2000 µS cm^{-1} (values limited by the calibration of the conductivity probe) for the months of May and June 2007 and January to May 2008, whilst the months July, August and September 2007 and June 2008 samples have significantly lower conductivity values of 26 and 32 µS cm^{-1} (July 2007), 22 and 24 µS cm^{-1} (August 2007), 22 and 23 µS cm^{-1} (September 2007) and 210 and 1337 µS cm^{-1} (July 2008) for Cha 05 and Cha 06, respectively.

The corresponding Zuari graphs are slightly more complicated due to the sampling of two tributaries, the Guloli River and the Kushavati River. The graphs have a single line joining the sampling locations Zua 01, Zua 02, Zua 04 and Zua 06 since these represent the main river channel. In addition to this main line, two independent points are plotted which represent the sampling sites Zua 03 located on the Guloli River tributary and Zua 05 opt located on the Kushavati River. Both graphs reveal a similar pattern to that of the near-estuarine sample locality (Zua 06), yielding a value of > 2000 µS cm^{-1} (again limited by the conductivity probe) for May and June 2007 and January to May 2008. Again July, August and September 2007 and June and July 2008 samples have lower conductivities of 278 µS cm^{-1} (July 2007), µS cm^{-1} (August 2007), 797 µS cm^{-1} (September 2007), 131 µS cm^{-1} (June 2008) and 74 µS cm^{-1} (July 2008). These observations are in agreement with the proposition that seasonal variation in precipitation, and hence river flow, limits the tidal range during the monsoon. Further it would appear that May and June 2007 and January to May 2008 had relatively low river flow, whereas July, August and September 2007 and June and July 2008 had relatively high flow. This is entirely consistent with the precipitation data recorded for

the sampling period, which shows that the monsoon rains began to fall around the beginning of June in both years, continuing until the end of September. However, the quantity falling prior to the June 2007 sampling date was significantly less than that falling prior to the June 2008 sampling date, thus explaining why high conductivity values for the near estuarine sampling localities are still prevalent for June 2007.

Therefore, when the data presented in Figures 7.3 and 7.4 are interpreted in conjunction with Figure 7.1, it becomes evident that the tides are capable of reaching similar elevations within each river system. Consistently low conductivity values (<100 µS cm^{-1}) are attained at Cha 04 on the Chapora River, and Zua 04 on the Zuari River; these equate to elevations of 10 m and 6 m, respectively. This compares well with conductivity values reported for the more northerly, west flowing rivers Arjuna, Gad, Sukh, Kasjli, Shashtri and Vashishthi which yield values ranging between 73 and 94 µS cm^{-1} (Das et al., 2005). These latter values were obtained by the authors from water samples collected during two consecutive monsoon seasons of 2001 and 2002.

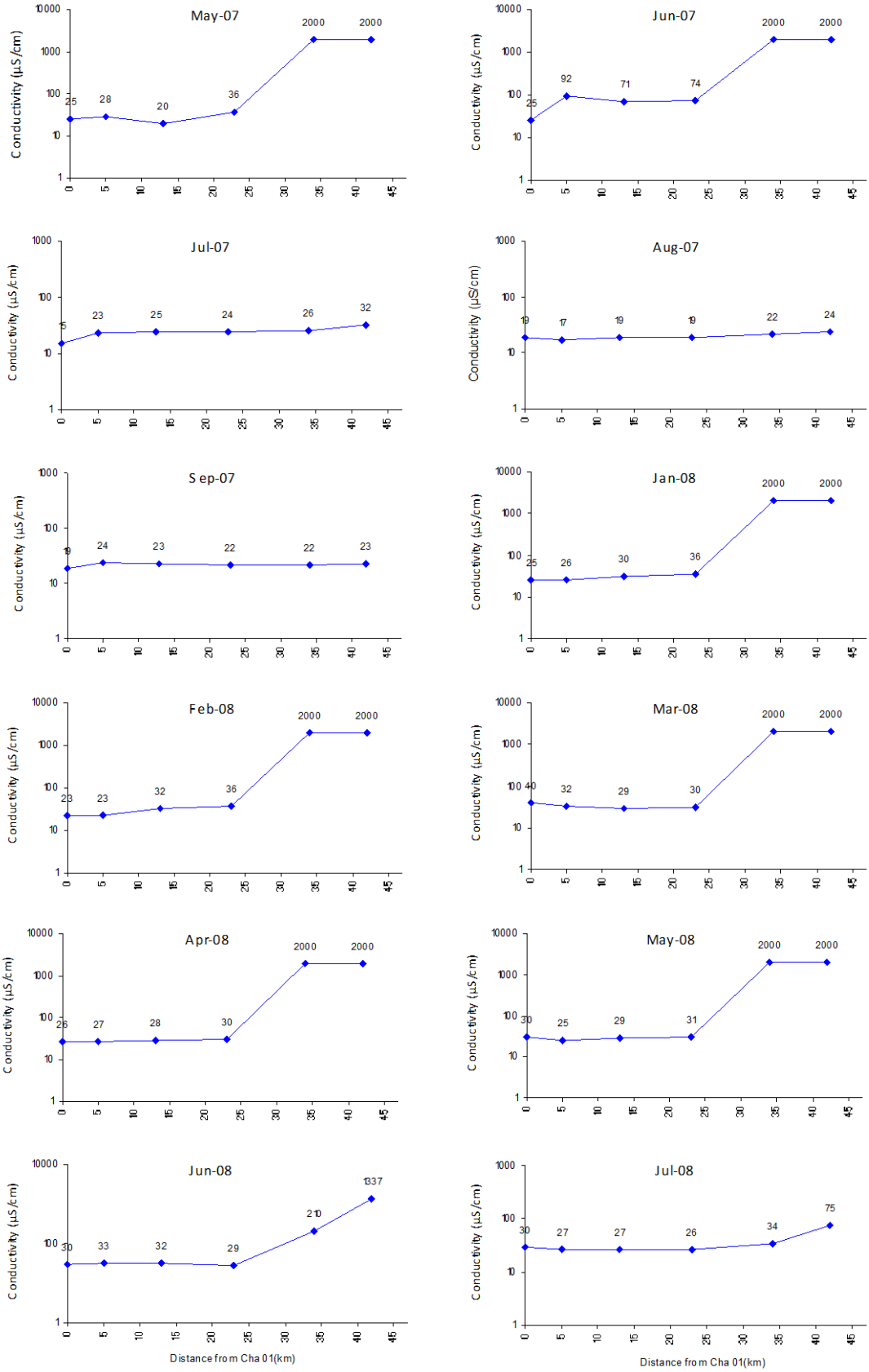

Figure 7.3 Spatial variation graphs of conductivity for the Chapora River for the months May 2007 to July 2008.

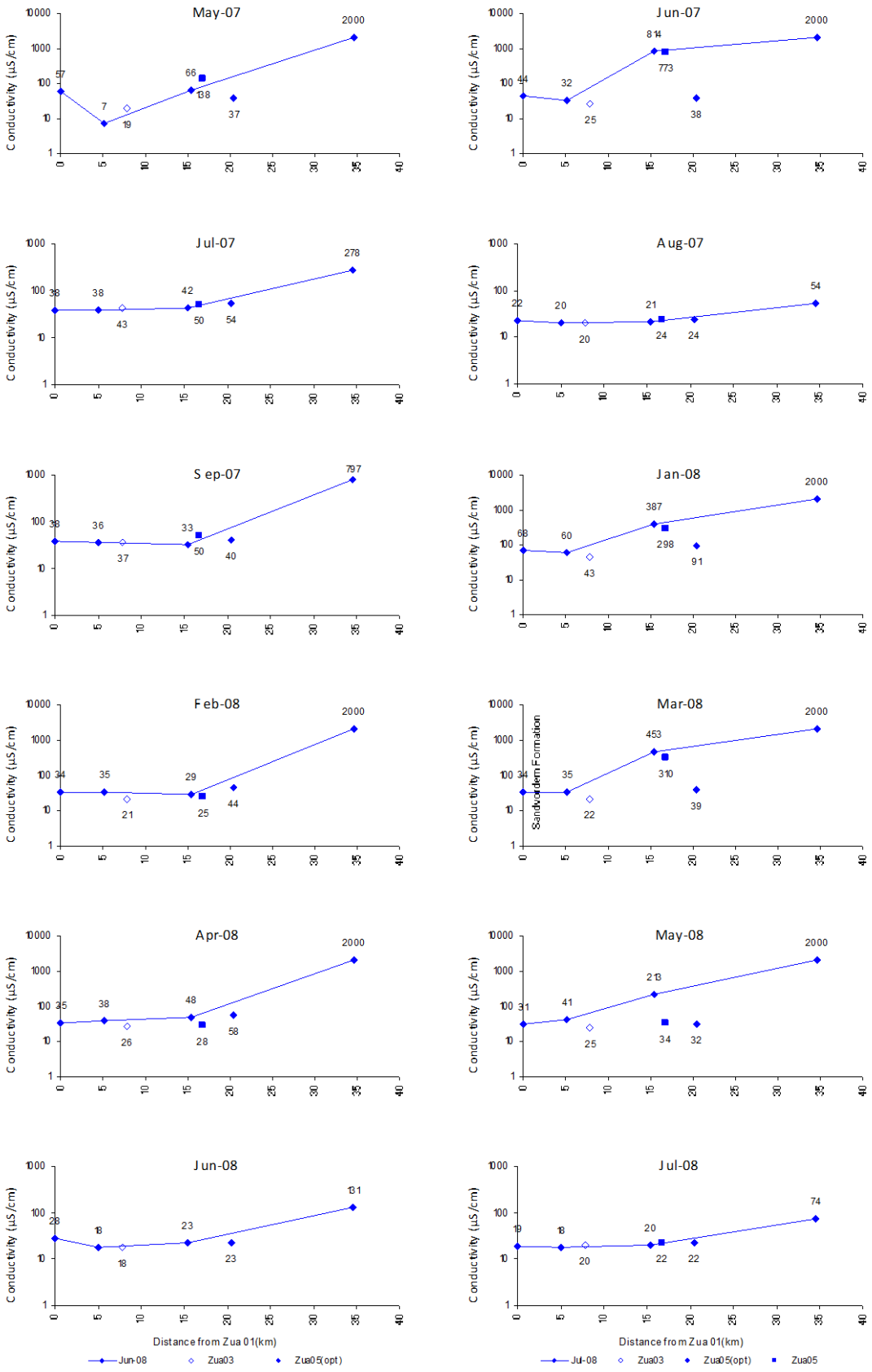

Figure 7.4 Spatial variation graphs of conductivity for the Zuari River for the months May 2007 to July 2008.

7.1.2. Rinse out effect

The term ‘rinse out effect’ is used here to describe the observed peaks in concentration of some elements shortly after the onset of the monsoon period (June) (c.f., Smolders et al., 2004). This phenomenon has also been described elsewhere in reference to acid rock drainage where it was termed as the ‘first flush’ and described the rapid rise in elemental concentrations during the rising limb of discharge following dry spells. As with the studies by Nordstrom, 2009 these peak concentrations are immediately followed by a fall to pre-monsoon values, or even lower. Analysis of the first four months worth of samples showed this phenomenon occurred for a selection of elements in June 2007; therefore the decision was made to increase the sampling regime to include June and July 2008 to investigate whether this was an annual, repeated, effect.

The elements that display the ‘rinse out effect’ during June 2007 include the major cations K, Mg, Ca, Si, and the anions HCO_3^-, SO_4 & Cl and the trace elements Rb, Sr, Cr, Mn, Fe and Co for the Chapora River, but only the major cations Mg & Si for the Zuari River (Figures 6.13 to 6.35). Although ‘rinse out effects’ are observed again for some elements during June 2008, including K, Mg, SO_4, NO_3, V, Co and Ni for the Chapora, and Rb, V, Cr, Mn, Fe, Co and Ni for the Zuari, there is insufficient evidence to demonstrate that the effect is annual. In fact, the only elements that show clear evidence of the ‘rinse out effect’ in both 2007 and 2008 are K, Mg, SO_4, and Co for the Chapora River; by contrast, no suite of elements show repeat rinse out effects in both years for the Zuari River (Table 7.2).

The fact that the rinse-out effect observed for the Chapora River coincides with a similar rinse-out feature for Cl for June 2007 could be indicative that some of the elements being rinsed-out may be derived from an estuarine source. Even though the EC values for Cha 01 – 04 for June 2007 are below 100 µS cm^{-1}, they are towards the higher end of the range with values between 71 – 92 µS cm^{-1}. The EC values for June 2008 are much lower, ranging between 29 and 33 µS cm^{-1} and the Cl concentration also remains fairly uniform at c. 5 mg l^{-1}. These two observations suggest that the Chapora localities Cha 01 – 04 are not estuarine influenced at the onset of the 2008 monsoon. It is also noteworthy that for many of the elements displaying a ‘rinse-out effect’ for the Chapora River, the concentrations are higher at the upstream localities (Cha 01 and Cha 02) and reduce downstream, which suggests that the source of these elements is most likely due to rock weathering as the upper localities do not display evidence of estuarine influence.

Interestingly, the Zuari River experienced a high EC value of 814 µS cm^{-1} for Zua 04 (Figures 6.3 & 7.4) in June 2007, which is very indicative of an estuarine signature. However, even with this signature the elements 'rinsed-out' in this month are limited to Mg & Si. The lack of other elemental peaks similar to those observed for the Chapora River for the same month could therefore be due to the dilution of the river water to a more estuarine signature which may mask the smaller changes in elemental composition expected due to chemical weathering.

Table 7. 2 Observations of 'rinse-out effects' during 2007 and 2008 for the Zuari and Chapora Rivers along with the range of Electrical Conductivity (EC) values for the upper four localities within each river, the values in brackets reflect the locality at which the EC value was derived.

Elements	Zuari River		Chapora River	
	June 2007	June 2008	June 2007	June 2008
Majors				
Na	×	×	×	×
K	×	×	✓	✓
Mg	✓	×	✓	✓
Ca	×	×	✓	×
Al	×	×	×	×
Si	✓	×	✓	×
HCO_3^-	×	×	✓	×
SO_4	×	×	✓	✓
F	×	×	×	×
Cl	×	×	✓	×
NO_3	×	×	×	✓
Traces				
Rb	×	✓	✓	×
Sr	×	×	✓	×
V	×	✓	×	✓
Cr	×	✓	✓	×
Mn	×	✓	✓	×
Fe	×	✓	✓	×
Co	×	✓	✓	✓
Ni	×	✓	×	✓
Cu	×	×	×	×
Zn	×	×	×	×
Pb	×	×	×	×
Ba	×	×	×	×
EC (location 01-04)	25 (03) – 814 (04)	18 (03) – 28 (01)	25 (01) – 92 (02)	29 (04) – 33 (02)

The ‘rinse out effect’ is believed to occur as a result of the strong seasonality between the dry season and the monsoon season (Smolders et al., 2004). During the dry season salts are precipitated on the sides of the river channels and within the pore spaces of the surrounding rocks and soil cover as the water table lowers. At the onset of the subsequent monsoon these salts are ‘rinsed out’ and taken into solution. Once this has occurred usually over a relatively short period of less than one month, the pre-monsoon concentrations return.

However, it is also worth noting that the rinse-out effect observed only demonstrates that certain elements have been taken into solution in the rivers as the water table rises close to the onset of the monsoon. It does not provide evidence of provenance for these elements. As mentioned above it is generally thought that these element concentrations are due to salt precipitation as the water table lowers and to chemical weathering in wetted pore spaces during the dry season, but some of these salts could equally be derived through infiltration of estuarine waters as the tides propagate further upstream during the dry season as is the case for Zua 04 in June 2007 and as could be the case for some of the lower locality Chapora samples also in June 2007. As mentioned previously, this study has attempted to address this potential issue by selecting river localities that are devoid of estuarine influence, which has been determined using both Cl concentration (Table 7.1 & Figure 7.2) and EC (Figures 6.3, 7.3 & 7.4).

The fact that the rinse-out effect does not appear to occur at the beginning of the 2008 monsoon requires further consideration. A likely possibility is that the ‘rinse out effect’ is so short lived that our sampling resolution is too infrequent. The precipitation data currently considered are based on a monthly resolution and it may be that during the 2008 monsoon season the ‘rinse out effect’ had already taken place prior to the river water samples being collected. Figure 6.5 shows the daily rainfall for the Goa area 73°E-75°E, 14°N-16°N for the sampling period of January 1st 2007 to December 31st 2008, while Figure 7.5 shows the daily precipitation for (a) May 1st 2007 to October 31st 2007 and (b) May 1st 2008 to October 31st 2008 (Acker and Leptoukh, 2007). Figure 7.5 clearly shows a greater level of precipitation for the 2007 monsoon compared with the 2008 monsoon; however, the graph also shows that precipitation started earlier in 2008 and was spread over a longer period. Figure 7.6 (a) and Figure 7.6 (b) shows the daily rainfall for just the 2007 and 2008 monsoon seasons, respectively, along with the sample collection dates for June for each year. Closer inspection of these plots suggests that there was more precipitation prior to the collection dates for the 2008 monsoon season compared with the 2007 season. In fact, c. 170 mm of rainfall was

recorded prior to the 2007 sampling, whereas c. 410 mm of rainfall was recorded prior to the 2008 sampling. This supports the theory that the 'rinse out effect' is short lived and was completed within <410 mm of rainfall in 2008 thus effectively 'missing' the monthly sampling event.

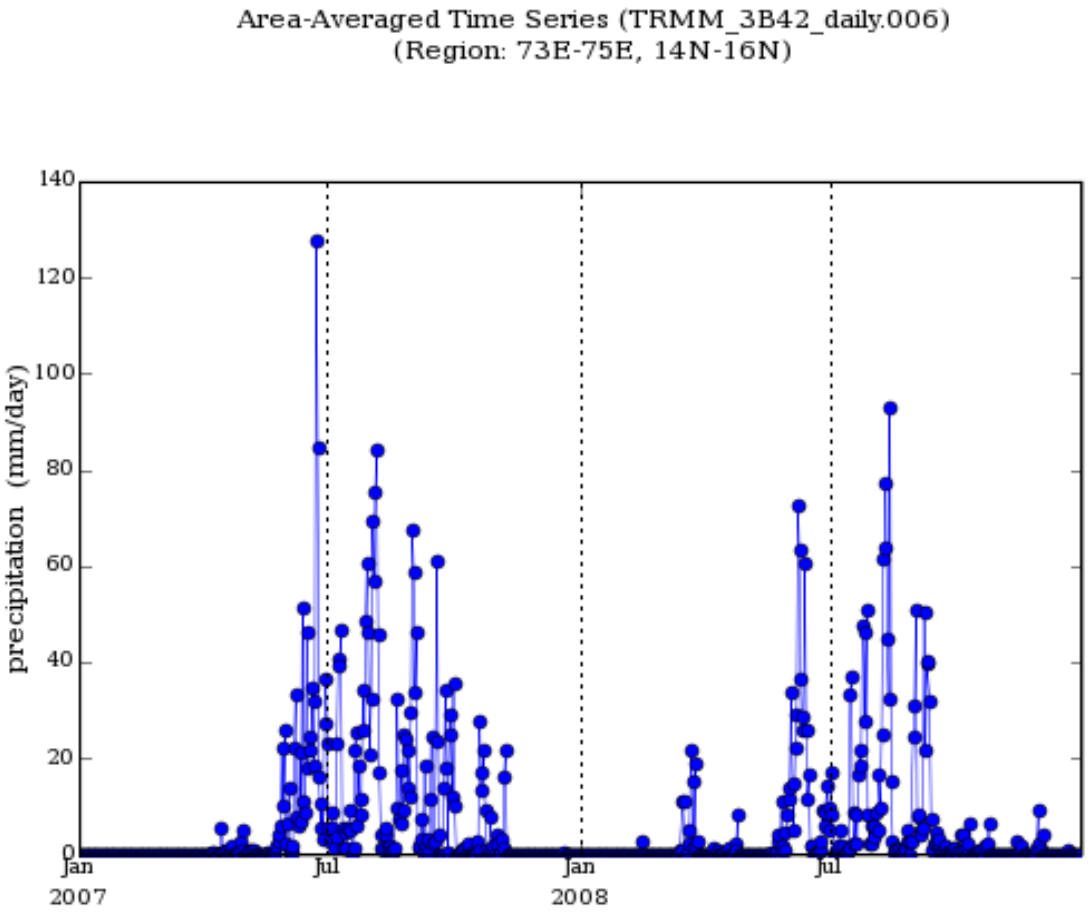

Figure 7.5 Precipitation graph for the area 73E-75E, 14N-16N from January 1st 2007 to December 31st 2008 (from Acker and Leptoukh, 2007).

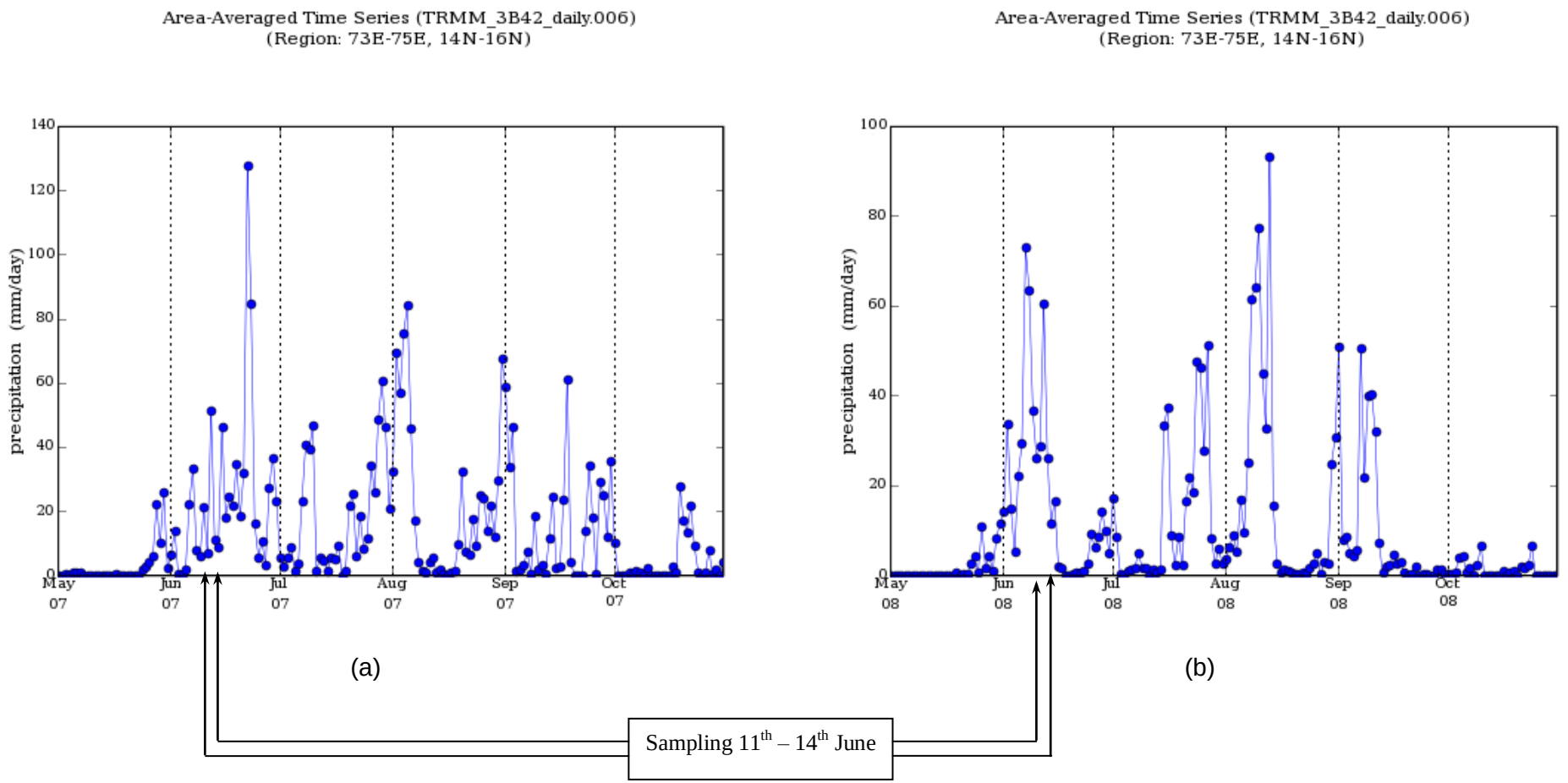

Figure 7.6 Precipitation graph for the area 73E-75E, 14N-16N from May 1st 2007 to October 31st 2007 and (b) Precipitation graph for the area 73E-75E, 14N-16N from May 1st 2008 to October 31st 2008 (from Acker and Leptoukh, 2007).

With reference to Figure 7.7, the element concentrations shown in Figures 6.5 to 6.27 can be explained as follows: Following the annual monsoon, the water table is at maximum saturation level but with every subsequent dry day the water table lowers. As it lowers, elements are either precipitated as salts within the pore spaces or the pore spaces retain moisture but without significant flow, although there will be some base level flow, however, this is not quantifiable within this study, in which case chemical weathering can continue. During the dry season there is almost no precipitation, and therefore the rivers do not have any significant flow and are essentially dominated by tidal influences and the previously mentioned base flow. It would seem that these tidal influences could also deliver ions to the drainage basins by salt deposition as the water percolates into the surrounding rocks as the tides ebb and flow. As discussed earlier measures were taken to minimise this effect but it may be that some component of the elemental composition of the river water may be estuarine derived. However, regardless of the provenance of the elements, during the onset of the subsequent monsoon the rainfall percolates through the pore spaces, and rinses out the precipitated elements as the water table rises once more. This 'rinse out effect' is temporally limited to the time it takes to rinse through the system, which is itself controlled by the lithology, the porosity of the substrate and the amount of rainfall over time.

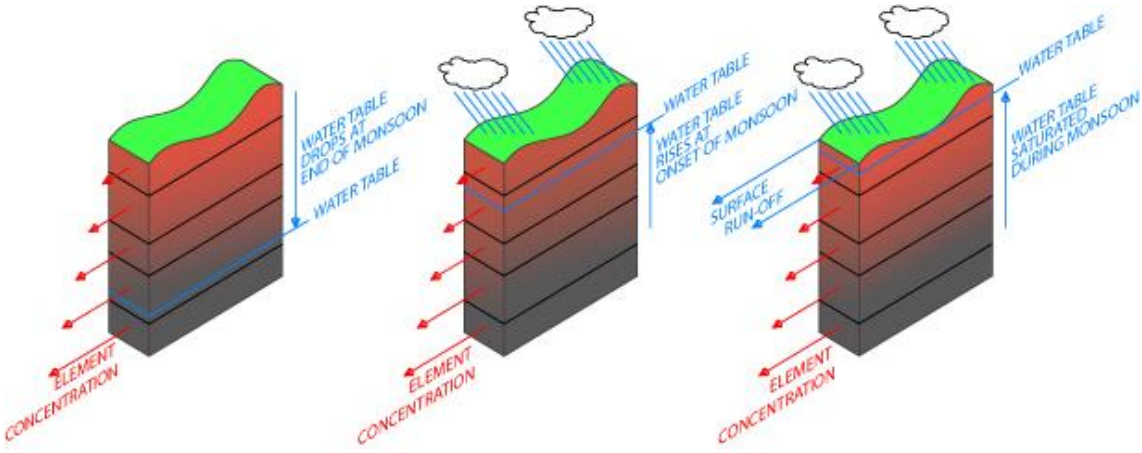

Figure 7.7 Effects of monsoonal rainfall on the water table, this figure is intended to represent the typical weathered lithology such as that documented for the Merces Quarry which has unaltered protolith at its base moving up profile through saprolite to indurated laterite at the upper surface.

Another observation that may be explained using Figure 7.7 is the relatively limited range of Ca + Mg values when plotted against HCO_3^- during the wet season (Figure 7.8). During the wet season Ca appears to be limited to between 200 - 300 µeq l^{-1} whilst Mg appears to be limited to between 100-150 µeq l^{-1}, albeit with a few notable exceptions. However, during the dry season Ca and Mg values increase relative to HCO_3^-. During silicate weathering all dissolved HCO_3^- originates from atmospheric/soil CO_2 (Dessert et al., 2001). Since the majority of the two drainage basins under observation are covered by laterite, it is logical to assume that the elemental concentrations observed in these fluvial systems are derived primarily from the lower levels of the lithological profile, which is demonstrated by the column experiment (Section 7.1.3). Accordingly, the red arrows on the left of the diagrams (Figure 6.7) are intended to represent the relative elemental contributions from the various depths within the lithological profile. If this behaviour has been correctly interpreted, then once the system has reached saturation only a fixed amount of flow can pass through the lithology, where it can react with the relatively unaltered or recently weathered minerals. The remainder of the rainfall flows into the rivers as surface and near-surface run-off. Further, this surface run-off passes through lithologies that have already been depleted of mobile elements and are thus preferentially enriched in immobile elements (lateritic materials).

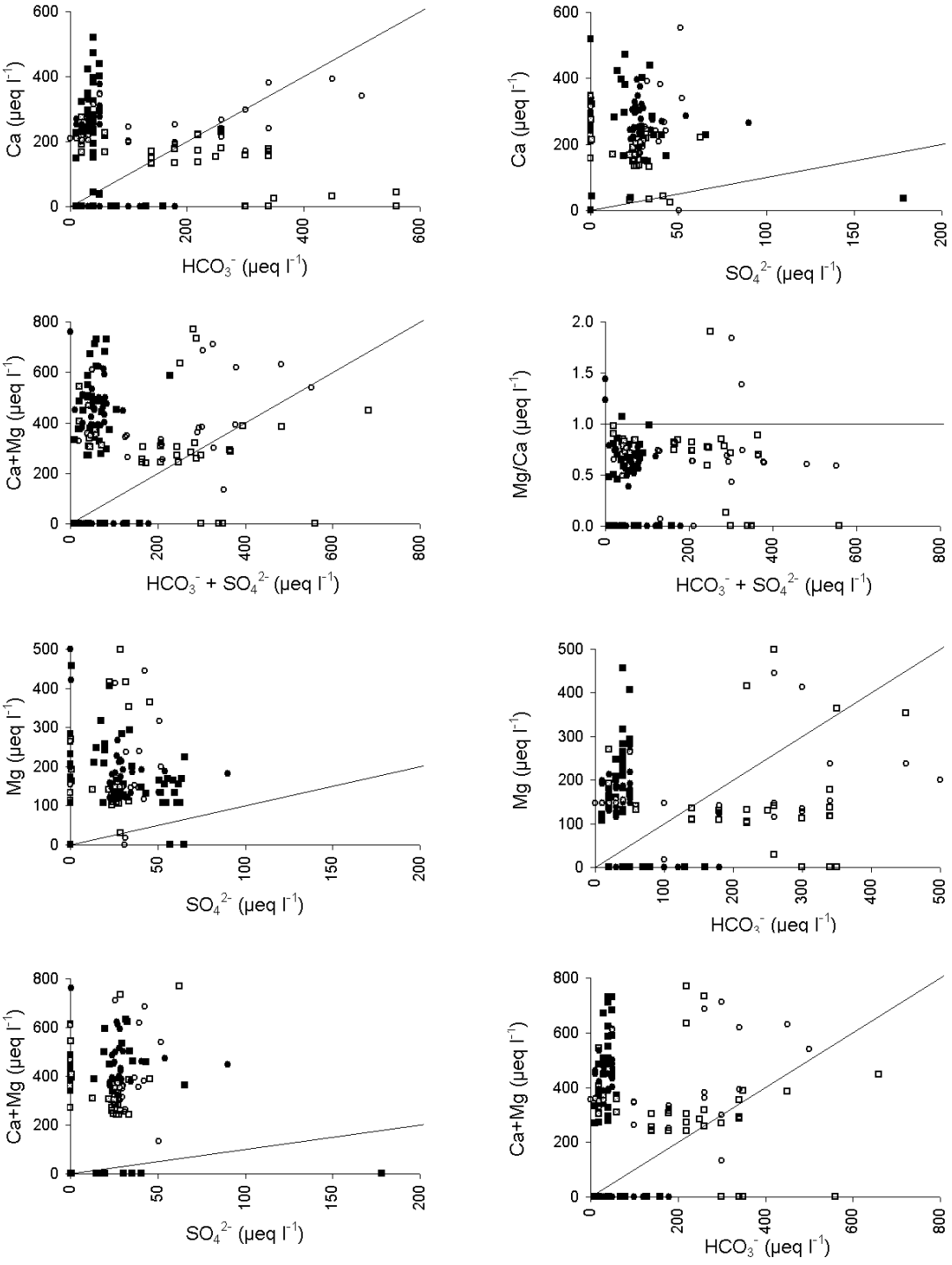

Figure 7.8 X-Y Plots plotting cations, Ca and Mg against anions HCO_3^- and SO_4^{2-}. Open symbols represent the monsoon period (June-07-Sept-07) closed symbols represent the dry Season (Oct-07-June-08) and shaded symbols represent the beginning of the 2008 monsoon season (July-08). Circular symbols represent the Chapora River and square symbols represent the Zuari River.

7.1.3. Column experiment

The column experiment described in Section 4.4 and discussed in Section 5.3 was designed to consider how the various zones within a weathering profile, the Merces Quarry profile, reacted in the presence of water in order to evaluate the relative reactivity of the various zones within a typical weathering profile. It was hypothesised that the relative reactivity would increase with depth through the profile as each zone is less weathered and therefore more enriched in mobile elements as we move down through the profile. Unfortunately, major and trace element analysis was not completed in time for inclusion in the thesis. Since element concentration is directly related to conductivity this can be used as a proxy for reactivity within the various columns, and is done so in the following discussion.

The experiment was conducted over a 16 week period and Figure 3.5 shows that conductivity diminished over time as expected. Also, as expected, the water samples obtained from column 1, unaltered protolith, report the highest conductivity. This was followed by column 6, the combination column, which is likely due to a contribution from unaltered protolith. The next highest conductivity was not attained for column 2 as predicted, but instead for column 3. Looking back at notes taken at the time this is likely due to the friable nature of the sample material used in this column. All column sample materials were crushed and sieved to create an approximately equal reactive surface area and permeability for all of the columns. However, the material used for this column was too friable to retain a consistent grain size and as such created a greater reactive surface area as well as slowing the progress of the water through the column, which took a few hours to drain, compared to a few minutes for the other 5 columns. In fact column 6 also showed a reduced permeability which suggests that the contribution from column 3 in this column has also had an effect on the conductivity values achieved for column 6. These two factors seem to have allowed columns 3 and 6 to achieve higher conductivity values than they would have achieved given a comparable surface area and permeability to the other columns. This observation is in broad agreement with the comments in the Section 7.1.4. Fluid residence time, which suggests that the residence time within the bedrock is likely an important control on solute concentrations.

Additionally, the XRF analysis of the Merces samples MQ1 - MQ17 can also be used to consider the depletion of mobile elements, such as the summed alkalis, Si, Rb, Sr and Ba and the subsequent preferential element enrichment of immobile elements such as Fe, Zr, Ti and Pb moving from the unaltered protolith up through the profile to the

indurated laterite cap. The graphs depicted in Figures 5.6 and 5.7 show a selection of element enrichment and depletion plots which, together with the conductivity discussion, support the view that water flowing through the upper zones of the weathered lithologies presently covering much of Goa is unlikely to generate and deliver significant elemental concentrations to the rivers. It is much more likely that the element concentrations entering the rivers are largely derived from weathering of relatively unaltered bedrock located at, or close to, the weathering front at significant depth, for the Merces Quarry profile this is located at c. 25 - 30 m below the surface. This weathering profile is made accessible due to the presence of the aggregate quarry, but it is important to realise that this weathering profile is typical and widespread across the region. This observation is can be thought of in terms of the Critical Zone (CZ) which extends from the vegetation canopy to the bottom of the ground water active zone and is where the complex interactions involving rock, water, air and living organisms occur (Brantley et al., 2007). However, mineral breakdown and element exchange are thought to occur within the deep CZ at the weathering front at the base of the regolith (Buss et al., 2013). The regolith is defined as the weathered rock material overlying pristine bedrock (Brantley et al., 2007). This is exactly in agreement with the conductivity data, where the highest conductivity was obtained from the protolith zone and generally diminished up profile, and the XRF data, which demonstrate a steady depletion of mobile elements from the base upwards with a marked depletion occurring around 25 m below the surface, this is accompanied by a concomitant rise in immobile elements as a result of preferential enrichment.

7.1.4. Fluid residence time

The above observations can be best understood in terms of the residence time of the fluid compared to the residence time required to reach chemical equilibrium (Maher, 2011). Catchments that show little variation in elemental concentration against variable discharge (chemostatic behaviour) are most likely to have fluid residence times that exceed the time required to reach chemical equilibrium. Conversely, decreases in concentration with increasing discharge can be explained by average residence times that are shorter than the time taken to achieve chemical equilibrium, which results in dilution (Maher, 2011). Therefore the residence time of water within the bedrock, saprolite and soil is likely an important control on solute concentrations because longer residence times will favour greater transfer of solute.

Tracer studies of small headwater catchments have yielded residence times ranging from a few months to several years, whilst residence times for larger rivers can approach decades due to longer flow paths (McGuire and McDonnell, 2006). The monsoonal climatic regime provides highly seasonal precipitation, therefore during the rainy season it is likely to lead to a very short residence time of just a few days with short transit pathways and high discharge; by contrast the dry season is characterised by long residence times due to sluggish or stagnated flow through the same transit pathways.

7.1.5. Spatial (downstream) variability

One of the most pronounced and ubiquitous observations from the graphical data is that the range of elemental concentrations for the selected localities for each river vary far more during the dry season that they do during the wet season. This suggests that during the wet season the river chemistry is dominated by precipitation and run-off with all localities reporting relatively similar concentrations, whilst during the dry season river chemistry is more locally controlled with each locality reporting quite different concentrations from its upstream or downstream neighbour. The major and trace element spatial variation graphs (Figure 7.9 – Figure 7.12) clearly support this for some elements (Ca, Mg, Rb, Sr, V and Ba), though but not for others (Na, K, Cl, SO_4 Co, Zn and Ni). For clarity, these graphs only consider data for a 2007 monsoon season month (August 2007), a 2008 dry season month (January 2008) and a 2008 monsoon season month (July 2008). However, referring to the temporal graphs (Figure 6.5 - Figure 6.27) for many elements the variability was at its greatest later in the year, around March or April and as such the graphs do not show this increased variability during the dry season.

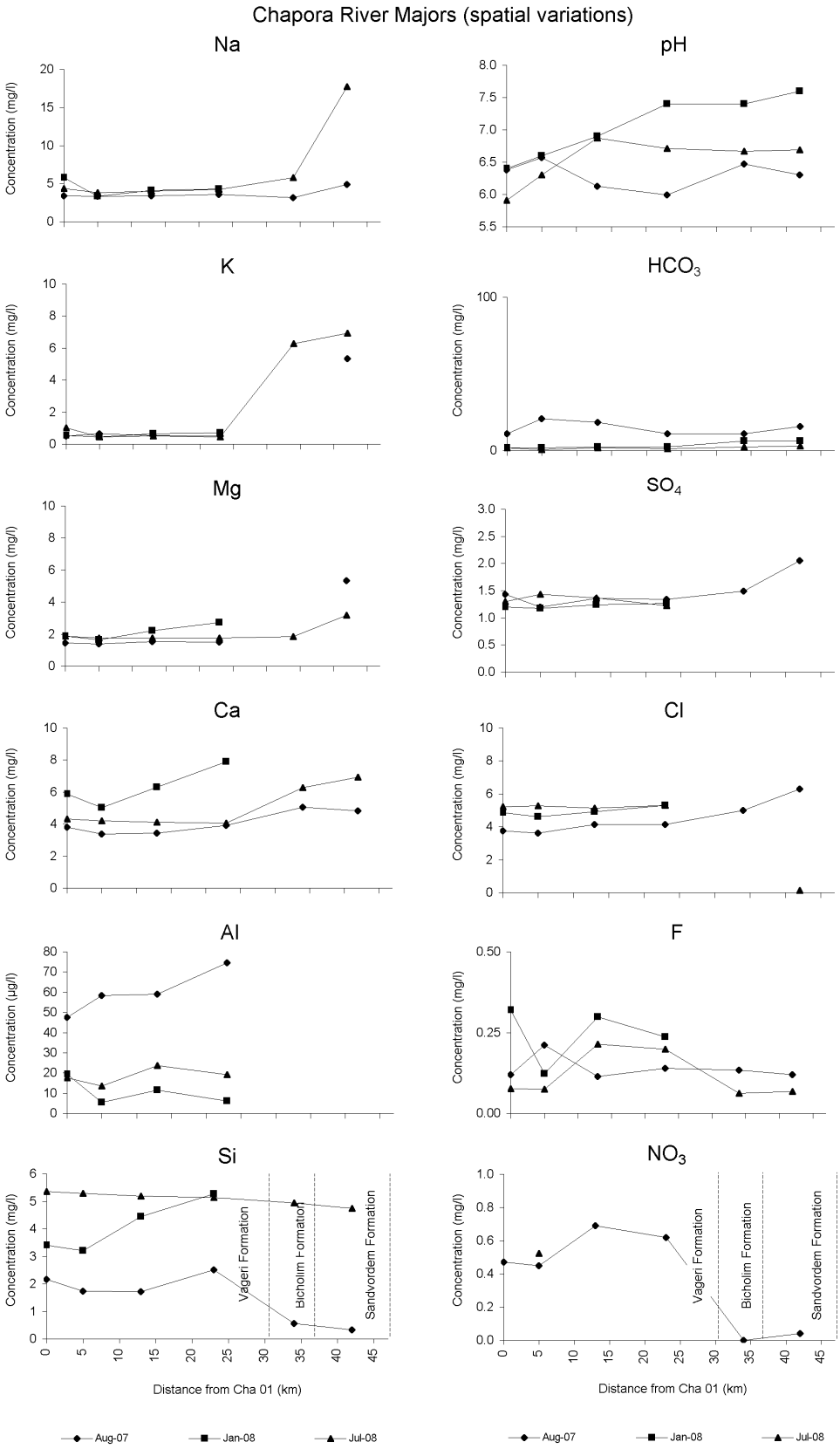

Figure 7.9 Spatial variation plots for the Chapora River showing the major cations, anions, pH and HCO_3^- concentrations for the months of August 2007, January 2008 and July 2008.

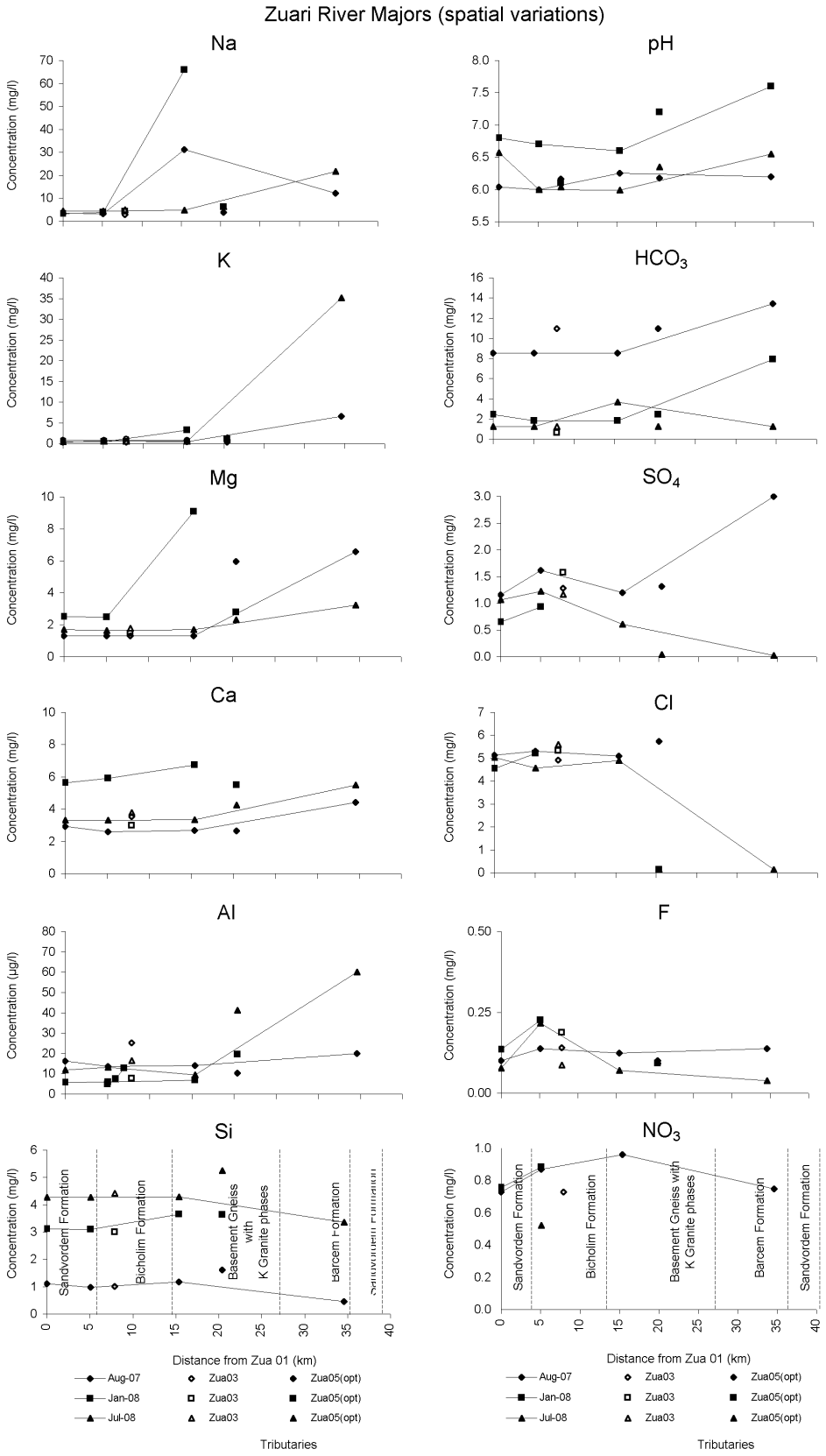

Figure 7.10 Spatial variation plots for the Zuari River showing the major cations, anions, pH and HCO_3^- concentrations for the months of August 2007, January 2008 and July 2008.

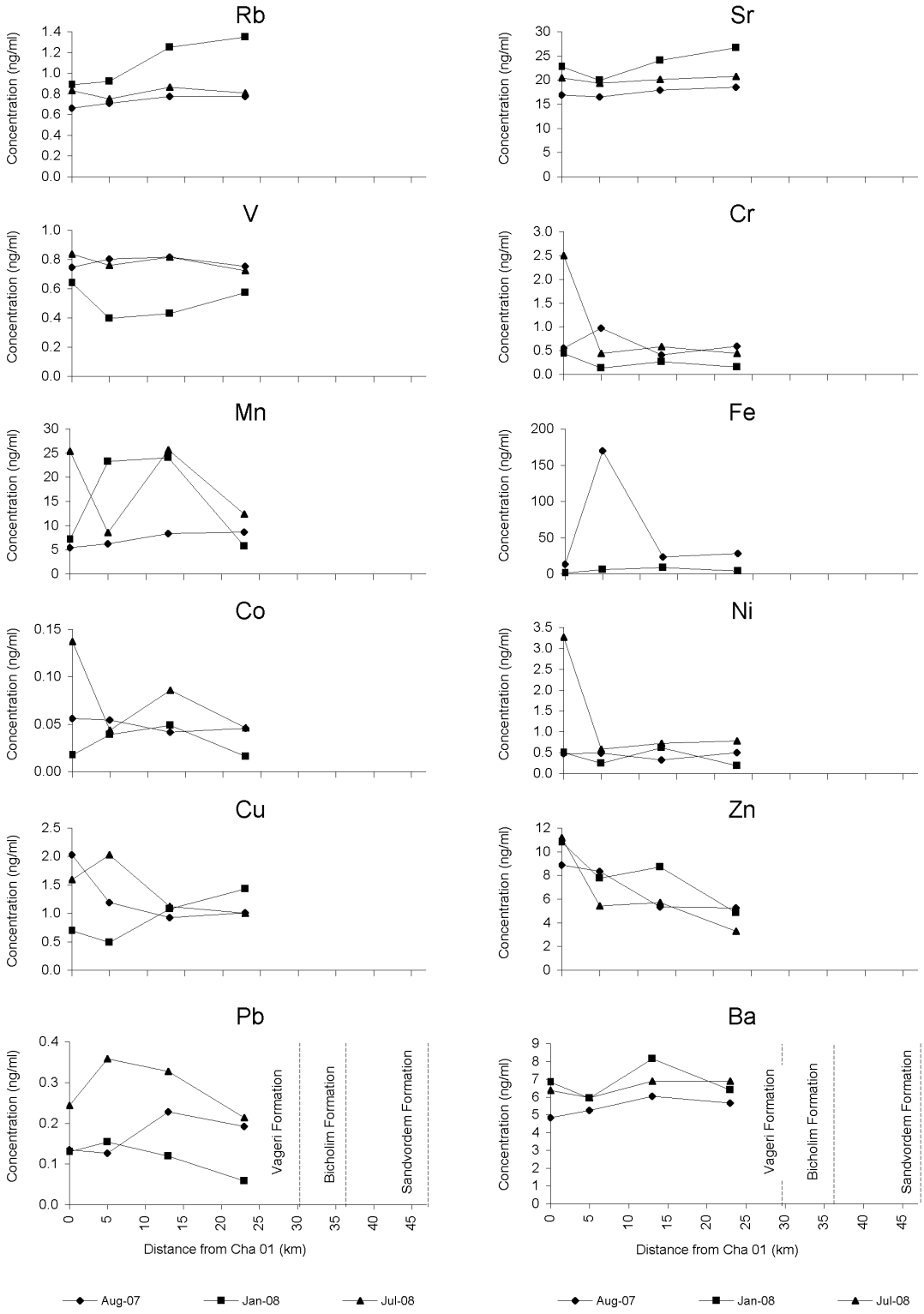

Figure 7.11 Spatial variation plots for the Chapora River showing trace element concentrations for the months of August 2007, January 2008 and July 2008.

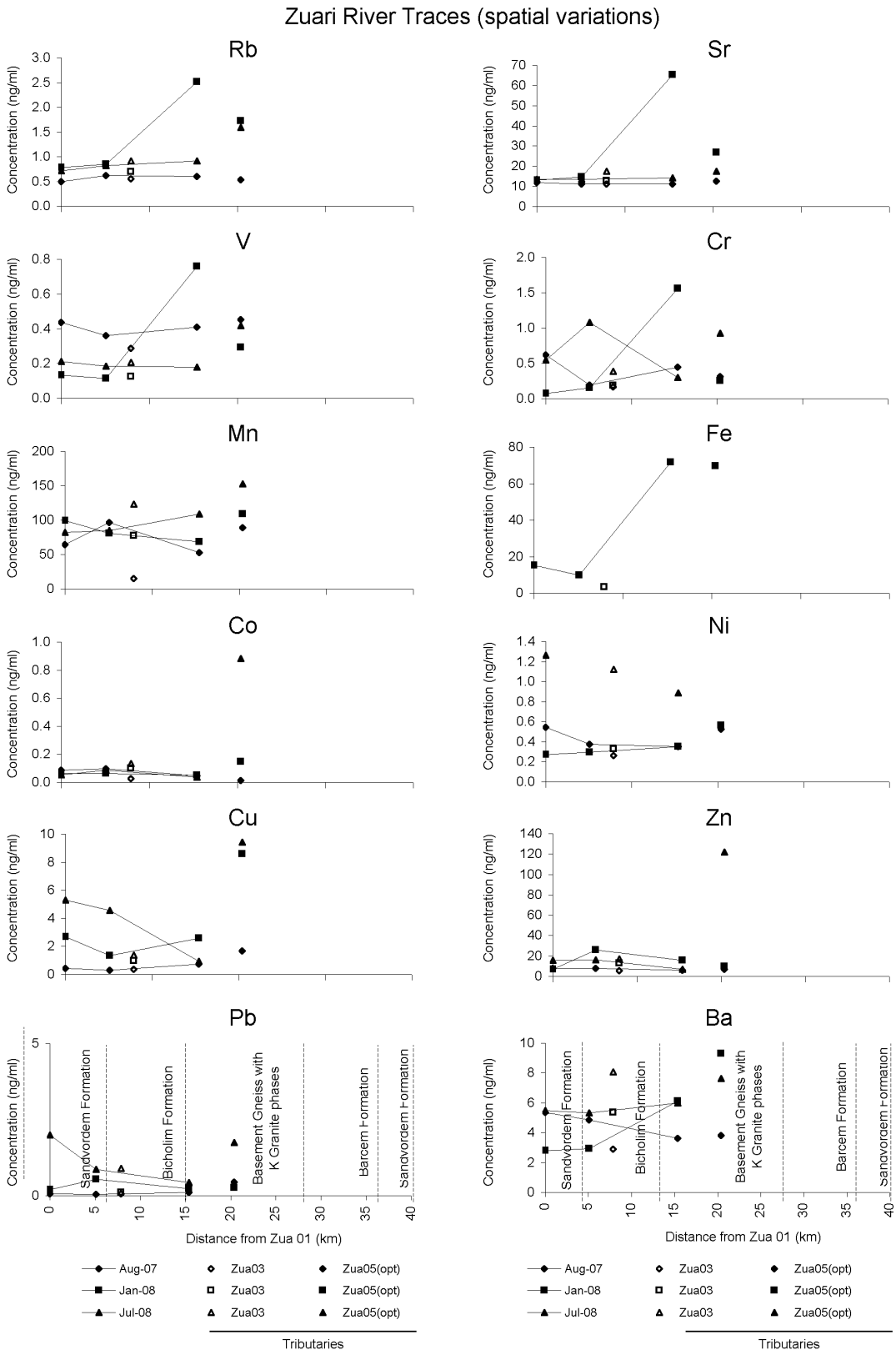

Figure 7.12 Spatial variation plots for the Zuari River showing trace element concentrations for the months of August 2007, January 2008 and July 2008.

7.1.6. Seasonal controls on river chemistry

Gibbs diagrams (Gibbs, 1970) are employed to determine elemental behaviour between the wet and dry season; these can also be used to indicate the dominant control for a given sample such as evaporation, rock and soil weathering, or precipitation-dominated. Gibbs diagrams were originally developed to plot Total Dissolved Solids (TDS) against relative proportions of cations (Na^++K^+) / (Na^++K^++Ca^{2+}) and / or anions, Cl / (Cl+HCO_3^-) for various surface waters from around the world, from which a curve with two distinct arms was created (Gibbs, 1970). Referring to Figures 7.13 and 7.14 the Gibbs plots have demarcated zones overlaid across the plot area in the shape of a V which has been rotated clockwise and positioned with its apex located centrally on the y axis. Travelling from left to right along the lower arm of the curve waters become lower in TDS concentrations and more relatively enriched in Cl and more representative of rain water. Rivers plotting in this zone are often tropical rivers draining thoroughly leached areas of low relief where the composition of the river water is controlled by dissolved salts supplied via precipitation. Whilst travelling from left to right along the upper arm of the curve waters become higher in TDS concentrations, with elements such as Cl and Na becoming dominant, representative of evaporation, which leads to increased salinity or TDS and the precipitation of $CaCO_3$ from solution increases the relative proportion of Na to Ca. Waters falling under this end member are generally located in hot, arid regions where often they show evolutionary paths starting near the Ca or rock weathering source changing in composition to the Na rich, high salinity end member as the river flow towards the ocean (Gibbs, 1970). Following these two arms to the left to their intersection, rock and soil weathering becomes the dominant control. Using this approach the appropriate Gibb's plots for the Chapora and Zuari Rivers (Figure 7.13 and Figure 7.14) reveal how the relative contributions of TDS against Cl/(Cl+HCO_3^-) vary throughout the year for each locality, and the following observations can be made.

As a general observation, TDS remains between 10 mg l^{-1} and 100 mg l^{-1} throughout the sampling period for all localities, with the highest values occurring during the 2007 wet season (June – September), with values for June being the highest for all the Chapora River localities and the three most upstream localities on the Zuari River which coincide with the onset of the monsoon. These also coincide with low (<0.4) values for Cl/(Cl+HCO_3^-) which are due to the higher HCO_3^- concentrations also occurring at this time as a direct result of enhanced weathering, thus placing the 2007 wet season values in the area of rock weathering dominance. These positions are

clearly linked to the peak concentrations occurring in June 2007 indicative of the rinse-out effect. However, the 2008 wet season months do not plot in the same sector of the graph as the 2007 wet season months as expected; but rather tend to plot with slightly lower TDS and significantly higher $Cl/(Cl+HCO_3^-)$ values in a similar sector of the graph along with most of the dry season samples. This is supportive of the observation discussed in section 7.1.2, that the 2008 sampling missed the rinse-out effect.

The 2007 wet season values (June – September) plot in a distinctly separate region from those for the 2008 dry season (January – May), and suggest that the wet season river chemistry is controlled by rock and soil weathering whereas the dry season river chemistry is controlled by precipitation. This, at first, may seem counter intuitive, with dry season chemistry being controlled by precipitation; however, it is in broad agreement with data presented for the Godavari River which are also presented on Gibbs plots (Jha et al., 2009). Here, samples were collected in March 2005 (pre-monsoon), December 2005 (post monsoon) and August 2006 (monsoon). These Gibbs plots also showed that for all three sample collection periods almost all of the data points plot within the rock weathering sector, regardless of the fact that 93-96% of all precipitation occurs during the monsoon period. That said, during the pre-monsoon, samples collected from the Sabri River, whose catchment area is devoid of basalt does fall under the precipitation dominance sector due to lower concentration of total dissolved solids. Under closer inspection of the Gibbs plots presented for the Godavari River data, the x-axis is represented by the cations $(Na^+ + K^+) / (Na^+ + K^+ + Ca^{2+})$, whilst the Gibbs plots used in this study the x-axis is represented by the anions $Cl / (Cl + HCO_3^-)$. Although, using different x-axes, similar observations are apparent between the Godavari data and the Chapora and Zuari data in that they are both predominantly controlled by rock dominance during the monsoon period whilst are precipitation dominated to some extent during the dry season. This is a feature that is typical of tropical rivers which drain heavily leached areas of low relief, resulting in a very low supply of dissolved salts from the lithology and where the rainfall is high and so the river chemistry becomes very similar to that of the precipitation chemistry.

However, as mentioned previously, the 2008 wet season months plot closer to those of the dry season values; this may be due to the slightly lower precipitation values for 2008 compared with 2007; alternatively, like the rinse-out observations, it could be due, simply to the timing and/or resolution of the sampling regime.

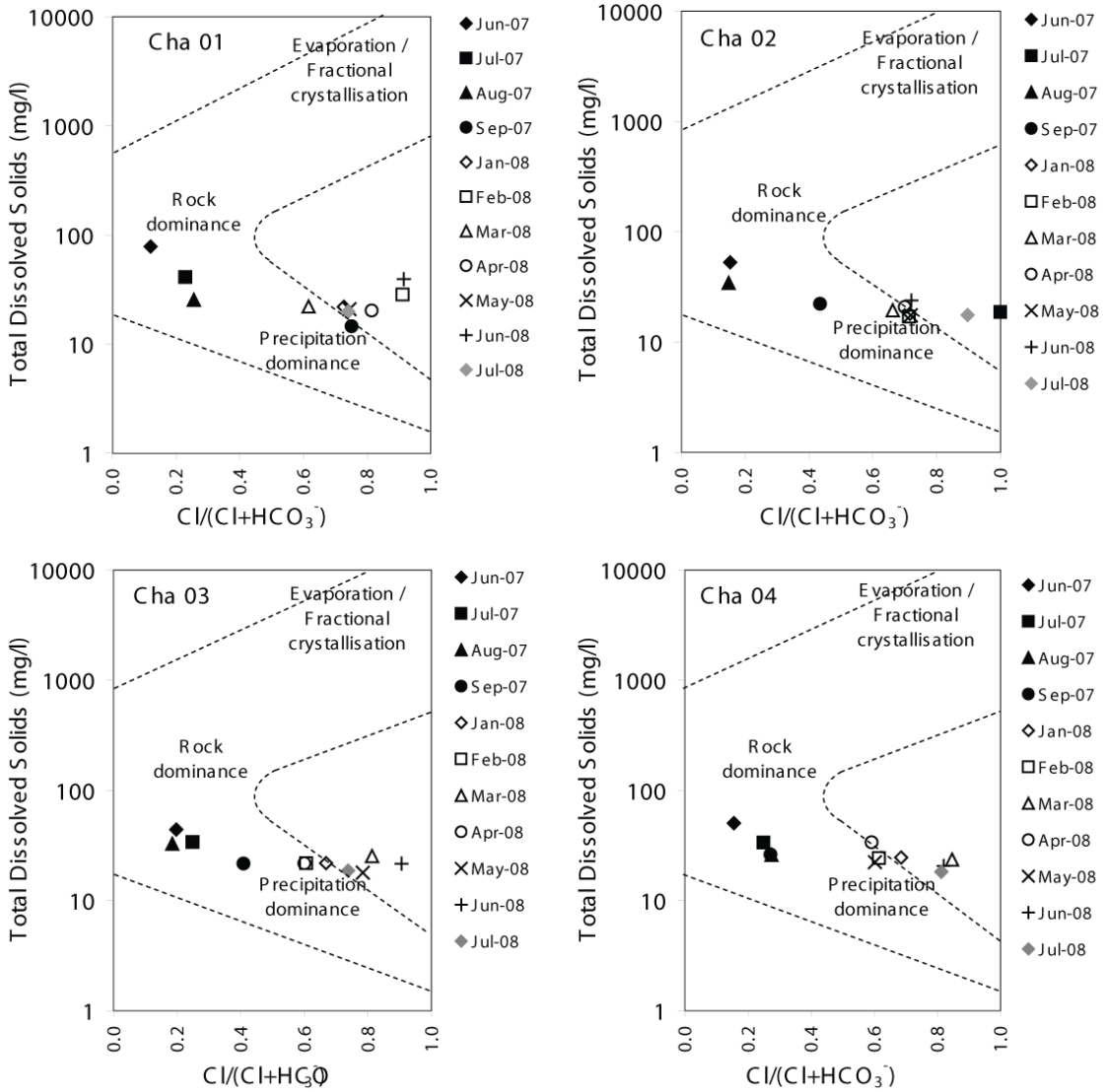

Figure 7.13 Gibbs diagram for the Chapora River plotting the monthly samples for each locality.

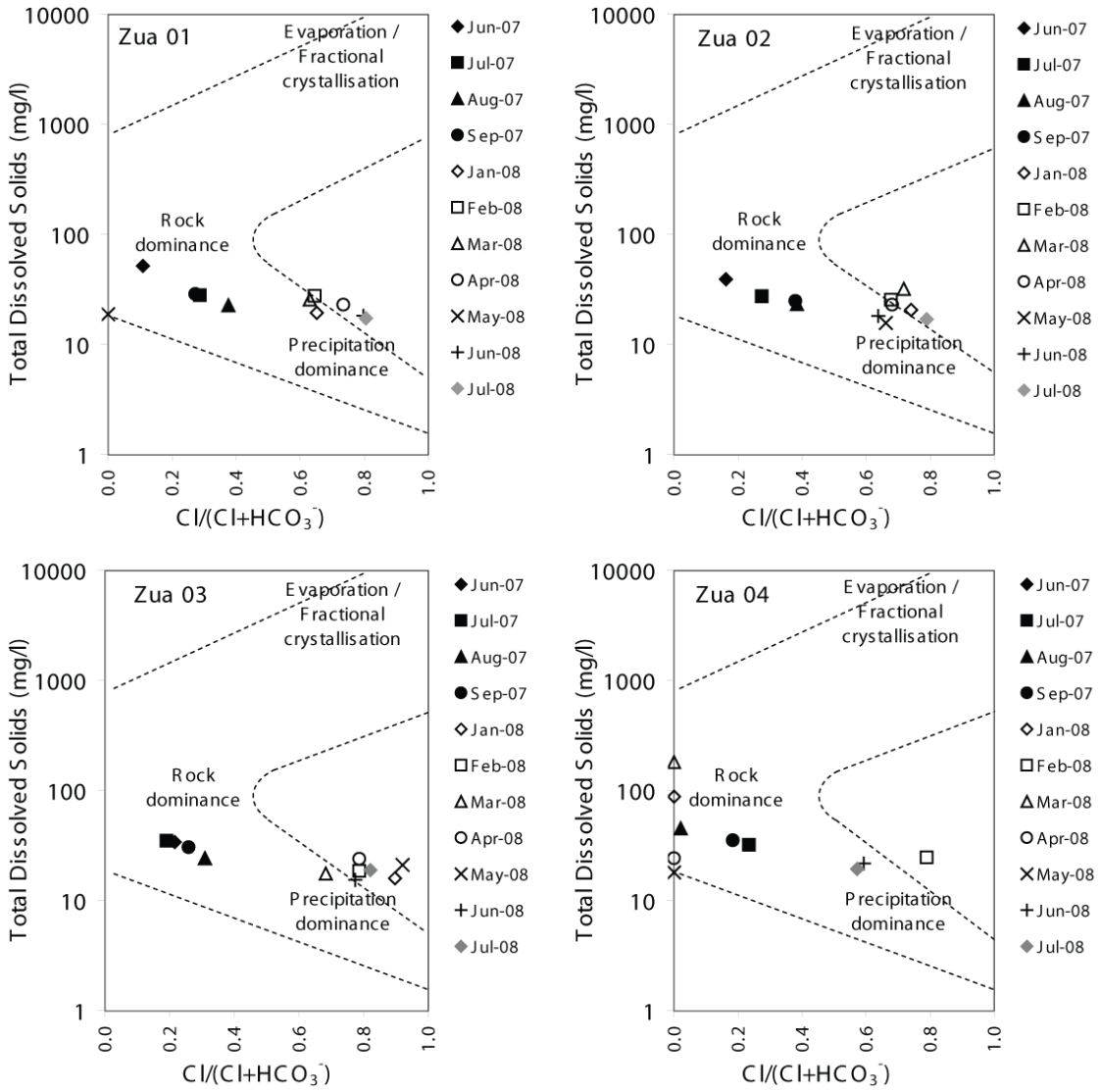

Figure 7.14 Gibbs diagram for the Zuari River plotting the monthly samples for each locality.

The following set of graphs (Figure 7.15 - Figure 7.18), show how HCO_3^- and Cl vary against $Cl/(Cl+HCO_3^-)$. These clearly demonstrate the dominance of HCO_3^- in controlling where each sample is plotted. Firstly considering the Cl graphs, these show that whilst Cl concentrations do vary between 3.61 mg l^{-1} for Cha 02 in Aug 2007 and 7.95 mg l^{-1} for Cha 03 in March 2008 (Figure 7.15) and between 4.19 mg l^{-1} for Zua 03 in June 2008 and 8.99 mg l^{-1} also for Zua 03 in April 2008 (Figure 7.16) they do not show a clear separation between the wet and dry months for Cl concentrations. However, they do show a clear separation along the x-axis with the wet season samples plotting further to the left and the dry season samples plotting further towards the right. This is due to increased HCO_3^- associated with the wet season driving the $Cl/(Cl+HCO_3^-)$ to lower values by dividing by larger values. For example, if HCO_3^- was zero this would plot at one as Cl/Cl would always equal one.

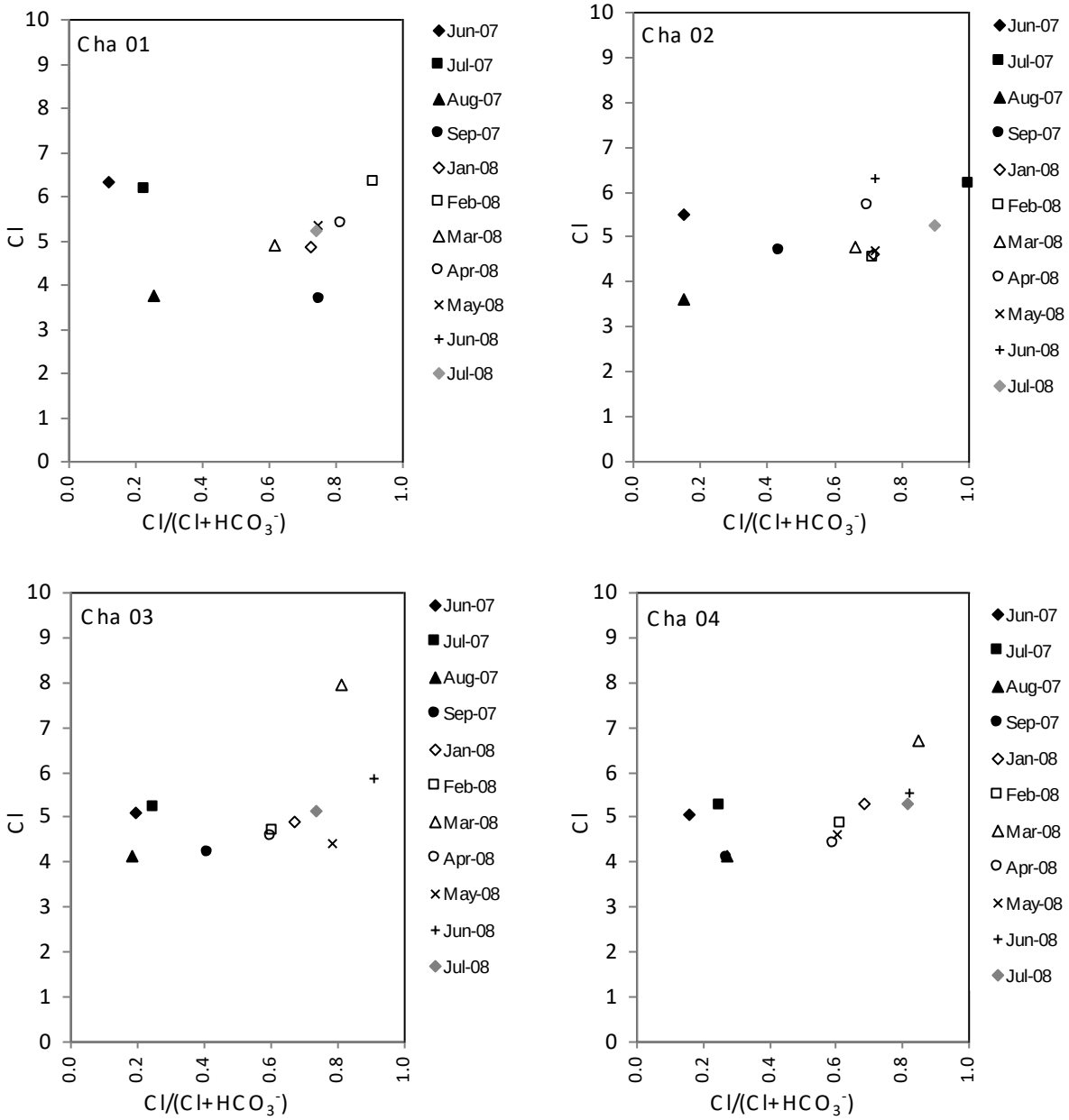

Figure 7.15 Graphs plotting Cl versus Cl/(Cl+HCO3$^-$) for the Chapora River sample localities, Cha 01 – Cha 04.

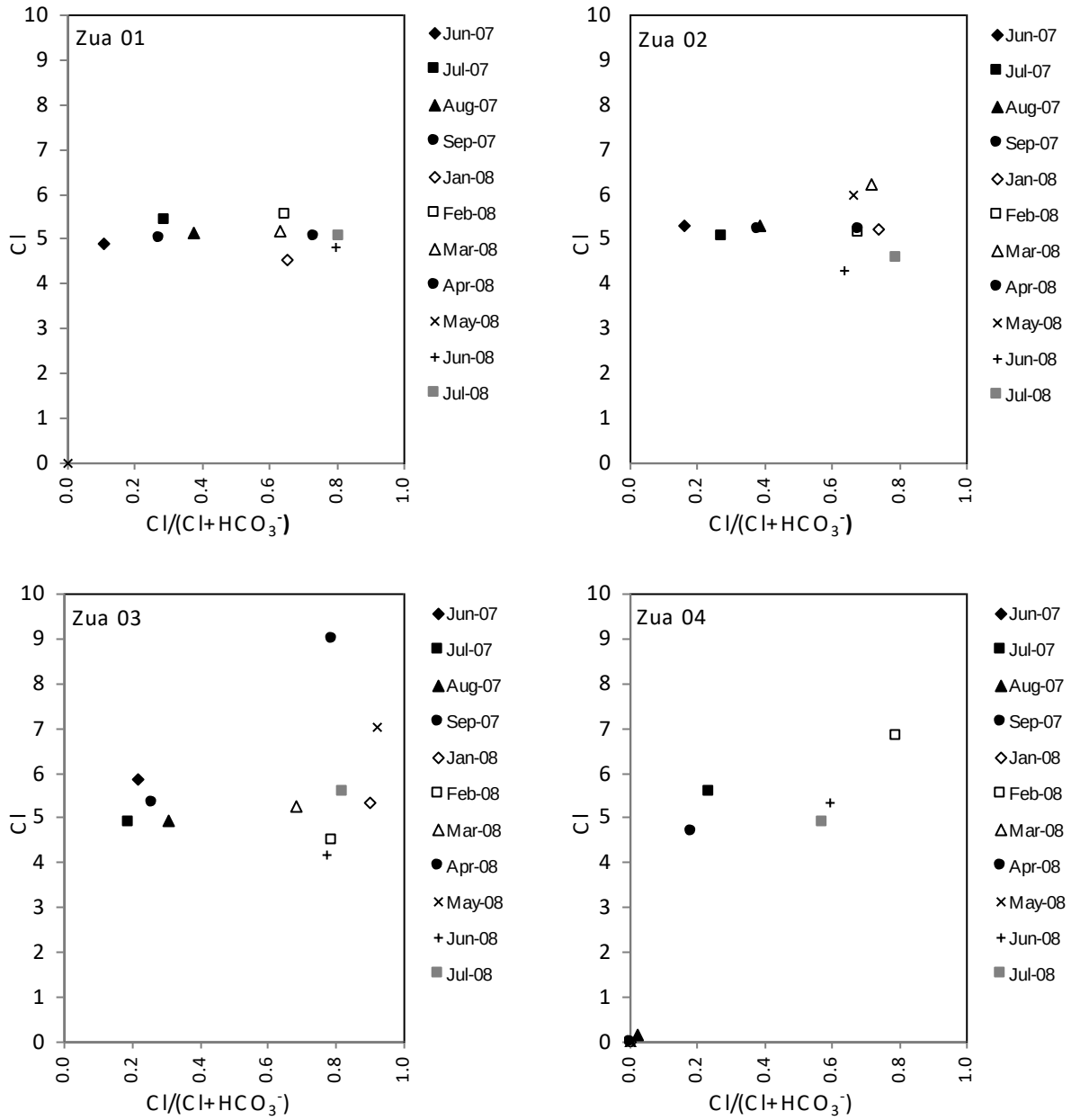

Figure 7.16 Graphs plotting Cl versus $Cl/(Cl+HCO_3^-)$ for the Zuari River sample localities, Zua 01 – Zua 04.

Regarding the HCO_3^- versus $Cl/(Cl+HCO_3^-)$ plots (Figures 7.17 and 7.18), these again clearly show a significant difference between the wet season samples and the dry season samples. The Chapora samples show the highest HCO_3^- occurring for June 2007 samples for all locations with the highest value of 46.37 mg l^{-1} occurring for Cha 01 and the next highest value of 30.51 mg l^{-1} occurring for Cha 02, although the values for Cha 03 and Cha 04 are not as expected with the Cha 04 sample reporting a higher value of 27.46 mg l^{-1} than that for Cha 03 of 20.74 mg l^{-1}.

The lowest values are represented by the dry season samples and the June and July 2008 wet season samples and these again plot towards the right of the graph due to the effect of low HCO_3^- values driving the x-axis towards one.

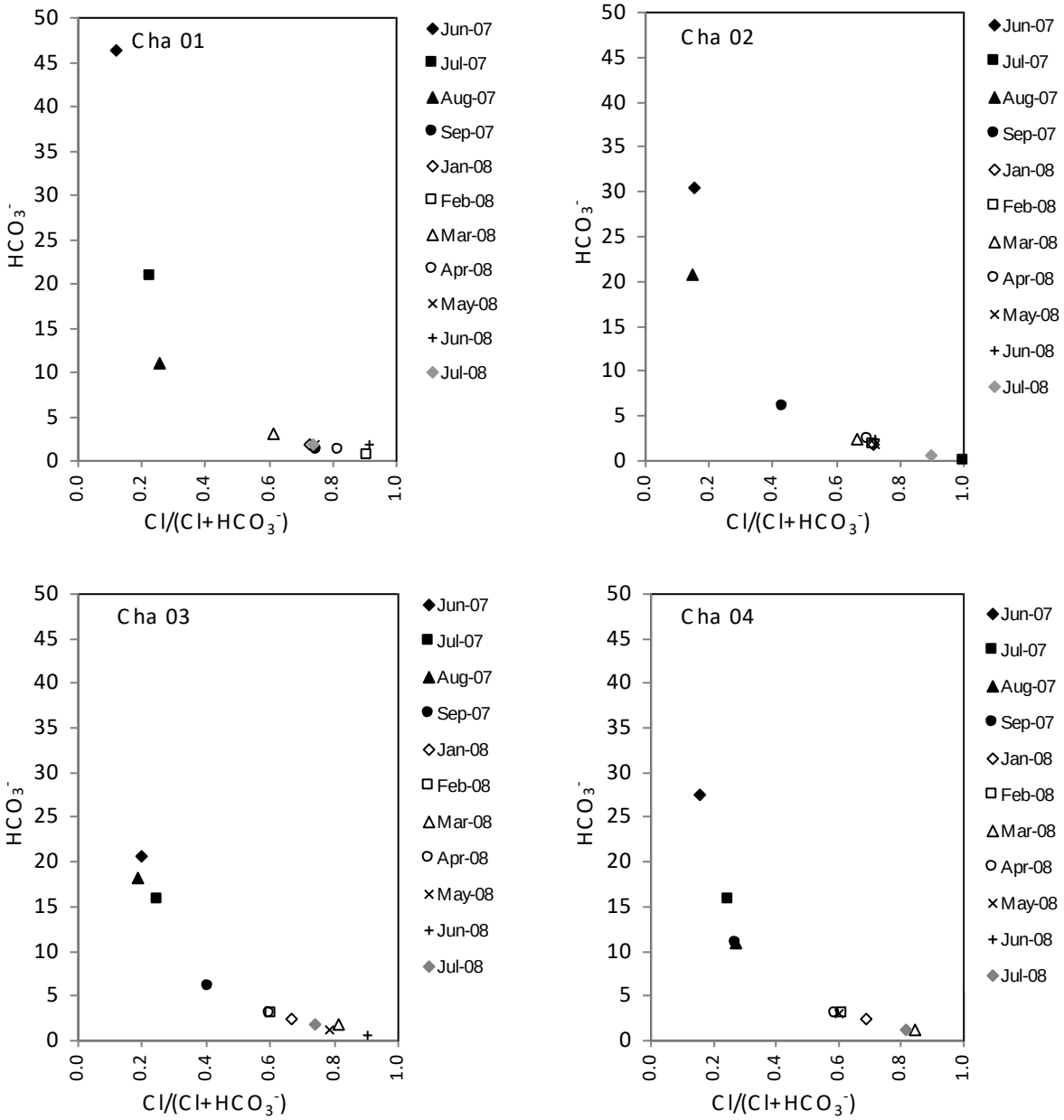

Figure 7.17 Graphs plotting HCO_3^-) versus Cl/(Cl+HCO_3^-) for the Chapora River sample localities, Cha 01 – Cha 04.

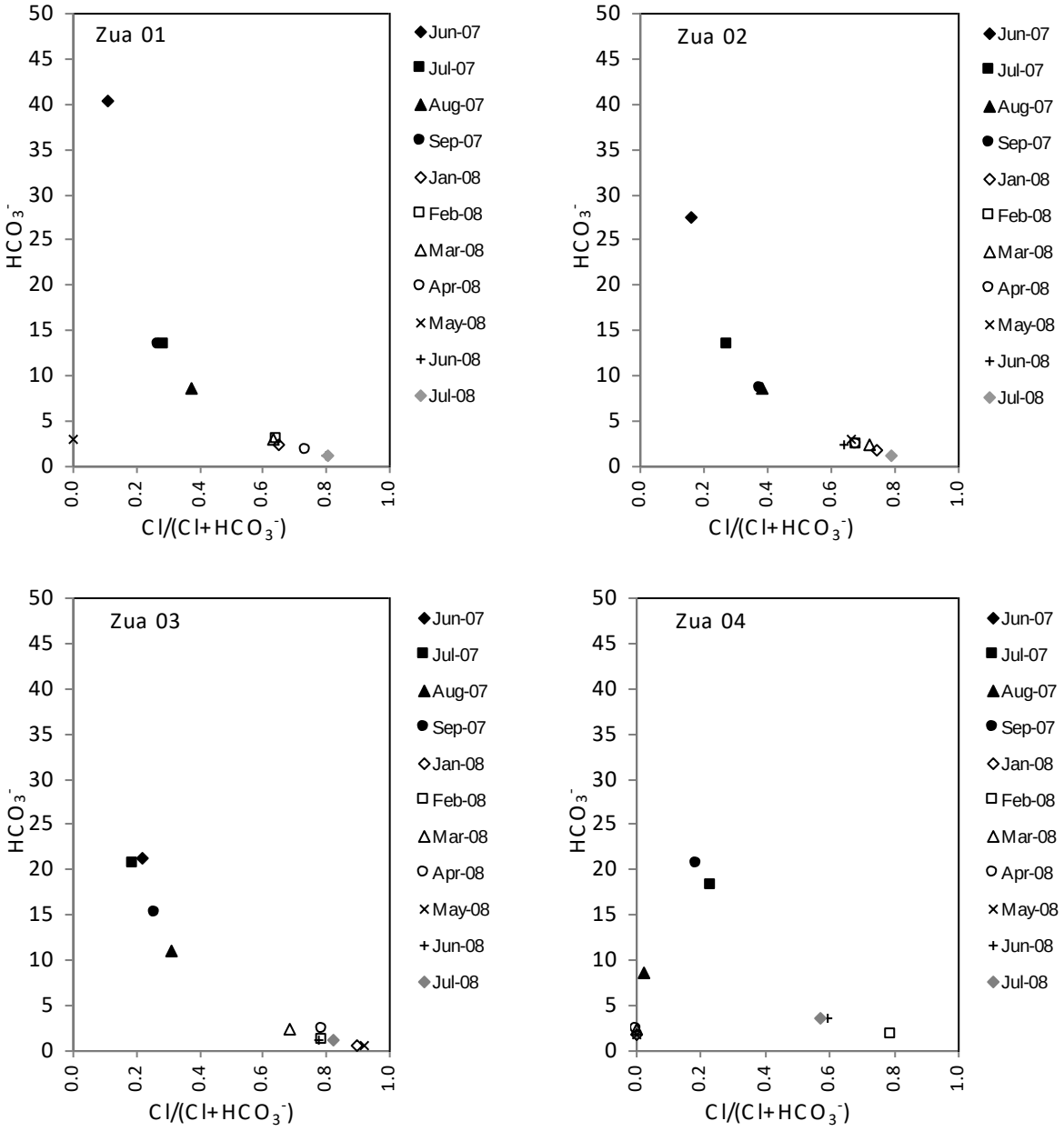

Figure 7.18 Graphs plotting HCO_3^- versus $Cl/(Cl+HCO_3^-)$ for the Zuari River sample localities, Zua 01 – Zua 04.

Considering Figures 7.15 to Figure 7.18 it is clear that Cl is relatively consistent for all of the sampling localities that are deemed unaffected by estuarine influence and that as expected, weathering is controlling the HCO_3^- concentrations with higher values occurring during the wet season and the highest occurring in June 2007 for all eight localities. Additionally, it appears that HCO_3^- concentrations reduce downstream suggesting that weathering is strongest in the upper reaches of both rivers.

7.2. Weathering Indices

The following section describes two weathering indices based on the lithological components collected from within the two drainage basins. The first is the Chemical Index of Alteration (CIA) and the second is the Mafic Index of Alteration (MIA).

7.2.1. Chemical Index of Alteration (CIA)

Given the recognised importance of chemical weathering in both catchment systems, and the associated fluvial chemistries, the nature of rock weathering is now explored.

Table 5.4 includes a calculated CIA value for the full suite of rock and sediment samples collected from the various river sampling localities. These are representative of the underlying lithologies present at each locality or in the case of the river borne samples, representative of lithologies known to be present in the upper reaches of the rivers. These CIA values range from 36.2 for sample Cha 03 S4 which is quartz chlorite schist to 97.6 for sample Zua 01 S1. This high CIA sample is a laterite which is dominated by a high percentage of Fe and Al (Figure 7.20a), and a low percentage of Ca, Na and K thus plotting close to the Al apex (Figure 7.20b) and indicating that the sample is extensively weathered. Other samples plotting close to the Al apex are Zua 03 S1 (red silt) and Zua 05 opt S2 (gravel and pebbles) these have CIA values of 86.8 and 91.2, respectively. Laterites plot towards the higher CIA values (>90) whereas aluminous laterites plot slightly lower (75 to 90) (Meshram and Randive, 2011). This reaffirms that these three high CIA samples are indeed lateritic (Zua 01 S1) or, in the case of the red silt (Zua 03 S1) and the gravel / pebbles (Zua 05 opt S2) are composed of lateritic components.

7.2.2. Mafic Index of Alteration (MIA)

For the suite of samples analysed the MIA values are almost always slightly higher than those calculated using the CIA method, with the notable exception of Cha 03 S3 which is a quartzite sample (Figure 7.19).

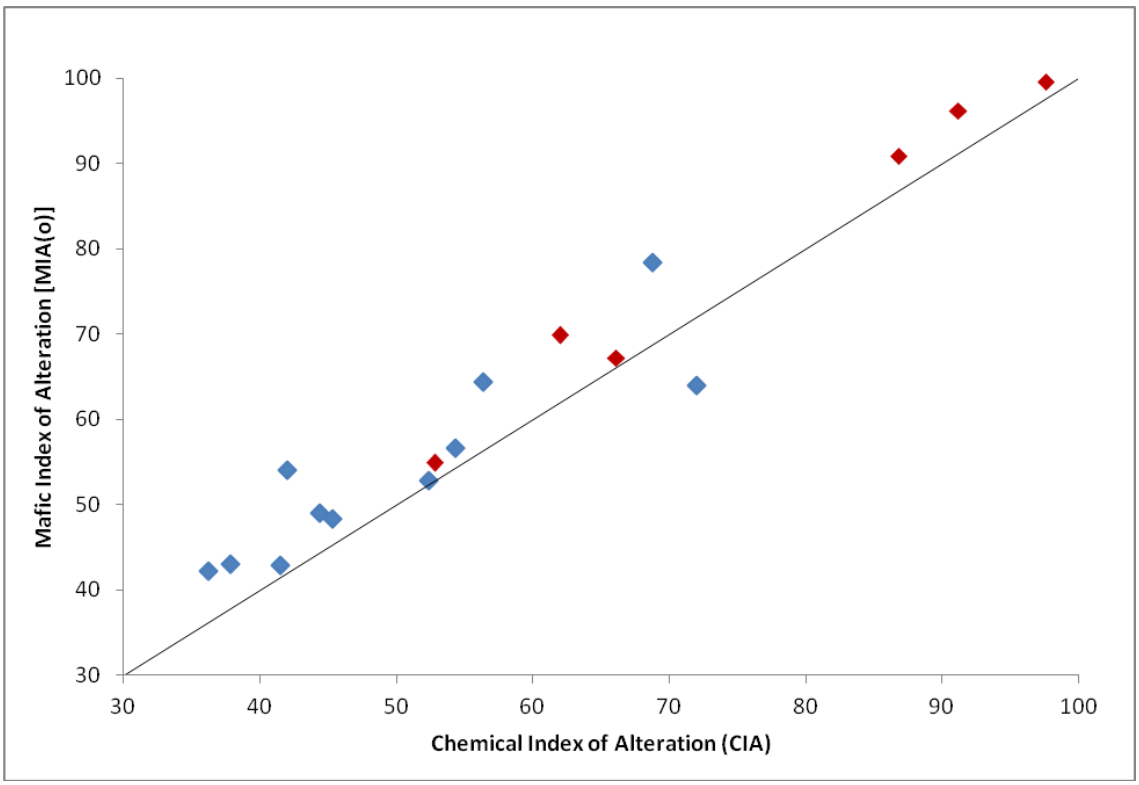

Figure 7.19 Comparison of the CIA and MIA(o) weathering indices for the Chapora and Zuari River samples. Blue data points represent the Chapora samples whilst red data points represent the Zuari samples, shown with a theoretical 1:1 line.

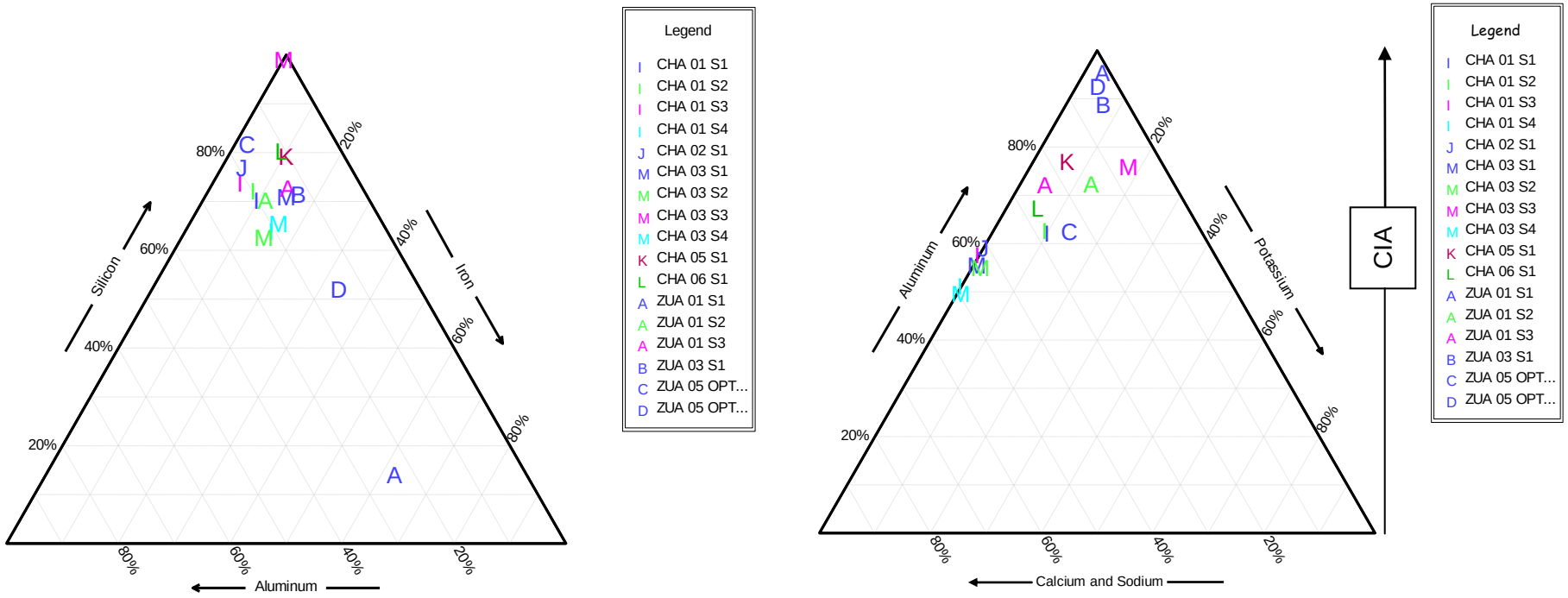

a b

Figure 7.20 Ternary diagrams, a) SiO_3, Fe_2O_3 and Al_2O_3 and b) Al_2O_3, K_2O and $CaO+Na_2O$. See legend for sample localities, and Section 5.1 for lithological interpretation.

7.3. Comparing and contrasting the Chapora and Zuari Rivers

As previously discussed in section 5.1, the lithology of the Chapora and Zuari drainage basins are broadly similar, in so much as they both drain significant amounts of Goa Group rocks, with the Chapora draining the Vageri, Bicholim and Sandvordem formations, and the Zuari draining the Bicholim, Sandvordem and Barcem formations. However, there are also significant differences between the two basins, with the Chapora River draining a small area (c.39 km^2) of Deccan basalt in its most upper reaches, and the Zuari having one tributary draining an area of (c.102 km^2) granite gneiss (Chandranath Granite). In addition to these lithological characteristics, both drainage basins have undergone significant weathering over the past millennia, which have resulted in the presence of extensive laterite cover; this weathering mantle is slightly more widespread for the Chapora River. In addition, the presence of Fe and Mg mines along Zuari River provides another potentially significant difference when compared to the Chapora River which has no mining influence.

Figures 7.21 and 7.22 display the major and trace element data for localities Cha 01 and Zua 01; these are designed to offer a better comparison of major and trace element temporal variations at comparative positions along the length of the two drainage basins. The following sections employ these figures to compare and contrast the two basins in terms of lithological and mining influence, and to explain observed similarities and differences.

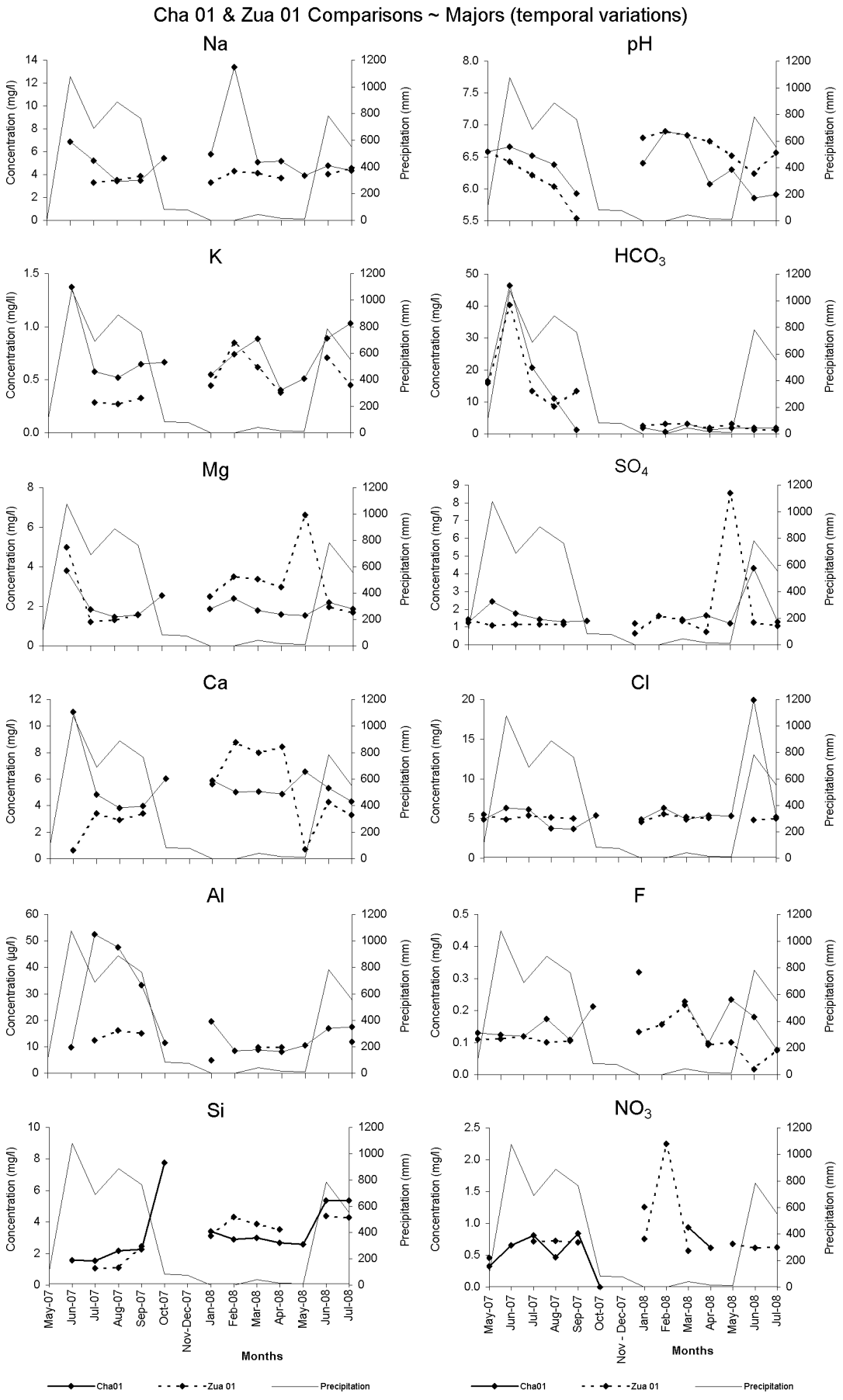

Figure 7.21 Major element plots showing the values for Cha 01 and Zua 01.

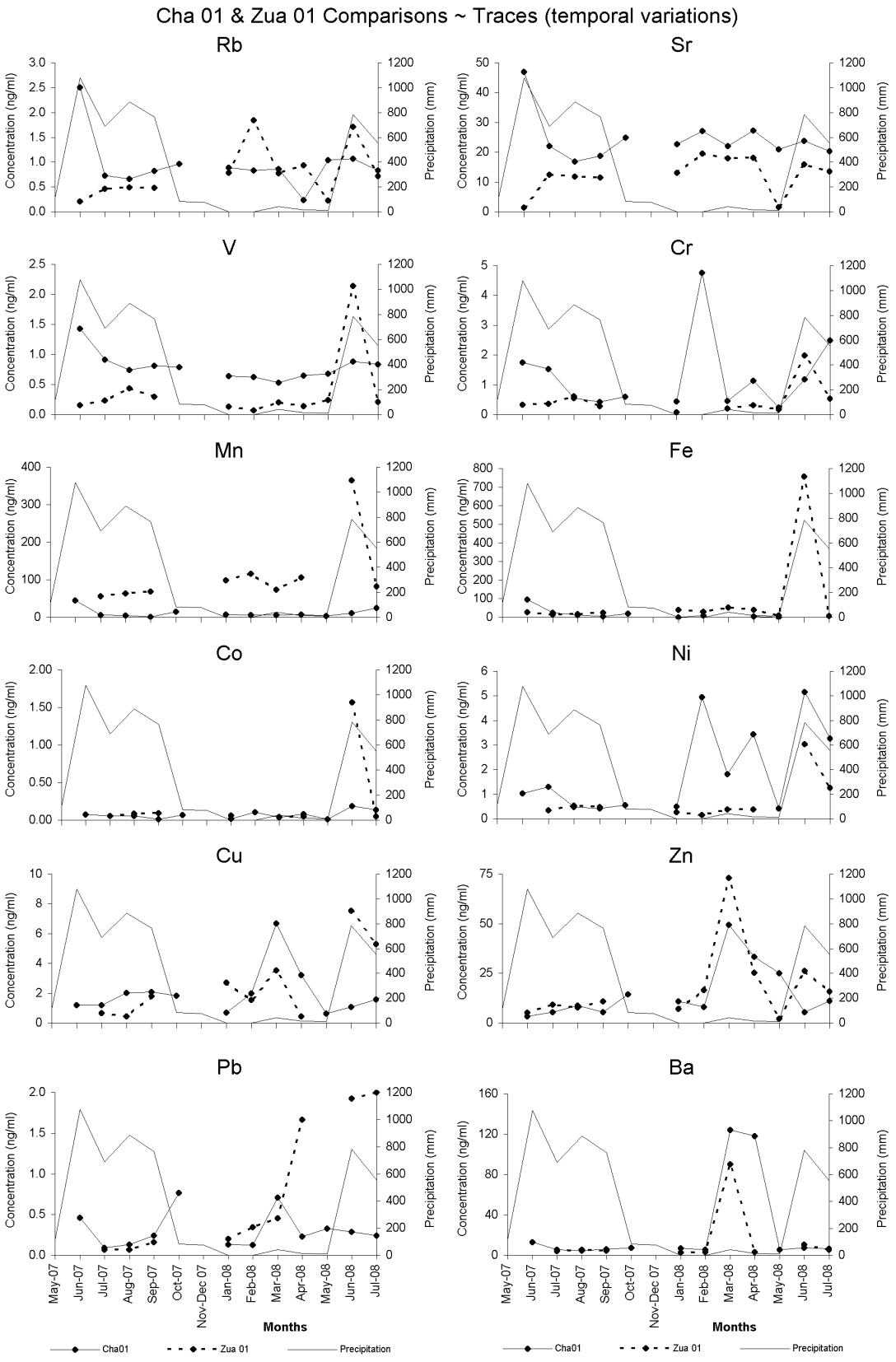

Figure 7.22 Trace element plots showing the values for Cha 01 and Zua 01.

7.3.1. Lithological influence

Figure 7.21 reveals that the plots for pH and HCO_3^- are very similar for the localities Cha 01 and Zua 01; however, pH values are slightly lower for Zua 01 during the wet 2007 season and higher during the dry season and the start of the 2008 wet season. The similarity in HCO_3^- indicates that a similar amount of chemical weathering has occurred in these two basins during the total observation period. The major cations, Na, K, Ca, Mg and Si display broadly similar trends with the occasional positive or negative deviation; the same can be said for the major anions. The most dramatic and potentially important difference occurs during the 2007 monsoon period with respect to Al; in this instance the Cha 01 values are significantly elevated throughout the whole wet season compared to those for Zua 01. These elevated Al values are possibly derived from weathering of feldspars within the Deccan basalt in the upper reaches of the Chapora River basin.

An additional method of comparing the fluvial chemistry of the two basins is by considering their Na normalised molar Ca/Mg ratios and comparing them to known silicate and carbonate end member domains; this method is considered in Figure 7.23.

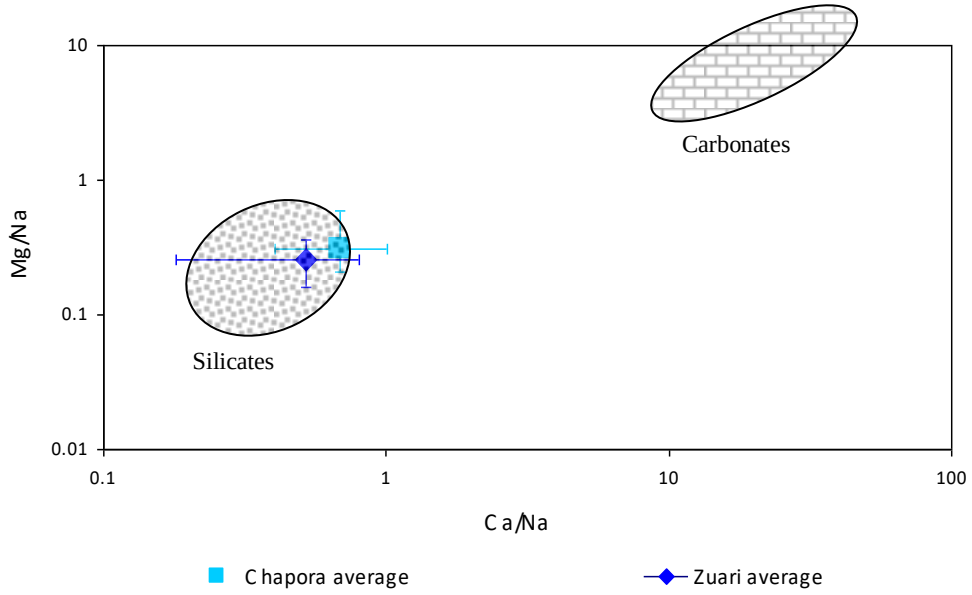

Figure 7.23 Na normalised molar Ca/Mg ratio plot showing the average values for all localities for the Chapora and Zuari Rivers, the error bars represent the extreme values for each ratio. The silicate and carbonate end member domains are taken from Gaillardet et al. (1999).

Figure 7.23 displays the combined average Na normalised molar Ca values for each river plotted against their respective combined average Na normalised molar Mg values. In broad terms this shows that the averaged composition of both river chemistries plot in a similar sector of the graph, and in close proximity to the silicate end member domain, although the error bars clearly show a range of values, however, these do still tend more towards the silicate end member domain. Additional plots showing the average molar Ca/Na v Mg/Na ratio values for each locality along with any rock or sediment samples collected at each locality are shown in Figure 7.24 and 7.25. It is evident from all the plots that the dominant influence is from the silicate end member. However, there does appear to be a small influence from the carbonate end member for Cha 05 and Zua 01; these could be due to influence from small outcrops of Mn-rich limestone within the Bicholim Fm.

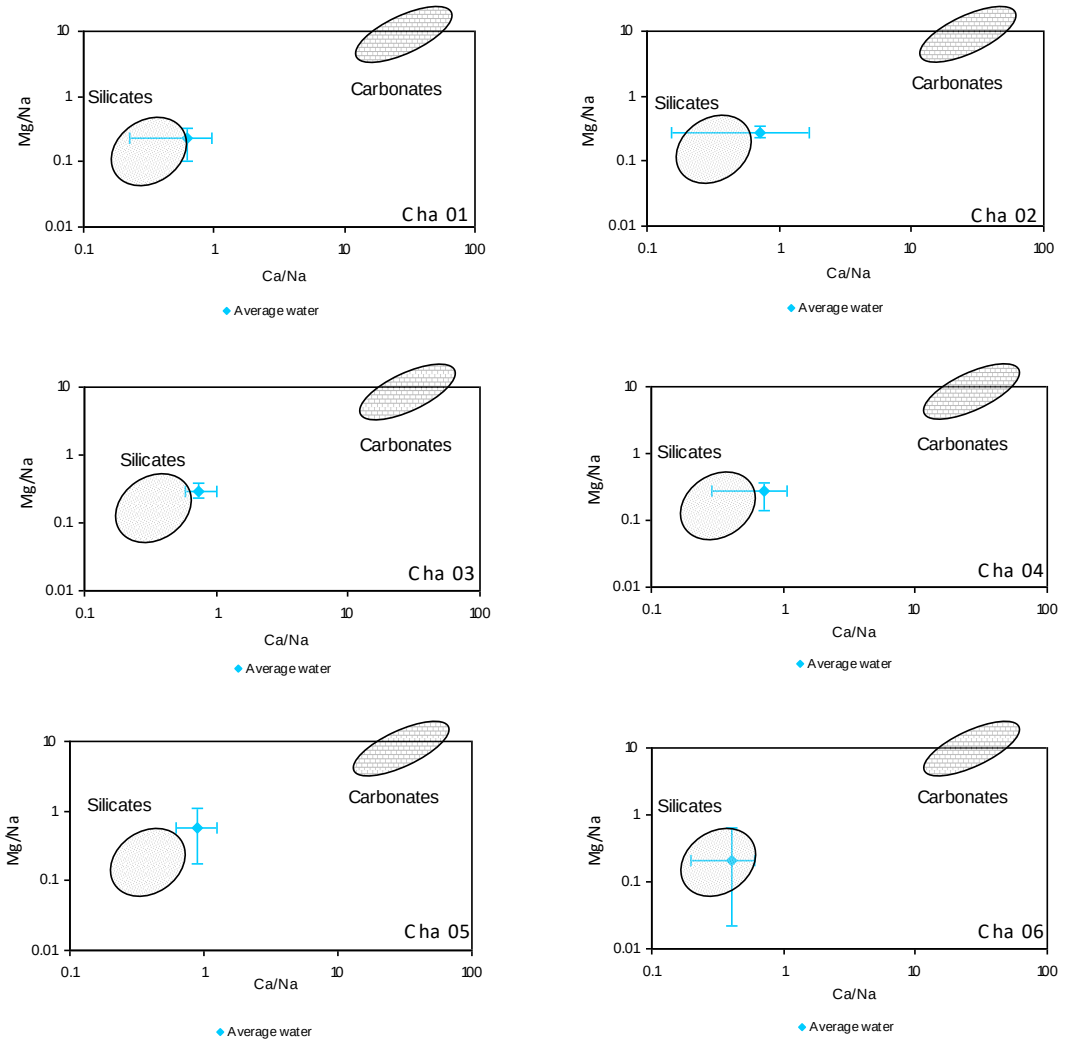

Figure 7.24 Na normalised molar Ca/Mg ratio plots for Zuari River localities (Zua 01 – 06), plots show the average water values with error bars representing the extreme values for each ratio.

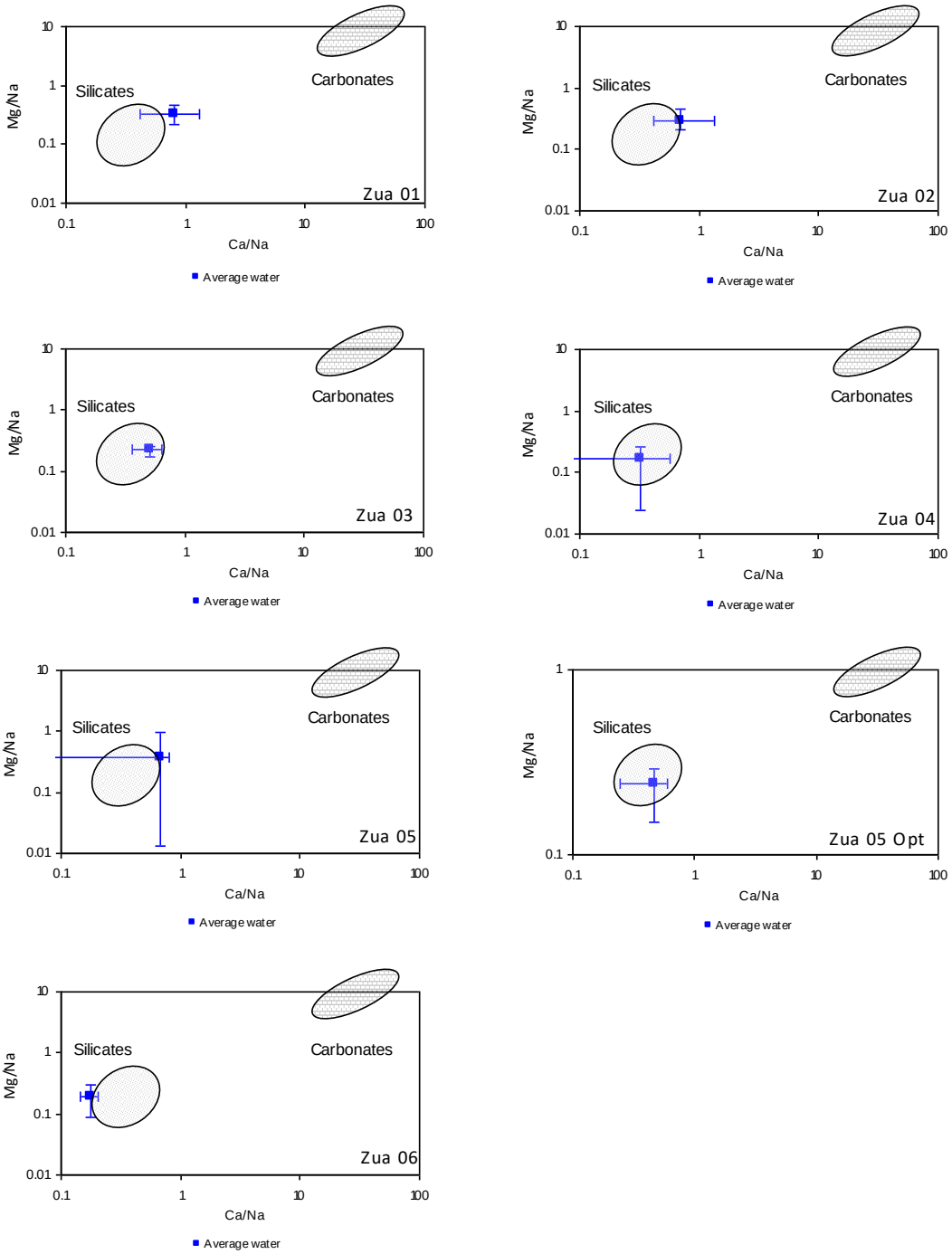

Figure 7.25 Na normalised molar Ca/Mg ratio plots for Chapora River localities (Cha 01 – 06), plots show the average water values with error bars representing the extreme values for each ratio.

7.3.2. Mining influence

As previously discussed (Section 4.1), the Zuari River was chosen for this study due to the presence of Fe and Mn mining throughout much of its basin; it is also used as a route for transporting the ore from the various mines to the bank side processing plants and out to the Arabian Sea where the ore is transferred to ocean-going bulk-carrier ships.

Accordingly, examination of the data may reveal differences in river chemistry resulting from these anthropogenic activities. Figures 7.21 and 7.22 indicate a number of obvious differences between the Zua 01 values and the Cha 01 values. In particular elevated peaks for Zua 01 are very apparent for the trace elements V, Mn, Fe, Co, Cu and Pb coinciding with the onset of the 2008 monsoon period. These elements could be derived from mining activities but could equally be due to weathering as they are showing elevated values at this time due to rinse-out effects close to the onset of the 2008 monsoon. Additionally, if hey were due to a mining source they would be present throughout the whole year rather than just as a rinse-out signature. However, the same observation is not apparent for the onset of the 2007 monsoon period; in fact many elements show the opposite with elevated concentrations for the Cha 01 values, such as Rb, Sr, V, Cr & Fe.

Likewise, the lack of sulphides present in the mine waste and the general lack of reactivity of this mine waste, which has already been heavily weathered to form laterite or comprises quartz rich inter bedded layers within the BIF formations also leads to the observation that it is difficult to identify clear differences between the rivers when considering the dissolved phase. It may be that differences may be more discernible in the suspended phase, since both Fe and Mn are insoluble in oxygenating environments; however, suspended sediments were not collected during this study.

In summary, it appears that the effects of mining within the Zuari River basin compared to the Chapora River basin are not clear within the existing dataset.

7.4. CO_2 drawdown

As discussed in chapters 1 and 2, silicate weathering is of fundamental importance to the global climate; for each equivalent of cation dissolution, a mole of CO_2 is drawn from the atmosphere and locked away in sediments. Accordingly, it is important to consider the various controls on silicate weathering rate, such as lithology, temperature, run-off, vegetation etc. Many researchers have studied silicate weathering rates on various lithologies and in different climatic localities; but these generally fall into two broad categories (a) small to medium sized watersheds (<100 km^2) where lithology is fairly uniform, and (b) large river basins where lithology is highly heterogeneous. In the Indian subcontinent, these studies have typically involved small rivers draining the relatively homogeneous Deccan Traps basalt or larger rivers draining the Himalayas. By contrast, until recently very little work had been done on smaller drainage basins such as those draining the Western Ghats escarpment on the west coast of India, these are important to the chemistry of the onshore Arabian Sea because they are subject to a highly seasonal climate, comprising high temperatures and high levels of precipitation high run-off during the monsoon seasons, and high temperatures but almost zero run-off during the dry season.

There are several approaches by which CO_2 drawdown may be calculated for river catchments. Of these, there are two main methods worthy of note. The first considers the chemistry of the river waters themselves, since these represent the element flux that is being transported out of the catchment. This rate of transport is subject to fundamental controls including discharge and discharge variability (i.e., climate): The second considers instead the weathering rate of the minerals present in the basement lithologies drained by the river. In this case, the nature and relative areas of lithologies comprising the catchment area need to be determined. Both methods are applied to the Chapora and Zuari River basins, and the results of the methodologies compared with each other. In addition, the results are also compared with those of a recent study of the Nethravati River basin (Kerala State) (Gurumurth et al., 2012) which lies in a broadly comparable geomorphological setting and climatic zone some 300 km to the south of the current study area. Additionally, a third method is considered based on estimating the volume of material removed due to the escarpment retreat over the past 60 Ma, again this is reliant on assuming a mono-lithological catchment and establishing a weathering rate for that chosen material, in this case metagreywacke has been selected due to its widespread presence within this basin.

7.4.1. CO_2 drawdown estimates by analysis of river chemistry

(Gurumurthy et al., 2012) provide an excellent account of weathering rates for a drainage basin (Nethravati River) on the west coast of India. The locality of the study mentioned above is c. 300 km south of the location chosen for the current study and since it is in effectively the same geomorphological domain (steep Ghats escarpment and low-lying coastal plain), it thus offers an excellent opportunity to compare this work with another in a similar climatic regime with similar topography and lithology.

Gurumurthy et al. (2012) calculate the silicate weathering rate (SWR) and the carbon dioxide consumption rate (CCR) for the Nethravati River and its tributaries based on data collected at five locations over a 12 month period from October 2006 to September 2007. The authors report a SWR of 42 t km^{-2} yr^{-1} and a CCR of 2.85 x 10^5 $mol.km^{-2}.yr^{-1}$ which they compare against a number of other Indian rivers such as the Gad, Kajili, Shashtri, Vashishtri (draining the Ghats westward), and Krishna and Bhima Rivers (draining the inland plateau eastward) as documented by Das et al. (2005).

Silicate weathering rate (SWR) and carbon dioxide consumption rate (CCR) are calculated as follows:

$$SWR = Q / A \times (\sum(Na^+ + K^+ + Mg^{2+} + Ca^{2+})_{sil} + SiO_2)$$

$$CCR = Q / A \times \sum(Na^+ + K^+ + Mg^{2+} + Ca^{2+})$$

where Q = the discharge in m^3 s^{-1} and A = the surface area of the drainage basin or watershed in km^2.

The CCR calculation method documented above and employed by Gurumurthy et al. (2012) has been used to calculate the CCR values for the Chapora and Zuari River basins. However, in order to first ensure a complete understanding of the method, the primary data for the Nethravati River was entered into the calculation to attempt to recreate the same answer as the one documented in their original paper.

In order to estimate the CCR for the Chapora and Zuari basins, it is first necessary to quantify the contribution of major ions from evaporites, anthropogenic sources and atmospheric sources. Since no evaporites are present within the studied drainage basins their contribution is nil. An anthropogenic Cl source would increase the Cl concentration of the rivers as well as decreasing the Na/Cl ratio, this is not identified

within either of the drainage basins, since the discharge weighted mean Na/Cl ratios of 0.76 and 0.68 for the Chapora and Zuari river waters, respectively, are similar to those of the Goa coastal rainwater ratio of 0.85 (Table 7.3). Finally, to quantify the chemical fluxes derived purely from rock weathering it is necessary to correct for atmospheric inputs; this is achieved by using Cl as a proxy, and upon the assumption that Cl in the Chapora and Zuari Rivers originates solely from rainfall. The rainfall corrected concentration of an element (X_r) is calculated following the relation (Stallard and Edmond, 1981, Negrel et al., 1993):

$$X_r = (X_{river} - Cl_{river}) \times (X/Cl)_{rainfall}$$

Where X_{river} and Cl_{river} are the molar concentrations in the river water and (X/Cl) rainfall is the molar ratio in the local rainfall.

Table 7. 3 Chemical composition of rainwater for a selection of locations in India. n = number of samples; all values are in µmol/L (Das et al., 2005).

Location	*n*	*Na*	*K*	*Mg*	*Ca*	*Cl*	*NO_3*	*SO_4*	*NH_4*	*Na/Cl*
Inland stations										
Pune	*12*	*41*	*2*	*9*	*27*	*50*	*8*	*11*	*11*	*0.82*
Sinhagad	*17*	*46*	*2*	*9*	*18*	*51*	*6*	*12*	*13*	*0.90*
Amboli Ghat	*1*	*17*	*8*	*-*	*9*	*11*	*0*	*3*	*47*	*1.55*
Sangameshwar	*1*	*26*	*4*	*-*	*10*	*28*	*6*	*8*	*0*	*0.93*
Mean		*42*	*2*	*9*	*21*	*48*	*7*	*11*	*13*	*0.88*
Coastal station										
Goa	*6*	*115*	*3*	*15*	*23*	*135*	*6*	*16*	*7*	*0.85*

The Goa coastal station concentrations provided above in Table 7.3 was used for the purposes of correcting for atmospheric inputs for this study.

Since Ca and Mg can also be derived from the weathering of carbonates, it is important to establish the proportion of Ca and Mg from each source. This is because the dissolution of Ca-Mg in carbonates is much faster than the Ca-Mg-Na in silicates and should therefore result in the enrichment of Ca and Mg relative to Na in the river water (higher Ca*/Na* and Mg*/Na* ratio) when compared to the bedrock. The relative contributions are usually determined by comparing Ca*/Na* and Mg*/Na* molar ratios of the river water with those of the local bedrock, with the relative excess of Ca and Mg being attributed to carbonate dissolution (Krishnaswami et al., 1999). Accordingly, the proportion of Ca and Mg attributed to Ca and Mg silicate weathering can be estimated as follows:

$Ca_{sil} = Na^* \times (Ca/Na)_{rock}$

$Mg_{sil} = Na^* \times (Mg/Na)_{rock}$

Where Na* is the weighted mean sodium concentration of the river water corrected for atmospheric inputs. Subscripts ‘sil’ and ‘rock’ refer to silicate origin and bedrock composition, respectively.

For the bedrock lithologies of the Chapora and Zuari basins the Ca/Na and Mg/Na molar ratios have been calculated by firstly converting the sample oxide wt. % (Section 5.1.15, Table 5.4) into an elemental wt. % by dividing the oxide wt. % by the (molecular mass of the oxide divided by the atomic mass of the element). Once converted this value is divided by the atomic mass of the element to obtain the number of moles.

For example; calculating the Ca/Na ratio for sample Cha 01 S1

Ca wt.% = 2.7 / (56.077/40.078) = 1.93	Na wt.% = 3.78 / (61.979/45.978) = 2.8
To calculate the number of mols	To calculate the number of mols
1.93 / 40.078 = 0.048 mols	2.8 / 22.989 = 0.122

Ca/Na ratio = 0.048/0.122 = 0.39

Table 7. 4 Major element abundance in main rock types of the Chapora and Zuari River basins. The table includes bedrock samples collected from the river basins and a selection of additional samples from *in situ* sampling (data extracted from Table 5.4).

Sample	*Description*	*SiO_2*	*CaO*	*MgO*	*K_2O*	*Na_2O*
				Wt%		
Cha 01 S1	*Meta greywacke*	*59.90*	*2.7*	*4.47*	*2.72*	*3.78*
Cha 01 S2	*Garnet Mica schist*	*62.79*	*3.07*	*3.21*	*2.55*	*3.40*
Cha 01 S3	*Meta greywacke*	*62.17*	*7.23*	*1.56*	*0.25*	*4.37*
Cha 01 S4	*Meta pellite*	*49.56*	*11.04*	*7.53*	*0.27*	*2.29*
Cha 02 S1	*Gneissic granite*	*66.12*	*9.01*	*1.32*	*0.18*	*1.26*
Cha 03 S1	*Meta greywacke*	*60.49*	*6.41*	*3.45*	*0.14*	*2.57*
Cha 03 S2	*Meta basite*	*48.68*	*10.52*	*7.93*	*0.49*	*2.55*
Cha 03 S3	*Quartzite*	*97.22*	*0.02*	*0.04*	*0.06*	*0.00*
Cha 03 S4	*Quartz chlorite schist*	*50.49*	*10.91*	*7.21*	*0.16*	*2.53*
Cha 05 S1	*Channel sediment*	*76.14*	*1.18*	*0.95*	*0.76*	*0.68*
Cha 06 S1	*Channel sediment*	*75.52*	*2.28*	*2.01*	*0.81*	*1.07*
Zua 01 S1	*Laterite*	*14.27*	*0.03*	*0.13*	*0.41*	*0.03*
Zua 01 S2	*Phyllite*	*64.00*	*0.17*	*2.66*	*2.87*	*2.90*
Zua 01 S3	*River bed sand*	*67.28*	*2.31*	*2.34*	*0.75*	*1.21*
Zua 03 S1	*Red silt*	*64.52*	*0.22*	*0.64*	*0.77*	*0.17*
Zua 05 opt S1	*Meta pellite*	*74.76*	*0.53*	*0.46*	*3.07*	*4.54*
Zua 05 opt S2	*Selection of pebbles*	*50.62*	*0.24*	*0.43*	*0.56*	*0.14*
Mean of 31 samples	*[1]Deccan Basalt (Mahabaleshwar)*	*49.42*	*10.2*	*5.77*	*0.47*	*2.49*
IND108	*[2]Chandranath Granite*	*71.61*	*1.79*	*0.64*	*4.43*	*3.88*
IND114	*[2]Chandranath Granite*	*74.07*	*1.42*	*0.29*	*4.54*	*3.75*
IND120	*[2]Chandranath Granite*	*73.49*	*1.65*	*0.47*	*3.72*	*4.19*
SQ2	*[2]Merces Quarry*	*67.7*	*0.95*	*3.07*	*3.68*	*3.31*

Note: [1]Data from Widdowson et al. (2005), [2]Data from Whimpenny et al. (2007).

Since the lithology of the Chapora and Zuari River basins is heterogeneous, it is necessary to account for the contribution of Ca and Mg from any carbonates present in the various rock types within each basin. The method chosen here is to simplify each major rock type or formation into a single lithology. To illustrate, the Vageri and Sandvordem Formations have been designated as metagreywacke, the Bicholim and Barcem Formations have been designated as phyllite, and the Deccan and Chandranath granites have been designated as basalt and granite, respectively. Then, in order to obtain the area weighted mean Ca/Na and Mg/Na ratios for each drainage basin the sum of the Ca/Na ratios and Mg/Na ratios for each major rock type have

been multiplied by their respective drainage basin areas and the results divided by the total basin area.

Additionally, to discount any estuarine influence (marine water influx by tidal action) only element concentrations from the furthest downstream locality which is completely unaffected by estuarine influence is used. For example, for the Chapora basin concentrations from locality Cha 04 are used along with the drainage basin area supplying this locality. This means that only two major lithologies are supplying elements to these sites, a small proportion of Deccan basalt (39 km^2) and the meta-greywacke of the Vageri Fm (308 km^2). Using this as an example the mean Ca/Na and Mg/Na ratios are calculated below:

Chapora River

Ca/Na_{mean} = ($Ca/Na_{Deccan\ mean}$ x $Area_{Deccan}$) + (Ca/Na_{Vageri} x $Area_{Vageri}$) / ∑ drainage basin areas =

Ca/Na_{mean} = 2.25 x 39 km^2 + 0.39 x 308 km^2 / 347 km^2 = 0.60

Mg/Na_{mean} = ($Mg/Na_{Deccan\ mean}$ x $Area_{Deccan}$) + (Mg/Na_{Vageri} x $Area_{Vageri}$) / ∑ drainage basin areas =

Mg/Na_{mean} = 1.18 x 39 km^2 + 0.91 x 308 km^2 / 347 km^2 = 0.94

Calculating for the Zuari basin is more complex due to it having a contribution from four different lithologies; again using those areas of the basin unaffected by estuarine influence, element concentrations from locality Zua 05opt have been used for the calculation along with the drainage basin area supplying this locality. Following the same principle the mean ratios are calculated as follows:

Zuari River

Ca/Na_{mean} = ($Ca/Na_{Chandranath}$ x $Area_{Chandranath}$) + ($Ca/Na_{Bicholim}$ x $Area_{Bicholim}$) + ($Ca/Na_{Sandvordem}$ x $Area_{Sandvordem}$) + (Ca/Na_{Barcem} x $Area_{Barcem}$) / ∑ drainage basin areas =

Ca/Na_{mean} = (0.23 x 102 km^2) + (0.03 x 304 km^2) + (0.39 x 120 km^2) + (0.03 x 200 km^2) / 726 km^2 = 0.12

Mg/Na_{mean} = ($Mg/Na_{Chandranath}$ x $Area_{Chandranath}$) + ($Mg/Na_{Bicholim}$ x $Area_{Bicholim}$) + ($Mg/Na_{Sandvordem}$ x $Area_{Sandvordem}$) + (Mg/Na_{Barcem} x $Area_{Barcem}$) / ∑ drainage basin areas =

Mg/Na_{mean} = (0.09 x 102 km^2) + (0.71 x 304 km^2) + (0.91 x 120 km^2) + (0.71 x 200 km^2) / 726 km^2 = 0.66

The discharge has also been recalculated according to the basin area supplying elements to the furthest downstream locality unaffected by estuarine influence, this equates to 347 km^2 for the Chapora Basin and 726 km^2 for the Zuari Basin. Using these values the CCR has been calculated as 6.62 x 10^5 mols km^{-2} yr^{-1} for the Chapora, and 9.05 x 10^5 mols km^{-2} yr^{-1} for the Zuari Basin. Compared with the values for the Nethravati River these values are 2.3 times higher for the Chapora and 3.1 times higher for the Zuari. This may be explained by the difference in lithology between the basins, since the Chapora has a small (39 km^2), but significant contribution from Deccan basalt in its upper reaches, whilst the Zuari has a significant (102 km^2) contribution from the Chandranath granite. Additionally, the other main lithologies present in the Chapora and Zuari Basins are metagreywacke and phyllite as compared to the migmatites and granodiorite-tonalite gneisses and charnockites of the Nethravati Basin. Other obvious differences are the basin areas with the Nethravati basin being 3657 km^2, over c.10 x larger than that of the Chapora and c.5 x larger than that of the Zuari. However, this latter difference in basin area is, in part mitigated by a similar difference in discharge; the discharge weighted mean (388 m^3 s^{-1}) for the Nethravati being c. 10 x higher than the discharge weighted mean (29.6 m^3 s^{-1}) of the Chapora and c.5 x higher than the discharge weighted mean (61.9 m^3 s^{-1}) of the Zuari. Therefore Q/A is remarkably similar for all three basins as follows:

Table 7. 5 Flow (Q) calculated as the discharge weighted mean, basin area (A) and Q/A for the Chapora and Zuari Rivers and the Nethravati River for comparison.

River	Nethravati	Chapora	Zuari
Q (m^3 s^{-1})	388	29.6	61.9
A (km^2)	3657	347	726
Q/A	0.106	0.085	0.085

Clearly, the similarity between Q/A values for the Chapora and Zuari Rivers is due to the discharge for these rivers being calculated based on precipitation multiplied by drainage basin area, but the similarity of these two values and that of the Nethravati Q/A value suggest that any difference in CCR or SWR is most likely derived from the geochemistry of the rivers, and thus their underlying lithologies; not from differences in basin area or river discharge.

Table 7. 6 Weathering characteristics for the Chapora and Zuari River basins, as calculated using the river water chemistry method, for a comparison the table also includes similar data for the Nethravati River as documented by Gurumurthy et al. (2012).

River basin	Area used in calculation (km^2)	Moles CO_2 per year	Moles CO_2 per year per km^2
Chapora	347	2.29×10^8	6.62×10^5
Zuari	726	6.57×10^8	9.05×10^5
Nethravati	3657	1.04×10^9	2.85×10^5

Table 7.6 reports values for CO_2 consumptions rates per square kilometre that are c. 2.3 times higher and c. 3.1 times higher for the Chapora and Zuari Rivers, respectively when compared to the Nethravati River. However, the much larger size of the Nethravati River basin more than makes up for this when comparing moles of CO_2 consumed per year with its contribution an order of magnitude higher.

Its is important to remember that the area used in this calculation has been reduced from that of the complete catchments in order to remove the influence of estuarine water, by only considering the discharge and area above and including Cha 04 on the Chapora River and Zua 05 opt on the Zuari River. Therefore, it is likely that the calculated values for the Chapora and Zuari River are under estimates as the lower portions of the drainage basins would also be subjected to the effects of weathering.

7.4.2. CO_2 drawdown estimates by analysis of catchment lithology

The predicted CO_2 drawdown resulting from the weathering of the various lithologies within the Chapora and Zuari drainage basins is next considered. To achieve this it is first necessary to estimate the area of each lithology within each basin (Table 7.7) and to identify the mineralogical composition of each lithology (Table 5.1). It is also necessary to have an understanding of the chemical weathering reactions, the rate constants for each mineral, and the determined number of moles of CO_2 sequestered for each mole of mineral weathered. The chemical weathering equations are documented previously along with the number of moles of CO_2 sequestered for each mole of mineral weathered (Table 2.3); the rate constants are discussed later in this section.

Area of each lithology within each drainage basin

For the Chapora and Zuari drainage basins, the area of each lithology within each basin has been estimated by overlaying a 1 km x 1 km grid over a correctly scaled geological map of Goa (Table 7.6). To simplify the natural complexity each formation is again assumed to be comprised of a single rock type: For example, the Vageri Fm and Sandvordem Fm are considered to be metagreywacke, the Bicholim Fm and Barcem Fm are represented by phyllite, whilst the Deccan Traps and Chandranath granite are considered to be basalt and granite, respectively.

Table 7. 7 Estimated areas for each major lithology within the Chapora and Zuari drainage basins.

Chapora drainage basin		**Zuari drainage basin**	
Deccan Basalt	39 km^2	Chandranath Granite	102 km^2
Vageri Fm	309 km^2	Sandvordem Fm	241 km^2
Bicholim Fm	78 km^2	Barcem Fm	415 km^2
Sandvordem Fm	160 km^2	Bicholim Fm	304 km^2
Total basin area	586 km^2	Total basin area	1062 km^2
Original estimate	588 km^2	Original estimate	1059 km^2

The original estimate mentioned in Table 7.7 refers to an initial aerial assessment conducted in a similar manner to that discussed above but considering the whole drainage basins for each river.

Rate constants

Rate constants are expressed as the number of moles of a mineral weathered per unit area per second (mols m^{-2} s^{-1}). These rate constants can vary depending on temperature and pH. To make the following calculations simpler, the following rate constants have been used which are based on 1 mm crystals at pH 5, as reported by Brantley (2003). In reality there will obviously be a wide range of crystal sizes present in each lithology as well as varying pH.

Table 7. 8 Rate constants for a range common minerals (Brantley et al., 2003), shown as most stable to least stable from top to bottom.

Mineral	Rate constant (mols m^{-2} s^{-1})
Quartz	4.1×10^{-14}
K-Feldspar	5.0×10^{-13}
Muscovite	3.2×10^{-13}
Phlogopite	3.2×10^{-13}
Albite	6.3×10^{-13}
Diopside	3.6×10^{-12}
Anorthite	4.0×10^{-12}
Enstatite	3.2×10^{-11}
Tremolite	1.1×10^{-11}
Forsterite	3.6×10^{-10}
Fayalite	3.6×10^{-10}
Calcite	5.0×10^{-5}

Rate constants for biotite and chlorite were not listed in Brantley et al. (2003) and therefore values have been derived from other sources. The value for biotite of 3.2×10^{-10} mol m^{-2} s^{-1} is employed here, but it should be noted that this was based on a study with pH varying between 1 and 4 (Kalinowski and Schweda, 1996). For chlorite a value of 5.0×10^{-12} mol m^{-2} s^{-1} at pH 5 has been adopted, based on Figure 3 in Lowson et al. (2005); this work provides a graph depicting how the rate constant for chlorite varies with pH. The rate constant for calcite is also included for comparison (Brantley, 2008), again this value is derived from a graph depicting how rate constant varies with pH and the value chosen is for pH 5. This clearly indicates how easily carbonates weather compared to silicates and therefore indicates their importance in contributing ions to the rivers where even small amounts of carbonate are present.

CO_2 drawdown from the Chapora and Zuari River basins

Based on the above discussions, the predicted CO_2 drawdown from these two basins is documented in Table 7.9 as follows, also included again for comparison are the equivalent data for the Nethravati River:

Table 7. 9 Area and weathering characteristics for the Chapora and Zuari River basins, as calculated using the catchment analysis method, for a comparison the table also includes similar data for the Nethravati River as documented by Gurumurthy et al. (2012).

River basin	Area used in calculation (km^2)	Moles CO_2 per year	Moles CO_2 per year per km^2
Chapora	586	9.99×10^6	1.70×10^4
Zuari	1,062	6.90×10^6	6.49×10^3
Nethravati	3,657	1.04×10^9	2.85×10^5

The following shows an example of the calculation for metagreywacke, an important lithology in both river basins:

According to Table 2.3, metagreywacke comprises 75% quartz, 15% Biotite, 5% Muscovite and 5% K-Feldspar assuming an area of 1 m^2 the percentage of each mineral within this 1 m^2 area is calculated. This is multiplied by the rate constant, for each mineral and then multiplied by the number of moles of CO_2 sequestered per mole of mineral weathered. This is multiplied by the number of seconds in a year to give moles m^{-2} yr^{-1} for each mineral component of each m^2 of rock type.

The following shows the calculations for each mineral identified within a metagreywacke sample.

Quartz - 1 m^2 x 0.75 x 4.1 x 10^{-14} mol m^{-2} s^{-1} x 0 x 31,536,000 s yr^{-1} = 0 moles m^{-2} yr^{-1}.

Biotite - 1 m^2 x 0.15 x 3.2 x 10^{-10} mol m^{-2} s^{-1} x 14 x 31,536,000 s yr^{-1} = 2.12 x 10^{-2} moles m^{-2} yr^{-1}.

Muscovite - 1 m^2 x 0.05 x 3.2 x 10^{-13} mol m^{-2} s^{-1} x 2 x 31,536,000 s yr^{-1} = 1.01 x 10^{-6} moles m^{-2} yr^{-1}.

K-Feldspar - 1 m^2 x 0.05 x 5.0 x 10^{-13} mol m^{-2} s^{-1} x 2 x 31,536,000 s yr^{-1} = 1.58 x 10^{-6} moles m^{-2} yr^{-1}.

These are added together to provide the number of moles of CO_2 sequestered per m^2 of each lithology. The calculation below is for metagreywacke.

2.12 x 10^{-2} + 1.01 x 10^{-6} + 1.58 x 10^{-6} = 2.12 x 10^{-2} moles m^{-2} yr^{-1}

This, along with the calculated CO_2 drawdown values for all other lithologies within each basin are then calculated as a function of the area for each single lithology. For example the Chapora drainage basin comprises 39 km^2 of Deccan Basalt, 309 km^2 of the Vageri Fm (metagreywacke), 78 km^2 of the Bicholim Fm (phyllite) and 160 km^2 of the Sandvordem Fm (metagreywacke).

Chapora drainage basin:

Deccan Basalt - 39 km^2 x 1,000,000 m^2 km^{-2} = 39,000,000 m^2 x 3.48 x 10^{-4} moles m^{-2} yr^{-1} = 1.36 x 10^4 moles CO_2 yr^{-1}.
Vageri Fm (metagreywacke) - 309 km^2 x 1,000,000 m^2 km^{-2} = 309,000,000 m^2 x 2.12 x 10^{-2} moles m^{-2} yr^{-1} = 6.56 x 10^6 moles CO_2 yr^{-1}.
Bicholim Fm (phyllite) - 78 km^2 x 1,000,000 m^2 km^{-2} = 78,000,000 m^2 x 4.80 x 10^{-4} moles m^{-2} yr^{-1} = 3.75 x 10^4 moles CO_2 yr^{-1}.
Sandvordem Fm (metagreywacke) - 160 km^2 x 1,000,000 m^2 km^{-2} = 160,000,000 m^2 x 2.12 x 10^{-2} moles m^{-2} yr^{-1} = 3.39 x 10^6 moles CO_2 yr^{-1}.

Total = 9.99 x 10^6 moles CO_2 yr^{-1}

Zuari drainage basin:

Chandranath granite - 102 km^2 x 1,000,000 m^2 km^{-2} = 102,000,000 m^2 x 1.41 x 10^{-2} moles m^{-2} yr^{-1} = 1.44 x 10^6 moles CO_2 yr^{-1}.
Barcem Fm (phyllite) - 415 km^2 x 1,000,000 m^2 km^{-2} = 415,000,000 m^2 x 4.80 x 10^{-4} moles m^{-2} yr^{-1} = 1.99 x 10^5 moles CO_2 yr^{-1}.
Bicholim Fm (phyllite) - 304 km^2 x 1,000,000 m^2 km^{-2} = 304,000,000 m^2 x 4.80 x 10^{-4} moles m^{-2} yr^{-1} = 1.46 x 10^5 moles CO_2 yr^{-1}.
Sandvordem Fm (metagreywacke) - 241 km^2 x 1,000,000 m^2 km^{-2} = 241,000,000 m^2 x 2.12 x 10^{-2} moles m^{-2} yr^{-1} = 5.11 x 10^6 moles CO_2 yr^{-1}.

Total = 6.90 x 10^6 moles CO_2 yr^{-1}

Nethravati drainage basin

The values for the Nethravati River are based on the 2.85 x 10^5 moles of CO_2 km^{-2} yr^{-1} from their paper and have been multiplied by the drainage basin area (3657 km^2) to obtain a value of 1.04 x 10^9 moles of CO_2 yr^{-1} for the drainage basin.

From Table 7.9 it can be seen that the moles of CO_2 per year per km^2 for the Chapora River basin is c. 20 times lower, whilst the moles of CO_2 per year per km^2 for the Zuari River basin is c. 40 times lower when compared to that for the Nethravati River basin. This may be as a result of the widespread presence of laterite in the Chapora and Zuari basins, and the fact that most of the rock across the Konkan plain has already reacted and been altered. Another explanation of this difference may be due the fact that this method of calculation does not account for vegetation whilst the method employed by Gurumurthy et al. (2012) is based on river chemistry and as such would incorporate any vegetation effects. Since vegetation is known to increase weathering rates due to both physical (root propagation) and chemical (organic acid) influence. However, the more likely reason for this disparity is the assumptions used and the use of laboratory based rate constants in this calculation method. This is discussed in later in the summary of this section.

7.4.3. CO_2 drawdown estimates by analysis of Scarp retreat

The origin and development of the Western Ghats escarpment has been discussed and outlined in Section 3.5.1. This section considers how this continental feature has controlled erosion in western peninsular India over geological, decadal and annual timescales.

In previous sections CO_2 drawdown in the two river catchments has been determined using river water chemistries and available catchment lithologies. Another, entirely independent method of assessing the amount of CO_2 consumption through silicate weathering is to calculate the volume of rock weathered during this escarpment retreat, and thus made available to the respective catchments and the erosion, transport and weathering processes acting therein. In effect, this approach should yield a maximum value of drawdown since it assumes that all material supplied annually by scarp retreat is fully reacted and thus available for CO_2 drawdown.

To calculate a first order estimate for scarp retreat per annum necessary for the CO_2 drawdown calculations on the time scales that are being considered in this current

work, it is first necessary to establish the distance of retreat of such 'great escarpments' per unit time. This can only be realistically achieved by first considering and estimating the retreat distance over geological durations. Several authors have attempted this for great escarpment features elsewhere. Particularly relevant to the current study are the estimates offered by Widdowson and Gunnell (1999, 2009; Table 7.10).

Table 7. 10 Retreat rates for a selection of Great Escarpments as determined by previous author's studies.

Escarpment	Estimated rate of scarp retreat	Reference
Colorado Plateaux	0.6 - 6.7 km Ma^{-1}	Schmidt (1989)
Great escarpment, Australia	2 km Ma^{-1}	Johnson (2009)
Cuesta escarpment, Morocco	1.3 km Ma^{-1}	Schmidt (1988)
Western Ghats, Goa, India	1.8 – 2.8 km Ma^{-1}	Widdowson and Gunnell (1999)

Using the simple method of Widdowson and Gunnell (1999) the scarp retreat of the Western Ghats inland of Goa (i.e., headwaters of the Chapora and Zuari Rivers) may be determined. This then yields the approximate volume of material that has been removed across the offshore shelf and Konkan lowlands since the separation the Seychelles from India c. 60 Ma.

The edge of the continental shelf is considered to mark the locus of continental separation; offshore this is taken to be where water depth increases dramatically, descending to the abyssal deep. Assuming the nascent escarpment originated as a major fault escarpment associated with the rifting event, then the total distance of retreat in c. 60 Ma is that distance between the edge of the shelf, and the current position of the Western Ghats inland of the current coastline. This distance may be measured at 70 – 100 km; accordingly, the rate of scarp retreat at this location may then be estimated as follows:

70 km / 60 Ma = 1.2 km Ma^{-1}

100 km / 60 Ma = 1.7 km Ma^{-1}

This range of values is entirely consistent with the values calculated by other authors for other similar escarpments (Table 7.10).

Now to consider the volume of material removed during this time, the length has been established above at 70 – 100 km, the height of the escarpment is estimated as 1 km and the width of the escarpment considering only the Chapora River drainage basin is estimated at between 10 – 15 km, both of these values have been estimated using Google Earth. Therefore the volume removed can be estimated as follows:

70,000 m x 10,000 m x 1,000 m / 60,000,000 yr = 11,667 m^3 yr^{-1}

100,000 m x 15,000 m x 1,000 m / 60,000,000 yr = 25,000 m^3 yr^{-1}

In order to estimate the CO_2 consumption resulting from this loss of material it is necessary to select an appropriate material and the rate at which this material will consume CO_2 during weathering and erosion. For simplicity a single lithology has been assumed and that all material is completely weathered. It is assumed that the material is metagreywacke and that it is consumed at a rate of 21.2 mols CO_2 m^{-3} yr^{-1}, this is derived from the catchment analysis section where it was calculated that the combined weathering rate for metagreywacke based on the rate constants and proportion of each mineral present was 2.12 x 10^{-2} m^2 yr^{-1}. This has been multiplied by 1000 to obtain the rate per cubic metre, since the rate constant used in the previous calculation is based on 1 mm diameter crystals / grains and there are 1000 mm in 1 m.

21.2 mols CO_2 m^{-3} yr^{-1} x 11,677 m^3 yr^{-1} = 2.47 x 10^5 mols CO_2 yr^{-1}

21.2 mols CO_2 m^{-3} yr^{-1} x 25,000 m^3 yr^{-1} = 5.30 x 10^5 mols CO_2 yr^{-1}

This compares against the following values for the Chapora River; based on rock weathering calculations and water chemistry of 9.99 x 10^6 mols CO_2 yr^{-1}, and 1.02 x 10^6 mols CO_2 yr^{-1}, respectively.

7.5. Summary

The three methods employed for the Chapora and Zuari River basins to determine the CO_2 drawdown resulting from silicate weathering have provided three very different values. Table 7.11 documents the results for the Chapora River using these three methods, along with the values for the Nethravati River for comparison.

Table 7. 11 Comparison of the results from the three methods employed to calculate CCR for the Chapora River basin, also listed as a comparison are similar values for the Nethravati River.

Method	CCR (mols CO_2 yr^{-1})	CCR (mols CO_2 yr^{-1} km^{-2})
Catchment Lithology	9.99×10^6	1.70×10^4
Water chemistry	2.29×10^8	6.62×10^5
Scarp retreat	2.47×10^5 - 5.30×10^5	2.47×10^4 – 3.53×10^4
Nethravati	1.04×10^9	2.85×10^5

It would seem that the method based on catchment lithology generates figures c. 16 times lower than those for the Nethravati, whilst the water chemistry method generates figures c. 2.3 times higher and the scarp retreat method generates figures c. 8 – 12 times lower than the Nethravati. However, when comparing the catchment lithology and scarp retreat results against the river water chemistry CCR result per year per km^2 calculated for the Chapora the catchment lithology result is 30 times lower and the scarp retreat method is 20-30 times lower.

The most plausible explanation for this extreme difference is that the calculations employed in the catchment lithology method are based on weathering rate constants measured in laboratory conditions for 1 mm mineral grains. It is well known that laboratory derived rate constants are often significantly different to those observed in the field. Moreover, to obtain a more realistic value based on this method it is necessary to consider a three dimensional model which incorporates realistic solute transport pathways through the various basin lithologies. These pathways will vary in all directions due to the fact that over time weathering and erosion has modified the rocks, depleting them of mobile elements and enriching them in immobile ones, leading to the formation of ever deepening weathering profiles which not only protect and buffer the fresh bedrock below with an overlying layer of relatively inert weathering residuum, but also alter the mineralogy and permeability of the bedrock both vertically and horizontally. This complex behaviour would provide a fascinating future area of research, but is outside the scope of this study.

The scarp retreat method should generate a theoretical maximum based on the complete, 100% weathering of the total volume of material lost during each year; in this instance this value is derived by time-averaging the recession rate over the past 60 Ma. However, it has, like the catchment lithology method, generated a suspiciously low

value when compared to that calculated by the more accepted river water chemistry method. It is therefore probable that using any method that relies purely on theoretical, laboratory-derived mineral weathering rates make overly simplistic assumptions regarding the mineralogically complex lithologies present, and thus that the proportion and manner by which these lithologies are weathered is not a suitable method for estimating CO_2 consumption in naturally variable systems.

Another plausible explanation is that the scarp retreat rate, currently calculated as an average for the past 60 Ma, is not consistent throughout this period: In fact it could be argued that it is more likely that the rate of retreat has changed over time, in response to climatic and tectonic changes. One such period of climatic change is due to the relatively recent inception of the India monsoon system which is closely related to the uplift of the Tibetan Plateau; this plateau reached its current elevation c.15 Ma (Spicer et al., 2003). Onset of monsoon would have had a disproportionate effect on the weathering and erosion of the Ghats escarpment, especially since this topography currently generates one the largest orographic gradients in the world. This would suggest that the rate of scarp retreat calculated above (Section 7.3.3.) is significantly lower than actuality. This is further complicated by the fact that the scarp doesn't retreat on a local scale as a single, linear entity, but rather as discrete drainage basin valley heads combining and coalescing in a sub-parallel orientation perpendicular to the continental divide; accordingly, this results in erosive material being supplied from the along the interfluves between these headward-sapping valleys. This then potentially provides a longer elevated source in addition to the escarpment from which material may be supplied. This additional supply could allow the scarp retreat estimate to be increased threefold; but even allowing for such extra supply, it would by no means account for the difference in the calculated values (i.e., the determined river water value).

In summary, it is entirely possible that the scarp retreat rate calculated as an average over the past 60 Ma is not sufficiently rapid to be representative of the modern day rate of retreat of this escarpment. Conversely, using laboratory-based rate constants and their associated assumptions discussed above to calculate CO_2 consumption in natural systems is not currently sufficiently well constrained to be of use, and consistently under estimates CO_2 drawdown by over an order of magnitude.

Finally, it should not be ignored that the river chemistry calculations could also be in error, especially since the basins being weathered are already heavily depleted. The potential error may be due to higher than expected carbonate contributions or due to the inclusion of elemental concentrations that have been derived from an estuarine source. Although every effort has been made to minimise this possibility by selecting rivers with low EC (<100 µS cm^{-1}) there is some evidence that some higher values close to this figure have been included. However, it is unlikely that these small contributions would account for any significant difference.

7.6. Global context

Clearly, the CO_2 consumption rate (CCR) calculated for the Chapora and Zuari River basins using the river chemistry method (Gurumurthy et al., 2012) is significantly higher than that calculated for the Nethravati River. Whilst this was initially surprising due to the low elemental concentrations observed within these catchments, these high CCR results may be accounted for by considering the elemental fluxes resulting from the highly seasonal rainfall experienced in the Chapora and Zuari catchments. First these calculated values should be placed into context with other major rivers for broader comparison (Table 7.9).

Table 7.12 CO_2 consumption rates (CCR) for the rivers of this study as calculated using the river chemistry method, tabulated with a selection of other major rivers for comparison.

River	CCR (mol km^{-2} yr^{-1})	Source
Chapora	0.62×10^6	This study
Zuari	0.91×10^6	This study
Nethravati	0.29×10^6	Gurumurthy et al. (2012)
Gad	0.57×10^6	Das et al. (2005)
Kajli	0.58×10^6	Das et al. (2005)
Shashtri	0.63×10^6	Das et al. (2005)
Vashistri	0.71×10^6	Das et al. (2005)
Krishna	0.42×10^6	Das et al. (2005)
Bhima	0.33×10^6	Das et al. (2005)
Narmada – Tapti	1.26×10^6	(Dessert et al. (2001)
Godavari	0.58×10^6	(Jha et al. (2009)
Ganges	0.45×10^6	(Jha et al. (2009)
Brahmaputra	0.15×10^6	(Jha et al. (2009)
Indus	0.054×10^6	Gaillardet et al. (1999)
Irrawady	0.832×10^6	Gaillardet et al. (1999)
Amazon	0.32×10^6	Gaillardet et al. (1999)

Table 7.11 reports that all the values listed are of the same order of magnitude (10^6) and that whilst the values for the Chapora and Zuari River systems are c. 2-3 times higher than those for the Nethravati River (Gurumurthy et al., 2012) they are not the highest. The highest values are reported for the Narmada-Tapti River (Dessert et al., 2001) with values of 1.26×10^6 mol km^{-2} yr^{-1}; with the next highest value being for the Irrawady River with a value of 0.832×10^6 mol km^{-2} yr^{-1}. The Narmada-Tapti River drains Deccan basalt terrain and therefore is likely to have high silicate weathering rates since basalt are known to have particularly high weathering rates. By contrast, the Irrawady River's high CO_2 consumption rate is largely due to the extreme relief and monsoonal rainfall resulting in high rates of physical weathering, supplying fresh mineral surfaces for chemical weathering and associated CO_2 consumption. As discussed in section 2.9 this does not necessarily happen *in-situ,* but is more likely to take place in depositional zones such where sufficient time is allowed for chemical weathering to take place. The study areas of the Chapora and Zuari River Basins are both subject to monsoonal rainfall and are also both characterised by zones of extreme orographic gradients in their upper reaches. Therefore, it is not unreasonable for them to achieve high CO_2 consumption rates.

7.7. Chapter Summary

- Estuarine influence varies greatly depending on the seasons. During the dry season the effects of the tides are felt many 10s of kilometres inland, however, during the monsoon season the tidal effects are driven back towards the estuary.

- 'Rinse out effects' describes the observed peaks in elemental concentration occurring close to the onset of the monsoon. This effect is not observed for all elements and is not observed in both the 2007 and 2008 monsoons.

- This effect is thought to be due to precipitation of salts on the sides of the river channels and in the pore spaces as the water table lowers during the dry season. The precipitated salts are flushed from the system as precipitation increases and the water table rises.

- The fact that the effect does not repeat during the 2008 monsoon is surprising. However, it appears that this may be due to the sampling resolution and the short lived nature of the effect.

- The range of Ca and Mg concentrations plotted against HCO_3^- concentrations suggests that there is a limiting factor during the wet season. It is thought that this is due to the permeability of the catchment. For example, only a certain amount of precipitation can flow through a given system, with any surplus flowing as surface flow.

- The spatial downstream variability suggests that during the wet season river chemistry is dominated by precipitation and run-off whilst during the dry season river chemistry is controlled by local lithology.

- Gibbs plots record the 2007 wet season values in the region of rock and soil weathering, whilst the dry season values plot in the region of precipitation dominance. This may seem counter intuitive, but it is in broad agreement with data for the Godavari River (Jha et al., 2009).

- Chemical Index of Alteration (CIA) and Mafic Index of Alteration (MIA) equations are described and have been used to evaluate the degree of weathering for the various rock and sediment samples collected. These were documented in Table 5.4.

- The MIA method is similar to the CIA method; however, it also incorporates the mafic elements Fe and Mg. It also takes account of oxidising and reducing environments with $MIA_{(O)}$ and $MIA_{(R)}$, respectively.

- In order to simplify the task of comparing and contrasting the two rivers, Figures 6.17 and 6.18 have been produced to plot Cha 01 and Zua 01 for each major and trace element on the same graphs.

- The main observation is that the Al values for Cha 01 are significantly elevated compared to those for Zua 01. This is likely due to lithological differences.

- Three methods of evaluating the CO_2 drawdown have been considered. The first one based on river chemistry, the second one based on rock mineral weathering reactions and the third one based on scarp retreat.

- The three methods yield very different values. When these are compared to values obtained for the Nethravati River which drains similar terrain and encounters a similar climate (Gurumurthy et al., 2012). The values for the first method are 2-3 times higher, whilst those from the second method are 20-40 times lower and those for the third are 8-12 times lower than those for the Nethravati River.

- Whilst the river chemistry values are slightly higher than those for the Nethravati River, when placed into a broader context they are not the highest and are of the same order of magnitude.

PART III: CONCLUSIONS AND RECOMMENDATIONS

Chapter 8. Conclusion

The main aim of this thesis was to determine the characteristics, controls, and effects on atmospheric CO_2 drawdown of chemical weathering in a sub-tropical, monsoonal climatic regime in high chemical weathering rate, westerly draining river basins of western peninsular India. The data collected from this extensive study have then been used to consider the specific objectives which are discussed in turn below.

Objective number one was to determine the variation in chemical composition of fluvial discharge into the Eastern Arabian Sea over a 15 month period from June 2007 to July 2008. This has been achieved by the monthly collection of river samples from 6 localities on the Chapora River and 7 localities on the Zuari River starting in June 2007 and ending in July 2008 in order to encompass the start of two monsoon seasons. The collected samples were analysed on site for water temperature, pH, dissolved oxygen (DO) and electrical conductivity (EC) and the collected samples were stored and transported back to the UK for subsequent analysis of major and trace element concentrations. These have been plotted, described and interpreted both temporally and spatially with the main observations being those of a rinse out effect and the ubiquitous observation of spatial variation showing element concentrations being more varied throughout the river basins during the dry season and more consistent throughout the basins during the wet season.

Objective number two was to determine the extent of tidal influence on river chemistry, spatially, throughout the drainage basins and temporally, throughout the sampling period in order to ensure that only riverine samples unaffected by estuarine influence are used in subsequent discussions. This objective has been achieved again via the sampling regime outlined above and more specifically by the interpretation of EC and Cl concentrations at the various localities at various times in the year. EC was found to vary dramatically throughout the drainage basins both temporally and spatially in response primarily to changes in river flow, with the tidal influence being identified further upstream during the dry months but being force seaward during the monsoon months. This extreme, seasonal variability in river flow is an important consideration in how these river basins weather as the river basins can be described as high energy or low energy depending on the time of year; this is discussed in the final summary of this chapter.

Objective number three was to determine the role of lithology on the elemental concentrations within the chosen fluvial systems. This objective was achieved by comparing the elemental composition of the two rivers first by comparing the major and trace element concentrations for Cha 01 and Zua 01 and secondly by mean of Na normalised plots for each locality. Both methods suggest strong similarities between the two rivers even though there are some minor differences in lithology, for example the small contribution from Deccan basalt in the upper reaches of the Chapora and the Chandranath granite in the Zuari. These differences may be evident in the elevated Al concentrations for Cha 01 compared to those for Zua 01.

Objective number four was to determine the effect of the laterite cover on the elemental concentrations within the chosen fluvial systems. It is recognised that much of the Konkan-Kanara coastal plain has already been heavily weathered over millions of years leaving behind an extensive laterite cover. This, mobile element depleted, laterite cover effectively protects the underlying, unweathered lithology. A column experiment was designed and undertaken over a 16 week period to establish the relative reactivity of the various zones within a weathering profile (Merces Quarry). This clearly demonstrated via EC values that the unweathered protolith was by far the most reactive and that in general the reactivity reduced up profile. Therefore the maturity of the regolith has to be another fundamental control in the weathering regime of these localities and other similar localities elsewhere. This is also discussed in more detail in the final summary of this chapter.

Objective number five was to determine the effect of Fe-Mn mining on dissolved riverine fluxes. Whilst this was considered, there was insufficient evidence to conclusively state that the influence of Fe-Mn mining of BIF within the Zuari basin was observable within the dissolved phase. However, it is highly likely that evidence would be forthcoming if the suspended sediment had been collected and analysed as both Fe and Mn are insoluble in oxidising environments.

Lastly, objective number six was to calculate the CO_2 drawdown resulting from the chemical weathering of the underlying lithology of the Chapora and Zuari River basins. This was achieved using three independent methods. The first method employed used the traditional approach of river water chemistry analysis which resulted in CO_2 drawdown values of the same order of magnitude as numerous other well documented rivers. Although, the values were 2-3 times higher than those for the Nethravati River some 300 km south of Goa which is a similar geomorphological setting and is subjected to a similar climatic regime. This is slightly surprising as it was predicted that

the CO_2 drawdown would be quite low due to the fact that the basins are already heavily weathered. This is supported by the Gibbs plots which show that both of the rivers plot along the precipitation – rock weathering arm, as is the case with many tropical rivers draining thoroughly weathered basins where the amount of rainfall is high relative to dissolved salts supplied from rock weathering. Therefore, two other methods were employed, which both utilise mineral weathering reactions and rate constants to estimate CO_2 drawdown. The first uses a simplified basin analysis where the basin is split into its main lithologies and each lithology is assumed to be a constant mineralogical composition, this method generated results that were 20-40 times lower than those for the Nethravati River. The third method assumed the complete weathering of all material removed due to the retreat of the Western Ghats escarpment over the past 60 Ma and was expected to generate a theoretical maximum. However, again this method yielded 8-12 times lower results than those for the Nethravati River. The low values of both of these methods may be due to issues with using laboratory based rate constants which are known to differ from those in real world environments, additionally, it is highly unlikely that the scarp retreat rate has been constant through time, in fact it is more likely to have increased in response to the development of the Indian monsoon. Overall, it is surprising that the CO_2 drawdown calculated using the river water chemistry method is as high as it is, especially considering the CIA and MIA values and for the collected rock and sediment samples and the results of the column experiment which both support the observation that much of the basin material is already heavily weathered. However, it is believed to represent the most reliable result and one that is at least in the correct order of magnitude to all the other rivers. This may in part be due to the provision of fresh material from the upper reaches of the basins each year as the hugely erosive monsoon waters flow down the rivers and deposit this material in the lower energy environments where chemical weathering has time to occur. Alternatively, it could in part be due to the presence of an additional, unidentified carbonate contribution or in some cases an estuarine influence.

Whilst some short comings have been observed as discussed in earlier chapters, the overall aims of the study have been met and the study has greatly enriched the understanding of the variability of river fluxes both spatially and temporally in the two catchments considered and provides a good basis for future work, especially in better constraining the temporal characteristics of the ‘rinse-out’ effect and interconnectedness of high energy physical weathering and erosion and the provision of fresh material to the low energy environments of the river systems.

Summary

At the start of the literature review, Figure 2.1 provided a schematic diagram of how high and low energy environments favour physical or chemical weathering and result in high or low total dissolves solids, respectively. In hindsight this diagram was too simplistic and failed to account for two fundamental features of the weathering mechanisms naturally occurring in these river systems. The first missing feature can be best described as the maturity of the regolith. It is well documented that the lithologies present within the catchments of the Zuari River and the Chapora River are extensively lateritised to substantial depths and therefore much of the landscape through which the rainwater is percolating has already been depleted of the majority of its soluble material. As discussed is section 6.1.2 it is now thought that the low element concentrations within the river water are derived from weathering of the protolith at or near to the weathering front at significant depth. Therefore 'Maturity of regolith' needs to be added to a revised Figure 2.1.

The second fundamental simplification is the lack of interconnectedness between the high energy and low energy parts of the diagram. The diagram currently depicts two completely independent systems, whilst in reality the two systems are at least spatially linked throughout the river system, with high energy environments being present in the upper reaches of the rivers in the Western Ghats where high rainfall and high relief combine to create high river flows. These high energy environments where physical weathering dominates would create new fresh surfaces on the *in situ* rock outcrops but would also deliver fresh material to lower energy environments throughout the river system, towards the estuary and out into the Arabian Sea. However, it is not sufficient to think only spatially; it is also necessary to think temporally. This is especially true for seasonal rivers like the ones studied here, as the whole river system changes from a high energy environment during the monsoon season to a low energy environment during the dry season, potentially making much of the river system a depositional environment. Therefore it is also necessary to revise Figure 2.1 to include a connection between sediment deposition and a low energy weathering environment (Figure 8.1).
This is also the case for Himalayan rivers as studied by Pogge Von Strandmann and Henderson, 2015 where they showed that increases in ^{7}Li are due to secondary mineral formation via weathering, which is taking place predominantly on the floodplains where fresh, eroded material has been deposited from the high Himalayas during the previous monsoon season.

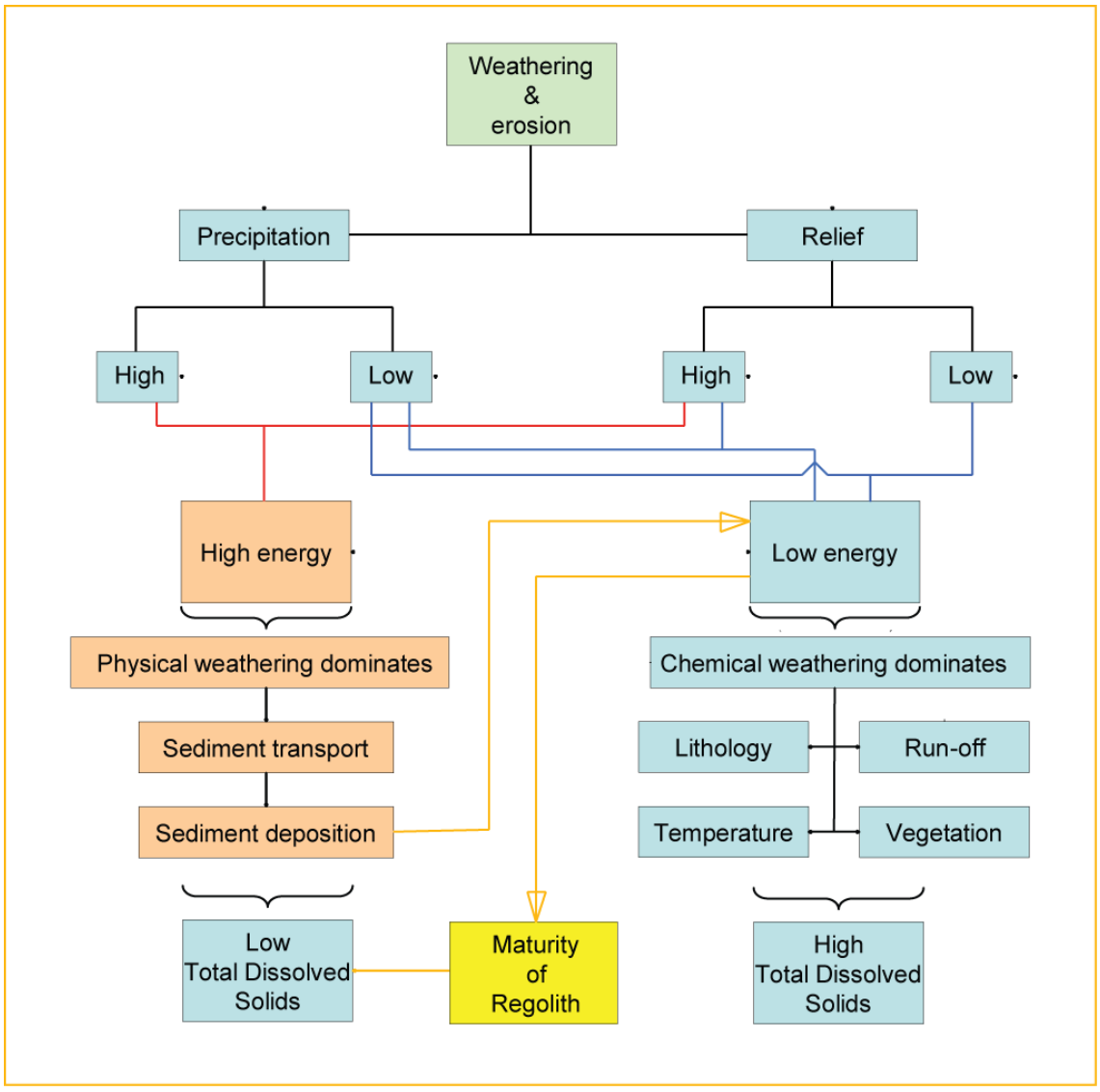

Figure 8.1 Revised diagram (based on Figure 2.1) depicting the interconnectedness of high energy and low energy weathering environments and the effect of maturity of regolith.

The weathering regime as can be better described as follows:

During the monsoon season high rainfall and high relief create a high energy environment which favours physical weathering and erosion. During this time chemical weathering is low due to the fact that there is generally insufficient contact time between the water and mineral surfaces. As the monsoon period starts to decline erosion products begin to be deposited with the larger / denser components falling out of suspension first, followed by the smaller / less dense components. This effect will also help distribute the various components within the river system. During the dry season some of these fresh erosion products are in constant contact with water and will undergo chemical weathering. The longer this dry season continues the higher the elemental concentrations will rise. Some of these erosion products will be within the remaining river flow, whilst others may have been deposited on the flood plains of the rivers as the river waters receded and the river channels narrowed. Chemical weathering will also still be occurring within the pore spaces of weathered lithology of the catchments. Additionally, it is highly possible that some elements could be supplied to these same areas of the basin by the ebb and flow of the tides. Regardless of the provenance of these elements at the onset of the subsequent monsoon rains the river flow will increase once more and will percolate through the system and encroach onto the lateral flood plains of the rivers where it will ‘rinse-out’ the now soluble minerals that have built up during the dry season. This, as discussed in detail earlier, occurs over a relatively short period of time (weeks), after which the river system reverts back to a high energy environment and concentrations once again decline throughout the monsoon season and then gradually start to increase once again through the subsequent dry season. It is also likely that some, small amounts of sub surface flow will continue during the dry season and will leach elements from the pore spaces with which it come into contact, delivering them to the river. Subsurface flow will also be a consideration during the wet season too as the water will flow laterally at all levels as long as the porosity of the lithology is such that it allows water to permeate. This will also move elements though the system and eventually into the rivers.

Chapter 9. Recommendations

The following observations are study specific but are also valid for future work on chemical weathering in river systems elsewhere in the world. In general they represent considerations that would enhance the results obtained should a similar project be undertaken.

9.1. Catchment selection

The present study considered two rivers, the Chapora and the Zuari from the coast to c. 50 km inland. These two rivers were chosen due to their similarities, in terms of their geomorphological setting, i.e., rivers originating in the Western Ghats providing extreme orographic gradients, in turn yielding substantial river flows which vary seasonally with the monsoons, and differences in respect of their lithologies, Deccan basalt present in the upper reaches of the Chapora basin and Chandranath granite present in the middle to upper reaches of the Zuari basin, as well as the extensive Banded Iron Formation (BIF) mining present along much of the Zuari river.

In reality, due to the low lying nature of the drainage basin, a significant length of the river was affected by tides and therefore river chemistry was highly influenced by sea water chemistry. Although the low lying nature of the Konkan plain was known, the extent of tidal influence was unexpected at the time of selecting the sampling localities. Whilst this provided an interesting addition to the study in terms of identifying which samples were affected and moreover, how this effect varies with season and hence river flux. In any future study it may be beneficial to extend to extra sampling stations further upstream in order to compare the weathering regimes in the higher reaches of the river systems. This would allow comparisons of high and low energy environments to be undertaken to evaluate how much chemical weathering takes place in each environment as it is expected that physical weathering and erosion will dominate in the high energy Western Ghats escarpment environment, whilst chemical weathering would be expected to dominate in the lower energy Konkan plain. This could also include the study of Li isotopes to further evaluate the congruency of weathering in the various parts of the catchment.

9.2. River Flow

The present study was concerned primarily with elemental concentration variation throughout the 15 month sampling period. The data can be summarised as displaying low element concentrations which, spatially (throughout the river basin) vary mostly during the dry season whilst displaying almost identical concentrations during the wet season. This observation suggests that during the dry season element concentrations at each locality are controlled by the local lithology, however, during the wet season the observation that the element concentrations are very similar throughout the basin suggests that at this time dilution and homogenisation of the river water takes place which essentially masks any local variations. These trends were additionally influenced by a 'rinse-out' which occurred close to the beginning of the monsoon season. However, due to the great disparity in river flow during the monsoon compared with the dry season all of these features would be obscured if the element flux was plotted instead of element concentration, in effect the only variation apparent would be in proportion with the river flow.

Additionally, attempts to locate river flow data for the chosen rivers via Indian Governmental websites such as the Central Water Commission were unsuccessful and attempts to measure the river flow in situ were flawed especially during the dry season where flow was almost non-existent. However, there is equipment that can measure and monitor river flow. These range in cost and complexity from the relatively simple vertical axis or horizontal axis mechanical meters where flow is recorded by counting rotations of an impeller, through electromagnetic meters which have no moving parts and where flow velocity is measured using Faraday's Law which states that a conductor (water) moving in a magnetic field (generated by the probe) produces a voltage that varies linearly with flow velocity (add ref Fulford et al) to meters such as the StreamPro Acoustic Doppler Current Meter (ADCM) which uses the principle of the Doppler effect. Al of these options would require more time during the sample collection period as well as regular maintenance and upkeep, all of which was not possible within the framework of this study. Also, once river flows are included it becomes necessary to consider how the flow varies throughout the river cross section as measurements of river flow at the surface are likely to exceed those at the base and sides of the river due to frictional losses. Therefore, it would be very useful to select rivers that have flow data available which account for this variability or to employ a suitable method to determine river flow for any future studies, ensuring that the flow measured is representative. Interestingly, the ADCM could possibly be left in place to monitor flow across the whole river cross section using a data logger, but would

arguably need one to be positioned at the very least in each river, but possibly at each sampling site to monitor how flow varied at each location.

9.3. Suspended sediment

At each locality two 30 ml water samples were collected, these were filtered sequentially through 5.0 µm and 0.2 µm Nucleopore filter papers. It would have been highly beneficial to have retained these filter papers for analysis of particulate matter as this could have been used to ascertain how the particulate matter varied in composition and concentration between the various localities within each river and how it varied between the two rivers. For example, this may have identified a greater proportion of particulate matter or possibly larger size fractions in the upper reaches of the rivers compared to the lower reaches as larger particles would remain buoyant at higher energy flows. Moreover, this may have been especially insightful in comparing the particulate matter between the Chapora and Zuari Rivers as much of the potential contaminants entering the Zuari River due to the effects of mining may well have been in the solid state rather than in solution.

9.4. Sample collection

At each locality a cation and an anion sample were collected every month. The cation sample was acidified with HNO_3 to c. pH~2. In addition to these a duplicate cation sample and a duplicate anion sample were also collected at localities Cha 02, Cha 03, Zua 02 and Zua 03 every month. Finally, a field blank sample was collected at each locality every month. Only when analysis of the cations and anions was in progress was it apparent that two field blank samples should have been collected, one acidified (cations analysis) and one un- acidified (anion analysis). Any future study would ensure that the correct number of field blanks are collected, one of which would be acidified with HNO_3 to c. pH~2.

9.5. Atmospheric correction

In order to calculate the CO_2 consumption rate due to silicate weathering for the two rivers it is necessary to account for any elemental contributions that are derived from atmospheric sources or anthropogenic sources as well as those derived from carbonates and evaporites. Correcting for atmospheric inputs was achieved using data published in the literature (Das et al., 2005). This paper provided elemental concentration data for precipitation from a variety of locations in close proximity to the study area and included inland and coastal data. It is clearly observed in these data

and widely acknowledged in the literature that the atmospheric elemental concentrations vary from a coastal source to a terrestrial source the further in land one moves. In hindsight it would have been beneficial to obtain a precipitation sample at each locality on each river at each sampling occasion where possible. These data could have then been used to see how the elemental concentration of the rainwater varied from location to location and from month to month at least throughout the monsoon period. This would have ensured that the most appropriate correction has been applied at each locality, although it is likely a very minor source of error.

9.6. Rinse-out

The observation of the 'Rinse-out' effect as discussed in section 7.1.2 was identified as being present for some elements and not for others and it also varied from year to year. To better quantify the 'Rinse-out' effect a higher resolution study over a shorter timescale would be advantageous. This would better constrain which elements are released and in which order, also repeating the study over subsequent years would prove or disprove the seasonality / regularity of these observations. Ideally the study would start just prior to the first rains, based on the 2007 and 2008 studies a start date of the 1st June would seem reasonable, samples would then be collected daily at the same time of day for at least 4 weeks, providing 28 cation samples and 28 anion samples per locality. In addition to these samples, duplicates and field blanks would also need to be collected, and should represent at least 10% of the total number of samples. Since this study is primarily concerned with identifying the longevity of the 'rinse-out' and the order in which the various elements are flushed from the system it is not necessary to collect samples from multiple localities on each river. Also, it is important to select a locality that is completely unaffected by the tides and therefore represents elemental concentrations derived solely from fluvial chemical weathering.

9.7. 3D weathering rate study

As discussed in Section 7.3 the method of calculating CO_2 drawdown by means of analysis of chemical weathering rates of the various minerals present in each lithology resulted in values substantially lower than those predicted by analysis of the river chemistry. Probably the most fundamental reason for this discrepancy is due to the need to simulate the weathering rates based on a three dimensional approach considering the variation in lithology and permeability both vertically and horizontally. As mentioned above this would prove a fascinating future study and could provide an

alternative approach for ascertaining the chemical weathering rates of catchments, but would ultimately require the application of simplifying assumptions in order to use the method over wide areas.

Additionally, using these same weathering calculations to determine CO_2 drawdown based on material removal via scarp retreat over the past 60 Ma also generates values significantly lower than those calculated using the more traditional river water chemistry method. Considering this study alone, one could be tempted to assume that because these weathering rate based methods generate similar values the river chemistry method is incorrect, however, if we compare all three sets of results with another similar river, such as the Nethravati River it seems that the river chemistry method generates the most acceptable result, albeit a little higher than expected.

Census 2011.

ACKER, J. G. & LEPTOUKH, G. (2007) Online analysis enhances use of NASA Earth science data. *Eos Trans. AGU,* 88.

AMIOTTE SUCHET, P. & PROBST, J. L. (1993) Modelling of atmospheric CO2 consumption by chemical weathering of rocks: Application to the Garonne, Congo and Amazon basins. *Chemical Geology,* 107**,** 205-210.

ANAND, S. P. & RAJARAM, M. (2004) Crustal structure of Narmada-Son Lineament: An aeromagnetic perspective. *Earth Planets Space,* 56**,** e9-e12.

BABECHUK, M. G., WIDDOWSON, M. & KAMBER, B. S. (2014) Quantifying chemical weathering intensity and trace element release from two contrasting basalt profiles, Deccan Traps, India. *Chemical Geology,* 363**,** 56-75.

BENJAMIN, M. T., JOHNSON, N. M. & NAESER, C. W. (1987) Recent rapid uplift in the Bolivian Andes: Evidence from fission-track dating. *Geology,* 15**,** 680-683.

BERNER, E. K. & BERNER, R. A. (2012) Global environment, water, air and geochemical cycles. *Princeton University Press*.

BERNER, E. K., BERNER, R. A., MOULTON, K. L., HEINRICH, D. H. & KARL, K. T. (2003) Plants and Mineral Weathering: Present and Past. *Treatise on Geochemistry.* Oxford, Pergamon.

BERNER, R. A. (2006a) GEOCARBSULF: A combined model for Phanerozoic atmospheric O2 and CO2. *Geochimica et Cosmochimica Acta,* 70**,** 5653-5664.

BERNER, R. A. (2006b) Inclusion of the Weathering of Volcanic Rocks in the GEOCARBSULF Model. *Am J Sci,* 306**,** 295-302.

BERNER, R. A. & CALDEIRA, K. (1997) The need for mass balance and feedback in the geochemical carbon cycle. *Geology,* 25**,** 955-956.

BERNER, R. A., LASAGA, A. C. & GARRELS, R. M. (1983) The carbonate-silicate geochemical cycle and its effect on atmospheric carbon dioxide over the past 100 million years. *American Journal of Science,* 283**,** 641-683.

BHANDARI, S., MAURYA, D. M. & CHAMYAL, L. S. (2005) Late Pleistocene alluvial plain sedimentation in Lower Narmada Valley, Western India: Palaeoenvironmental implications. *Journal of Asian Earth Sciences,* 24**,** 433-444.

BICKLE, M. J. (1996) Metamorphic decarbonation, silicate weathering and the longâ€• term carbon cycle. *Terra Nova,* 8**,** 270-276.

BONDRE, N. Â R., HART, W. Â K. & SHETH, H. Â C. (2006) Geology and Geochemistry of the Sangamner Mafic Dike Swarm, Western Deccan Volcanic Province, India: Implications for Regional Stratigraphy. *The Journal of Geology,* 114**,** 155-170.

BOURMAN, R. P. & OLLIER, C. D. (2002) A critique of the Schellmann definition and classification of [`]laterite'. *CATENA,* 47**,** 117-131.

BOURMAN, R. P. & OLLIER, C. D. (2003) Reply to the Discussion of "A critique of the Schellmann definition and classification of laterite" by R.P. Bourman and C.D. Ollier (Catena 47, 117-131). *CATENA,* 52**,** 81-83.

BRADY, P. V., DORN, R. I., BRAZEL, A. J., CLARK, J., MOORE, R. B. & GLIDEWELL, T. (1999) Direct measurement of the combined effects of lichen, rainfall, and temperature onsilicate weathering. *Geochimica et Cosmochimica Acta,* 63**,** 3293-3300.

BRANTLEY, S. L. (2008) Kinetics of mineral dissolution. *Kinetics of water-rock interaction.* Springer.

BRANTLEY, S. L., EDITORS-IN-CHIEF:Â Â HEINRICH, D. H. & KARL, K. T. (2003) 5.03 - Reaction Kinetics of Primary Rock-forming Minerals under Ambient Conditions. *Treatise on Geochemistry.* Oxford, Pergamon.

BRANTLEY, S. L., GOLDHABER, M. B. & RAGNARSDOTTIR, K. V. (2007) Crossing disciplines and scales to understand the critical zone. *Elements,* 3**,** 307-314.

BUCHANAN, F. (1807) A Journey from Madras through the counries of Mysore, Kanara and Malabar. *East India Co., London,* Vol. 2:436-461, Vol. 3: 66, 89, 251. 258, 378.

BUSS, H. L., BRANTLEY, S. L., SCATENA, F. N., BAZILIEVSKAYA, E. A., BLUM, A., SCHULZ, M., JIMÃ©NEZ, R., WHITE, A. F., ROTHER, G. & COLE, D. (2013) Probing the deep critical zone beneath the Luquillo Experimental Forest, Puerto Rico. *Earth Surface Processes and Landforms,* 38**,** 1170-1186.

CAMPANILE, D., NAMBIAR, C. G., BISHOP, P., WIDDOWSON, M. & BROWN, R. (2008) Sedimentation record in the Konkan–Kerala Basin: implications for the evolution of the Western Ghats and the Western Indian passive margin. *Basin Research,* 20**,** 3-22.

CASTOR, S. B. & HEDRICK, J. B. (2006) Industrial minerals and rocks: Commodities, markets, and uses. Kogel, JE.

CHENET, A.-L., QUIDELLEUR, X., FLUTEAU, F. D. R., COURTILLOT, V. & BAJPAI, S. (2007) 40 Kâ€“40 Ar dating of the Main Deccan large igneous province: Further evidence of KTB age and short duration. *Earth and Planetary Science Letters,* 263**,** 1-15.

COLLIER, J. S., SANSOM, V., ISHIZUKA, O., TAYLOR, R. N., MINSHULL, T. A. & WHITMARSH, R. B. (2008) Age of Seychelles-India break-up. *Earth and Planetary Science Letters,* 272**,** 264-277.

COURTILLOT, V. E. & RENNE, P. R. (2003) On the ages of flood basalt events. *Comptes Rendus Geoscience,* 335**,** 113-140.

COX, K. G. & SUMMERFIELD, M. A. (1989) The role of mantle plumes in the development of continental drainage patterns.

DAS, A., KRISHNASWAMI, S., SARIN, M. M. & PANDE, K. (2005) Chemical weathering in the Krishna Basin and Western Ghats of the Deccan Traps, India: Rates of basalt weathering and their controls. *Geochimica et Cosmochimica Acta,* 69**,** 2067-2084.

DECONTO, R. M. & POLLARD, D. (2003) Rapid Cenozoic glaciation of Antarctica induced by declining atmospheric CO2.

DESSAI, A. (2011) The Geology of Goa Group: Revisited. *Journal Geological Society of India,* 78**,** 233-242.

DESSERT, C., DUPRE, B., FRANCOIS, L. M., SCHOTT, J., GAILLARDET, J., CHAKRAPANI, G. & BAJPAI, S. (2001) Erosion of Deccan Traps determined by river geochemistry: impact on the global climate and the 87Sr/86Sr ratio of seawater. *Earth and Planetary Science Letters,* 188**,** 459-474.

DESSERT, C., DUPRE, B., GAILLARDET, J., FRANCOIS, L. M. & ALLEGRE, C. J. (2003) Basalt weathering laws and the impact of basalt weathering on the global carbon cycle. *Chemical Geology,* 202**,** 257-273.

DHOUNDIAL, D. P., PAUL, D. K., SARKAR, A., TRIVEDI, J. R., GOPALAN, K. & POTTS, P. J. (1987) Geochronology and geochemistry of precambrian granitic rocks of goa, sw india. *Precambrian Research,* 36**,** 287-302.

DREVER, J. I. (1994) The effect of land plants on weathering rates of silicate minerals. *Geochimica et Cosmochimica Acta ; Vol/Issue: 58:10***,** Pages: 2325-2332.

DRURY, S. A. (1984) A Proterozoic intra-cratonic basin, dike swarms and thermal evolution in South India. *Geological Survey of India,* 25**,** 437-449.

DUPRE, B., DESSERT, C., OLIVA, P., GODDERIS, Y., VIERS, J., FRANCOIS, L., MILLOT, R. & GAILLARDET, J. (2003) Rivers, chemical weathering and Earth's climate. *Comptes Rendus Geosciences,* 335**,** 1141-1160.

FEDO, C. M., WAYNE NESBITT, H. & YOUNG, G. M. (1995) Unraveling the effects of potassium metasomatism in sedimentary rocks and paleosols, with implications for paleoweathering conditions and provenance. *Geology,* 23**,** 921-924.

FERNANDES, O. A. (2009) Physiography and Geoogy of Goa. IN MASCARENHAS, A. A. K., GLENN (Ed.) *Natural Resources of Goa: A perspective. .* India: Geological Society of Goa.

FRANCE-LANORD, C. & DERRY, L. A. (1997) Organic carbon burial forcing of the carbon cycle from Himalayan erosion. *Nature,* 390**,** 65-67.

GALY, V., BEYSSAC, O., FRANCE-LANORD, C. & EGLINTON, T. (2008) Recycling of graphite during Himalayan erosion: A geological stabilization of carbon in the crust. *Science,* 322**,** 943-945.

GANERÃ¸D, M., TORSVIK, T. H., VAN HINSBERGEN, D. J. J., GAINA, C., CORFU, F., WERNER, S., OWEN-SMITH, T. M., ASHWAL, L. D., WEBB, S. J. & HENDRIKS, B. W. H. Palaeoposition of the Seychelles microcontinent in relation to the Deccan Traps and the Plume Generation Zone in Late Cretaceous-Early Palaeogene time. *Geological Society, London, Special Publications,* 357**,** 229-252.

GANEROD, M., TORSVIK, T. H., VAN HINSBERGEN, D. J. J., GAINA, C., CORFU, F., WERNER, S., OWEN-SMITH, T. M., ASHWAL, L. D., WEBB, S. J. & HENDRIKS, B. W. H. Palaeoposition of the Seychelles microcontinent in relation to the Deccan Traps and the Plume Generation Zone in Late Cretaceous-Early Palaeogene time. *Geological Society, London, Special Publications,* 357**,** 229-252.

GIBBS, R. J. (1970) Mechanisms Controlling World Water Chemistry. *Science,* 170**,** 1088-1090.

GOKUL, A. R. (1985) Structure and tectonics of Goa. Earth Resources for Goa's development. *Goa Seminar Volume. Geological Survey of India***,** 14-21.

GOLDICH, S. S. (1938) A Study in Rock-Weathering. *The Journal of Geology,* 46**,** 17-58.

GOUDIE, A. S. & VILES, H. A. (2012) Weathering and the global carbon cycle: Geomorphological perspectives. *Earth-Science Reviews,* 113**,** 59-71.

GOVERNMENT OF INDIA (2010) Ground water information booklet, South Goa District, Goa State. IN RESOURCES, M. O. W. (Ed.).

GSI (1996) Geological and Mineralogical Map of Goa. Government of India.

GUNNELL, Y. & FLEITOUT, L. (1998) Shoulder uplift of the Western Ghats passive margin, India: a denudational model. *Earth Surface Processes and Landforms,* 23**,** 391-404.

GURUMURTHY, G. P., BALAKRISHNA, K., RIOTTE, J., BRAUN, J.-J., AUDRY, S. P., SHANKAR, H. N. U. & MANJUNATHA, B. R. (2012) Controls on intense silicate

weathering in a tropical river, southwestern India. *Chemical Geology,* 300â€“301**,** 61-69.

HAMDAN, J. & BURNHAM, C. P. (1996) The contribution of nutrients from parent material in three deeply weathered soils of Peninsular Malaysia. *Geoderma,* 74**,** 219-233.

HARNOIS, L. (1988) The CIW index: A new chemical index of weathering. *Sedimentary Geology,* 55**,** 319-322.

HILLEY, G. E. & PORDER, S. (2008) A framework for predicting global silicate weathering and CO2 drawdown rates over geologic time-scales. *Proceedings of the National Academy of Sciences,* 105**,** 16855-16859.

HINSINGER, P., FERNANDES BARROS, O. N., BENEDETTI, M. F., NOACK, Y. & CALLOT, G. (2001) Plant-induced weathering of a basaltic rock: experimental evidence. *Geochimica et Cosmochimica Acta,* 65**,** 137-152.

HOLDEN, J. (2005) *Introduction to physical geography and the environment,* Harlow, England; New York, Pearson-Prentice Hall.

HOUSE, W. A. & WARWICK, M. S. (1998) Hysteresis of the solute concentration/discharge relationship in rivers during storms. *Water Research,* 32**,** 2279-2290.

JAY, A. E., NIOCAILL, C. M., WIDDOWSON, M., SELF, S. & TURNER, W. (2009) New palaeomagnetic data from the Mahabaleshwar Plateau, Deccan Flood Basalt Province, India: implications for the volcanostratigraphic architecture of continental flood basalt provinces. *Journal of the Geological Society,* 166**,** 13-24.

JAY, A. E. & WIDDOWSON, M. (2008) Stratigraphy, structure and volcanology of the SE Deccan continental flood basalt province: implications for eruptive extent and volumes. *Journal of the Geological Society,* 165**,** 177-188.

KALINOWSKI, B. E. & SCHWEDA, P. (1996) Kinetics of muscovite, phlogopite, and biotite dissolution and alteration at pH 1â€“4, room temperature. *Geochimica et Cosmochimica Acta,* 60**,** 367-385.

KATZ, M. E., WRIGHT, J. D., MILLER, K. G., CRAMER, B. S., FENNEL, K. & FALKOWSKI, P. G. (2005) Biological overprint of the geological carbon cycle. *Marine Geology,* 217**,** 323-338.

KERRICK, D. M. & CALDEIRA, K. (1998) Metamorphic CO 2 degassing from orogenic belts. *Chemical Geology,* 145**,** 213-232.

KISAKUREK, B., JAMES, R. H. & HARRIS, N. B. W. (2005) Li and [delta]7Li in Himalayan rivers: Proxies for silicate weathering? *Earth and Planetary Science Letters,* 237**,** 387-401.

KLEMM, V., LEVASSEUR, S., FRANK, M., HEIN, J. R. & HALLIDAY, A. N. (2005) Osmium isotope stratigraphy of a marine ferromanganese crust. *Earth and Planetary Science Letters,* 238**,** 42-48.

KRISHNASWAMI, S. & SINGH, S. K. (2005) Chemical weathering in the river basins of the Himalaya, India. *Current Science,* 89**,** 841-849.

KRISHNASWAMI, S., SINGH, S. K. & DALAI, T. K. (1999) Silicate weathering in the Himalaya: Role in contributing to major ions and radiogenic Sr to the Bay of Bengal. *Ocean Science, Trends and Future Directions***,** 23-51.

LABRECQUE, J. & SCHORIN, II (1987) Z. Geomorph. NF Suppl.-Bd. 64 j 33-38 I Berlin-Stuttgart-] uni 1987. *Laterites: Some Aspects of Current Research***,** 33.

LEMARCHAND, E., CHABAUX, F. O., VIGIER, N., MILLOT, R. & PIERRET, M.-C. (2010) Lithium isotope systematics in a forested granitic catchment (Strengbach, Vosges Mountains, France). *Geochimica et Cosmochimica Acta,* 74**,** 4612-4628.

LI, G. & ELDERFIELD, H. (2013) Evolution of carbon cycle over the past 100 million years. *Geochimica et Cosmochimica Acta,* 103**,** 11-25.

LOVELOCK, J. & MARGULIS, L. (1996) The Gaia Hypothesis.

LUCAS, Y. (2001) The role of plants in controlling rates and products of weathering: Importance of biological pumping. *Annual Review of Earth and Planetary Sciences,* 29**,** 135-163.

MAHER, K. (2011) The role of fluid residence time and topographic scales in determining chemical fluxes from landscapes. *Earth and Planetary Science Letters,* 312**,** 48-58.

MAHONEY, J. J. (1988) Deccan Traps. IN MACDOUGAL, J. D. (Ed.) *Continental Flood Basalts.* Kluwer Dordrecht.

MCARTHUR, J. M., HOWARTH, R. J. & BAILEY, T. R. (2001) Strontium isotopes stratigraphy: LOWESS Version 3. Best-fit line to the marine Sr-isotope curve for 0 to 509 Ma and accompanying look-up table for deriving numerical age. *Journal of Geology,* 109**,** 155-169

MCFARLANE, M. J. (1976) *Laterite and landscape*, Academic Press.

MCGUIRE, K. J. & MCDONNELL, J. J. (2006) A review and evaluation of catchment transit time modeling. *Journal of Hydrology,* 330**,** 543-563.

MESHRAM, R. R. & RANDIVE, K. R. (2011) Geochemical study of laterites of the Jamnagar district, Gujarat, India: Implications on parent rock, mineralogy and tectonics. *Journal of Asian Earth Sciences,* 42**,** 1271-1287.

MESQUITA, A. & KAISARY, S. (2007) Distribution of iron and manganese. National Institute of Oceanography, India.

MEYBECK, M. (1986) Composition chimique des ruisseaux non pollues de France. *Sci. Geol. Bull. (Strasbourg),* **39,** 3-77.

MILLOT, R., VIGIER, N. & GAILLARDET, J. R. M. (2010) Behaviour of lithium and its isotopes during weathering in the Mackenzie Basin, Canada. *Geochimica et Cosmochimica Acta,* 74**,** 3897-3912.

MISRA, S. & FROELICH, P. N. (2012) Lithium Isotope History of Cenozoic Seawater: Changes in Silicate Weathering and Reverse Weathering. *Science,* 335**,** 818-823.

MITCHELL, C. & WIDDOWSON, M. (1991) A geological map of the southern Deccan Traps, India and its structural implications. *Journal of the Geological Society,* 148**,** 495-505.

MULLER, R. D., SDROLIAS, M., GAINA, C., STEINBERGER, B. & HEINE, C. (2008) Long-Term Sea-Level Fluctuations Driven by Ocean Basin Dynamics. *Science,* 319**,** 1357-1362.

NAIR, M., JOSEPH, T., BALACHANDRAN, K.K., NAIR, K.K.C. & PAIMPILLIL, J.S. (2003) Arsenic enrichment in estuarine sediments - impact of iron and manganese mining. IN AHMED, M. F. A., M.A.; ADEEL, Z. (Ed.) *(Int. Symp. on Fate of Arsenic in the Environment; ;). International Training Network (ITN).* Dhaka; Bangladesh.

NAQVI, S. M. & ROGERS, J. J. W. (1987) *Precambrian geology of India,* New York, Oxford Univ. Press [u.a.].

NARAIN, H. & SUBRAHMANYAM, C. (1986) Precambrian Tectonics of the South Indian Shield Inferred from Geophysical Data. *The Journal of Geology,* 94**,** 187-198.

NASH, D. J. & MCLAREN, S. J. (2011) *Geochemical sediments and landscapes*, John Wiley & Sons.

NEGREL, P., ALLEGRE, C. J., DUPRE, B. & LEWIN, E. (1993) Erosion sources determined by inversion of major and trace element ratios and strontium isotopic ratios in river water: The Congo Basin case. *Earth and Planetary Science Letters,* 120**,** 59-76.

NESBITT, H. W. & YOUNG, G. M. (1982) Early Proterozoic climates and plate motions inferred from major element chemistry of lutites. *Nature,* 299**,** 715-717.

NESBITT, H. W. & YOUNG, G. M. (1984) Prediction of some weathering trends of plutonic and volcanic rocks based on thermodynamic and kinetic considerations. *Geochimica et Cosmochimica Acta,* 48**,** 1523-1534.

NOAA (2012).

OHTA, T. & ARAI, H. (2007) Statistical empirical index of chemical weathering in igneous rocks: A new tool for evaluating the degree of weathering. *Chemical Geology,* 240**,** 280-297.

OLIVER, L., HARRIS, N., BICKLE, M., CHAPMAN, H., DISE, N. & HORSTWOOD, M. (2003) Silicate weathering rates decoupled from the 87Sr/86Sr ratio of the dissolved load during Himalayan erosion. *Chemical Geology,* 201**,** 119-139.

PARKER, A. (1970) An Index of Weathering for Silicate Rocks. *Geological Magazine,* 107**,** 501-504.

PARKHURST, D. L., AND APELLO, C.A.J. (2013) Description of input and examples for PHREQC version 3 - A computer program for speciation, batch-reaction, one-dimensional transport and inverse geochemical calculations. *U.S. Geological Survey Techniques and Methods, book 6.*

PASCOE, E. H. (1964) *A manual of the Geology of India and Burma.*, Government of India Press, Calcutta.

PATRO, B. P. K., HARINARAYANA, T., SASTRY, R. S., RAO, M., MANOJ, C., NAGANJANEYULU, K. & SARMA, S. V. S. (2005) Electrical imaging of Narmadaâ€"Son Lineament Zone, Central India from magnetotellurics. *Physics of the Earth and Planetary Interiors,* 148**,** 215-232.

PIPER, D., BAU, M. (2013) Normalised Rare Earth Elements in Water, Sediments, and Wine: Identifying Sources and Environmental Redox Conditions. *American Journal of Analytical Chemistry,* 4**,** 69-83.

PISTINER, J. S. & HENDERSON, G. M. (2003) Lithium-osotope fractionation during continental weathering processes. *Earth and Planetary Science Letters,* 214**,** 327-339.

POGGE VON STRANDMANN, P. A. E., BURTON, K. W., JAMES, R. H., VAN CALSTEREN, P. & GISLASON, S. U. R. (2010) Assessing the role of climate on uranium and lithium isotope behaviour in rivers draining a basaltic terrain. *Chemical Geology,* 270**,** 227-239.

POGGE VON STRANDMANN, P. A. E. & HENDERSON, G. M. (2015) The Li isotope response to mountain uplift. *Geology,* 43**,** 67-70.

POGGE VON STRANDMANN, P. A. E., JENKYNS, H. C. & WOODFINE, R. G. (2013) Lithium isotope evidence for enhanced weathering during Oceanic Anoxic Event 2. *Nature Geosci,* 6**,** 668-672.

PRICE, J. R. & VELBEL, M. A. (2003) Chemical weathering indices applied to weathering profiles developed on heterogeneous felsic metamorphic parent rocks. *Chemical Geology,* 202**,** 397-416.

PURNACHANDRA RAO, V., SHYNU, R., KESSARKAR, P. M., SUNDAR, D., MICHAEL, G. S., NARVEKAR, T., BLOSSOM, V. & MEHRA, P. (2011) Suspended sediment dynamics on a seasonal scale in the Mandovi and Zuari estuaries, central west coast of India. *Estuarine, Coastal and Shelf Science,* 91**,** 78-86.

RAVAL, U. & VEERASWAMY, K. (2011) Mapping of tectonic corridors through hidden parts of the Greater Dharwar Terrane, Southern India. *Journal of Asian Earth Sciences,* 42**,** 1210-1225.

RAVIZZA, G. & PEUCKER-EHRENBRINK, B. (2003) Chemostratigraphic evidence of Deccan volcanism from the marine osmium isotope record. *Science,* 302**,** 1392-1395.

RAYMO, M. E. & RUDDIMAN, W. F. (1992) Tectonic forcing of late Cenozoic climate. *Nature,* 359**,** 117-122.

RAYMO, M. E., RUDDIMAN, W. F. & FROELICH, P. N. (1988) Influence of late Cenozoic mountain building on ocean geochemical cycles. *Geology,* 16**,** 649-653.

RICHARDS, M. A., ALVAREZ, W., SELF, S., KARLSTROM, L., RENNE, P. R., MANGA, M., SPRAIN, C. J., SMIT, J., VANDERKLUYSEN, L. C. & GIBSON, S. A. (2015) Triggering of the largest Deccan eruptions by the Chicxulub impact. *Geological Society of America Bulletin***,** B31167. 1.

ROGERS, J. J. W. (1986) The Dharwar Craton and the Assembly of Peninsular India. *The Journal of Geology,* 94**,** 129-143.

RUDDIMAN, W. F. (1997) *Tectonic uplift and climate change,* New York, Plenum Press.

SAHASRABUDHE, Y. S. & DESHMUKH, S. S. (1981) The Laterites of Maharashtra State. . *Proceedings of the International Seminar on Lateritisation Processes.* Trivandrum, India 11-14 December, 1979.

SARIN, M. M. (2001) Biogeochemisrty of Himalayan rivers as an agent of climate change. *Current Science,* 81**,** 1146-1450.

SCHELLMANN, W. (2003) Discussion of "A critique of the Schellmann definition and classification of laterite" by R.P. Bourman and C.D. Ollier (Catena 47, 117-131). *CATENA,* 52**,** 77-79.

SCOTESE, C. R. (2001) Atlas of Earth History, Volume 1,Paleogeography, PALEOMAP Project, Arlington, Texas, 52 pp.

SMOLDERS, A. J. P., HUDSON-EDWARDS, K. A., VAN DER VELDE, G. & ROELOFS, J. G. M. (2004) Controls on water chemistry of the Pilcomayo river (Bolivia, South-America). *Applied Geochemistry,* 19**,** 1745-1758.

SPICER, R. A., HARRIS, N. B. W., WIDDOWSON, M., HERMAN, A. B., GUO, S., VALDES, P. J., WOLFE, J. A. & KELLEY, S. P. (2003) Constant elevation of southern Tibet over the past 15 million years. *Nature,* 421**,** 622-624.

STALLARD, R. F. & EDMOND, J. M. (1981) Geochemistry of the Amazon: 1. Precipitation chemistry and the marine contribution to the dissolved load at the time of peak discharge. *Journal of Geophysical Research: Oceans (1978â€“2012),* 86**,** 9844-9858.

STALLARD, R. F. & EDMOND, J. M. (1983) GEOCHEMISTRY OF THE AMAZON 2. THE INFLUENCE OF GEOLOGY AND WEATHERING ENVIRONMENT ON THE DISSOLVED LOAD. *J. Geophys. Res.,* 88**,** 9671-9688.

STOREY, M., MAHONEY, J. J., SAUNDERS, A. D., DUNCAN, R. A., KELLEY, S. P. & COFFIN, M. F. (1995) Timing of Hot Spot Related Volcanism and the Breakup of Madagascar and India. *Science,* 267**,** 852-855.

SUBRAMANIAN, V. (2000) *Water : quantity-quality perspective in south Asia,* Surrey, U.K., Kingston International.

SUMMERFIELD, M. A. (1991) *Global Geomorphology*, Prentice Hall.

SWAMI NATH, J. & RAMAKRISHNAN, M. (1976) Dharwar stratigraphic model and Karnataka craton evolution. *Geological Survey of India,* 107**,** 149-175.

TAYLOR, A. S. & LASAGA, A. C. (1999) The role of basalt weathering in the Sr isotope budget of the oceans. *Chemical Geology,* 161**,** 199-214.

THOMAS, M. F. (1994) *Geomorphology of the tropics,* Chichester, Wiley.

TORRES, M. A., WEST, A. J. & LI, G. (2014) Sulphide oxidation and carbonate dissolution as a source of CO2 over geological timescales. *Nature,* 507**,** 346-349.

UNESCO (1993) Discharge of selected rivers of the world. *UNESCO*.

UNNIKRISHNAN, A. S., SHETYE, S. R. & GOUVEIA, A. D. (1997) Tidal Propagation in the Mandovi-Zuari Estuarine Network, West Coast of India: Impact of Freshwater Influx. *Estuarine, Coastal and Shelf Science,* 45**,** 737-744.

VANDAMME, D., COURTILLOT, V., BESSE, J. & MONTIGNY, R. (1991) Paleomagnetism and age determinations of the Deccan Traps (India): Results of a Nagpur-Bombay Traverse and review of earlier work. *Rev. Geophys.,* 29**,** 159-190.

VELBEL, M. A. (1993) Temperature dependence of silicate weathering in nature; how strong a negative feedback on long-term accumulation of atmospheric CO 2 and global greenhouse warming? *Geology,* 21**,** 1059-1062.

VIERS, J., OLIVA, P., DANDURAND, J. L., DUPRÃ©, B., GAILLARDET, J., EDITORS-IN-CHIEF:Â Â HEINRICH, D. H. & KARL, K. T. (2007) 5.20 - Chemical Weathering Rates, CO2 Consumption, and Control Parameters Deduced from the Chemical Composition of Rivers. *Treatise on Geochemistry.* Oxford, Pergamon.

WALKER, J. C. G., HAYS, P. B. & KASTING, J. F. (1981) A negative feedback mechanism for the long-term stabilization of Earth's surface temperature. *Journal of Geophysical Research: Oceans,* 86**,** 9776-9782.

WATTS, A. B. & COX, K. G. (1989) The Deccan Traps: an interpretation in terms of progressive lithospheric flexure in response to a migrating load. *Earth and Planetary Science Letters,* 93**,** 85-97.

WEST, A. J., GALY, A. & BICKLE, M. (2005) Tectonic and climatic controls on silicate weathering. *Earth and Planetary Science Letters,* 235**,** 211-228.

WIDDOWSON, M. (1997) Tertiary palaeosurfaces of the SW Deccan, Western India: implications for passive margin uplift. *Geological Society, London, Special Publications,* 120**,** 221-248.

WIDDOWSON, M. (2008) Laterite and Ferricrete. *Geochemical Sediments and Landscapes.* Blackwell Publishing Ltd.

WIDDOWSON, M. (2009) Evolution of Laterite in Goa. IN MASCARENHAS, A. A. K., GLENN (Ed.) *Natural Resources of Goa: A geological perspective. .* India: Geological Society of Goa.

WIDDOWSON, M. & COX, K. G. (1996) Uplift and erosional history of the Deccan Traps, India: Evidence from laterites and drainage patterns of the Western Ghats and Konkan Coast. *Earth and Planetary Science Letters,* 137**,** 57-69.

WIDDOWSON, M. & GUNNEL, Y. (1999) Lateritization, geomorphology and geodynamics of a passive continental margin: the Konkan and Kanara lowlands of western peninsular India. *Spec. Publs int. Ass. Sediment,* 27**,** 245-274.

WIDDOWSON, M., PRINGLE, M. S. & FERNANDEZ, O. A. (2000) A Post K-T Boundary (Early Palaeocene) Age for Deccan-type Feeder Dykes, Goa, India. *J. Petrology,* 41**,** 1177-1194.

WIMPENNY, J., GÃSLASON, S. U. R., JAMES, R. H., GANNOUN, A., POGGE VON STRANDMANN, P. A. E. & BURTON, K. W. (2010) The behaviour of Li and Mg isotopes during primary phase dissolution and secondary mineral formation in basalt. *Geochimica et Cosmochimica Acta,* 74**,** 5259-5279.

Appendix A – Sampling record sheet

SAMPLING RECORD SHEET

Date:	01/09/07	Time:	10.05	Sample site:	CHA 01
Weather conditions:		Raining			
Comments:					
Air temperature:	25.9 ºC	Flow rate:	Fast		
Dissolved Oxygen:	101.0 %	Water temperature:	24.2 ºC	Pressure:	995 mbar
Conductivity:	19 µS cm^{-1}	Water temperature:	24.0 ºC	pH:	5.93
Bicarbonate: 1st run 100ml		Bicarbonate: 2nd run 100ml		Bicarbonate: 3rd run 100ml	
pH	Units	pH	Units	pH	Units
6.56	0	6.19	0	6.44	0
3.84	5	5.04	2	5.02	2
3.53	10	4.33	4	4.61	4
3.39	15	4.08	6	4.09	6
3.29	20	3.91	8	3.92	8
3.29	25	3.72	10	3.83	10
		3.67	12	3.78	12
		3.57	14	3.77	14
		3.55	16	3.72	16
		3.50	18	3.67	18
		3.41	20	3.56	20

Appendix B - Sampling methodology

B.1 Dissolved Oxygen:

- Switch on:
- Message 'O_2 Sensor 0 days remaining' is displayed – press the tick button to clear
- Remove the cap from the probe (Note there is silica gel in the cap)
- Place the probe into the running water and press the tick button again – meter shows the word 'stabilizing' eventually the meter will beep 3 times.
- Record the percentage O_2, the water temperature and the atmospheric pressure on the record sheet supplied.
- If you wish to do another reading press the tick button.

To Calibrate the Dissolved Oxygen meter:

This shouldn't need to be done too often (say once every 6 months). The calibration needs to be done on water with 100% O_2. This can be achieved using a fish tank and electric pump to aerate the water for a couple of hours.

- Press button 5.
- Scroll to 'O_2 calibration' and press the tick button.
- Insert probe into aerated water and press the tick button.
- Dry the probe with a tissue and replace cap.
- Switch meter off.

B. 2 Conductivity meter: (Small blue meter)

- Press the on/mode button.
- Screen immediately shows battery condition and then changes to show temperature and µS.
- Remove the cap and place probe into sample and stir gently <u>(do not submerge below waterproof line).</u>
- Record value in µS cm^{-1} on record sheet provided.
- Rinse with distilled water and dry off with a tissue.
- Replace cap and ensure the meter is switched off.

B. 3 pH meter: (Calibrate every day!)

- Switch the meter ‘on’.
- Carefully remove the electrode from its pH4 solution.
- Rinse the electrode in distilled water.
- Press the ‘cal’ button.
- Submerge probe in 1st buffer (use pH7 first) and press read, it will beep when it has finished.
- The meter then asks for standard 2, submerge in second buffer (pH4) and press read, again the meter will beep when finished.
- The meter then asks for a 3rd standard, this is usually pH10 but will not be required here – press exit.
- Screen comes up with slope (theoretical is -58.0) if satisfied press ‘read’ to store the calibration.
- Rinse probe in distilled water, dry with a tissue and make certain the meter is switched off.
- Carefully re-insert probe into its pH4 solution.

Taking readings:

- Switch on.
- Press ‘read’.
- Insert probe into sample and stir gently (the probe is very fragile take great care)
- The meter should beep when stabilized; however, an average can be taken if the reading appears to fluctuate slightly.
- Rinse the probe with distilled water between samples (not necessary during titration)
- Always carefully store the probe in the pH4 solution to keep the probe ‘sharp’

B. 4 Titration: (Wear gloves for this as acid is quite strong)

- Carefully slide 1.6N H_2SO_4 acid bottle onto the end of titrator.
- Rotate ¼ turn to lock in place.
- Remove cap and insert tube half to 2/3 into end of acid bottle.
- Rotate the small screw on the end to push acid through the tube.
- Make sure a steady flow of acid drips from the end and no air bubbles are present.
- Reset the meter to zero using the screw on the acid bottle side of the titrator.

- You are now set to go!

- Add 50ml of sample water to the glass beaker.
- Measure and record the pH on the record sheet provided.
- Add say 20 units of acid to the beaker.
- Measure and record the pH on the record sheet provided.
- Continue as above until the pH reads 4.88 or less.
- Add a further 20 units of acid to ensure the reading continues to decrease.

- Obtain a fresh sample and repeat for 2nd run, but now add acid units to say 20 below previous 4.88 reading then add 2 units at a time. This should produce an accurate record of the inflection point.

- Obtain a fresh sample and repeat as above.

B. 5 Water sampling:

It is imperative that duplicates and blanks are taken at each sampling session. One session is taken to mean the sampling of all sites on one river. The following regime is suggested:

It is intended that there are at least 6 sites per river. Of these 6 sites 4 should be sampled for just anions and cations and the other 2 sites should be sampled for anions, cations, a duplicate of each and a blank. The blank will be deionised water.

- Prepare two bottles; one for anions and one for cations. (Duplicates and blanks as required).
- Add two drops of 50% Nitric acid to the cation bottle/bottles prior to adding the sample.

- The sampled water should be drawn into the syringe and filtered into the bottles through a 5µm filter and a 2µm filter (passing through the 5µm filter first). The filters should not need to be replaced every time!
- It is important to overfill the bottle to make sure that no bubbles are left in the sample.
- Place a sheet of cling film over the bottle and firmly secure the screw top lid.
- Label the bottle using the sticky labels provided and tape over them using clear tape.
- Place in a samples bag and label the sample bag.

Appendix C – Geomorphological survey sheet

GEOMORPHOLOGY SURVEY SHEET							
Date: 13/03/09		Time: 11.05		Sample site: Cha 01			
GPS location: 15º 47.805' N : 74º 06.074' E							
Comments:							
Elevation							
GPS	91 m	Barometric	104 m	Map		Google	
River morphology							
Width	75 strides	Upstream direction	64 º	Downstream Direction	208 º		
River bed sediment							
The river bed is dominated by large cobbles, boulders and pebbles of various lithologies and coarse sand. Cha 01 S1 09 is a sample of this sand. Cha 01 S2 09 is a sample of a small in-situ outcrop located on the left bank of the river when looking upstream.							
Samples retrieved							
Cha 01 S1 09	Cha 01 S2 09						
Vegetation							
Sparse		Moderate		Dense	X		
Vegetation type							
Plantation		Rice field		Jungle	X		
Vegetation description							
Mainly jungle with 2-3% banana & palm plantation. The pebble bars are heavily vegetated with c.1.5 m tall shrubs / bushes.							
Local geomorphological setting (>km scale)							
Upstream the foothills of the Western Ghats can be seen							
Local geomorphological setting (<km scale)							
There are range of hills running parallel to the river at this location on the left looking upstream							
Other							

Appendix D – Ion Chromatography tray template

Birkbeck UNIVERSITY OF LONDON		Ion Chromatography tray template						Birkbeck UNIVERSITY OF LONDON	
Standard 1	Standard 2	Standard 3							Standard 3
1	2	3	4	5	6	7	8	9	10
Ion 96.3									Standard 3
11	12	13	14	15	16	17	18	19	20
Lab Blank 1									Standard 3
21	22	23	24	25	26	27	28	29	30
Ion 96.3									Standard 3
31	32	33	34	35	36	37	38	39	40
Lab Blank 1									Standard 3
41	42	43	44	45	46	47	48	49	50
Ion 96.3									Standard 3
51	52	53	54	55	56	57	58	59	60
Lab Blank 1									Standard 3
61	62	63	64	65	66	67	68	69	70
Ion 96.3									Standard 3
71	72	73	74	75	76	77	78	79	80
Lab Blank 1									Standard 3
81	82	83	84	85	86	87	88	89	90
Ion 96.3									Standard 3
91	92	93	94	95	96	97	98	99	100

Appendix E – ICP-MS tray template

Birkbeck UNIVERSITY OF LONDON	ICP-MS tray template							Birkbeck UNIVERSITY OF LONDON	
Standard									
1	2	3	4	5	6	7	8	9	10
11	12	13	14	15	16	17	18	19	20
									Standard
21	22	23	24	25	26	27	28	29	30
31	32	33	34	35	36	37	38	39	40
41	42	43	44	45	46	47	48	49	50
									Standard
51	52	53	54	55	56	57	58	59	60

Appendix F – Comparison of Duplicates

Table F1: Precision of duplicates for major anions and cations for April 2008

Sample	Anions (mg l)				Major Cations (ppb or µg/l)					
	F	**Cl**	**NO_3**	**SO_4**	**Na**	**K**	**Mg**	**Ca**	**Al**	**Si**
CHA 2A	0.0983	5.709	-	1.4066	4054	494.4	1592	5116	6.448	2101
CHA 2A DUP	-	-	-	-	3871	492.8	1543	5058	5.983	2025
% DIFF	-	-	-	-	-5	0	-3	-1	-8	-4
STDEV/AV	-	-	-	-	3	0	2	1	5	3
CHA 3A	0.1814	4.5927	0.4734	1.3786	4558	827.2	1865	5516	7.365	3545
CHA 3A DUP	0.1075	4.6162	0.4303	1.9298	3900	679.2	2022	5703	3.957	3842
% DIFF	-69	1	-10	29	-17	-22	8	3	-86	8
STDEV/AV	36	0	7	24	11	14	6	2	43	6
ZUA 2A	0.0986	5.2378	0.4127	0.9484	3564	422.7	2904	7616	2.56	3385
ZUA 2A DUP	0.0826	5.1834	0.7623	1.056	3285	394.6	2668	7134	1.85	3070
% DIFF	-19	-1	46	10	-8	-7	-9	-7	-38	-10
STDEV/AV	12	1	42	8	6	5	6	5	23	7
ZUA 3A	0.1	9.0892	0.4516	2.1002	5267	517.7	1564	3278	10.2	2638
ZUA 3A DUP	0.082	8.6136	-	2.0323	5120	614.2	1521	3151	6.051	3202
% DIFF	-22	-6	-	-3	-3	16	-3	-4	-69	18
STDEV/AV	14	4	-	2	2	12	2	3	36	14
RANGE: % DIFF	19 - 9	1 - 6	10 - 46	3 - 29	3 - 17	0 - 22	3 -9	1 - 7	8 -86	4 -18
RANGE :STDEV/AV	12 - 36	0 - 4	7 - 42	2 - 24	3 - 11	0 - 14	2 - 6	1 -5	5 - 43	3 - 14

Table F2: Precision of duplicates for major anions and cations for May 2008

Sample	Anions (mg l)				Major Cations (ppb or µg/l)					
	F	**Cl**	**NO_3**	**SO_4**	**Na**	**K**	**Mg**	**Ca**	**Al**	**Si**
CHA 2A	0.3151	4.6875	-	1.0903	3201	427.3	1444	4861	7.395	1402
CHA 2A DUP	0.2532	4.9576	-	1.8466	3213	442.5	1438	4796	7.797	1412
% DIFF	-24	5	-	41	0	3	0	-1	5	1
STDEV/AV	15	4	-	36	0	2	0	1	4	1
CHA 3A	0.2222	4.4275	-	1.3188	3574	656	1699	5024	4.539	2931
CHA 3A DUP	0.2214	4.5339	-	1.135	3618	568.4	1857	5349	3.975	3115
% DIFF	0	2	-	-16	1	-15	9	6	-14	6
STDEV/AV	0	2	-	11	1	10	6	4	9	4
ZUA 2A	0.2973	6.0328	0.642	1.1183						
ZUA 2A DUP	0.1175	6.1498	0.525	1.0911						
% DIFF	-153	2	-22	-2						
STDEV/AV	61	1	14	2						
ZUA 3A	0.0891	7.0247	0.6836	1.7312						
ZUA 3A DUP	0.0668	7.223	0.3207	1.7426						
% DIFF	-33	3	-113	1						
STDEV/AV	20	2	51	0						
RANGE: % DIFF	0 - 153	2 - 5	22-113	1 - 41	0 -1	3 - 15	0 - 9	1 - 6	5 - 14	1 - 6
RANGE :STDEV/AV	0 - 61	1 - 4	14 - 51	0 - 36	0 -1	2 -10	0 - 6	1 - 4	4 - 9	1 - 4

Table F3: Precision of duplicates for major anions and cations for June 2008

Sample	Anions (mg l)				Major Cations (ppb or µg/l)					
	F	**Cl**	**NO_3**	**SO_4**	**Na**	**K**	**Mg**	**Ca**	**Al**	**Si**
CHA 2A	0.2201	6.2871	1.6436	1.6938	4671	997.7	2241	5485	16.54	5447
CHA 2A DUP	0.0791	6.2546	-	1.8776	4363	994.3	2089	4917	18.87	4986
% DIFF	-178	-1	-	10	-7	0	-7	-12	12	-9
STDEV/AV	67	0	-	7	5	0	5	8	9	6
CHA 3A	0.0879	5.8642	2.5581	1.9558	4483	962.1	2302	5395	8.917	5404
CHA 3A DUP	0.1083	5.8598	1.1798	1.9814	4670	974.1	2026	5635	9.531	5605
% DIFF	19	0	-117	1	4	1	-14	4	6	4
STDEV/AV	15	0	52	1	3	1	9	3	5	3
ZUA 2A	0.0834	4.3462	0.3257	1.3073	3960	801.2	1595	3870	17.62	3735
ZUA 2A DUP	0.0939	4.2282	0.5484	1.276	3909	811.3	1652	3990	5.643	4317
% DIFF	11	-3	41	-2	-1	1	3	3	-212	13
STDEV/AV	8	2	36	2	1	1	2	2	73	10
ZUA 3A	0.1254	4.1721	-	0.9112	3510	1040	1271	3287	42.79	3032
ZUA 3A DUP	0.2366	4.042	-	1.3336	3322	1032	1289	3214	60	3752
% DIFF	47	-3	-	32	-6	-1	1	-2	29	19
STDEV/AV	43	2	-	27	4	1	1	2	24	15
RANGE: % DIFF	1 - 178	0 - 3	41-117	1 - 32	1 - 7	0 - 1	1 - 14	2 - 12	6 - 212	4 - 19
RANGE :STDEV/AV	8 - 67	0 - 2	36 - 52	1 - 27	1 - 5	0 - 1	1 - 9	2 - 8	5 - 73	3 - 15

Table F4: Precision of duplicates for major anions and cations for July 2008

Sample	Anions (mg l)				Major Cations (ppb or µg/l)					
	F	**Cl**	**NO_3**	**SO_4**	**Na**	**K**	**Mg**	**Ca**	**Al**	**Si**
CHA 2A	0.0759	5.3306	0.5273	1.4469	3839	463	1771	4202	13.47	5288
CHA 2A DUP	0.0783	5.0127	-	1.3686	3913	444.6	1786	4194	10.02	5378
% DIFF	3	-6	-	-6	2	-4	1	0	-34	2
STDEV/AV	2	4	-	4	1	3	1	0	21	1
CHA 3A	0.2142	5.1549	-	1.3623	3972	503.2	1772	4115	23.6	5182
CHA 3A DUP	0.1387	5.4105	-	1.246	3838	459	1778	4095	11.6	5240
% DIFF	-54	5	-	-9	-3	-10	0	0	-103	1
STDEV/AV	30	3	-	6	2	6	0	0	48	1
ZUA 2A	0.2156	4.5725	-	1.2217	4503	515.9	1643	3325	13.14	4265
ZUA 2A DUP	0.0628	4.8485	0.6388	1.0416	4507	521.4	1674	3339	3.722	4271
% DIFF	-243	6	-	-17	0	1	2	0	-253	0
STDEV/AV	78	4	-	11	0	1	1	0	79	0
ZUA 3A	0.087	5.6782	-	1.1806	4968	516.7	1778	3796	16.53	4424
ZUA 3A DUP	0.0635	5.2826	-	1.1111	4669	498.7	1703	3642	7.185	4272
% DIFF	-37	-7	-	-6	-6	-4	-4	-4	-130	-4
STDEV/AV	22	5	-	4	4	3	3	3	56	2
RANGE: % DIFF	3 - 243	3 - 7	-	4 - 17	0 - 6	1 - 10	0 - 4	0 - 4	34 - 253	0 - 4
RANGE :STDEV/AV	2 - 78	3 - 5	-	4 - 11	0 - 4	1 - 6	0 - 3	0 - 3	21 - 79	0 - 2

Table F5: Precision of duplicates for trace elements for April 2008

Sample	Rb	Sr	V	Cr	Mn	Fe	Co	Ni	Cu	Zn	Pb	Ba
CHA 2	0.7856	20.82	0.5773	0.1419	10.58	7.309	0.0298	0.3176	0.7261	17.42	0.04591	47.93
CHA 2 DUP	0.4861	20.11	0.5403	0.2807	10.64	8.081	0.03014	0.4097	0.743	55.07	0.08028	140.7
% DIFF	-62	-4	-7	49	1	10	1	22	2	68	43	66
STDEV/AV	33	2	5	46	0	7	1	18	2	73	39	70
CHA 3	0.7286	23.55	0.4402	0.5112	31.77	10.12	0.09209	4.358	2.438	53.35	0.2854	175.2
CHA 3 DUP	0.9752	23.57	0.459	0.2113	33.21	13.45	0.04588	0.8835	1.12	33.68	0.126	112.3
% DIFF	25	0	4	-142	4	25	-101	-393	-118	-58	-127	-56
STDEV/AV	20	0	3	59	3	20	47	94	52	32	55	31
ZUA 2	1.097	19.42	0.09445	0.1244	157.7	13.61	0.03088	0.26	1.153	7.737	0.1267	3.202
ZUA 2 DUP	1.037	18.13	0.07771	0.06221	147.6	10.91	0.02673	0.2321	1.117	6.099	0.1037	3.091
% DIFF	-6	-7	-22	-100	-7	-25	-16	-12	-3	-27	-22	-4
STDEV/AV	4	5	14	47	5	16	10	8	2	17	14	2
ZUA 3	0.8182	15.03	0.1743	0.09181	61.02	16.38	0.03703	0.7069	1.365	20.2	0.4017	5.273
ZUA 3 DUP	0.9428	14.31	0.1073	0.1472	111	16.36	0.1367	0.4574	1.437	22.25	0.3435	5.288
% DIFF	13	-5	-62	38	45	0	73	-55	5	9	-17	0
STDEV/AV	10	3	34	33	41	0	81	30	4	7	11	0
RANGE: % DIFF	6 - 62	0 - 7	4 - 62	38 - 142	1 - 45	0 - 25	1 - 101	12 - 393	2 - 118	9 - 68	17 - 127	0 - 66
RANGE :STDEV/AV	4 - 33	0 - 5	3 - 34	33 - 59	0 - 41	0 - 20	1 - 47	8 - 94	2 - 52	7 - 73	11 - 55	0 - 70

Table F6: Precision of duplicates for REE for April 2008

Sample	La	Ce	Pr	Nd	Sm	Eu	Gd	Tb	Dy	Ho	Er	Tm	Yb	Lu
CHA 2	0.0047	0.0079	0.0014	0.0043	0.0009	0.0016	0.0008	0.0003	0.0029	0.0000	0.0003	-	0.0013	0.0003
CHA 2 DUP	0.0067	0.0069	0.0007	0.0048	0.0018	0.0058	0.0022	0.0003	0.0020	0.0001	-	-	0.0008	0.0000
% DIFF	29	-15	-94	11	50	72	63	25	-42	50	-	-	-75	700
STDEV/AV	24	10	45	8	47	80	64	20	24	47	-	-	39	198
CHA 3	0.0099	0.0151	0.0021	0.0082	0.0051	0.0048	0.0019	0.0003	0.0015	0.0006	0.0004	0.0002	0.0035	0.0004
CHA 3 DUP	0.0074	0.0117	0.0015	0.0050	0.0018	0.0044	0.0022	0.0002	0.0022	0.0001	0.0001	0.0001	0.0029	0.0002
% DIFF	-34	-28	-41	-65	-183	-10	12	-60	31	-333	-200	-67	-20	-80
STDEV/AV	20	18	24	35	68	6	9	33	26	88	71	35	13	40
ZUA 2	0.0128	0.0050	0.0012	0.0017	0.0028	0.0009	0.0000	0.0001	0.0001	0.0000	-	0.0003	0.0017	0.0002
ZUA 2 DUP	0.0105	0.0041	0.0012	0.0009	0.0015	0.0005	-	0.0000	0.0015	0.0002	0.0002	-	0.0020	0.0002
% DIFF	-22	-20	0	-100	-83	-71	-	-200	90	75	-	-	17	17
STDEV/AV	14	13	0	47	42	37	-	71	116	85	-	-	13	13
ZUA 3	0.0293	0.0430	0.0047	0.0222	0.0045	0.0017	0.0042	0.0003	0.0019	0.0005	0.0023	0.0005	0.0022	0.0004
ZUA 3 DUP	0.0215	0.0289	0.0039	0.0173	0.0028	0.0012	0.0033	0.0001	0.0033	0.0005	0.0003	0.0003	0.0008	0.0001
% DIFF	-36	-49	-21	-28	-64	-44	-29	-200	41	-8	-567	-33	-160	-233
STDEV/AV	22	28	14	18	34	25	18	71	36	5	105	20	63	76
RANGE: % DIFF	22 - 36	15 - 49	0 - 94	11 - 100	50 - 183	10 - 72	12 - 63	25 - 200	31 - 90	8 - 333	200 - 567	33 - 67	17 - 160	17 - 700
RANGE :STDEV/AV	14 - 24	10 - 28	0 - 45	8 - 47	34 - 68	6 - 80	9 - 64	20 - 71	24 - 116	5 - 88	71 - 105	20 - 35	13 - 63	13 - 198

Table F7: Precision of duplicates for trace elements for May 2008

Sample	Rb	Sr	V	Cr	Mn	Fe	Co	Ni	Cu	Zn	Pb	Ba
CHA 2	0.9554	18.95	0.4675	0.1505	6.856	2.31	0.01046	0.226	1.064	6.613	0.2531	4.377
CHA 2 DUP	0.9556	18.46	0.4702	0.1953	7.238	6.817	0.01181	0.2518	1.169	11.14	0.194	4.08
% DIFF	0	-3	1	23	5	66	11	10	9	41	-30	-7
STDEV/AV	0	2	0	18	4	70	9	8	7	36	19	5
CHA 3	1.25	20.96	0.4268	0.318	13.73	15.13	0.01945	0.2402	0.7701	5.771	0.273	6.545
CHA 3 DUP	1.19	22.21	0.4323	0.1163	14.79	25.4	0.01799	0.1802	0.5405	4.798	0.04206	6.84
% DIFF	-5	6	1	-173	7	40	-8	-33	-42	-20	-549	4
STDEV/AV	3	4	1	66	5	36	6	20	25	13	104	3
ZUA 2												
ZUA 2 DUP												
% DIFF												
STDEV/AV												
ZUA 3												
ZUA 3 DUP												
% DIFF												
STDEV/AV												
RANGE: % DIFF	0 - 5	3 - 6	1	23 - 173	5 - 7	40 - 66	8 - 11	10 - 33	9 - 42	20 - 41	30 - 549	4 - 7
RANGE :STDEV/AV	0 - 3	2 - 4	0 - 1	18 - 66	4 - 5	36 - 70	6 - 9	8 - 20	7 - 25	13 - 36	19 - 104	3 - 5

Table F8: Precision of duplicates for REE for May 2008

Sample	La	Ce	Pr	Nd	Sm	Eu	Gd	Tb	Dy	Ho	Er	Tm	Yb	Lu
CHA 2	0.0121	0.0073	0.0013	0.0035	0.0030	0.0005	0.0030	0.0002	0.0012	0.0001	0.0001	-	0.0017	-
CHA 2 DUP	0.0138	0.0065	0.0013	0.0045	0.0024	0.0009	0.0019	0.0003	0.0015	0.0002	-	0.0003	0.0027	-
% DIFF	12	-13	3	22	-25	45	-57	43	22	25	-	-	36	-
STDEV/AV	9	9	2	18	16	42	31	39	18	20	-	-	31	-
CHA 3	0.0111	0.0131	0.0013	0.0060	0.0036	0.0009	0.0019	0.0003	0.0027	0.0004	-	0.0002	0.0021	-
CHA 3 DUP	0.0094	0.0116	0.0013	0.0058	0.0009	0.0010	0.0038	0.0003	0.0024	0.0003	-	0.0000	0.0023	-
% DIFF	-17	-13	3	-4	-300	8	50	25	-14	-50	-	600	8	-
STDEV/AV	11	8	2	3	85	6	47	20	9	28	-	212	6	-
ZUA 2	2.7965	0.0205	0.0068	0.0023	0.0078	0.0036	0.0019	0.0012	0.0019	0.0060	0.0026	0.0021	0.0033	-
ZUA 2 DUP	2.9377	0.0278	0.0098	0.0032	0.0065	0.0013	0.0014	0.0025	0.0031	0.0040	0.0030	0.0032	0.0020	0.0008
% DIFF	5	26	31	29	-19	-186	-37	52	37	-49	16	35	-64	-
STDEV/AV	3	21	26	24	12	68	22	50	32	28	12	30	34	-
ZUA 3	7.4680	0.0287	0.0422	0.0082	0.0297	0.0064	0.0043	0.0050	0.0061	0.0093	0.0043	0.0085	0.0044	-
ZUA 3 DUP	6.8494	0.0162	0.0281	0.0055	0.0107	-0.0006	0.0033	0.0018	0.0049	0.0040	0.0033	0.0022	0.0051	0.0004
% DIFF	-9	-77	-50	-49	-177	1125	-32	-173	-24	-131	-29	-293	15	-
STDEV/AV	6	39	28	28	66	172	20	66	15	56	18	84	11	-
RANGE: % DIFF	5 - 17	13 - 77	3 - 50	4 - 49	19 - 300	8 - 1125	32 - 57	25 - 173	14 - 37	25 - 131	16 - 29	35 - 600	8 - 64	-
RANGE :STDEV/AV	3 - 11	8 - 39	2 - 28	3 - 28	12 - 85	6 - 172	20 - 47	20 - 66	9 - 32	20 - 56	12 - 18	30 - 212	6 - 34	-

Table F9: Precision of duplicates for trace elements for June 2008

Sample	Rb	Sr	V	Cr	Mn	Fe	Co	Ni	Cu	Zn	Pb	Ba
CHA 2	1.066	23.79	0.8648	0.2216	22.53	-	0.1202	1.892	0.9968	4.231	0.2857	7.383
CHA 2 DUP	1.313	21.95	0.7946	3.346	22.91	6.559	0.2561	5.533	1.323	11.52	0.2389	7.186
% DIFF	19	-8	-9	93	2	-	53	66	25	63	-20	-3
STDEV/AV	15	6	6	124	1	-	51	69	20	65	13	2
CHA 3	1.362	23.58	0.693	0.6155	24.6	-	0.1269	2.268	1.34	4.985	0.1564	9.054
CHA 3 DUP	1.421	24.47	0.7365	0.6697	25.23	-	0.1136	1.794	1.33	4.005	0.1393	9.33
% DIFF	4	4	6	8	2	-	-12	-26	-1	-24	-12	3
STDEV/AV	3	3	4	6	2	-	8	17	1	15	8	2
ZUA 2	1.544	14.85	0.1581	0.2916	213	4.544	0.2379	1.461	1.575	13.29	0.2673	5.574
ZUA 2 DUP	1.544	14.72	0.1117	-	220.2	4.571	0.2208	0.7399	1.219	9.732	0.2474	5.486
% DIFF	0	-1	-42	-	3	1	-8	-97	-29	-37	-8	-2
STDEV/AV	0	1	24	-	2	0	5	46	18	22	5	1
ZUA 3	1.703	16.33	0.7241	2.185	188.5	40.29	0.3402	1.809	1.431	9.057	0.4197	9.976
ZUA 3 DUP	1.715	15.8	0.5551	1.662	188.7	60.87	0.309	0.9983	1.053	5.707	0.3023	9.714
% DIFF	1	-3	-30	-31	0	34	-10	-81	-36	-59	-39	-3
STDEV/AV	0	2	19	19	0	29	7	41	22	32	23	2
RANGE: % DIFF	0 - 19	1 - 8	6 - 42	8 - 93	0 - 3	1 - 34	8 - 53	26 - 97	1 - 36	24 - 63	8 - 39	2 - 3
RANGE :STDEV/AV	0 - 15	1 - 6	4 - 24	6 - 124	0 - 2	0 - 29	5 - 51	17 - 69	1 - 22	15 - 65	5 - 23	1 - 2

Table F10: Precision of duplicates for REE for June 2008

Sample	La	Ce	Pr	Nd	Sm	Eu	Gd	Tb	Dy	Ho	Er	Tm	Yb	Lu
CHA 2	0.0554	0.0633	0.0102	0.0366	0.0087	0.0034	0.0098	0.0016	0.0147	0.0007	0.0048	0.0013	0.0068	-
CHA 2 DUP	0.0626	0.0605	0.0082	0.0386	0.0106	0.0047	0.0098	0.0010	0.0079	0.0017	0.0048	0.0009	0.0050	0.0002
% DIFF	12	-5	-24	5	18	29	0	-60	-86	58	0	-46	-38	-
STDEV/AV	9	3	15	4	14	24	0	33	43	58	0	27	22	-
CHA 3	0.0487	0.0545	0.0096	0.0337	0.0067	0.0028	0.0098	0.0003	0.0109	0.0011	0.0029	0.0003	0.0068	0.0000
CHA 3 DUP	0.0518	0.0726	0.0102	0.0498	0.0063	0.0036	0.0067	0.0010	0.0087	0.0013	0.0050	0.0007	0.0053	0.0001
% DIFF	6	25	6	32	-8	22	-47	67	-25	21	42	60	-29	100
STDEV/AV	4	20	4	27	5	18	27	71	16	17	37	61	18	141
ZUA 2	0.0422	0.0368	0.0090	0.0322	0.0095	0.0064	0.0139	0.0056	0.0065	0.0058	0.0058	-0.0163	0.0090	0.0039
ZUA 2 DUP	0.0196	0.0177	0.0068	0.0216	0.0136	0.0027	0.0139	0.0026	0.0062	0.0027	0.0023	-0.0262	0.0030	0.0011
% DIFF	-116	-108	-32	-49	30	-135	0	-118	-5	-118	-150	38	-200	-264
STDEV/AV	52	50	20	28	25	57	0	53	3	52	61	-33	71	80
ZUA 3	0.1353	0.2474	0.0278	0.1217	0.0325	0.0076	0.0266	0.0042	0.0205	0.0068	0.0120	-	0.0097	0.0024
ZUA 3 DUP	0.1498	0.2803	0.0339	0.1494	0.0361	0.0068	0.0368	0.0047	0.0202	0.0071	0.0130	-	0.0130	0.0021
% DIFF	10	12	18	19	10	-12	28	11	-2	4	7	-	26	-14
STDEV/AV	7	9	14	14	7	8	23	9	1	3	5	-	21	9
RANGE: % DIFF	6 - 112	5 - 108	6 - 32	5 - 49	8 - 30	12 - 135	0 - 47	11 - 118	2 - 86	4 - 118	0 - 150	38 - 60	26 - 200	14 - 264
RANGE :STDEV/AV	4 - 52	3 - 50	4 - 20	4 - 28	5 - 25	8 - 57	0 - 27	9 - 71	1 - 43	3 - 58	0 - 61	27 - 61	18 - 71	9 - 141

Table F11: Precision of duplicates for trace elements for July 2008

Sample	Rb	Sr	V	Cr	Mn	Fe	Co	Ni	Cu	Zn	Pb	Ba
CHA 2	0.7538	19.35	0.7606	0.4408	8.607	-	0.04357	0.5795	2.027	5.406	0.3586	5.952
CHA 2 DUP	0.7166	19.48	0.7703	0.5486	8.457	-	0.03902	0.5649	1.969	4.043	0.331	6.165
% DIFF	-5	1	1	20	-2	-	-12	-3	-3	-34	-8	3
STDEV/AV	4	0	1	15	1	-	8	2	2	20	6	2
CHA 3	0.8642	20.15	0.8168	0.588	25.7	-	0.08586	0.7239	1.119	5.727	0.3269	6.885
CHA 3 DUP	0.7668	19.7	0.8601	0.3482	25.66	-	0.07828	0.4605	0.8623	3.046	0.1158	6.676
% DIFF	-13	-2	5	-69	0	-	-10	-57	-30	-88	-182	-3
STDEV/AV	8	2	4	36	0	-	7	31	18	43	67	2
ZUA 2	0.8168	13.42	0.1834	1.077	84.87	10.87	0.08629	38.92	4.568	16.36	0.8708	5.319
ZUA 2 DUP	0.8485	13.35	0.2024	0.2604	85.01	-	0.02013	0.6892	1.584	16.03	0.3608	5.89
% DIFF	4	-1	9	-314	0	-	-329	-5547	-188	-2	-141	10
STDEV/AV	3	0	7	86	0	-	88	136	69	1	59	7
ZUA 3	0.9126	17.4	0.2064	0.3874	123	33.86	0.1332	1.125	1.363	17.13	0.8921	8.084
ZUA 3 DUP	0.8577	16.59	0.146	0.3208	119.9	16.53	0.1265	1.419	1.352	20.88	0.952	8.012
% DIFF	-6	-5	-41	-21	-3	-105	-5	21	-1	18	6	-1
STDEV/AV	4	3	24	13	2	49	4	16	1	14	5	1
RANGE: % DIFF	4 - 13	1 - 5	1 - 41	20 - 314	0 - 3	105	5 - 329	3 - 5547	1 - 188	2 - 88	6 - 182	1 - 10
RANGE :STDEV/AV	3 - 8	0 - 3	1 - 24	13 - 86	0 - 2	49	4 - 88	2 - 136	1 - 69	1 - 43	5 - 67	1 - 7

Table F12: Precision of duplicates for REE for July 2008

Sample	La	Ce	Pr	Nd	Sm	Eu	Gd	Tb	Dy	Ho	Er	Tm	Yb	Lu
CHA 2	0.0688	0.0302	0.0059	0.0217	0.0060	0.0020	0.0073	0.0010	0.0034	0.0009	0.0028	0.0005	0.0029	0.0003
CHA 2 DUP	0.0854	0.0248	0.0050	0.0141	0.0023	0.0012	0.0038	0.0006	0.0015	0.0006	0.0018	0.0006	0.0022	0.0004
% DIFF	19	-22	-17	-55	-167	-59	-94	-80	-130	-44	-50	13	-31	22
STDEV/AV	15	14	11	30	64	32	45	40	56	25	28	9	19	18
CHA 3	0.0811	0.0506	0.0058	0.0309	0.0098	0.0015	0.0047	0.0005	0.0048	0.0011	0.0024	0.0007	0.0036	0.0002
CHA 3 DUP	0.0373	0.0385	0.0052	0.0207	0.0060	0.0020	0.0066	0.0007	0.0043	0.0010	0.0009	0.0006	0.0025	0.0003
% DIFF	-117	-31	-11	-49	-62	25	29	30	-10	-4	-163	-12	-40	14
STDEV/AV	52	19	7	28	34	20	24	25	7	3	63	8	24	11
ZUA 2	0.1097	0.0564	0.0108	0.0402	0.0171	0.0059	0.0192	0.0034	0.0072	0.0054	0.0074	-	0.0050	0.0050
ZUA 2 DUP	0.0852	0.0375	0.0045	0.0236	0.0101	0.0010	0.0080	0.0009	0.0053	0.0020	0.0028	-	-	0.0011
% DIFF	-29	-50	-139	-70	-71	-517	-140	-300	-35	-165	-167	-	-	-333
STDEV/AV	18	28	58	37	37	102	58	85	21	64	64	-	-	88
ZUA 3	0.0866	0.0625	0.0097	0.0453	0.0118	0.0032	0.0075	0.0016	0.0093	0.0032	0.0037	-	0.0070	0.0016
ZUA 3 DUP	0.0916	0.0562	0.0074	0.0342	0.0065	0.0017	0.0069	0.0005	0.0022	0.0015	-	-	0.0020	0.0008
% DIFF	5	-11	-31	-32	-82	-82	-8	-186	-329	-116	-	-	-250	-91
STDEV/AV	4	7	19	20	41	41	5	68	88	52	-	-	79	44
RANGE: % DIFF	5 - 117	11 - 50	11 - 139	32 - 70	62 - 167	25 - 517	8 - 140	30 - 300	10 - 329	4 - 165	50 - 167	12 - 13	31 - 250	14 - 333
RANGE :STDEV/AV	4 - 52	7 - 28	7 - 58	20 - 37	34 - 64	20 - 102	5 - 58	2 - 85	7 - 88	3 - 64	28 - 64	8 - 9	19 - 79	11 - 88

Appendix G – Elemental concentrations for the Chapora and Zuari Rivers.

The following pages provide major element concentration data for the Chapora River sampling sites Cha 01 to Cha 06 and the Zuari River sampling sites Zua 01 – Zua 06, and trace element and REE concentration data for localities Cha 01 to Cha 04 and Zua 01 to Zua 05 opt since no samples were analysed for Cha 05, Cha 06, Zua 05 or Zua 06 due to the observed estuarine influence at these localities.

Table G1 – Major element data for Chapora River sites Cha 01 – Cha 02.

Date of sampling	Discharge ($m^3 s^{-1}$)	T (°C)	pH	DO (%)	TDS (mg L^{-1})	EC (µS cm^{-1})	Na	K	Ca	Mg	F	Cl	NO_3^-	SO_4^{2-}	HCO_3^-	SiO_2	TZ^+	TZ^-	NICB (%)
							(µmol L^{-1})										(µeq L^{-1})		
Cha 01, (Lat:15° 47.795'N Long: 74° 06.072'E)																			
Jun- 07	153±24	28.5	6.66	81.8	79	47	298.0	35.3	275.7	156.3	6.3	178.0	10.6	25.5	760	56	1197.4	1005.9	9
Jul-07	95±15	25.3	6.52	102.1	44	15	227.1	14.6	120.3	74.9	6.3	173.8	13.1	18.4	340	55	631.9	569.9	5
Aug-07	123±19	24.0	6.38	102.2	26	19	149.2	13.3	95.3	60.1	8.9	106.1	7.6	14.9	180	77	473.3	332.3	17
Sep-07	109±17	24.0	5.93	101.0	17	19	151.4	16.6	99.3	63.8	5.8	104.1	13.5	13.3	20	81	494.2	170.1	49
Oct-07	11±2	-	-	-	21	-	235.8	17.1	150.7	104.1	11.1	151.8	-	13.9	-	277	762.5	190.7	60
Nov-07	11±2	-	-	-	-	-	-	-	-	-	-	-	-	-	-	-	-	-	-
Dec-07	0.1±0.02	23.8	6.93	100.3	-	42	-	-	-	-	-	-	-	-	-	-	-	-	-
Jan-08	0	23.0	6.40	94.6	24	25	251.0	14.1	147.0	76.5	16.8	137.4	20.3	12.5	30	121	712.0	229.5	51
Feb-08	0	21.6	6.90	91.7	28	23	582.9	18.9	125.5	97.9	-	178.3	-	-	10	104	1048.7	188.3	70
Mar-08	6±1	23.6	6.84	94.5	23	40	221.4	22.8	126.0	73.6	12.1	137.9	15.2	13.8	50	107	643.5	242.9	45
Apr-08	2±0.3	28.3	6.08	98.5	21	26	225.3	10.2	121.5	65.4	5.3	152.0	10.0	17.3	20	96	609.4	221.9	47
May-08	1.4±0.2	27.8	6.30	94.8	19	30	170.1	13.0	114.3	63.4	12.6	150.3	-	12.7	30	92	538.4	218.4	42
Jun-08	112±18	26.4	5.86	101.4	39	25	208.8	22.8	132.7	89.7	9.5	563.0	-	45.0	30	190	676.4	692.4	-1
Jul-08	77±12	26.0	5.91	100.9	20	28	189.7	26.3	108.0	76.5	4.2	147.5	0.0	13.5	30	191	585.1	208.8	47
Cha 02, (Lat:15° 45.999'N Long: 74° 04.746'E)																			
Jun- 07	195±24	29.0	6.76	70.0	54	92	174.9	30.2	169.4	98.7	6.8	155.1	16.0	26.0	500	12	741.4	730.0	1
Jul-07	121±15	25.9	6.47	105.5	36	23	182.7	14.1	104.3	72.4	11.1	174.0	16.9	19.5	260	87	550.2	500.9	5
Aug-07	156±19	25.6	6.57	107.7	35	17	146.2	16.6	84.3	57.6	5.8	101.8	7.3	12.5	340	62	446.7	479.8	-4
Sep-07	139±17	24.7	6.57	104.6	23	24	164.9	11.0	100.6	72.8	15.3	132.3	8.1	14.9	100	73	522.6	285.4	29
Oct-07	14±2	-	-	-	18	-	181.0	17.1	116.8	80.6	10.5	129.2	10.5	13.9	-	209	592.9	178.1	54
Nov-07	14±2	-	-	-	-	-	-	-	-	-	-	-	-	-	-	-	-	-	-
Dec-07	0.2±0.02	26.2	6.52	108.2	-	34	-	-	-	-	-	-	-	-	-	-	-	-	-
Jan-08	0	24.6	6.60	107.9	19	26	145.7	11.8	125.3	67.9	6.3	130.3	18.5	12.3	30	114	543.8	209.7	44
Feb-08	0	23.6	6.90	102.1	18	23	139.2	11.0	111.3	57.2	11.6	128.3	15.3	12.1	30	93	487.1	209.4	40
Mar-08	8±1	25.6	6.83	99.6	22	32	164.9	14.6	121.8	73.2	12.6	134.8	37.7	12.1	40	82	569.4	249.3	39
Apr-08	3±0.3	30.6	6.95	105.0	21	27	176.2	12.5	127.8	65.4	5.3	161.1	-	14.7	40	75	575.0	235.7	42
May-08	2±0.2	29.7	6.86	112.2	18	25	139.2	11.0	121.3	59.2	16.8	132.3	-	11.3	30	50	511.2	201.8	43
Jun-08	142±18	27.4	6.82	102.5	26	33	203.1	25.6	137.0	92.2	11.6	177.4	26.6	17.6	40	194	687.0	290.8	41
Jul-08	97±12	26.5	6.30	104.8	18	27	167.0	11.8	104.8	72.8	4.2	148.9	8.4	14.9	10	188	534.0	201.3	45

Est. = Estuarine influenced, <dl = below detection limit, - = no sample collected

Table G2 – Major element data for Chapora River sites Cha 03 – Cha 04.

Date of sampling	Discharge ($m^3 s^{-1}$)	T (°C)	pH	DO (%)	TDS (mg L^{-1})	EC (µS cm^{-1})	Na	K	Ca	Mg	F	Cl	NO_3^-	SO_4^{2-}	HCO_3^-	SiO_2	TZ^+	TZ^-	NICB (%)
							(µmol L^{-1})										(µeq L^{-1})		
Cha 03, (Lat:15° 44.097'N Long: 74° 01.169'E)																			
Jun- 07	153±24	30.1	6.47	90.6	45	71	207.1	30.7	190.4	117.7	6.3	143.6	13.4	19.8	340	46	853.8	542.7	22
Jul-07	95±15	26.7	6.50	103.1	35	25	179.7	16.6	116.8	72.4	5.8	147.5	16.0	17.3	260	84	574.6	463.8	11
Aug-07	123±19	25.1	6.13	104.3	34	19	149.2	14.1	86.1	63.4	5.8	116.5	11.1	14.2	300	61	462.2	461.6	0
Sep-07	109±17	25.1	6.38	102.2	22	23	160.1	15.3	98.3	72.4	6.8	119.0	9.7	13.2	100	61	516.9	262.0	33
Oct-07	11±2	-	-	-	16	-	172.3	16.1	107.3	78.6	10.0	112.3	-	11.5	-	221	560.1	145.2	59
Nov-07	11±2	-	-	-	-	-	-	-	-	-	-	-	-	-	-	-	-	-	-
Dec-07	0.1±0.02	28.1	6.70	97.0	-	35	-	-	-	-	-	-	-	-	-	-	-	-	-
Jan-08	0	25.6	6.90	91.2	22	30	177.9	16.9	157.4	90.5	15.8	138.5	-	12.9	40	158	690.7	220.1	52
Feb-08	0	25.6	6.60	90.1	23	32	150.9	15.3	154.4	94.6	-	132.6	15.3	15.0	50	182	664.4	227.9	49
Mar-08	6±1	28.7	6.58	93.9	26	29	184.9	16.9	143.0	113.6	14.2	224.2	15.0	27.1	30	132	714.8	337.6	36
Apr-08	2±0.3	31.3	6.90	95.9	22	28	198.4	21.2	137.7	76.9	9.5	129.5	7.6	14.4	50	126	648.9	225.2	48
May-08	1.4±0.2	30.3	6.76	94.2	18	29	155.3	16.9	125.3	69.9	11.6	125.0	-	13.7	20	104	562.6	184.0	51
Jun-08	112±18	27.5	6.61	94.5	24	32	194.9	24.6	134.7	94.6	4.7	165.3	41.3	20.4	10	192	678.2	262.0	44
Jul-08	77±12	26.8	6.87	96.7	19	27	172.7	12.8	102.8	72.8	11.1	145.3	-	14.2	30	184	536.7	214.6	43
Cha 04, (Lat:15° 42.761'N Long: 73° 57.411'E)																			
Jun- 07	153±24	30.5	6.84	102.8	51	74	205	24	196	117	7	142	10	16	450	54	855.1	641.9	14
Jul-07	95±15	26.8	6.17	103.1	34	24	183	16	107	73	7	148	1	15	260	54	559.5	446.6	11
Aug-07	123±19	25.2	5.99	105.0	27	19	156	13	98	62	7	117	10	14	180	90	490.0	341.7	18
Sep-07	109±17	25.9	6.19	103.5	28	22	163	13	96	70	6	116	24	14	180	59	507.8	353.4	18
Oct-07	11±2	-	-	-	17	-	171	15	109	80	10	115	13	13	-	214	563.8	164.1	55
Nov-07	11±2	-	-	-	-	-	-	-	-	-	-	-	-	-	-	-	-	-	-
Dec-07	0.1±0.02	28.4	6.12	102.6	-	32	-	-	-	-	-	-	-	-	-	-	-	-	-
Jan-08	0	28.0	7.40	108.7	25	36	186	18	197	112	13	150	-	13	40	188	822.2	228.8	56
Feb-08	0	26.7	7.90	119.2	25	36	177	19	187	107	7	137	11	14	50	167	785.9	234.0	54
Mar-08	6±1	28.9	6.78	107.1	24	30	193	20	160	105	7	190	9	15	20	152	745.0	255.3	49
Apr-08	2±0.3	32.6	6.98	161.3	34	30	589	32	173	132	11	125	8	14	50	149	1231.8	221.2	70
May-08	1.4±0.2	31.4	6.85	106.8	22	31	190	22	152	89	8	130	-	12	50	133	694.5	212.1	53
Jun-08	112±18	27.3	6.84	104.3	22	29	191	26	124	86	12	156	16	14	20	182	635.1	232.5	46
Jul-08	77±12	27.9	6.71	101.6	18	26	184	12	102	73	11	149	-	13	20	183	544.3	205.3	45

Est. = Estuarine influenced, <dl = below detection limit, - = no sample collected

Table G3 – Major element data for Chapora River sites Cha 05 – Cha 06.

Date of sampling	Discharge ($m^3 s^{-1}$)	T (°C)	pH	DO (%)	TDS (mg L^{-1})	EC (µS cm^{-1})	Na	K	Ca	Mg	F	Cl	NO_3^-	SO_4^{2-}	HCO_3^-	SiO_2	TZ^+	TZ^-	NICB (%)
							(µmol L^{-1})										(µeq L^{-1})		
Cha 05, (Lat:15° 40.973'N Long: 73° 53.001'E)																			
Jun- 07	153±24	30.1	6.49	89.4	59	2000	Est.	Est.	Est.	Est.	Est.	Est.	Est.	Est.	960	Est.	0.0	959.9	-100
Jul-07	95±15	25.7	6.44	100.1	37	26	197.9	<dl	133.0	57.2	6.8	200.5	12.7	21.0	260	16	578.3	522.1	5
Aug-07	123±19	25.2	6.47	103.5	26	22	137.9	<dl	126.3	0.0	6.8	141.0	0.0	15.5	180	20	390.4	358.8	4
Sep-07	109±17	25.6	6.28	101.3	44	22	143.5	126.9	148.7	204.1	6.3	129.7	9.2	12.9	300	19	976.0	471.0	35
Oct-07	11±2	-	-	-	23	-	137.9	153.2	173.2	246.9	4.7	3.7	3.7	-	-	154	1131.1	12.1	98
Nov-07	11±2	-	-	-	-	-	-	-	-	-	-	-	-	-	-	-	-	-	-
Dec-07	0.1±0.02	26.6	6.43	96.2	-	2000	-	-	-	-	-	-	-	-	-	-	-	-	-
Jan-08	0	27.6	7.40	93.2	6	2000	Est.	Est.	Est.	Est.	Est.	Est.	Est.	Est.	100	Est.	0.0	100.0	-100
Feb-08	0	28.1	7.60	123.0	3	2000	Est.	Est.	Est.	Est.	Est.	Est.	Est.	Est.	50	Est.	0.0	50.0	-100
Mar-08	6±1	30.0	7.03	89.6	6	2000	Est.	Est.	Est.	Est.	Est.	Est.	Est.	Est.	100	Est.	0.0	100.0	-100
Apr-08	2±0.3	32.5	6.77	106.2	6	2000	Est.	Est.	Est.	Est.	Est.	Est.	Est.	Est.	100	Est.	0.0	100.0	-100
May-08	1.4±0.2	32.4	6.76	94.8	6	2000	Est.	Est.	Est.	Est.	Est.	Est.	Est.	Est.	100	Est.	0.0	100.0	-100
Jun-08	112±18	27.8	6.82	96.9	2	210	Est.	Est.	Est.	Est.	Est.	Est.	Est.	Est.	30	Est.	0.0	30.0	-100
Jul-08	77±12	28.5	6.67	99.0	2	34	251.9	160.4	156.4	76.1	3.2	0.0	0.0	0.0	40	176	877.3	43.1	91
Cha 06, (Lat:15° 38.932'N Long: 73° 50.174'E)																			
Jun- 07	153±24	31.1	7.06	92.3	80	2000	Est.	Est.	Est.	Est.	Est.	Est.	Est.	Est.	1310	Est.	0.0	1310.0	-100
Jul-07	95±15	26.8	6.13	100.8	43	32	254.9	91.6	<dl	66.2	6.3	281.8	15.6	25.2	300	26	744.9	654.0	6
Aug-07	123±19	24.5	6.30	107.1	45	24	213.6	136.6	120.5	219.7	7.9	178.0	0.6	21.3	260	12	1030.6	489.1	36
Sep-07	109±17	25.6	5.96	98.7	25	23	202.3	5.4	122.5	8.6	7.4	185.3	10.3	15.8	100	19	469.9	334.6	17
Oct-07	11±2	-	-	-	36	-	836.5	129.2	169.9	207.8	2.1	3.9	3.7	0.3	-	205	1721.0	10.4	99
Nov-07	11±2	-	-	-	-	-	-	-	-	-	-	-	-	-	-	-	-	-	-
Dec-07	0.1±0.02	25.8	6.88	97.7	-	2000	-	-	-	-	-	-	-	-	-	-	-	-	-
Jan-08	0	28.8	7.60	95.3	6	2000	Est.	Est.	Est.	Est.	Est.	Est.	Est.	Est.	100	Est.	0.0	100.0	-100
Feb-08	0	28.4	7.80	107.7	7	2000	Est.	Est.	Est.	Est.	Est.	Est.	Est.	Est.	120	Est.	0.0	120.0	-100
Mar-08	6±1	32.9	7.03	93.0	11	2000	Est.	Est.	Est.	Est.	Est.	Est.	Est.	Est.	180	Est.	0.0	179.9	-100
Apr-08	2±0.3	31.7	7.46	124.1	10	2000	Est.	Est.	Est.	Est.	Est.	Est.	Est.	Est.	160	Est.	0.0	160.0	-100
May-08	1.4±0.2	31.3	7.04	105.6	8	2000	Est.	Est.	Est.	Est.	Est.	Est.	Est.	Est.	130	Est.	0.0	130.0	-100
Jun-08	112±18	27.9	6.88	91.3	2	1337	Est.	Est.	Est.	Est.	Est.	Est.	Est.	Est.	30	Est.	0.0	30.0	-100
Jul-08	77±12	28.7	6.69	99.5	3	75	771.2	177.0	172.7	130.8	3.7	3.7	-	-	50	169	1555.2	57.3	93

Est. = Estuarine influenced, <dl = below detection limit, - = no sample collected

Table G4 – Major element data for Zuari River sites Zua 01 – Zua 02.

Date of sampling	Discharge ($m^3 s^{-1}$)	T (°C)	pH	DO (%)	TDS (mg L^{-1})	EC (µS cm^{-1})	Na	K	Ca	Mg	F	Cl	NO_3^-	SO_4^{2-}	HCO_3^-	SiO_2	TZ^+	TZ^-	NICB (%)
							(µmol L^{-1})										(µeq L^{-1})		
Zua 01, (Lat:15° 14.079'N Long: 74° 11.066'E)																			
Jun- 07	277±44	29.4	6.43	95.1	52	44	<dl	<dl	15	205	6	138	-	11	660	-	440.7	826.4	-30
Jul-07	172±27	26.5	6.22	99.1	29	38	144	7	85	49	6	153	12	12	220	39	420.2	414.4	1
Aug-07	221±35	26.8	6.04	98.5	24	22	153	7	73	54	5	145	12	12	140	40	414.2	325.8	12
Sep-07	197±31	25.9	5.54	99.4	30	38	168	8	85	65	6	142	11	12	220	87	477.5	402.8	8
Oct-07	20±3	-	-	-	-	-	-	-	-	-	-	-	-	-	-	-	-	-	-
Nov-07	20±3	-	-	-	-	-	-	-	-	-	-	-	-	-	-	-	-	-	-
Dec-07	0.2±0.04	26.0	6.45	94.3	-	55	-	-	-	-	-	-	-	-	-	-	-	-	-
Jan-08	0	25.7	6.80	90.8	20	68	143	11	140	103	7	129	12	7	40	111	641.0	201.2	52
Feb-08	0	27.3	6.90	86.5	30	34	188	22	219	144	8	157	36	17	50	154	935.3	285.4	53
Mar-08	11±2	26.1	6.84	89.3	27	34	180	16	200	139	12	146	9	15	50	138	872.8	246.7	56
Apr-08	4±0.5	29.9	6.75	86.4	24	35	161	17	211	122	5	143	-	8	30	126	844.7	192.9	63
May-08	3±0.5	29.8	6.52	87.7	20	31	<dl	<dl	17	272	5	-	11	89	50	<dl	579.7	244.4	41
Jun-08	202±32	25.9	6.24	93.7	19	28	176	18	107	81	1	135	10	13	20	157	569.7	192.9	49
Jul-08	138±22	26.4	6.57	97.7	18	19	198	12	83	70	4	142	10	11	20	152	513.7	198.8	44
Zua 02, (Lat:15° 13.972'N Long: 74° 09.077'E)																			
Jun- 07	277±44	30.3	6.29	91.6	40	32	<dl	<dl	16	174	6	150	10	17	450	-	380.0	649.9	-26
Jul-07	172±27	26.6	6.09	98.6	28	38	144	8	68	52	5	143	14	14	220	37	392.2	409.4	-2
Aug-07	221±35	26.7	6.00	95.7	24	20	146	15	65	54	7	150	14	17	140	35	399.7	344.9	7
Sep-07	197±31	25.2	6.09	101.4	25	36	178	23	84	67	6	147	13	-	140	53	502.0	305.3	24
Oct-07	20±3	-	-	-	-	-	-	-	-	-	-	-	-	-	-	-	-	-	-
Nov-07	20±3	-	-	-	-	-	-	-	-	-	-	-	-	-	-	-	-	-	-
Dec-07	0.2±0.04	25.9	6.42	92.8	1	54	-	-	-	-	-	-	-	10	-	-	0.0	19.6	0
Jan-08	0	25.5	6.70	87.0	22	60	170	12	147	102	12	147	14	10	30	110	681.0	223.2	51
Feb-08	0	28.2	6.60	92.8	27	35	173	13	236	127	11	145	16	9	40	144	911.1	229.0	60
Mar-08	11±2	27.3	6.73	87.5	33	35	448	22	197	156	5	175	-	10	40	134	1177.5	239.7	66
Apr-08	4±0.5	30.8	6.81	80.2	24	38	155	11	190	119	5	147	7	11	40	121	784.2	221.8	56
May-08	3±0.5	31.6	6.82	92.9	17	41	<dl	<dl	19	200	15	168	10	13	50	-	437.3	270.8	24
Jun-08	202±32	25.3	5.90	94.5	19	18	172	20	97	66	4	121	5	13	40	133	517.5	196.0	45
Jul-08	138±22	25.9	6.00	95.9	16	18	196	13	83	67	12	129	-	-	20	152	510.2	160.5	52

Est. = Estuarine influenced, <dl = below detection limit, - = no sample collected

Table G5 – Major element data for Zuari River sites Zua 03 – Zua 04.

Date of sampling	Discharge ($m^3 s^{-1}$)	T (°C)	pH	DO (%)	TDS (mg L^{-1})	EC (µS cm^{-1})	Na	K	Ca	Mg	F	Cl	NO_3^-	SO_4^{2-}	HCO_3^-	SiO_2	TZ^+	TZ^-	NICB (%)
							(µmol L^{-1})										(µeq L^{-1})		
Zua 03, (Lat:15° 13.612'N Long: 74° 08.728'E)																			
Jun- 07	277±44	29.7	6.15	89.8	35	25	<dl	<dl	11	179	10	166	11	23	350	-	381.7	582.8	-21
Jul-07	172±27	28.4	6.17	109.3	36	43	133	9	84	58	6	138	15	13	340	28	424.8	525.6	-11
Aug-07	221±35	27.4	6.16	120.0	25	20	130	7	66	53	7	139	12	13	180	36	377.4	364.5	2
Sep-07	197±31	28.5	6.29	121.0	31	37	153	16	76	64	6	150	10	14	250	63	450.1	444.0	1
Oct-07	20±3	-	-	-	-	-	-	-	-	-	-	-	-	-	-	-	-	-	-
Nov-07	20±3	-	-	-	-	-	-	-	-	-	-	-	-	-	-	-	-	-	-
Dec-07	0.2±0.04	27.4	6.41	92.3	-	51	-	-	-	-	-	-	-	-	-	-	-	-	-
Jan-08	0	26.3	6.10	89.8	16	43	159	11	74	60	10	150	-	16	10	106	437.9	203.0	37
Feb-08	0	27.7	6.00	98.7	20	21	182	11	114	72	7	127	16	20	20	135	564.8	210.8	46
Mar-08	11±2	27.1	6.30	95.1	19	22	159	7	75	62	16	148	11	15	40	113	440.4	245.9	28
Apr-08	4±0.5	29.2	6.36	93.7	25	26	229	13	82	64	5	254	7	22	40	94	534.4	349.4	21
May-08	3±0.5	31.7	6.65	97.5	22	25	<dl	<dl	113	299	5	198	11	18	10	<dl	824.8	259.7	52
Jun-08	202±32	26.3	6.48	91.9	16	18	153	27	82	52	7	118	-	9	20	108	448.0	164.0	46
Jul-08	138±22	26.9	6.04	93.1	19	20	216	13	95	73	5	158	-	12	20	157	565.4	206.8	46
Zua 04, (Lat:15° 16.014'N Long: 74° 06.678'E)																			
Jun- 07	277±44	30.1	6.34	86.4	34	814	<dl	<dl	327	0	Est.	Est.	Est.	Est.	350	0	653.7	349.9	30
Jul-07	172±27	28.2	6.12	97.8	33	42	148	10	79	55	6	158	19	0	300	31	425.6	482.5	-6
Aug-07	221±35	27.2	6.25	110.4	52	21	1360	11	67	54	6	144	15	12	140	42	1612.1	330.3	66
Sep-07	197±31	28.1	6.12	108.2	37	33	163	10	77	68	5	132	15	13	340	53	463.0	516.5	-5
Oct-07	20±3	-	-	-	0	-	-	-	-	-	-	-	-	-	-	-	-	-	-
Nov-07	20±3	-	-	-	0	-	-	-	-	-	-	-	-	-	-	-	-	-	-
Dec-07	0.2±0.04	27.5	6.48	103.5	0	63	-	-	-	-	-	-	-	-	-	-	-	-	-
Jan-08	0	26.5	6.60	80.3	90	387	2995	82	168	373	Est.	Est.	Est.	Est.	30	130	4159.6	30.0	99
Feb-08	0	29.4	7.10	94.1	26	29	252	15	141	99	12	193	10	18	30	136	748.0	280.7	45
Mar-08	11±2	28.6	7.42	86.7	182	453	6286	150	258	790	Est.	Est.	Est.	Est.	40	115	8532.2	40.0	99
Apr-08	4±0.5	32.0	7.39	95.4	24	48	469	19	113	110	6	0	0	33	40	95	935.0	112.1	79
May-08	3±0.5	32.0	6.58	96.8	18	213	<dl	<dl	118	473	Est.	Est.	Est.	Est.	30	<dl	1182.0	30.0	95
Jun-08	202±32	26.3	6.67	92.2	22	23	194	20	108	77	5	150	0	15	60	153	583.6	245.7	41
Jul-08	138±22	27.2	5.99	94.3	20	20	208	13	84	70	4	138	0	6	60	153	527.5	214.6	42

Est. = Estuarine influenced, <dl = below detection limit, - = no sample collected

Table G6 – Major element data for Zuari River sites Zua 05 – Zua 05 opt.

Date of sampling	Discharge ($m^3 s^{-1}$)	T (°C)	pH	DO (%)	TDS (mg L^{-1})	EC (µS cm^{-1})	Na	K	Ca	Mg	F	Cl	NO_3^-	SO_4^{2-}	HCO_3^-	SiO_2	TZ^+	TZ^-	NICB
							(µmol L^{-1})										(µeq L^{-1})		(%)
Zua 05, (Lat:15° 15.460'N Long: 74° 03.457'E)																			
Jun- 07	277±44	30.0	6.48	76.7	34	773	Est.	Est.	Est.	Est.	Est.	Est.	Est.	Est.	560	Est.	0.0	560.0	-100
Jul-07	172±27	28.0	6.18	99.6	40	50	134	127	109	205	6	190	18	16	220	Est.	888.7	466.0	31
Aug-07	221±35	27.5	6.20	99.7	45	24	158	153	117	246	6	174	17	14	260	14	1036.4	486.0	36
Sep-07	197±31	27.9	6.14	99.4	35	50	152	89	114	14	7	167	-	14	260	12	497.4	463.3	4
Oct-07	20±3	-	-	-	0	-	-	-	-	-	-	-	-	-	-	-	-	-	-
Nov-07	20±3	-	-	-	0	-	-	-	-	-	-	-	-	-	-	-	-	-	-
Dec-07	0.2±0.04	28.4	6.22	105.1	0	66	-	-	-	-	-	-	-	-	-	-	-	-	-
Jan-08	0	27.9	6.40	89.9	2	298	Est.	Est.	Est.	Est.	Est.	Est.	Est.	Est.	40	Est.	0.0	40.0	-100
Feb-08	0	30.3	6.70	98.3	22	25	218	143	174	79	7	6	-	-	30	106	865.4	43.3	90
Mar-08	11±2	28.8	6.89	89.7	1	310	Est.	Est.	Est.	Est.	Est.	Est.	Est.	Est.	20	Est.	0.0	20.0	-100
Apr-08	4±0.5	31.5	6.59	97.2	101	28	3901	21	160	80	6	11	-	0.4	20	114	4402.2	37.9	98
May-08	3±0.5	30.9	6.82	99.6	18	34	184	64	146	85	3	-	-	-	50	113	710.6	52.6	86
Jun-08	202±32	25.9	6.11	93.5	15	-	160	133	112	53	4	-	-	-	11	116	623.0	15.0	95
Jul-08	138±22	27.2	6.07	103.6	13	22	147	0	113	65	5	3	-	-	60	150	501.7	68.1	76
Zua 05 opt, (Lat:15° 12.935'N Long: 74° 04.348'E)																			
Jun- 07	277±44	29.5	6.30	98.6	53	38	<dl	<dl	21	393	7	174	9	21	560	0	828.8	791.2	2
Jul-07	172±27	27.6	6.19	100.2	34	54	175	8	89	69	6	173	16	13	260	51	499.0	481.2	2
Aug-07	221±35	26.6	6.18	99.7	28	24	166	8	88	64	5	162	16	14	180	58	478.0	390.9	10
Sep-07	197±31	27.0	6.28	99.8	40	40	192	9	88	87	7	159	20	18	340	65	551.7	562.4	-1
Oct-07	20±3	-	-	-	-	-	-	-	-	-	-	-	-	-	-	-	-	-	-
Nov-07	20±3	-	-	-	-	-	-	-	-	-	-	-	-	-	-	-	-	-	-
Dec-07	0.2±0.04	25.2	6.01	98.9	-	72	-	-	-	-	-	-	-	-	-	-	-	-	-
Jan-08	0	23.6	7.20	87.9	19	91	290	26	137	114	5	4	-	-	40	129	819.6	48.7	89
Feb-08	0	26.1	7.80	95.2	19	44	268	27	161	130	4	4	-	-	40	156	877.1	48.4	90
Mar-08	11±2	25.1	7.13	99.5	25	39	551	22	132	139	5	5	-	-	40	136	1116.3	49.8	91
Apr-08	4±0.5	29.2	6.77	94.8	16	58	236	14	121	102	4	19	-	-	30	109	693.9	52.3	86
May-08	3±0.5	30.1	6.64	98.3	9	32	<dl	<dl	21	225	4	9	-	0.5	40	<dl	492.0	53.5	80
Jun-08	202±32	25.9	5.64	93.8	13	23	193	19	104	83	-	-	-	-	20	154	584.1	20.0	93
Jul-08	138±22	26.9	6.35	97.6	16	22	276	35	106	95	5	4	-	0.4	20	187	714.4	29.8	92

Est. = Estuarine influenced, <dl = below detection limit, - = no sample collected

Table G7 – Major element data for Zuari River site Zua 06.

Date of sampling	Discharge ($m^3 s^{-1}$)	T (°C)	pH	DO (%)	TDS (mg L^{-1})	EC (µS cm^{-1})	Na	K	Ca	Mg	F	Cl	NO_3^-	SO_4^{2-}	HCO_3^-	SiO_2	TZ^+	TZ^-	NICB
							(µmol L^{-1})										(µeq L^{-1})		(%)
Zua 06, (Lat:15° 20.993'N Long: 74° 00.179'E)																			
Jun- 07	277±44	30.2	7.09	73.4	95	2000	Est.	Est.	Est.	Est.	Est.	Est.	Est.	Est.	1560	Est.	0.0	1559.9	-100
Jul-07	172±27	28.0	6.05	94.8	21	278	Est.	Est.	Est.	Est.	Est.	Est.	Est.	Est.	340	Est.	0.0	339.9	-100
Aug-07	221±35	27.5	6.20	101.2	41	54	534	168	110	0	7	-	12	31	220	16	922.6	301.9	51
Sep-07	197±31	28.9	6.53	99.4	176	797	5265	-	-	271	3	-	-	314	300	10	5806.1	930.4	72
Oct-07	20±3	-	-	-	-	-	-	-	-	-	-	-	-	-	-	-	-	-	-
Nov-07	20±3	-	-	-	-	-	-	-	-	-	-	-	-	-	-	-	-	-	-
Dec-07	0.2±0.04	30.2	6.40	90.1	-	2000	-	-	-	-	-	-	-	-	-	-	-	-	-
Jan-08	0	29.5	7.60	93.7	8	2000	Est.	Est.	Est.	Est.	Est.	Est.	Est.	Est.	130	Est.	0.0	130.0	-100
Feb-08	0	30.8	7.40	97.4	5	2000	Est.	Est.	Est.	Est.	Est.	Est.	Est.	Est.	80	Est.	0.0	80.0	-100
Mar-08	11±2	30.8	7.32	97.6	5	2000	Est.	Est.	Est.	Est.	Est.	Est.	Est.	Est.	80	Est.	0.0	80.0	-100
Apr-08	4±0.5	32.5	7.41	115.1	4	2000	Est.	Est.	Est.	Est.	Est.	Est.	Est.	Est.	70	Est.	0.0	70.0	-100
May-08	3±0.5	30.9	6.91	134.1	10	2000	Est.	Est.	Est.	Est.	Est.	Est.	Est.	Est.	160	Est.	0.0	160.0	-100
Jun-08	202±32	26.7	6.71	87.4	1	131	Est.	Est.	Est.	Est.	Est.	Est.	Est.	Est.	10	Est.	0.0	10.0	-100
Jul-08	138±22	27.8	6.35	94.4	67	74	941	899	137	133	2	4	0	0.3	20	120	2380.4	26.4	98

Est. = Estuarine influenced, <dl = below detection limit, - = no sample collected

Table G8 – Trace element data for Chapora River sites Cha 01 - Cha 04.

Date of Sampling	Rb	Sr	V	Cr	Mn	Fe	Al	Co	Ni	Cu	Zn	Pb	Ba
						(ng ml^{-1})							
Cha 01, (Lat:15° 47.795'N Long: 74° 06.072'E)													
Jun- 07	2.5	46.96	1.43	1.75	45.04	95.38	9.82	0.07	1.04	1.21	3.20	0.46	13.15
Jul-07	0.73	22.09	0.91	1.53	5.89	26.06	52.39	0.05	1.29	1.21	5.44	0.09	5.38
Aug-07	0.66	16.92	0.75	0.56	5.42	13.27	47.64	0.06	0.48	2.03	8.86	0.14	4.85
Sep-07	0.83	18.77	0.81	0.43	1.75	3.87	33.29	0.01	0.42	2.07	5.38	0.24	6.12
Oct-07	0.97	24.99	0.79	0.60	14.82	19.65	11.51	0.07	0.55	1.84	14.52	0.77	7.48
Nov-07	-	-	-	-	-	-	-	-	-	-	-	-	-
Dec-07	-	-	-	-	-	-	-	-	-	-	-	-	-
Jan-08	0.89	22.79	0.64	0.44	7.11	1.13	19.49	0.02	0.50	0.69	10.80	0.13	6.83
Feb-08	0.83	27.15	0.62	4.76	6.37	9.51	8.37	0.11	4.96	1.99	8.04	0.13	5.69
Mar-08	0.86	22.15	0.53	0.46	5.90	<dl	8.87	0.04	1.81	6.69	49.47	0.71	124.4
Apr-08	0.24	27.28	0.65	1.14	7.05	4.41	8.10	0.08	3.43	3.21	33.25	0.23	118.3
May-08	1.04	20.97	0.68	0.23	3.56	0.48	10.61	0.01	0.43	0.62	25.07	0.33	5.39
Jun-08	1.07	23.79	0.89	1.19	11.47	<dl	17.01	0.19	5.17	1.08	5.41	0.29	7.38
Jul-08	0.83	20.40	0.84	2.5	25.35	<dl	17.48	0.14	3.27	1.59	11.19	0.24	6.38
Cha 02, (Lat:15° 45.999'N Long: 74° 04.746'E)													
Jun- 07	1.96	32.21	0.57	0.36	102.1	74.47	22.42	0.14	0.52	0.80	3.89	0.19	13.5
Jul-07	0.76	19.03	1.26	0.66	6.29	26.66	56.08	0.04	0.42	1.27	5.99	0.13	5.51
Aug-07	0.71	16.56	0.80	0.97	6.27	169.7	58.31	0.05	0.49	1.19	8.35	0.13	5.26
Sep-07	0.69	18.10	0.74	0.54	15.10	10.75	35.78	0.06	0.33	1.20	5.76	0.14	5.54
Oct-07	1.02	21.36	0.70	0.26	24.95	15.70	39.48	0.08	0.36	1.32	8.86	0.17	6.34
Nov-07	-	-	-	-	-	-	-	-	-	-	-	-	-
Dec-07	-	-	-	-	-	-	-	-	-	-	-	-	-
Jan-08	0.92	19.96	0.40	0.13	23.21	6.32	5.36	0.04	0.25	0.49	7.77	0.15	5.93
Feb-08	0.84	18.56	0.40	0.14	22.27	5.68	6.00	0.05	0.34	1.87	4.86	0.09	4.92
Mar-08	0.93	20.48	0.42	0.12	17.83	<dl	5.75	0.04	0.27	3.89	12.59	0.34	27.71
Apr-08	0.79	20.82	0.58	0.14	10.58	7.31	6.45	0.03	0.32	0.73	17.42	0.05	47.93
May-08	0.96	18.95	0.47	0.15	6.86	2.31	7.40	0.01	0.23	1.06	6.61	0.25	4.38
Jun-08	1.34	23.83	0.86	0.22	22.53	<dl	16.54	0.12	1.89	1.00	4.23	0.13	7.78
Jul-08	0.75	19.35	0.76	0.44	8.61	<dl	13.47	0.09	0.58	2.03	5.41	0.36	5.95
Cha 03, (Lat:15° 44.097'N Long: 74° 01.169'E)													
Jun- 07	2.11	33.31	0.75	0.87	30.55	32.84	22.91	0.07	0.63	1.51	10.74	0.15	11.11
Jul-07	0.88	20.81	0.93	0.61	7.38	28.76	74.90	0.05	0.47	1.37	6.10	0.10	6.26
Aug-07	0.77	17.90	0.82	0.41	8.37	23.65	59.07	0.04	0.32	0.92	5.34	0.23	6.05
Sep-07	0.76	19.45	0.73	0.39	6.54	14.43	45.21	0.05	0.31	0.86	4.67	0.14	5.86
Oct-07	1.00	21.86	0.69	0.26	15.80	5.58	23.83	0.06	0.22	0.76	3.94	0.06	6.09
Nov-07	-	-	-	-	-	-	-	-	-	-	-	-	-
Dec-07	-	-	-	-	-	-	-	-	-	-	-	-	-
Jan-08	1.25	24.09	0.43	0.26	24.11	8.71	11.52	0.05	0.61	1.08	8.73	0.12	8.15
Feb-08	1.12	24.13	0.37	0.15	41.34	13.58	2.98	0.08	0.25	1.12	2.74	0.05	8.66
Mar-08	0.95	24.18	0.52	0.18	16.33	<dl	7.58	0.03	0.34	1.39	32.97	0.14	116.7
Apr-08	0.73	23.55	0.44	0.51	31.77	10.12	7.37	0.09	4.36	2.44	53.35	0.29	175.2
May-08	1.25	20.96	0.43	0.32	13.73	15.13	4.54	0.02	0.24	0.77	5.77	0.27	6.55
Jun-08	1.36	23.58	0.69	0.62	24.60	<dl	8.92	0.13	2.27	1.34	4.99	0.16	9.05
Jul-08	0.86	20.15	0.82	0.59	25.70	<dl	23.60	0.09	0.72	1.12	5.73	0.33	6.89
Cha 04, (Lat:15° 42.761'N Long: 73° 57.411'E)													
Jun- 07	1.78	29.06	0.63	0.84	26.86	30.60	8.65	0.08	0.60	1.47	7.36	0.14	7.90
Jul-07	0.88	20.42	1.03	0.58	8.60	35.04	68.76	0.04	0.42	0.71	5.44	0.06	6.45
Aug-07	0.77	18.57	0.75	0.60	8.63	28.19	74.59	0.05	0.50	1.01	5.25	0.19	5.67
Sep-07	0.77	19.44	0.63	0.42	6.29	22.52	49.94	0.04	0.22	1.02	6.20	0.74	5.86
Oct-07	0.98	21.57	0.72	0.22	13.98	13.05	36.88	0.07	0.26	1.39	3.58	0.07	5.80
Nov-07	-	-	-	-	-	-	-	-	-	-	-	-	-
Dec-07	-	-	-	-	-	-	-	-	-	-	-	-	-
Jan-08	1.35	26.64	0.57	0.15	5.76	3.96	6.05	0.02	0.18	1.43	4.86	0.06	6.39
Feb-08	1.30	23.93	0.54	0.39	28.49	15.66	10.19	0.04	0.88	2.38	3.52	0.17	4.13
Mar-08	1.44	22.89	0.55	0.30	22.40	6.07	24.66	0.05	0.48	2.91	6.19	1.40	8.83
Apr-08	1.57	36.13	0.65	2.85	23.48	20.08	16.59	0.10	2.98	2.30	14.64	0.52	33.69
May-08	1.49	22.05	0.51	0.28	11.81	26.45	7.98	0.03	0.71	1.46	19.33	0.09	6.40
Jun-08	1.43	22.45	0.81	0.40	13.66	21.86	66.99	0.10	1.59	0.89	2.49	0.13	9.20
Jul-08	0.81	20.73	0.72	0.44	12.37	<dl	19.17	0.05	0.78	1.01	3.30	0.21	6.89

<dl = below detection limit

Table G9 – Trace element data for Zuari River sites Zua 01 - Zua 05opt.

Date of Sampling	Rb	Sr	V	Cr	Mn	Fe	Al	Co	Ni	Cu	Zn	Pb	Ba
	(ng ml^{-1})												
Zua 01, (Lat:15° 14.079'N Long: 74° 11.066'E)													
Jun- 07	0.20	1.36	0.16	0.33	<dl	26.64	<dl	<dl	<dl	<dl	5.28	<dl	<dl
Jul-07	0.47	12.51	0.24	0.36	56.47	15.37	12.48	0.06	0.35	0.67	9.13	0.07	4.13
Aug-07	0.49	11.87	0.44	0.62	64.14	17.34	16.23	0.09	0.54	0.44	7.71	0.07	5.38
Sep-07	0.49	11.54	0.29	0.29	68.63	25.75	15.10	0.09	0.49	1.79	10.93	0.16	4.54
Oct-07	-	-	-	-	-	-	-	-	-	-	-	-	-
Nov-07	-	-	-	-	-	-	-	-	-	-	-	-	-
Dec-07	-	-	-	-	-	-	-	-	-	-	-	-	-
Jan-08	0.78	13.17	0.13	0.07	99.06	41.24	4.82	0.06	0.27	2.70	7.11	0.20	2.81
Feb-08	1.85	19.54	0.07	<dl	116.8	29.72	<dl	<dl	0.16	1.54	16.56	0.35	3.30
Mar-08	0.78	17.94	0.20	0.21	73.99	52.06	9.81	0.05	0.38	3.54	73.11	0.45	90.12
Apr-08	0.93	18.16	0.14	0.32	106.0	40.80	9.69	0.05	0.38	0.44	25.34	0.66	3.34
May-08	0.27	1.59	0.24	0.17	<dl	9.75	-	<dl	<dl	<dl	2.01	<dl	<dl
Jun-08	1.72	15.87	2.14	1.99	364.6	757.8	-	1.57	3.03	7.53	26.31	1.92	10.84
Jul-08	0.72	13.53	0.21	0.54	82.16	8.00	11.76	0.05	1.26	5.30	15.78	2.00	5.48
Zua 02, (Lat:15° 13.972'N Long: 74° 09.077'E)													
Jun- 07	0.153	1.43	0.20	0.25	<dl	15.23	-	<dl	<dl	<dl	0.59	<dl	<dl
Jul-07	0.54	10.90	0.35	0.19	74.83	16.80	11.73	0.07	0.36	0.31	8.28	0.06	4.39
Aug-07	0.62	11.20	0.36	0.19	96.89	13.00	13.62	0.10	0.38	0.30	7.97	0.05	4.87
Sep-07	1.22	11.96	0.25	0.41	83.40	29.46	16.13	0.10	2.56	10.00	37.57	0.43	4.98
Oct-07	-	-	-	-	-	-	-	-	-	-	-	-	-
Nov-07	-	-	-	-	-	-	-	-	-	-	-	-	-
Dec-07	-	-	-	-	-	-	-	-	-	-	-	-	-
Jan-08	0.84	14.59	0.11	0.16	81.07	38.39	7.55	0.06	0.30	1.34	26.00	0.54	2.94
Feb-08	1.11	20.20	0.09	0.01	122.3	19.66	8.49	<dl	0.12	0.39	43.66	0.33	4.34
Mar-08	1.20	24.21	0.19	0.39	209.1	55.07	14.70	0.14	0.57	1.59	10.51	0.43	11.75
Apr-08	1.10	19.42	0.09	0.12	157.7	13.61	2.56	0.03	0.26	1.15	7.74	0.13	3.20
May-08	0.21	1.83	0.21	0.08	<dl	<dl	-	<dl	<dl	<dl	2.21	<dl	<dl
Jun-08	1.54	14.85	0.16	0.29	213.0	4.54	17.62	0.24	1.46	1.58	13.29	0.27	5.57
Jul-08	0.82	13.42	0.18	1.08	84.87	10.87	13.14	0.09	-	4.57	16.36	0.87	5.32
Zua 03, (Lat:15° 13.612'N Long: 74° 08.728'E)													
Jun- 07	0.18	1.03	0.17	0.20	<dl	23.56	-	<dl	<dl	<dl	1.29	<dl	<dl
Jul-07	0.78	12.67	0.31	0.10	60.39	5.74	8.13	0.05	0.23	0.35	4.50	0.06	3.47
Aug-07	0.55	11.25	0.29	0.17	15.10	5.36	10.37	0.03	0.26	0.38	5.47	0.06	2.90
Sep-07	0.65	12.29	0.27	0.17	18.89	10.74	5.88	0.03	0.28	1.25	8.57	0.15	2.70
Oct-07	-	-	-	-	-	-	-	-	-	-	-	-	-
Nov-07	-	-	-	-	-	-	-	-	-	-	-	-	-
Dec-07	-	-	-	-	-	-	-	-	-	-	-	-	-
Jan-08	0.70	12.92	0.13	0.19	77.23	23.72	7.66	0.10	0.33	0.96	12.92	0.10	5.35
Feb-08	0.77	17.04	0.18	0.12	119.9	16.88	<dl	0.07	0.23	1.00	32.41	0.18	7.31
Mar-08	0.51	13.29	0.12	0.19	89.16	29.26	7.13	0.10	0.31	0.40	3.73	0.09	5.58
Apr-08	0.82	15.03	0.12	0.29	110.8	28.46	10.20	0.14	1.06	1.37	20.20	0.40	5.27
May-08	0.15	2.50	0.27	0.14	<dl	22.26	-	<dl	<dl	<dl	3.92	<dl	<dl
Jun-08	1.70	16.33	0.72	2.19	188.5	40.29	42.79	0.34	1.81	1.43	9.06	0.42	9.98
Jul-08	0.91	17.40	0.21	0.39	123.0	33.86	16.53	0.13	1.13	1.36	17.13	0.89	8.08
Zua 04, (Lat:15° 16.014'N Long: 74° 06.678'E)													
Jun- 07	0.79	6.92	0.21	0.39	<dl	19.77	<dl	<dl	<dl	<dl	12.09	<dl	<dl
Jul-07	0.71	12.47	0.20	0.19	103.3	21.46	13.54	0.07	0.34	0.70	4.69	0.11	4.84
Aug-07	0.60	11.30	0.41	0.45	52.99	18.37	10.97	0.05	0.35	0.73	5.79	0.11	3.64
Sep-07	0.62	12.53	0.33	0.20	53.05	56.66	11.33	0.04	0.29	0.65	7.58	1.38	3.58
Oct-07	-	-	-	-	-	-	-	-	-	-	-	-	-
Nov-07	-	-	-	-	-	-	-	-	-	-	-	-	-
Dec-07	-	-	-	-	-	-	-	-	-	-	-	-	-
Jan-08	2.51	65.31	0.76	1.56	68.47	94.42	12.67	0.05	0.35	2.59	15.57	0.23	6.11
Feb-08	1.01	20.52	0.10	0.06	12.49	<dl	<dl	<dl	<dl	0.79	13.71	0.18	3.79
Mar-08	2.76	128.0	1.15	3.23	97.71	38.24	6.53	0.06	0.70	3.76	8.40	0.13	8.40
Apr-08	1.06	24.11	0.17	0.22	13.39	0.07	3.31	0.04	0.71	0.87	11.98	0.12	2.71
May-08	0.52	3.26	0.11	0.42	<dl	11.90	<dl	<dl	<dl	<dl	3.86	<dl	<dl
Jun-08	1.42	17.48	0.28	0.71	123.5	16.21	6.04	0.09	1.42	0.81	5.41	0.19	7.32
Jul-08	0.92	14.27	0.18	0.30	109.1	13.99	9.35	0.04	0.89	0.92	6.85	0.43	6.00
Zua 05 opt, (Lat:15° 12.935'N Long: 74° 04.348'E)													
Jun- 07	0.25	1.54	0.19	0.53	<dl	23.46	<dl	<dl	<dl	<dl	5.51	<dl	<dl
Jul-07	0.48	13.91	0.31	0.28	86.55	74.20	19.35	0.07	0.46	0.79	4.39	0.42	3.65
Aug-07	0.54	12.65	0.45	0.31	89.12	20.91	25.14	0.01	0.53	1.67	7.11	0.44	3.82
Sep-07	0.47	13.82	0.34	0.22	72.01	31.75	19.59	0.08	0.34	0.41	6.33	0.66	3.42
Oct-07	-	-	-	-	-	-	-	-	-	-	-	-	-
Nov-07	-	-	-	-	-	-	-	-	-	-	-	-	-
Dec-07	-	-	-	-	-	-	-	-	-	-	-	-	-
Jan-08	1.72	26.78	0.29	0.25	109.2	90.89	19.56	0.15	0.56	8.60	9.55	0.26	9.31
Feb-08	1.73	26.42	0.23	0.08	92.07	53.59	<dl	0.04	0.47	4.43	13.00	0.30	6.87
Mar-08	0.86	28.91	0.23	0.36	76.74	44.57	4.27	0.08	0.38	0.87	20.08	0.11	78.41
Apr-08	1.08	19.99	0.17	0.09	61.02	16.38	2.74	0.03	0.43	0.61	4.95	0.10	3.88
May-08	0.26	1.71	0.15	0.24	<dl	1.57	<dl	<dl	<dl	<dl	3.01	<dl	<dl
Jun-08	1.11	17.96	0.36	0.15	120.3	7.24	11.96	0.09	1.55	1.58	7.85	0.35	6.35
Jul-08	1.59	17.49	0.42	0.93	152.5	37.85	41.22	0.88	-	9.43	121.9	1.75	7.64

<dl = below detection limit

Table G10– Rare Earth Element data for Chapora River sites Cha 01 - Cha 04.

Date of Sampling	Y	La	Ce	Pr	Nd	Sm	Eu	Gd	Tb	Dy	Ho	Er	Tm	Yb	Lu
	(ppb or ng ml^{-1})														
Cha 01, (Lat:15° 47.795 'N Long: 74° 06.072 'E)															
Jun- 07	0.013	0.026	0.027	0.004	0.013	0.004	0.002	0.005	0.000	0.001	0.001	0.001	0.001	0.000	0.000
Jul-07	0.038	0.038	0.044	0.006	0.029	0.006	0.003	0.007	0.001	0.008	0.001	0.005	0.001	0.003	0.000
Aug-07	0.048	0.121	0.065	0.012	0.045	0.010	0.003	0.011	0.002	0.009	0.002	0.005	0.001	0.003	0.000
Sep-07	0.036	0.290	0.054	0.011	0.036	0.008	0.003	0.010	0.001	0.008	0.001	0.003	0.001	0.003	0.000
Oct-07	0.013	0.157	0.016	0.003	0.013	0.003	0.002	0.003	0.001	0.003	0.000	0.001	0.000	0.001	0.000
Nov-07	-	-	-	-	-	-	-	-	-	-	-	-	-	-	-
Dec-07	-	-	-	-	-	-	-	-	-	-	-	-	-	-	-
Jan-08	0.010	0.192	0.010	0.002	0.006	0.002	0.001	0.003	0.000	0.002	0.001	0.001	0.000	0.003	0.000
Feb-08	0.008	0.059	0.009	0.002	0.005	0.001	0.001	0.001	0.000	0.002	0.000	<dl	0.000	0.001	0.000
Mar-08	0.008	0.013	0.018	0.003	0.006	0.005	0.009	<dl	0.000	0.005	0.000	0.001	0.000	0.003	0.000
Apr-08	0.011	0.012	0.014	0.002	0.010	0.003	0.004	0.001	0.000	0.002	0.001	0.000	0.000	0.001	0.000
May-08	0.009	0.023	0.007	0.001	0.004	0.001	0.001	0.002	0.000	0.003	0.001	0.000	0.000	0.003	0.000
Jun-08	0.039	0.035	0.045	0.006	0.033	0.009	0.002	0.012	0.000	0.008	0.001	0.003	0.001	0.008	<dl
Jul-08	0.023	0.205	0.031	0.005	0.019	0.006	0.001	0.004	0.001	0.004	0.001	0.002	0.001	0.003	0.000
Cha 02, (Lat:15° 45.999 'N Long: 74° 04.746 'E)															
Jun- 07	0.029	0.065	0.071	0.010	0.033	0.007	0.003	0.007	0.001	0.009	0.001	0.003	0.001	0.003	0.000
Jul-07	0.036	0.051	0.050	0.008	0.033	0.008	0.002	0.010	0.002	0.010	0.001	0.005	0.001	0.004	0.000
Aug-07	0.065	0.188	0.070	0.012	0.048	0.010	0.002	0.018	0.002	0.014	0.002	0.007	0.001	0.007	0.001
Sep-07	0.018	0.104	0.026	0.003	0.015	0.006	0.002	0.002	0.001	0.003	0.001	0.001	0.001	0.000	0.000
Oct-07	0.026	0.067	0.037	0.005	0.023	0.007	0.002	0.007	0.001	0.004	0.001	0.004	0.001	0.000	0.000
Nov-07	-	-	-	-	-	-	-	-	-	-	-	-	-	-	-
Dec-07	-	-	-	-	-	-	-	-	-	-	-	-	-	-	-
Jan-08	0.006	0.031	0.007	0.001	0.004	0.003	0.001	0.003	0.000	0.002	0.000	<dl	0.000	0.002	0.000
Feb-08	0.006	0.032	0.008	0.002	0.007	0.005	0.001	0.002	0.001	0.001	0.000	0.000	0.000	0.001	0.000
Mar-08	0.010	0.012	0.015	0.001	0.006	0.003	0.002	0.002	0.000	0.005	0.000	<dl	0.000	0.002	0.000
Apr-08	0.006	0.005	0.008	0.001	0.004	0.001	0.002	0.001	0.000	0.003	0.000	0.000	0.000	0.001	0.000
May-08	0.005	0.012	0.007	0.001	0.004	0.003	0.001	0.003	0.000	0.001	0.000	0.000	0.000	0.002	0.000
Jun-08	0.046	0.055	0.063	0.010	0.037	0.009	0.003	0.010	0.002	0.015	0.001	0.005	0.001	0.007	<dl
Jul-08	0.021	0.069	0.030	0.006	0.022	0.006	0.002	0.007	0.001	0.003	0.001	0.003	0.001	0.003	0.000
Cha 03, (Lat:15° 44.097 'N Long: 74° 01.169 'E)															
Jun- 07	0.029	0.045	0.052	0.007	0.027	0.005	0.002	0.007	0.001	0.004	0.001	0.003	0.001	0.002	0.000
Jul-07	0.049	0.059	0.061	0.011	0.046	0.011	0.003	0.011	0.001	0.012	0.002	0.006	0.001	0.003	0.001
Aug-07	0.037	0.076	0.067	0.009	0.035	0.008	0.002	0.010	0.001	0.007	0.002	0.003	0.001	0.004	0.001
Sep-07	0.023	0.075	0.040	0.005	0.023	0.005	0.002	0.003	0.001	0.003	0.001	0.004	0.001	0.001	0.000
Oct-07	0.019	0.034	0.031	0.005	0.018	0.005	0.001	0.007	0.001	0.004	0.000	0.001	0.001	0.003	0.000
Nov-07	-	-	-	-	-	-	-	-	-	-	-	-	-	-	-
Dec-07	-	-	-	-	-	-	-	-	-	-	-	-	-	-	-
Jan-08	0.007	0.035	0.011	0.001	0.005	0.001	0.001	0.004	0.000	0.001	0.001	0.000	0.000	0.002	0.000
Feb-08	0.008	0.017	0.010	0.001	0.008	0.001	0.001	0.002	0.000	0.002	0.000	0.000	0.000	0.003	0.000
Mar-08	0.010	0.012	0.016	0.002	0.004	0.001	0.008	0.003	0.000	0.001	0.001	0.000	0.000	0.001	0.000
Apr-08	0.011	0.010	0.015	0.002	0.008	0.005	0.005	0.002	0.000	0.002	0.001	0.000	0.000	0.003	0.000
May-08	0.007	0.011	0.013	0.001	0.006	0.004	0.001	0.002	0.000	0.003	0.000	0.000	0.000	0.002	0.000
Jun-08	0.038	0.049	0.055	0.010	0.034	0.007	0.003	0.010	0.000	0.011	0.001	0.003	0.000	0.007	0.000
Jul-08	0.022	0.081	0.051	0.006	0.031	0.010	0.002	0.005	0.001	0.005	0.001	0.002	0.001	0.004	0.000
Cha 04, (Lat:15° 42.761 'N Long: 73° 57.411 'E)															
Jun- 07	0.008	0.024	0.018	0.002	0.013	0.001	0.001	0.004	0.000	0.002	0.000	0.001	0.000	0.000	0.000
Jul-07	0.045	0.048	0.064	0.010	0.041	0.010	0.003	0.009	0.001	0.009	0.002	0.006	0.001	0.004	0.000
Aug-07	0.040	0.072	0.078	0.010	0.047	0.010	0.003	0.008	0.002	0.006	0.002	0.004	0.001	0.002	0.000
Sep-07	0.024	0.063	0.045	0.006	0.028	0.006	0.002	0.007	0.001	0.005	0.001	0.002	0.001	0.003	0.000
Oct-07	0.027	0.041	0.049	0.007	0.026	0.005	0.002	0.006	0.001	0.006	0.001	0.004	0.001	0.001	0.000
Nov-07	-	-	-	-	-	-	-	-	-	-	-	-	-	-	-
Dec-07	-	-	-	-	-	-	-	-	-	-	-	-	-	-	-
Jan-08	0.005	0.022	0.006	0.001	0.002	0.002	0.001	0.000	0.000	0.003	0.000	<dl	0.000	0.002	0.000
Feb-08	0.009	0.065	0.016	0.002	0.008	0.001	0.001	0.002	0.000	0.001	0.001	<dl	0.000	0.004	0.000
Mar-08	0.018	0.028	0.029	0.003	0.017	0.000	0.001	0.002	0.000	0.004	0.001	0.003	0.000	0.003	0.000
Apr-08	0.010	0.028	0.019	0.003	0.010	0.006	0.002	0.004	0.001	0.002	0.001	0.001	0.000	0.004	0.000
May-08	0.007	0.025	0.008	0.002	0.007	0.001	0.001	0.001	0.000	0.001	0.000	0.001	0.000	0.002	0.000
Jun-08	0.070	0.078	0.159	0.018	0.077	0.012	0.005	0.008	0.002	0.016	0.002	0.006	0.000	0.007	0.001
Jul-08	0.020	0.093	0.061	0.008	0.027	0.008	0.003	0.005	0.001	0.003	0.002	0.003	0.000	0.006	0.001

<dl = below detection limit, - = no sample

Table G11 – Rare Earth Element data for Zuari River sites Zua 01 - Zua 05opt.

Date of Sampling	Y	La	Ce	Pr	Nd	Sm	Eu	Gd	Tb	Dy	Ho	Er	Tm	Yb	Lu
	(ppb or ng ml^{-1})														
Zua 01, (Lat:15° 14.079'N Long: 74° 11.066'E)															
Jun- 07	26.66	2.810	0.031	0.023	0.004	0.015	0.005	0.001	0.002	0.002	0.000	0.002	0.000	0.001	0.000
Jul-07	0.016	0.027	0.028	0.003	0.014	0.004	0.001	0.007	0.000	0.004	0.000	0.002	0.000	0.002	0.000
Aug-07	0.017	0.037	0.036	0.006	0.015	0.004	0.002	0.002	0.000	0.002	0.000	0.002	0.000	0.003	0.000
Sep-07	0.015	0.038	0.030	0.003	0.018	0.008	0.001	0.002	0.001	0.004	0.000	0.000	0.000	0.004	0.000
Oct-07	-	-	-	-	-	-	-	-	-	-	-	-	-	-	-
Nov-07	-	-	-	-	-	-	-	-	-	-	-	-	-	-	-
Dec-07	-	-	-	-	-	-	-	-	-	-	-	-	-	-	-
Jan-08	0.006	0.041	0.018	0.004	0.004	<dl	0.001	0.000	0.000	0.003	0.000	<dl	0.000	0.002	<dl
Feb-08	0.006	0.031	0.026	0.002	0.018	0.005	0.001	0.006	0.002	0.002	0.003	0.003	<dl	0.003	0.001
Mar-08	0.011	0.017	0.034	0.003	0.020	0.010	0.003	<dl	0.001	0.001	0.000	0.000	0.001	<dl	0.001
Apr-08	0.007	0.017	0.019	0.002	0.007	0.005	0.001	0.000	0.000	0.002	0.000	0.000	0.001	0.002	0.000
May-08	30.22	3.488	0.012	0.016	0.003	0.009	0.005	0.001	0.002	0.003	0.007	0.002	0.001	0.003	<dl
Jun-08	0.562	0.869	2.275	0.206	0.881	0.182	0.047	0.176	0.027	0.136	0.029	0.078	<dl	0.056	0.010
Jul-08	0.025	0.612	0.076	0.010	0.039	0.009	0.001	0.013	0.001	0.006	0.003	0.003	<dl	0.001	0.001
Zua 02, (Lat:15° 13.972'N Long: 74° 09.077'E)															
Jun- 07	21.20	3.407	0.023	0.014	0.003	0.009	0.003	0.003	0.007	0.003	0.003	0.003	0.001	0.003	0.001
Jul-07	0.017	0.028	0.035	0.005	0.017	0.004	0.002	0.005	0.001	0.002	0.000	0.001	0.000	0.002	0.000
Aug-07	0.016	0.029	0.036	0.005	0.022	0.007	0.001	0.004	0.000	0.004	0.001	0.004	0.000	0.002	0.000
Sep-07	0.016	0.050	0.027	0.004	0.015	0.006	0.000	0.002	0.001	0.001	0.000	0.000	0.000	0.001	0.000
Oct-07	-	-	-	-	-	-	-	-	-	-	-	-	-	-	-
Nov-07	-	-	-	-	-	-	-	-	-	-	-	-	-	-	-
Dec-07	-	-	-	-	-	-	-	-	-	-	-	-	-	-	-
Jan-08	0.007	0.046	0.017	0.003	0.005	0.004	0.002	<dl	<dl	0.005	0.000	0.001	0.000	0.000	0.000
Feb-08	0.001	0.018	0.013	0.002	0.011	0.001	0.002	0.005	0.001	0.004	0.002	0.001	<dl	0.001	0.001
Mar-08	0.009	0.025	0.028	0.003	0.008	0.005	0.002	0.001	0.001	0.000	0.001	0.000	0.000	0.002	0.000
Apr-08	0.002	0.013	0.005	0.001	0.002	0.003	0.001	0.000	0.000	0.000	0.000	<dl	0.000	0.002	0.000
May-08	26.47	2.797	0.021	0.007	0.002	0.008	0.004	0.002	0.001	0.002	0.006	0.003	0.002	0.003	<dl
Jun-08	0.019	0.042	0.037	0.009	0.032	0.009	0.006	0.014	0.006	0.007	0.006	0.006	<dl	0.009	0.004
Jul-08	0.024	0.110	0.056	0.011	0.040	0.017	0.006	0.019	0.003	0.007	0.005	0.007	<dl	0.005	0.005
Zua 03, (Lat:15° 13.612'N Long: 74° 08.728'E)															
Jun- 07	19.07	4.343	0.031	0.027	0.003	0.018	0.002	0.002	0.000	0.002	0.006	0.002	0.001	0.004	<dl
Jul-07	0.011	0.017	0.014	0.003	0.009	0.004	0.000	0.002	0.000	0.003	0.001	0.000	0.000	0.001	0.000
Aug-07	0.009	0.020	0.013	0.002	0.010	0.003	0.000	0.001	0.000	0.004	0.000	0.001	0.000	0.002	0.000
Sep-07	0.005	0.026	0.008	0.002	0.010	0.002	0.000	<dl	0.001	<dl	<dl	0.001	0.000	<dl	0.000
Oct-07	-	-	-	-	-	-	-	-	-	-	-	-	-	-	-
Nov-07	-	-	-	-	-	-	-	-	-	-	-	-	-	-	-
Dec-07	-	-	-	-	-	-	-	-	-	-	-	-	-	-	-
Jan-08	0.015	0.034	0.042	0.006	0.022	0.000	0.001	0.006	0.000	0.004	0.001	0.000	0.000	0.003	0.000
Feb-08	0.009	0.046	0.044	0.008	0.030	0.005	0.002	0.012	0.001	0.004	0.001	0.002	<dl	0.001	0.000
Mar-08	0.009	0.019	0.026	0.004	0.016	0.004	0.002	0.008	0.002	0.001	0.000	0.000	0.000	0.003	0.000
Apr-08	0.012	0.029	0.043	0.005	0.022	0.005	0.002	0.004	0.000	0.002	0.001	0.002	0.000	0.002	0.000
May-08	19.81	7.468	0.029	0.042	0.008	0.030	0.006	0.004	0.005	0.006	0.009	0.004	0.008	0.004	<dl
Jun-08	0.089	0.135	0.247	0.028	0.122	0.033	0.008	0.027	0.004	0.021	0.007	0.012	<dl	0.010	0.002
Jul-08	0.021	0.087	0.062	0.010	0.045	0.012	0.003	0.007	0.002	0.009	0.003	0.004	<dl	0.007	0.002
Zua 04, (Lat:15° 16.014'N Long: 74° 06.678'E)															
Jun- 07	302.5	13.17	0.060	0.021	0.003	0.014	0.000	0.002	0.009	0.002	0.003	0.003	0.003	0.004	<dl
Jul-07	0.014	0.028	0.032	0.004	0.016	0.004	0.001	0.003	0.001	0.004	0.001	0.001	0.000	0.002	0.000
Aug-07	0.011	0.024	0.026	0.004	0.016	0.004	0.001	0.003	0.000	0.003	0.001	0.002	0.000	0.004	0.000
Sep-07	0.011	0.028	0.032	0.004	0.021	0.007	0.001	0.009	0.002	0.003	0.000	0.000	0.000	<dl	0.000
Oct-07	-	-	-	-	-	-	-	-	-	-	-	-	-	-	-
Nov-07	-	-	-	-	-	-	-	-	-	-	-	-	-	-	-
Dec-07	-	-	-	-	-	-	-	-	-	-	-	-	-	-	-
Jan-08	0.024	0.071	0.083	0.009	0.034	0.013	0.003	0.002	0.001	0.006	0.001	0.002	0.001	0.007	0.000
Feb-08	<dl	0.025	0.009	0.002	0.008	0.007	0.000	0.003	0.001	0.000	0.003	0.003	<dl	0.002	0.001
Mar-08	0.009	0.039	0.021	0.002	0.007	0.001	<dl	0.002	0.001	0.003	0.000	0.001	0.000	<dl	0.000
Apr-08	0.003	0.027	0.005	0.001	0.002	0.002	0.001	0.000	0.000	0.003	0.000	0.001	0.000	0.002	0.000
May-08	119.2	5.364	0.022	0.020	0.006	0.008	0.004	0.003	0.006	0.003	0.006	0.003	0.005	0.004	0.000
Jun-08	0.037	0.069	0.106	0.018	0.061	0.007	0.005	0.017	0.004	0.015	0.005	0.003	<dl	0.007	0.002
Jul-08	0.013	0.108	0.053	0.006	0.041	0.007	0.001	0.010	0.001	0.005	0.002	0.003	<dl	0.004	0.001
Zua 05 opt, (Lat:15° 12.935'N Long: 74° 04.348'E)															
Jun- 07	31.23	5.569	0.093	0.017	0.004	0.011	0.008	0.001	<dl	0.002	0.006	0.002	0.003	0.003	0.000
Jul-07	0.015	0.030	0.040	0.004	0.016	0.003	0.002	0.006	0.000	0.003	0.001	0.001	0.000	0.002	0.000
Aug-07	0.019	0.050	0.044	0.005	0.021	0.006	0.001	0.003	0.001	0.004	0.001	0.001	0.001	0.003	0.000
Sep-07	0.007	0.015	0.018	0.002	0.011	0.003	0.001	0.000	0.002	0.003	0.000	0.000	0.000	<dl	0.000
Oct-07	-	-	-	-	-	-	-	-	-	-	-	-	-	-	-
Nov-07	-	-	-	-	-	-	-	-	-	-	-	-	-	-	-
Dec-07	-	-	-	-	-	-	-	-	-	-	-	-	-	-	-
Jan-08	0.033	0.056	0.082	0.011	0.051	0.006	0.004	0.003	0.001	0.009	0.001	0.002	0.000	0.007	0.000
Feb-08	0.011	0.055	0.043	0.006	0.022	0.008	0.004	0.011	0.002	0.005	0.003	0.002	<dl	0.003	0.004
Mar-08	0.009	0.015	0.022	0.002	0.012	0.000	0.004	<dl	0.001	0.003	0.000	0.002	0.001	0.000	0.001
Apr-08	0.003	0.010	0.008	0.001	0.004	0.003	0.001	0.001	0.000	0.001	0.000	<dl	0.000	0.002	0.000
May-08	26.85	4.713	0.023	0.012	0.005	0.007	0.003	0.003	0.002	0.003	0.006	0.003	0.005	0.006	<dl
Jun-08	0.034	0.068	0.097	0.013	0.051	0.017	0.005	0.016	0.003	0.012	0.005	0.008	<dl	0.006	0.003
Jul-08	0.127	8.092	0.187	0.023	0.091	0.021	0.010	0.026	0.007	0.022	0.008	0.018	<dl	0.009	0.005

<dl = below detection limit, - = no sample

Appendix H – Saturation Indices for Chapora and Zuari sites (Cha 01 – 04 and Zua 01 – 04)

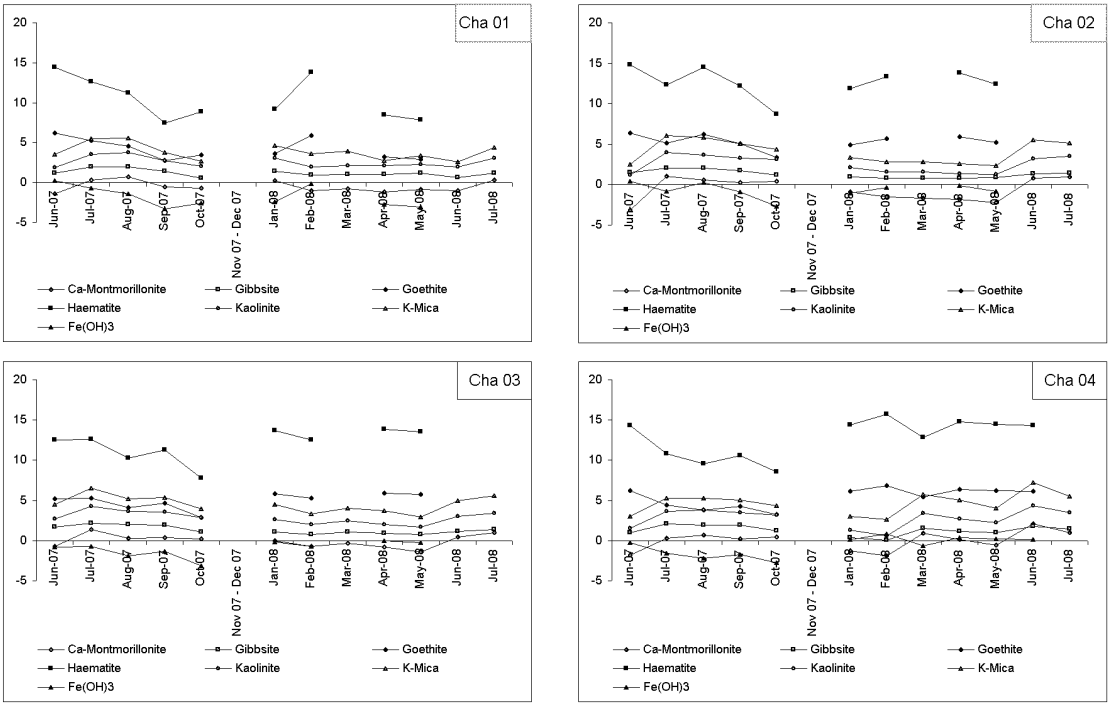

Figure H1: Saturation Indices for Chapora River localities (Cha 01 – 04).

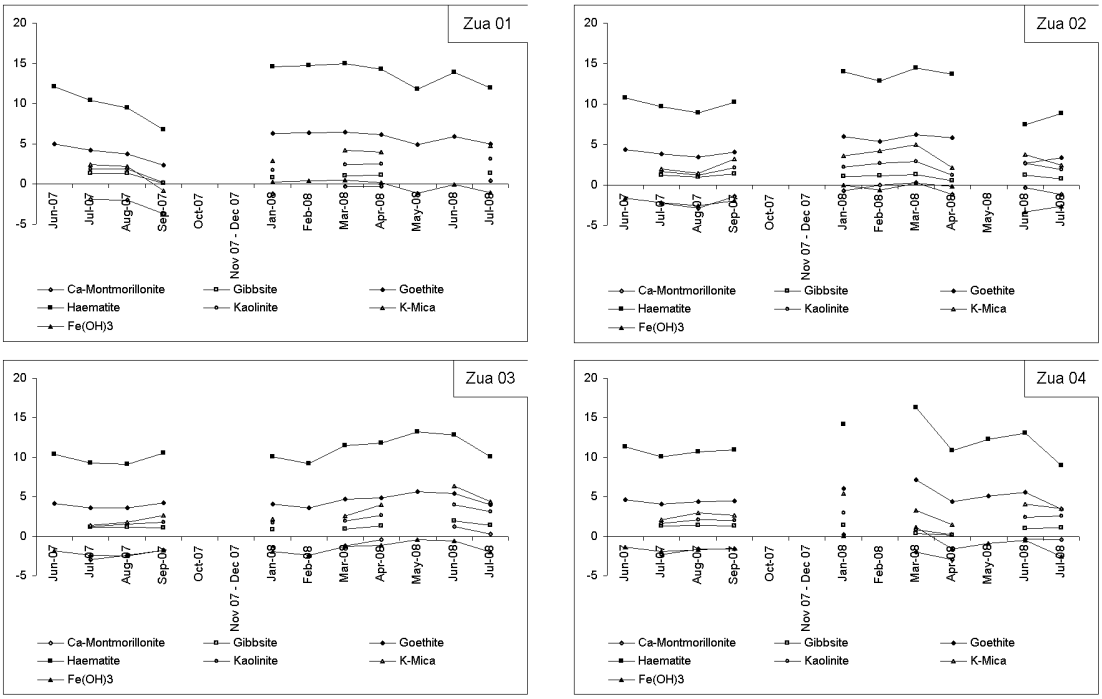

Figure H2: Saturation Indices for Zuari River localities (Zua 01 – 04).

Appendix J – Goldschmidt 2015 Abstracts 1263 – presented 09.30 session 05b in Terrace 1

Controls on seasonal elemental variation in tropical rivers in Goa, India

C. HIBBERT1*, K. A. HUDSON-EDWARDS1 AND
M. WIDDOWSON2

1Birkbeck University of London, Malet Street, London, WC1E 7HZ (*correspondence: chris.hibbert4@ntlworld.com; k.hudson-edwards@bbk.ac.uk)
2Geography, Environment and Earth Sciences Department, University of Hull, Hull HU6 7RX, UK (Mike.Widdowson@open.ac.uk)

Silicate weathering is of primary importance in the long term global climate due to associated CO^2 sequestration. This study aimed to determine the controls on chemical weathering over a 15 month period (May 2007 – July 2008) in a subtropical, monsoonal climatic regime in western India. Here, highly seasonal rivers rising at the Western Ghats escarpment discharge into the Arabian Sea. The Ghats present a topographical barrier to the SW monsoon, and thus generate one of the world's highest orographic gradients. Two river basins were selected for this study, the Zuari and the Chapora, both characterised by high seasonal precipitation and run-off, with c. 85% occurring during the monsoon months (June – September). The rivers flow steeply down the Ghats then across the low-lying Konkan - Kanara coastal plateaux much of which is heavily weathered and covered by laterite. The water samples (n = 13 per month) were collected from seven sites along the Zuari River and six sites along the Chapora River. The samples were analysed using ICP-MS for cations and ion chromatography for anions. Major and trace element concentrations were found to be very low throughout both basins, although a marked increase was observed for various elements (e.g., Ca, K, Mg, Na, Rb, Sr, V, Cr, Mn, Fe, Co, $HCO3^-$) shortly after the onset of the monsoon. We interpret this as a 'rinse-out effect'. Despite absolute concentrations decreasing with increasing river runoff, total element fluxes increase during the monsoon.
Additionally, due to the low elevation of the coastal plain, tidal effects are observed c. 40 km inland becoming forced seaward during the monsoon by high river flows. Continental weathering is controlled by numerous factors, including lithology, climate, vegetation and anthropogenic effects; it is highest in the humid tropics due to high temperatures and precipitation. This study shows that the degree of weathering and the extent of weathering residuum are also major limiting factors for elemental fluxes in tropical catchments.